EVALUATING WETLAND EXTENT TRENDS USING REMOTE SENSING: CASE STUDIES IN THE CANADIAN ROCKIES

ITALO SAMPAIO RODRIGUES
M. Eng. Federal University of Ceará, 2020

A Thesis
Submitted in Partial Fulfillment of the
Requirements for the Degree

DOCTOR OF PHILOSOPHY

in

EARTH, SPACE, AND PHYSICAL SCIENCE

Department of Geography and Environment
University of Lethbridge
LETHBRIDGE, ALBERTA, CANADA

EVALUATING WETLAND EXTENT TRENDS USING REMOTE SENSING: CASE STUDIES IN THE CANADIAN ROCKIES

ITALO SAMPAIO RODRIGUES

Date of Defense: April 4, 2025

Dr. Chris Hopkinson Thesis Supervisor	Professor	Ph.D.
Dr. Laura Chasmer Thesis Examination Committee Member Department of Geography and Environment	Associate Professor	Ph.D.
Dr. Ryan MacDonald Thesis Examination Committee Member MacDonald Hydrology Consultants Ltd.	Senior Hydrologist	Ph.D.
Dr. Suzanne Bayley Thesis Examination Committee Member University of Alberta	Emeritus Professor	Ph.D.
Dr. Hester Jiskoot Internal External Examiner Department of Geography and Environment	Professor	Ph.D.
Dr. Alain Pietroniro External Examiner Department of Civil Engineering University of Calgary	Professor	PhD
Dr. Kevin McGeough Chair, Thesis Examination Committe Department of Geography and Environment	Professor	Ph.D.

Abstract

Mountainous wetlands provide critical ecosystem services, but their sustainability is increasingly threatened by climate change impacts on river flow, runoff regimes, and landscape dynamics. The main objective of this thesis is to investigate how wetland hydrology and land cover in two mountainous regions, the Upper Columbia floodplain in British Columbia and the Eastern Slopes of Alberta (ES), are changing over time and how they could react under future climate scenarios. The specific aims of this thesis are to: 1) Evaluate historical and projected changes in wetland land cover and hydrology in the Upper Columbia River floodplain (1984–2040); 2) Apply and expand these methods to the ES (1984–2023); 3) Quantify open water evaporation relative to forest ecosystem evapotranspiration volumes, and assess seasonal variations between the snowmelt- and rainfall-dominated periods.

Results on Objective 1 indicate that from 1984 to 2022 the Upper Columbia floodplain has already undergone significant hydrological and ecological changes. Peak river discharge now occurs eleven days earlier and with shorter duration, so generating greater peak flows over a shorter period. These shifts have matched a drying trend in wetland habitats and a transition to woody and shrubby vegetation. Under both RCP 4.5 and RCP 8.5, projected data (2020s–2040s) show a continuous reduction in late-summer open water areas; the seasonal peak shifts earlier into spring (April to mid-May). Applying a similar analytical approach to the ES in Objective 2 revealed both parallel and contrasting trends. In the snowmelt-dominated period (late May to mid-July), subalpine (≤2300 m) and alpine (>2300 m) regions experienced increases in open water, non-woody, and woody/shrub vegetation while barren land decreased. On the other hand, the rainfall-dominated period (late July to mid-September) revealed a decline in open water area and an increase in barren land, so suggesting possible seasonal water constraints and vegetation changes. For Objective 3, the estimated proportion (P%) of open water evaporation in relation to volumes of forest ecosystem evapotranspiration. Historically, P% was 2.4% during the snowmelt-dominated period and 2.1% during the rainfall-dominated period. Especially in earlier stages of the hydrologic year, these trends indicate rising contributions of surface water bodies to total evapotranspiration. The consequences comprise changed water availability, habitat changes, and the long-term viability of wetland ecosystem services. The noted seasonality of hydrological changes and acceleration highlights the need for adaptive water management and conservation strategies considering local and regional dynamics.

Keywords: Open water; Climate change; Land cover trends; Forecast; Water resources; Landsat archive

To my grandparents Divani (*in memoriam*) and Gilberto &

to my parents Lucia and Dary.

Acknowledgements

I thank God, Our Lady Mary, and Jesus Christ for the gift of life and all the daily blessings I have received.

To my eternal girlfriend and wife, Brenda Lopes, which accepted to come to Canada with me, giving up her dreaming job, family, and friends back in Brazil. I love you today, and always little Peta. May God bless us for many more days, months, years and decades together S2. To my mother, Lucia, who, regardless of the difficulties, has always supported me unconditionally in everything I do or intended to do. To my father, Dary, who, even from a distance, always shows constant support in everything I do in my life. To my brother, Daniel, we had a blast during the childhood to adult life and having you all here in Canada was simply outstanding. Love you brother! To my entire family and relatives (Tio Diogenes, Tia Ana, Ceiça, Elmo) who constantly listens to me, shared good and bad moments, I love you!

To my brother Caio Alencar and sister-in-law Thais Costa and friends of life Pedro Fernandes, Suelen Pitombeira and Glauber Rodrigues for always being by my side in moments of joy, difficulty and perseverance.

To my fantastic Brazilian (Murilo, Maria, Preto and Felipe, Daniel and Felipe, Julia and Marcelo), Canadian (Ben Pearse, Celeste Barnes, Jessica, Emily, Joe), and international (Paula, Saeid, Farnoosh, Oshini, Josh, Kristin) friends, thanks for making this PhD journey smother.

To my supervisor, Professor Chris Hopkinson, thank you for the company, trust, and exceptional hydrological and remote sensing chats. Thank you for your time and dedication to this project, despite our many challenging circumstances; in particular, thank you for your patience with my English writing. I will always be grateful to you for the opportunity you gave me in the PhD since the beginning (even do not knowing me), you changed my life for the best man, and I will never forget it. The concluding of this work would not be possible without your advice and constant questions.

To my committee members, Professor Laura Chasmer, Professor Suzanne Bayley, and Dr Ryan MacDonald for the valuable contributions that certainly helped me in the completion of this work and in my academic education.

To the University of Lethbridge, which through its professors, staff and

outsourced workers made this work possible.

To the funding sources: NSERC (grant no. 2017-04362), Alberta Innovates, the Nexen Fellowship in Water Resources, Columbia Wetlands Stewardship Partners, School of Graduate Students Tuition Scholarship, and the Shuswap Band's Columbia Headwaters Aquatic Restoration Secwépemc Strategy (CHARS) project, without them all, this research would not be possible.

To the Federal University of Ceará Professors, especially to Professors Carlos Alexandre, José Carlos, Pedro Medeiros, Iran Lima Neto and Adunias Teixeira for their collaboration and constant advice. I have great admiration for you all, not only as researchers or professors, but essentially as human beings.

To my friends of HIDROSED, who I was glad of sharing coffees and friendship; I will carry you all with me for the rest of my life, specially: Adão, Suzi, Ariana, Brenno, Christine, Gabriela, Jairo, Juliana, Maiany, Thales and Alisson.

I thank everyone who believed in me during this cycle.

Contribution of Authors

This thesis consists of four scientific manuscripts, of which to date two are published within peer-reviewed, open access academic journals. Thesis Chapters 2 and 3 were published as open-access, peer-reviewed journal articles. Thesis Chapters 4 and 5 will be submitted for publication after thesis defense. This work is the result of multiple collaborative efforts, with specific contributions listed below.

Chapter 2: Multi-decadal floodplain classification and trend analysis in the Upper Columbia River valley, British Columbia

Citation:
Rodrigues, I. S., Hopkinson, C., Chasmer, L., MacDonald, R. J., Bayley, S. E., & Brisco, B. (2024). Multi-decadal floodplain classification and trend analysis in the Upper Columbia River valley, British Columbia. Hydrology and Earth System Sciences, 28(10), 2203-2221. https://doi.org/10.5194/hess-28-2203-2024

Author Contributions:
Italo Sampaio Rodrigues: investigation, formal analysis, data curation, conceptualization, and writing – original draft.
Chris Hopkinson: investigation, formal analysis, data curation, conceptualization, and writing – original draft, review, and editing.
Laura Chasmer: visualization, supervision, conceptualization, and writing – review and editing.
Ryan MacDonald: visualization, supervision, methodology, and writing – review and editing.
Suzanne Bayley: visualization, supervision, resources, project administration, funding acquisition, conceptualization, and writing – review and editing.
Brian Brisco: conceptualization and writing – review and editing.

All of the authors have read and agreed to the published version of the manuscript.

Chapter 3: Warmer air temperatures predicted to result in wetland drying in the Upper Columbia River Valley, British Columbia, Canada

Citation:
Rodrigues, I. S., Hopkinson, C., Chasmer, L., MacDonald, R. J., & Bayley, S. E. (2025). Warmer air temperatures predicted to result in wetland drying in the Upper Columbia River Valley, British Columbia, Canada. *Science of The Total Environment*, *959*, 178261. https://doi.org/10.1016/j.scitotenv.2024.178261

Author Contributions:
Italo Sampaio Rodrigues: investigation, formal analysis, data curation, validation, conceptualization, writing, and methodology – original draft, review and editing.
Chris Hopkinson: investigation, formal analysis, data curation, software, resources, methodology, conceptualization, supervision, funding acquisition, and writing – original draft, review, and editing.
Laura Chasmer: conceptualization, investigation, methodology, supervision, writing – review & editing.
Ryan MacDonald: conceptualization, supervision, writing – review & editing.
Suzanne Bayley: funding acquisition, investigation, project administration, supervision, writing – review & editing.

All of the authors have read and agreed to the published version of the manuscript.

Chapter 4: Aquatic and Riparian Land Cover Trends across Mountainous Headwater Basins in Alberta, Canada

Chapter 4: This chapter is in preparation for submission to a journal that is yet to be determined.

Author Contributions:
Italo Sampaio Rodrigues: investigation, formal analysis, data curation, validation, conceptualization, writing, and methodology – original draft, review and editing.
Chris Hopkinson: investigation, formal analysis, data curation, software, resources, methodology, conceptualization, supervision, funding acquisition, and writing – original draft, review, and editing.

Chapter 5: Trends in the extent of water bodies related to evapotranspiration rates in the Eastern Slopes of Alberta, Canada

Chapter 5: This chapter is in preparation for submission to a journal that is yet to be determined.

Author Contributions:
Italo Sampaio Rodrigues: investigation, formal analysis, data curation, validation, conceptualization, writing, and methodology – original draft, review and editing.
Chris Hopkinson: investigation, formal analysis, data curation, software, resources, methodology, conceptualization, supervision, funding acquisition, and writing – original draft, review, and editing.

During my PhD (2020 – 2025), I was involved in the following manuscripts which were not included in this thesis:

- **Rodrigues, I. S.**, Costa, C. a. G., Teixeira, A. D. S., Neto, I. E. L., Lopes, F. B., & De Araújo, J. C. (2025). Effects of floating macrophytes on open-water evaporation in a Brazilian tropical reservoir. *Journal of South American Earth Sciences*, *164*, 105683. (https://doi.org/10.1016/j.jsames.2025.105683)

- Rodrigues, G. P., Brosinsky, A., **Rodrigues, I. S.**, Mamede, G. L., & de Araújo, J. C. (2024). Impact of reservoir evaporation on future water availability in north-eastern Brazil: a multi-scenario assessment. *Hydrology and Earth System Sciences*, 28(14), 3243-3260. (https://doi.org/10.5194/hess-28-3243-2024)

- **Rodrigues, I. S.**, Rodrigues, G. P., Costa, C. A. G., Hopkinson, C., & de Araújo, J. C. (2024). Connectivity of evapotranspiration processes in a Brazilian dryland reservoir using remote sensing. *Agricultural and Forest Meteorology*, 351, 110017. (https://doi.org/10.1016/j.agrformet.2024.110017)

- Rodrigues, G. P., **Rodrigues, I. S.**, Raabe, A., Holstein, P., & de Araújo, J. C. (2023). Direct measurement of open-water evaporation: a newly developed sensor applied to a Brazilian tropical reservoir. *Hydrological Sciences Journal*, 68(3), 379-394. (https://doi.org/10.1080/02626667.2022.2157278)

- Rocha, S. M., Molinas, E., **Rodrigues, I. S.**, & Neto, I. E. L. (2023). Assessment of total evaporation rates and its surface distribution by tridimensional modelling and remote sensing. *Journal of Environmental Management*, 327, 116846. (https://doi.org/10.1016/j.jenvman.2022.116846)

- **Rodrigues, I. S.**, Costa, C. A. G., Raabe, A., Medeiros, P. H. A., & de Araújo, J. C. (2021). Evaporation in Brazilian dryland reservoirs: Spatial variability and impact of riparian vegetation. *Science of The Total Environment*, 797, 149059 (https://doi.org/10.1016/j.scitotenv.2021.149059).

- **Rodrigues, I. S.**, Costa, C. A. G., Neto, I. E. L., & Hopkinson, C. (2021). Trends of evaporation in Brazilian tropical reservoirs using remote sensing. *Journal of Hydrology*, 598, 126473. (https://doi.org/10.1016/j.jhydrol.2021.126473)

Table of Contents

List of Figures

Fig. 5.9. A conceptual representation illustrating the historical environmental challenges in the Eastern Slopes of Alberta.

List of Tables

List of Abbreviations

%RMSE	Percent Root Mean Square Error
%TE	Total Percentage Errors
AGV	Aboveground Vegetation
ANN	Artificial Neural Networks
AP	Aerial Photos
BC	British Columbia
CA	Cellular Automata
CanESM5	Canadian Earth System Model version 5
CMIP6	Coupled Model Intercomparison Project Phase 6
DEM	Digital Elevation Model
Dfc	Subarctic
ENVI	Environment for Visualizing Imagery
ES	Eastern Slopes of Alberta
Est	Estimated Historical Monthly
ET	Evapotranspiration
ETM+	Enhanced Thematic Mapper Plus
GCMs	Global Climate Models
GEE	Google Earth Engine
IPCC	Intergovernmental Panel on Climate Change
LC	Land Cover
Lidar	Light Detection and Ranging
LS	Late Summer
LS5	Landsat 5 archive
LSM	Linear Scaling Method
M	Marsh
M – Ow	Marsh to Open Water
M – Wm	Marsh to Wet Meadow
M – Ws	Marsh to Woody/Shrub
MNDWI	Modified Normalized Difference Water Index
MODIS	Moderate-Resolution Imaging Spectroradiometer
MOLUSCE	Modules for Land Use Change Simulations
MSS	Multispectral Scanner
NIR	Near Infra Red
NSE	Nash-Sutcliffe Coefficient
NDVI	Normalized Difference Vegetation Index
NDWI	Normalized Difference Water Index
Obs	Historical Monthly
OLI	Operational Land Imager
OW	Open Water
OW – M	Open Water to Marsh
Ow – Wm	Open Water to Wet Meadow
Ow – Ws	Open Water to Woody/Shrub
P%	Proportion
$P\%_A$	Average P%
PCA	Principal Component Analysis
PDO	Pacific Decadal Oscillation
PDFs	Probability Density Functions
PFA	Permanent Forest Area

PNA	Pacific North America
R^2	Coefficient of Determination
RCM	Regional Climate Models
RCP	Representative Concentration Pathway
RF	Random Forests
RMSE	Root Mean Square Error
RPAS	Remotely Pilot Airborne System
RS	Remote Sensing
S	Spring
S2	Sentinel 2 archive
SAR	Synthetic Aperture Radar
SM	Snowmelt-dominated Period
SSP2	Shared Socioeconomic Pathways 2
SSP5	Shared Socioeconomic Pathways 5
Su	Summer
SWIR	Short Wave Infra Red
SVM	Support Vector Machine
TCT	Tasseled Cap Transform
Td	Tundra
TE	Total Error
TM	Thematic Mapper
TPI	Topographic Position Index
UAV	Unmanned Aerial Vehicle
UCRW	Upper Columbia River Wetlands
WM	Wet Meadow
Wm – M	Wet Meadow to Marsh
Wm – Ow	Wet Meadow to Open Water
Wm – Ws	Wet Meadow to Woody/Shrub
WS	Woody/Shrub
Ws – M	Woody/Shrub to Marsh
Ws – Ow	Woody/Shrub to Open Water
Ws – Wm	Woody/Shrub to Wet Meadow

Chapter 1: Remote Sensing as a Tool to Assess Trends and Changes in Temperate Montane Wetlands: A Review

Abstract

Montane wetlands are undergoing change; however, their remote locations and limited field observations, particularly in smaller or emerging areas (like high-elevation benchlands), have hindered comprehensive monitoring. While remotely sensed data offers extensive historical datasets dating back to the 1980s, such as the Landsat archive, a challenge arises due to the inability to accurately resolve wetlands and transitional areas at this spatial resolution of 30 meters, leading to uncertainty about the changes that have occurred. On the other hand, while higher spatial resolution imagery, such as Sentinel-2, is great, it lacks long time frames. To effectively quantify long-term (multi-decadal) and seasonal dynamics, systematic observations at higher spatial (e.g., <30 m) and temporal (e.g., weekly to monthly) resolutions are essential over a minimum period of 10–20 years to differentiate trends from natural variability. This study reviews the use of remote sensing (RS) to assess trends and change in the extents of temperate montane wetlands, with an emphasis on the Canadian Cordilleran contexts of Alberta and British Columbia. The tools, such as active and passive remote sensing sensors, along with techniques including field-based methods and both supervised and unsupervised algorithms, utilised in studies of montane wetlands are reviewed. For regional or large-area assessments, Landsat 5 and 8 are the most cost-effective tool to evaluate trends and changes, due to consistent and continuous data collection. Although the maximum likelihood algorithm has been the commonly used image landcover classifier, RS indices are frequently employed for change detection. This region has also been impacted by rapid transformation, as the continuous increase of air temperature normals accelerates the melting of snowpack, glaciers, permafrost, and rocky glaciers, changing stream and river discharge, potentially increasing evapotranspiration rates. This reduces late-summer moisture reserves, prolonging dry spells and increasing the likelihood of drought.. Overall, this review identifies a) technologies and methods for quantifying changes in wetlands using remotely sensed data and b) the changes in wetlands that have occurred in this region as observed using remotely sensed data.

Keywords: Mountain Wetlands; Drought Vulnerability; Hydrological Trends; Land Cover Change; Climate Change

1.1 Introduction

Wetlands are dynamic ecosystems characterized by saturated soils, standing water, and unique vegetation adapted to aquic conditions. According to the National Wetlands Working Group (1997) wetlands are generally separated into open water wetlands (shallow ponds or lakes with submerged vegetation), swamps (forested wetlands dominated by trees or shrubs), bogs (rain-fed, acidic peatlands with sphagnum moss), and fens (groundwater-fed, mineral-rich peatlands supporting sedges and grasses). Often separated, marshes are herbaceous wetlands with emergent plants including cattails (Keddy, 2010). From carbon sequestration (Hrach et al., 2021) to flood control (Westbrook et al., 2010), these ecosystems offer vital services; however, their structure and purpose change greatly depending on geography, hydrology, and temperature (Gorham, 1991).

In the Canadian Cordillera, temperate montane wetlands are unique in their elevation-dependent hydrology and biodiversity. Unlike lowland wetlands, they mostly depend on snowmelt and groundwater discharge, producing patchy, small-scale systems including alpine marshes (seasonally inundated meadows) and benchland fens (peatlands on terraced slopes). Temperate montane headwater wetlands influence downstream eco-hydrology (Chatterjee et al., 2010) by storing water during wet periods and often maintaining downstream runoff during dry periods (Brinson and Malvárez, 2002). However, these wetlands are particularly vulnerable to climate change, as warming temperatures alter snowpack duration and precipitation patterns, threatening specialist species like the endangered Whitebark Pine (*Pinus albicaulis*) that depend on these habitats (Stewart et al., 2020). As ecosystems (i.e., integrated communities of organisms interacting with their physical environment) montane wetlands support food webs spanning aquatic insects to grizzly bears (*Ursus arctos*), underscoring their role as biodiversity hotspots in mountainous regions (Russell and Bauer, 2000; Hood and Bayley, 2009; Díaz et al., 2014; Cooper et al., 2017).

The Canadian Cordilleran region of Alberta and British Columbia (BC) is undergoing landcover changes due to climate change (Schnorbus et al., 2012; Trant et al., 2020). While deglaciation and treeline expansion are known and expected changes (MacDonald et al., 1993; Hopkinson and Young, 1998; Rhemtulla et al., 2002; Stockdale et al., 2015; McCaffrey and Hopkinson, 2020a), impacts to wetlands are less obvious or well understood. There is a need to evaluate the spatial and temporal patterns and trends associated with wetland loss, expansion, or genesis in these environments. Montane and alpine wetlands are primarily nourished by local groundwater resurgence, snowmelt, and rainfall, but unlike valley floodplain wetlands, they lack

cumulative water inputs from large upslope areas (Carlson et al., 2020). Their hydrology is characterized by high spatiotemporal variability, as they often depend on limited upstream contributions (e.g., a single snowfield or hillslope seep) (Hayashi, 2020). In contrast, valley wetlands integrate water from entire watersheds, buffering them against local variability (Lee et al., 2015). However, climate change is expected to alter water supply magnitudes and timing, which will impact the frequency of drought (e.g. Kienzle, 2006) in montane and alpine regions, as a consequence of changing precipitation trends (Musselman et al., 2018), timing of snow and glacial melt (Milner et al., 2017), as well as warming and evapotranspiration (Helbig et al., 2020).

Wetland changes can be evaluated using repeat field assessments (Zhang et al., 2018a; Gibson et al., 2022), though the effort can be costly and labor-intensive, and limits the number of possible site visits. Remote wetlands, where access limits measurements over the whole spectrum of ecological variability, aggravate these difficulties. Furthermore, the need for repeat visits depends on the research goals since some studies (e.g., baseline inventories) may need only a single assessment while others (e.g., hydrological trend analyses) demand longitudinal data. Moreover, wetland changes sometimes develop gradually over decades, a timescale that usually surpasses the length of funding cycles, which makes continuous monitoring challenging. For instance, Zhang et al. (2018a) collected 120 soil samples from the Karuola Glacier wetlands over several seasons on the Qinghai-Tibetan Plateau (China) and then used X-ray fluorescence spectrometry to look at metals including cadmium and lead. Comparing samples from grazing paths, tourist sites, and unspoiled areas, the authors evaluated the effect of human activity on metal concentrations and found trailside soils with lead levels three times higher than those in undisturbed areas. Gibson et al. (2022), in the Oil Sands Region (Athabasca, Canada), used isotopic "fingerprints" to separate industrial impacts from natural water balance fluctuations by methodical water sampling of 67 wetlands. Their results highlighted a notable change in hydrology as oil sands wetlands held 40% less water than undisturbed sites.

On the other hand, RS approaches are well-suited to assessing wetland changes (e.g., vegetation- and/or water-extent dynamics) over time. For example, the Landsat program has been collecting data since the MSS era (1972–1992) through TM/ETM+ (1982–2022) and into the current OLI sensors (2013-present), providing a continuous sequence of satellite images that can span over 40 years (Senay et al. 2017) and even longer using ground or airborne photography (Luo et al., 2019). Field measurements and RS techniques can be integrated to quantify and better

understand wetland changes across spatial and temporal scales (Dahl, 2006). The integration of these methods results in essential baseline data that informs a variety of applications, ranging from monitoring hydrological changes to aiding in habitat conservation and restoration efforts.

The primary objective of this review is to evaluate the use of remote sensing (RS) -based assessment of temperate montane wetland changes in the Canadian Cordillera, to support climate change impact assessment, regional planning, and resource management. Additionally, to demonstrate how this region has been threatened through time, along with the primary causes and effects. The main objective of this review is to describe the use of RS for understanding wetland change in the Canadian Rockies. To do this, the review is structured as follows: (1) defining the study area (section 1.2), (2) cataloguing wetland mapping methods (section 1.3), (3) evaluating RS change-detection techniques (section 1.4), and (4) describing montane wetland trajectories in the Canadian Cordillera (section 1.5). This review will guide selecting appropriate RS methodologies for monitoring mountainous wetland dynamics, using global examples to contextualize Canadian findings.

1.2 Temperate Montane Wetland in Canada

Temperate montane wetlands remain less affected by anthropogenic impacts compared to those in lowlands/valleys, where land development, and water withdrawals have caused wetland losses over the past two centuries (Dahl, 1990). Therefore, temperate montane wetlands are an important indicator landcover for identifying climate change-induced hydrological process dynamics over time (Lee et al., 2015).

In Canada, temperate montane wetlands are located in the Montane Cordillera Ecozone, which is located in an area of approximately 470,000 km² between central British Columbia and western Alberta (Figure 1.1) where montane wetlands cover approximately 8,200 km² or almost 2% of the land area (Environment and Climate Change Canada, 2016). Despite the small relative area, these wetland landcovers provide essential hydro-ecological functions to proximal and downstream ecosystems as well as transient animal communities, among other services.

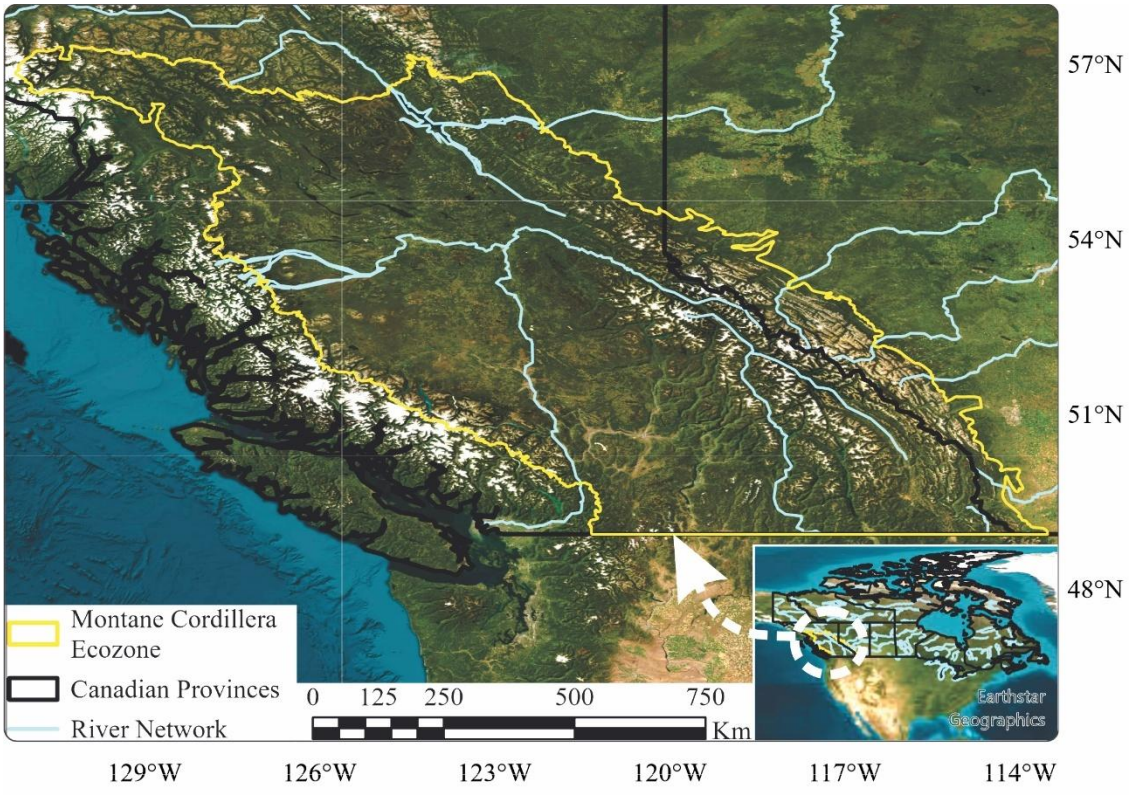

Fig. 1.1. Extent of the Montane Cordillera Ecozone in Canada.

The impact of climate change in these regions will lead to increasing air temperatures, more rapid snow- and glacier-melt which further altering stream and river flow, lake levels and open water areas, decreasing water availability in late summer through increased evapotranspiration (i.e., combination of evaporation from soil, water bodies, and transpiration through plant stoma during photosynthesis), which further increases the potential for drought (Johnson et al., 2005; Kienzle, 2006). In this region, drought appears as extended periods of soil moisture shortages that prevent wetland functionality, characterized by significant drops in the water table (over 30 cm) and vegetation stress persisting for 60 days or more (Bonsal and Regier, 2007). Montane wetlands face significant vulnerability, with reduced snowmelt and increased evaporation potentially leading to a 15–40% reduction in wetland area during dry spells (Schindler and Donahue, 2006). This decline poses a threat to species such as the harlequin duck (*Histrionicus histrionicus*), which relies on these essential habitats.

Research has been conducted in the Canadian Rock mountains (Luckman, 1990; Luckman and Kavanagh, 2000; Trant et al., 2020; Danby and Hik, 2007) as well as over worldwide temperate

mountain wetlands (Fassnacht et al., 2018; Leppi et al., 2011; Pederson et al., 2010; Valeo et al., 2007) to assess how local meteorological shifts and land use change have affected these ecosystems. The Canadian Rockies have been an indicator of environmental shifts, as per Luckman (1990), which used field photographic and observations comparisons to assess mountain land cover change, by capturing glacial retreat and shifts in vegetation that servers as indicators of climate change. Building on this method, Luckman and Kavanagh (2000) combined dendrochronological analysis with geomorphological assessments to show how past climate changes have left tangible marks on both the physical environment and living communities. Recent studies by Trant et al. (2020) utilized historical photographs, and vegetation surveys to measure the rate of ecosystem change over a century. In addition, Danby and Hik (2007) used spatial analysis of tree establishment patterns alongside microclimate monitoring to explore site-specific elements influencing treeline dynamics.

Worldwide, Kandel and Acharya (2024) used remote sensing and geographic information system techniques to identify changes in land cover in the Rara Wetland of Nepal. Sun et al. (2020) examined satellite imagery and climate records from the Qinghai–Tibetan Plateau to investigate how alpine wetland productivity reacts to air temperature. Their findings revealed that vegetation indices are more influenced by thermal variations than by changes in precipitation. In the southern Appalachian region, Zhou et al. (2016) utilized vegetation indices obtained from remotely sensed imagery to assess net primary productivity in montane wetlands, providing essential data for ecological forecasting. In North Africa, Zerai and Mahdavi (2024) combined satellite imagery, field surveys, and hydrological modelling to examine the impacts of drought on the Ichkeul Lake–Bizerte Lagoon system. Andrade et al. (2020) explored spectral vegetation indices to observe the dynamics of high-altitude wetlands in the North Andes, enabling more focused ecological monitoring. Together, these studies highlight the crucial importance fieldwork and remote sensing technologies to assess mountain wetlands around the world as they adapt to shifting climatic conditions.

1.3 Methods for Wetland Identification

1.3.1 Linking Fieldwork to Remote Sensing Methods

In environmental monitoring, fieldwork fulfills three main purposes, such as, baseline ecological data collecting (e.g., species richness, biodiversity metrics), validation of remote sensing observations, and hydrological and ecological model calibration (Munge et al., 2017). Although

fundamental, field campaigns have natural scaling difficulties when combined with moderate-resolution satellite data (e.g., Landsat, Sentinel-2, MODIS). Strong upscaling techniques are necessary to guarantee accurate sensor calibration and validation in the spatial mismatch between point-based ground measurements (usually <1 m^2) and pixel sizes (900 m^2 for MODIS, 100 m^2 for Sentinel). In heterogeneous montane wetlands, where microtopographic changes affect ecological conditions at sub-pixel levels, this scaling problem is especially severe.

Effective wetland evaluation in the Canadian Cordillera begins with accurate observation and land cover classification of these dynamic regions. Supporting remote sensing applications depends on field validation, which generates ground-truth data enhancing the accuracy of assessments of vegetation structure, hydroperiod detection, and land cover classification. For instance, to create a comprehensive 10-m resolution wetland inventory for Canada, the Canadian Wetland Inventory Map Version 3A combined environmental features and in situ validation with multi-source imagery, including Sentinel-1, Sentinel-2, and ALOS PALSAR-2 (Pouliot et al., 2023). However, it is essential to understand the temporal dynamics of wetland inundation. Using Sentinel-1 SAR coherence data between 2017 and 2020, Amani et al. (2022) observed in Alberta that most wetlands were flooded less than 50% of the time. Furthermore, tools such as Lidar have enhanced the ability to conduct fine-scale, three-dimensional mapping of wetland vegetation, which complements multispectral satellite data and aids in the quantification of vegetation structure and phenology (White et al., 2013).

Tracking changes in wetlands across time calls for a combination of satellite archives, in situ observations, and aerial historical images. Examining four decades of Landsat images (1984–2020) in Alberta, Amani et al. (2021) found notable land cover changes connected to human activity and climate, so indicating trends in wetland extent. Moreover, emerging technologies such as hyperspectral remote sensing offer new opportunities to monitor wetland biogeochemistry. Fraser et al. (2014) for example showed that in wetland environments, hyperspectral data, when calibrated with in situ measurements, can reasonably estimate parameters including chlorophyll content and plant stress.

Remotely piloted airborne system (RPAS coupled with multispectral, hyperspectral, lidar, and thermal sensors) are an alternative to validate land cover classification as it may be deployed on an 'as needed' basis beneath cloud cover. The main advantages of RPAS are the changeable spatial and radiometric resolutions (i.e., as the camera/sensor can be changed between multispectral,

thermal, lidar or hyperspectral, based on the needs of the survey), independent data acquisition (i.e. the images can be gathered based on user availability and favourable weather conditions, particularly on days with clear skies and lower wind speed), and easily deployable and user-friendly (i.e., the software to operate RPAS and process the data tend to be intuitive and user-friendly). Holden et al. (2020) used a combination of geolocated photos and RPAS imagery to assign training and validation pixels for a land cover classification using Sentinel-2 imagery. Overall, combining these complementary data sources, historical, satellite, and field-based, scientists and managers can develop a multidimensional knowledge of wetland function, so enabling more efficient conservation and adaptive management in the face of continuous environmental change.

1.3.2 Multispectral image classification for montane wetlands

Classification methods are crucial for identifying land cover types; moreover, they can reveal changes over time on a long-term basis. There are two methods for land cover algorithms, unsupervised and supervised. Unsupervised classifications are unguided by any reference information, so the classification is performed by analysis of data features (i.e., digital number of the pixel) by software (e.g., ArcGIS, ENVI, etc.) (Ozesmi and Bauer, 2002). This type of classification is ideal to be used where no validation (or little) data are available (Montgomery et al., 2021). They are easy to perform, and their computational requirements are linearly proportional with the number of objects to be classified (Garcia-Dias et al., 2018). The main disadvantage of this kind of classification is that the user needs to choose the number of land cover classes before the application, therefore, a knowledge of the study area is required before the classifier running.

There are three main unsupervised classification methods used for imagery analysis: Iso-clustering, K-Means, and Fuzzy K-Means. The Iso-clustering algorithm is an iterative process where every cell is assigned to the closest of these means. New means are recalculated for each cluster based on the attribute distances of the cells that belong to the cluster after the first iteration. The user can specify the number of iterations of the process. When increasing the number of clusters, the number of iterations should also increase (Richards, 2008). Using a minimum distance technique, K-Means unsupervised classification iteratively clusters the pixels into the closest class by calculating starting class means evenly dispersed throughout the data space. Every iteration updates the class means and reclassifies the pixels in accordance with the updated means. Unless a standard deviation or distance limitation is given, all pixels are assigned to the closest class;

otherwise, some pixels may be unclassified if they do not fulfil the chosen criterion. This method continues until either the maximum number of iterations is reached or the number of pixels in each class change by less than the chosen pixel change threshold (Tou and Gonzalez, 1974). K-Means can effectively detect abrupt shifts, such as the formation of new water bodies, even in the absence of prior labels (Pekel et al., 2016). However, it faces challenges when dealing with mixed pixels in diverse landscapes (Tiner et al., 2016). Fuzzy K-Means is the same algorithm as K-means, the only difference is, instead of assigning a point exclusively to only one cluster, it can have some sort of fuzziness or overlap between two or more clusters.

Even though unsupervised classifiers may not be the more accurate approach for land cover classification, it has been successfully applied for wetland land cover, as performed by Whitfield et al., (2020), which characterized hydrological and landscape changes (e.g., vegetation, water, and snow extent) in mountains and prairies of the Western Canada using Landsat series images using K-Means from 1985 to 2010. The Fuzzy K-means and K-Means classifier were also used to create a national river classification (Dallaire et al., 2019) and 23-class land cover of the forested area of Canada (Wulder et al., 2008), respectively, using the Landsat 7.

The land cover change would be the next step after the image classification, in fact Dong and Chen, (2021) assessed the vegetation changes in the Hailar River wetlands (China) between 1987 and 2019 using the Landsat 5 (using images from 1987, 2001, and 2010) and 8 (using images from 2019) imagery using the Iso-clustering algorithm. A direct comparison of land cover class areas, such as marsh versus woody/shrub encroachment, over the 32-year gap revealed specific types of change, including a 23% shift from marshes to woody/shrub Pertiwi et al. (2021) investigated the spring flood processes in the Lena Delta, Eastern Siberia. The authors combined Iso-clustering method to separate the land cover classes and to create the training input for the Random Forest classifier. The model accuracy assessed by comparing the multi-temporal satellite data (TerraSAR-X/TanDEM-X, RapidEye, and Landsat 8) with modeled flood areas resulting in a high kappa coefficients (0.78-0.97). Nonetheless, their methodology presents significant concerns; in particular, using an unsupervised method to create training data for a supervised classifier could lead to increased uncertainties. When these unsupervised classification outputs are utilized as reference datasets for training and validation in a Random Forest model, any initial misclassification may carry through the supervised land cover classification process, potentially distorting the final land cover maps. This method could still achieve high overall accuracy because

of class dominance or restricted validation areas; however, it may undermine confidence in minority classes or more fleeting features. To address these issues, it is advisable to validate unsupervised land cover classification results with field data or expert interpretation prior to incorporating them into supervised training workflows.

Supervised classification approaches require a reference or 'training' dataset, that is selected/identified by the user to represent a physical landscape feature of interest for the classification (e.g., water, vegetation, or soil extent). The Maximum Likelihood, Support vector machine, Decision tree, and Random Forest are the most reliable supervised algorithms for imagery classification.

The Maximum Likelihood classifier calculates the mean and variance for each class by calculating the interested region's statistics, and then establishes a classification function. To produce the classification, each pixel in the image is categorised and then substituted into the classification function of each class (Myung, 2003). This algorithm has widely been used in wetland classification, as demonstrated by Teferi et al., (2010), which quantified the wetland loss in the Choke Mountain range, headwater region of the river Nile. Landsat 5 and 7 were used and the Maximum Likelihood classifier was employed for land cover classification. The results showed that 607 km^2 of seasonal wetland with low moisture and 22.4 km^2 of open water are lost in the study area during the period 1986 to 2005.

The Support vector machine (SVM) can also be another reliable method for wetland delineation, as it is based on statistical learning frameworks proposed by Cortes and Vapnik, (1995). A binary linear classifier that allocates new instances to one class or the other is created by the SVM training method. In order to maximise the distance between the two classes, the SVM maps training examples to points in space. Then, based on which side of the gap they fall, new samples are projected into that same area and predicted to belong to a category. For example, Hung et al. (2020) classified land cover based on WorldView-2 imagery using SVM in the High Arctic territory of Nunavut (Canada), resulting in a Kappa coefficient of 0.89. Using multispectral imagery and lidar, Pittman and Hu (2023) classified forest species in the boreal forests of Northern Ontario, Canada, using SVM classifiers. With a Kappa coefficient of 0.69 this method produced a modest degree of classification accuracy in the complex forested environment. Through the use of SVM with SPOT-5 imagery, Ullah et al. (2017) classified land cover in the Hindu Kush Mountain Ranges of Northern Pakistan. With a Kappa coefficient of 0.86, the study revealed strong classification

accuracy on steep and difficult terrain. Employing Sentinel-2 images, Amin et al. (2024) classified land cover in the complex mountainous terrain by means of SVM in the Himalayas (Pakistan part). The study turned up an average Kappa coefficient of 0.65. Han et al., (2017) investigated the floodplain change in China using the SVM method from 1995-2015 by Landsat 5 and 8. The Kappa coefficient reached 0.94, based on field sample points.

Depending on the region and training data, the most accurate supervised classifier is probably Random Forest, an ensemble learning technique for categorising images that works by building a large number of decision trees during training (Breiman, 2001). The Random Forest output is the class that the majority of the trees choose, and it also tends to rectify the overfitting of the training set. Although overfitting is a regular problem in machine learning, Random Forest is especially made to more successfully solve this problem than single decision trees (Breiman, 2001). By averaging predictions (in regression) or gathering majority votes (in classification), the ensemble character of random forest, where many trees are built using bootstrapped subsets of both the data and feature space, helps lower variance and avoid overfitting (Breiman, 2001). Furthermore, Random Forest lowers correlation between trees by choosing at random a subset of features at every node split, so lowering the chance of generally fitting noise in the data. Furthermore, Random Forest exhibits resilience to noisy, multi-temporal satellite data such as Landsat and Sentinel-2 (Millard and Richardson, 2015), ensuring high accuracy (>89% overall) for wetland classification in Eastern Slopes of Alberta. By improving the management of mixed pixels at ecotones (specifically, the boundaries between wetlands and forests), Random Forest reduces errors by 12–18% in montane regions when compared to SVM (DeLancey et al., 2019). Random Forest was also applied to the forthcoming nSight-2 hyperspectral and the WorldView-2 data for wetland plant species differentiation in Verloren Vallei Nature Reserve, South Africa (Gasela et al., 2022). For this purpose, field spectrometer data (in situ sensing) of various wetland plant species were used for validation, resulting with high accuracies of 78-84%. Recent ensemble methods such as XGBoost and deep learning approaches like ResUNet are now comparable to RF for specific applications, such as mapping small (<0.1 ha) emergent wetlands (Jafarzadeh et al., 2022). Overall, the selection of a land cover classification method is determined by the availability of data, as well as the specific type of wetland and its hydrological characteristics. In montane wetland regions, where hydrology is frequently influenced by Variable Source area and fill-and-spill dynamics (Devito et al., 2012), gradual changes in land cover were effectively captured by the Random Forest

algorithm and Mann-Kendall trend analysis test. While arctic peatlands might require adjusted Mann-Kendall tests, such as the seasonal Kendall test, to account for non-linear changes induced by permafrost (Minayeva et al., 2018), coastal wetlands require the use of the Random Forest algorithm combined with radar integration to distinguish mangroves from water (Purwanto et al., 2022). Therefore, integrating multi-sensor data, such as Landsat imagery archives alongside radar sensors, with localized hydrological characteristics yields the most reliable insights regarding particular types of wetlands.

Although supervised classifiers tend to perform high classification accuracy, these methods, cannot independently cluster data by identifying its features, hence overtraining of the decision boundary may result. Unreliable training samples or too big datasets used to build the classifier could compromise model accuracy (Ramezan et al., 2021). Furthermore, choosing a suitable supervised classification method for big-scale data can provide difficulties since both training and classification procedures usually require for significant computational time (Amin et al., 2024). Moreover, misclassification might arise in case an input does not match any predefined class in the training data (Xu et al., 2024).

The pixel-based image analysis is constrained by the fact that: image pixels are not real geographic objects and the pixel topology is constrained; this method largely disregards some aspects of the images, such as texture, context, and shape; and the increased variability implicit in high spatial resolution imagery confuses traditional pixel-based classifiers, leading to lower classification accuracies (Gao and Mas, 2008).

Supervised algorithms typically adopt a pixel-based approach for training data, relying solely on the spectral information associated with each individual or group of pixels. They are usually regions where ground-truth data were collected or is available. This training sample would be in the form of an n-dimensional vector, where n was the number of spectral bands in the image data. In contrast to pixel-based classification methods that classify individual pixels directly, object-based classification first aggregates image pixels into spectrally homogenous image objects using an image segmentation algorithm and then classifies the individual objects (Liu and Xia, 2010). This object-based classification approach was used in the Yellow-River-Source National Park aiming to detect wetlands changes (Ma et al., 2022). The authors combined a variety of image features (spectrum, geometry, texture, and context) to aggregate the pixels. The wetland area demonstrated a decreasing trend, primarily due to the significant decrease in the marsh wetlands.

The object-based method, on the other hand, has its own drawbacks: over-segmentation and under-segmentation (Möller et al. 2006). Under-segmentation produces image objects that cover more than one class, which introduces classification errors because all pixels in each mixed image object must be assigned to the same class. Additionally, features extracted from mis-segmented image objects with over-segmentation or under-segmentation errors do not accurately represent the characteristics of real objects on the Earth's surface (Song et al. 2005).

While traditional object-based methods struggle with segmentation errors, modern neural network approaches offer solutions. Using vision transformer architecture, the Segment Anything Model (Kirillov et al., 2023) demonstrates potential for wetland mapping through its zero-shot generalization; however, its effectiveness on small montane wetlands (<0.5 ha) has yet to be evaluated in peer-reviewed research. On the other hand, deep learning approaches, such as U-Net (Ronneberger et al., 2015) and DeepLabv3+ (Chen et al., 2018), have been tested in wetlands, and the results indicated that these models outperformed traditional machine learning methods (i.e., Random Forest and SVM) (Mahdianpari et al., 2018). These approaches require substantial training data; furthermore, models developed under particular conditions are unable to generalize across varying seasons, sensor types, or geographic locations without further fine-tuning, which impacts their usability in different environmental conditions (Ma et al., 2019; Su et al., 2021).Overall, wetland classification can be challenging due to there being many associated landcover classes that can vary in time (e.g., water, vegetation, and soil extent) over small areas. These characteristics can result in spectral confusion or mixing of the targets, requiring RS data with high spatial resolution (e.g., Airborne Lidar, RPAS, etc.) for spatially accurate class definitions.

1.4 Wetland Change detection

1.4.1 Methods for change detection assessment

To assess and identify such rapid environmental changes (natural, anthropogenic, or event-based), change detection methods are essential, for example: algebra-based change, transform-based change, classification-based change, advanced models, neural network and fuzzy approach.

In the algebra-based change detection each image pixel is subjected to mathematical operations (image differencing, regression, rationing, vegetation/water index differencing, and so on) resulting in a different image. The advantages are these techniques are uncomplicated, simple to use, and easy to interpret. The disadvantages are in choosing the right threshold to recognise the specific

change areas, in addition, the selection of appropriate image bands is difficult. For example, Xiong et al. (2012) employed a technique for change detection based on the likelihood ratio obtained from the joint Probability Density Function of the synthetic-aperture radar images. The likelihood ratio is the comparison of two Synthetic Aperture Radar (SAR) images' joint probability density functions (PDFs). The change detection measure's histogram, which is derived from the likelihood ratio, contains a single, steep peak that can be utilised to establish the change detection threshold accurately and quickly under the assumption that both PDFs follow the gamma distribution. The suggested change detection technique is easy to use and efficient at spotting changes, according to analyses of SAR image pairs from various platforms.

The transform-based methods technique, to determine whether the image has altered, the pixels of the image are transformed (Asokan and Anitha, 2019), which includes four methods, the Principal Component Analysis (PCA), Tasseled Cap Transform (TCT), and the Chi-Square Transform. The first, PCA, is a method for analysing multi-dimensional datasets with many dimensions or characteristics per observation, improving the interpretability of data while maintaining the most information, and enabling the presentation of multidimensional data (Jolliffe and Cadima, 2016). Secondly, the TCT is a technique for converting the spectral data from satellite measurements into spectral indicators (Kauth and Thomas, 1976). The inversion of the linear mixture model is a linear transformation that changes from pixel to pixel based on its placement inside the mixing space, whereas the TCT is a single rotation (affine transformation) that is applied uniformly to every pixel. As a result, the linear mixture model successfully orthogonalizes the substrate and plant fractions, addressing one of the main drawbacks of the TCT in that it cannot distinguish between the contributions of the soil and vegetation to mixed reflectance. The last one, the chi-squared distribution transform with k degrees of freedom (number of bands) represents the distribution of the sum of k independent standard normal random variables (Vázquez-jiménez et al., 2017). A transform-based change detection technique decomposes the image on many scales using the transform technique. The independent component is then split into a separate component of the data, which is then converted into a component of the image (Asokan and Anitha, 2019). Then, by threshold segmenting change components, a change map is produced. The key benefit is that it emphasises different information in derived components while reducing redundancy between bands, and the main drawback is that it is unable to obtain precise change information. However, the change per pixel can be reconstructed based on the loading patterns (Huang et al., 2009).

The landcover classification-based differencing is based on the classification of the image, and to provide accurate classification results, although, the quality and amount of the training data are crucial. For example, post-classification comparison, spectral–combined temporal analysis, unsupervised change detection, ANN, and hybrid change detection. The first one compares independently classified images from multiple time periods with changes in land cover maps (Lu et al., 2004). Second, spectral-temporal analysis reduces reliance on training data by detecting changes without full classification using time-series data (e.g., NDVI trends), depending on consistent radiometric calibration (Zhu and Woodcock, 2014). Third, unsupervised change detection finds pixel value changes (e.g., image differencing) without reference datasets for training land cover classes, so challenging the assignment of meaningful land cover classes to changes (Singh et al., 1989). Later on, the ANN can replicate detailed spectral patterns but depends on large training datasets to prevent overfitting, a significant challenge in heterogeneous mountainous areas (Zhang et al., 2018c). Ultimately, hybrid approaches, that is, unsupervised methods to flag changes, then classification to identify their land cover class, balance strengths but add complexity (Chen et al., 2003). All techniques have trade-offs between training data needs and interpretability; for example, Rutchey and Vilchek (1994) showed how misclassified pixels in wetland mapping inflated false change detection by 20–30%, so highlighting the need for representative training samples, particularly in topographically complex areas where spectral mixing is common. The advantage of these methods is that they can provide a change information matrix; nevertheless, choosing a high-quality and sizable collection of training samples for image classification is challenging, and overfitting is a possibility.

In the advanced models approach, the correlation of the image reflectance values is used to translate to physically based parameters or fractions using linear or nonlinear models. A linear model assumes that parameters are incorporated in a linear manner (e.g., ordinary least squares), even when predictors (i.e., independent and dependent variables) have a nonlinear relationship with the response. This is evident in Generalized Linear Models, where link functions (e.g., logit) introduce nonlinearity while maintaining the linearity of the parameters (McCullagh and Nelder, 1989). For example, wetland reflectance might have a nonlinear relationship with soil moisture, yet a GLM with a logarithmic link maintains linearity in its parameters. Nonlinear models, such as neural networks, allow parameters to interact in exponential or multiplicative ways, facilitating them capture complex spectral relationships in wetlands that linear models miss (Mahdianpari et al.,

2018). However, in the absence of sufficient data, nonlinearity can lead to overfitting, which can be avoided by using regularization techniques (e.g., ridge regression for nearly linear systems) (James et al., 2021).

For instance, they comprise the biophysical parameter estimation models, the spectral mixture models, and the Li–Strahler reflectance models. The biophysical models use a regression analysis, which seeks to find the relationship between one or more independent variables (e.g., reflectance) and a dependent variable (e.g., fieldwork sample measurements) (Thenkabail et al., 2011). Though the spectral mixture model is conceptually comparable to the TCT approach, they are fundamentally different (Adams, 1995). The Li–Strahler reflectance models emphasizes that the Lambertian condition (i.e., when the surface luminance is the same regardless of angle of view) may prevail within the pixel, while non-Lambertian signatures will exist at the pixel scale overall (Liu et al., 2018). The advanced models methods are easier to comprehend than the spectral signature and are capable of extracting vegetation information (Li et al., 1995). However, these approaches are time-demanding and difficult process of developing suitable models for conversion of image reflectance values to biophysical parameters (Lu et al., 2004).

On the other hand, it could be interesting to search for subtle/slow changes in the distribution of RS data over time when analysing time-ordered observations. For signal change testing, the Bayesian analysis (i.e., parametric technique, student t-test) can be used. This method entails combining existing prior knowledge with the RS data to create the posterior distribution and provide a consistent framework for estimating complicated statistical models in conjunction with Markov Chain Monte Carlo techniques (AghaKouchak et al., 2013). The Markov Chain Monte Carlo methods offer both point estimates and intervals, which are crucial for observing ecosystems that experience slow, subtle, or spatially diverse changes, thereby encompassing the entire spectrum of possible changes (Denison, 2002). However, Bayesian methods depend on distributional assumptions, e.g., normality, that might not always hold for RS data, particularly in non-Gaussian or noisy environments (e.g., mountainous terrain with shadow effects) (Zhao et al., 2019). When parametric assumptions are violated, non-parametric can be used, such as bootstrapping or permutation tests (Lunetta et al., 2006).

A non-parametric method known as the Wilcoxon signed-rank test is used to compare two related samples, in this case remote sensing data on land cover, or to perform a paired difference test using repeated measurements on a single sample to determine whether the two samples differ

(Scheff, 2016). This test's main drawback is that it can only identify a single change point, in contrast to the non-parametric Sequential Mann-Kendall test (Kendall, 1975; Mann, 1945), which is particularly useful for Sequential Step Change Analysis. The Mann-Kendall test works for all distributions and identifies a trend in a series for three hypotheses: no trend, positive trend, negative trend.

The Mann-Kendall method is a robust methodology for monotonic and continuous/gradual trends and have been used to assess mountain wetlands area trends (Zhang et al., 2018b; Zimba et al., 2018; Msofe et al., 2019; Luo et al., 2020). However, it misses short-term disturbances like hydrological droughts (Arra et al., 2024). For short-term trends, the change/breakpoint analysis (Killick et al., 2012) should be considered, as it allows observation of episodic changes that deviate from the normal pattern, as it depicts the approximate time and the number/amount of change (Killick et al., 2010). This technique has been applied to examine changes in Canadian Taiga Plains ecozone using Airborne Lidar (Chasmer and Hopkinson, 2016a) and Landsat data (Chasmer et al., 2016b) in boreal wetlands while other studies, for example Chasmer et al. (2018) used the change point analysis to determine anomalies or disturbances in vegetation pixel time series (Landsat 5 imagery using the Modified Soil Adjusted Vegetation Index.

In addition, some work has been done combining both trend and change methods in temperate mountain wetlands worldwide, as showed by Feizizadeh et al. (2021), which utilized machine learning algorithms (e.g., Support Vector Machine, Random Forest, and Classification and Regression Tree) on the Google Earth Engine (using Landsat satellite image time series 2000 – 2020) for land use mapping and trend detection analysis (Mann-Kendall test) in the Urmia Lake Basin, Northern Iran. The authors found a reduction of water area by 2% and an increase in the area of vegetation by about 10%. Negative water surface trends were also observed in the Mongolian Plateau, with a disappearance of 208 lakes from 1976 to 2013, which were evaluated by Zhang et al. (2016) using Landsat 5, 7, and 8 imagery. In contrast, the authors discovered a counterintuitive trend in the nearby Tibetan Plateau, with 99 new lakes and lake expansion. The Yellow River's headwaters of Tibet also experienced an increase in surface water area (3.4 km^2 from 1986 to 2019), which was associated with a rise in precipitation and permafrost thaw, followed by the building of hydropower reservoirs near the river's outlet. This finding was made through Luo et al. (2020) using the Google Earth Engine (Landsat TM/ETM+/OLI, Sentinel-2A, and MODIS) based on automatic extraction of the Normalized Difference Water Index (NDWI) and the Modified Normalized

Difference Water Index (MNDWI).

The Landsat time series are the most frequently used remote sensing data to assess changes and trends in wetland area variations. The combination of trend and change methods may be the best practice to assess the wetlands disturbance over time. The Mann-Kendall trend test has been widely used and might be the most popular and effective approach for trend analysis when wetland time series are monotonic and continuous, for other types, the change point analysis should be used.

1.4.2 Applications of the change detection methods

The identification and mapping of temperate montane wetland change started in the 1940s, using aerial photography. This approach identifies distinct topographic and vegetation patterns characteristic of wetlands through the stereoscopic analysis of overlapping aerial images, such as organic soil textures, hydrophilic vegetation, and surface water signatures. Analysts define wetland boundaries by recognizing visual indicators in time-series photographs, which allows for the monitoring of area changes, hydroperiod variations, and shifts in vegetation succession (Tiner, 2016). For example, Carli and Bayley (2015) used air photos to observe changes from the 1940s to 2004 over the Columbia Wetlands, BC Canada. They found that open water increased by 77% while there was a decrease of marsh (14.5%) and shrub (40%) vegetation extent. The shadow cast by the mountains on the landscape, which can reduce the amount of light needed for quality photography, is one of the key limitations of aerial photogrammetry in mountainous environments.

Wulder et al. (2018) assessed wetland land-cover change across Canada using the Landsat multispectral image archive (33 years). The overall accuracy of the supervised classification was 71%, and they found the extent of wetlands was stable. In the montane regions of Alberta, Canada, Hilker et al. (2009) introduced a Tasseled Cap transformations of both MODIS and Landsat TM/ETM data, demonstrating that land cover (e.g., woody forest; wetlands, barren, and water) change could be mapped with high accuracy (93%). In the temperate montane wetlands of Canada, Lee (2011) applied a Maximum likelihood classification to Landsat data (1976 – 2008) to quantify a 4.8% loss of wetland cover due primarily to commercial forestry. In the Montane Cordillera Ecozones of Western Canada, Ireland and Petropoulos (2015) applied a Decision-Tree classification to the Landsat series from 2003 to 2011 to show that 60% of vegetation was in a state of recovery from previous wildfires. Other sources of multispectral image data were also used to detect change in montane wetlands worldwide, such as, Sentinel 2 in France (Carlson et al., 2020) and Italy (Praticò et al., 2021), Worldview series in Czech Republic (Stych et al., 2019) and China (Deng et

al., 2014), Rapid Eye in Austria (Polychronaki et al., 2020) and Tanzania (Thonfeld et al., 2020), etc.

Hyperspectral sensors can be used to classify and observe change in temperate montane wetlands around the world (Cristóbal et al., 2021; Marcinkowska-Ochtyra et al., 2018; Tong et al., 2013) but has not been implemented over Canadian temperate montane wetlands. This type of sensor may collect hundreds of spectral bands across a broad spectral range, but wetlands can be spatially heterogeneous, having water-vegetation-soil in close proximity, which can produce spectrally mixed pixels. In the context of spectral mixing, wetlands show spatial heterogeneity, producing mixed pixels with vegetation (~700 nm NDVI peak), water (characterized by the 810 nm reflectance minimum), and organic soils (which show a spectral signature between 500-1800 nm) all within individual pixels (Dalponte et al., 2012). Another factor relates to the data time limit since, despite the proven success of sensors such AVIRIS-NG (5 m spatial resolution) in montane wetlands of Alaskan regions, there have been no systematic airborne or spaceborne hyperspectral campaigns covering Canadian montane wetlands (Miller et al., 2024).

SAR is another method for mapping wetland change. SAR was the first active sensor used for terrain imaging in 1951, and it has since been utilised to map wetlands, among other land cover types (Brisco et al., 2011; White et al., 2015). SAR's all-weather, day/night imaging capability is essential for consistent monitoring of cloudy montane regions like the Canadian Rockies where optical data often fails (Darychuk et al., 2023). Particularly useful in hydrologic applications, the sensitivity of the SAR in evaluating water and vegetation structure (such as detecting open water through low backscatter and flooded forests via double-bounce effects) enables it to be longer wavelengths (L-/P-band) enhance its value further by penetrating forest canopies to map subsurface water in peatlands and soil moisture (Kasischke et al., 2009). SAR has been assessed for temperate montane wetland monitoring in Canada (Hopkinson et al., 2020; Wulder et al., 2018; Mahdianpari et al., 2020a,b) and other areas worldwide (Attarchi and Gloaguen, 2014; Reschke et al., 2012; Endo et al., 2020) demonstrating the utility of SAR to support wetland management. However, SAR has limitations, for instance, speckle noise that complicates classification, complex backscatter interpretation dependent on polarization and surface conditions, and inability to directly evaluate water quality or specific vegetation types like hyperspectral sensors (Singh et al., 2022).

Remotely piloted airborne system (RPAS) has been employed for montane wetland change assessment, as demonstrated by Hird et al. (2017a), who used RPAS data to monitor the recovery of

forest vegetation over petroleum well sites in Alberta Canada's Boreal and Rocky Mountain regions. The authors observed vegetation area increases after ~ 20 years of reclamation indicating long disturbance recovery periods. Animals can also modify wetlands, as was found by Puttock et al. (2015) in the Tamar River catchment, Southwest England. They used RPAS photogrammetric data to assess the impact of reintroduced beavers, which increased water extent due to the creation of dams and changes in vegetation structure caused by beaver tree-felling activity. Moreover, the RPAS platform has been frequently used to monitor mountain wetlands change worldwide, for example. However, no studies were found that utilized remotely piloted aircraft systems (RPAS) platforms or data to evaluate temporal changes in Canadian temperate montane wetlands..

Possibly the most accurate and efficient method for wetland classification and change detection is using multi-spectral (usually three wavelengths: 532 nm, 1064 nm, and 1550 nm) Lidar data (Chasmer et al., 2020). By acquiring high-resolution elevation data (horizontal resolution <1 m), Lidar efficiently defines wetland boundaries and hydrological features, so proving its value for wetland classification (Chasmer et al., 2016b). However, because of high expenses and limited coverage, it is not ideal for continuous monitoring; hence, it is less accessible for frequent monitoring or large-scale applications. Studies have demonstrated that the integration of Lidar with multispectral imaging can enhance classification accuracy by as much as 20% (Bork and Su, 2007). Lidar is a useful instrument, but its best results come from combining other remote sensing techniques catered to particular landscape conditions with it (Kalacska et al., 2017).

Airborne Lidar technology became popular through the 2000's, making important contributors to the development of wetland data acquisition, including water extent and hydroperiod (Marti-Cardona et al., 2013; Montgomery et al., 2018), and topography and vegetation structure (Hopkinson et al., 2005; Zlinszky et al., 2012). In the boreal forest of North America, Margolis et al. (2015) have used airborne and spaceborne Lidar to map and model aboveground vegetation (AGV) attributes. The authors used airborne Lidar metrics gathered with 1000 geolocated forest inventory sample plots for biophysical model training and validation, then to extrapolate the AGV model using the ICESat-GLAS Lidar data. The distribution of the AGV boreal forest in North America was 47% in western Canada, 44% in eastern Canada, and 9% in Alaska, with relative errors usually below 4% in all three regions.

Airborne Lidar data have also been used to evaluate changes in temperate montane wetlands. For example, Loh et al. (2020) employed Lidar for wetland change detection in tropical

montane forest of northern Borneo between 2000 and 2012. The multitemporal maps depicted an overall increase rate of 10.44 Mg ha^{-1} $year^{-1}$, which was attributed to natural regeneration. Hopkinson and Demuth (2006), used Lidar to assess surface changes in the Peyto Glacier, Canadian Rocky Mountains. The study compared two Lidar images collected 23 months apart (2000 and 2002), it was found that there was a reduction in volume totaling 33×10^6 m^3, which implies a reduction in downstream runoff of ~22×10^6 m^3 or ~16% of total basin runoff. Decreasing water extent due to local precipitation reduction may increase terrestrial vegetation area in montane regions, observed by Leipe and Carey, (2021). They used airborne Lidar data to measure changes in shrub vegetation cover in a headwater catchment in Yukon Territory, Canada. Airborne Lidar data were collected at two periods: in August 2007 and 2018, and results showed an average expansion in area of 5.8%.

Another approach to evaluate vegetation extent change uses data fusion. The use of airborne Lidar data (for validation) and terrestrial oblique photography (to identify land cover changes) from 1914 – 2006 were used in the Westcastle Watershed, Alberta, Canada, to map changes in canopy cover in McCaffrey and Hopkinson, (2020b). They showed a decrease in canopy cover on warm, fire-exposed aspects at high elevations, and an increase in canopy cover on cool, non-fire-exposed conditions (McCaffrey and Hopkinson, 2020b). In another study (McClelland et al., 2019), Landsat 5, 7 and 8 and MODIS were used to map high temporal and spatial resolution treeline change in montane regions of Alberta, Canada, from 2000 to 2018, using a landcover classification-based differencing, which showed an earlier spring green-up caused by an increase of soil moisture over the years.

In contrast, Rhemtulla et al. (2002) used oblique terrestrial photographs (taken in 1915 and 1997) and repeat aerial photographs (flown in 1949 and 1991) to assess changes in vegetation composition and distribution in the montane ecoregion of Jasper National Park, Rocky Mountains of Alberta, Canada. Between pairwise combinations of all the various classifications between 1915 and 1997, a transition matrix was produced, summarizing the directions and amounts of change by adding the pixels in each individual photograph by land cover type between 1915 and 1997. The results indicated a shift towards late-successional vegetation types and grasslands, shrubs, juvenile forest, while open forests decreased in extent and closed-canopy forests became more prevalent. Changes in vegetation patterns were likely largely attributable to shifts in the fire regime over the last century.

The combination of different sensors may enable multiple estimates of change in wetland water extents, as suggested in Hopkinson et al. (2020) for the Upper Columbia River (Canada). They used Radarsat 2 and Landsat 5 and 8 data to map changing wetland hydroperiod using a frequency analysis approach. The authors found a ~16% loss of area of permanent water, equivalent to ~ 3.5% of the entire wetland floodplain area. The results from Hopkinson et al. (2020) were aligned with those of Pekel et al. (2016), who used Landsat 5, 7, and 8 to map global permanent surface water between 1984 and 2015, observing a general reduction, though new permanent water bodies have also emerged.

Emerging cloud-based computing platforms (e.g., Google Earth Engine, Amazon Web Services, etc.) are increasing the availability of regional to global-scale land use maps at moderate spatial resolutions (e.g., Amani et al., 2020). Amani et al. (2019) created the first Canada wetland inventory using Google Earth Engine, resulting in an overall classification accuracy of 71%. Even though the source data in these free cloud-based platforms are typically not of a high spatial resolution (<5m), such platforms have been used to assess changes in Canadian temperate montane wetlands (Hird et al., 2017b) as well as worldwide (Long et al., 2021; Wang et al., 2018). Ultimately, there are trade offs between the needs for large area coverages that are useful for policy or national reporting, and the spatial detail and classification accuracy needed at localised scales for land management decision making (Gardner and Davidson, 2011). Although land cover change may be evaluated through field-based mapping, RS provides the basis for consistent, longer time periods and funding cycles, as well as cost-effective methods, which are particularly useful in remote or difficult to access areas like temperate montane floodplain and bench land wetlands.

1.5 Wetland Threats and Change in the Temperate Montane Canadian Cordillera

Temperate montane wetlands are often regarded as sentinels of global environmental change (Erwin, 2008). These ecosystems rely on snow, glacier melt, and rainfall that contribute to runoff, which flows into wetlands; however, many of these wetlands are also formed in areas with springs (these areas offer a reliable supply of water, frequently sourced from groundwater) (Ruddy and Williams, 1991; Sundeen et al., 1989; Carlson et al., 2020). Apart from continuous water sources, particular environmental conditions affect the accumulation and persistence of water in temperate montane wetlands. For instance, topographic features including depressions, moderate slopes, and valley bottoms help to retain water by reducing runoff and so promoting groundwater

discharge (Borderieux et al., 2025). These landforms create microclimates with reduced solar radiation and cooler temperatures, which in turn reduce evapotranspiration rates (Fridley et al., 2021). These conditions help to preserve wetland hydrology especially in dry times (Scherrer and Körner, 2011). For mountainous regions, studies have shown that topography-induced microclimatic cooling preserves favorable moisture conditions, so supporting the survival of cold-adapted plant communities (Scherrer and Körner, 2011). Microclimatic buffering provided by understory vegetation and landscape physiography helps to further stabilize near-ground temperatures and hence enhance water retention in these ecosystems (Fridley et al., 2021).

However, the availability of water can vary with climate change, which may impact the soil-water-vegetation dynamics (Lee et al., 2015). Climate change affects wetland ecosystems; nevertheless, local environmental conditions help in regulating their resilience. By controlling hydrology and soil moisture, topographic features, microclimatic buffering (e.g., cool-air pooling in depressions) and vegetation feedback (e.g., peat accumulation) can help enhance stability (Erwin, 2009; Johnson et al., 2015). On slopes with limited recharge, for example, low-lying wetlands (areas often saturated with water, either permanently or seasonally) may change to meadows or shrublands as moisture thresholds are exceeded; on the other hand, strong groundwater connectivity helps these wetlands to often resist drought by preserving water tables (Winter, 2000). Rarely driven by climate alone, such changes arise from interacting pressures including altered precipitation, evaporation rates, and biological invasions (non-native vegetation species enter and flourish in an ecosystem) (Poff et al., 2015). Moreover, early signals of ecosystem tipping points are changes in vegetation, including loss of wetland species (e.g., *Carex spp.*, known as sedges) or invasion of upland plants (*Betula nana*, known as dwarf birch) (Müller and Joos, 2021). Thus, predicting these transitions involves the integration of topographic features, hydrological and ecological variables with regional climate projections.

For instance, Stewart et al. (2004), used measured river discharge (i.e., stream gage) to observe trends from 1948 to 2000 and to project future shifts in the period of springtime snowmelt and its effects on river flow in the Rocky Mountain Cordillera in Canada and the USA from 1995 to 2099. The streamflow timing trends showed an earlier springtime snowmelt of 10 – 20 days relative to historical observations, with future flow peaks likely being up to 30 – 40 days earlier.

In the Elbow River Watershed, Alberta, Valeo et al. (2007) evaluated regional climate trends (>30 years) and found a positive trend in air temperature of +0.03 ºC $year^{-1}$, rainfall and

snowfall showed an increase of +0.43 mm year^{-1} and a decrease of 0.22 mm year^{-1}, respectively, while river discharge produced higher volumes during early spring. In the Upper Columbia River, Moore et al. (2020) observed a decrease of glacier cover, by up to 2% (1985 – 2013), with catchment water yield increasing during early spring corresponding with a ~13% decline in river discharge during late summer (Brahney et al., 2017). Other trends were also analysed in different parts of the Canadian Rocky Mountain region related with air temperature (Fassnacht et al., 2018; McGuire et al., 2012; Bunnell et al., 2011), snowpack (Brown and Mote, 2008; Fassnacht et al., 2018; Shea et al., 2006), the advance of trees throughout the short growing season (Luckman, 1990; Luckman and Kavanagh, 2000; Danby and Hick, 2007), river siltation (i.e., the accumulation of sediment in rivers, lakes, and water bodies) (Schiefer et al., 2013) glacial melt/change (Hopkinson and Young, 1998; Demuth et al., 2003; Tennant and Menounos, 2013), and river discharge (Stahl and Moore, 2006; Rood et al., 2007). These trends have also been observed in other temperate montane regions around the world (Alonso-González et al., 2022; Li et al., 2011; Mostowik et al., 2019).

Continued hydroclimatic changes are likely to result in more rapid spring snowmelt, which impacts river flow, lake (Hauer et la., 1997) and ground water levels (Millar et al., 2018), as well as herbaceous water-dependent vegetation (non-woody plants, e.g., grasses and sedges) (Shen et la., 2018). Meanwhile, water availability in late summer may be reduced due to increased evapotranspiration (Fernandes et al., 2007; Helbig et al., 2020), with increased potential for drought (Johnson et al., 2005). Three synergistic factors explain the increased potential for drought: (i) atmospheric changes (reduced summer precipitation and increased evapotranspiration from rising temperatures); (ii) soil moisture deficits from prolonged dry periods that inhibit wetland recharge; and (iii) landscape position where groundwater-disconnected wetlands on glacial till plains are particularly vulnerable (Johnson et al., 2005). Moreover, Johnson et al. (2005) emphasized that in the Northern prairie wetlands of central North America, drought results from climate-mediated hydrological thresholds rather than from soil conditions alone; that is, when precipitation is below 350 mm year-1 and air temperatures rise above 20°C, wetlands enter ephemeral states. These results highlight the need to measure local hydrology (for example, river discharge, ground water level, evapotranspiration, etc.) as well as macroclimatic trends (such as jet stream changes lowering spring rains) to estimate wetland resilience. Thus, changes in the major climate variables of air temperature and precipitation are expected to alter the hydrological cycle of precipitation inputs,

ground, lake and vegetation storages and evaporative outputs; those changes associated with soil moisture deficits and particular landscape position (such as groundwater-disconnected wetlands) can also impact nutrient and, sediment fluxes, biological systems, and food-web dynamics (Firth and Fisher, 2012). For wetlands in mountainous ecozones, an increase in wetland extent was observed (Wulder et al., 2018) which may be related to an acceleration of glacier-melt due to global warming (Moore et al., 2020; Tennant and Menounos, 2013).

In response to warmer air temperatures there is a positive trend of vegetation encroachment in the higher altitude regions of North American, and specifically in the Canadian Cordillera an increase of 3.0% in 29 years, as evaluated by Ju and Masek, (2016), who used Landsat 5 and 7 to derive an NDVI trend during the peak-summer. This greening trend correlates strongly with alpine shrub encroachment (*Salix spp.* and *Betula glandulosa*), which has expanded upslope at rates of 1–3 m per decade in the region, as documented by Myers-Smith et al. (2020) using repeat aerial photography and field surveys. Together, these studies underscore how NDVI trends, while valuable for detecting change, must be interpreted alongside fieldwork data to predict long-term ecosystem trajectories. Furthermore, these vegetation shifts change the carbon dynamics of the area; for example, more shrub cover increases summer CO_2 uptake, however it also decreases surface albedo, which increases localized warming (Lantz et al., 2019).

Although shrub encroachment impacts terrestrial carbon dynamics in the Canadian Cordillera, these changes have cascading effects on nearby wetland ecosystems, which are vital in the regional carbon cycle. Wetlands perform a key function in absorbing and transferring CO_2 from atmospheric to in situ and downstream aquatic and terrestrial carbon pools (Shukla et al., 2019). Wetland vegetation captures CO_2 through photosynthesis, storing 2–5 kg C m^{-2} $year^{-1}$ as organic carbon in waterlogged peat soils, where anaerobic conditions decrease decomposition (Vitt et al., 1994). Microbial activity transforms a portion of this carbon into methane (CH_4), which is either oxidized in aerobic zones (Lai et al., 2009) or emitted into the atmosphere.

Down gradient rivers, wetlands and soils can act either as sinks or sources of CO_2 and CH_4 (Hao et al., 2011; Kang et al., 2014) as well as dissolved organic carbon can be released into streams and adjacent water bodies (Lou et al., 2014). Nonetheless, the carbon storage capacity in these ecosystems is potentially projected to decline (Bisbing et al., 2010; Bartowitz et al., 2019) as a result of climate change, since this phenomenon will likely increase the frequency of extreme weather events (e.g., severe storms), which could alter local hydrology in montane wetlands

(Westerling, 2016). Severe storms have become powerful agents of change in the Canadian Montane Cordillera, reshaping wetlands in ways that ripple through the entire ecosystem. For instance, torrential rain on mountain slopes starts a chain reaction: floodwaters scour fragile peatlands, removing centuries of accumulated carbon in days, while landslides bury whole wetlands under suffocating layers of sediment (Buttle et al., 2016). However, nature shows its amazing adaptability; groundwater-fed bogs remain like subterranean reservoirs and returning beavers create new water traps that rebuild carbon stores (Hood and Larson, 2013). This dynamic landscape demonstrates that pockets of resilience endure and provide hope and direction for conservation in an era of climate extremes.

While storms reshape wetland hydrology, their climatic drives also create the conditions for another transforming power: wildfire. By encouraging rapid vegetation growth, which generates plenty of fuel loads that later dry under summer droughts, the same strong rainfall events that erode peatlands in spring can increase the likelihood of wildfire (Buttle et al., 2012). This cycle is intensifying in the Canadian Montane Cordillera (Coogan et al., 2019); groundwater-dependent wetlands may remain refugia (Hood and Larson, 2014), but nearby forests and shrublands are becoming increasingly flammable. Drought-stressed vegetation becomes prone to ignition by late summer; wildfires may thus turn carbon-storing ecosystems into emission sources (Gerrand et al., 2021).

In the future, an average annual air temperature increase of 3°C is forecasted by 2100 in the Columbia headwaters (Carver 2017), which is predicted to result in increasing evaporation rates and decreasing glacial melt runoff contributions (Moore et al., 2009; Moore et al., 2020). The projected 3°C increase in air temperatures by 2100 starts a series of events that will drastically affect water availability. Warming first speeds glacial melt, producing a brief run-off surge. But this is a temporary; as glaciers shrink past a threshold levels (referred to “peak water”, i.e., the point when a glacier has melted enough that its annual contribution to streamflow begins to decline permanently), their impact on rivers reduces (Moore et al., 2020). Retraction of glaciers reveals darker rock that absorbs more heat, so accelerating additional melting (Zemp et al., 2025). Meanwhile, more precipitation falls as rain instead of snow, so reducing natural water storage from nature system and forcing water to flow downstream in winter rather than be steadily released through summer (Dibike et al., 2018). Most climate change scenarios project higher temperature in summer (Schnorbus et al., 2012), reduced annual snowfall at higher elevations (Carver et al., 2017),

which are critical to late-season streamflow water supply. Pederson et al. (2010) investigated climatological trends (1969 – 2007) from 25 snow telemetry stations, stream gauge records from 14 rivers, and 37 meteorological stations across the same region. The trends showed warmer spring temperatures coupled with increases in mean spring precipitation, and snowmelt occurring an average of 8 days earlier, 14 fewer days of seasonal snow cover, and an increase in peak streamflow of ~24%.

In late summer glaciers are a dominant water source (Penna et al., 2014), supplying streamflow during periods when snowmelt and rainfall are reduced (Viviroli et al., 2003). For instance, Jiskoot and Mueller (2012) state that 25% of the late-summer streamflow from the Upper Columbia River Basin is glacially fed. However, warmer air temperatures in late summer have resulted in increased glacier wastage in the Central Rocky Mountains of North America, leading to a contemporary reduction in river discharge from 1950 to 2008 (Leppi et al., 2011).

Furthermore, the ecohydrological future of temperate montane wetlands is uncertain (Demuth et al., 2008; Strack et al., 2019) as glaciers retreat and snowpacks reduce across mountain areas (Moore et al., 2008). Projections indicate significant declines in glacial meltwater contributions (up to 60% in Eastern Slopes of Alberta by 2100) threatening the late-summer flows sustaining these ecosystems (Anderson and Radič, 2020). While shrinking water volumes change aquatic habitats, drying soil provide opportunities for woody and shrub vegetation to encroach into previously waterlogged areas, so coinciding with observable changes in wetland extent and vegetation (Teferi et al., 2010; Rai et al., 2018). Particularly in late summer when risks of drought rise, the compounding effects of glacial loss, lower snow accumulation, and earlier melt seasons (Fickas et al., 2016; Yu et al., 2017) could force wetlands toward irreversible ecological transitions. Targeted research is therefore necessary since the full consequences for biodiversity, carbon storage, and watershed stability are yet poorly known (Tong et al., 2014; Reza et al., 2020). Figure 1.2 shows a schematic picture of what is occurring in temperate montane wetlands around the world.

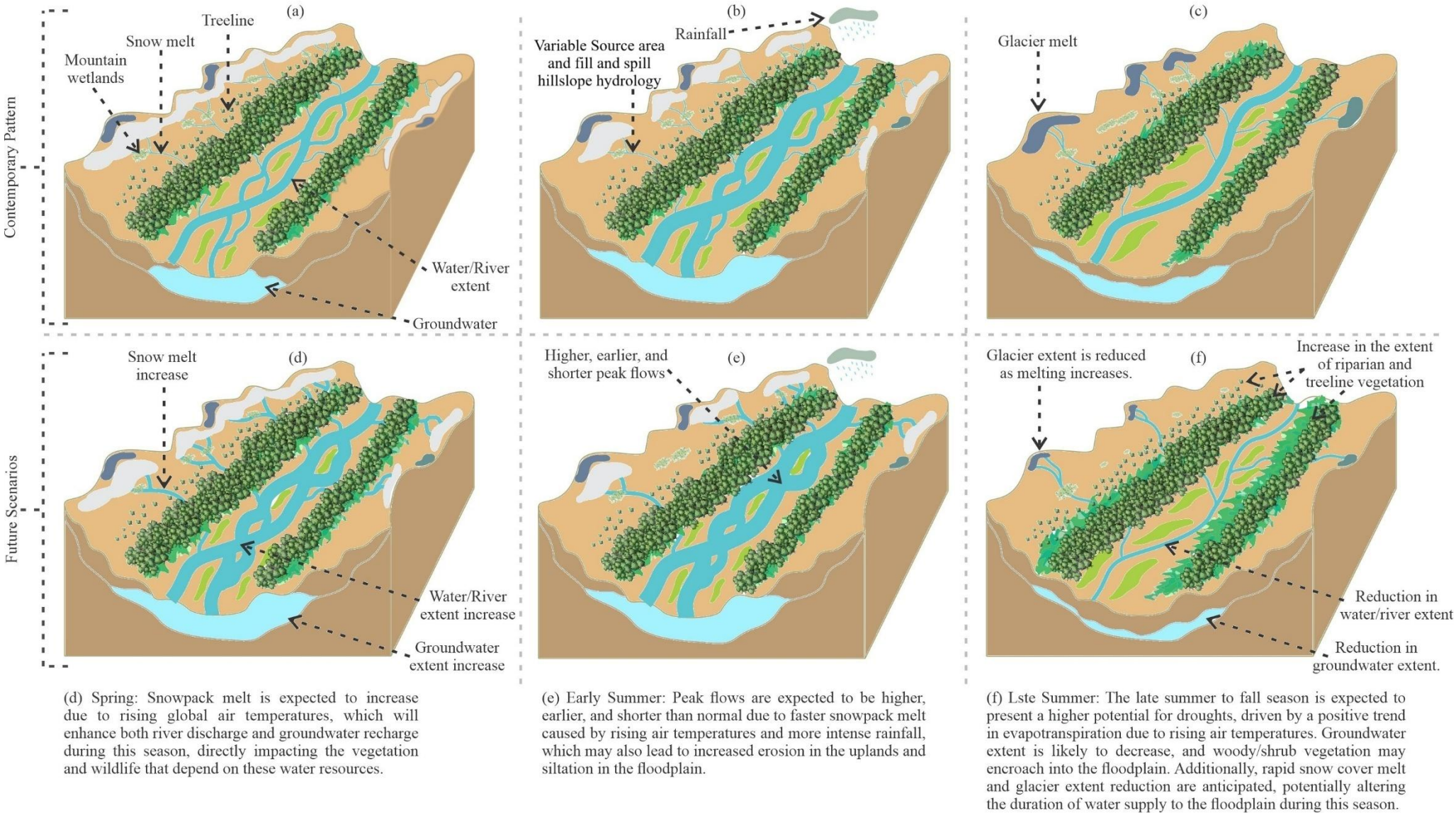

Fig. 1.2. A schematic showing the contemporary pattern in temperate montane wetlands during Spring (a), Summer (b), and Late Summer (c), and future scenarios over the Spring (d), Summer (e), and Late Summer (f)

1.6 Conclusion and recommendations

This literature review combines recent studies on temperate montane wetlands and forests, focusing on identifying the study area in Canada (specifically, temperate montane wetland regions), methods for mapping, techniques for detecting changes, and the environmental changes seen in Canada's mountainous areas. The study area (Objective 1) emphasizes the ecological significance of temperate montane wetlands in the mountainous Canadian regions, showing how these ecosystems are sensitive to both climatic and topographic influences and play a vital role in regional hydrology and biodiversity. Regarding wetland mapping methods (Objective 2), Landsat 5 and 8 imagery have dominated because of their consistency, moderate spatial resolution (30 meters), and long-term availability (>40 years). Traditional techniques for classifying land cover, particularly the maximum likelihood classifier, are still frequently used. However, more accurate machine learning methods, such as Random Forest, are still underused in Canadian montane wetlands, likely because of their computational requirements.

The vegetation and water indices commonly used, like NDVI, NDWI, and MNDWI, for detecting changes from a distance (Objective 3) are simple and don't need much computer power. While they might miss some complex changes in the landscape, these methods offer easy ways to understand how the land is changing. While they may overlook more intricate spectral and structural alterations, these methods provide readily accessible ways to assess landscape dynamics. However, the review pointed out a significant methodological gap: it discovered a lack of Canadian studies utilizing hyperspectral or RPAS platforms to detect long-term changes in montane wetland ecosystems.

In describing montane wetland trajectories (Objective 4), the literature repeatedly records hydrological changes driven by climate. Increasing air temperatures have accelerated snowfall and glacier melt, resulting in increased spring runoff while diminishing water availability by late summer. These factors elevate evapotranspiration, thereby heightening drought risk, and promote the encroachment of woody and shrub vegetation into drying wetlands. While there is growing evidence of climate impacts in regions such as the Montane Cordillera, our understanding of how these ecosystems respond to the dual pressures of land use and climate change remains limited. This underscores the need for more integrated, data-driven methods to track and predict these shifts.

The results presented provide a foundation for the subsequent phases of the thesis, which will integrate techniques for supervised land cover classification with climate projection models to

explore the trends of wetland ecosystems in the Upper Columbia Wetlands in British Columbia and Eastern Slopes of Alberta.

1.7 Thesis Research Objectives and Hypotheses

This thesis explores long-term land cover changes in montane wetlands spanning two important mountainous Canadian regions—the Upper Columbia River Basin (British Columbia) and the Eastern Slopes of Alberta—to better understand how hydrological variability and climate change are altering these sensitive ecosystems. This work will integrate machine learning and hydroclimatic modelling with 40+ years of satellite observations to:

- Chapter 2: to quantify the floodplain wetland response to changing hydroclimatic conditions within the Upper Columbia River Wetlands (UCRW) in Canada during the past 39 years (1984 – 2022).

- Hypothesis of Chapter 2: From 1984 and 2022, the extent and composition of floodplain wetlands in the UCRW will experience changes, characterized by the gradual encroachment of woody and shrub species that have replacing marsh and wet-meadow land covers, resulting in a reduction of open-water areas. These wetlands will become wetter in spring and early summer, while experiencing drier conditions in late summer, influenced by shifts in snowmelt timing, river discharge, and precipitation patterns.

- Chapter 3: to forecast (2023 – 2040) and describe the effects of climate change on Open Water, Marsh, Wet Meadow, and Woody/Shrub LCs in the UCRW, Canada using Landsat image archive time series and hydroclimatic models.

- Hypothesis of Chapter 3: Climate change is expected to lead to a decrease in Open Water and Marsh areas, while promoting an increase in Woody/Shrub cover in the UCRW from 2023 to 2040, especially under higher CO_2 emission scenarios. Although open water extent is projected to increase in the spring and early summer as a result of earlier snowmelt and changes in peak flow timing.

- Chapter 4: to quantify and assessing multi-decadal wetlands land cover extent (i.e., open water, riparian non-woody, riparian woody/shrub, and barren) trends on large spatial scale of the Eastern Slopes of Alberta (ES) from 1984 to 2023.

- Hypothesis of Chapter 4: In the Eastern Slopes of Alberta, there will be a noticeable increase in open water during the snowmelt-dominated period (nival). However, during the rainfall-dominated period (pluvial), a trend toward woody and shrub encroachment will emerge, along with a decline in open water areas within montane wetlands, which will be influenced by seasonal climate variability.

- Chapter 5: to investigate the long-term historical (1984 to 2023) analysis of the open water area and evaporation rates on the ES. Moreover, the historical proportion of open water evaporation volume compared to the evapotranspiration volumes of the forest ecosystem in the Eastern Slopes of Alberta was estimated.

- Hypothesis of Chapter 5: Warmer air temperature altered open water area dynamics throughout ES from 1984 to 2023. This resulted in an expansion of open water during the snowmelt-dominated period and a reduction during the late-summer rainfall-dominated period, accompanied by positive historical trends in evaporation rates. Furthermore, the proportion of open water evaporation volume to historical forest ecosystem evapotranspiration volume was higher during the snowmelt-dominated period than in the rainfall-dominated period, as consequence of positive trends of open water areas and evaporation during the nival period.

Overall, this thesis explores how historical and projected hydroclimatic changes are impacting montane wetlands in two important areas of Canada: Eastern Slopes of Alberta (ES) and UCRW (BC). The historical dynamics of the UCRW are quantified in Chapter 2 to evaluate how wetland composition has changed over almost four decades with variations in snowmelt and river discharge. Based on Chapter 2 datasets, Chapter 3 forecasts future land cover changes in the UCRW

to reflect the ecological effects of ongoing climate forcing. Chapter 4 employs methods akin to those in Chapter 2, utilizing long-term Landsat records to identify trends in wetland class transitions, thereby expanding the spatial focus to the Eastern Slopes. To grasp how warming might change hydrological processes in the ES, Chapter 5 finally combines historical open water areas with evapotranspiration modelling. These chapters taken together seek to quantify, predict, and contextualize wetland change under climate change across two mountain areas with ecological and hydrological importance.

1.8 Thesis Structure

This thesis has been written using the "research paper" style with an introductory Chapter 1 based on a literature review of existing knowledge on temperate montane wetlands, the Upper Columbia River Floodplain and, previous studies on the wetlands of the Eastern Slopes of Alberta, trends in the Montane ecosystems and relevant remote sensing methods to detect environmental changes. Chapters 2, 3, 4, and 5 are the major outcomes of this research. The concluding chapter 6, "Thesis Conclusion and Recommendations", summarizes key contributions, and proposes potential areas for future research.

1.9 References

Adams, J. (1995). Classification of multispectral images based on fractions of endmembers: Application to land-cover change in the Brazilian Amazon. *Remote Sensing of Environment*, *52*(2), 137–154. https://doi.org/10.1016/0034-4257(94)00098-8

Alonso-González, E., Revuelto, J., Fassnacht, S. R., & López-Moreno, J. I. (2022). Combined influence of maximum accumulation and melt rates on the duration of the seasonal snowpack over temperate mountains. *Journal of Hydrology*, *608*, 127574. https://doi.org/10.1016/j.jhydrol.2022.127574

Anderson, S., & Radić, V. (2020). Identification of local water resource vulnerability to rapid deglaciation in Alberta. *Nature Climate Change*, *10*(10), 933–938. https://doi.org/10.1038/s41558-020-0863-4

AghaKouchak, A. (2013). Extremes in a changing climate : detection, analysis and uncertainty. In *Springer eBooks*. http://ci.nii.ac.jp/ncid/BB11290672

Amani, M., Ghorbanian, A., Ahmadi, S. A., Kakooei, M., Moghimi, A., Mirmazloumi, S. M., Moghaddam, S. H. A., Mahdavi, S., Ghahremanloo, M., Parsian, S., Wu, Q., & Brisco, B. (2020). Google Earth Engine Cloud Computing Platform for Remote Sensing Big Data Applications: A Comprehensive Review. *IEEE Journal of Selected Topics in Applied Earth Observations and Remote Sensing*, *13*, 5326–5350. https://doi.org/10.1109/jstars.2020.3021052

Amani, M., Brisco, B., Warren, R., DeLancey, E. R., Seydi, S. T., & Poncos, V. (2022). Wetland Hydroperiod analysis in Alberta using INSAR Coherence data. *Remote Sensing*, *14*(14), 3469. https://doi.org/10.3390/rs14143469

Amani, M., Mahdavi, S., Kakooei, M., Ghorbanian, A., Brisco, B., DeLancey, E., Toure, S., & Reyes, E. L. (2021). Wetland change analysis in Alberta, Canada using four decades of Landsat imagery. *IEEE Journal of Selected Topics in Applied Earth Observations and Remote Sensing*, *14*, 10314–10335. https://doi.org/10.1109/jstars.2021.3110460

Amani, M., Mahdavi, S., Afshar, M., Brisco, B., Huang, W., Mirzadeh, S. M. J., White, L., Banks, S., Montgomery, J., & Hopkinson, C. (2019). Canadian Wetland Inventory using Google Earth Engine: The First Map and Preliminary Results. *Remote Sensing*, *11*(7), 842. https://doi.org/10.3390/rs11070842

Amin, G., Imtiaz, I., Haroon, E., Saqib, N. U., Shahzad, M. I., & Nazeer, M. (2024). Assessment of machine learning algorithms for land cover classification in a complex mountainous landscape. *Journal of Geovisualization and Spatial Analysis*, *8*(2). https://doi.org/10.1007/s41651-024-00195-z

Andrade, C., Borrás, J., Cordero, J. M., & Parra, H. (2020). Use of Spectral Vegetation Indices for Detecting Changes in High-Altitude Wetlands of the North Andean Region. International Archives of the Photogrammetry, Remote Sensing and Spatial Information Sciences, XLII-3/W12, 13–18. https://doi.org/10.5194/isprs-archives-XLII-3-W12-2020-13-2020

Arra, A. A., Alashan, S., & Şişman, E. (2024). Trends of meteorological and hydrological droughts and associated parameters using innovative approaches. *Journal of Hydrology*, *640*, 131661. https://doi.org/10.1016/j.jhydrol.2024.131661

Asokan, A., & Anitha, J. (2019). Change detection techniques for remote sensing applications: a survey. *Earth Science Informatics*, *12*(2), 143–160. https://doi.org/10.1007/s12145-019-00380-5

Attarchi, S., & Gloaguen, R. (2014). Classifying Complex Mountainous Forests with L-Band SAR and Landsat Data Integration: A Comparison among Different Machine Learning Methods in the Hyrcanian Forest. *Remote Sensing*, *6*(5), 3624–3647. https://doi.org/10.3390/rs6053624

Bartowitz, K. J., Higuera, P. E., Shuman, B. N., McLauchlan, K. K., & Hudiburg, T. W. (2019). Post-Fire Carbon Dynamics in Subalpine Forests of the Rocky Mountains. *Fire*, *2*(4), 58. https://doi.org/10.3390/fire2040058

Bisbing, S., Alaback, P., & DeLuca, T. (2010). Carbon storage in old-growth and second growth fire-dependent western larch (Larix occidentalis Nutt.) forests of the Inland Northwest, USA. *Forest Ecology and Management*, *259*(5), 1041–1049. https://doi.org/10.1016/j.foreco.2009.12.018

Bonsal, B. R., & Regier, M. (2007). Historical comparison of the 2001/2002 drought in the Canadian Prairies. *Climate Research, 33*(3), 229–242. https://doi.org/10.3354/cr033229

Borderieux, J., De Lombaerde, E., De Pauw, K., Sanczuk, P., Vangansbeke, P., Vanneste, T., De Frenne, P., Gégout, J., & Serra-Diaz, J. (2025). Cool topoclimates promote cold-adapted plant diversity in temperate mountain forests. Peer Community Journal, 5. https://doi.org/10.24072/pcjournal.519

Brahney, J., Weber, F., Foord, V., Janmaat, J., & Curtis, P. J. (2017). Evidence for a climate-driven hydrologic regime shift in the Canadian Columbia Basin. *Canadian Water Resources Journal / Revue Canadienne Des Ressources Hydriques*, *42*(2), 179–192. https://doi.org/10.1080/07011784.2016.1268933

Breiman, L. (2001). Random forests. *Machine Learning*, *45*(1), 5–32. https://doi.org/10.1023/a:1010933404324

Brinson, M. M., & Malvárez, A. I. (2002). Temperate freshwater wetlands: types, status, and threats. *Environmental Conservation*, *29*(2), 115–133. https://doi.org/10.1017/s0376892902000085

Brisco, B., Kapfer, M., Hirose, T., Tedford, B., & Liu, J. (2011). Evaluation of C-band polarization diversity and polarimetry for wetland mapping. *Canadian Journal of Remote Sensing*, *37*(1), 82–92. https://doi.org/10.5589/m11-017

Brown, R. D., & Mote, P. W. (2008). The Response of Northern Hemisphere Snow Cover to a Changing Climate*. *Journal of Climate*, *22*(8), 2124–2145. https://doi.org/10.1175/2008jcli2665.1

Bunnell, F. L., Kremsater, L. L., Moy, A., & Wells, R. W. (2011). Future vegetation structure and vertebrate distributions based on changes in moisture balance and temperature. Final Report, FSP

Y113120.

Buttle, J., Boon, S., Peters, D., Spence, C., Van Meerveld, H., & Whitfield, P. (2012). An overview of temporary stream hydrology in Canada. *Canadian Water Resources Journal / Revue Canadienne Des Ressources Hydriques*, *37*(4), 279–310. https://doi.org/10.4296/cwrj2011-903

Buttle, J. M., Allen, D. M., Caissie, D., Davison, B., Hayashi, M., Peters, D. L., Pomeroy, J. W., Simonovic, S., St-Hilaire, A., & Whitfield, P. H. (2016). Flood processes in Canada: Regional and special aspects. Canadian Water Resources Journal / Revue Canadienne Des Ressources Hydriques, 41(1–2), 7–30. https://doi.org/10.1080/07011784.2015.1131629

Carli, C.M., & Bayley, S.E. (2015). River connectivity and road crossing effects on floodplain vegetation of the upper Columbia River, Canada. Ecoscience, 22(2–4), 97–107. https://doi.org/10.1080/11956860.2015.1121705

Carlson, B. Z., Hébert, M., Van Reeth, C., Bison, M., Laigle, I., & Delestrade, A. (2020). Monitoring the Seasonal Hydrology of Alpine Wetlands in Response to Snow Cover Dynamics and Summer Climate: A Novel Approach with Sentinel-2. *Remote Sensing*, *12*(12), 1959. https://doi.org/10.3390/rs12121959

Carver, M. (2017) Water Monitoring and Climate Change in the Upper Columbia Basin: Summary of Current Status and Opportunities; Columbia Basin Trust: Castlegar, BC, Canada.

Chasmer, L., Cobbaert, D., Mahoney, C., Millard, K., Peters, D., Devito, K., Brisco, B., Hopkinson, C., Merchant, M., Montgomery, J., Nelson, K., & Niemann, O. (2020). Remote Sensing of Boreal Wetlands 1: Data Use for Policy and Management. *Remote Sensing*, *12*(8), 1320. https://doi.org/10.3390/rs12081320

Chasmer, L., Devito, K., Hopkinson, C., & Petrone, R. (2018). Remote sensing of ecosystem trajectories as a proxy indicator for watershed water balance. *Ecohydrology*, *11*(7). https://doi.org/10.1002/eco.1987

Chasmer, L., & Hopkinson, C. (2016a). Threshold loss of discontinuous permafrost and landscape evolution. *Global Change Biology*, *23*(7), 2672–2686. https://doi.org/10.1111/gcb.13537

Chasmer, L., Hopkinson, C., Montgomery, J., & Petrone, R. (2016b). A physically based terrain morphology and vegetation structural classification for wetlands of the Boreal Plains, Alberta, Canada. *Canadian Journal of Remote Sensing,* *42*(1), 1–20. https://doi.org/10.1080/07038992.2016.1196583

Chatterjee, A., Blom, E., Gujja, B., Jacimovic, R., Beevers, L., O'Keeffe, J., Beland, M., & Biggs, T. (2010). WWF Initiatives to Study the Impact of Climate Change on Himalayan High-altitude Wetlands (HAWs). Mountain Research and Development, 30(1), 42–52. https://doi.org/10.1659/mrd-journal-d-09-00091.1

Chen, L., Zhu, Y., Papandreou, G., Schroff, F., & Adam, H. (2018). Encoder-Decoder with Atrous Separable Convolution for Semantic Image Segmentation. In *Lecture notes in computer science* (pp. 833–851). https://doi.org/10.1007/978-3-030-01234-2_49

Chen, J., Gong, P., He, C., Pu, R., & Shi, P. (2003). Land-Use/Land-Cover change detection using improved Change-Vector analysis. *Photogrammetric Engineering & Remote Sensing*, *69*(4), 369–379. https://doi.org/10.14358/pers.69.4.369

Coogan, S. C., Robinne, F., Jain, P., & Flannigan, M. D. (2019). Scientists' warning on wildfire — a Canadian perspective. *Canadian Journal of Forest Research*, *49*(9), 1015–1023. https://doi.org/10.1139/cjfr-2019-0094

Cooper, D. J., Kaczynski, K. M., Sueltenfuss, J., Gaucherand, S., & Hazen, C. (2017). Mountain wetland restoration: The role of hydrologic regime and plant introductions after 15 years in the Colorado Rocky Mountains, U.S.A. *Ecological Engineering*, *101*, 46–59. https://doi.org/10.1016/j.ecoleng.2017.01.017

Cortes, C., & Vapnik, V. (1995). Support-vector networks. *Machine Learning*, *20*(3), 273–297. https://doi.org/10.1007/bf00994018

Cristóbal, J., Graham, P., Prakash, A., Buchhorn, M., Gens, R., Guldager, N., & Bertram, M. (2021). Airborne Hyperspectral Data Acquisition and Processing in the Arctic: A Pilot Study Using the Hyspex Imaging Spectrometer for Wetland Mapping. *Remote Sensing*, *13*(6), 1178. https://doi.org/10.3390/rs13061178

Dahl, T. E. (2006). Remote sensing as a tool for monitoring wetland habitat change. US fish and wildlife service, Branch of Habitat Assessment, Fish and Wildlife Resource Centre, 555.

Dahl, T. E. (1990). *Wetlands Losses in the United States, 1780's to 1980's*. US Department of the Interior, Fish and Wildlife Service.

Dallaire, C. O., Lehner, B., & Creed, I. (2019). Multidisciplinary classification of Canadian river reaches to support the sustainable management of freshwater systems. *Canadian Journal of Fisheries and Aquatic Sciences*, *77*(2), 326–341. https://doi.org/10.1139/cjfas-2018-0284

Dalponte, M., Bruzzone, L., & Gianelle, D. (2012). Tree species classification in the Southern Alps based on the fusion of very high geometrical resolution multispectral/hyperspectral images and LiDAR data. *Remote Sensing of Environment*, *123*, 258–270. https://doi.org/10.1016/j.rse.2012.03.013

Danby, R. K., & Hik, D. S. (2007). Variability, contingency and rapid change in recent subarctic alpine tree line dynamics. *Journal of Ecology*, *95*(2), 352–363. https://doi.org/10.1111/j.1365-2745.2006.01200.x

Dibike, Y., Eum, H., & Prowse, T. (2018). Modelling the Athabasca watershed snow response to a changing climate. *Journal of Hydrology Regional Studies*, *15*, 134–148. https://doi.org/10.1016/j.ejrh.2018.01.003

DeLancey, E. R., Simms, J. F., Mahdianpari, M., Brisco, B., Mahoney, C., & Kariyeva, J. (2019). Comparing deep learning and shallow Learning for Large-Scale Wetland classification in Alberta, Canada. *Remote Sensing*, *12*(1), 2. https://doi.org/10.3390/rs12010002

Demuth, M., Pinard, V., Pientroniro, A., Luckman, B., Hopkinson, C., Dornes, P., & Comeau, L. (2008). Recent and past-century variations in the glacier resources of the Canadian Rocky Mountains – Nelson River system. *Terra Glacialis*, *11*. http://scholar.ulethbridge.ca/hopkinson/publications/recent-and-past-century-variations-glacier-

resources-canadian-rocky-mountains

Demuth, M. N., & Pietroniro, A. (2003). The impact of climate change on the glaciers of the Canadian Rocky Mountain eastern slopes and implications for water resource related adaptation in the Canadian prairies:“Phase I”–headwaters of the North Saskatchewan River Basin. Geological Survey of Canada Open File, 4322, 96.

Deng, S., Katoh, M., Guan, Q., Yin, N., & Li, M. (2013). Interpretation of Forest Resources at the Individual Tree Level at Purple Mountain, Nanjing City, China, Using WorldView-2 Imagery by Combining GPS, RS and GIS Technologies. *Remote Sensing*, *6*(1), 87–110. https://doi.org/10.3390/rs6010087

Denison, D. G. T. (2002). *Bayesian methods for nonlinear classification and regression*. http://ci.nii.ac.jp/ncid/BA56543296

Devito, K., Mendoza, C., & Qualizza, C. (2012). Conceptualizing Water Movement in the Boreal Plains. Implications for Watershed Reconstruction. *ERA: Education and Research Archive*. https://doi.org/10.7939/r32j4h

Díaz, S., Demissew, S., Carabias, J., Joly, C., Lonsdale, M., Ash, N., Larigauderie, A., Adhikari, J. R., Arico, S., Báldi, A., Bartuska, A., Baste, I. A., Bilgin, A., Brondizio, E., Chan, K. M., Figueroa, V. E., Duraiappah, A., Fischer, M., Hill, R., Zlatanova, D. (2014). The IPBES Conceptual Framework — connecting nature and people. *Current Opinion in Environmental Sustainability*, *14*, 1–16. https://doi.org/10.1016/j.cosust.2014.11.002

Dong, X., & Chen, Z. (2021). Digital Examination of Vegetation Changes in River Floodplain Wetlands Based on Remote Sensing Images: A Case Study Based on the Downstream Section of Hailar River. *Forests*, *12*(9), 1206. https://doi.org/10.3390/f12091206

Endo, Y., Halabisky, M., Moskal, L. M., & Koshimura, S. (2020). Wetland Surface Water Detection from Multipath SAR Images Using Gaussian Process-Based Temporal Interpolation. *Remote Sensing*, *12*(11), 1756. https://doi.org/10.3390/rs12111756

Environment and Climate Change Canada (2016) Canadian Environmental Sustainability Indicators: Extent of Canada's Wetlands. Consulted on November 25, 2021. Available at: www.ec.gc.ca/indicateurs-indicators/default.asp?lang=en&n=69E2D25B-1.

Erwin, K. L. (2008). Wetlands and global climate change: the role of wetland restoration in a changing world. *Wetlands Ecology and Management*, *17*(1), 71–84. https://doi.org/10.1007/s11273-008-9119-1

Fassnacht, S. R., Venable, N. B., McGrath, D., & Patterson, G. G. (2018). Sub-Seasonal Snowpack Trends in the Rocky Mountain National Park Area, Colorado, USA. *Water*, *10*(5), 562. https://doi.org/10.3390/w10050562

Feizizadeh, B., Omarzadeh, D., Garajeh, M. K., Lakes, T., & Blaschke, T. (2021). Machine learning data-driven approaches for land use/cover mapping and trend analysis using Google Earth Engine. *Journal of Environmental Planning and Management*, *66*(3), 665–697.

https://doi.org/10.1080/09640568.2021.2001317

Fernandes, R., Korolevych, V., & Wang, S. (2007). Trends in Land Evapotranspiration over Canada for the Period 1960–2000 Based on In Situ Climate Observations and a Land Surface Model. *Journal of Hydrometeorology*, *8*(5), 1016–1030. https://doi.org/10.1175/jhm619.1

Fickas, K. C., Cohen, W. B., & Yang, Z. (2015). Landsat-based monitoring of annual wetland change in the Willamette Valley of Oregon, USA from 1972 to 2012. *Wetlands Ecology and Management*, *24*(1), 73–92. https://doi.org/10.1007/s11273-015-9452-0

Firth, P., & Fisher, S. G. (2012). *Global Climate Change and Freshwater Ecosystems*. Springer Science & Business Media.

Fraser, R., Olthof, I., Kokelj, S., Lantz, T., Lacelle, D., Brooker, A., Wolfe, S., & Schwarz, S. (2014). Detecting landscape changes in high latitude environments using LandsAT Trend Analysis: 1. Visualization. *Remote Sensing*, *6*(11), 11533–11557. https://doi.org/10.3390/rs61111533

Fridley, J. D., Sanders, N. J., & Klass, J. R. (2021). Microclimatic buffering by vegetation in a changing climate: A meta-analysis. Landscape Ecology, 36(8), 2157–2172. https://doi.org/10.1007/s10980-021-01195-w

Gao, Y., & Mas, J. F. (2008). A comparison of the performance of pixel-based and object-based classifications over images with various spatial resolutions. Online journal of earth sciences, 2(1), 27-35.
https://citeseerx.ist.psu.edu/document?repid=rep1&type=pdf&doi=a5ea97fa6421b57a4963a0beed0ebad210dcf99c

Gardner, R. C., & Davidson, N. (2011). The Ramsar Convention. In *Springer eBooks* (pp. 189–203). https://doi.org/10.1007/978-94-007-0551-7_11

Gasela, M., Kganyago, M., & De Jager, G. (2022). Testing the utility of the resampled nSight-2 spectral configurations in discriminating wetland plant species using Random Forest classifier. *Geocarto International*, *37*(26), 11830–11845. https://doi.org/10.1080/10106049.2022.2060326

Garcia-Dias, R., Prieto, C. A., Almeida, J. S., & Ordovás-Pascual, I. (2018). Machine learning in APOGEE - Unsupervised spectral classification with K-means. *Astronomy and Astrophysics*, *612*. https://doi.org/10.1051/0004-6361/201732134

Gerrand, S., Aspinall, J., Jensen, T., Hopkinson, C., Collingwood, A., & Chasmer, L. (2021). Partitioning carbon losses from fire combustion in a montane Valley, Alberta Canada. *Forest Ecology and Management*, *496*, 119435. https://doi.org/10.1016/j.foreco.2021.119435

Gibson, J., Eby, P., Birks, S., Twitchell, C., Gray, C., & Kariyeva, J. (2022). Isotope-based water balance assessment of open water wetlands across Alberta: Regional trends with emphasis on the oil sands region. *Journal of Hydrology Regional Studies*, *40*, 101036. https://doi.org/10.1016/j.ejrh.2022.101036

Gorham, E. (1991). Northern peatlands: Role in the carbon cycle and probable responses to climatic

warming. *Ecological Applications*, *1*(2), 182-195. https://doi.org/10.2307/1941811

Government of Alberta (2015). Alberta Wetland Identification and Delineation Directive. Water Policy Branch, Alberta Environment and Parks. Edmonton, Alberta.

Han, X., Pan, J., & Devlin, A. T. (2017). Remote sensing study of wetlands in the Pearl River Delta during 1995–2015 with the support vector machine method. *Frontiers of Earth Science*, *12*(3), 521–531. https://doi.org/10.1007/s11707-017-0672-x

Hao, Y. B., Cui, X. Y., Wang, Y. F., Mei, X. R., Kang, X. M., Wu, N., Luo, P., & Zhu, D. (2011). Predominance of Precipitation and Temperature Controls on Ecosystem CO2 Exchange in Zoige Alpine Wetlands of Southwest China. *Wetlands*, *31*(2), 413–422. https://doi.org/10.1007/s13157-011-0151-1

Hauer, F. R., Baron, J. S., Campbell, D. H., Fausch, K. D., Hostetler, S. W., Leavesley, G. H., Leavitt, P. R., Mcknight, D. M., & Stanford, J. A. (1997). Assessment of climate change and freshwater ecosystems of the Rocky Mountains, USA and Canada. *Hydrological Processes*, *11*(8), 903–924. https://doi.org/10.1002/(sici)1099-1085(19970630)11:8

Hayashi, M. (2020). Alpine hydrogeology: The critical role of groundwater in sourcing the headwaters of the world. *University of Calgary*. Retrieved from https://live-ucalgary.ucalgary.ca/sites/default/files/teams/371/Hayashi2020.pdf

Hrach, D. M., Petrone, R. M., Green, A., & Khomik, M. (2021). Analysis of growing season carbon and water fluxes of a subalpine wetland in the Canadian Rocky Mountains: Implications of shade on ecosystem water use efficiency. *Hydrological Processes*, *36*(1). https://doi.org/10.1002/hyp.14425

Helbig, M., Waddington, J. M., Alekseychik, P., Amiro, B. D., Aurela, M., Barr, A. G., Black, T. A., Blanken, P. D., Carey, S. K., Chen, J., Chi, J., Desai, A. R., Dunn, A., Euskirchen, E. S., Flanagan, L. B., Forbrich, I., Friborg, T., Grelle, A., Harder, S., Zyrianov, V. (2020). Increasing contribution of peatlands to boreal evapotranspiration in a warming climate. *Nature Climate Change*, *10*(6), 555–560. https://doi.org/10.1038/s41558-020-0763-7

Hilker, T., Wulder, M. A., Coops, N. C., Linke, J., McDermid, G., Masek, J. G., Gao, F., & White, J. C. (2009). A new data fusion model for high spatial- and temporal-resolution mapping of forest disturbance based on Landsat and MODIS. *Remote Sensing of Environment*, *113*(8), 1613–1627. https://doi.org/10.1016/j.rse.2009.03.007

Hird, J., Montaghi, A., McDermid, G., Kariyeva, J., Moorman, B., Nielsen, S., & McIntosh, A. (2017a). Use of Unmanned Aerial Vehicles for Monitoring Recovery of Forest Vegetation on Petroleum Well Sites. *Remote Sensing*, *9*(5), 413. https://doi.org/10.3390/rs9050413

Hird, J., DeLancey, E., McDermid, G., & Kariyeva, J. (2017b). Google Earth Engine, Open-Access Satellite Data, and Machine Learning in Support of Large-Area Probabilistic Wetland Mapping. *Remote Sensing*, *9*(12), 1315. https://doi.org/10.3390/rs9121315

Holden, P. B., Rebelo, A. J., & New, M. G. (2020). Mapping invasive alien trees in water towers: A

combined approach using satellite data fusion, drone technology and expert engagement. *Remote Sensing Applications Society and Environment*, *21*, 100448. https://doi.org/10.1016/j.rsase.2020.100448

Hood, G. A., & Larson, D. G. (2013). Beaver-Created habitat heterogeneity influences aquatic invertebrate assemblages in Boreal Canada. Wetlands, 34(1), 19–29. https://doi.org/10.1007/s13157-013-0476-z

Hood, G. A., & Larson, D. G. (2014). Ecological engineering and aquatic connectivity: a new perspective from beaver-modified wetlands. *Freshwater Biology*, *60*(1), 198–208. https://doi.org/10.1111/fwb.12487

Hopkinson, C., Fuoco, B., Grant, T., Bayley, S. E., Brisco, B., & MacDonald, R. (2020). Wetland Hydroperiod Change Along the Upper Columbia River Floodplain, Canada, 1984 to 2019. *Remote Sensing*, *12*(24), 4084. https://doi.org/10.3390/rs12244084

Hopkinson, C., & Demuth, M. N. (2006). Using airborne lidar to assess the influence of glacier downwasting on water resources in the Canadian Rocky Mountains. *Canadian Journal of Remote Sensing*, *32*(2), 212–222. https://doi.org/10.5589/m06-012

Hopkinson, C., Chasmer, L. E., Sass, G., Creed, I. F., Sitar, M., Kalbfleisch, W., & Treitz, P. (2005). Vegetation class dependent errors in lidar ground elevation and canopy height estimates in a boreal wetland environment. *Canadian Journal of Remote Sensing*, *31*(2), 191–206. https://doi.org/10.5589/m05-007

Hopkinson, C., & Young, G. J. (1998). The effect of glacier wastage on the flow of the Bow River at Banff, Alberta, 1951–1993. *Hydrological Processes*, *12*(10–11), 1745–1762. https://doi.org/10.1002/(sici)1099-1085(199808/09)12:10/11

Huang, C., Goward, S. N., Masek, J. G., Thomas, N., Zhu, Z., & Vogelmann, J. E. (2009). An automated approach for reconstructing recent forest disturbance history using dense Landsat time series stacks. *Remote Sensing of Environment*, *114*(1), 183–198. https://doi.org/10.1016/j.rse.2009.08.017

Hung, J. K., & Treitz, P. (2020). Environmental land-cover classification for integrated watershed studies: Cape Bounty, Melville Island, Nunavut. *Arctic Science*, *6*(4), 404–422. https://doi.org/10.1139/as-2019-0029

Ireland, G., & Petropoulos, G. P. (2014). Exploring the relationships between post-fire vegetation regeneration dynamics, topography and burn severity: A case study from the Montane Cordillera Ecozones of Western Canada. *Applied Geography*, *56*, 232–248. https://doi.org/10.1016/j.apgeog.2014.11.016

Jafarzadeh, H., Mahdianpari, M., Gill, E. W., Brisco, B., & Mohammadimanesh, F. (2022). Remote sensing and machine learning tools to support Wetland Monitoring: A Meta-Analysis of three decades of research. *Remote Sensing*, *14*(23), 6104. https://doi.org/10.3390/rs14236104

James, G., Witten, D., Hastie, T., & Tibshirani, R. (2021). An introduction to statistical learning (2nd ed.). Springer. https://doi.org/10.1007/978-1-0716-1418-1

Jiskoot, H., & Mueller, M. (2012). Glacier fragmentation effects on surface energy balance and runoff. *Hydrological Processes, 26*(12), 1861–1875. https://doi.org/10.1002/hyp.9288

Johnson, W. C., Millett, B. V., Gilmanov, T., Voldseth, R. A., Guntenspergen, G. R., & Naugle, D. E. (2005). Vulnerability of Northern Prairie Wetlands to Climate Change. *BioScience*, *55*(10), 863. https://doi.org/10.1641/0006-3568(2005)055

Johnson, W. C., Werner, B., & Guntenspergen, G. R. (2015). Non-linear responses of glaciated prairie wetlands to climate warming. *Climatic Change*, *134*(1–2), 209–223. https://doi.org/10.1007/s10584-015-1534-8

Jolliffe, I. T., & Cadima, J. (2016). Principal component analysis: a review and recent developments. *Philosophical Transactions of the Royal Society a Mathematical Physical and Engineering Sciences*, *374*(2065), 20150202. https://doi.org/10.1098/rsta.2015.0202

Ju, J., & Masek, J. G. (2016). The vegetation greenness trend in Canada and US Alaska from 1984–2012 Landsat data. *Remote Sensing of Environment*, *176*, 1–16. https://doi.org/10.1016/j.rse.2016.01.001

Kalacska, M., Chmura, G., Lucanus, O., Bérubé, D., & Arroyo-Mora, J. (2017). Structure from motion will revolutionize analyses of tidal wetland landscapes. *Remote Sensing of Environment*, *199*, 14–24. https://doi.org/10.1016/j.rse.2017.06.023

Kandel, D. R., & Acharya, D. (2024). Monitoring Land Use and Land Cover Change in Rara Wetland Using Remote Sensing and GIS Techniques. SSRN Electronic Journal. https://doi.org/10.2139/ssrn.4911218

Kang, X., Wang, Y., Chen, H., Tian, J., Cui, X., Rui, Y., Zhong, L., Kardol, P., Hao, Y., & Xiao, X. (2014). Modeling Carbon Fluxes Using Multi-Temporal MODIS Imagery and CO2 Eddy Flux Tower Data in Zoige Alpine Wetland, South-West China. *Wetlands*, *34*(3), 603–618. https://doi.org/10.1007/s13157-014-0529-y

Kasischke, E. S., Bourgeau-Chavez, L. L., Rober, A. R., Wyatt, K. H., Waddington, J. M., & Turetsky, M. R. (2009). Effects of soil moisture and water depth on ERS SAR backscatter measurements from an Alaskan wetland complex. Remote Sensing of Environment, 113(9), 1868–1873. https://doi.org/10.1016/j.rse.2009.04.006

Kauth, R. J. and Thomas, G. S., "The Tasselled Cap -- A Graphic Description of the Spectral-Temporal Development of Agricultural Crops as Seen by LANDSAT" (1976). *LARS Symposia*. Paper 159. http://docs.lib.purdue.edu/lars_symp/159 Kendall, M. G. (1948). Rank correlation methods.

Keddy, P. A. (2010). *Wetland ecology: Principles and conservation* (2nd ed.). Cambridge University Press.

Kienzle, S. W. (2006). The Use of the Recession Index as an Indicator for Streamflow Recovery After a Multi-Year Drought. *Water Resources Management*, *20*(6), 991–1006. https://doi.org/10.1007/s11269-006-9019-1

Killick, R., Fearnhead, P., & Eckley, I. A. (2012). Optimal Detection of Changepoints With a Linear Computational Cost. *Journal of the American Statistical Association*, *107*(500), 1590–1598. https://doi.org/10.1080/01621459.2012.737745

Killick, R., Eckley, I. A., Ewans, K., & Jonathan, P. (2010). Detection of changes in variance of oceanographic time-series using changepoint analysis. *Ocean Engineering*, *37*(13), 1120–1126. https://doi.org/10.1016/j.oceaneng.2010.04.009

Kirillov, A., Mintun, E., Ravi, N., Mao, H., Rolland, C., Gustafson, L., Xiao, T., Whitehead, S., Berg, A. C., Lo, W., Dollár, P., & Girshick, R. (2023). Segment anything. *arXiv (Cornell University)*. https://doi.org/10.48550/arxiv.2304.02643

Lantz, T. C., Marsh, P., & Kokelj, S. V. (2019). Recent shrub proliferation in the Mackenzie Delta uplands and microclimatic implications. Ecosystems, 16(1), 47–59. https://doi.org/10.1007/s10021-012-9595-2

Lee, S. (2011). *Detecting Wetland Change through Supervised Classification of Landsat Satellite Imagery within the Tunkwa Watershed of British Columbia, Canada*. http://www.pancroma.com/downloads/FULLTEXT01.pdf

Lee, S., Ryan, M. E., Hamlet, A. F., Palen, W. J., Lawler, J. J., & Halabisky, M. (2015). Projecting the Hydrologic Impacts of Climate Change on Montane Wetlands. *PLoS ONE*, *10*(9), e0136385. https://doi.org/10.1371/journal.pone.0136385

Leipe, S. C., & Carey, S. K. (2021). Rapid shrub expansion in a subarctic mountain basin revealed by repeat airborne LiDAR. *Environmental Research Communications*, *3*(7), 071001. https://doi.org/10.1088/2515-7620/ac0e0c

Leppi, J. C., DeLuca, T. H., Harrar, S. W., & Running, S. W. (2011). Impacts of climate change on August stream discharge in the Central-Rocky Mountains. *Climatic Change*, *112*(3–4), 997–1014. https://doi.org/10.1007/s10584-011-0235-1

Li, X., Strahler, A. H., & Woodcock, C. E. (1995). A hybrid geometric optical-radiative transfer approach for modeling albedo and directional reflectance of discontinuous canopies. *IEEE Transactions on Geoscience and Remote Sensing*, *33*(2), 466–480. https://doi.org/10.1109/tgrs.1995.8746028

Li, Z., He, Y., Wang, C., Wang, X., Xin, H., Zhang, W., & Cao, W. (2010). Spatial and temporal trends of temperature and precipitation during 1960–2008 at the Hengduan Mountains, China. *Quaternary International*, *236*(1–2), 127–142. https://doi.org/10.1016/j.quaint.2010.05.017

Liu, D., & Xia, F. (2010). Assessing object-based classification: advantages and limitations. *Remote Sensing Letters*, *1*(4), 187–194. https://doi.org/10.1080/01431161003743173

Liu, Q., Yan, G., Jiao, Z., Xiao, Q., Wen, J., Liang, S., Wang, J., Schaaf, C., & Strahler, A. (2018).

From Geometric-Optical Remote sensing modeling to Quantitative Remote Sensing Science—In memory of academician Xiaowen Li. *Remote Sensing*, *10*(11), 1764. https://doi.org/10.3390/rs10111764

Loh, H. Y., James, D., Ioki, K., Wong, W. V. C., Tsuyuki, S., & Phua, M. (2020). Aboveground Biomass Changes in Tropical Montane Forest of Northern Borneo Estimated Using Spaceborne and Airborne Digital Elevation Data. *Remote Sensing*, *12*(22), 3677. https://doi.org/10.3390/rs12223677

Long, X., Li, X., Lin, H., & Zhang, M. (2021). Mapping the vegetation distribution and dynamics of a wetland using adaptive-stacking and Google Earth Engine based on multi-source remote sensing data. *International Journal of Applied Earth Observation and Geoinformation*, *102*, 102453. https://doi.org/10.1016/j.jag.2021.102453

Lou, X., Zhai, S., Kang, B., Hu, Y., & Hu, L. (2014). Rapid Response of Hydrological Loss of DOC to Water Table Drawdown and Warming in Zoige Peatland: Results from a Mesocosm Experiment. *PLoS ONE*, *9*(11), e109861. https://doi.org/10.1371/journal.pone.0109861

Lu, D., Mausel, P., Brondízio, E., & Moran, E. (2004). Change detection techniques. *International Journal of Remote Sensing*, *25*(12), 2365–2401. https://doi.org/10.1080/0143116031000139863

Luckman, B., & Kavanagh, T. (2000). Impact of Climate Fluctuations on Mountain Environments in the Canadian Rockies. *AMBIO*, *29*(7), 371. https://doi.org/10.1639/0044-7447(2000)029

Luckman, B. H. (1990). Mountain Areas and Global Change: A View from the Canadian Rockies. *Mountain Research and Development*, *10*(2), 183. https://doi.org/10.2307/3673428

Lunetta, R. S., Knight, J. F., Ediriwickrema, J., Lyon, J. G., & Worthy, L. D. (2006). Land-cover change detection using multi-temporal MODIS NDVI data. *Remote Sensing of Environment*, *105*(2), 142–154. https://doi.org/10.1016/j.rse.2006.06.018

Luo, D., Jin, H., Du, H., Li, C., Ma, Q., Duan, S., & Li, G. (2020). Variation of alpine lakes from 1986 to 2019 in the Headwater Area of the Yellow River, Tibetan Plateau using Google Earth Engine. *Advances in Climate Change Research*, *11*(1), 11–21. https://doi.org/10.1016/j.accre.2020.05.007

Luo, L., Wang, X., Guo, H., Lasaponara, R., Zong, X., Masini, N., Wang, G., Shi, P., Khatteli, H., Chen, F., Tariq, S., Shao, J., Bachagha, N., Yang, R., & Yao, Y. (2019). Airborne and spaceborne remote sensing for archaeological and cultural heritage applications: A review of the century (1907–2017). *Remote Sensing of Environment*, *232*, 111280. https://doi.org/10.1016/j.rse.2019.111280

Ma, L., Liu, Y., Zhang, X., Ye, Y., Yin, G., & Johnson, B. A. (2019). Deep learning in remote sensing applications: A meta-analysis and review. ISPRS Journal of Photogrammetry and Remote Sensing, 152, 166–177. https://doi.org/10.1016/j.isprsjprs.2019.04.015

Ma, T., She, Y., Zhao, L., Hu, B., Feng, X., Zhao, J., & Zhao, Z. (2022). Alpine Wetland Evolution and Their Response to Climate Change in the Yellow-River-Source National Park from 2000 to 2020. *Water*, *14*(15), 2351. https://doi.org/10.3390/w14152351

MacDonald, G. M., Edwards, T. W. D., Moser, K. A., Pienitz, R., & Smol, J. P. (1993). Rapid response of treeline vegetation and lakes to past climate warming. *Nature*, *361*(6409), 243–246. https://doi.org/10.1038/361243a0

Mahdianpari, M., Salehi, B., Rezaee, M., Mohammadimanesh, F., & Zhang, Y. (2018). Very deep convolutional neural networks for complex land cover mapping using multispectral remote sensing imagery. Remote Sensing, 10(7), 1119. https://doi.org/10.3390/rs10071119

McCullagh, P., & Nelder, J. A. (1989). Generalized linear models (2nd ed.). Chapman and Hall.

McGuire, C. R., Nufio, C. R., Bowers, M. D., & Guralnick, R. P. (2012). Elevation-Dependent Temperature Trends in the Rocky Mountain Front Range: Changes over a 56- and 20-Year Record. *PLoS ONE*, *7*(9), e44370. https://doi.org/10.1371/journal.pone.0044370

Mahdianpari, M., Salehi, B., Mohammadimanesh, F., Brisco, B., Homayouni, S., Gill, E., DeLancey, E. R., & Bourgeau-Chavez, L. (2020a). Big Data for a Big Country: The First Generation of Canadian Wetland Inventory Map at a Spatial Resolution of 10-m Using Sentinel-1 and Sentinel-2 Data on the Google Earth Engine Cloud Computing Platform. *Canadian Journal of Remote Sensing*, *46*(1), 15–33. https://doi.org/10.1080/07038992.2019.1711366

Mahdianpari, M., Brisco, B., Granger, J. E., Mohammadimanesh, F., Salehi, B., Banks, S., Homayouni, S., Bourgeau-Chavez, L., & Weng, Q. (2020b). The Second Generation Canadian Wetland Inventory Map at 10 Meters Resolution Using Google Earth Engine. *Canadian Journal of Remote Sensing*, *46*(3), 360–375. https://doi.org/10.1080/07038992.2020.1802584

Mann, H. B. (1945). Nonparametric Tests Against Trend. Econometrica, 13(3), 245. https://doi.org/10.2307/1907187

Marcinkowska-Ochtyra, A., Zagajewski, B., Raczko, E., Ochtyra, A., & Jarocińska, A. (2018). Classification of High-Mountain Vegetation Communities within a Diverse Giant Mountains Ecosystem Using Airborne APEX Hyperspectral Imagery. *Remote Sensing*, *10*(4), 570. https://doi.org/10.3390/rs10040570

Margolis, H. A., Nelson, R. F., Montesano, P. M., Beaudoin, A., Sun, G., Andersen, H., & Wulder, M. A. (2015). Combining satellite lidar, airborne lidar, and ground plots to estimate the amount and distribution of aboveground biomass in the boreal forest of North America. *Canadian Journal of Forest Research*, *45*(7), 838–855. https://doi.org/10.1139/cjfr-2015-0006

Marti-Cardona, B., Dolz-Ripolles, J., & Lopez-Martinez, C. (2013). Wetland inundation monitoring by the synergistic use of ENVISAT/ASAR imagery and ancilliary spatial data. *Remote Sensing of Environment*, *139*, 171–184. https://doi.org/10.1016/j.rse.2013.07.028

McCaffrey, D., & Hopkinson, C. (2020a). Repeat Oblique Photography Shows Terrain and Fire-Exposure Controls on Century-Scale Canopy Cover Change in the Alpine Treeline Ecotone. *Remote Sensing*, *12*(10), 1569. https://doi.org/10.3390/rs12101569

McCaffrey, D. R., & Hopkinson, C. (2020b). Modeling Watershed-Scale Historic Change in the Alpine Treeline Ecotone Using Random Forest. *Canadian Journal of Remote Sensing*, *46*(6), 715–

732. https://doi.org/10.1080/07038992.2020.1865792

McClelland, C. J. R., Coops, N. C., Berman, E. E., Kearney, S. P., Nielsen, S. E., Burton, A. C., & Stenhouse, G. B. (2019). Detecting changes in understorey and canopy vegetation cycles in West Central Alberta using a fusion of Landsat and MODIS. *Applied Vegetation Science*, *23*(2), 223–238. https://doi.org/10.1111/avsc.12466

Mei, A., Manzo, C., Fontinovo, G., Bassani, C., Allegrini, A., & Petracchini, F. (2015). Assessment of land cover changes in Lampedusa Island (Italy) using Landsat TM and OLI data. *Journal of African Earth Sciences*, *122*, 15–24. https://doi.org/10.1016/j.jafrearsci.2015.05.014

Mercer, J. J. (2018). *Insights into mountain wetland resilience to climate change: An evaluation of the hydrological processes contributing to the hydrodynamics of alpine wetlands in the Canadian Rocky Mountains*. https://harvest.usask.ca/bitstream/10388/11257/1/MERCER-THESIS-2018.pdf (Doctoral dissertation, University of Saskatchewan).

Miller, C.E., R.O. Green, D.R. Thompson, A.K. Thorpe, M. Eastwood, I.B. Mccubbin, W. Olson-Duvall, M. Bernas, C.M. Sarture, S. Nolte, L.M. Rios, M.A. Hernandez, B.D. Bue, and S.R. Lundeen. 2024. ABoVE: AVIRIS-NG Imaging Spectroscopy for Alaska, Canada, and Iceland, 2017-2022, V3. ORNL DAAC, Oak Ridge, Tennessee, USA. https://doi.org/10.3334/ORNLDAAC/2362

Millar, D. J., Cooper, D. J., & Ronayne, M. J. (2018). Groundwater dynamics in mountain peatlands with contrasting climate, vegetation, and hydrogeological setting. *Journal of Hydrology*, *561*, 908–917. https://doi.org/10.1016/j.jhydrol.2018.04.050

Millard, K., & Richardson, M. (2015). On the Importance of Training Data Sample Selection in Random Forest Image Classification: A Case Study in Peatland Ecosystem Mapping. *Remote Sensing*, *7*(7), 8489–8515. https://doi.org/10.3390/rs70708489

Milner, A. M., Khamis, K., Battin, T. J., Brittain, J. E., Barrand, N. E., Füreder, L., Cauvy-Fraunié, S., Gíslason, G. M., Jacobsen, D., Hannah, D. M., Hodson, A. J., Hood, E., Lencioni, V., Ólafsson, J. S., Robinson, C. T., Tranter, M., & Brown, L. E. (2017). Glacier shrinkage driving global changes in downstream systems. *Proceedings of the National Academy of Sciences*, *114*(37), 9770–9778. https://doi.org/10.1073/pnas.1619807114

Minayeva, T., Sirin, A., Kershaw, P., Bragg, O. (2018). Arctic Peatlands. In: Finlayson, C., Milton, G., Prentice, R., Davidson, N. (eds) *The Wetland Book*. Springer, Dordrecht. https://doi.org/10.1007/978-94-007-4001-3_109

Montgomery, J., Mahoney, C., Brisco, B., Boychuk, L., Cobbaert, D., & Hopkinson, C. (2021). Remote Sensing of Wetlands in the Prairie Pothole Region of North America. *Remote Sensing*, *13*(19), 3878. https://doi.org/10.3390/rs13193878

Montgomery, J. S., Hopkinson, C., Brisco, B., Patterson, S., & Rood, S. B. (2018). Wetland hydroperiod classification in the western prairies using multitemporal synthetic aperture radar. *Hydrological Processes*, *32*(10), 1476–1490. https://doi.org/10.1002/hyp.11506

Moore, R. D., Fleming, S. W., Menounos, B., Wheate, R., Fountain, A., Stahl, K., Holm, K., & Jakob, M. (2008). Glacier change in western North America: influences on hydrology, geomorphic hazards and water quality. *Hydrological Processes*, *23*(1), 42–61. https://doi.org/10.1002/hyp.7162

Moore, R. D., Pelto, B., Menounos, B., & Hutchinson, D. (2020). Detecting the Effects of Sustained Glacier Wastage on Streamflow in Variably Glacierized Catchments. Frontiers in Earth Science, 8. https://doi.org/10.3389/feart.2020.00136 Morrison, A., Westbrook, C. J., & Bedard-Haughn, A. (2015). Distribution of Canadian Rocky Mountain wetlands impacted by beaver. Wetlands, 35(1), 95-104.

Mostowik, K., Siwek, J., Kisiel, M., Kowalik, K., Krzysik, M., Plenzler, J., & Rzonca, B. (2019). Runoff trends in a changing climate in the Eastern Carpathians (Bieszczady Mountains, Poland). *CATENA*, *182*, 104174. https://doi.org/10.1016/j.catena.2019.104174

Möller, M., Lymburner, L., & Volk, M. (2006). The comparison index: A tool for assessing the accuracy of image segmentation. *International Journal of Applied Earth Observation and Geoinformation*, *9*(3), 311–321. https://doi.org/10.1016/j.jag.2006.10.002

Msofe, N., Sheng, L., & Lyimo, J. (2019). Land Use Change Trends and Their Driving Forces in the Kilombero Valley Floodplain, Southeastern Tanzania. *Sustainability*, *11*(2), 505. https://doi.org/10.3390/su11020505

Müller, J., & Joos, F. (2021). Committed and projected future changes in global peatlands – continued transient model simulations since the Last Glacial Maximum. *Biogeosciences*, *18*(12), 3657–3687. https://doi.org/10.5194/bg-18-3657-2021

Musselman, K. N., Lehner, F., Ikeda, K., Clark, M. P., Prein, A. F., Liu, C., Barlage, M., & Rasmussen, R. (2018). Projected increases and shifts in rain-on-snow flood risk over western North America. *Nature Climate Change*, *8*(9), 808–812. https://doi.org/10.1038/s41558-018-0236-4

Munge, B., Thomas, G., & Heck, D. (2017). Outdoor Fieldwork in Higher Education: Learning From Multidisciplinary Experience. *Journal of Experiential Education*, *41*(1), 39–53. https://doi.org/10.1177/1053825917742165

Myung, I. J. (2003). Tutorial on maximum likelihood estimation. *Journal of Mathematical Psychology*, *47*(1), 90–100. https://doi.org/10.1016/s0022-2496(02)00028-7
Ozesmi, S. L., & Bauer, M. E. (2002). Satellite remote sensing of wetlands. Wetlands ecology and management, 10(5), 381-402.

National Wetlands Working Group. (1997). *The Canadian wetland classification system* (2nd ed.). Wetlands Research Centre, University of Waterloo.

Pederson, G. T., Gray, S. T., Ault, T., Marsh, W., Fagre, D. B., Bunn, A. G., Woodhouse, C. A., & Graumlich, L. J. (2010). Climatic Controls on the Snowmelt Hydrology of the Northern Rocky Mountains. *Journal of Climate*, *24*(6), 1666–1687. https://doi.org/10.1175/2010jcli3729.1

Pekel, J., Cottam, A., Gorelick, N., & Belward, A. S. (2016). High-resolution mapping of global surface water and its long-term changes. *Nature*, *540*(7633), 418–422.

https://doi.org/10.1038/nature20584

Penna, D., Engel, M., Mao, L., Dell'Agnese, A., Bertoldi, G., & Comiti, F. (2014). Tracer-based analysis of spatial and temporal variations of water sources in a glacierized catchment. *Hydrology and Earth System Sciences*, *18*(12), 5271–5288. https://doi.org/10.5194/hess-18-5271-2014

Pertiwi, A. P., Roth, A., Schaffhauser, T., Bhola, P. K., Reuß, F., Stettner, S., Kuenzer, C., & Disse, M. (2021). Monitoring the Spring Flood in Lena Delta with Hydrodynamic Modeling Based on SAR Satellite Products. *Remote Sensing*, *13*(22), 4695. https://doi.org/10.3390/rs13224695

Pittman, R. C., & Hu, B. (2023). Contribution of topographic features and categorization uncertainty for a tree species classification in the boreal biome of Northern Ontario. *GIScience & Remote Sensing*, *60*(1). https://doi.org/10.1080/15481603.2023.2214994

Poff, N. L., Brown, C. M., Grantham, T. E., Matthews, J. H., Palmer, M. A., Spence, C. M., Wilby, R. L., Haasnoot, M., Mendoza, G. F., Dominique, K. C., & Baeza, A. (2015). Sustainable water management under future uncertainty with eco-engineering decision scaling. *Nature Climate Change*, *6*(1), 25–34. https://doi.org/10.1038/nclimate2765

Polychronaki, A., Spindler, N., Stoinschek, B., Schmidt, A., Zebisch, M., Renner, K., ... & Sonnenschein, R. (2020) Habitat mapping and monitoring in Alpine regions using multi-temporal RapidEye data. https://www.earsel.org/symposia/2013-symposium-Matera/pdf_proceedings/EARSeL-Symposium-2013_9_3_Polychronaki.pdf

Praticò, S., Solano, F., Di Fazio, S., & Modica, G. (2021). Machine Learning Classification of Mediterranean Forest Habitats in Google Earth Engine Based on Seasonal Sentinel-2 Time-Series and Input Image Composition Optimisation. *Remote Sensing*, *13*(4), 586. https://doi.org/10.3390/rs13040586

Purwanto, A. D., Wikantika, K., Deliar, A., & Darmawan, S. (2022). Decision tree and random forest classification algorithms for mangrove forest mapping in Sembilang National Park, Indonesia. *Remote Sensing*, *15*(1), 16. https://doi.org/10.3390/rs15010016

Puttock, A., Cunliffe, A., Anderson, K., & Brazier, R. (2015). Aerial photography collected with a multirotor drone reveals impact of Eurasian beaver reintroduction on ecosystem structure. *Journal of Unmanned Vehicle Systems*, *3*(3), 123–130. https://doi.org/10.1139/juvs-2015-0005

Rai, R., Zhang, Y., Paudel, B., Acharya, B., & Basnet, L. (2018). Land Use and Land Cover Dynamics and Assessing the Ecosystem Service Values in the Trans-Boundary Gandaki River Basin, Central Himalayas. *Sustainability*, *10*(9), 3052. https://doi.org/10.3390/su10093052

Ramezan, C. A., Warner, T. A., Maxwell, A. E., & Price, B. S. (2021). Effects of training set size on supervised Machine-Learning Land-Cover classification of Large-Area High-Resolution remotely sensed data. *Remote Sensing*, *13*(3), 368. https://doi.org/10.3390/rs13030368

Reschke, J., Bartsch, A., Schlaffer, S., & Schepaschenko, D. (2012). Capability of C-Band SAR for Operational Wetland Monitoring at High Latitudes. *Remote Sensing*, *4*(10), 2923–2943.

https://doi.org/10.3390/rs4102923

Reza, N. P. Z. A., Aliakba, H., Saeid, P., Omid, B. K., & Rasoul, G. (2020). Detection and Prediction of Water Body and Aquatic Plants Cover Changes of Choghakhor International Wetland, Using Landsat Imagery and the Cellular Automata–Markov Model. *Contemporary Problems of Ecology*, *13*(5), 545–555. https://doi.org/10.1134/s1995425520050091

Rhemtulla, J. M., Hall, R. J., Higgs, E. S., & Macdonald, S. E. (2002). Eighty years of change: vegetation in the montane ecoregion of Jasper National Park, Alberta, Canada. Canadian Journal of Forest Research, 32(11), 2010-2021.

Richards, J. A. (2008). *Remote Sensing Digital Image Analysis: An Introduction*. https://ci.nii.ac.jp/ncid/BB12871218

Röder, A., Udelhoven, T., Hill, J., Del Barrio, G., & Tsiourlis, G. (2008). Trend analysis of Landsat-TM and -ETM+ imagery to monitor grazing impact in a rangeland ecosystem in Northern Greece. *Remote Sensing of Environment*, *112*(6), 2863–2875. https://doi.org/10.1016/j.rse.2008.01.018

Ronneberger, O., Fischer, P., & Brox, T. (2015). U-NET: Convolutional Networks for Biomedical Image Segmentation. In Lecture notes in computer science (pp. 234–241). https://doi.org/10.1007/978-3-319-24574-4_28

Rood, S. B., Pan, J., Gill, K. M., Franks, C. G., Samuelson, G. M., & Shepherd, A. (2007). Declining summer flows of Rocky Mountain rivers: Changing seasonal hydrology and probable impacts on floodplain forests. *Journal of Hydrology*, *349*(3–4), 397–410. https://doi.org/10.1016/j.jhydrol.2007.11.012

Rutchey, K., & Vilchek, L. (1994). Development of an Everglades vegetation map using a SPOT image and the Global Positioning System. Photogrammetric Engineering and Remote Sensing, 60(6), 767-775. https://www.asprs.org/wp-content/uploads/pers/1994journal/jun/1994_jun_767-775.pdf

Russell, A. P., & Bauer, A. M. (2000). The amphibians and reptiles of Alberta: A field guide and primer of boreal herpetology. University of Calgary Press.

Scheff, S. W. (2016). Fundamental Statistical Principles for the Neurobiologist : A Survival Guide. In *Elsevier eBooks*. https://international.scholarvox.com/book/88831984

Scherrer, D., & Körner, C. (2011). Topographically controlled thermal-habitat differentiation buffers alpine plant diversity against climate warming. Journal of Biogeography, 38(2), 406–416. https://doi.org/10.1111/j.1365-2699.2010.02407.x

Schiefer, E., Petticrew, E. L., Immell, R., Hassan, M. A., & Sonderegger, D. L. (2013). Land use and climate change impacts on lake sedimentation rates in western Canada. *Anthropocene*, *3*, 61–71. https://doi.org/10.1016/j.ancene.2014.02.006

Schindler, D. W., & Donahue, W. F. (2006). An impending water crisis in Canada's western prairie

provinces. *Proceedings of the National Academy of Sciences, 103*(19), 7210–7216. https://doi.org/10.1073/pnas.0601568103

Schnorbus, M., Werner, A., & Bennett, K. (2012). Impacts of climate change in three hydrologic regimes in British Columbia, Canada. *Hydrological Processes*, *28*(3), 1170–1189. https://doi.org/10.1002/hyp.9661

Senay, G. B., Schauer, M., Friedrichs, M., Velpuri, N. M., & Singh, R. K. (2017). Satellite-based water use dynamics using historical Landsat data (1984–2014) in the southwestern United States. *Remote Sensing of Environment*, *202*, 98–112. https://doi.org/10.1016/j.rse.2017.05.005

Shea, J. M., & Marshall, S. J. (2006). Atmospheric flow indices, regional climate, and Glacier mass balance in the Canadian Rocky mountains. *International Journal of Climatology*, *27*(2), 233–247. https://doi.org/10.1002/joc.1398

Shen, X., Xue, Z., Jiang, M., & Lu, X. (2018). Spatiotemporal Change of Vegetation Coverage and its Relationship with Climate Change in Freshwater Marshes of Northeast China. *Wetlands*, *39*(3), 429–439. https://doi.org/10.1007/s13157-018-1072-z

Shukla, P. R., Skeg, J., Buendia, E. C., Masson-Delmotte, V., Pörtner, H., Roberts, D. C., Zhai, P., Slade, R., Connors, S., Van Diemen, S., Ferrat, M., Haughey, E., Luz, S., Pathak, M., Petzold, J., Pereira, J. P., Vyas, P., Huntley, E., Kissick, K., Malley, J. (2019). Climate Change and Land: an IPCC special report on climate change, desertification, land degradation, sustainable land management, food security, and greenhouse gas fluxes in terrestrial ecosystems. In *IPCC (Intergovernmental Panel on Climate Change)*. https://philpapers.org/rec/SHUCCA-2

Singh, P., Shankar, A., & Diwakar, M. (2022). Review on nontraditional perspectives of synthetic aperture radar image despeckling. *Journal of Electronic Imaging*, *32*(02). https://doi.org/10.1117/1.jei.32.2.021609

Singh, A. (1989). Review Article Digital change detection techniques using remotely-sensed data. *International Journal of Remote Sensing*, *10*(6), 989–1003. https://doi.org/10.1080/01431168908903939

Song, M., Civco, D. L., & Hurd, J. D. (2005). A competitive pixel-object approach for land cover classification. *International Journal of Remote Sensing*, *26*(22), 4981–4997. https://doi.org/10.1080/01431160500213912

Stahl, K., & Moore, R. D. (2006). Influence of watershed glacier coverage on summer streamflow in British Columbia, Canada. *Water Resources Research*, *42*(6). https://doi.org/10.1029/2006wr005022

Stewart, I. T., Cayan, D. R., & Dettinger, M. D. (2004). Changes in Snowmelt Runoff Timing in Western North America under a `Business as Usual' Climate Change Scenario. *Climatic Change*, *62*(1–3), 217–232. https://doi.org/10.1023/b:clim.0000013702.22656.e8

Stewart, R. I. A., Dossena, M., Bohan, D. A., Jeppesen, E., Kordas, R. L., Ledger, M. E., ... & Woodward, G. (2020). Mesocosm experiments as a tool for ecological climate-change research.

Advances in Ecological Research, *48*, 71–181. https://doi.org/10.1016/B978-0-12-417199-2.00002-1

Stockdale, C. A., Bozzini, C., Macdonald, S. E., & Higgs, E. (2015). Extracting ecological information from oblique angle terrestrial landscape photographs: Performance evaluation of the WSL Monoplotting Tool. *Applied Geography*, *63*, 315–325. https://doi.org/10.1016/j.apgeog.2015.07.012

Strack, M., Hayne, S., Lovitt, J., McDermid, G. J., Rahman, M. M., Saraswati, S., & Xu, B. (2019). Petroleum exploration increases methane emissions from northern peatlands. *Nature Communications*, *10*(1). https://doi.org/10.1038/s41467-019-10762-4

Stych, P., Jerabkova, B., Lastovicka, J., Riedl, M., & Paluba, D. (2019). A Comparison of WorldView-2 and Landsat 8 Images for the Classification of Forests Affected by Bark Beetle Outbreaks Using a Support Vector Machine and a Neural Network: A Case Study in the Sumava Mountains. *Geosciences*, *9*(9), 396. https://doi.org/10.3390/geosciences9090396

Su, Z., Li, W., Ma, Z., & Gao, R. (2021). An improved U-Net method for the semantic segmentation of remote sensing images. Applied Intelligence, 52(3), 3276–3288. https://doi.org/10.1007/s10489-021-02542-9

Sun, Z., Wu, Y., Tang, Y., & Zhao, Y. (2020). Exploring the relationships between climate change and alpine wetlands on the Qinghai-Tibetan Plateau using remote sensing. Journal of Earth Science, 31(4), 859–872. https://doi.org/10.1007/s11769-020-1107-2

Teferi, E., Uhlenbrook, S., Bewket, W., Wenninger, J., & Simane, B. (2010). The use of remote sensing to quantify wetland loss in the Choke Mountain range, Upper Blue Nile basin, Ethiopia. *Hydrology and Earth System Sciences*, *14*(12), 2415–2428. https://doi.org/10.5194/hess-14-2415-2010

Tennant, C., & Menounos, B. (2013). Glacier change of the Columbia Icefield, Canadian Rocky Mountains, 1919–2009. *Journal of Glaciology*, *59*(216), 671–686. https://doi.org/10.3189/2013jog12j135

Thenkabail, P., Lyon, J., & Huete, A. (2011). Advances in hyperspectral remote sensing of vegetation and agricultural croplands. In *CRC Press eBooks* (pp. 3–36). https://doi.org/10.1201/b11222-3

Thonfeld, F., Steinbach, S., Muro, J., & Kirimi, F. (2020). Long-Term Land Use/Land Cover Change Assessment of the Kilombero Catchment in Tanzania Using Random Forest Classification and Robust Change Vector Analysis. *Remote Sensing*, *12*(7), 1057. https://doi.org/10.3390/rs12071057

Tiner, R. W. (2016). *Wetland Indicators: A Guide to Wetland formation, identification, delineation, classification, and mapping, second edition*. https://www.taylorfrancis.com/books/9781315374710

Tong, L., Xu, X., Fu, Y., & Li, S. (2014). Wetland Changes and Their Responses to Climate Change in the “Three-River Headwaters” Region of China since the 1990s. *Energies*, *7*(4), 2515–

2534. https://doi.org/10.3390/en7042515

Tong, Q., Xue, Y., & Zhang, L. (2013). Progress in Hyperspectral Remote Sensing Science and Technology in China Over the Past Three Decades. *IEEE Journal of Selected Topics in Applied Earth Observations and Remote Sensing*, *7*(1), 70–91. https://doi.org/10.1109/jstars.2013.2267204

Tou, J. T., & Gonzalez, R. C. (1974). *Pattern Recognition Principles*. Addison Wesley Publishing Company, Reading, Massachusetts

Trant, A., Higgs, E., & Starzomski, B. M. (2020). A century of high elevation ecosystem change in the Canadian Rocky Mountains. *Scientific Reports*, *10*(1). https://doi.org/10.1038/s41598-020-66277-2

Ullah, S., Shafique, M., Farooq, M., Zeeshan, M., & Dees, M. (2017). Evaluating the impact of classification algorithms and spatial resolution on the accuracy of land cover mapping in a mountain environment in Pakistan. *Arabian Journal of Geosciences*, *10*(3). https://doi.org/10.1007/s12517-017-2859-6

Valeo, C., Xiang, Z., Bouchart, F., Yeung, P., & Ryan, M. C. (2007). Climate Change Impacts in the Elbow River Watershed. *Canadian Water Resources Journal / Revue Canadienne Des Ressources Hydriques*, *32*(4), 285–302. https://doi.org/10.4296/cwrj3204285

Vázquez-Jiménez, R., Romero-Calcerrada, R., Novillo, C. J., Ramos-Bernal, R. N., & Arrogante-Funes, P. (2017). Applying the chi-square transformation and automatic secant thresholding to Landsat imagery as unsupervised change detection methods. *Journal of Applied Remote Sensing*, *11*(1), 016016. https://doi.org/10.1117/1.jrs.11.016016

Viviroli, D., Weingartner, R., & Messerli, B. (2003). Assessing the Hydrological Significance of the World's Mountains. *Mountain Research and Development*, *23*(1), 32–40. https://doi.org/10.1659/0276-4741(2003)023

Wang, C., Jia, M., Chen, N., & Wang, W. (2018). Long-Term Surface Water Dynamics Analysis Based on Landsat Imagery and the Google Earth Engine Platform: A Case Study in the Middle Yangtze River Basin. *Remote Sensing*, *10*(10), 1635. https://doi.org/10.3390/rs10101635

Westbrook, C. J., Cooper, D. J., & Baker, B. W. (2010). Beaver assisted river valley formation. *River Research and Applications*, *27*(2), 247–256. https://doi.org/10.1002/rra.1359

Westerling, A. L. (2016). Increasing western US forest wildfire activity: sensitivity to changes in the timing of spring. *Philosophical Transactions of the Royal Society B Biological Sciences*, *371*(1696), 20150178. https://doi.org/10.1098/rstb.2015.0178

White, L., Brisco, B., Dabboor, M., Schmitt, A., & Pratt, A. (2015). A Collection of SAR Methodologies for Monitoring Wetlands. *Remote Sensing*, *7*(6), 7615–7645. https://doi.org/10.3390/rs70607615

Whitfield, P. H., Kraaijenbrink, P. D. A., Shook, K. R., & Pomeroy, J. W. (2020). The Spatial Extent of Hydrological and Landscape Changes across the Mountains and Prairies of the

Saskatchewan and Mackenzie Basins. *Hydrology and Earth System Sciences Discussions*. https://doi.org/10.5194/hess-2019-671

Winter, T. C. (2000). The vulnerability of wetlands to climate change: A hydrologic landscape perspective. *JAWRA Journal of the American Water Resources Association*, *36*(2), 305–311. https://doi.org/10.1111/j.1752-1688.2000.tb04269.x

Wu, W., Shi, Y., Cai, K., Li, K., Cering, L., & Gong, Z. (2021). Using an explicit multi-feature decision tree for wetland information extraction in Qomolangma national nature reserve. *Remote Sensing Letters*, *12*(1), 68–78. https://doi.org/10.1080/2150704x.2021.1875145

Wulder, M., Li, Z., Campbell, E., White, J., Hobart, G., Hermosilla, T., & Coops, N. (2018). A National Assessment of Wetland Status and Trends for Canada's Forested Ecosystems Using 33 Years of Earth Observation Satellite Data. *Remote Sensing*, *10*(10), 1623. https://doi.org/10.3390/rs10101623

Wulder, M. A., White, J. C., Cranny, M., Hall, R. J., Luther, J. E., Beaudoin, A., Goodenough, D. G., & Dechka, J. A. (2008). Monitoring Canada's forests. Part 1: Completion of the EOSD land cover project. *Canadian Journal of Remote Sensing*, *34*(6), 549–562. https://doi.org/10.5589/m08-066

Xiong, B., Chen, J. M., & Kuang, G. (2011). A change detection measure based on a likelihood ratio and statistical properties of SAR intensity images. *Remote Sensing Letters*, *3*(3), 267–275. https://doi.org/10.1080/01431161.2011.572093

Xu, X., Li, D., Liu, H., Zhao, G., Cui, B., Yi, Y., Yang, W., & Du, J. (2024). Comparative Validation and Misclassification Diagnosis of 30-Meter Land cover datasets in China. *Remote Sensing*, *16*(22), 4330. https://doi.org/10.3390/rs16224330

Yu, H., Zhang, F., Kung, H., Johnson, V. C., Bane, C. S., Wang, J., Ren, Y., & Zhang, Y. (2017). Analysis of land cover and landscape change patterns in Ebinur Lake Wetland National Nature Reserve, China from 1972 to 2013. *Wetlands Ecology and Management*, *25*(5), 619–637. https://doi.org/10.1007/s11273-017-9541-3

Zerai, A. H., & Mahdavi, A. (2024). Monitoring the Impact of Drought on Ichkeul Lake-Bizerte Lagoon Wetlands Using Remote Sensing and Hydrological Modeling. Environmental Challenges, 100105. https://doi.org/10.1016/j.envc.2024.100105

Zemp, M., Jakob, L., Dussaillant, I., Nussbaumer, S. U., Gourmelen, N., Dubber, S., A, G., Abdullahi, S., Andreassen, L. M., Berthier, E., Bhattacharya, A., Blazquez, A., Vock, L. F. B., Bolch, T., Box, J., Braun, M. H., Brun, F., Cicero, E., Colgan, W., . . . Zheng, W. (2025). Community estimate of global glacier mass changes from 2000 to 2023. *Nature*. https://doi.org/10.1038/s41586-024-08545-z

Zimba, H., Kawawa, B., Chabala, A., Phiri, W., Selsam, P., Meinhardt, M., & Nyambe, I. (2018). Assessment of trends in inundation extent in the Barotse Floodplain, upper Zambezi River Basin: A remote sensing-based approach. *Journal of Hydrology Regional Studies*, *15*, 149–170. https://doi.org/10.1016/j.ejrh.2018.01.002

Zhang, Z., Zheng, D., Xue, Z., Wu, H., & Jiang, M. (2018a). Identification of anthropogenic contributions to heavy metals in wetland soils of the Karuola Glacier in the Qinghai-Tibetan Plateau. *Ecological Indicators*, *98*, 678–685. https://doi.org/10.1016/j.ecolind.2018.11.052

Zhang, F., Yushanjiang, A., & Jing, Y. (2018b). Assessing and predicting changes of the ecosystem service values based on land use/cover change in Ebinur Lake Wetland National Nature Reserve, Xinjiang, China. *The Science of the Total Environment*, *656*, 1133–1144. https://doi.org/10.1016/j.scitotenv.2018.11.444

Zhang, C., Sargent, I., Pan, X., Li, H., Gardiner, A., Hare, J., & Atkinson, P. M. (2018c). Joint Deep Learning for land cover and land use classification. *Remote Sensing of Environment*, *221*, 173–187. https://doi.org/10.1016/j.rse.2018.11.014

Zhang, G., Yao, T., Piao, S., Bolch, T., Xie, H., Chen, D., Gao, Y., O'Reilly, C. M., Shum, C. K., Yang, K., Yi, S., Lei, Y., Wang, W., He, Y., Shang, K., Yang, X., & Zhang, H. (2016). Extensive and drastically different alpine lake changes on Asia's high plateaus during the past four decades. *Geophysical Research Letters*, *44*(1), 252–260. https://doi.org/10.1002/2016gl072033

Zhao, K., Wulder, M. A., Hu, T., Bright, R., Wu, Q., Qin, H., Li, Y., Toman, E., Mallick, B., Zhang, X., & Brown, M. (2019). Detecting change-point, trend, and seasonality in satellite time series data to track abrupt changes and nonlinear dynamics: A Bayesian ensemble algorithm. *Remote Sensing of Environment*, *232*, 111181. https://doi.org/10.1016/j.rse.2019.04.034

Zhou, Y., Zhou, D., Zhao, M., & Su, Y. (2016). Estimating Net Primary Productivity of Montane Wetlands in the Southern Appalachian Region Using Remote Sensing Vegetation Indices. Open Journal of Ecology, 6(5), 284–295. https://doi.org/10.4236/oje.2016.65028

Zlinszky, A., Mücke, W., Lehner, H., Briese, C., & Pfeifer, N. (2012). Categorizing Wetland Vegetation by Airborne Laser Scanning on Lake Balaton and Kis-Balaton, Hungary. *Remote Sensing*, *4*(6), 1617–1650. https://doi.org/10.3390/rs4061617

Zhu, Z., & Woodcock, C. E. (2014). Continuous change detection and classification of land cover using all available Landsat data. *Remote Sensing of Environment*, *144*, 152–171. https://doi.org/10.1016/j.rse.2014.01.011

Chapter 2: Multi-decadal Floodplain Classification and Trend Analysis in the Upper Columbia River Valley, British Columbia

Abstract

Temperate montane floodplain wetlands ecosystems experience significant seasonal water fluctuation over the year, resulting in a dynamic hydroperiod, with a range of vegetation community responses. This paper assesses trends and changes in landcover and hydro-climatological variables, including air temperature, river discharge, and water level in the Upper Columbia River Wetlands (UCRW), British Columbia, Canada. A time series landcover classification from the Landsat image archive was generated using a Random Forest algorithm from 1984 to 2022. Peak river flow timing, duration, and anomalies were examined to evaluate temporal coincidence with observed land cover trends. The land cover classifier used to segment changes in wetland area and open water performed well (Kappa = 0.82). Over the last four decades, observed river discharge and air temperature have increased, precipitation has decreased, the timing of peak flow is earlier, and flow duration has been reduced. The frequency of both high discharge events and dry years have increased, indicating a shift towards more extreme floodplain flow behavior. These hydrometeorological changes are associated with a shift in the timing of snow melt from April to mid-May and are associated with seasonal changes in the vegetative communities over the 39-year period. Thus, woody shrubs (+6% to +12%) have expanded as they gradually replaced marsh and wet meadow landcovers with a reduction in open water area. This suggests that increasing temperatures have already impacted regional hydrology, wetland hydroperiod and floodplain land cover in the Upper Columbia Valley. Overall, there is substantial variation in seasonal and annual land cover reflecting the dynamic nature of floodplain wetlands, but the results show that the wetlands are drying out with increasing areas of woody/shrubby habitat and loss of aquatic habitat. The results suggest that floodplain wetlands, particularly marsh and open water habitats are vulnerable to climatic and hydrological changes that could further reduce their areal extent in the future.

Keywords: Montane; Floodplain Wetlands; Hydrology; Climate Change; Landsat; Landcover Classification; Seasonal Change

Citation:
Rodrigues, I. S., Hopkinson, C., Chasmer, L., MacDonald, R. J., Bayley, S. E., & Brisco, B. (2024). Multi-decadal floodplain classification and trend analysis in the Upper Columbia River valley, British Columbia. *Hydrology and Earth System Sciences*, 28(10), 2203-2221. https://doi.org/10.5194/hess-28-2203-2024

Supplementary materials 1, 2, and 3 of Chapter 2:
Supplement of Hydrol. Earth Syst. Sci., 28, 2203–2221, 2024 https://doi.org/10.5194/hess-28-2203-2024-supplement

Author Contributions:
Italo Sampaio Rodrigues: investigation, formal analysis, data curation, conceptualization, and writing – original draft.
Chris Hopkinson: investigation, formal analysis, data curation, conceptualization, and writing – original draft, review, and editing.
Laura Chasmer: visualization, supervision, conceptualization, and writing – review and editing.
Ryan MacDonald: visualization, supervision, methodology, and writing – review and editing.
Suzanne Bayley: visualization, supervision, resources, project administration, funding acquisition, conceptualization, and writing – review and editing.
Brian Brisco: conceptualization and writing – review and editing.

All the authors have read and agreed to the published version of the manuscript.

2.1.Introduction

Many temperate montane floodplain wetlands have a short history of establishment due to the short period since the deglaciation of lower elevation areas (Cooper et al. 2012) and are minerotrophic, making them highly sensitive to changes in surface and ground-water hydrology (Hathaway et al., 2022; Wang et al., 2016; Wang et al., 2018; Remmer et al., 2022). Large climatic gradients occur within relatively short distances due to elevational changes, which can amplify the effects of climate (MacDonald et al., 1993; Hopkinson and Young, 1998; Loeffler et al., 2011; McCaffrey and Hopkinson, 2020).

Over the last several decades, climatic changes and the amplifying effects of large elevational gradients on micro-climatology in the Canadian Rocky Mountains have resulted in significant changes to short- (Marshall, 2014) and long-term hydrology (Edwards et al., 2008; Jost et al., 2012), runoff (Stewart et al., 2004), and water storage (Mote et al., 2005; Whitfield, 2001). These changes impact minerotrophic wetlands, which can be sensitive to variations in hydrology, for example, since the 1950s the montane cordilleran ecozone has experienced precipitation decreases in southern (20 ~ 50%) and increases (30 ~ 50%) in northern regions (DeBeer et al., 2015). Changes in the phase of precipitation have also been observed over the last 60 years by Zhang et al. (2000), Schnorbus et al. (2014), and Vincent et al. (2015). On an annual basis, the authors found that the ratio of seasonal snowfall decreased by about 8% in the south and increased by ~12% in the north. The major changes occurred during spring, with reductions of ~20% for the entire region. Furthermore, snow accumulation and duration have also decreased due to a positive trend in air temperature (+1ºC since 1900s) (Zhang et al., 2000; Valeo et al., 2007; Whitfield, 2014), which is leading to earlier and faster snow- and glacier-melt during spring, resulting in high and shortened peak flows.

By mid-century, peak flows are predicted to increase with a shift to earlier spring runoff. For example, DeBeer et al., (2021) suggest that the timing of runoff could occur up to two to four weeks earlier by 2100. Earlier snowmelt increases the length of the summer period with associated higher air temperatures and evaporative losses (Foster et al., 2016; Leppi et al., 2012). Greater drying potential and diminished summer and autumn stream flow could have broad impacts on flora and fauna of minerotrophic montane wetlands (Stewart, 2008).

Montane floodplains and the wetlands that exist within them are governed by pulses or short intervals of water runoff, which contribute to flooding (i.e., flood pulses) (Junk et al., 1989).

The flood pulse enhances biological productivity and diversity in these ecosystems (Hughes, 1997) associated with the combined effects of the flood timing, water temperature, nutrient content, turbidity, and hydrological connectivity (Stanford et al., 2005; Lacoul and Freedman 2006; Bayley and Guimond 2008). Higher amplitude events that occur over shorter time periods or earlier in the season can inhibit the growth of some species or may initiate succession (Bayley, 1995). For example, during high flood events (wet years) Amoros and Bornette (2002) observed that fast flowing river discharge can carry away organic nutrients and deposit silt in the basins, which according to Sparks et al. (1990) and Bayley and Guimond (2009), may lead to decreases or loss of biodiversity, marsh burial, and a change in the wetland. However, in following years, marshes can grow back as the tubers remain and can regenerate following flooding (Hernandez and Mitsch, 2006). In contrast, periodic dry periods enhance shrub growth, which can be decimated during wet periods (Takaoka and Swanson, 2008).

It is crucial to ascertain whether there is a longer-term trend in the changes that are occurring to these montane floodplains or if there are events of such magnitude that cause this environment to move into a new ecosystem state. Recent trajectories in montane floodplain wetland landcovers remains a source of uncertainty, which raises questions over how floodplain riparian vegetation, permanent open water, and discharge properties have increased or decreased over recent decades. Wetland land cover mapping, management and change assessments typically employ field observation and data collection (Millar et al., 2018; Ray et al., 2019; Windell and Segelquist, 1986); however, this approach is costly, labor-intensive, and unable to represent past conditions (Chasmer et al., 2020).

In this context, remote sensing (RS) data and especially the Landsat time-series, can assist in wetland trend and change analysis by providing at least four decades of data (Ju and Masek, 2016; Wulder et al., 2022). The Landsat archive, which is now longer than pulses of seasonal or interannual hydro-climatological anomalies, permits evaluation of longer-term trends across large and spatially continuous areas, to help us better understand the patterns, direction, rates and drivers of change in dynamic montane wetland ecosystems.

The Columbia River floodplain in Canada represents a unique environment to assess wetland ecosystem changes over time associated with climatic and land-use changes. Wetlands of the Columbia River Basin provide important ecosystem services, such as critical habitats for flora and fauna, such as spawning grounds of fish (Cooper et al., 2017), support food webs (Díaz et al.,

2015), filter and store sediment from runoff erosion events (Lottig et al., 2013), and accumulate and release carbon (Hrach et al., 2022). A better understanding of the trends and changes in this study region will serve as an important reference for other similar wetlands in the Rocky Mountains.

The primary goal of this study is to quantify temperate montane floodplain wetlands response to changing hydroclimatic conditions within the Upper Columbia River Wetlands (UCRW) in Canada during the past 39 years (1984 - 2022). The objectives are to quantify and evaluate the historical trends and changes in i) areal floodplain landcover (open water, marsh, wet meadow, and riparian shrubs and trees) extents within the UCRW, and ii) the peak flow conditions in the Columbia River over the last 39 years in terms of discharge, water level, maximum inundation extent, timing, and duration using remote sensing and river runoff observations. To achieve this, seasonal land cover classifications from Landsat 5 and 8 were generated using a Random Forest algorithm, and local hydroclimatic data were examined to help explain the observed landcover trends. This study provides a framework for evaluating effects of climate change in the UCRW, supporting regional decision-makers as part of a strategic planning for the local biota and water resource management for the entire Canadian Columbia River.

2.2. Methods

2.2.1. Study Area

This study focusses on a ~ 120 km stretch of the Upper Columbia River floodplain (188 km²) between Donald and Invermere within the Rocky Mountain Trench, British Columbia, Canada (Figure 2.1). The region drains an upstream area of ~6,660 km², presents historical averages of: air temperature 3ºC, precipitation 800 mm $year^{-1}$ (MacDonald and Chernos, 2020), wind speed ~1 m s^{-1}, relative humidity 55% (Hersbach et al., 2020) and annual average peak flow of 512 m^3 s^{-1} (Carli and Bayley, 2015).

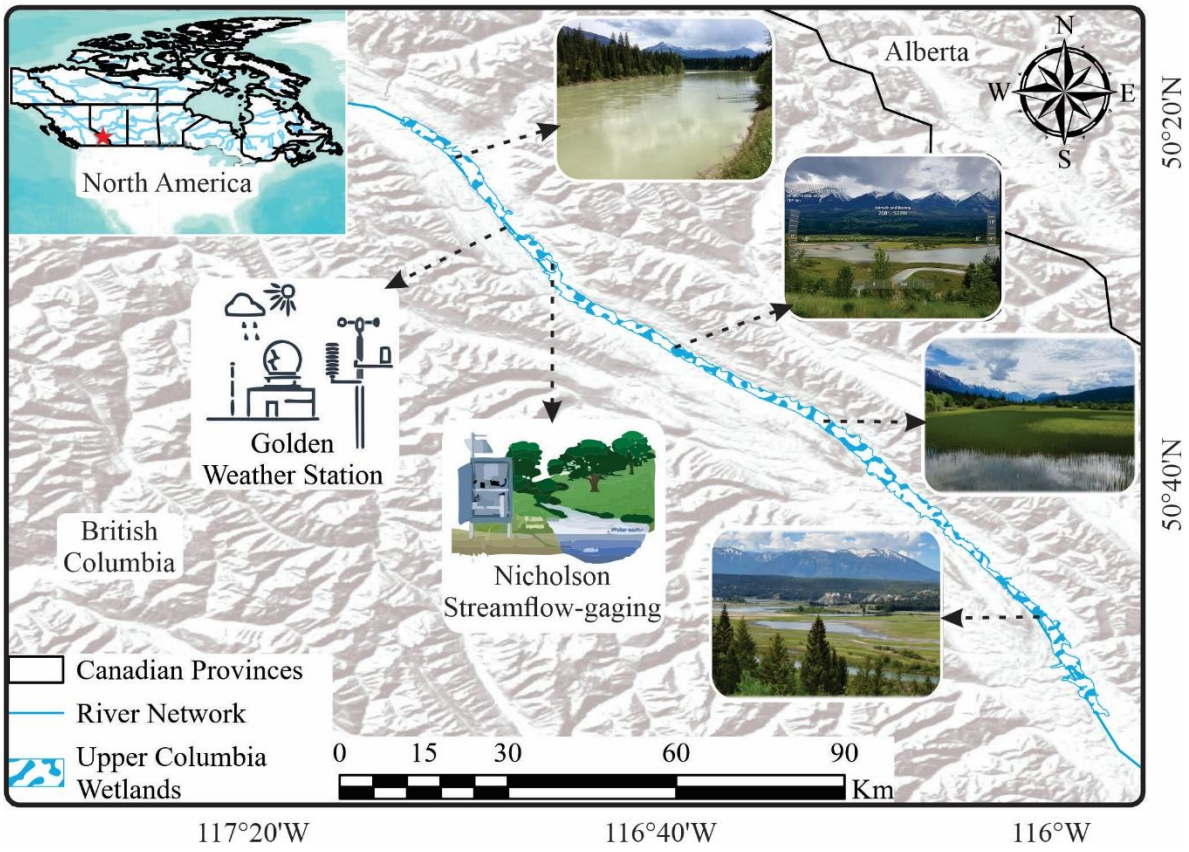

Fig. 2.1. Study area and approximate location of the streamflow-gaging and weather station

2.2.2. Remote sensing and hydroclimatic data input

The investigation period was 1984 to 2022, based on the Landsat 5 (Thematic Mapper – TM) and 8 (Operational Land Imager – OLI) Collection 2, Tier 1, Level 2 reflectance archives available via the Google Earth Engine (GEE). GEE contains the Landsat processing methods to compute at-sensor surface reflectance, and cloud-free composites. Higher spatial resolution (e.g. Sentinel 2, European Space Agency; Airborne LiDAR – Columbia Wetlands Stewardship Partners and the Provincial Government; UAV LiDAR, and geotagged oblique photos; historical aerial photographs (BC Government, 2022), and the historical land cover classification of Canada (Hermosilla et al., 2022) were used together as a reference dataset. To determine the 'best available pixel' cloud-free pixels were selected and the median reflectance product was calculated to generate three composition images for each year: 1. prior to seasonal flooding (April to mid-May) – Spring; 2. during the peak discharge period (late-May to end July) – Summer; and 3. late summer hydroperiod (August to mid-September) – Late summer. Air temperature and precipitation data for

Golden, BC (1984 - 2022) (Golden A, 1173209; Location: 51° 17' 57" N, 116° 58' 56" W) (Environment Canada, 2022a), and river discharge and water level at the Nicholson gauge (Columbia River at Nicholson, 08NA002; Location: 51° 14' 36" N, 116° 54' 46" W) (Environment Canada. 2022b) on the Columbia River (1903 - 2022) were obtained from the Environment Canada online data archives.

2.2.3. Workflow

The UCRW trend and change analysis workflow adopted seven steps, as shown in Fig. 2.2: i) acquisition of remote sensing data, and ii) hydroclimatic data; iii) reference dataset (i.e., Higher spatial resolution) for classification training purposes; iv) land cover classification; v) validation of land covers; vi) trend analysis; vii) and land cover change assessment.

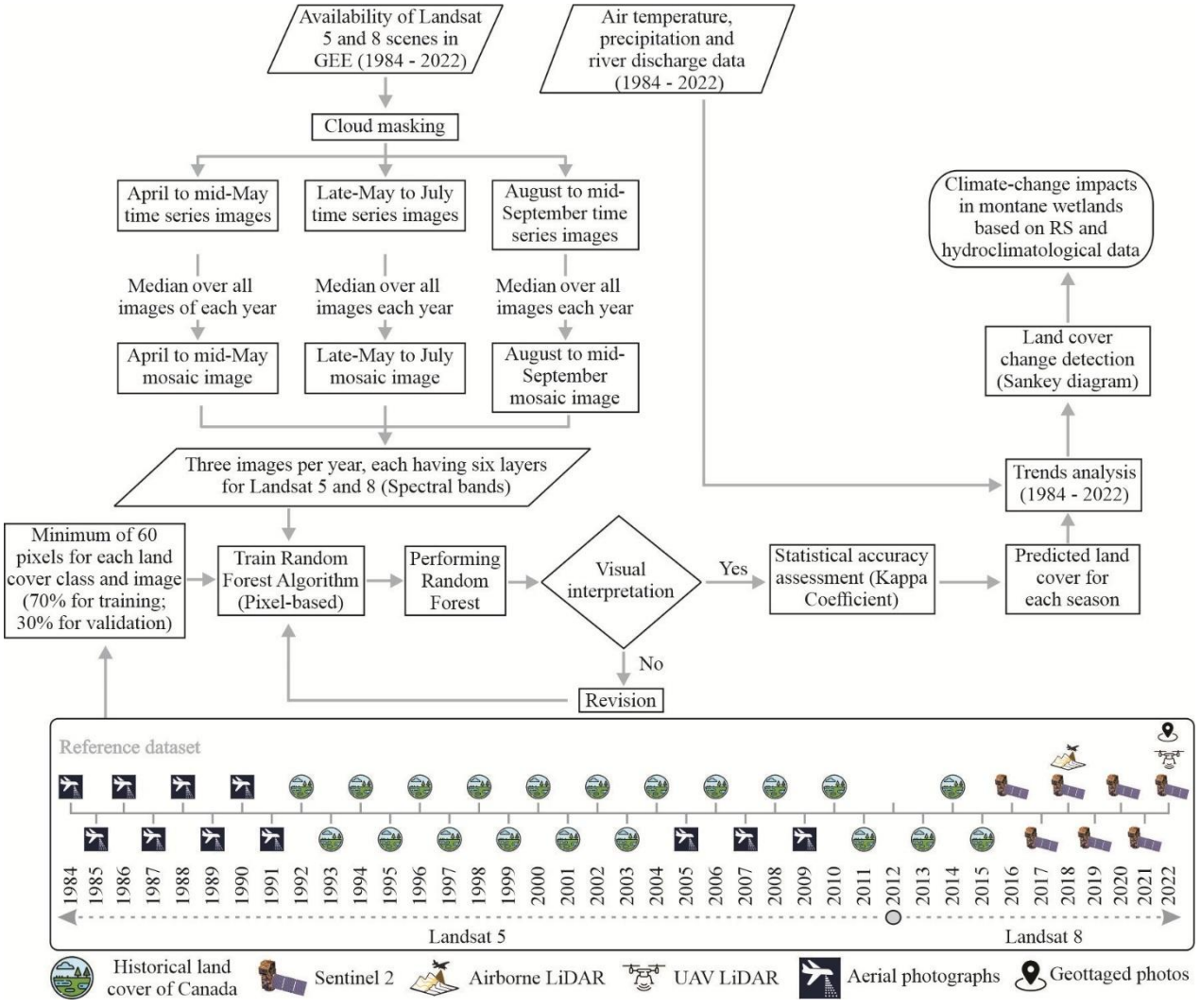

Fig. 2.2. Methodological workflow for the spatial-temporal (1984 - 2022) analysis of vegetated and water landcover classes using remote sensing and hydro-climatological data.

2.2.4. Random Forest algorithm and training data collection

To determine changes in the vegetation- and water-extent over time, a random forest (RF) classification (Breiman, 2001) was performed using GEE. RF is a supervised machine learning algorithm that generates multiple decision trees to create and predict a raster classification, in this case four classes: Open water, Marsh (i.e., Bulrush – *Schoenoplectus tabernaemontani* ,and Cattail Marsh – *Typha latifolia*), Wet meadow (e.g., Beaked Sedge – *Carex rostrata*, Water Sedge - *Carex aquatilis*, Horsetail - *Equisetum arvense*), Woody/Shrub vegetation (e.g. Woody: Cottonwood – *Populus*, Norway Spruce – *Picea abies*, and Dogwood – *Cornus* spp.; Shrub: Sitka Willow - *Salix sitchensis*, Red – Osier Dogwood – *Cornus sericea*, Horsetail – *Equisetum* spp.). RF was used because it is non-parametric and does not rely on a priori knowledge of the ecological drivers or characteristics of the prediction/classification outputs (Menze et al., 2009).

Training data collection, however, can be challenging over large or mountainous regions, as these ecosystems have dynamic or unpredictable weather, are remote and difficult to enter (e.g. Inglada et al., 2017). Moreover, access to training data is difficult to acquire over time because data may not be available for the period of assessment; land cover classes or observations could also be different from the current study, making it difficult to compare. This research utilizes a variety of reference remote sensing data sources: UAV and Airborne LiDAR, aerial photographs, geotagged photos, Sentinel 2, and historical classified land cover (Hermosilla et al., 2022) to generate training samples per each year (Figure 2.1).

To extract or determine the most reliable training pixels within areas of unchanging landcover class, the time series classification of Hermosilla et al. (2022) was used. Land cover permanence was calculated by summing the number of times each land cover class pixel was identified in the same pixel location. Reference rasters contain a numerical pixel value (i.e. 1 – open water; 2 – marsh; 3 – wet meadow; 4 – woody/shrub) that corresponds to each land cover in the input rasters. The 1984 land cover raster was chosen as the reference raster because this was the first year of the record, thereby providing a baseline or starting point from which to compare. The permanent land cover raster was then used within GEE to mask out permanent zones within the study floodplain that showed potential as training areas. Training pixels were then allocated within

these training areas and used over the whole time-series. However, in the years with available higher resolution imagery (i.e., sporadically throughout the time series: Aerial photographs – 1984 to 1991, 2005, 2007, and 2009; Sentinel 2 – 2016 to 2022; Airborne LiDAR – 2018; UAV LiDAR and geotagged photos – 2022), which by expert interpretive identification of land cover class was possible to increase the number of training pixels in these years with more reference datasets.

To reduce the uncertainty in the training data associated with classification errors in the historical land cover classification (Hermosilla et al. 2022), pixels within land cover patches were selected. Therefore, training pixels had to be at least 90m from adjacent landcovers (to reduce the potential for edge effects and mixed pixels) (Pelletier et al. 2016). The RF model was trained using 1500 trees (as per Millard and Richardson, 2015), and each class sample had a minimum of 60 pixels identified (60 pixels per land cover class; a total of 240 for the four land cover classes), and in the years with available higher resolution imagery, >40 pixels per land cover class were allocated (about 100 pixels per land cover class; a total of 400 assuming the four land cover classes), with 70% used for training and 30% reserved for validation. Pixels reserved for training within the RF model were those that were furthest in distance from clouds or cloud shadow boundaries, as applied in White et al. (2014). The training pixels were randomly distributed across the study floodplain with each scene mosaic. Classification was performed using the five following Landsat TM and OLI bands: Blue (Band 2 in OLI; Band 1 in TM), Green (Band 3 in OLI; Band 2 in TM), Red (Band 4 in OLI; Band 3 in TM), Near Infra Red (NIR, Band 5 in OLI; Bands 4 and 5 in TM), and Short Wave Infra Red (SWIR, Bands 6 and 7 in OLI; Band 7 in TM). Figure 2.3 illustrates the training and validation steps and the location of the training sites.

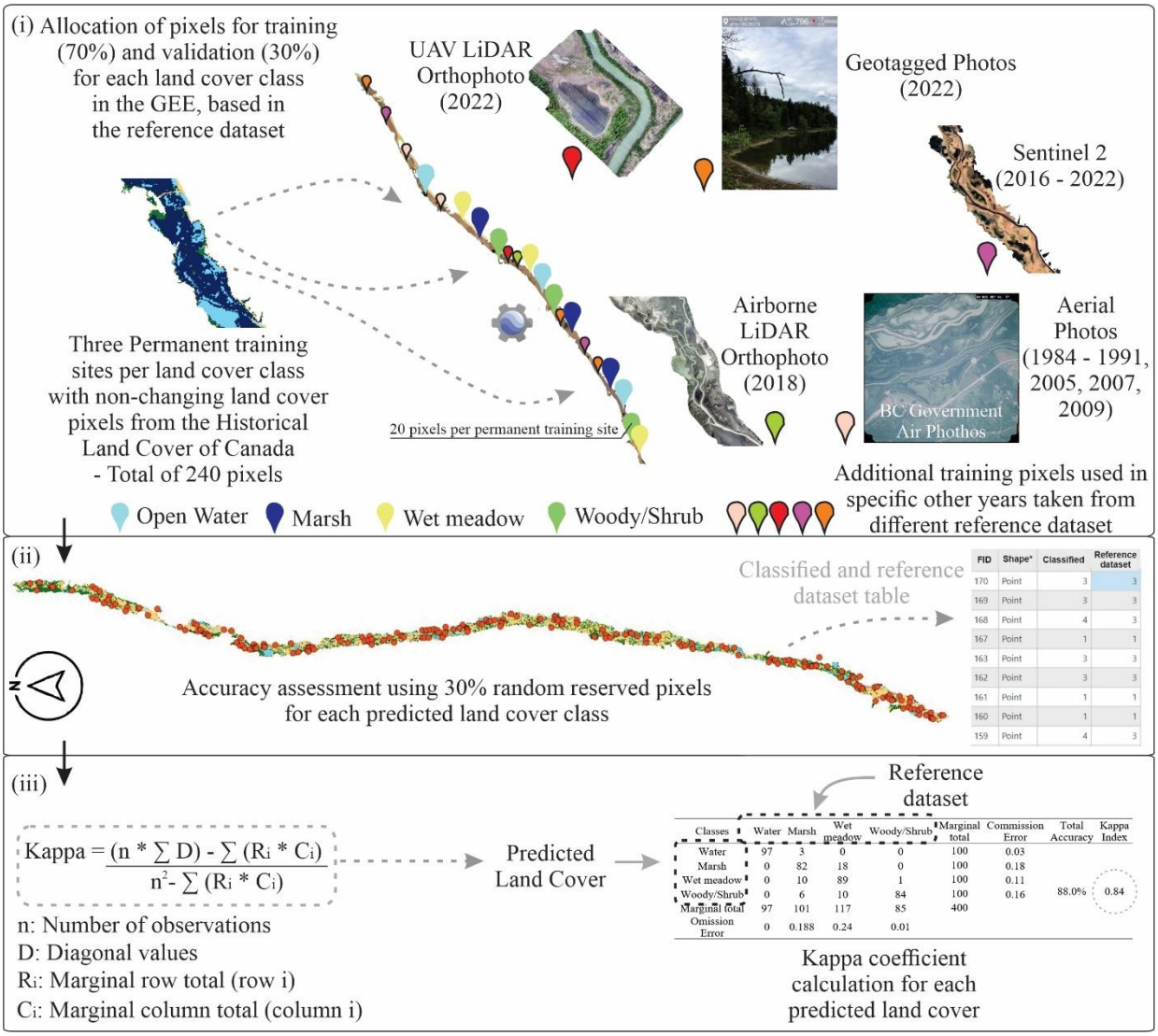

Fig. 2.3. Steps for land cover prediction: (i) Allocation of training pixels method; (ii) Accuracy assessment for the predicted land cover; (iii) Statistical evaluation using the Kappa coefficient.

2.2.5. Reference dataset and accuracy measurement

The higher spatial resolution RS, such as UAV and airborne LiDAR, aerial photographs, Sentinel 2, geotagged photos, and the non-changing pixels of the Historical Land Cover of Canada created by Hermosilla et al. (2022) (supplementary material 1 of Chapter 2) (Rodrigues et al. 2024) were used to allocate the training pixels/polygons. Thereafter, the Kappa coefficient was calculated to estimate the accuracy of the random forest simulated land cover.

According to Congalton and Green (2019), 50 random ground sample points are enough for each land cover category, though, a minimum of two-hundred samples were used per mosaic

image. The results of the kappa accuracy assessment were then summarized in a confusion matrix with omissions and commissions for all classes and periods. Furthermore, as discharge and open water area are expected to covary, a linear regression between these two variables was performed: i) as an additional check on the open water classification; and ii) to create a discharge-based model of floodplain inundation area.

2.2.6. Trend and change analysis

To assess the trends over 39 years in the wetland area classification and the hydroclimatic data, the Mann-Kendall test (Mann, 1945; Kendall, 1975) as well as Sen's slope method (Sen, 1968) were performed using pyMannKendall (Hussain and Mahmud, 2019). The Mann-Kendall method is a nonparametric test used to identify a trend in a series. To evaluate changes in wetland extent, three hypotheses were tested based on trends over the period of data observation: i) no trend exists over the time period; ii) a positive trend exists; and iii) a negative trend exists. A significance level or p-value ≤ 0.05 was assumed. For the land cover change assessment, the Change Detection Wizard in ArcGIS Pro was used with a pixel value change method to assess the shift during 1984 ~ 2022 raster datasets. This method provides a systematic way to identify changes between land cover classes (e.g., open water to marsh, marsh to woody/shrub, etc.). This method was utilized to determine the changes first between the seasonal images of 1984 and 2002 and then again from 2002 to 2022.

2.2.7. Discharge timing, duration, frequency, hydrograph, and anomaly assessment

To understand how hydro-climate variability might have influenced or altered wetland extents throughout the time of study, the use of direct observation (stream-gaging) methods is an appropriate way to evaluate river-based wetland changes. The timing and length of the peak flow (i.e., daily maximum flows) were determined using the historical streamflow-gaging station from Nicholson (1903–2022). The data were divided using a twenty-five-year time interval to assess when the peak flow occurred and how it has changed since 1903 (compared groups: 1903 to 1928, 1929 to 1953, 1954 to 1978, 1979 to 2003, and 2004 to 2022). This time interval was chosen because the Pacific Decadal Oscillation (PDO) influences precipitation and air temperature in the central-eastern Rockies (Linsley et al., 2015), and the PDO periodicities/cycles were most energetic/perceptive within a 25 year interval average (Mantua and Hare, 2002). To determine

whether the peak flow is occurring earlier or later, an average of the Julian day peak flow for each group was calculated and then compared.

The 10% highest flow (relative to peak flow) for each year was determined for the peak flow duration/length, and the number of days. To ascertain if the number of peak flow days is increasing or decreasing, the data were further divided into the five groups. The average of the number of peak flow days per 25-year time interval was determined and then compared.

To define the distribution of river discharge and how it changed over the course of a century, a frequency (%) curve from the daily and peak discharge was built, using the same five groups (1903 to 1928, 1929 to 1953, 1954 to 1978, 1979 to 2003, and 2004 to 2022), to show the frequency of each flow discharge, and the frequency with which it is overcome. Additionally, a peak flow hydrograph analysis was carried out for the five groups using the 25-year period interval average to compare shape and how it has altered since 1903. To separate the peak- from base-flow the recession method (Brutsaert and Nieber, 1977) was used (Equation 2.1).

$$Q_t = Q_0 K^t \tag{2.1}$$

Where Q_t is the baseflow (the threshold utilized was 50 $m^3.s^{-1}$ because it was observed that the discharge normally only increased beyond this value), Q_0 is the initial baseflow (at the beginning of the storm event, time = 0), k = exponential decay constant (ratio of the baseflow at time t = 0 to the baseflow one day earlier), and t is the number of days after the start of the peak flow. This method is used to discover the daily baseflow during the peak flow, and Equation 2.2 is used to determine the peak flow runoff (Q_{PR}).

$$Q_{PR} = Q - Q_t \tag{2.2}$$

After finding Q_{PR}, the values were plotted to create a hydrograph, an exponential model (Equation 2.3) was generated for each hydrograph to determine the recession constant (α) where a larger α represents a steeper decline (Berhail et al., 2012).

$$Q_a = Q_i e^{-\propto t} \tag{2.3}$$

Q_a is the discharge at time *t* after recession, Q_i represents the discharge at the start of recession, *e* is Euler's number (2.71828). In terms of the anomaly evaluation, it was used to identify how climate change affected peak discharge. The anomaly assessment was also used to detect the predominant PDO pattern (i.e., warm, normal, or cold) in each 25 years interval in the UCRW. The study implemented the straightforward technique proposed by Genz and Luz (2012). The anomaly for the peak flow was determined as follows in Equation 2.4:

$$Anomaly = \frac{(Q_i - Q_m)}{\sigma} \quad (2.4)$$

Q_i is the annual peak flow ($m^3.s^{-1}$) in a year, Q_m is the historical average of peak flow ($m^3.s^{-1}$), and σ is the standard deviation ($m^3.s^{-1}$). The Anomaly can be classified as: Wet > 0.5; Normal year ±0.5; Dry < -0.5. The Mann-Kendall trend test was then used to assess the anomalies to determine whether or not the peak flow anomaly was increasing or decreasing.

2.3. Results

2.3.1. Random Forest classification accuracy

A RF classification was used to determine the land cover extent per season in the UCRW since 1984 to 2022. To do this, 100 supervised classifications were performed for each period of Spring (37), Summer (29), and Late summer (34), using a total of 32,880 pixels for all seasonal images (23,016 for training, and 9,864 for validation). The average Kappa coefficient for all land cover classes and from each study period was 0.83 (April to mid-May; Table S1 to S37), 0.85 (late-May to July; Table S38 to S66), and 0.78 (August to mid-September; Table S67 to S100), which results in an average for all images of 0.82 (all Confusion Matrix with total accuracy, omission and commission for all classes and periods, and its corresponding classified raster are attached in the supplementary material 2 of Chapter 2 (Rodrigues et al., 2024), Table S1 to S100). Furthermore, the area of open water was correlated with river discharge for each year (Figure 2.4), varying from R^2 of 0.75 (April to mid-May and August to mid-September) to 0.82 (late-May to July). This is not a direct validation of the open water classification; however, as river discharge increases, open water extent across the floodplain also increases.

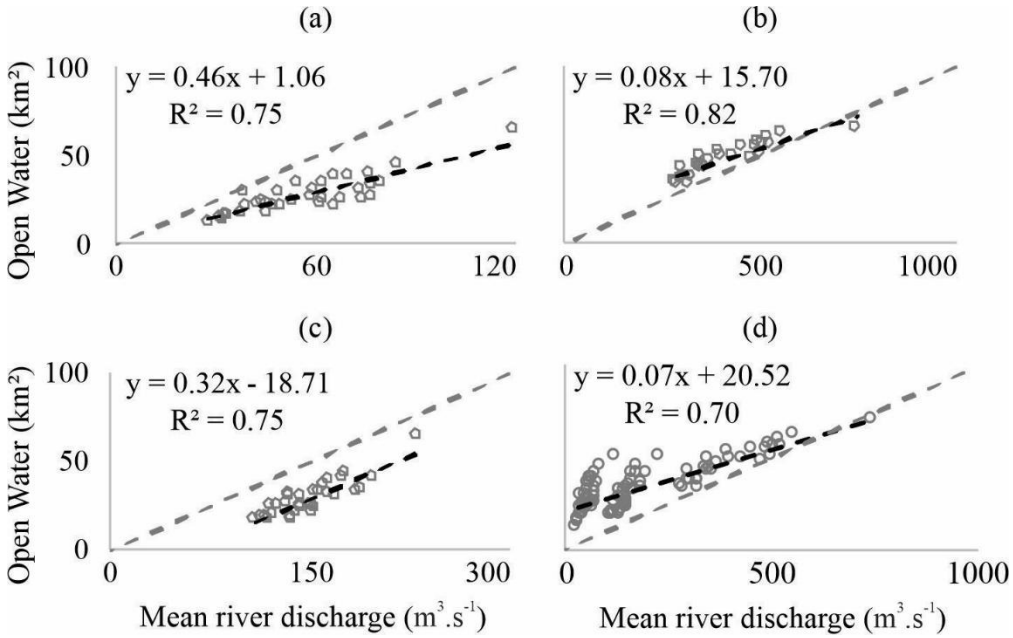

Fig. 2.4. Linear regression between area of open water and mean river discharge in April to mid-May (a), late-May to July (b), August to mid-September (c), annual basis (d).

2.3.2. Changes in the Upper Columbia floodplain from 1984 to 2022

The area of open water decreased from April to mid-May (-0.11 km².year^{-1}; -5 km^2 or -3% in 39 years, compared to the UCRW area) and from August to mid-September (-0.28 km².year^{-1}; -11 km^2 or -6%), which might be related with an overall reduction in precipitation (-0.75 mm.year^{-1}; p-value = 0.01) and an increase in air temperature (0.02°C.year^{-1}; p-value = 0.02) since 1984. The decrease in precipitation may have resulted in a loss of marsh areas of -1.39 km².year^{-1} (-55 km^2 or -29% during spring) and -0.24 km².year^{-1} (-9 km^2 or -5% by late summer), and an increase of wet meadow area during spring (1.28 km².year^{-1}; +48 km$^{2;}$ +26%) and reduction in the late summer (-0.12 km².year^{-1};-4 km^2 ;-2%). In contrast, woody/shrub vegetation increased in area over the spring, peak flow period and late summer by 0.26 km².year^{-1} (+11 km^2; +6%), by 0.50 km².year^{-1} (+20 km^2; +11%) and 0.57 km².year^{-1} (22 km^2 ; +12%) respectively.

During the peak flow season (late-May to July), the open water extent showed a positive tendency (0.13 km².year^{-1}; +3%), likely due to the increase in peak discharge (0.58 m³.s^{-1}.year^{-1}; p-value = 0.02) and water level (0.63 cm.year^{-1}; p-value = 0.02), and may be related to the increase in air temperature, which influences the beginning of the snowmelt period. This rapid and earlier rise in open water during the summer may have a negative impact on marsh growth which may explain

the negative trend of -0.90 km².year^{-1} in marsh area in this period (-19%) in the floodbasin. The marsh areas declined and were replaced by more open water (0.13 km².year-1; +3%), and an increase in the area of wet meadow (0.30 km^2.year-1; +7%) and woody/shrub (0.50 km^2.year-1; +11%) over the 39 years in the summer period.

The trends of the land cover extent and hydroclimatological indicators are shown in Figure 2.5 and Table 2.1, respectively. The overall annual trends show that open water (-0.03 km².year^{-1}) and marsh (-0.10 km².year^{-1}) extent are decreasing, whereas wet meadow (0.06 km².year^{-1}) and woody/shrub (0.17 km².year^{-1}) areas are expanding (Figure 2.5d). The relatively small annual changes compared to the larger seasonal changes (Figure 2.5 d vs 2.5 a,b,c) demonstrates the importance of the seasonal evaluation in detecting changes in the UCRW. The spatial context and the percentage of change during spring, summer, and late summer in Figures 2.6, 2.7, and 2.8, shows how each land cover has changed over 39 years in the floodplain. The location/coordinates of the main changes are provided in the supplementary materials 3 of Chapter 2 file (Tables S101 to S104) (Rodrigues et al., 2024).

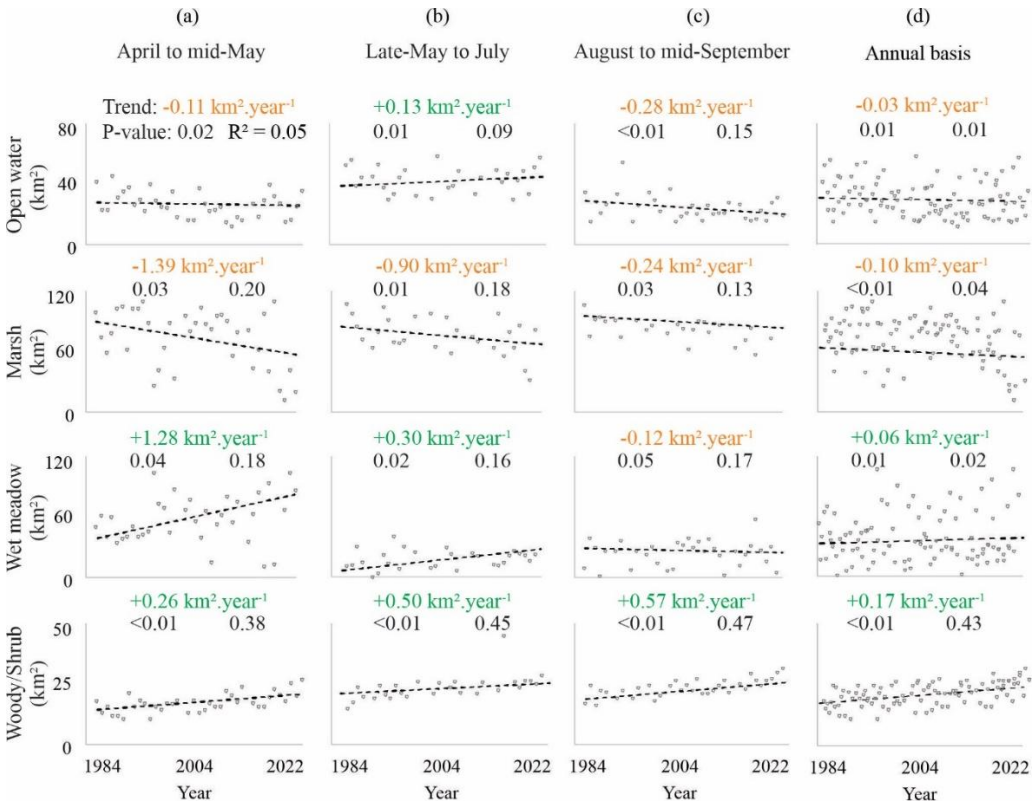

Green – Positive trends; Orange – Negative trends.

Fig. 2.5. Trends of land cover extent during April to mid-May (a), late-May to July (b), August to mid-September (c) and in on annual basis (d) (1984 – 2022)

Table 2.1. Historical and trends of hydroclimate variables (1984 - 2022).

Variable	Air temperature	Precipitation	Discharge		Water level	
			Annual	Peak flow	Annual	Peak level
Min.	-30.10 °C	301.40 mm	12.70 $m^3.s^{-1}$	283 $m^3.s^{-1}$	10.10 cm	232.20 cm
Mean	5.22 °C	463.80 mm	104.97 $m^3.s^{-1}$	428.18 $m^3.s^{-1}$	106.20 cm	320.70 cm
Max.	25.70 °C	641.40 mm	748 $m^3.s^{-1}$	748 $m^3.s^{-1}$	421.40 cm	421.40 cm
τ	0.02	-0.08	0.02	0.04	0.06	0.07
S	1197480	-62	1382135	25	5098418	45
p-value	0.02*	0.01*	<0.01*	0.02*	<0.01*	0.02*
Slope	0.02 °C.$year^{-1}$	-0.75 mm.$year^{-1}$	0.01 $m^3.s^{-1}$ $year^{-1}$	0.58 $m^3.s^{-1}$ $year^{-1}$	0.01 cm.$year^{-1}$	0.63 cm.$year^{-1}$

Min. – Minimum; Max. – Maximum; * – There is a significant temporal trend at the 5% level; S and τ – indicate the trend (negative or positive); Slope – represents the 39 years increase/decrease of the variable; p-value – trend significance ≤ 0.05 high significance.

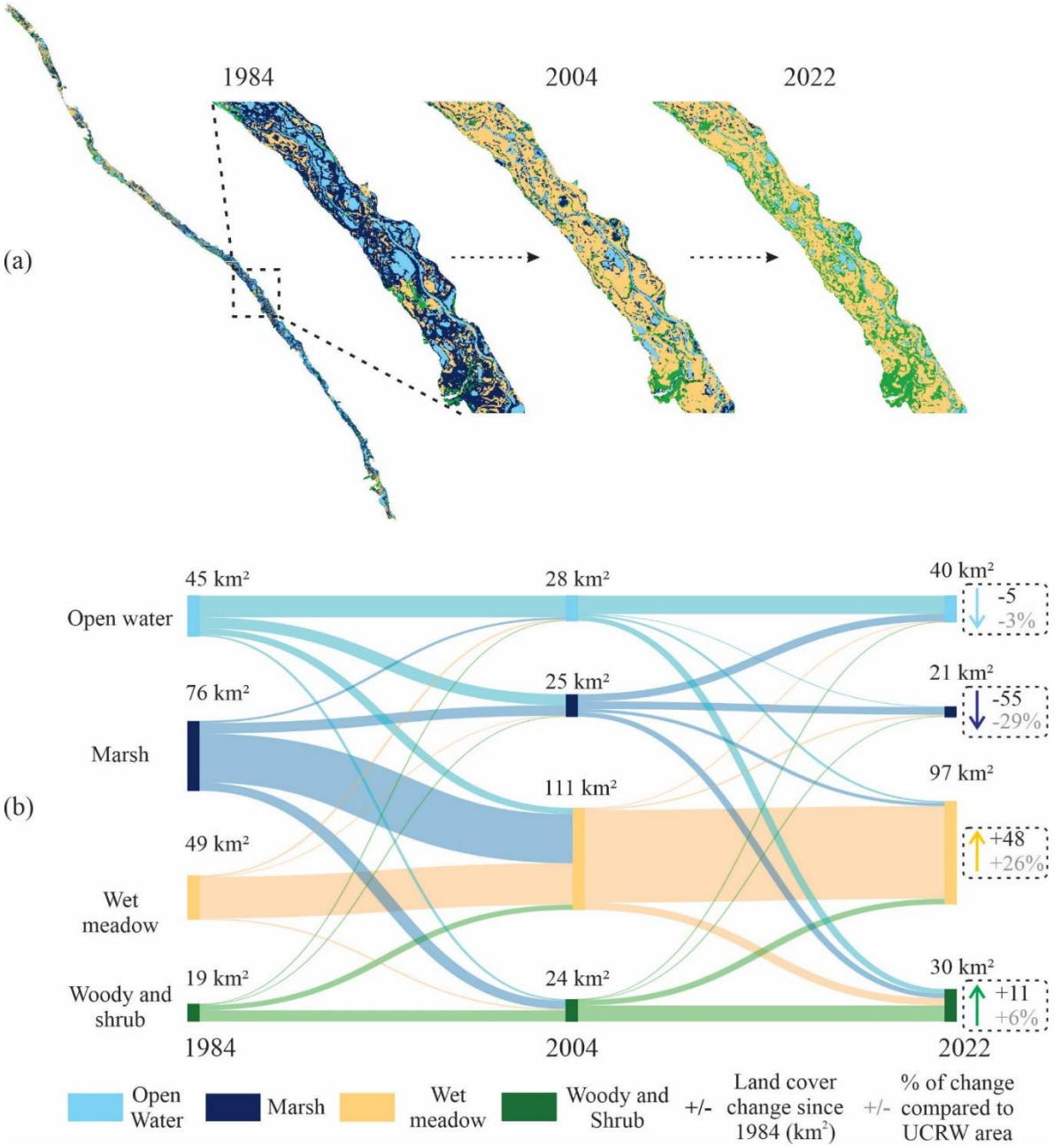

Fig. 2.6: The Upper Columbia River floodplain distribution of land cover change from April to mid-May. Map insets (a) indicate changes in land cover for sample regions. Sankey diagram (b) of the changes in land cover from 1984 to 2004 (left) and 2004 to 2022 (right), the land cover change since 1984, and the percentage of change compared to the Columbia wetlands area (188 km^2).

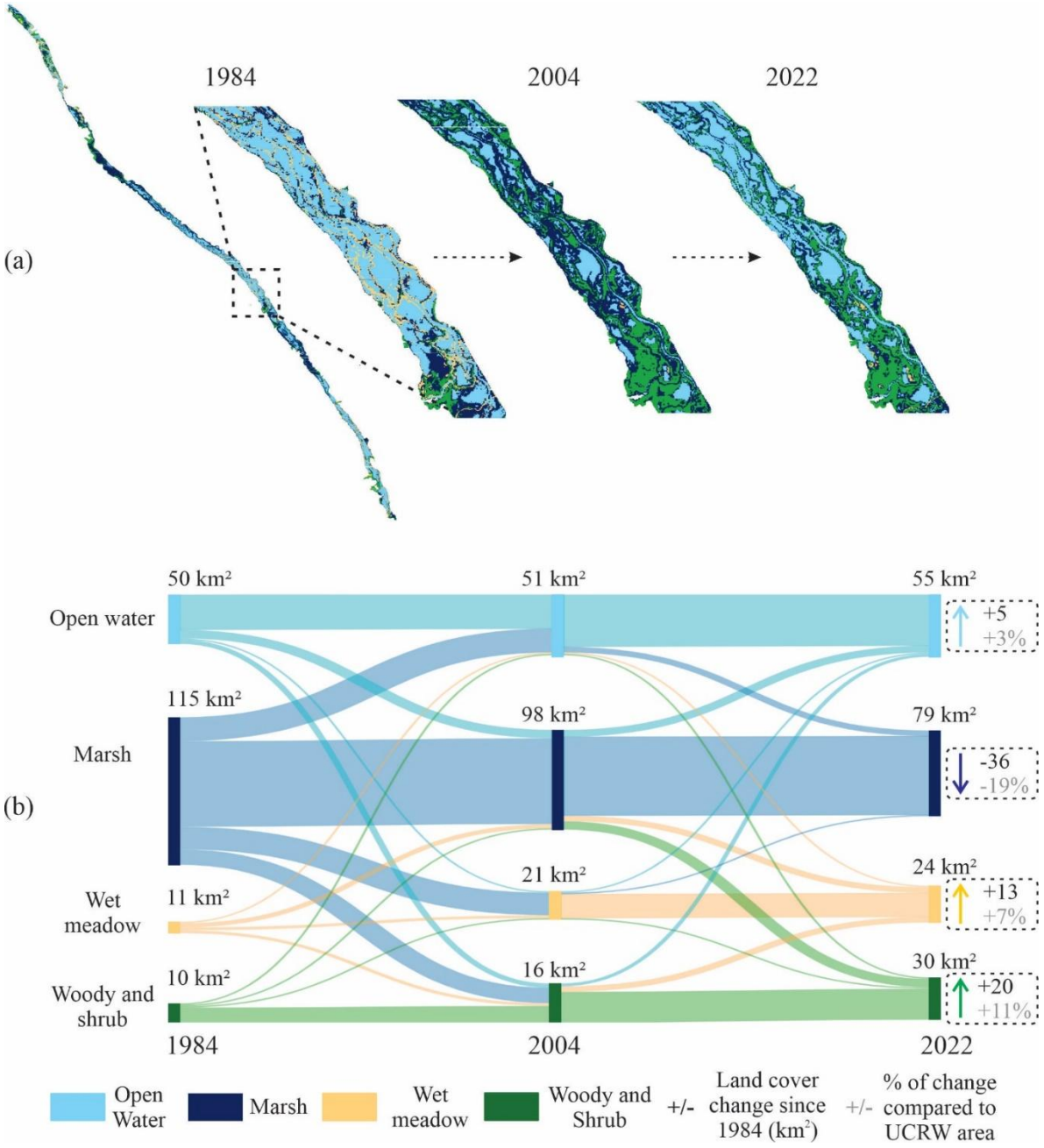

Fig. 2.7: The Upper Columbia River floodplain distribution of land cover change from late-May to July. Map insets (a) indicate changes in land cover for sample regions. Sankey diagram (b) of the changes in land cover from 1984 to 2004 (left) and 2004 to 2022 (right), the land cover change since 1984, and the percentage of change compared to the Columbia wetlands area (188 km^2).

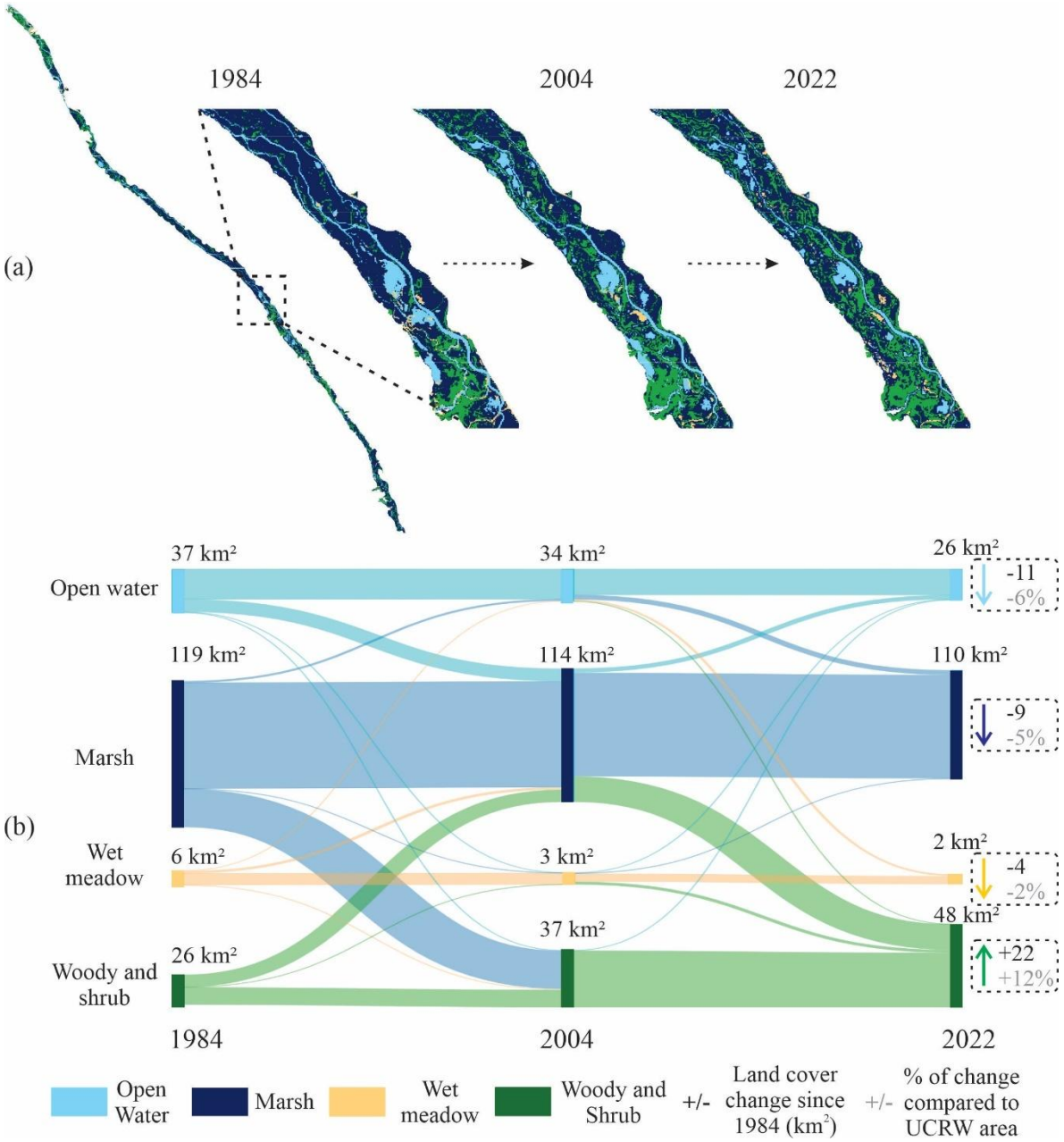

Fig. 2.8: The Upper Columbia River floodplain distribution of land cover change from August to mid-September. Map insets (a) indicate changes in land cover for sample regions. Sankey diagram (b) of the changes in land cover from 1984 to 2004 (left) and 2004 to 2022 (right), the land cover change since 1984, and the percentage of change compared to the Columbia wetlands area (188 km^2).

2.3.3. Upper Columbia River discharge

The average discharge (Q_m) of the Upper Columbia River was 428.2 $m^3.s^{-1}$, with standard deviation (σ) of 105.9 $m^3.s^{-1}$ and these values were used to classify the peak discharge in the anomaly assessment. The twenty-five-year interval represented well the cold and warm Pacific Decadal Oscillation (PDO) pattern at the UCRW, and how this atmospheric teleconnection affected local river discharge. Figure 2.9 shows the standardized anomaly time series of streamflow values in the Upper Columbia River. Classification of the annual events by the anomaly method resulted in forty-one normal years, thirty-seven wet years, and forty-one dry years. Additionally, analysis of the anomaly values with the Mann-Kendall test yields a negative trend of -0.08 (p-value = 0.02; τ = -0.03; S = -209), showing a dry tendency, which is consistent with the decline of open water area and increase in woody/shrub vegetation during the 1984 to 2022 period.

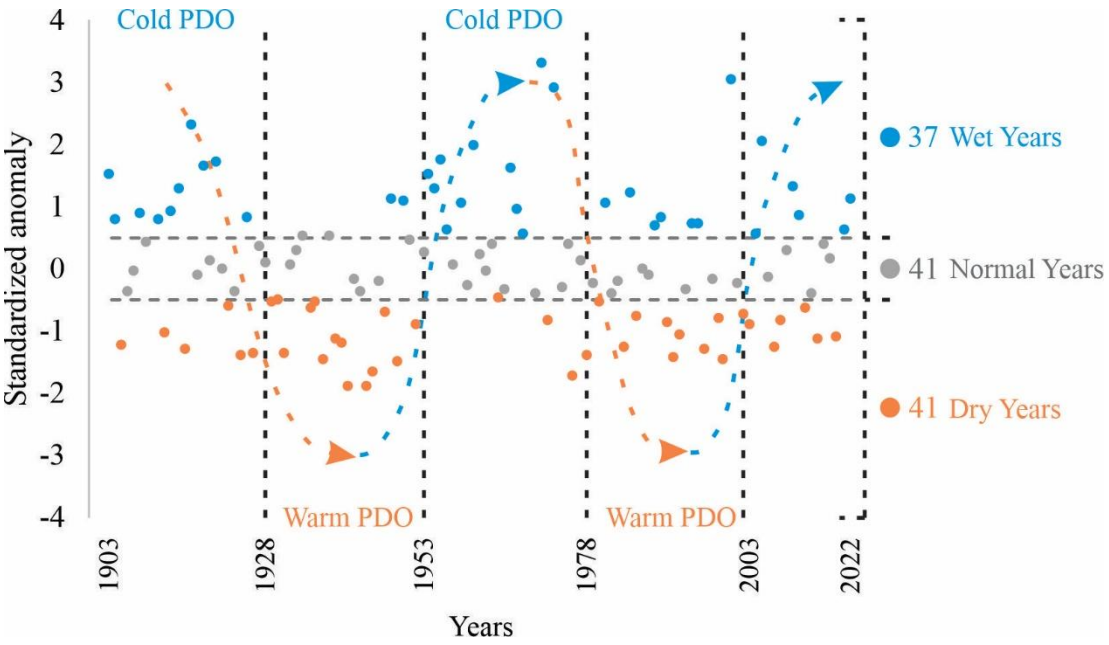

Fig. 2.9: Standardized anomaly time series of annual peak flow of the Upper Columbia River at Nicholson (08NA002), British Columbia, Canada, and the predominant PDO phase in each 25 years

The timing of the peak flow (Julian peak flow days) may be explained by the predominant PDO phase since 1903 (Table 2.2). Peaks flows tended to be late in the Cold PDO (June 26, June 22, and June 15; as consequence of colder air temperatures) and earlier during the Warm PDO (June 20, and June 16; due to higher air temperatures). However overall, regardless of the PDO phase, the Julian peak flow day is starting earlier in the season (Table 2.2).

Table 2.2 summarizes the peak flow day for the Upper Columbia River and its duration since 1903. From 1903 to 1928, June 26 (Julian Day 178) was found to be the approximate day of annual peak flow. From 2004 to 2022, peak flow occurred on average on June 15 (Julian Day 169), eleven days earlier than in the past (i.e., 1903 to 1928). Peak flow duration also changed from an average of 22 days from 1903 – 1928 to 11 days after 2003. In contrast, if 1979 to 2003 is compared with 2004 to 2022 (the period of our remote sensing dataset), the peak flow was only earlier by one day, and its duration was shortened by one day. Thus, in the last century, the peak flows have gotten earlier in the season and the duration of peak flow shorter resulting in a dryer floodplain during the summer growing season.

Table 2.2. Annual average peak flow day for each PDO group (1903 to 1928, 1929 to 1953, 1954 to 1978, 1979 to 2003, and 2004 to 2022) and the duration/length of each peak flow period.

	Julian peak flow day (date)	Var.	SD	Duration/Length of peak flow period (days)	Var.	SD
1903 - 1928	178 (June 26)	218	15	22	115	11
1929 - 1953	172 (June 20)	224	15	15	80	9
1954 - 1978	174 (June 22)	177	13	12	46	7
1979 - 2003	168 (June 16)	166	13	12	56	8
2004 - 2022	167 (June 15)	133	11	11	51	7

Var. – Variance; SD – Standard deviation

The frequency analysis revealed that higher peaks appeared more frequently during 1903 – 1978, since the highest peak was 770 $m^3.s^{-1}$, while the lowest peak after 2003 was 305 $m^3.s^{-1}$, which was 233% lower (Figure 2.10a). Moreover, the daily discharge frequency (Figure 2.10b) revealed that 1903 – 1928 period had a higher discharge rate than post-2003 in terms of frequencies between 10% and 60%.

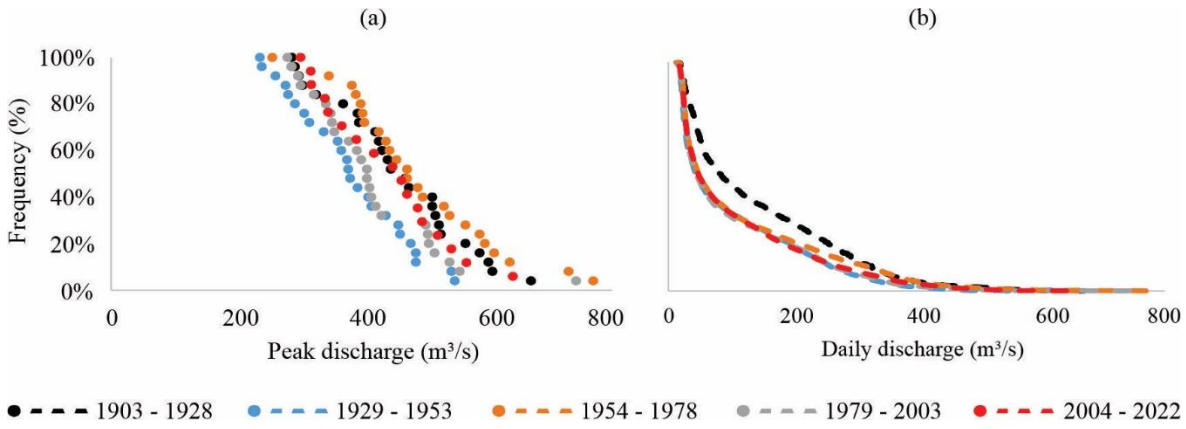

Fig. 2.10. Frequency assessment of the Upper Columbia River peak (a) and daily discharge (b) from 1903 to 2022

Figure 2.11a shows that the baseflow had a decrease (average of -1.5%) from October to April since 1903, and the peak flow hydrograph had a broader shape during the intervals of 1903 to 1928 and 1929 to 1953, with a lower discharge, before becoming steeper with larger flows in a shorter amount of time. The positive trend in the recession constant coefficient over time, which is depicted in Figure 11b, can also explain this pattern.

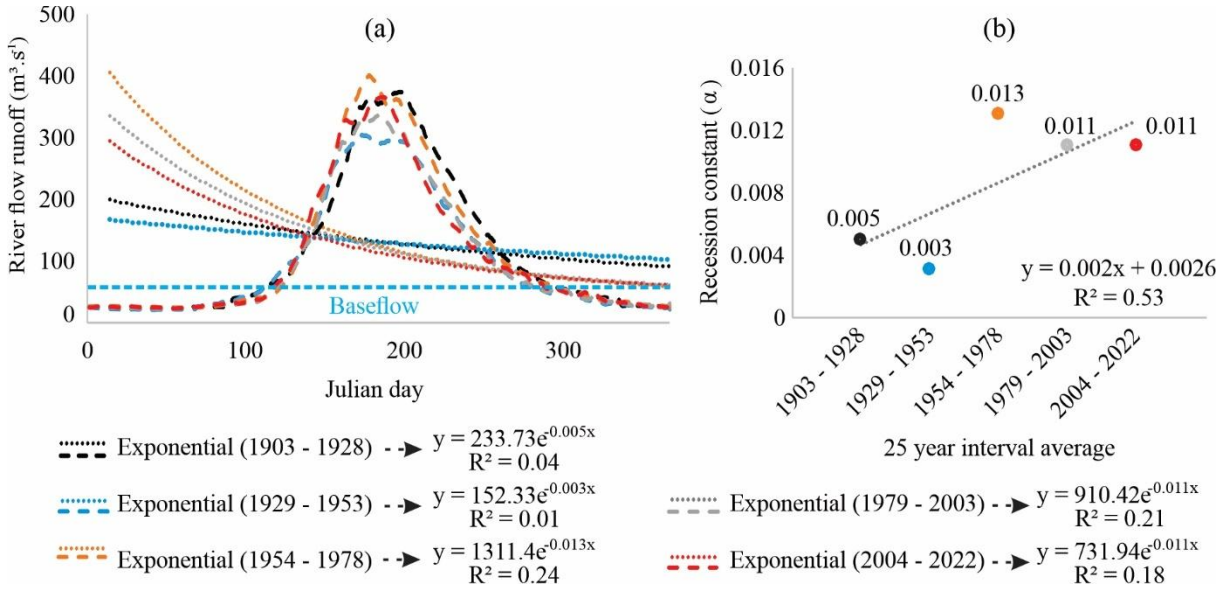

Fig. 2.11. Twenty-five-year interval average river discharge hydrograph of the Upper Columbia River (a), and hydrograph recession constant tendency from the peak flow runoff (b) (1903 to 1928, 1929 to 1953, 1954 to 1978, 1979 to 2003, and 2004 to 2022)

2.4. Discussion

2.4.1. Classification evaluation

The land cover classification used in this study was made possible by the utilisation of various types of data for calibration and validation, resulting in the annual kappa average of 82%, with higher accuracy during April to mid-May and the peak discharge period. At the beginning of the growing season (April to mid-May) the four classes (Open water, Marsh, Wet meadow, and Woody/Shrub) were easier to distinguish. During the peak flow period, the floodplain surface is mostly covered by water, marsh, and woody vegetation, with a small area of wet meadow visible since the water levels were often so high that the dominant wetland meadow vegetation was covered. During the late summer (August to mid-September) there is higher greening in the Marsh and Woody/Shrub vegetation, which creates some confusion between the vegetated classes. Moreover, marsh and wet meadow merge, which might be contributing for the lower kappa during April to mid-May and August to mid-September. Furthermore, the years with supplementary available imagery (1984 to 1991, 2005, 2007, 2009, 2016, 2018, 2022) for additional training and validation were those where RF performed better (average Kappa of 0.84). This illustrates how the increase in high quality training/validation sites improves the land cover classification.

In addition, based on the high correlation between river discharge and open water in the Upper Columbia River floodplain, the open water area can be estimated from river discharge. This result is consistent with Hopkinson et al., (2020), which also found similar relationship over a smaller part of the UCRW, R^2 0.87. However, the moderate correlation (R^2 0.70) may be explained as the floodplain contains hundreds of wetlands that flood during peak flow and retain water during late summer and spring. There is substantial variation spatially and temporally in flood depth because in some years the flood peak overtops the natural levees into all the wetlands while in other years, water reaches into the wetlands through natural channels or gaps in the natural levees (Leven, 2024). This results in a highly dynamic hydroperiod that influences vegetation communities in a wide range of ways.

Each year in early spring, the wetland water levels are at their lowest levels, when the Columbia River drops to 0.3 meters (Environment Canada. 2022b), and according to our results there is a negative trend of open water during this season. If the open water areas keep shrinking, marsh and wet meadows would be expected to reduce their area as well, and woody/shrub vegetation would be expected to encroach in the floodplain, which is what has been observed in all seasons. In contrast, when the flood pulse rises 2 – 4 meters, much of the wet meadow vegetation is

covered by the turbid floodwaters.

The UCRW has connected and non-connected wetlands, with both types experiencing variation in water levels and areal extent as the river rises and falls; however, more isolated wetland water bodies may suffer permanent level and extent changes as a result of overbank flooding, slow drainage, loss to evapotranspiration (MacDonald and Chernos, 2020; Carli and Bayley, 2015), and climate change (Bürger et al., 2011; Carver, 2017; Jost et al., 2012). The aforementioned effects have primarily been seen between April and mid-May, and August to mid-September, when open water is shrinking, and woody/shrub vegetation is encroaching within the floodplain.

2.4.2. Hydrometeorological changes in the upper Columbia River Basin

The positive trend of air temperature in the UCRW (0.02 ºC $year^{-1}$) is consistent with an increase in global air temperatures during the same period (Hansen et al., 2010; Ohmura and Wild, 2002). Between 1900 and 1998, Western Canada warmed by ~ 1 ºC (Zhang et al., 2000), and since the early 1960s, the trend on the eastern slopes of the Canadian Rockies has been warmer than the regional norm (2.6 – 3.6 ºC) (Harder et al., 2015). The proportion of rainfall to total precipitation is predicted to increase as air temperatures increase while the proportion of precipitation that falls as snow tends to decrease (Lapp et al., 2005). For the Canadian Rockies, trends in precipitation are mixed, with some studies reporting increasing trends of roughly 14% during the period 1948–2012 (Vincent et al., 2015) and other studies finding neither trends nor change (Valeo et al., 2007), as well as a declining trend (-0.75 mm $year^{-1}$) as was observed in this study.

Streamflow is the basin-scale integrated response to these hydrometeorological changes, and in high elevation headwater regions with limited meteorological monitoring, streamflow is a readily observable indicator that can be used to gauge hydroclimatic change (Harder et al., 2015). In the past century, several natural annual stream flows in the southern Canadian Rockies have decreased (Rood et al., 2004; Brahney et al 2017), and peak streamflow events have been observed in some rivers to arrive earlier and with less flow volume, with late summer flows dropping and winter flows rising (Rood et al., 2007). The positive trend in the annual basin discharge and peak flow was also seen in the UCRW, indicating that the peak flow had shifted to eleven days earlier and that the peak flow duration had decreased by eleven days (compared with pre-1928).

Although there is a positive trend in the peak discharge, according to the frequency analysis the highest peak (770 m^3 s^{-1}) was observed during 1903 – 1978. The lower peak discharges

during post-1978 (compared with pre-1978) may be a result of the negative precipitation trend from 1984 to 2022. Furthermore, a negative trend was observed when it comes to daily discharge (which relates to the decrease in the baseflow since 1903), mostly in frequencies between 10% and 60% which refers to the start and end of the peak discharge, respectively. According to the historical analysis of the peak flow runoff hydrograph, the reduction of these flows (between 10% and 60%) typically leads to faster and higher peak discharge over fewer days, which is consistent with the positive tendency of the recession constant value, and in accordance with Brahney et al. (2017), who in the same area observed an 11% decline in river flow between 1947 and 2011, predominantly in late summer.

Another explanation for this pattern is through the anomaly assessment, which showed that dry or warm PDO phases are becoming drier, essentially post-1978, as per Newton et al. (2014), who since the 1970s observed a more severe dry PDO phase over the Canadian Cordillera. This suggests that the peak flow is shortening, while the magnitude of the discharge is increasing, causing higher discharges over fewer days, and it may impact the water availability through the year (specifically over the late summer), which relates to the downward annual basis open water area trend. These results agree with Hopkinson et al. (2020), who used Landsat data to calculate water extent and hydroperiod change from 1984 to 2019 in a portion of the Canadian Columbia wetlands. They found a reduction of the permanent water area extent by ~16% (or ~3.5% of the floodplain), which is higher than the decrease in open water found in this research (-6%) for the entire Columbia River valley over the year. Those aforementioned results are in accordance with other snow-driven montane ecosystems in western Canada (Burn, 1994; Burn et al., 2004; Cutforth et al., 1999; Whitfield, 2001; Barnett et al., 2005; Stewart et al., 2005).

Under current and future climate change, earlier and faster snowmelt is expected, directly affecting the snow accumulation- and melt-dominated watersheds (Steger et al., 2012; Pörtner et al., 2019). The positive trend of the air temperature is probably the cause for the earlier snowpack melt, which increases peak flow volumes, while shortening the duration (DeBeer et al., 2021). The rapid rise of the peak flow will enhance the open water area during spring and summer, which when combined with positive air temperature trends may increase the evaporative demand, which will impact the amount of water that is lost to the atmosphere and whether or not these wetlands will shift into other land cover types, which can further enhance evapotranspiration (e.g. shrubs), essentially in late summer (Kienzle, 2006; Rasouli et al., 2022). The reduction of marsh and open

water, as well as the increase in wet meadow and woody/shrub vegetation from August to mid-September, are also reflected in this pattern.

2.4.3. Hydroclimatic trends as drivers of land cover change

Hydrological changes may be a key factor in this trend of UCRW expansion of woody/shrub cover. Changes to the late winter flow regime will affect ice formation and break-up, a fluvial geomorphic process that creates sites for seedling colonisation by the riparian vegetation, encouraging clonal suckering (Rood et al., 2007). The woody/shrub vegetation is increasing as the land is drier for longer and thus the floodplain water table is lower, which leads to a drier root zone, which allows the spread of woody vegetation (Liu et al., 2022; Pellerin et al., 2015).

Regarding trends of woody encroachment, Barger et al. (2011) found positive trends of 0.8% cover $year^{-1}$ in the Northern US Rocky Mountains over a 30-year period. In the central region of the Rock Mountains of Alberta, Glines (2012) observed a positive encroachment trend of 0.9% cover $year^{-1}$ since 1952 to 2003. In Niwot Ridge, south of the Rocky Mountains, Formica et al. (2014) reported a positive woody encroachment trend of 0.2% cover $year^{-1}$ over 62 years, which was the same rate found by Tape et al., (2006) in Northern Alaska. The average annual positive trend (0.17% km $year^{-1}$) of woody/shrub encroachment in the UCRW study is in accordance with other studies. Moreover, the woody ecotone advance has the potential to interfere with almost all regional components of the hydrological cycle: higher evapotranspiration by woodlands (Donohue et al., 2007); increase of the rainwater interception by the canopy trees (Owens et al., 2006); lower runoff (Bonan, 2008); decreases of the groundwater recharge, streamflow (recharge below the rhizosphere) (Tennesen, 2008). The progression of wetland communities from herbaceous to woody plants is considered a natural succession (Vogl, 1969; Mitsch and Gosselink, 2000), although, climate change has accelerated the woody ecotone encroachment in some mountain wetlands (Politti, et al., 2014).

In addition to the possible effects of climate change, atmospheric teleconnection influences like El Niño and La Niña may significantly alter streamflow and impact land cover as has been found in other studies across western Canada (Gobena and Gan, 2006; St Jacques et al., 2012; Fleming and Sauchyn, 2012; Chasmer and Hopkinson, 2016). El Niño appears to impact the UCRW as the frequency of this phenomenon has increased since 1980s (Cai et al., 2021; Zhou et al., 2014), which may explain the predominantly dry pattern in this region (Yang et al., 2019; Yang et al.,

2021) (number of years by anomaly: thirteen normal years, thirteen wet years, and sixteen dry years), justifying the downward trend for open water on an annual basis.

The historical air temperature and precipitation record of the UCRW, resampled for El Niño and La Niña occurrences, can be used to overlay climate projections from general circulation models, which may result in more pronounced future changes to the region's precipitation and temperature. According to the projections of the Special Report on Emissions Scenarios (Byers et al., 2022; IPCC, 2007) climate scenarios for the 2050s, the average annual precipitation of the Canadian Rocky Mountains could further decrease by about 5% while the average annual temperature could marginally increase by about 0.3ºC under the potential combined impact of both climate change and El Niño. In contrast, based on the predictions of the Special Report on Emissions Scenarios of 2050s (Byers et al., 2022; IPCC, 2007), La Niña years might see an additional 9% increase in average precipitation while a 0.3ºC decrease in average temperature. The drying effect of climate change on the UCRW should be partly mitigated by a future La Niña year, but that effect could worsen in an El Niño year. These findings support those of Gobena and Gan (2006), who found that, in south-western Canada, El Niño and La Niña occurrences, respectively, cause large negative and positive streamflow anomalies.

In western Canada, the Pacific North America (PNA) pattern is the active atmospheric teleconnection that has the greatest impact on the local climate and hydrology (Newton et al., 2014). The PNA pattern has a positive (i.e., relates to the Pacific warm episodes, El Niño, and characterized by above-average air temperatures), and a negative (i.e., associated with Pacific cold events, La Niña, marked by low-average air temperatures) phase (Lopez and Kirtman, 2019). The increased frequency of the positive phase of PNA has been noticed over the years (Gan et al., 2023; Wang et al., 2017), and the main reason might be the continuous emissions of greenhouse warming (Cai et al., 2014). A more frequent positive phase of PNA may lead to higher air temperatures, which leads to reductions in the seasonal snowpack (Mote et al., 2005; Brown and Robinson, 2011), and earlier spring runoff (Stewart et al., 2004).

Overall, the dominant changing seasonal hydrological processes within the UCRW include: shortening of snowmelt period due to increasing air temperatures, which will boost the river discharge as well as the groundwater (essentially during summer season); increasing and shortening of peak flows in summer due to shortening period of snowmelt combined with higher intensity rainfall and greater wetland flooding (Figure 2.12b) (Musselman et al., 2018), which may

also cause increased erosion in the uplands and siltation of the floodplain (Zhang et al., 2022); by late summer, water has moved through wetlands, causing them to dry, resulting in shrubification and enhanced water losses from evapotranspiration (Li et al., 2020) (Figure 2.12c).

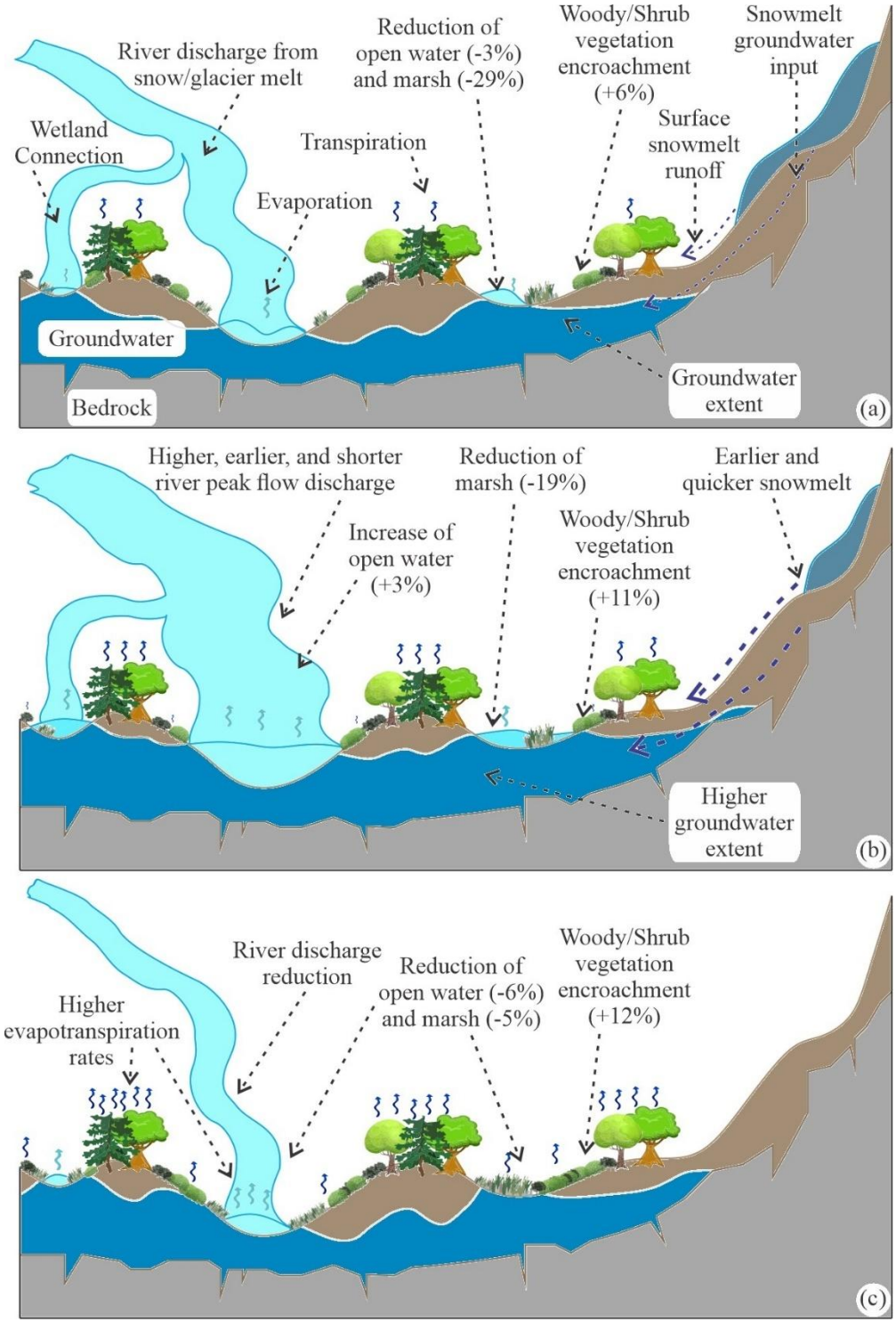

Fig. 2.12. Updated conceptual understanding of the hydrological processes conditions for the UCRW during Spring (a), Summer (b), and late Summer (c).

The UCRW has changed over the past 39 years as a result of the rise in air temperature and decrease in precipitation, which has caused significant changes in the floodplain. Remote sensing was used in this work to identify areas with low, moderate, and large shifts since 1984 and to evaluate the spatial distribution of land cover trends and changes. The results obtained illustrate the potential for the fusion of remote sensing and hydroclimatological data for the assessment changing montane wetland environments.

2.5. Sources of uncertainty

Although the Random Forest algorithm demonstrated acceptable accuracy, several sources of uncertainty may be present regarding the training and validation data sources, and the spatial resolution of the Landsat imagery. It would be ideal to train and verify landcover classes using historical measured in-situ field data. However, due to the constraints over temporal data availability, different remote sensing data sources were necessary for model calibration and validation in this historical LC classification. The additional training pixels allocated using the higher resolution dataset are in the beginning (1984 to 1991), part of middle (2005, 2007, and 2009), and in the late of the time series (2016 to 2022), which tends to reduce the inaccuracies caused by the less accurate data in other years (i.e., unchanging pixels). Sixty unchanging pixels per LC class from the historical land cover classification of Canada (Hermosilla et al., 2022) (overall accuracy of 80%) were used as reference dataset for all years, therefore, any errors here could be propagated into the UCRW LC classification. However, the distribution of most reliable training and validation pixels (using higher resolution datasets) over time has enabled accurate results, which when compared to independent data sources, confirm the encroachment of woody/shrub vegetation (Politti, et al., 2014; Primack, 2000; Theurillat and Guisan, 2001), and reduction of open water during late summer (Rood et al., 2004; Kienzle, 2006; Rood et al., 2007) in montane wetlands.

Regarding the spatial resolution of the Landsat time series, 30 meters is not the ideal resolution for classifying wetlands because this habitat is typically mixed, with variable width ecotones and vegetation inside open water and vice versa. In this study, the use of complementary

remote sensing data sources has enabled temporal calibration and validation but further enhancements may be possible by the addition of new data sources. For example, combining the multispectral sensors with synthetic aperture radar (SAR) may increase the accuracy up to 85% (Loosvelt et al., 2012; Mahdianpari et al., 2017; Muro et al., 2020), since SAR is an effective tool to identify permanent open water (Montgomery et al., 2018).

2.6. Conclusion

This study analyzed temporal trends and changes of land-cover in the Upper Columbia River Wetlands using remote sensing and a Random Forest classification routine for a 39 year-period. The classifier delivered a reasonable level of accuracy (Kappa 82%). 39 years of rising air temperature resulted in an increase in the Columbia River discharge. During the peak flow period, open water extent showed a positive tendency (0.10 $km^2.year^{-1}$), while on an annual basis open water area is declining (-0.03 $km^2.year^{-1}$). Furthermore, the peak flow occurs one day earlier now than ~40 years ago, while peak flow duration has decreased by one day. However, since 2003, the peak flow has occurred eleven days earlier than 1903 – 1928, and its duration has reduced by eleven days, which has resulted in higher discharges in a shorter time. It also means that the summer period is drier and the land cover vegetation subject to drier conditions. According to the anomaly assessment approach, dry years have been increasingly frequent since 1984.

Open water areas of the floodplain have decreased in size during the April to mid-May period, while a large area of floodplain marsh has been replaced by wet meadow. In the same period, shrub and woody vegetation have increased during the 39 years by 11 km^2. The peak flow period shows a decline in marsh regions and an increase in wet meadow, woody/shrub, and open water, the latter of which revealed a moderate increase. From August to mid-September, there was a decline in the amount of open water, marsh, and wet meadow, but a significant increase in the amount of woody/shrub species.

Overall, the future of the Upper Columbia River Wetlands and their ecohydrological services are at risk due to the altered runoff regime that favors drying of the floodplain. Expansion of riparian shrub and treed ecotones are gradually replacing marsh and wet meadow landcovers commensurate with a reduction in permanent open water area, which may lead to higher evapotranspiration, mainly during late summer, thus raising the potential for drought. While new floodplain riparian ecosystem habitats are being created, these come at the expense of lost open

water/aquatic habitat.

Code availability. Code available in the link: https://github.com/italosrodrigues/GEE-RF-LC-code

Acknowledgements

The authors acknowledge funding provided by the Natural Sciences and Engineering Research Council of Canada (NSERC) (2017-04362), Alberta Innovates, the Nexen Fellowship in Water Resources, the Columbia Wetlands Stewardship Partners and the Shuswap Band's project Columbia Headwaters Aquatic Restoration Secwépemec Strategy (CHARS).

2.7. References

Amoros, C., and Bornette, G. (2002). Connectivity and biocomplexity in waterbodies of riverine floodplains. *Freshwater biology*, 47(4), 761-776, https://doi.org/10.1046/j.1365-2427.2002.00905.x

Barger, N. N., Archer, S. R., Campbell, J. L., Huang, C., Morton, J. A., & Knapp, A. K. (2011). Woody plant proliferation in North American drylands: A synthesis of impacts on ecosystem carbon balance. *Journal of Geophysical Research Atmospheres*, *116*. https://doi.org/10.1029/2010jg001506

Barnett, T. P., Adam, J. C., & Lettenmaier, D. P. (2005). Potential impacts of a warming climate on water availability in snow-dominated regions. *Nature*, *438*(7066), 303–309. https://doi.org/10.1038/nature04141

Bayley, P. B. (1995). Understanding Large River: Floodplain Ecosystems. *BioScience*, *45*(3), 153–158. https://doi.org/10.2307/1312554

Bayley, S. E., & Guimond, J. K. (2009). Aboveground biomass and nutrient limitation in relation to river connectivity in montane floodplain marshes. *Wetlands*, *29*(4), 1243–1254. https://doi.org/10.1672/08-227.1

Bayley, S. E., & Guimond, J. K. (2008b). Effects of river connectivity on marsh vegetation community structure and species richness in montane floodplain wetlands in Jasper National Park, Alberta, Canada. *Ecoscience*, *15*(3), 377–388. https://doi.org/10.2980/15-3-3084

BC Government.: "Digital Air Photos of B.C." Province of British Columbia. Accessed January, 2022. https://www2.gov.bc.ca/gov/content/data/geographic-data-services/digital-imagery/air-photos, 2022

Berhail, S., Ouerdachi, L., & Boutaghane, H. (2012). The Use of the Recession Index as Indicator for Components of Flow. *Energy Procedia*, *18*, 741–750. https://doi.org/10.1016/j.egypro.2012.05.090

Bonan, G. B. (2008). Forests and Climate Change: Forcings, Feedbacks, and the Climate Benefits of Forests. *Science*, *320*(5882), 1444–1449. https://doi.org/10.1126/science.1155121

Brahney, J., Weber, F., Foord, V., Janmaat, J., & Curtis, P. J. (2017). Evidence for a climate-driven hydrologic regime shift in the Canadian Columbia Basin. *Canadian Water Resources Journal / Revue Canadienne Des Ressources Hydriques*, *42*(2), 179–192. https://doi.org/10.1080/07011784.2016.1268933

Breiman, L.: Random forests. Machine learning, 45(1), 5-32, https://doi.org/10.1023/A:1010933404324, 2001.

Brutsaert, W., & Nieber, J. L. (1977). Regionalized drought flow hydrographs from a mature glaciated plateau. *Water Resources Research*, *13*(3), 637–643. https://doi.org/10.1029/wr013i003p00637

Burn, D. H., Aziz, O. I. A., & Pietroniro, A. (2004). A Comparison of Trends in Hydrological Variables for Two Watersheds in the Mackenzie River Basin. *Canadian Water Resources Journal /*

Revue Canadienne Des Ressources Hydriques, *29*(4), 283–298. https://doi.org/10.4296/cwrj283

Burn, D. H. (1994). Hydrologic effects of climatic change in west-central Canada. *Journal of Hydrology*, *160*(1–4), 53–70. https://doi.org/10.1016/0022-1694(94)90033-7

Bürger, G., Schulla, J., & Werner, A.T. (2011). Estimates of future flow, including extremes, of the Columbia River headwaters. Water Resources Research, 47(10). https://doi.org/10.1029/2010wr009716

Byers, E., Krey, V., Kriegler, E., Riahi, K., Schaeffer, R., Kikstra, J., Lamboll, R., Nicholls, Z., Sandstad, M., Smith, C., Van Der Wijst, K., Lecocq, F., Portugal-Pereira, J., Saheb, Y., Stromann, A., Winkler, H., Auer, C., Brutschin, E., Lepault, C., Skeie, R. (2022). AR6 Scenarios Database [Dataset]. In *Zenodo (CERN European Organization for Nuclear Research)*. https://doi.org/10.5281/zenodo.5886912

Cai, W., Santoso, A., Collins, M. *et al.* Changing El Niño–Southern Oscillation in a warming climate. *Nat Rev Earth Environ* 2, 628–644 (2021). https://doi.org/10.1038/s43017-021-00199-z

Cai, W., Borlace, S., Lengaigne, M., Van Rensch, P., Collins, M., Vecchi, G., Timmermann, A., Santoso, A., McPhaden, M. J., Wu, L., England, M. H., Wang, G., Guilyardi, E., & Jin, F. (2014). Increasing frequency of extreme El Niño events due to greenhouse warming. *Nature Climate Change*, *4*(2), 111–116. https://doi.org/10.1038/nclimate2100

Carli, C. M., and Bayley, S. E.: River connectivity and road crossing effects on floodplain vegetation of the upper Columbia River, Canada. Ecoscience, 22(2-4), 97-107, https://doi.org/10.1080/11956860.2015.1121705, 2015.

Carver, M.: Water monitoring and climate change in the upper Columbia Basin: Summary of current status and opportunities. Columbia Basin Trust, 2017.

Chasmer, L., Cobbaert, D., Mahoney, C., Millard, K., Peters, D., Devito, K., Brisco, B., Hopkinson, C., Merchant, M., Montgomery, J., Nelson, K., & Niemann, O. (2020). Remote Sensing of Boreal Wetlands 1: Data Use for Policy and Management. *Remote Sensing*, *12*(8), 1320. https://doi.org/10.3390/rs12081320

Chasmer, L., Hopkinson, C., Veness, T., Quinton, W., & Baltzer, J. (2014). A decision-tree classification for low-lying complex land cover types within the zone of discontinuous permafrost. *Remote Sensing of Environment*, *143*, 73–84. https://doi.org/10.1016/j.rse.2013.12.016

Congalton, R. G., & Green, K. (2019). *Assessing the Accuracy of Remotely Sensed Data: Principles and Practices, Third Edition*. CRC Press.

Cooper, D. J., Chimner, R. A., and Merritt, D. M.: Western Mountain wetlands (pp. 313-328). University of California Press: Berkeley, CA, USA, 2012.

Cooper, D. J., Kaczynski, K. M., Sueltenfuss, J., Gaucherand, S., & Hazen, C. (2017). Mountain wetland restoration: The role of hydrologic regime and plant introductions after 15 years in the Colorado Rocky Mountains, U.S.A. *Ecological Engineering*, *101*, 46–59. https://doi.org/10.1016/j.ecoleng.2017.01.017

Chasmer, L., & Hopkinson, C. (2016). Threshold loss of discontinuous permafrost and landscape

evolution. *Global Change Biology*, *23*(7), 2672–2686. https://doi.org/10.1111/gcb.13537

Cutforth, H. W., McConkey, B. G., Woodvine, R. J., Smith, D. G., Jefferson, P. G., & Akinremi, O. O. (1999). Climate change in the semiarid prairie of southwestern Saskatchewan: Late winter–early spring. *Canadian Journal of Plant Science*, *79*(3), 343–350. https://doi.org/10.4141/p98-137

DeBeer, C.M., Wheater, H.S., Pomeroy, J.W., Barr, A.G., Baltzer, J.L., Johnstone, J. F., Turetsky, M.R., Stewart, R.E., Hayashi, M., Van Der Kamp, G., Marshall, S., Campbell, E., Marsh, P., Carey, S.K., Quinton, W.L., Li, Y., Razavi, S., Berg, A., McDonnell, J.J., Pietroniro, A. (2021). Summary and synthesis of Changing Cold Regions Network (CCRN) research in the interior of western Canada – Part 2: Future change in cryosphere, vegetation, and hydrology. Hydrology and Earth System Sciences, 25(4), 1849–1882. https://doi.org/10.5194/hess-25-1849-2021

DeBeer, C.M., Wheater, H.S., Carey, S.K., & Chun, K.P. (2015). Recent climatic, cryospheric, and hydrological changes over the interior of western Canada: a synthesis and review. Hydrology and Earth System Sciences. https://doi.org/10.5194/hessd-12-8615-2015Díaz, S., Demissew, S., Carabias, J., Joly, C., Lonsdale, M., Ash, N., and Zlatanova, D.: The IPBES Conceptual Framework—connecting nature and people. Current opinion in environmental sustainability, 14, 1-16, https://doi.org/10.1016/j.cosust.2014.11.002, 2015.

Donohue, R. J., Roderick, M. L., & McVicar, T. R. (2007). On the importance of including vegetation dynamics in Budyko's hydrological model. *Hydrology and Earth System Sciences*, *11*(2), 983–995. https://doi.org/10.5194/hess-11-983-2007

Edwards, T. W., Birks, S. J., Luckman, B. H., & MacDonald, G. M. (2008). Climatic and hydrologic variability during the past millennium in the eastern Rocky Mountains and northern Great Plains of western Canada. *Quaternary Research*, *70*(2), 188–197. https://doi.org/10.1016/j.yqres.2008.04.013

Environment Canada.: "Historical climate data." Environment Canada. Accessed November, 2022. https://climate.weather.gc.ca/historical_data/search_historic_data_e.html, 2022a

Environment Canada.: "HYDAT database". Environment Canada. Accessed November, 2022. https://wateroffice.ec.gc.ca/search/historical_e.html, 2022b

Fleming, S. W., & Sauchyn, D. J. (2012). Availability, volatility, stability, and teleconnectivity changes in prairie water supply from Canadian Rocky Mountain sources over the last millennium. *Water Resources Research*, *49*(1), 64–74. https://doi.org/10.1029/2012wr012831

Formica, A., Farrer, E. C., Ashton, I. W., & Suding, K. N. (2014). Shrub Expansion Over the Past 62 Years in Rocky Mountain Alpine Tundra: Possible Causes and Consequences. *Arctic Antarctic and Alpine Research*, *46*(3), 616–631. https://doi.org/10.1657/1938-4246-46.3.616

Foster, L. M., Bearup, L. A., Molotch, N. P., Brooks, P. D., & Maxwell, R. M. (2016). Energy budget increases reduce mean streamflow more than snow–rain transitions: using integrated modeling to isolate climate change impacts on Rocky Mountain hydrology. *Environmental Research Letters*, *11*(4), 044015. https://doi.org/10.1088/1748-9326/11/4/044015

Gan, R., Liu, Q., Huang, G., Hu, K., & Li, X. (2023). Greenhouse warming and internal variability

increase extreme and central Pacific El Niño frequency since 1980. *Nature Communications*, *14*(1). https://doi.org/10.1038/s41467-023-36053-7

Genz, F., & Luz, L. (2012). Distinguishing the effects of climate on discharge in a tropical river highly impacted by large dams. *Hydrological Sciences Journal*, *57*(5), 1020–1034. https://doi.org/10.1080/02626667.2012.690880

Glines, L. M. (2012). *Woody plant encroachment into grasslands within the Red Deer River drainage, Alberta*. https://doi.org/10.7939/r33h5v

Gobena, A. K., & Gan, T. Y. (2006). Low-frequency variability in Southwestern Canadian stream flow: links with large-scale climate anomalies. *International Journal of Climatology*, *26*(13), 1843–1869. https://doi.org/10.1002/joc.1336

Hansen, J., Ruedy, R., Sato, M., & Lo, K. (2010). GLOBAL SURFACE TEMPERATURE CHANGE. *Reviews of Geophysics*, *48*(4). https://doi.org/10.1029/2010rg000345

Harder, P., Pomeroy, J. W., & Westbrook, C. J. (2015). Hydrological resilience of a Canadian Rockies headwaters basin subject to changing climate, extreme weather, and forest management. *Hydrological Processes*, *29*(18), 3905–3924. https://doi.org/10.1002/hyp.10596

Hathaway, J. M., Westbrook, C. J., Rooney, R. C., Petrone, R. M., & Langs, L. E. (2022). Quantifying relative contributions of source waters from a subalpine wetland to downstream water bodies. *Hydrological Processes*, *36*(9). https://doi.org/10.1002/hyp.14679

Hermosilla, T., Wulder, M. A., White, J. C., & Coops, N. C. (2022). Land cover classification in an era of big and open data: Optimizing localized implementation and training data selection to improve mapping outcomes. *Remote Sensing of Environment*, *268*, 112780. https://doi.org/10.1016/j.rse.2021.112780

Hernandez, M. E., & Mitsch, W. J. (2006). Influence of hydrologic pulses, flooding frequency, and vegetation on nitrous oxide emissions from created riparian marshes. *Wetlands*, *26*(3), 862–877. https://doi.org/10.1672/0277-5212(2006)26

Hersbach, H., Bell, B., Berrisford, P., Hirahara, S., Horányi, A., Muñoz-Sabater, J., Nicolas, J., Peubey, C., Radu, R., Schepers, D., Simmons, A., Soci, C., Abdalla, S., Abellan, X., Balsamo, G., Bechtold, P., Biavati, G., Bidlot, J., Bonavita, M., . . . Thépaut, J. (2020). The ERA5 global reanalysis. *Quarterly Journal of the Royal Meteorological Society*, *146*(730), 1999–2049. https://doi.org/10.1002/qj.3803

Hopkinson, C., Fuoco, B., Grant, T., Bayley, S. E., Brisco, B., & MacDonald, R. (2020). Wetland Hydroperiod Change Along the Upper Columbia River Floodplain, Canada, 1984 to 2019. *Remote Sensing*, *12*(24), 4084. https://doi.org/10.3390/rs12244084

Hopkinson, C., & Young, G. J. (1998). The effect of glacier wastage on the flow of the Bow River at Banff, Alberta, 1951–1993. *Hydrological Processes*, *12*(10–11), 1745–1762. https://doi.org/10.1002/(sici)1099-1085(199808/09)12:10/11

Hrach, D. M., Petrone, R. M., Green, A., & Khomik, M. (2021). Analysis of growing season carbon

and water fluxes of a subalpine wetland in the Canadian Rocky Mountains: Implications of shade on ecosystem water use efficiency. *Hydrological Processes*, *36*(1). https://doi.org/10.1002/hyp.14425

Hughes, F. M. (1997). Floodplain biogeomorphology. *Progress in Physical Geography Earth and Environment*, *21*(4), 501–529. https://doi.org/10.1177/030913339702100402

Hussain, M., & Mahmud, I. (2019). pyMannKendall: a python package for non parametric Mann Kendall family of trend tests. *The Journal of Open Source Software*, *4*(39), 1556. https://doi.org/10.21105/joss.01556

Inglada, J., Vincent, A., Arias, M., Tardy, B., Morin, D., & Rodes, I. (2017). Operational High Resolution Land Cover Map Production at the Country Scale Using Satellite Image Time Series. *Remote Sensing*, *9*(1), 95. https://doi.org/10.3390/rs9010095

IPCC, 2007. Climate Change, Intergovernmental Panel on Climate Change Fourth Assessment Report, 2007.

Jost, G., Moore, R. D., Menounos, B., & Wheate, R. (2012). Quantifying the contribution of glacier runoff to streamflow in the upper Columbia River Basin, Canada. *Hydrology and Earth System Sciences*, *16*(3), 849–860. https://doi.org/10.5194/hess-16-849-2012

Ju, J., & Masek, J. G. (2016). The vegetation greenness trend in Canada and US Alaska from 1984–2012 Landsat data. *Remote Sensing of Environment*, *176*, 1–16. https://doi.org/10.1016/j.rse.2016.01.001

Junk, W. J., Bayley, P. B., and Sparks, R. E. (1989). The flood pulse concept in river-floodplain systems. Canadian special publication of fisheries and aquatic sciences, 106(1), 110-127. https://ftp.cs.ru.nl/toinesmits/Recommended_readings_IWRM_2009/Water_Ecomorphological_principles/1989JunkThe%20flood%20pulse%20concept%20in.pdf

Kendall, M.G. (1957). Rank Correlation Methods. Biometrika, 44(1/2), 298. https://doi.org/10.2307/2333282

Kienzle, S.W. (2006). The Use of the Recession Index as an Indicator for Streamflow Recovery After a Multi-Year Drought. Water Resources Management, 20(6), 991–1006. https://doi.org/10.1007/s11269-006-9019-1

Lacoul, P., & Freedman, B. (2006). Environmental influences on aquatic plants in freshwater ecosystems. *Environmental Reviews*, *14*(2), 89–136. https://doi.org/10.1139/a06-001

Lapp, S., Byrne, J., Townshend, I., & Kienzle, S. (2005). Climate warming impacts on snowpack accumulation in an alpine watershed. *International Journal of Climatology*, *25*(4), 521–536. https://doi.org/10.1002/joc.1140

Leppi, J. C., DeLuca, T. H., Harrar, S. W., & Running, S. W. (2011). Impacts of climate change on August stream discharge in the Central-Rocky Mountains. *Climatic Change*, *112*(3–4), 997–1014. https://doi.org/10.1007/s10584-011-0235-1

Leven, C. (2024). Wetland hydrology and the impacts of beaver dams in the Upper Columbia River

floodplain wetlands. (Master's thesis, University of Waterloo).

Li, Z., Wang, S., & Li, J. (2020). Spatial variations and long-term trends of potential evaporation in Canada. *Scientific Reports*, *10*(1). https://doi.org/10.1038/s41598-020-78994-9

Linsley, B. K., Wu, H. C., Dassié, E. P., & Schrag, D. P. (2015). Decadal changes in South Pacific sea surface temperatures and the relationship to the Pacific decadal oscillation and upper ocean heat content. *Geophysical Research Letters*, *42*(7), 2358–2366. https://doi.org/10.1002/2015gl063045

Liu, Y., Cui, Z., Huang, Z., López-Vicente, M., Zhao, J., Ding, L., & Wu, G. (2022). Shrub encroachment in alpine meadows increases the potential risk of surface soil salinization by redistributing soil water. *CATENA*, *219*, 106593. https://doi.org/10.1016/j.catena.2022.106593

Loeffler, J., Anschlag, K., Baker, B., Finch, O., Wundram, D., Diekkrüger, B., Schröder, B., Pape, R., & Lundberg, A. (2011). Mountain ecosystem response to global change. *Erdkunde*, *65*(2), 189–213. https://doi.org/10.3112/erdkunde.2011.02.06

Loosvelt, L., Peters, J., Skriver, H., De Baets, B., & Verhoest, N. E. C. (2012). Impact of Reducing Polarimetric SAR Input on the Uncertainty of Crop Classifications Based on the Random Forests Algorithm. *IEEE Transactions on Geoscience and Remote Sensing*, *50*(10), 4185–4200. https://doi.org/10.1109/tgrs.2012.2189012

Lopez, H., & Kirtman, B. P. (2018). ENSO influence over the Pacific North American sector: uncertainty due to atmospheric internal variability. *Climate Dynamics*, *52*(9–10), 6149–6172. https://doi.org/10.1007/s00382-018-4500-0

Lottig, N. R., Buffam, I., & Stanley, E. H. (2013). Comparisons of wetland and drainage lake influences on stream dissolved carbon concentrations and yields in a north temperate lake-rich region. *Aquatic Sciences*, *75*(4), 619–630. https://doi.org/10.1007/s00027-013-0305-8

McCaffrey, D. R., & Hopkinson, C. (2020). Modeling Watershed-Scale Historic Change in the Alpine Treeline Ecotone Using Random Forest. *Canadian Journal of Remote Sensing*, *46*(6), 715–732. https://doi.org/10.1080/07038992.2020.1865792

MacDonald, R., and M. Chernos. (2020). *Hydrological Assessment of the Upper Columbia River Watershed*, 64. Cranbrook, BC, Canada: MacHydro Consultants Ltd.

MacDonald, G. M., Edwards, T. W. D., Moser, K. A., Pienitz, R., & Smol, J. P. (1993). Rapid response of treeline vegetation and lakes to past climate warming. *Nature*, *361*(6409), 243–246. https://doi.org/10.1038/361243a0

Mahdianpari, M., Salehi, B., Mohammadimanesh, F., & Brisco, B. (2017). An Assessment of Simulated Compact Polarimetric SAR Data for Wetland Classification Using Random Forest Algorithm. *Canadian Journal of Remote Sensing*, *43*(5), 468–484. https://doi.org/10.1080/07038992.2017.1381550

Mann, H. B. (1945). Nonparametric Tests Against Trend. Econometrica, 13(3), 245. https://doi.org/10.2307/1907187

Mantua, N. J., & Hare, S. R. (2002). The Pacific Decadal Oscillation. *Journal of Oceanography*,

58(1), 35–44. https://doi.org/10.1023/a:1015820616384

Marshall, S. J. (2014). Meltwater run-off from Haig Glacier, Canadian Rocky Mountains, 2002–2013. *Hydrology and Earth System Sciences*, *18*(12), 5181–5200. https://doi.org/10.5194/hess-18-5181-2014

Menze, B. H., Kelm, B. M., Masuch, R., Himmelreich, U., Bachert, P., Petrich, W., & Hamprecht, F. A. (2009). A comparison of random forest and its Gini importance with standard chemometric methods for the feature selection and classification of spectral data. *BMC Bioinformatics*, *10*(1). https://doi.org/10.1186/1471-2105-10-213

Millar, D. J., Cooper, D. J., & Ronayne, M. J. (2018). Groundwater dynamics in mountain peatlands with contrasting climate, vegetation, and hydrogeological setting. *Journal of Hydrology*, *561*, 908–917. https://doi.org/10.1016/j.jhydrol.2018.04.050

Millard, K., & Richardson, M. (2015). On the Importance of Training Data Sample Selection in Random Forest Image Classification: A Case Study in Peatland Ecosystem Mapping. *Remote Sensing*, *7*(7), 8489–8515. https://doi.org/10.3390/rs70708489

Mitch, W. J., and Gosselink, J. G.: Wetlands 3rd ed, 2000.

Montgomery, J. S., Hopkinson, C., Brisco, B., Patterson, S., & Rood, S. B. (2018). Wetland hydroperiod classification in the western prairies using multitemporal synthetic aperture radar. *Hydrological Processes*, *32*(10), 1476–1490. https://doi.org/10.1002/hyp.11506

Mote, P. W., Hamlet, A. F., Clark, M. P., & Lettenmaier, D. P. (2005). Declining mountain snowpack in Western North America*. *Bulletin of the American Meteorological Society*, *86*(1), 39–50. https://doi.org/10.1175/bams-86-1-39

Muro, J., Varea, A., Strauch, A., Guelmami, A., Fitoka, E., Thonfeld, F., Diekkrüger, B., & Waske, B. (2020). Multitemporal optical and radar metrics for wetland mapping at national level in Albania. *Heliyon*, *6*(8), e04496. https://doi.org/10.1016/j.heliyon.2020.e04496

Musselman, K. N., Lehner, F., Ikeda, K., Clark, M. P., Prein, A. F., Liu, C., Barlage, M., & Rasmussen, R. (2018). Projected increases and shifts in rain-on-snow flood risk over western North America. *Nature Climate Change*, *8*(9), 808–812. https://doi.org/10.1038/s41558-018-0236-4

Newton, B. W., Prowse, T. D., & Bonsal, B. R. (2014). Evaluating the distribution of water resources in western Canada using synoptic climatology and selected teleconnections. Part 2: summer season. *Hydrological Processes*, *28*(14), 4235–4249. https://doi.org/10.1002/hyp.10235

Ohmura, A., & Wild, M. (2002). Is the Hydrological Cycle Accelerating? *Science*, *298*(5597), 1345–1346. https://doi.org/10.1126/science.1078972

Owens, M. K., Lyons, R. K., & Alejandro, C. L. (2006). Rainfall partitioning within semiarid juniper communities: effects of event size and canopy cover. *Hydrological Processes*, *20*(15), 3179–3189. https://doi.org/10.1002/hyp.6326

Pekel, J., Cottam, A., Gorelick, N., & Belward, A. S. (2016). High-resolution mapping of global surface water and its long-term changes. *Nature*, *540*(7633), 418–422.

https://doi.org/10.1038/nature20584

Pellerin, S., Lavoie, M., Boucheny, A., Larocque, M., & Garneau, M. (2015). Recent Vegetation Dynamics and Hydrological Changes in Bogs Located in an Agricultural Landscape. *Wetlands*, *36*(1), 159–168. https://doi.org/10.1007/s13157-015-0726-3

Pelletier, C., Valero, S., Inglada, J., Champion, N., & Dedieu, G. (2016). Assessing the robustness of Random Forests to map land cover with high resolution satellite image time series over large areas. *Remote Sensing of Environment*, *187*, 156–168. https://doi.org/10.1016/j.rse.2016.10.010

Politti, E., Egger, G., Angermann, K., Rivaes, R., Blamauer, B., Klösch, M., Tritthart, M., & Habersack, H. (2014). Evaluating climate change impacts on Alpine floodplain vegetation. *Hydrobiologia*, *737*(1), 225–243. https://doi.org/10.1007/s10750-013-1801-5

Pörtner, H. O., Roberts, D. C., Masson-Delmotte, V., Zhai, P., Tignor, M., Poloczanska, E., and Weyer, N. M. (2019). The ocean and cryosphere in a changing climate. IPCC Special Report on the Ocean and Cryosphere in a Changing Climate, https://doi.org/10.1017/9781009157964

Primack, A. G. B. (2000). Simulation of climate-change effects on riparian vegetation in the Pere Marquette River, Michigan. *Wetlands*, *20*(3), 538–547. https://doi.org/10.1672/0277-5212(2000)020

Rasouli, K., Pomeroy, J. W., & Whitfield, P. H. (2022). The sensitivity of snow hydrology to changes in air temperature and precipitation in three North American headwater basins. *Journal of Hydrology*, *606*, 127460. https://doi.org/10.1016/j.jhydrol.2022.127460

Ray, A. M., Sepulveda, A. J., Irvine, K. M., Wilmoth, S. K., Thoma, D. P., & Patla, D. A. (2019). Wetland drying linked to variations in snowmelt runoff across Grand Teton and Yellowstone national parks. *The Science of the Total Environment*, *666*, 1188–1197. https://doi.org/10.1016/j.scitotenv.2019.02.296

Remmer, C. R., Rooney, R., Bayley, S., & Leven, C. (2023). The importance of groundwater to the upper Columbia River floodplain wetlands. *Canadian Water Resources Journal / Revue Canadienne Des Ressources Hydriques*, *49*(2), 204–218. https://doi.org/10.1080/07011784.2023.2234869

Rood, S. B., Pan, J., Gill, K. M., Franks, C. G., Samuelson, G. M., & Shepherd, A. (2007). Declining summer flows of Rocky Mountain rivers: Changing seasonal hydrology and probable impacts on floodplain forests. *Journal of Hydrology*, *349*(3–4), 397–410. https://doi.org/10.1016/j.jhydrol.2007.11.012

Rood, S. B., Samuelson, G., Weber, J., & Wywrot, K. (2004). Twentieth-century decline in streamflows from the hydrographic apex of North America. *Journal of Hydrology*, *306*(1–4), 215–233. https://doi.org/10.1016/j.jhydrol.2004.09.010

Schnorbus, M., Werner, A., & Bennett, K. (2012). Impacts of climate change in three hydrologic regimes in British Columbia, Canada. *Hydrological Processes*, *28*(3), 1170–1189. https://doi.org/10.1002/hyp.9661

Sen, P. K. (1968). Estimates of the regression coefficient based on Kendall's TAU. *Journal of the American Statistical Association*, *63*(324), 1379–1389.

https://doi.org/10.1080/01621459.1968.10480934

Sparks, R. E., Bayley, P. B., Kohler, S. L., & Osborne, L. L. (1990). Disturbance and recovery of large floodplain rivers. *Environmental Management*, *14*(5), 699–709. https://doi.org/10.1007/bf02394719

St Jacques, J., Lapp, S. L., Zhao, Y., Barrow, E. M., & Sauchyn, D. J. (2012). Twenty-first century central Rocky Mountain river discharge scenarios under greenhouse forcing. *Quaternary International*, *310*, 34–46. https://doi.org/10.1016/j.quaint.2012.06.023

Stanford, J. A., Lorang, M. S., & Hauer, F. R. (2005). The shifting habitat mosaic of river ecosystems. *SIL Proceedings 1922-2010*, *29*(1), 123–136. https://doi.org/10.1080/03680770.2005.11901979

Steger, C., Kotlarski, S., Jonas, T., & Schär, C. (2012). Alpine snow cover in a changing climate: a regional climate model perspective. *Climate Dynamics*, *41*(3–4), 735–754. https://doi.org/10.1007/s00382-012-1545-3

Stewart, I. T. (2008). Changes in snowpack and snowmelt runoff for key mountain regions. *Hydrological Processes*, *23*(1), 78–94. https://doi.org/10.1002/hyp.7128

Stewart, I. T., Cayan, D. R., & Dettinger, M. D. (2005). Changes toward Earlier Streamflow Timing across Western North America. *Journal of Climate*, *18*(8), 1136–1155. https://doi.org/10.1175/jcli3321.1

Stewart, I. T., Cayan, D. R., & Dettinger, M. D. (2004). Changes in Snowmelt Runoff Timing in Western North America under a `Business as Usual' Climate Change Scenario. *Climatic Change*, *62*(1–3), 217–232. https://doi.org/10.1023/b:clim.0000013702.22656.e8

Takaoka, S., & Swanson, F. J. (2008). Change in Extent of Meadows and Shrub Fields in the Central Western Cascade Range, Oregon∗. *The Professional Geographer*, *60*(4), 527–540. https://doi.org/10.1080/00330120802212099

Tape, K., Sturm, M., & Racine, C. (2006). The evidence for shrub expansion in Northern Alaska and the Pan-Arctic. *Global Change Biology*, *12*(4), 686–702. https://doi.org/10.1111/j.1365-2486.2006.01128.x

Tennesen, M. (2008). When Juniper and Woody Plants Invade, Water May Retreat. *Science*, *322*(5908), 1630–1631. https://doi.org/10.1126/science.322.5908.1630

Theurillat, J., & Guisan, A. (2001). Potential Impact of Climate Change on Vegetation in the European Alps: A Review. *Climatic Change*, *50*(1/2), 77–109. https://doi.org/10.1023/a:1010632015572

Valeo, C., Xiang, Z., Bouchart, F., Yeung, P., & Ryan, M. C. (2007). Climate Change Impacts in the Elbow River Watershed. *Canadian Water Resources Journal / Revue Canadienne Des Ressources Hydriques*, *32*(4), 285–302. https://doi.org/10.4296/cwrj3204285

Vincent, L. A., Zhang, X., Brown, R. D., Feng, Y., Mekis, E., Milewska, E. J., Wan, H., & Wang, X. L. (2015). Observed Trends in Canada's Climate and Influence of Low-Frequency Variability Modes. *Journal of Climate*, *28*(11), 4545–4560. https://doi.org/10.1175/jcli-d-14-00697.1

Vogl, R. J. (1969). One Hundred and Thirty Years of Plant Succession in a Southeastern Wisconsin Lowland. *Ecology*, *50*(2), 248–255. https://doi.org/10.2307/1934852

Wang, X., Shaw, E. L., Westbrook, C. J., & Bedard-Haughn, A. (2018). Beaver Dams Induce Hyporheic and Biogeochemical Changes in Riparian Areas in a Mountain Peatland. *Wetlands*, *38*(5), 1017–1032. https://doi.org/10.1007/s13157-018-1059-9

Wang, G., Cai, W., Gan, B., Wu, L., Santoso, A., Lin, X., Chen, Z., & McPhaden, M. J. (2017). Continued increase of extreme El Niño frequency long after 1.5 °C warming stabilization. *Nature Climate Change*, *7*(8), 568–572. https://doi.org/10.1038/nclimate3351

Wang, X., Helgason, B., Westbrook, C., & Bedard-Haughn, A. (2016). Effect of mineral sediments on carbon mineralization, organic matter composition and microbial community dynamics in a mountain peatland. *Soil Biology and Biochemistry*, *103*, 16–27. https://doi.org/10.1016/j.soilbio.2016.07.025

White, J. C., Wulder, M. A., Hobart, G. W., Luther, J. E., Hermosilla, T., Griffiths, P., Coops, N. C., Hall, R. J., Hostert, P., Dyk, A., & Guindon, L. (2014). Pixel-Based Image Compositing for Large-Area Dense Time Series Applications and Science. *Canadian Journal of Remote Sensing*, *40*(3), 192–212. https://doi.org/10.1080/07038992.2014.945827

Whitfield, P. H. (2014). Climate Station Analysis and Fitness for Purpose Assessment of 3053600 Kananaskis, Alberta. *Atmosphere-Ocean*, *52*(5), 363–383. https://doi.org/10.1080/07055900.2014.946388

Whitfield, P. H. (2001). Linked hydrologic and climate variations in British Columbia and Yukon. *Environmental Monitoring and Assessment*, *67*(1/2), 217–238. https://doi.org/10.1023/a:1006438723879

Windell, J. T., and Segelquist, C. (1986). An ecological characterization of Rocky Mountain montane and subalpine wetlands (Vol. 86, No. 11). Fish and Wildlife Service, US Department of the Interior.

Wulder, M. A., Roy, D. P., Radeloff, V. C., Loveland, T. R., Anderson, M. C., Johnson, D. M., Healey, S., Zhu, Z., Scambos, T. A., Pahlevan, N., Hansen, M., Gorelick, N., Crawford, C. J., Masek, J. G., Hermosilla, T., White, J. C., Belward, A. S., Schaaf, C., Woodcock, C. E., Cook, B. D. (2022). Fifty years of Landsat science and impacts. *Remote Sensing of Environment*, *280*, 113195. https://doi.org/10.1016/j.rse.2022.113195

Yang, Y., Gan, T. Y., & Tan, X. (2021). Recent changing characteristics of dry and wet spells in Canada. *Climatic Change*, *165*(3–4). https://doi.org/10.1007/s10584-021-03046-8

Yang, Y., Gan, T. Y., & Tan, X. (2019). Spatiotemporal changes of drought characteristics and their dynamic drivers in Canada. *Atmospheric Research*, *232*, 104695. https://doi.org/10.1016/j.atmosres.2019.104695

Zhang, T., Li, D., East, A. E., Walling, D. E., Lane, S., Overeem, I., Beylich, A. A., Koppes, M., & Lu, X. (2022). Warming-driven erosion and sediment transport in cold regions. *Nature Reviews Earth & Environment*, *3*(12), 832–851. https://doi.org/10.1038/s43017-022-00362-0

Zhang, X., Vincent, L. A., Hogg, W., & Niitsoo, A. (2000). Temperature and precipitation trends in Canada during the 20th century. *Atmosphere-Ocean*, *38*(3), 395–429. https://doi.org/10.1080/07055900.2000.9649654

Zhou, Z., Xie, S., Zheng, X., Liu, Q., & Wang, H. (2014). Global Warming–Induced Changes in El Niño Teleconnections over the North Pacific and North America. *Journal of Climate*, *27*(24), 9050–9064. https://doi.org/10.1175/jcli-d-14-00254.1

Chapter 3: Warmer air temperatures predicted to result in wetland drying in the Upper Columbia River Valley, British Columbia, Canada

Abstract

Climatic warming is likely to affect the Canadian Rockies, leading to changes in the land cover (LC) and hydrological cycles. This study estimates climate-induced changes in LC (open water, marsh, wet meadow, and woody/shrub) in the Upper Columbia River Wetlands (UCRW), British Columbia, Canada, from 1984 to 2040. An artificial Neural Network (ANN) approach was used with Landsat series archive data from 1984 to 2022 to project seasonal LC change from 2020s to 2040s. Concurrently, hydroclimatic-based models (using air temperature and precipitation to predict river discharge at the UCRW, 1984-2022) were developed (average Nash Sutcliffe: training 0.75 and validation of 0.70) to predict (1984-2040) river discharge forced by Representative Concentration Pathway (RCP) 4.5 and 8.5. The 1984–2022 regression between river discharge and UCRW open water area was forced by RCP scenario river discharge results, calculating open water area for both scenarios. ANN-predicted LC with a Kappa of 0.85 (average of all seasons) for 2020s reference and projected LC, and 0.82 for reference and projected LC change maps (2000s–2020s). From 2020s to 2040s, the ANN projected a reduction (-5%) of open water areas during late summer (August to mid-September) in the UCRW, consistent with RCP 4.5 forecasts. The peak of the open water area in the UCRW is projected to shift from summer (late-May to July) to spring (April to mid-May) in both RCP scenarios. The projected changing hydrological conditions reduced the marsh area (-1% to -12%) and increased the wet meadow (+1% to +4%) mostly in the summer and late summer. Meanwhile, woody and shrubby vegetation on the floodplain increased (3% to 5%), indicating that the floodplain is projected to dry out.

Keywords: Ecohydrology; Remote sensing; Machine Learning; Climate change; Montane ecosystems

Citation:
Rodrigues, I. S., Hopkinson, C., Chasmer, L., MacDonald, R. J., & Bayley, S. E. (2025). Warmer air temperatures predicted to result in wetland drying in the Upper Columbia River Valley, British Columbia, Canada. *Science of The Total Environment*, *959*, 178261. https://doi.org/10.1016/j.scitotenv.2024.178261

Supplementary materials A, B, C and D of Chapter 3:
Supplement of Science of Total Environment:
https://view.officeapps.live.com/op/view.aspx?src=https%3A%2F%2Fars.els-cdn.com%2Fcontent%2Fimage%2F1-s2.0-S0048969724084195-mmc1.docx&wdOrigin=BROWSELINK

Author Contributions:
Italo Sampaio Rodrigues: investigation, formal analysis, data curation, validation, conceptualization, writing, and methodology – original draft, review and editing.
Chris Hopkinson: investigation, formal analysis, data curation, software, resources, methodology, conceptualization, supervision, funding acquisition, and writing – original draft, review, and editing.
Laura Chasmer: conceptualization, investigation, methodology, supervision, writing – review & editing.
Ryan MacDonald: conceptualization, supervision, writing – review & editing.
Suzanne Bayley: funding acquisition, investigation, project administration, supervision, writing – review & editing.

All the authors have read and agreed to the published version of the manuscript.

3.1. Introduction

Montane wetlands act as sentinels of environmental change (Williamson et al., 2008; Moser et al., 2019) because they experience a significant elevational gradient where isotherms change quickly in space and time, altering seasonal freeze – thaw cycles (Edwards et al., 2008; Löffler et al., 2011), precipitation/runoff (Stewart, 2009), and therefore, vegetation change (Hrach et al., 2022). Montane wetlands also influence downstream hydrology and ecology (Chatterjee et al., 2010) by storing water during wet periods and supplying downstream flows during dry periods (Brinson and Malvárez, 2002). They also provide critical habitats for local biota (Cooper et al., 2017), provide support for food chains (Díaz et al., 2015), filter and store sediment and nutrients from runoff erosion events (Lottig et al., 2013), and store and emit carbon (Hrach et al., 2022).

Climate-mediated changes in hydrology have had numerous ecological implications in montane wetlands. For example, satellite time-series data over the Upper Colombia River Wetlands (UCRW) showed that open water extent decreased (1984 to 2022), and the encroachment of woody vegetation increased across the floodplain (Rodrigues et al., 2024). In the Rocky Mountains of Alberta, Glines (2012) documented a positive woody and shrub trend of 0.9% cover·year^{-1} from 1952 to 2003. A positive woody and shrub encroachment trend of 0.2% cover year^{-1} over 62 years was also reported by Formica et al. (2014) in Niwot Ridge, south of the Rocky Mountains. Woody vegetation expansion influences hydrology (DeBeer et al., 2021; Leipe and Carey, 2021) by increasing canopy interception (Zwieback et al., 2019), evapotranspiration (Aguirre et al., 2020), and water infiltration (VanShaar et al., 2002).

Higher air temperatures are predicted over the Columbia River headwaters in the future (Flannigan et al., 2009; Schnorbus et al., 2012; Carver 2017; Wang et al., 2017), which is expected to increase rates of snow and glacier melt (Moore et al., 2020), annual river flow, and lake size (Johnson et al., 2005). During late summer, glacier melt can increase river discharge and connected wetland area (e.g., open water) (Stahl and Moore, 2006; Jost et al., 2012). However, climate change-driven glacier melt in western Canada may disrupt local wetland hydrology and dependent biota since they will no longer supply water for this environment in the future (Clarke et al., 2015; Tsuruta and Schnorbus, 2021). Furthermore, the anticipated increase in evapotranspiration during late summer due to atmospheric warming (Moore et al., 2008) is expected to elevate the risk of drought (Harrington and Flannigan, 1993; Girardin et al., 2006; Kienzle, 2006; Wang et al., 2020). Consequently, there is uncertainty regarding the future of these wetlands and whether the associated

ecosystems can be sustained under a changing climate regime.

The process of projecting the climate response of a watershed frequently involves the use of a hydrological model forced by climate scenarios (Tsuruta and Schnorbus, 2021). Since the 2014 IPCC Fifth Assessment Report, greenhouse gas concentration scenarios are based on Representative Concentration Pathways (RCP), which express atmospheric radiative forcing associated with different greenhouse gas emission scenarios predicted to 2100. Frequently used scenarios for climate change studies are RCP 4.5 (business-as-usual emissions; radiative forcing reaches 4.5 W m^{-2} by 2050, stabilizing early after 2100 (Thomson et al., 2011)) and RCP 8.5 (extreme baseline emissions, radiative forcing grows to 8.5 $W.m^{-2}$ by 2100 (Bjørnaes, 2013)).

Another method of examining the effects of climate change is to project land cover (LC) and river discharge (Gomes et al., 2020; Tsuruta and Schnorbus, 2021). Remote sensing (RS) is an effective tool to detect LC changes (e.g. there is at least 40 years of satellite imagery data using the moderate resolution satellite series: Landsat) (Amani et al., 2021; Wulder et al., 2022). Historical LC data can be utilized to project future LC by using the Artificial Neural Networks (ANN) approach (Rahman et al., 2017; Kamaraj and Rangarajan, 2022). The spatial visualization of the projected LC allows decision-makers to act in these specific vulnerable locations that are expected to change over time. Alternatively, empirical hydroclimatic-based models driven by air temperature and precipitation can be used to simulate the past and project the future of river discharge (Zhang et al., 2011; Diomede et al., 2008).

In this context, hydroclimatic-based models forced by RCM data can be used to project the river discharge in different RCP scenarios. Also, the integration of ANN with RS data (particularly the Landsat time-series) can aid in the prediction of spatial wetland trends and changes. Both approaches enable an evaluation of past and potential future trends across vast areas, thereby facilitating a deeper understanding of changes in montane wetland ecosystems.

This research aimed to forecast and describe the effects of climate change on Open Water, Marsh, Wet Meadow, and Woody/Shrub LCs in the Upper Columbia River Wetlands (UCRW) in British Columbia (BC), Canada using Landsat image archive time series and hydroclimatic models. The specific objectives are (i) to linearly project observed historical LC changes into the future up to 2040s; (ii) to compare / verify the projected open water LC by independently modeling the discharge and open water extents using RCP 4.5; (iii) to quantify and evaluate the projected trends and changes in areal floodplain land cover extents within the UCRW. Meanwhile, RCP 8.5 provides

an upper estimate of wetland changes. Outputs of the research will assist in the strategic planning and management of local wetlands in the Columbia Valley for future water and habitat management by developing a methodology to assess the possible effects of future climate change on montane floodplain landscapes.

3.2. Materials and Methods

3.2.1. Study Area

The Upper Columbia River Wetlands are in Southeastern British Columbia, Canada, spanning a ~120 km stretch of the Columbia River floodplain (188 km^2) between the towns of Donald and Invermere (Figure 3.1). The open-water areas of these floodplain wetlands are distinguished by collections of emergent and submerged aquatic plants (Marsh and Wet meadow), which provide essential habitat and other resources for fish, invertebrates, amphibians, and birds (Rooney et al., 2013). The study area has a humid continental mild summer climate (Köppen climate classification), with cold winters, and short, cool summers. For Golden, B.C., the mean annual average air temperature is 3ºC, and total precipitation ~800 mm $year^{-1}$ (Environment Canada, 2022a). The annual average peak river flow at Nicholson, upstream of Golden, is 512 $m^3 s^{-1}$ (Carli and Bayley, 2015). Annual air temperature is predicted to increase by 0.02 and 0.03 deg C $year^{-1}$ by 2040 based on RCP 4.5 and 8.5 scenarios (Swart et al 2019; ECCC 2021) (Figure 1c – see below).

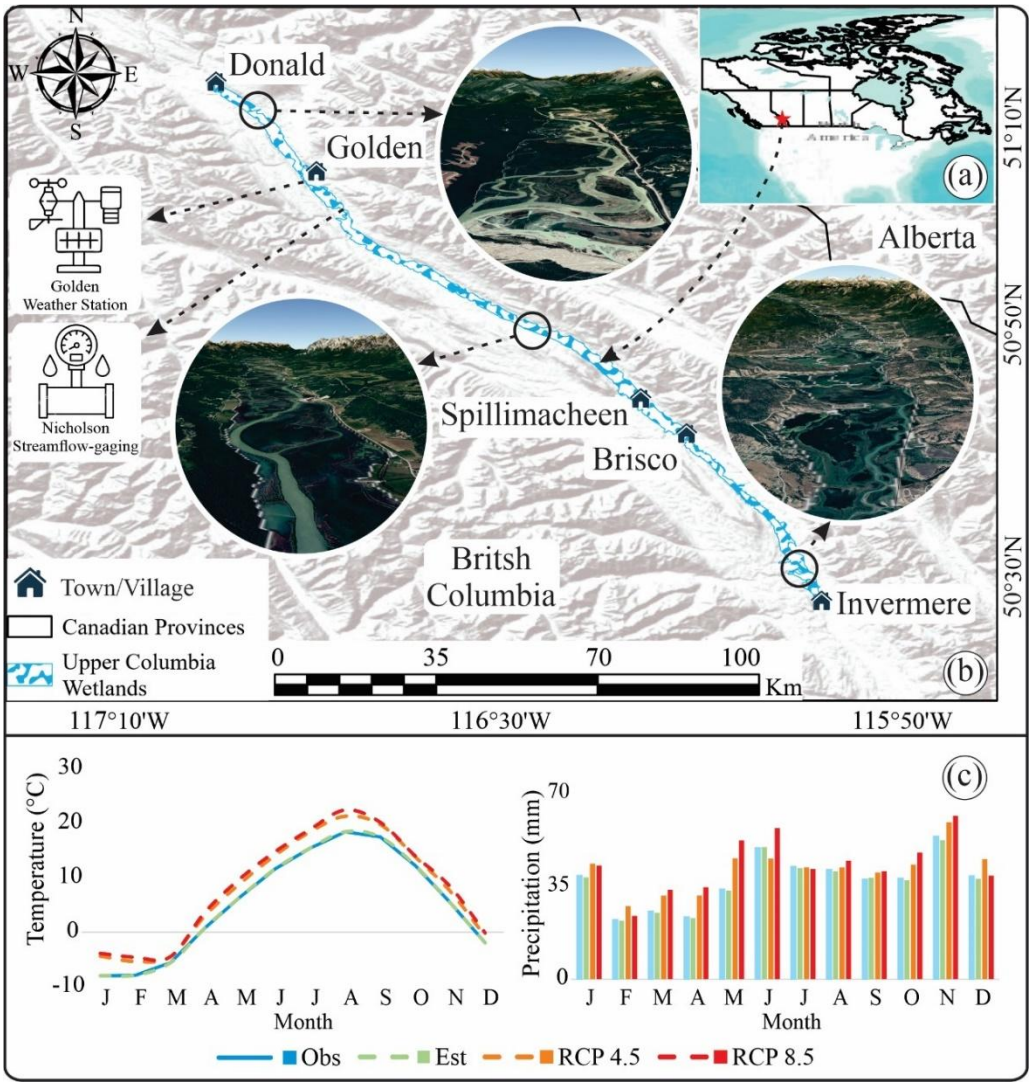

Fig. 3.1. a) The study location in Canada; b) Upper Columbia River Wetlands study area; c) observed, estimated and predicted meteorological data for Golden, BC where, Obs – Historical monthly averages at Golden meteorological station (1984 to 2022); Est – Estimated Historical monthly averages with bias correction by CanESM5 (1984 to 2014); RCP 4.5 – Projected (2015 to 2040) monthly averages with bias correction (Linear Scaling Method – LSM) by CanESM5 under RCP 4.5; RCP 8.5 – Projected (2015 to 2040) monthly averages with bias correction (LSM) by CanESM-2 under RCP 8.5

3.2.2. Data

The historical (1984 – 2022) river discharge data were acquired from the Nicholson gauge (Environment Canada, 2022b; Columbia River at Nicholson, 08NA002; Location: 51° 14' 36" N,

116° 54' 46" W). Historical (1984 – 2022) air temperature (T_{air}) and precipitation (P), data were obtained from the Golden Weather station (Environment Canada, 2022a; Golden A, 1173209; Location: 51° 17' 57" N, 116° 58' 56" W; Elevation: 784.9 m a.s.l.). This station was chosen due to its extensive historical record and its location within the main valley of the study area.

The projected daily T_{air} and P were obtained from a subset of the Canadian CanESM5 model (Swart et al., 2019), which is part of the Coupled Model Intercomparison Project Phase 6 (CMIP6) global climate models (GCMs) (Environment and Climate Change Canada, 2021). The grids were established with a longitude and latitude of 2.8125°, which corresponds to a spatial resolution of ~312 km. Outputs from GCMs are subject to systematic scale-based deviations from location-specific values, therefore, bias-correction is recommended to ensure simulation reliability (Teutschbein and Seibert, 2012). The Linear Scaling Method (LSM) was used to correct bias, as this method has proven effective for bias-correction in mountain environments (Teutschbein and Seibert, 2012; Chen et al., 2013; Shrestha et al., 2017). Temperature for a given time 't' ($T_{(t)}$) is corrected with an additive factor ($\overline{T}_m$- $\overline{T}_s$, Equation 3.1, where $\overline{T}_m$ is the average monthly historical air temperature observed at the reference weather station, and $\overline{T}_s$ represents the average monthly historical air temperature simulated by the CanESM5 for the grid cell occupied by the observation station), whereas the precipitation variables ($P_{(t)}$), are corrected with a multiplicative factor ($\overline{P}_m$ / $\overline{P}_s$, Equation 3.2, where $\overline{P}_m$ is the historical monthly hydroclimatic data average measured at the reference weather station, and $\overline{P}_s$ represents the monthly average simulated by the CanESM5). The use of additive (to correct the bias on the air temperature) and multiplicative (to correct the bias on other hydroclimatic variables) factors has been used in studies of hydrological impacts due to climate change (Teutschbein and Seibert, 2012; Fiseha et al., 2014; Althoff et al., 2020). Thus, bias-correction through the LSM was performed for both the baseline (1984-2014) and scenario (2015-2040) periods using Equations 3.1 and 3.2 (* represents the bias-corrected variable):

$$T^*_{(t)} = T_{(t)} + \overline{T}_m - \overline{T}_s \quad (3.1)$$

$$P^*_{(t)} = P_{(t)} \left(\frac{\overline{P}_m}{\overline{P}_s}\right) \quad (3.2)$$

Moreover, the seasonal (Spring: April 01 to May 15; Summer: May 16 to July 31; Late Summer: August 01 to September 15) historical LC (maps were obtained from Rodrigues et al.

(2024)), from 1984 to 2022, which were used in the Artificial Neural Network (ANN) algorithm to project seasonal spatial LC. The four LC classes are: Open water; Marsh (*Schoenoplectus tabernaemontani* – Bulrush, and *Typha latifolia* – Cattail Marsh*);* Wet meadow (*Carex rostrata* – Beaked Sedge, *Carex aquatilis* – Water Sedge, *Equisetum arvense* – Horsetail*)*; Woody/Shrub vegetation (Woody species: Cottonwood – *Populus*, Norway Spruce – *Picea abies*, and Dogwood – *Cornus* spp.; Shrub species: Sitka Willow – *Salix sitchensis*, Red – Osier Dogwood – *Cornus sericea*, Horsetail – *Equisetum* spp.). In addition, the ANN model incorporated terrain driving factors such as elevation (from the NASA SRTM Digital Elevation Model – DEM), slope, topographic position index (TPI – the difference between the elevation of each pixel and the average elevation of its neighbouring pixels (De Reu et al., 2012)), and aspect (suggested by Kamaraj and Rangarajan, 2022). The driving factors were created from the DEM using the Spatial Analyst tool in ArcGIS Pro v3.3.1. The ANN learns and applies spatial relationships between LC types, driving factors, and LC change across the study area, thus improving predictions (Gharaibeh et al., 2020).

The following is a succinct explanation of the terrain driving factors that were used in the ANN routine: elevation affects vegetation and land cover, with locally high elevations (e.g., on the riverbank) tending to display distinct vegetation types (e.g., woody and shrub) compared to nearby or adjacent low elevations (e.g., marsh). Slope affects floodplain land cover since taller dense vegetation is more prevalent on sloped terrain, for example, whereas open water is found in flat areas. Aspect can provide an index of local growing conditions due to solar radiation receipt, for example. TPI can provide a local proxy of hillslope-scale moisture conditions in flatter terrain, with local lowlands tending to be wetter and local uplands tending to be drier.

3.2.3. Modelling Framework

The research was conducted in four stages (Figure 3.2). First, an artificial neural network (ANN) approach, MOLUSCE (NextGIS, 2017) was used to project the spatial land cover (LC) using historical LC classification data from the UCRW (Rodrigues et al., 2024). Second, linear LC (i.e., Open Water, Marsh, Wet Meadow, and Woody/Shrub) simulation was performed using ANN. Third, hydroclimate-based models were created to project river discharge using T_{air} and P from the RCP 4.5 and 8.5 scenarios. Finally, trend analyses were performed to assess the impact of climate change based on the linear LC change and RCP scenarios.

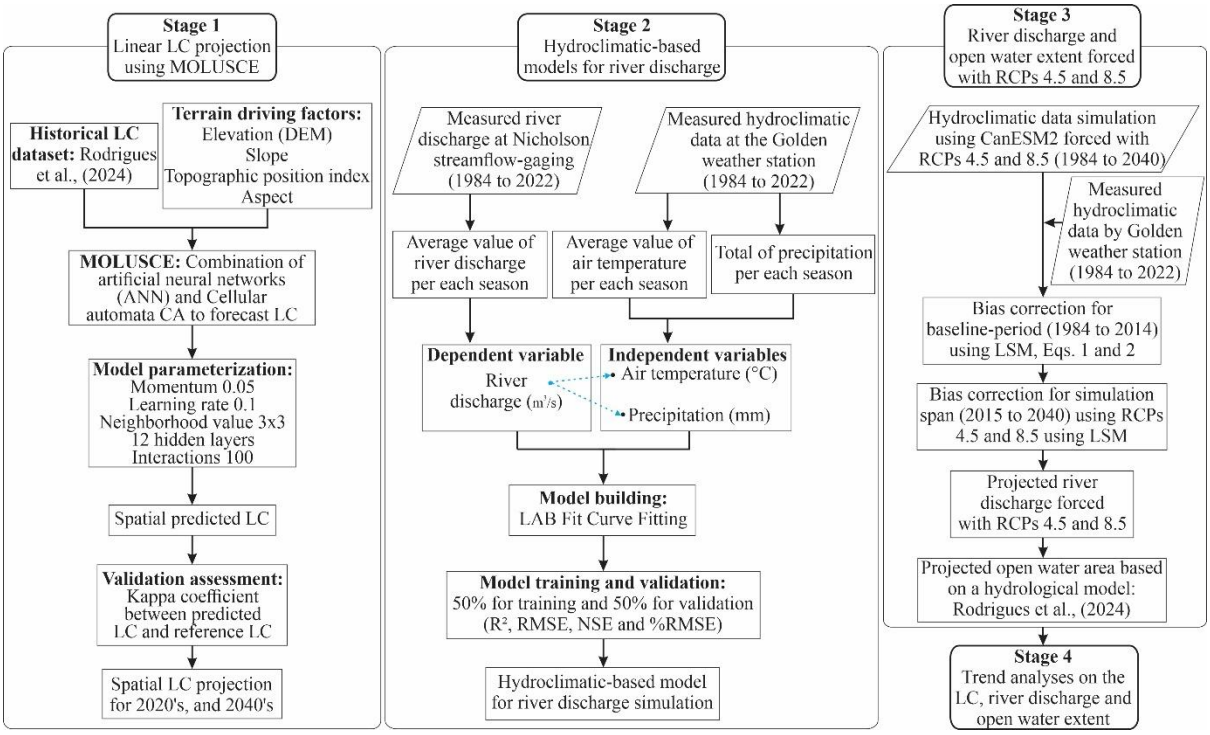

Fig. 3.2. Methodological flowchart for assessing climate change impacts in the LC and river discharge in the UCRW.

3.2.4. Stage 1: Linear LC projection using MOLUSCE

The MOLUSCE plug-in, integrated into the QGIS software (version 2.18), was employed to forecast changes in land cover (LC) of the UCRW until the 2040s. Historical seasonal LC maps (Rodrigues et al., 2024) were used along with terrain driving factors (Figure S1A) to predict landcover change. This projection utilises a hybrid approach combining artificial neural networks (ANN) and Cellular automata (CA). The Cellular Automata (CA) functionality in QGIS is implemented using the Markov chain technique, which predicts future land cover based on past and current land cover (Yatoo et al., 2020). This model integrates seasonal historical and current land cover maps with spatial terrain driving factors (i.e., elevation, slope, topographic position index, and aspect; Figure S1 in supplementary material A of Chapter 3) (Rodrigues et al. 2025) to provide estimates of future changes as tables and maps (Gašparović and Jogun, 2017). Moreover, the ANN algorithm in MOLUSCE was used since it tends to be more accurate than other techniques for LC prediction (Gharaibeh et al., 2020; Ahmad et al., 2023).

The parametrization of MOLUSCE begins with the transition potential model (i.e., the potential of a pixel to change from one land cover class to another), which was trained using a

momentum of 0.05 (varying from 0 to 1), a learning rate of 0.01 (range between 0 to 1) to stabilise the learning graph (as per Alshari and Gawali, 2022; Kamaraj and Rangarajan, 2022) and was trained for 100 iterations to prevent overfitting. The learning rate, momentum, and iterations are called the learning parameters. High learning rate and momentum enable quick yet unstable learning; Small learning rate and momentum suggest steady yet sluggish learning. The number of iterations should avoid overfitting, which may be determined via testing and simulations. (NextGIS, 2017). A neighbourhood value (counts the pixels around the current pixel: size = 1 indicates 9 pixels, or 3 × 3 region; size = 2 implies 25 pixels, or 5 × 5 region, etc.) of 3 (i.e., which implies 49 pixels, or 7 × 7 region, from the historical LC dataset) was employed to train the ANN algorithm using change observations occurring within a 90-meter radius around each LC cell. The model had 12 hidden layers (as per Muhammad et al., 2022), which were neurons that learned linear and non-linear relationships between the input (LC and terrain driving factors) and the output (projected LC). Each hidden layer neuron gets inputs from all previous layer neurons, multiplies them by their weights, adds a bias term, and sends the output via an activation function. Neuron output feeds the next layer (NextGIS, 2017). The projected LC pixel was decided based on the present state of a neighbouring cell, the changes in the surrounding cells, and by the relationships with the terrain driving factors in the CA framework (Lau and Kam, 2005; Koomen and Beurden, 2011).

The ANN-CA simulation was subsequently followed by the validation process, which allows for the verification, comparison, and validation of the projected LC. The validation process involved comparing the projected seasonal LC with the reference seasonal LC maps (Rodrigues et al., 2024). To avoid noise in the trends, approximate 20-year periods (1980s to 2020s) were used to forecast seasonal LC maps during the period from 2020 to 2040. The mode of the seasonal LC maps from the 1984 to 1988 (herein referred to as 1980s) and the 2002 to 2006 period (herein referred to as 2000s) was utilised to project the seasonal mode LC map from the 2018 to 2022 period (herein referred to as 2020s). This approach avoids the selection of a dry or wet year and instead uses ‘typical’ characteristics on a per pixel basis. Furthermore, the rationale for using these past intervals and years was based on an analysis of the Pacific Decadal Oscillation, which pinpointed normal, dry and wet years in the UCRW, as detailed by Rodrigues et al. (2024). For instance, in the 1980s, there were two normal years (1984 and 1988), two dry years (1985 and 1987), and one wet year (1986). In the 2000s, there was one normal year (2003), two dry years (2004 and 2005), and two wet years (2002 and 2006). In the end, ensuring a well-balanced combination of all floodplain

conditions.

The mode of the LC maps was determined in the Google Earth Engine using the "*.mode()*" tool. Hence, the LC map for the year 2020 was derived utilising the reference LC mode and change maps from the 1980s and 2000s, and the terrain driving variables, as the input data using the prediction methodology described above. The predicted seasonal mode map of 2020's, was compared to the reference seasonal mode map of 2020's. The Kappa coefficient was employed to assess the level of accuracy between the reference and projected LC. Specifically, 100 pixels per land cover class were evenly random dispersed throughout the whole domain of the UCRW, resulting in a total of 400 pixels across the four land cover classes: open water, marsh, wet meadow, and woody/shrub. In addition, the Kappa coefficient was used to assess the accuracy between the projected land cover changes and the actual changes throughout the entire UCRW. This involved randomly selecting 100 points per class (1200 total), evenly random distributed across twelve LC change classes: 1) open water to marsh, 2) open water to wet meadow, 3) open water to woody/shrub, 4) marsh to open water, 5) marsh to wet meadow, 6) marsh to woody/shrub, 7) wet meadow to open water, 8) wet meadow to marsh, 9) wet meadow to woody/shrub, 10) woody/shrub to open water, 11) woody/shrub to marsh, and 12) woody/shrub to wet meadow. The analysis focused on the land cover areas that underwent change by excluding areas that retained the same LC class through time. The comparison was made between the reference land cover change map from the 2000s to the 2020s, and the land cover change map between the reference land cover from the 2000s and the projected land cover for the 2020s.

To extend the forecasts beyond 2020, the reference seasonal mode LC map from the 2000s and 2020s was used to forecast the seasonal mode LC map for the 2040s (i.e. 2038 to 2042). Figure 3.3 illustrates the implementation of the cascade projection method.

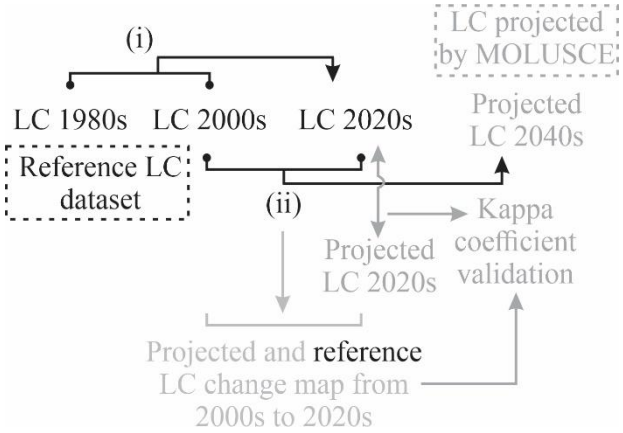

Fig. 3.3. LC forecast approach using MOLUSCE (i and ii: the steps and datasets used to project LC over the future)

3.2.5. Stage 2: Hydroclimatic-based models for river discharge

Hydroclimatic models based on average monthly air temperature (T_{air}) (°C) and monthly total precipitation (P) (mm) were created to estimate monthly river discharge in the UCRW, since glacier melt, snow melt, and rainfall are the main drivers of river discharge (Diomede et al., 2008; Zhang et al., 2011; Tsuruta and Schnorbus, 2021). The seasonal (spring, summer, and late summer) models to simulate monthly river discharge were developed based on observed river discharge at Nicholson streamflow-gauge (from 1984 to 2022) as the response variable, T_{air} and P as inputs. T_{air} and river discharge were averaged, and cumulative P was totalised for each season (Spring; Summer; Late Summer). Average discharge (in $m^3.s^{-1}$) was projected for each season.

The seasonal models were created using the LABFit software (Silva et al., 2004), which uses the Levenberg-Marquardt optimisation technique (Levenberg, 1944; Marquardt, 1963) (also referred to as damped least-squares). This method is considered powerful because it combines a gradient descent algorithm, which is a machine learning approach used to find the coefficients of a function that minimises a cost function, with a Gauss-Newton algorithm, which solves non-linear least squares problems found by the minimum residual of the chosen non-linear function (Silva et al., 2004). The optimal non-linear regression form between the T_{air} and P and river discharge was determined based on the reduced chi-square (i.e., a non-linear function around 1 is ideal) using the LABFit library, which offers over 500 pre-defined non-linear regression functions. The river discharge data from 1984 to 2022 were divided into two equal parts: 50% for training (even years 1984, 1986, etc.) and the remaining 50% (odd years) for validation. Training and validation were sampled from alternating years to mitigate the influence of anomalous multi-year periods, and due

to a noticeable shift in the UCRW river flow patterns around the year 2000 (Rodrigues et al., 2024).

3.2.6. Stage 3: River discharge and open water extent forced with RCPs 4.5 and 8.5

The seasonal hydroclimatic-based models from section 3.2.5, were driven by the bias corrected T_{air} and P from CanESM5 (from historical, 1984 – 2014, and projected 2015 – 2040). The river discharge was examined using two distinct atmospheric forcing scenarios: a hydroclimatic-based model driven by the RCPs 4.5 (SSP2) and 8.5 (SSP5). To evaluate if projected river flow was representative of true discharge, GCM-modelled discharge at RCP 4.5 and 8.5 was compared (using Nash-Sutcliffe coefficient) against observed discharge during the period of overlap from 1984 to 2022.

Total floodplain open water extent for each season was estimated for both RCP 4.5 and 8.5 scenarios using previously generated empirical models (Rodrigues et al., 2024) of open water area based on river discharge (i.e., river discharge vs open water regression; herein referred to as regression model). GCM-modelled open water extent was compared to the open water extent projected by the ANN approach for 2040, which determined the RCP pathway that the linear projection of the UCRW followed in the future.

3.2.7. Stage 4: Trend analyses

The Mann-Kendall method (Kendall, 1975; Mann, 1945) was used to conduct a trend analysis on the projected LC extent, GCM-modelled river discharge, open water area, air temperature and precipitation in pyMannKendall (Hussain and Mahmud, 2019). The Mann-Kendall method evaluates three hypotheses: i) the absence of a trend (null hypothesis), ii) a positive trend, iii) a negative trend. A significance threshold of p-value = 0.05 was adopted. The magnitude of the changes was evaluated by the nonparametric Sen's slope and Kendall's tau (τ) coefficient, which quantifies the association between the variables.

3.2.8. Statistical comparison

In section 3.2.4, the reference and projected LC extent (in square kilometres) for the 2020's were compared using two statistical techniques: Total error (TE) and Total Percentage Error (%TE).

In section 3.2.5, the hydroclimatic model performances were assessed using the coefficient of determination (R^2), RMSE, the Nash-Sutcliffe coefficient (NSE) as proposed by Nash and

Sutcliffe (1970), and the percent RMSE (%RMSE).

In section 3.2.6, the open water extent projected by RCP 4.5 and 8.5 was compared to the open water extent projected by the ANN approach utilizing the RMSE and %RMSE. This comparison determined the RCP pathway that the linear projection of the UCRW followed in the future.

3.3. Results

3.3.1. Spatial LC projection accuracy

The seasonal kappa coefficients of the predicted raster for the 2020's (using the LC of 1980's and 2000's from each season) over the spring, summer and late summer seasons was 0.86, 0.88, and 0.81, respectively. The seasonal confusion matrix with total accuracy, omission and commission errors of the reference and projected land cover of 2020s are shown in Supplementary material B of Chapter 3 (Table S1 to S3) (Rodrigues et al. 2025). Moreover, Figure 3.4 illustrates the seasonal (spring, summer, and late summer) predicted LC for each floodplain land cover compared to the reference dataset.

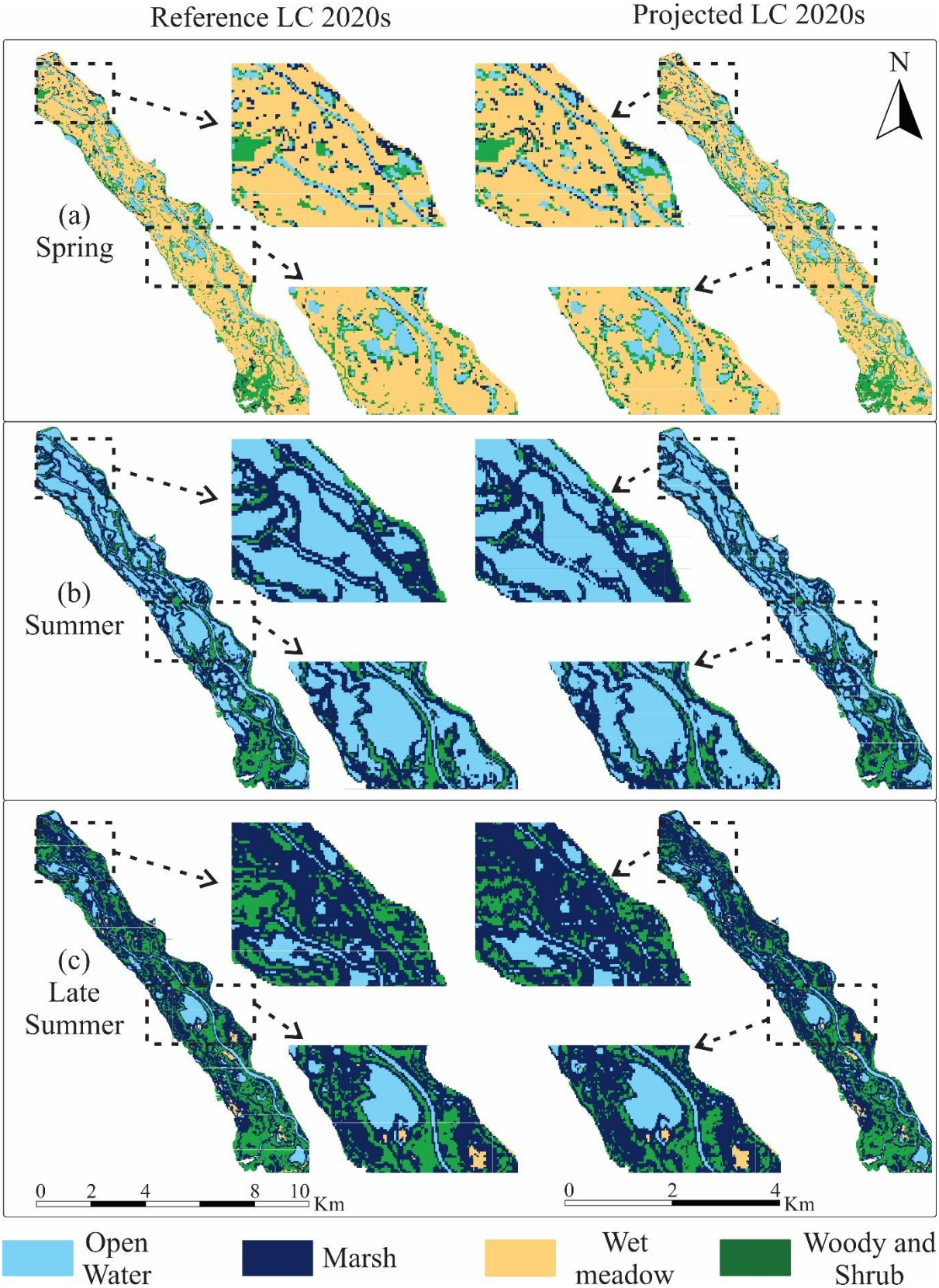

Fig. 3.4. Comparison of central section (portion of Spillimacheen to Golden, spanning a ~14 km

stretch) of the Upper Columbia River floodplain reference and projected LC for 2020's during the spring (a), summer (b), and late summer (c).

More importantly, the seasonal kappa coefficients of the LC change maps (i.e., between the reference and projected 2000's and 2020's) during spring, summer, and late summer was 0.78, 0.84, and 0.86, respectively. Tables 3.1 to 3.3 describe the seasonal (spring, summer, and late summer) confusion matrix with total accuracy, omission and commission errors of the reference and projected land cover change maps from 2000s to 2020s. In addition, Figure 3.5 illustrates the seasonal (spring, summer, and late summer) predicted LC change map for each floodplain land cover compared to the reference LC change map dataset.

Table 3.1. Confusion Matrix with commission and omission errors between the reference and projected land cover change of 2020's during spring (i.e., April to mid-May)

Classes	OW–M	OW–WM	OW–WS	M–OW	M–WM	M–WS	WM–OW	WM–M	WM–WS	WS–OW	WS–M	WS–WM	Marginal total	Comission Error	Total Accuracy	Kappa Index
OW–M	74	2	2	4	2	4	2	1	2	2	3	2	100	0.26		
OW–WM	3	74	1	3	4	3	1	3	2	1	3	2	100	0.26		
OW–WS	2	0	80	3	4	3	3	1	1	0	2	1	100	0.20		
M–OW	2	3	1	76	1	3	3	2	2	3	3	1	100	0.24		
M–WM	1	3	2	3	80	3	5	2	1	0	0	0	100	0.20		
M–WS	2	2	2	1	1	79	2	2	3	2	2	2	100	0.21		
WM–OW	0	2	1	1	3	0	80	2	3	3	3	2	100	0.20		
WM–M	1	2	2	2	1	1	2	80	2	2	3	2	100	0.20	79.9%	0.78
WM–WS	2	2	3	2	2	2	1	2	79	2	1	2	100	0.21		
WS–OW	0	0	2	1	1	2	0	2	2	84	3	3	100	0.16		
WS–M	0	1	2	1	1	2	1	3	1	2	86	0	100	0.14		
WS–WM	0	1	2	2	3	1	0	0	1	2	1	87	100	0.13		
Marginal total	87	92	100	99	103	103	100	100	99	103	110	104	1200			
Omission Error	0.15	0.20	0.20	0.23	0.22	0.23	0.20	0.20	0.20	0.18	0.22	0.16				

1) OW – M: open water to marsh; 2) OW – WM: open water to wet meadow; 3) OW – WS: open water to woody/shrub; 4) M – OW: marsh to open water; 5) M – WM: marsh to wet meadow; 6) M – WS: marsh to woody/shrub; 7) WM – OW: wet meadow to open water; 8) WM – M: wet meadow to marsh; 9) WM – WS: wet meadow to woody/shrub; 10) WS – OW: woody/shrub to open water; 11) WS – M: woody/shrub to marsh; and 12) WS – WM: woody/shrub to wet meadow

Table 3.2. Confusion Matrix with commission and omission errors between the reference and projected land cover change of 2020's during summer (i.e., late-May to July)

Classes	OW–M	OW–WM	OW–WS	M–OW	M–WM	M–WS	WM–OW	WM–M	WM–WS	WS–OW	WS–M	WS–WM	Marginal total	Comission Error	Total Accuracy	Kappa Index
OW–M	83	2	1	1	2	1	2	1	2	2	1	2	100	0.17		
OW–WM	3	84	1	1	2	1	1	1	2	1	1	2	100	0.16		
OW–WS	2	0	81	2	4	3	3	1	1	0	2	1	100	0.19		
M–OW	1	1	1	86	1	0	0	2	2	2	3	1	100	0.14		
M–WM	1	3	2	3	84	3	1	2	1	0	0	0	100	0.16		
M–WS	0	2	0	1	1	89	2	2	1	0	0	2	100	0.11		
WM–OW	0	2	1	1	3	0	84	1	2	2	2	2	100	0.16		
WM–M	1	1	0	1	1	1	2	86	2	2	1	2	100	0.14	85.1%	0.84
WM–WS	1	1	1	1	2	1	1	2	85	2	1	2	100	0.15		
WS–OW	0	0	2	1	1	2	0	2	2	84	3	3	100	0.16		
WS–M	0	1	2	1	1	2	1	3	1	2	86	0	100	0.14		
WS–WM	2	1	2	1	1	1	1	2	2	2	1	84	100	0.15		
Marginal total	94	98	94	100	103	104	98	105	103	99	101	101	1200			
Omission Error	0.12	0.14	0.14	0.14	0.18	0.14	0.14	0.18	0.18	0.15	0.15	0.17				

Table 3.3. Confusion Matrix with commission and omission errors between the reference and projected land cover change of 2020's during late summer (i.e., August to late-September)

Classes	OW–M	OW–WM	OW–WS	M–OW	M–WM	M–WS	WM–OW	WM–M	WM–WS	WS–OW	WS–M	WS–WM	Marginal total	Comission Error	Total Accuracy	Kappa Index
OW–M	86	1	1	1	1	1	2	1	1	2	1	2	100	0.14		
OW–WM	3	84	1	1	2	1	1	1	2	1	1	2	100	0.16		
OW–WS	2	0	85	1	1	3	3	1	1	0	2	1	100	0.15		
M–OW	1	1	1	86	1	0	0	2	2	2	3	1	100	0.14		
M–WM	1	3	1	2	89	1	1	1	1	0	0	0	100	0.11		
M–WS	0	2	0	1	1	89	2	2	1	0	0	2	100	0.11		
WM–OW	0	2	1	1	1	0	86	1	2	2	2	2	100	0.14		
WM–M	1	1	0	1	1	1	2	86	2	2	1	2	100	0.14	86.8%	0.86
WM–WS	1	1	1	1	2	1	1	2	85	2	1	2	100	0.15		
WS–OW	0	0	2	1	1	2	0	1	2	89	1	1	100	0.11		
WS–M	0	1	2	1	1	2	1	3	1	2	86	0	100	0.14		
WS–WM	0	1	1	0	1	2	1	1	1	1	1	90	100	0.10		
Marginal total	95	97	96	97	102	103	100	102	101	103	99	105	1200			
Omission Error	0.09	0.13	0.11	0.11	0.13	0.14	0.14	0.16	0.16	0.14	0.13	0.14				

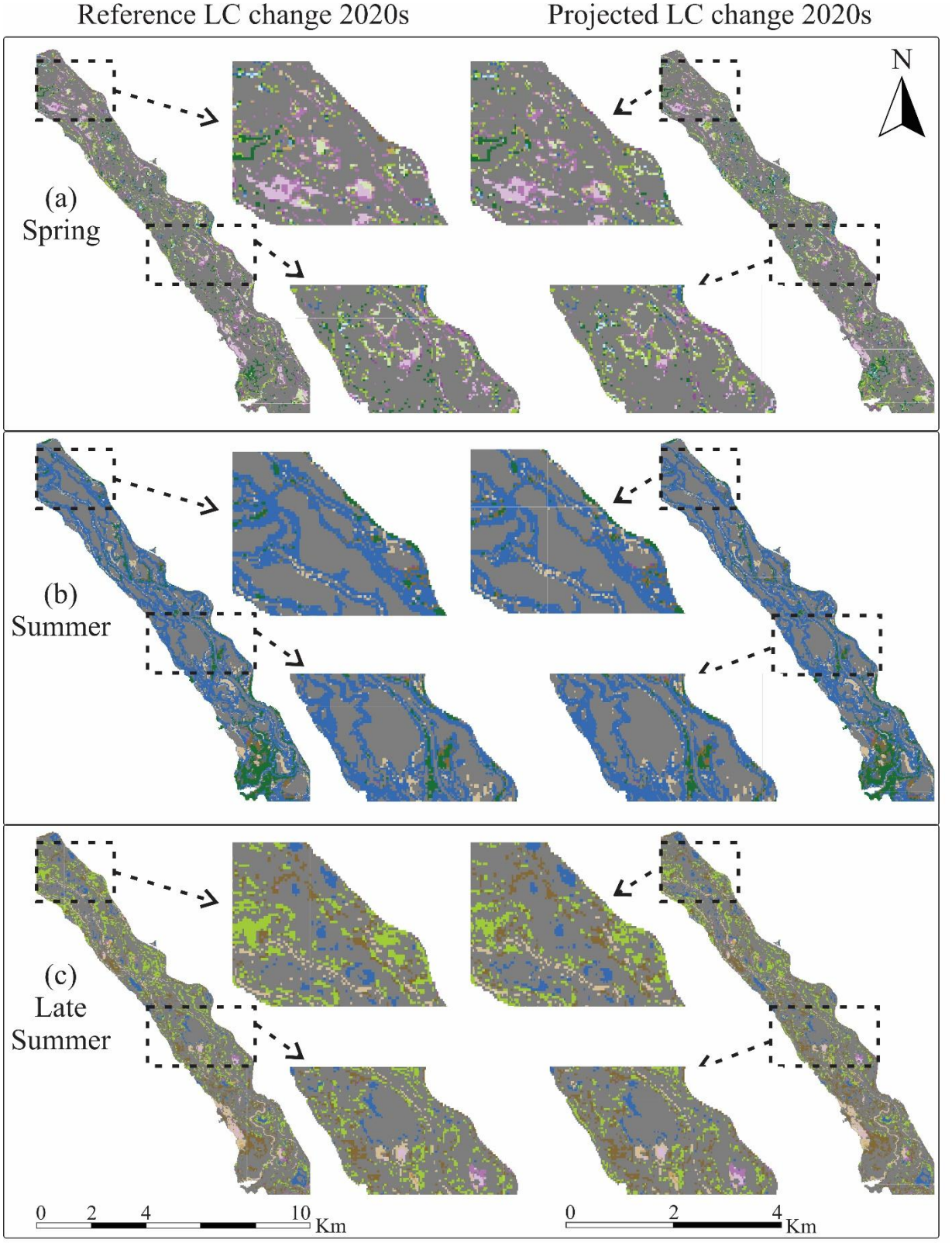
Reference LC change 2020s
Projected LC change 2020s
N
(a)
Spring
(b)
Summer
(c)
Late
Summer
0 2 4 10 Km
0 2 4 Km
M –> OW
WM –> OW
WS –> OW
No Change
WS –> M
WM –> M
OW –> M
WS –> WM
M –> WM
OW –> WM
WM –> WS
M –> WS
OW –> WS
OW: Open Water
M: Marsh
WM: Wet Meadow
WS: Woody and Shrub

Fig. 3.5. Comparison of the reference and projected land cover change map of central section (portion of Spillimacheen to Golden, spanning a ~14 km stretch) of the Upper Columbia River floodplain from 2000's to 2020 during spring (a), summer (b), and late summer.

M –> OW: marsh to open water; WM –> OW: wet meadow to open water; WS –> OW: woody/shrub to open water; WS –> M: woody/shrub to marsh; WM –> M: wet meadow to marsh; OW –> M: open water to marsh; WS –> WM: woody/shrub to wet meadow; M –> WM: marsh to wet meadow; OW –> WM: open water to wet meadow; OW –> WS: open water to woody/shrub; M –> WS: marsh to woody/shrub; and WM –> WS: wet meadow to woody/shrub.

Table 3.4 shows that the projected LC of 2020's total errors (TE) between -0.8 and +1.0 km^2 (average: +0.03 km^2), with total percentage errors (%TE) varying from -15% to +12.5% (average: -0.1%). The best projected land cover change classes were as follows: Spring: wet meadow to open water; Summer: marsh to woody/shrub; Late summer: open water to marsh. Also, in Spring, open water to marsh and wet meadow change trajectories were overestimated, while during Summer there was an under-estimation of the open water to woody/shrub change class. In Late Summer an overestimation of marsh to wet meadow and marsh to woody/shrub was found. These results match commission and omission outcomes, i.e., Tables 3.1 to 3.3. Therefore, the projected LC extents are a reasonable representation of the reference (or true) LC.

Table 3.4. Comparison of the reference and projected LC change extent maps from the 2000s to 2020s in the Upper Columbia River floodplain.

LC change classes	Reference LC Change (km^2) (Rodrigues et al. 2024)			Projected LC Change (km^2)			TE (km^2)			%TE (%)		
	S	Su	LS	S	Su	LS	S	Su	LS	S	Su	LS
OW (No Change)	22.10	46.00	24.70	22.00	46.20	24.30	-0.10	0.20	-0.40	-0.45	0.4	-1.6
OW –> M	0.40	4.30	7.80	0.45	4.45	8.00	0.05	0.15	0.20	12.50	3.5	2.6
OW –> WM	2.00	0.90	1.40	2.20	0.95	1.30	0.20	0.05	-0.10	10.00	5.6	-7.1
OW –> WS	3.10	0.80	0.10	2.95	0.68	0.11	-0.15	-0.12	0.01	-4.84	-15.0	10.0
M (No Change)	11.30	73.00	102.00	11.50	73.40	101.20	0.20	0.40	-0.80	1.77	0.5	-0.8
M –> OW	5.90	5.80	1.40	5.50	6.20	1.30	-0.40	0.40	-0.10	-6.78	6.9	-7.1
M –> WM	3.40	5.90	1.10	3.30	5.80	1.20	-0.10	-0.10	0.10	-2.94	-1.7	9.1
M –> WS	4.00	13.30	8.50	3.80	13.10	9.30	-0.20	-0.20	0.80	-5.00	-1.5	9.4
WM (No Change)	87.00	18.00	0.60	88.00	17.80	0.57	1.00	-0.20	-0.03	1.15	-1.1	-5.0
WM –> OW	9.10	0.90	0.50	9.00	0.85	0.47	-0.10	-0.05	-0.03	-1.10	-5.6	-6.0
WM –> M	6.90	0.70	0.20	6.60	0.65	0.21	-0.30	-0.05	0.01	-4.35	-7.1	5.0
WM –> WS	8.00	1.40	2.30	7.80	1.50	2.32	-0.20	0.10	0.02	-2.50	7.1	0.9
WS (No Change)	14.40	13.00	36.70	14.60	13.20	36.30	0.20	0.20	-0.40	1.39	1.5	-1.1
WS –> OW	2.80	2.10	0.10	2.68	2.00	0.10	-0.12	-0.10	-0.01	-4.29	-4.8	-5.0
WS –> M	2.20	1.90	0.10	2.28	2.00	0.09	0.08	0.10	-0.01	3.64	5.3	-10.0
WS –> WM	5.10	0.20	0.10	5.20	0.21	0.11	0.10	0.01	0.00	1.96	5.0	5.0

S – spring; Su – summer; LS – late summer; OW: open water; M: marsh; WM: wet meadow; WS: woody/shrub; OW –> M: open water to marsh; OW –> WM: open water to wet meadow;

3.3.2. Projected floodplain landcover change from 2020 to 2040

From 2020 to 2040, the area of open water is predicted to decrease in spring (April to mid-May) (-3 km^2 or -2% of the total floodplain area) and late summer (August to mid-September), while an increase is expected during summer season (late-May to July) (-9 km^2 or -5%) Marsh areas are projected to decrease during the spring (-1 km^2 or -1%), summer (-19 km^2 or -12%), and late summer (-2 km^2 or -1%). Wet meadow area is projected to decrease during spring (-2 km^2 or -1%) and increase in the summer (+6 km^2 or +4%), and late summer (+1 km^2 or -1%). In contrast, woody/shrub vegetation increased in area over the spring (+6 km^2 or +4%), summer (+7 km^2 or +4%), and late summer (+10 km^2 or +5%). The air temperature and precipitation are projected to increase. The changes per season of the land cover extent are depicted in Figure 3.6, 3.7, and 3.8, and the trends in the hydro-climatological parameters are shown in Supplementary Material C of Chapter 3 (Rodrigues et al. 2025) (Table S4).

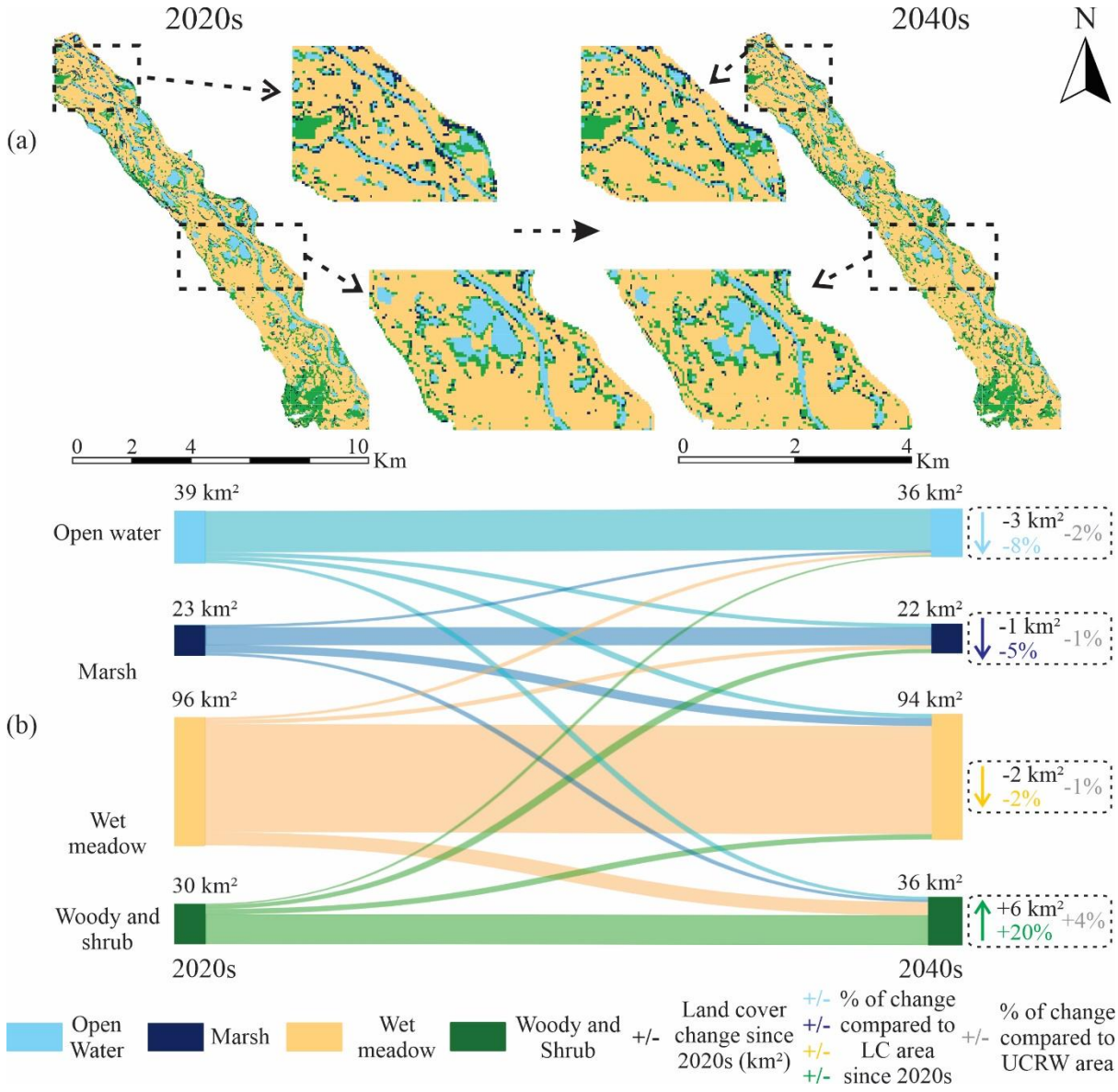

Fig. 3.6. Projected Upper Columbia River floodplain distribution of land cover change from April to mid-May. Insets: a) illustrate changes in land cover for a central sample region (~14 km stretch portion of Spillimacheen to Golden) of the overall floodplain. b) Sankey diagram of the changes in land cover from 2020 to 2040, the land cover change since 2020, and the percentage of change compared to each individual land cover since 2020, and the Columbia wetlands area (188 km^2).

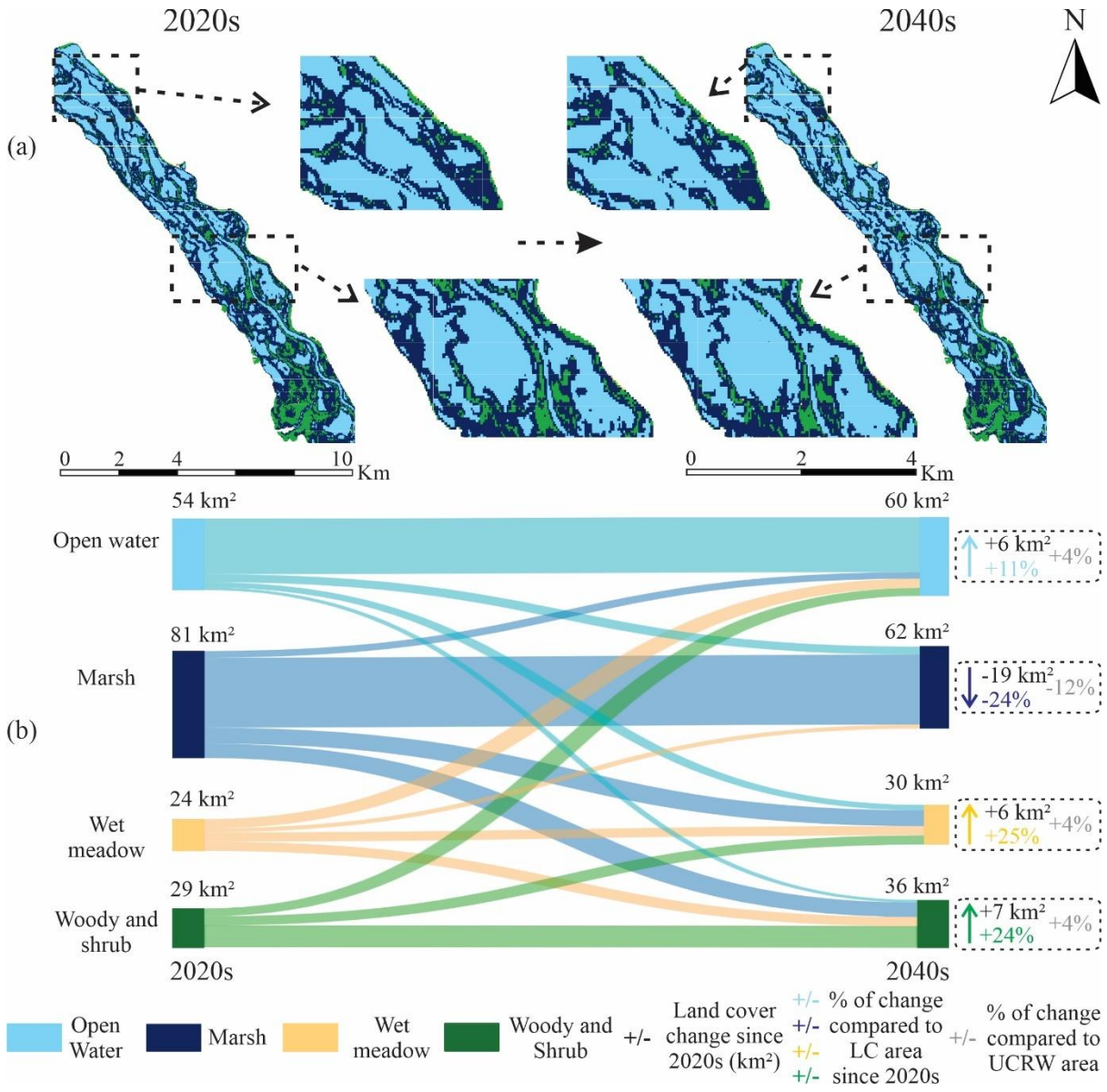

Fig. 3.7. Projected Upper Columbia River floodplain distribution of land cover change from late-May to July. Insets: a) illustrate changes in land cover for a central sample region (~14 km stretch portion of Spillimacheen to Golden) of the overall floodplain. b) Sankey diagram of the changes in land cover from 2020 to 2040, the land cover change since 2020, and the percentage of change compared to each individual land cover since 2020, and the Columbia wetlands area (188 km^2).

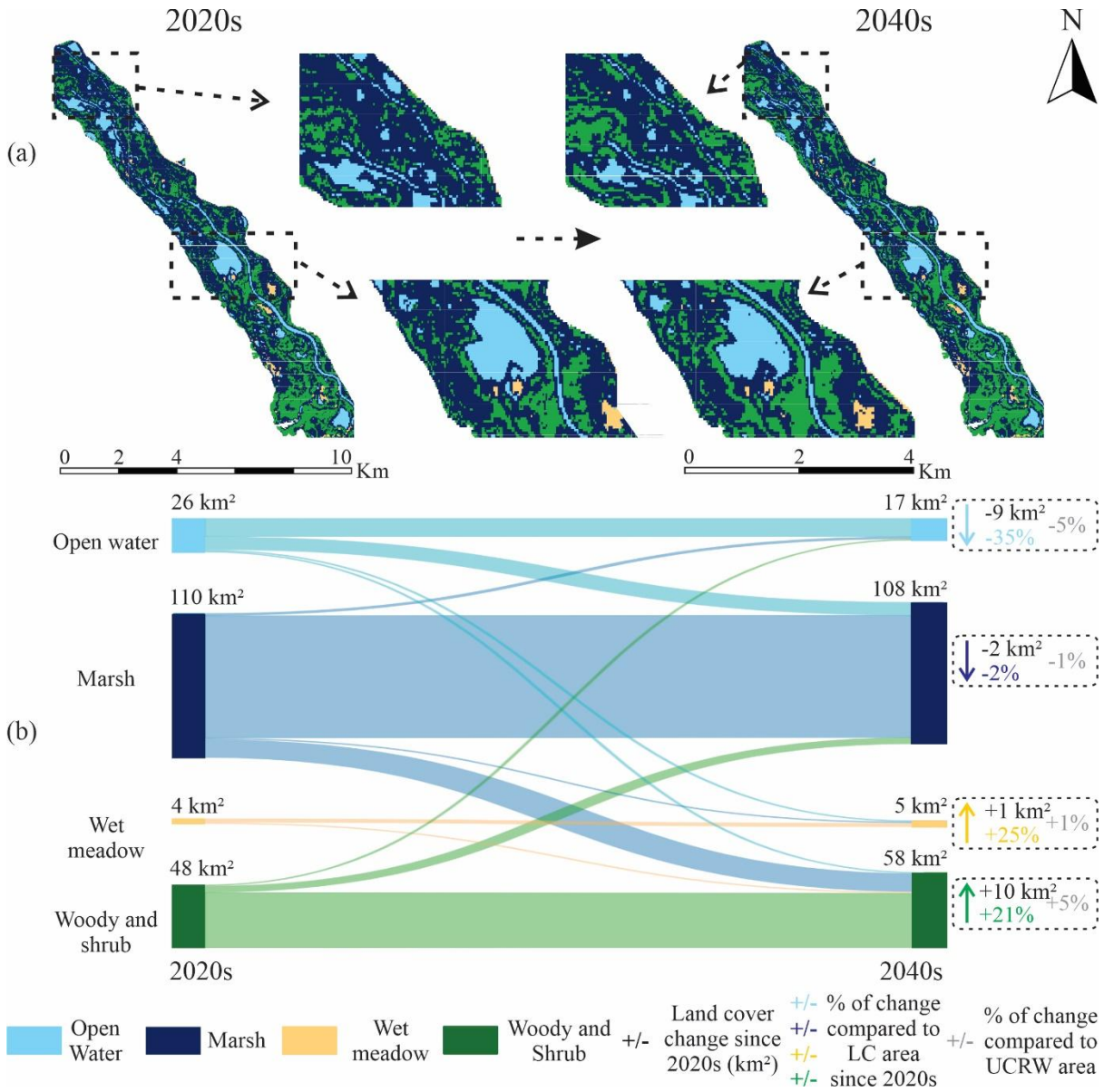

Fig. 3.8. Projected Upper Columbia River floodplain distribution of land cover change from August to mid-September. Insets: a) illustrate changes in land cover for a central sample region (~14 km stretch portion of Spillimacheen to Golden) of the overall floodplain. b) Sankey diagram of the changes in land cover from 2020 to 2040, the land cover change since 2020, and the percentage of change compared to each individual land cover since 2020, and the Columbia wetlands area (188 km^2).

A section-based evaluation (i.e., Invermere to Brisco, Brisco to Spillimacheen, Spillimacheen to Golden, Golden to Donald) of the UCRW was conducted, showing the projected changes per river reach section of the floodplain from 2020 to 2040. Based on this, the most

vulnerable section of the UCRW is from Spillimacheen to Golden (Figures S2 in supplementary material D of Chapter 3) (Rodrigues et al. 2025), which during spring is projected to have larger decreases in open water, marsh, and wet meadow, and increases in woody/shrub. During the summer, open water, wet meadow, and woody/shrub are likely to increase, while marsh areas will decrease. Meanwhile, in late summer, open water and marsh are expected to decline, while wet meadow and woody/shrub encroachment will increase. In addition, the second most vulnerable section is from Brisco to Spillimacheen, followed by Invermere to Brisco, and Golden to Donald. The other projected land cover changes per section and season results are described in supplementary material D of Chapter 3 (Rodrigues et al. 2025), Figures S3 (Invermere to Brisco), S4 (Brisco to Spillimacheen) and S5 (Golden to Donald).

3.3.3. River discharge model

Figure 3.9 (a, b, c) presents the training and validation performance of the seasonal Upper Columbia River discharge models trained from monthly air temperature and precipitation. The model for spring had the highest accuracy, followed by late summer, then summer. Figure 3.10d shows a visual comparison between modeled versus reference values of river discharge at the Upper Columbia River. The higher accuracy of the hydroclimatic models during spring is due to low flow variation during this season, which makes it simpler to simulate. While in late summer and summer, river flow is more dynamic. Overall, the results suggest that the seasonal hydroclimatic-based models captured the river dynamic throughout the 1984 to 2022 period.

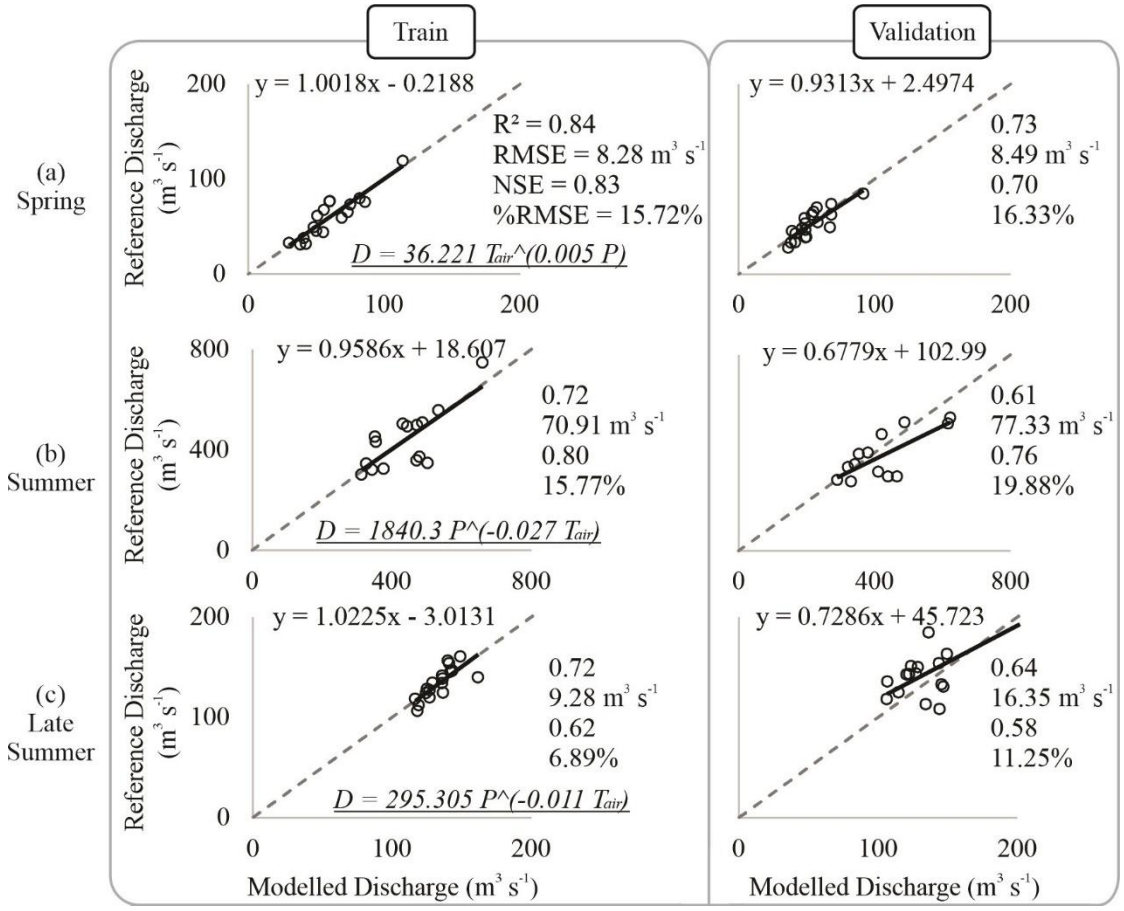

Fig. 3.9. Performance (i.e., R^2, RMSE, NSE, and %RMSE) of the seasonal hydroclimatic-based models for spring (a), summer/peak flow (b), and late summer (c), and the annual variation of reference and seasonal modeled (i.e., train and validation data) river discharge (d) from 1984 to 2022

3.3.4. Projected discharge trends forced by RCP 4.5 and 8.5

The projected Upper Columbia River discharge changes from 1984 to 2040 are illustrated in Figure 3.10 during the spring (Figure 3.11a), summer (Figure 3.11b), late summer (Figure 3.11c). In the spring, the Upper Columbia River discharge tends to increase under RCP 4.5 (+0.78 m^3 s^{-1} $year^{-1}$) and 8.5 (+1.85 m^3 s^{-1} $year^{-1}$). However, the river discharge during summer (RCP 4.5: -1.13 m^3 s^{-1} $year^{-1}$; RCP 8.5: -1.32 m^3 s^{-1} $year^{-1}$) and late summer (RCP 4.5: -0.03 m^3 s^{-1} $year^{-1}$; RCP 8.5: -0.21 m^3 s^{-1} $year^{-1}$) season are projected to reduce. Overall, regardless of the scenarios and season, almost all river discharge projections out to 2040 (except for the RCP 4.5 in late summer) are statistically significant ($p < 0.05$).

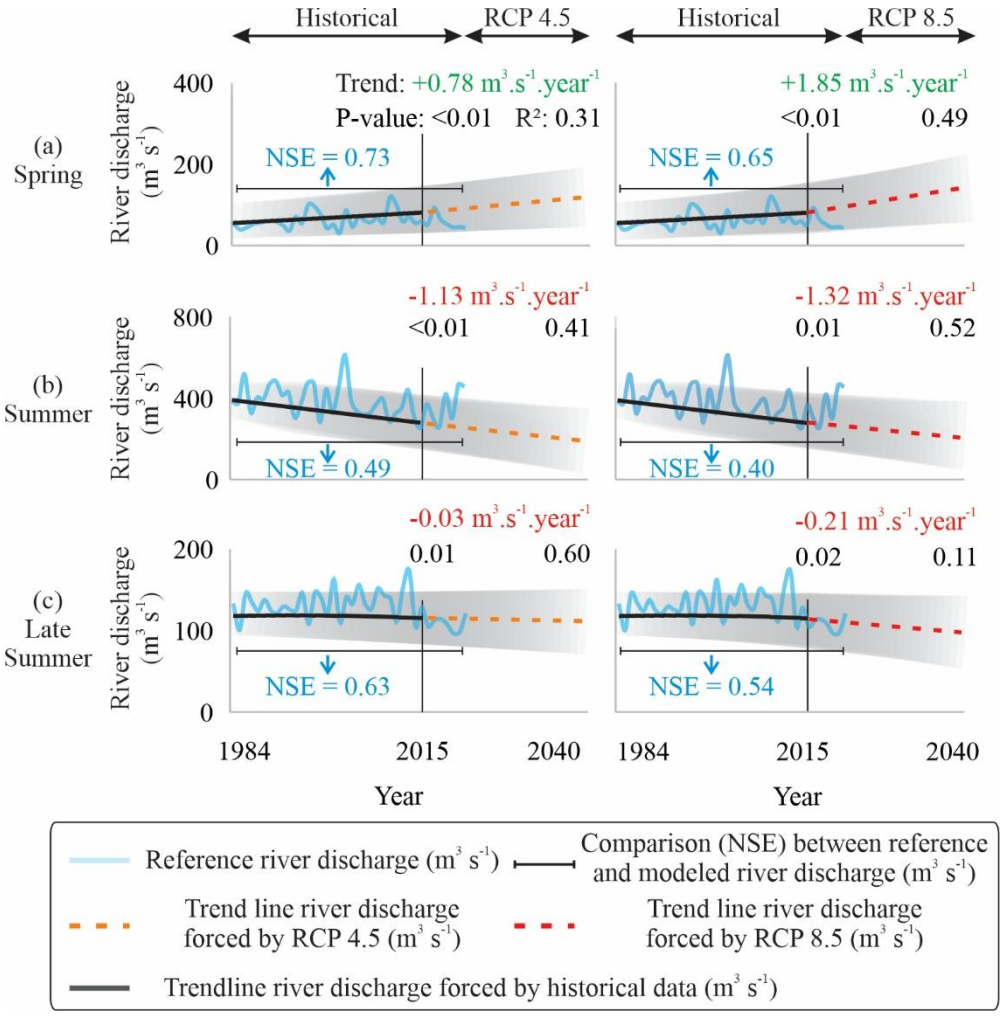

Fig. 3.10. Projected trends (1984 – 2040) of river discharge during spring (a), summer/peak flow (b), late summer (c) and forced by the RCPs 4.5 and 8.5, and a comparison (NSE) between reference and modelled river discharge (1984 – 2022). Shaded areas indicate the 95% confidence intervals for the projected river discharge for each decade.

Furthermore, when comparing the modelled and measured overlapping period of river discharge (i.e., from 1984 to 2022), during spring, the RCP 4.5 (NSE 0.73) better represented the reference river discharge, followed by the RCP 8.5 (R^2 0.65) projections. In summer, the RCP 4.5 paths better reflected the reference discharge, with NSE of 0.49, while RCP 8.5 projections had a lower accuracy, NSE of 0.40. Over the late summer, the RCP 4.5 (NSE 0.63) were better associated with the reference river discharge, and a low representation by the RCP 8.5 (NSE 0.54).

3.3.5. Projected floodplain open water area trends forced by RCPs 4.5 and 8.5

The open water extent of the UCRW from 1984 to 2040 is shown in Figure 3.11, during the spring (Figure 3.11a), summer (Figure 3.11b), late summer (Figure 3.11c). In the spring, the open water area will increase according to the RCP 4.5 (+0.21 km^2 $year^{-1}$) and 8.5 (+0.30 km^2 $year^{-1}$). In contrast, the open water extent during summer (RCP 4.5: -0.05 km^2 $year^{-1}$; RCP 8.5: -0.06 km^2 $year^{-1}$) and late summer (RCP 4.5: -0.07 km^2 $year^{-1}$; RCP 8.5: -0.10 km^2 $year^{-1}$) season will decrease. Overall, all projected trends of open water extent are statistically significant ($p < 0.05$), independent of the scenarios and seasons with the exception of the late summer period.

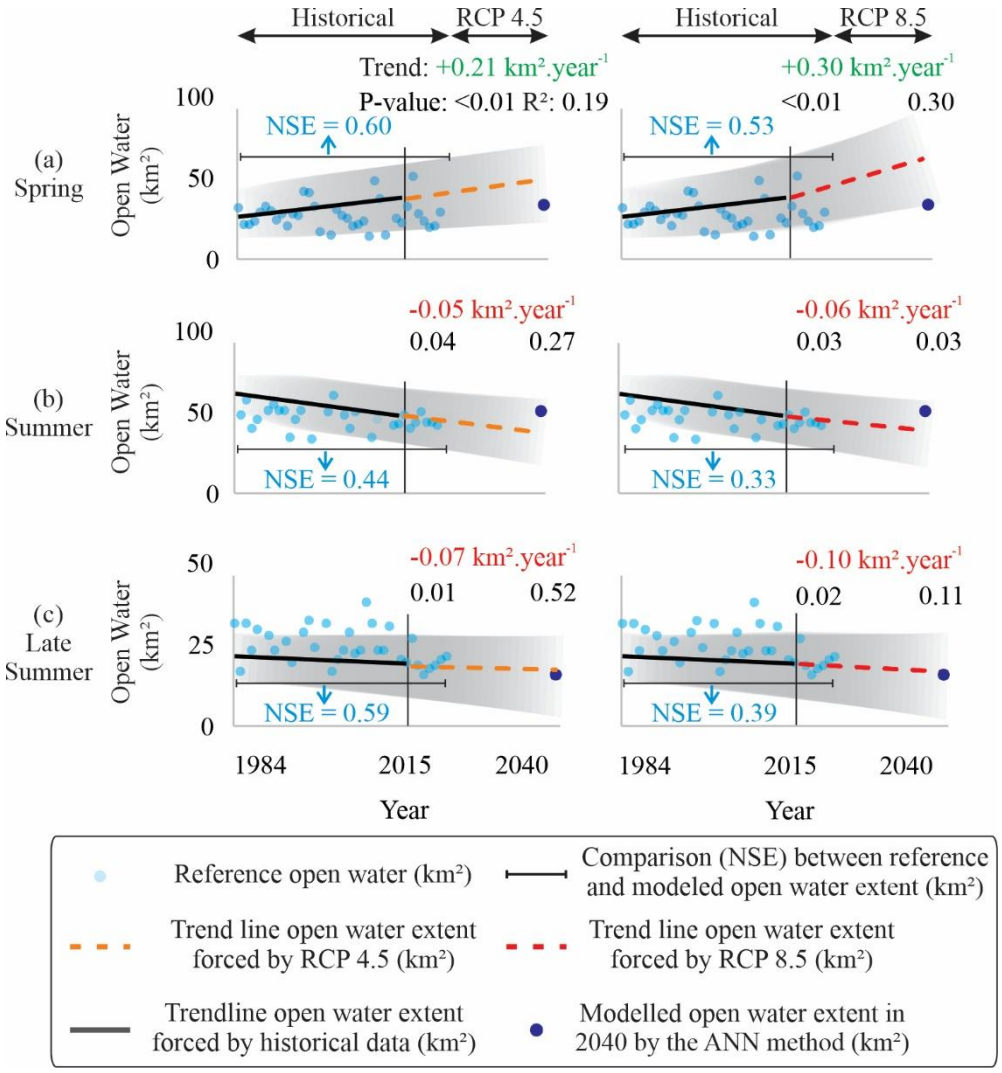

Fig. 3.11. Projected trends (1984 – 2040) of open water extent during spring (a), summer/peak flow (b), and late summer (c) forced by the RCPs 4.5 and 8.5, and a comparison (NSE) between reference and open water extent (1984 – 2022) and the ANN method in 2040. Shaded areas indicate the 95% confidence intervals for the projected open water extent for each decade.

Figure 3.11 illustrates the comparison between the predicted open water extent determined by the Artificial Neural Networks (ANN) findings and the open water projected by both RCPs paths. Overall, the open water LC extent based on ANN were well within the 95% confidence limits of the RCP 4.5 open water area during spring, summer, and late summer. The ANN seasonal open water LC projections deviated further from the RCP 8.5 open water trend line with spring showing the greatest negative deviation.

Moreover, comparing the modelled and measured overlapping period of open water (i.e., from 1984 to 2022), RCP 4.5 better represented the reference open water extent in all seasons (NSE: spring 0.60, summer 0.44, and late summer 0.59) (Figure 11 a,b,c). Meanwhile, the RCP 8.5 paths showed lower accuracy over the spring (NSE 0.53), summer (NSE 0.33) and late summer (NSE 0.39) (Figure 3.11a,b,c).

3.4. Discussion

3.4.1. MOLUSCE as a tool for land cover projection

The overall average kappa coefficient for the predicted LC made by the ANN method was 0.85, which is considered a good accuracy for wetlands (Alam et al. 2021; Aneesha Satya et al. 2020; Rahman et al. 2017), as this ecosystem tends to be very dynamic and difficult to predict. In the spring, open water, marsh, wet meadow, and woody/shrub were easier to discern. In summer, the floodplain is largely covered by water, marsh, and woody vegetation, with a small area of wet meadow visible since high water levels cover the dominant wetland meadow vegetation. In late summer, marsh and woody/shrub vegetation greens up, confusing the vegetated groups. Furthermore, marsh and wet meadow merge, which may diminish late summer kappa values.

Regarding the 2000s – 2020s seasonal LC change maps comparison, overall average kappa coefficient between the reference and predicted LC by the ANN method was 0.82. However, during the Spring (0.78) and Summer (0.84) presented the lowest kappa. This may be explained as LCs changes throughout Spring and Summer are more complex (i.e., with earlier shift of the peak discharge from summer to spring) than in Late Summer (kappa coefficient was the greatest, 0.86), when drying patterns are more predictable (as open water and marsh decrease, wet meadow and woody/shrub grow).

In addition, the projected open water areas in 2040 by the ANN approach and the regression model (i.e., river discharge vs open water) are better aligned with the RCP 4.5

predictions, exhibiting a historical (1984 to 2022) average NSE of 0.54. The results highlight the accuracy of the ANN in projecting the LC extent in the UCRW. Solely relying on the ANN technique would suggest that the wetlands will have reduced open water areas in spring and late summer, while experiencing increased open water throughout summer. However, as the ANN predictions are for a specific time interval (i.e., 2020s and 2040s), the real trend can be masked as wetlands are a fluctuating ecosystem, experiencing both dry and wet periods depending on the season and year. This variability is illustrated in Figure 3.10, which displays the fluctuations in open water areas across the projected seasons and timeframe.

3.4.2. Climate change impacts on the Upper Columbia River floodplain

The projected increase of river discharge and open water during spring in the Upper Columbia River Wetlands (UCRW) are influenced by regional air temperature and precipitation, which since 2015 tend to increase by 0.5 °C and 3 mm, respectively, in the 2040s under RCP 4.5 and 0.8 °C and 5 mm in the 2040s under RCP 8.5. This pattern in the spring season may influence the timing of snowmelt in the UCRW, which usually starts in April (spring) and achieves a peak in June ~ July (summer), and then decreases through August and September (late summer).

The onset of snowmelt may shift to earlier in April as has been observed by Rodrigues et al., (2024) in the same region, who suggested that the peak flow occurred six days earlier in 2022 than in 1984, in addition, the peak flow duration has shortened by ~ one day, with a higher frequency of high discharge events showing more rapid onset. In the UCRW, an earlier shift of the peak discharge from summer to spring is expected in under the RCP 4.5 and RCP 8.5 scenarios. In fact, in 2023, peak discharge in the Nicholson gauge occurred from May 9th to May 25th (as per Environment Canada, 2022c). Tsuruta and Schnorbus (2021) employed a sophisticated hydrological model that incorporated factors such as snow and glacier melt, as well as rainfall, to forecast river discharge in the Mica Basin, north of the UCRW, until the year 2100. The authors found that spring discharge will likely increase under both RCP 4.5 and 8.5 scenarios while summer and late summer discharge are projected to decrease in both scenarios, which aligns with our findings. In Keremeos Creek watershed, southern British Columbia (Canada), Mirmasoudi et al. (2019) observed an earlier timing of snowmelt regarding RCP 4.5 and 8.5 which is to be expected as a function of increasing air temperature. Thus, for RCP 4.5 in the 2040s, snowmelt may start earlier in March and peak in May. However, RCP 8.5 in the 2040s may cause snowmelt to begin sooner (February~May) and

peak in April. In the Columbia watershed (above Donald), Bürger et al. (2011) projected an earlier snowpack melting, resulting in June peak discharges instead of July. The projected warming in this watershed is changing its hydrology from snow-melt-dominated (nival) river discharge to rainfall-driven (pluvial) discharge. In consequence, river discharge in August and September is projected to decrease. In the Spillimacheen, Schnorbus et al. (2012) projected in both scenarios an earlier spring freshet (April and May) and a peak discharge shift from July to June. As a result, July, August, and September 2050s river discharge is expected to decrease substantially.

The river reach section from Spillimacheen to Golden has changed the most, which is likely due to the discharge of the Spillimacheen river and Bugaboo snow and glacier melt streams, where there are a large number of downstream connected wetlands that can quickly respond to river discharge fluctuations. In the Columbia River Basin, glacier runoff generates 25–35% of surface flows during late summer river discharge (Jost et al. 2012), supplying downstream wetlands (Fleming and Dahlke 2014; Milner et al. 2017). However, from 1985 to 2005, Columbia Basin glaciers lost 15% of their area (Bolch et al. 2010) and have been projected to decline 35% to 100% by 2100 (Clarke et al. 2015). These historical and forecast declines in glacier volume and area decreases threaten Columbia River tributaries and wetlands.

Worldwide, climate change will also impact river floodplain ecosystems, for instance, Moradkhani et al. (2010) employed the Soil and Water Assessment Tool in the Tualatin River floodplain (USA) to forecast river flow for a 50-year recurrence interval. The findings indicated a significant decrease (~ –200 m^3 s^{-1}) for low and middle emissions scenarios, while a notable increase (~ +200 m^3 s^{-1}) under high emissions scenario. In rainfall-driven river floodplains, multi-model projections (50–100 years) indicate that by mid-century, mean annual precipitation and runoff are expected to decrease by 10–30% in certain dry subtropical and tropical regions, such as West Africa, Central America, and northeast Brazil, while an increase of 10–40% is projected in some wet tropical regions, including equatorial Africa, the La Plata River, southern Asia, and northern Australia (Milly et al., 2005; Nohara et al., 2006; Li et al., 2007; Bates et al., 2008; Weiland et al., 2012). In the context of extensive river systems and using hydrological simulations, Booij (2004) in the Meuse River (which flows through France, Belgium, and the Netherlands) observed a small reduction in average discharge and a slight rise in discharge variability during extreme events. Meanwhile, Middelkoop et al., (2001) demonstrate that global warming will shift the Rhine River basin (Europe) from a combined rainfall and snowmelt regime to one that is

predominantly dominated by rainfall. This shift is expected to result in higher winter discharge, more intense and earlier peak flows in spring, decreased summer discharge, and prolonged low flow during late summer.

The projected reduction of the river discharge is also a function of decreases in the ratio of snow to total monthly precipitation due to air temperature increases in all RCP projections (Flannigan et al., 2009; Schnorbus et al., 2012; Carver 2017; Wang et al., 2017). If increased precipitation falls as rain, snow accumulation- and melt-dominated watersheds may be more controlled by rainwater runoff (Barnett et al., 2005; Stewart et al., 2005; Knowles et al., 2006; Hamlet et al., 2013; MacDonald et al., 2010), which may also increase the erosion in the mountains (Zhang et al., 2022a) enhancing siltation within the floodplain. Yet, recent studies observed the discharge response to positive trends of temperature, consequently, lower discharges were found during summer and late summer due to increased evaporation rates and a shift in the snow dynamics (Bach et al., 2018; Teuling et al., 2019), which may explain the decrease in permanent water bodies in the UCRW during late summer (Hopkinson et al., 2020).

The projected trends over the discharge and open water may directly affect marsh areas, which are located around these water bodies. Air temperature and precipitation are the main drivers for marsh extent, which may be explained as they react rapidly to hydrological and climatological changes (Keddy, 2011). The positive trends of rainfall and faster snowmelt in the UCRW may create larger open water areas but reduce the marsh fringe area essentially during spring and summer, as the floodplain will have a rapid overflow, submerging the whole marsh area (Keddy and Reznicek, 1986; Keddy, 2011; Van Der Valk, 2005) and a portion of small riparian woody and shrub vegetation (Sparks, 1995; Fischenich and Copeland, 2001; Steiger et al., 2005). Marsh zones may also be influenced by animals, for example beavers as they may control the open water pattern in some regions building dams, which can retain water regardless of the season (Hood and Bayley, 2008).

The close connection between floodplain open water and marsh areas suggests that if open water dries out, marshes will disappear, which has been observed by negative projected annual trend for both land covers. This negative trend in open water and marsh land covers will make room for wet meadow, which is forecasted to increase during summer and late summer and reduce in the spring (Clair et al. 1998; Kołos et al. 2013). Wet meadow area may increase during summer and late summer because the projected precipitation changes during spring (DeBeer et al., 2015, DeBeer et

al., 2021), which will result in faster flooding in a shorter time period. In addition, increasing evaporation rates (Werner et al., 2013; Bach et al., 2018; Teuling et al., 2019) could reduce the area of open water, which may open some space for wet meadow in the end of summer and late summer when the open water levels will tend to be low.

Wet Meadow is an important ecosystem in the UCRW, providing many ecosystem services, for example, carbon sequestration (Wang et al., 2005), nutrient cycle (Zhang et al., 2022b), and aquifer recharge (McClymont et al., 2010). Nevertheless, due to drier conditions, woody/shrub encroachment in this region has been advancing since 1980s (Rodrigues et al., 2024), and according to the projections will continue, which may alter the community composition and structure of the floodplain's flora. The transition from herbaceous (i.e., marshes and wet meadows), to woody or shrub vegetation is not immediate (from one year to the next). Herbaceous plants can be perennials or annuals, and the ecological succession to a woody or shrub state may be dependent on previous conditions (wet or dry) of the floodplain and could exhibit delays, potentially spanning years (Rood et al., 2003). For instance, seeds of the cottonwood species are typically dispersed following the annual peak in river flows, when the receding flood exposes moist areas that are favorable for the seeds to land and germinate (Mahoney and Rood, 1998; Peters et al., 2015). Projected earlier peak discharge (in May or June instead of July) and flood pulse shrink can promote the seedling during summer season, since the cottonwood seedling occurs from May to July (Braatne et al., 1996) and they need exposes moist areas to germinate. However, in the late summer, reduced flow discharges may hinder the initial establishment of cottonwood seedlings at streambank elevations, leading to higher mortality rates among small seedlings (Rood et al., 1998). This is because the post-flood period is crucial for seedling recruitment (Rood et al., 2005; Polzin and Rood, 2006). However, projected increases in rainfall during the late summer could mitigate these adverse effects by raising soil moisture levels. Furthermore, the encroachment of woody shrubs may also impact water movement and the evapotranspiration (Cui et al., 2022), which may also lead to a decrease in soil moisture (Deng et al., 2021).

These projected changes described here may also affect the animals that live within the floodplain. Drier and more shrubby wetlands may be less hospitable for fish and amphibians, which may decline as the open water areas shrink (Hof et al., 2011). Climate-altered wetlands with less open water areas may also reduce the habitat for migratory waterbirds, as they use these wet regions on their way north or for reproduction (Haig et al., 2019). Furthermore, the habitat heterogeneity

and interspersion of herbaceous, woody and shrub vegetation can impact the recruitment and establishment of cottonwood seedlings surrounded by herbaceous plant neighbors. This is because cottonwood seedlings are shade-intolerant (require full sunlight to grow) and experience negative impacts from adult conspecific neighbors, in this case, the herbaceous ones (Comita and Hubbell, 2009; Yin et al., 2023).

In summary, the projected changes for the UCRW include an increase in peak discharge of the Upper Columbia River and a shift in the peak open water area from summer to spring, and reduction by late summer (Figure 3.12). The marsh areas are projected to decrease in all seasons. The wet meadow is projected to decrease in size throughout the spring, but it is expected to expand during the summer and late summer. Woody and shrub encroachment is projected to increase through all seasons.

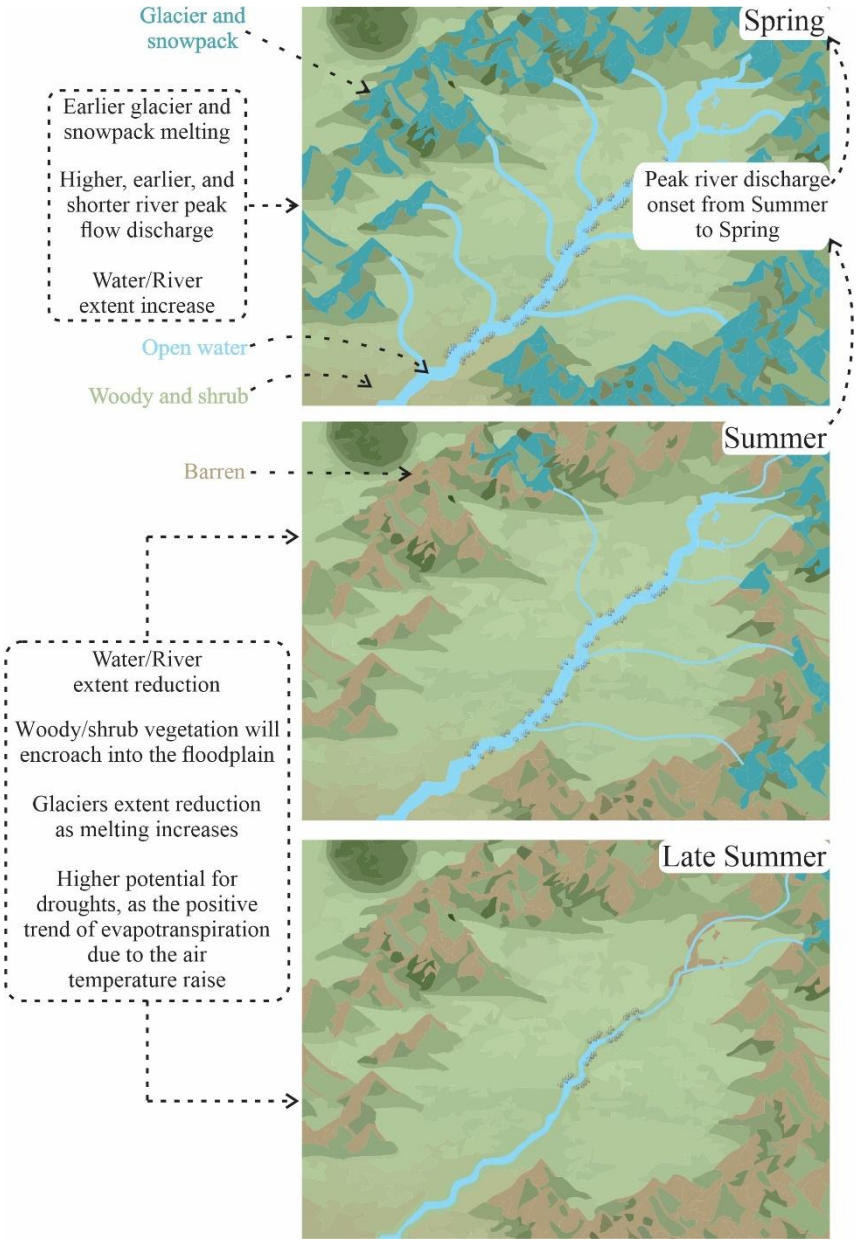

Fig. 3.12. Projected hydrological processes and land cover changes by season for the UCRW.

3.5. Challenges and limitations of river discharge and LC projections

Multiple studies have identified uncertainties and ambiguity in regression models in accurately forecasting and predicting river flow in locations where snow processes play a significant role in driving the runoff and river discharge patterns (Alexander et al., 2016). The primary concern is around the timing of snowmelt in the future and the subsequent response and adaptation of the land and its biota to this shift. Utilising additional hydroclimatological factors, such as surface temperature, ground water, and shortwave or long wave radiation, have the potential

to improve the accuracy of river discharge projections. Moreover, incorporating air temperature and total precipitation from previous months, such as February and March, could potentially enhance model performance, as river discharge reflects prior hydroclimatic conditions. Nonetheless, before spring and after late summer, only baseflow occurs (as per Rodrigues et al., 2024). Incorporating additional one or two months could potentially enhance the performance of hydroclimatic models by providing the model with more degrees of freedom. However, this improvement is likely attributable to the inclusion of periods with lower flows, which simplifies the estimation process.

Utilising GCMs to assess the potential effects of future climate change introduces additional uncertainty, as these models simulate several climatic scenarios known as RCPs. The objective of employing bias correction techniques is to minimise the discrepancy between model simulations and actual measurements within a specified reference period (in our case from 1984 to 2015). The validity of a bias correction strategy for the historical validation/reference period implies its continued validity for future periods (Zheng et al., 2020). This premise has garnered widespread acceptance in research on the effects of climate change (Fiseha et al., 2014; Kundzewicz et al., 2018; Teutschbein and Seibert, 2012).

The main uncertainty about artificial neural networks (ANN) is the only use of two-time steps, i.e., spatial land cover of the past (T1) and present (T2), to predict the future (T3), not allowing the use of other time steps between T1 and T2, which could theoretically improve learning. Nevertheless, terrain drivers enable the ANN to learn spatial correlations between land cover types and change throughout the floodplain, enhancing predictions (Gharaibeh et al., 2020). One potential method for improving the projections involves utilizing additional time periods (for instance, T1 from 1984 to 1988, T2 from 1989 to 1993, to project T3, which spans 1994 to 1998, followed by assessing the accuracy of the projection against the reference dataset; thereafter, using T2 and T3 to estimate T4, covering 1999 to 2003, and so on), providing higher control over the projected land cover. However, the use of extra periods for land cover projections could lead to increased “trend noise”. This occurs as specific periods over time may primarily represent either dry or wet years, thereby affecting the land cover projections with a clear pattern (either wet or dry). Employing T1 (past) and T2 (present) aids in reducing the influence of trend noise. However, it is essential to ensure that both time points selected for the projections are representative periods, avoiding of any specific wet or dry conditions. The ANN algorithm in MOLUSCE is not flawless; however, it is generally more precise than other techniques for spatial land cover prediction

(Gharaibeh et al., 2020; Ahmad et al., 2023). Ultimately, the ANN is consistent with the projected open water areas.

The higher uncertainty in the seasonal hydroclimatic models is (in theory) subject to their simplicity compared to full hydrological models (e.g., Raven hydrological modelling; Craig et al., 2020). Running a full hydrological model is intended to improve analysis, however seasonal parsimonious hydroclimatic models can be used in data-poor places such as montane regions. Finally, a comparison of the uncertainties of the hydroclimatic and full hydrological models would assist in determining whether the parsimonious model can accurately represent river discharge compared with a more complex model. This assessment would show the limit of when a more sophisticated or simpler model is valid.

Another factor that introduces uncertainty in the projections is the behaviour of animals, specifically beaver populations and beaver dams. Beaver dams may significantly expand the area of open water. For instance, it may be presumed that the increase in open water in the wetland is due to the faster melting of snow, however beavers, can play a crucial role in the local hydrology and often increase the area of open water in wetlands (Hood and Bayley, 2008; Hood and Larson, 2013).

3.6. Conclusion

This study employed an Artificial Neural Network (ANN) approach to evaluate linearly projected land-cover trends and changes (from 2020 to 2040) and compared against an independent open water projection for RCP 4.5 and 8.5 climate scenarios based on an empirical river discharge model in the Upper Columbia River Wetlands (UCRW). The ANN predicted land cover with a Kappa of 0.85 for 2020s comparing the reference and projected LC, and a Kappa of 0.82 for 2020s reference and projected LC change maps during the training phase. Significant changes were projected from 2020s to 2040s by the ANN, with a reduction of open water areas during late summer (August to mid-September), which are consistent with RCP 4.5 projections. Furthermore, the peak open water area in the UCRW is expected to transition from summer (late-May to July) to spring (April to mid-May) under both RCP scenarios. Rising air temperatures, with the anticipated associated changes to precipitation amounts, phase and earlier snowmelt, are projected to shift the Columbia River peak discharge from summer to spring under both RCP scenarios. Expected floodplain changes are a reduction in marsh area and increased wet meadow, particularly during

summer and late summer. The area of woody/shrubs was projected to continue increasing across all seasons which is aligned with a general trend of floodplain drying. Projected land cover trends using MOLUSCE assist in determining likely land cover gains and losses, and therefore can support mitigation measures to maintain ecological integrity or ecosystem services within the floodplain. Overall, the UCRW is projected to become greener (woody/shrub) and drier with less open water, especially during late summer.

Acknowledgements

The authors received funding provided by the Natural Sciences and Engineering Research Council of Canada (NSERC; grant no. 2017-04362), Alberta Innovates, the Nexen Fellowship in Water Resources, the Columbia Wetlands Stewardship Partners and the Shuswap Band's Columbia Headwaters Aquatic Restoration Secwépemc Strategy (CHARS) project.

3.7. References

Aguirre, D., Benhumea, A.E., & McLaren, J.R. (2020). Shrub encroachment affects tundra ecosystem properties through their living canopy rather than increased litter inputs. *Soil Biology and Biochemistry*, *153*, 108121. https://doi.org/10.1016/j.soilbio.2020.108121

Ahmad, H., Abdallah, M., Jose, F., Elzain, H.E., Bhuyan, M.S., Shoemaker, D.J., & Selvam, S. (2023). Evaluation and mapping of predicted future land use changes using hybrid models in a coastal area. *Ecological Informatics*, *78*, 102324. https://doi.org/10.1016/j.ecoinf.2023.102324

Alshari, E.A., & Gawali, B.W. (2022). Modeling Land Use Change in Sana'a City of Yemen with MOLUSCE. *Journal of Sensors*, *2022*, 1–15. https://doi.org/10.1155/2022/7419031

Alam, N., Saha, S., Gupta, S., & Chakraborty, S. (2021). Prediction modelling of riverine landscape dynamics in the context of sustainable management of floodplain: a Geospatial approach. *Annals of GIS*, *27*(3), 299–314. https://doi.org/10.1080/19475683.2020.1870558

Alexander, P., Prestele, R., Verburg, P.H., Arneth, A., Baranzelli, C., Silva, F.B.E., Brown, C., Butler, A., Calvin, K., Dendoncker, N., Doelman, J. C., Dunford, R., Engström, K., Eitelberg, D., Fujimori, S., Harrison, P.A., Hasegawa, T., Havlik, P., Holzhauer, S., Rounsevell, M.D.A. (2016). Assessing uncertainties in land cover projections. *Global Change Biology*, *23*(2), 767–781. https://doi.org/10.1111/gcb.13447

Amani, M., Mahdavi, S., Kakooei, M., Ghorbanian, A., Brisco, B., DeLancey, E., Toure, S., & Reyes, E.L. (2021). Wetland Change Analysis in Alberta, Canada Using Four Decades of Landsat Imagery. *IEEE Journal of Selected Topics in Applied Earth Observations and Remote Sensing*, *14*,

10314–10335. https://doi.org/10.1109/jstars.2021.3110460

Althoff, D., Rodrigues, L.N., & Da Silva, D.D. (2020). Impacts of climate change on the evaporation and availability of water in small reservoirs in the Brazilian savannah. *Climatic Change*, *159*(2), 215–232. https://doi.org/10.1007/s10584-020-02656-y

Bach, A.F., Van Der Schrier, G., Melsen, L.A., Tank, A. M.G.K., & Teuling, A.J. (2018). Widespread and Accelerated Decrease of Observed Mean and Extreme Snow Depth Over Europe. *Geophysical Research Letters*, *45*(22). https://doi.org/10.1029/2018gl079799

Barnett, T.P., Adam, J.C., & Lettenmaier, D.P. (2005). Potential impacts of a warming climate on water availability in snow-dominated regions. *Nature*, *438*(7066), 303–309. https://doi.org/10.1038/nature04141

Bates, B. C., Kundzewicz, Z. W., Wu, S., Arnell, N., Burgett, V., & Räisänen, J. (2008). Climate change and water: technical paper of the intergovernmental panel on climate change. *IPCC Secretariat, Geneva*. https://researchportal.helsinki.fi/sv/publications/climate-change-and-water-technical-paper-of-the-intergovernmental

Bjørnæs, C. (2013). A guide to representative concentration pathways. CICERO. Center for International Climate and Environmental Research, 351-357.

Booij, M. J. (2004). Impact of climate change on river flooding assessed with different spatial model resolutions. *Journal of Hydrology*, *303*(1–4), 176–198. https://doi.org/10.1016/j.jhydrol.2004.07.013

Braatne, J. H., Rood, S. B., & Heilman, P. E. (1996). Life history, ecology, and conservation of riparian cottonwoods in North America. *Biology of Populus and its Implications for Management and Conservation*, (Part I), 57-85.

Brinson, M.M., & Malvárez, A.I. (2002). Temperate freshwater wetlands: types, status, and threats. *Environmental Conservation*, *29*(2), 115–133. https://doi.org/10.1017/s0376892902000085

Bucton, B. G. B., Shrestha, S., Kc, S., Mohanasundaram, S., Virdis, S. G., & Chaowiwat, W. (2022b). Impacts of climate and land use change on groundwater recharge under shared socioeconomic pathways: A case of Siem Reap, Cambodia. *Environmental Research*, *211*, 113070. https://doi.org/10.1016/j.envres.2022.113070

Bürger, G., Schulla, J., & Werner, A.T. (2011). Estimates of future flow, including extremes, of the Columbia River headwaters. *Water Resources Research*, *47*(10). https://doi.org/10.1029/2010wr009716

Carli, C.M., & Bayley, S.E. (2015). River connectivity and road crossing effects on floodplain vegetation of the upper Columbia River, Canada. *Ecoscience*, *22*(2–4), 97–107. https://doi.org/10.1080/11956860.2015.1121705

Carver, M. (2017) Water Monitoring and Climate Change in the Upper Columbia Basin: Summary

of Current Status and Opportunities; Columbia Basin Trust: Castlegar, BC, Canada.

Chatterjee, A., Blom, E., Gujja, B., Jacimovic, R., Beevers, L., O'Keeffe, J., Beland, M., & Biggs, T. (2010). WWF Initiatives to Study the Impact of Climate Change on Himalayan High-altitude Wetlands (HAWs). *Mountain Research and Development*, *30*(1), 42–52. https://doi.org/10.1659/mrd-journal-d-09-00091.1

Chen, J., Brissette, F.P., Chaumont, D., & Braun, M. (2013). Finding appropriate bias correction methods in downscaling precipitation for hydrologic impact studies over North America. *Water Resources Research*, *49*(7), 4187–4205. https://doi.org/10.1002/wrcr.20331

Clair, T. A., Warner, B.G., Robarts, R., Murkin, H., Lilley, J., Mortsch, L., ... & Avis, W. (1998). Canadian inland wetlands and climate change. The Canada country study: climate impacts and adaptation. National sectoral volume. Environment Canada, Ottawa, Ontario, Canada, 189-218.

Clarke, G.K.C., Jarosch, A.H., Anslow, F.S., Radić, V., & Menounos, B. (2015). Projected deglaciation of western Canada in the twenty-first century. *Nature Geoscience*, *8*(5), 372–377. https://doi.org/10.1038/ngeo2407

Comita, L. S., & Hubbell, S. P. (2009). Local neighborhood and species' shade tolerance influence survival in a diverse seedling bank. *Ecology*, *90*(2), 328–334. https://doi.org/10.1890/08-0451.1

Cooper, D.J., Kaczynski, K.M., Sueltenfuss, J., Gaucherand, S., & Hazen, C. (2017). Mountain wetland restoration: the role of hydrologic regime and plant introductions after 15 years in the Colorado Rocky Mountains, USA. *Ecological Engineering*, 101, 46-59. https://doi.org/10.1016/j.ecoleng.2017.01.017

Craig, J.R., Brown, G., Chlumsky, R., Jenkinson, R.W., Jost, G., Lee, K., Mai, J., Serrer, M., Sgro, N., Shafii, M., Snowdon, A.P., & Tolson, B.A. (2020). Flexible watershed simulation with the Raven hydrological modelling framework. *Environmental Modelling & Software*, *129*, 104728. https://doi.org/10.1016/j.envsoft.2020.104728

Cui, J., Lian, X., Huntingford, C., Gimeno, L., Wang, T., Ding, J., He, M., Xu, H., Chen, A., Gentine, P., & Piao, S. (2022). Global water availability boosted by vegetation-driven changes in atmospheric moisture transport. *Nature Geoscience*, *15*(12), 982–988. https://doi.org/10.1038/s41561-022-01061-7

DeBeer, C.M., Wheater, H.S., Pomeroy, J.W., Barr, A.G., Baltzer, J.L., Johnstone, J. F., Turetsky, M.R., Stewart, R.E., Hayashi, M., Van Der Kamp, G., Marshall, S., Campbell, E., Marsh, P., Carey, S.K., Quinton, W.L., Li, Y., Razavi, S., Berg, A., McDonnell, J.J., Pietroniro, A. (2021). Summary and synthesis of Changing Cold Regions Network (CCRN) research in the interior of western Canada – Part 2: Future change in cryosphere, vegetation, and hydrology. *Hydrology and Earth System Sciences*, *25*(4), 1849–1882. https://doi.org/10.5194/hess-25-1849-2021

DeBeer, C.M., Wheater, H.S., Carey, S.K., & Chun, K.P. (2015). Recent climatic, cryospheric, and hydrological changes over the interior of western Canada: a synthesis and review. *Hydrology and Earth System Sciences*. https://doi.org/10.5194/hessd-12-8615-2015

De Reu, J., Bourgeois, J., Bats, M., Zwertvaegher, A., Gelorini, V., De Smedt, P., Chu, W., Antrop, M., De Maeyer, P., Finke, P., Van Meirvenne, M., Verniers, J., & Crombé, P. (2012). Application of the topographic position index to heterogeneous landscapes. *Geomorphology*, *186*, 39–49. https://doi.org/10.1016/j.geomorph.2012.12.015

Deng, Y., Li, X., Shi, F., & Hu, X. (2021). Woody plant encroachment enhanced global vegetation greening and ecosystem water-use efficiency. *Global Ecology and Biogeography*, *30*(12), 2337–2353. https://doi.org/10.1111/geb.13386

Díaz, S., Demissew, S., Carabias, J., Joly, C., Lonsdale, M., Ash, N., Larigauderie, A., Adhikari, J.R., Arico, S., Báldi, A., Bartuska, A., Baste, I.A., Bilgin, A., Brondizio, E., Chan, K.M., Figueroa, V.E., Duraiappah, A., Fischer, M., Hill, R., Zlatanova, D. (2014). The IPBES Conceptual Framework — connecting nature and people. *Current Opinion in Environmental Sustainability*, *14*, 1–16. https://doi.org/10.1016/j.cosust.2014.11.002

Diomede, T., Davolio, S., Marsigli, C., Miglietta, M.M., Moscatello, A., Papetti, P., Paccagnella, T., Buzzi, A., & Malguzzi, P. (2008). Discharge prediction based on multi-model precipitation forecasts. *Meteorology and Atmospheric Physics*, *101*(3–4), 245–265. https://doi.org/10.1007/s00703-007-0285-0

Edwards, T.W., Birks, S.J., Luckman, B.H., & MacDonald, G.M. (2008). Climatic and hydrologic variability during the past millennium in the eastern Rocky Mountains and northern Great Plains of western Canada. *Quaternary Research*, *70*(2), 188–197. https://doi.org/10.1016/j.yqres.2008.04.013

Environment Canada.: "Historical climate data." Environment Canada. Accessed November, 2022. https://climate.weather.gc.ca/historical_data/search_historic_data_e.html, 2022a

Environment Canada.: "HYDAT database". Environment Canada. Accessed November, 2022. https://wateroffice.ec.gc.ca/search/historical_e.html, 2022b

Environment Canada.: "HYDAT database". Environment Canada. Accessed November, 2023. https://wateroffice.ec.gc.ca/report/historical_e.html?stn=08NA002, 2022c

Environment and Climate Change Canada/Environnement et Changement Climatique Canada. (2021). CMIP6 ensemble of daily predictor variables (Version 1) [Dataset]. Canadian Climate Data and Scenarios. https://climate-scenarios.canada.ca/?page=pred-cmip6

Fischenich, J.C., & Copeland, R.R. (2001). Environmental considerations for vegetation in flood control channels. *This Digital Resource Was Created in Microsoft Word and Adobe Acrobat*. https://erdc-library.erdc.dren.mil/jspui/bitstream/11681/8536/1/12654.pdf

Fiseha, B., Setegn, S., Melesse, A., Volpi, E., & Fiori, A. (2014). Impact of Climate Change on the Hydrology of Upper Tiber River Basin Using Bias Corrected Regional Climate Model. *Water Resources Management*, *28*(5), 1327–1343. https://doi.org/10.1007/s11269-014-0546-x

Flannigan, M.D., Krawchuk, M.A., de Groot, W.J., Wotton, B.M., & Gowman, L.M. (2009). Implications of changing climate for global wildland fire. *International journal of wildland fire*,

18(5), 483-507. https://doi.org/10.1071/WF08187

Fleming, S.W., & Dahlke, H.E. (2014). Modulation of linear and nonlinear hydroclimatic dynamics by mountain glaciers in Canada and Norway: Results from information-theoretic polynomial selection. *Canadian Water Resources Journal / Revue Canadienne Des Ressources Hydriques*, *39*(3), 324–341. https://doi.org/10.1080/07011784.2014.942164

Formica, A., Farrer, E.C., Ashton, I.W., and Suding, K.N.: Shrub expansion over the past 62 years in Rocky Mountain alpine tundra: possible causes and consequences. Arctic, Antarctic, and Alpine Research, 46(3), 616-631, https://doi.org/10.1657/1938-4246-46.3.616, 2014.

Gharaibeh, A., Shaamala, A., Obeidat, R., & Al-Kofahi, S. (2020). Improving land-use change modeling by integrating ANN with Cellular Automata-Markov Chain model. *Heliyon*, *6*(9), e05092. https://doi.org/10.1016/j.heliyon.2020.e05092

Gašparović, M., & Jogun, T. (2017). The effect of fusing Sentinel-2 bands on land-cover classification. *International Journal of Remote Sensing*, *39*(3), 822–841. https://doi.org/10.1080/01431161.2017.1392640

Girardin, M.P., Tardif, J.C., Flannigan, M.D., & Bergeron, Y. (2006). Forest Fire-Conducive Drought Variability in the Southern Canadian Boreal Forest and Associated Climatology Inferred from Tree Rings. *Canadian Water Resources Journal / Revue Canadienne Des Ressources Hydriques*, *31*(4), 275–296. https://doi.org/10.4296/cwrj3104275

Glines, L.M. (2012). Woody plant encroachment into grasslands within the Red Deer River drainage, Alberta. *ERA: Education and Research Archive*. https://doi.org/10.7939/r33h5v

Gomes, L., Bianchi, F., Cardoso, I., Schulte, R., Arts, B., & Filho, E.F. (2020). Land use and land cover scenarios: An interdisciplinary approach integrating local conditions and the global shared socioeconomic pathways. *Land Use Policy*, *97*, 104723. https://doi.org/10.1016/j.landusepol.2020.104723

Haig, S.M., Murphy, S.P., Matthews, J.H., Arismendi, I., & Safeeq, M. (2019). Climate-Altered Wetlands Challenge Waterbird Use and Migratory Connectivity in Arid Landscapes. *Scientific Reports*, *9*(1). https://doi.org/10.1038/s41598-019-41135-y

Hamlet, A.F., Elsner, M.M., Mauger, G. S., Lee, S., Tohver, I., & Norheim, R.A. (2013). An Overview of the Columbia Basin Climate Change Scenarios Project: Approach, Methods, and Summary of Key Results. *ATMOSPHERE-OCEAN*, *51*(4), 392–415. https://doi.org/10.1080/07055900.2013.819555

Harrington, J., & Flannigan, M. (1993). A Model for the Frequency of Long Periods of Drought at Forested Stations in Canada. *Journal of Applied Meteorology*, *32*(11), 1708–1716. https://doi.org/10.1175/1520-0450(1993)032

Hof, C., Araújo, M.B., Jetz, W., & Rahbek, C. (2011). Additive threats from pathogens, climate and land-use change for global amphibian diversity. *Nature*, *480*(7378), 516–519.

https://doi.org/10.1038/nature10650

Hood, G. A., & Larson, D. G. (2013). Beaver-Created Habitat Heterogeneity Influences Aquatic Invertebrate Assemblages in Boreal Canada. *Wetlands*, *34*(1), 19–29. https://doi.org/10.1007/s13157-013-0476-z

Hood, G.A., & Bayley, S.E. (2008). Beaver (Castor canadensis) mitigate the effects of climate on the area of open water in boreal wetlands in western Canada. *Biological Conservation*, *141*(2), 556–567. https://doi.org/10.1016/j.biocon.2007.12.003

Hopkinson, C., Fuoco, B., Grant, T., Bayley, S.E., Brisco, B., & MacDonald, R. (2020). Wetland Hydroperiod Change Along the Upper Columbia River Floodplain, Canada, 1984 to 2019. *Remote Sensing*, *12*(24), 4084. https://doi.org/10.3390/rs12244084

Hrach, D.M., Petrone, R.M., Green, A., & Khomik, M. (2022). Analysis of growing season carbon and water fluxes of a subalpine wetland in the Canadian Rocky Mountains: implications of shade on ecosystem water use efficiency. Hydrological Processes, 36(1), e14425.

Hussain, M., & Mahmud, I. (2019). pyMannKendall: a python package for non parametric Mann Kendall family of trend tests. *The Journal of Open Source Software*, *4*(39), 1556. https://doi.org/10.21105/joss.01556

IPCC, 2014: Climate Change 2014: Synthesis Report. Contribution of Working Groups I, II and III to the Fifth Assessment Report of the Intergovernmental Panel on Climate Change [Core Writing Team, R.K. Pachauri and L.A. Meyer (eds.)]. IPCC, Geneva, Switzerland, 151 pp.

IPCC, 2021: Summary for Policymakers. In: Climate Change 2021: The Physical Science Basis. Contribution of Working Group I to the Sixth Assessment Report of the Intergovernmental Panel on Climate Change [Masson-Delmotte, V., P. Zhai, A. Pirani, S. L. Connors, C. Péan, S. Berger, N. Caud, Y. Chen, L. Goldfarb, M. I. Gomis, M. Huang, K. Leitzell, E. Lonnoy, J.B.R. Matthews, T. K. Maycock, T. Waterfield, O. Yelekçi, R. Yu & B. Zhou (eds.)]. Cambridge University Press. In Press.

Johnson, W.C., Millett, B.V., Gilmanov, T., Voldseth, R.A., Guntenspergen, G. R., & Naugle, D.E. (2005). Vulnerability of Northern Prairie Wetlands to Climate Change. *BioScience*, *55*(10), 863. https://doi.org/10.1641/0006-3568(2005)055

Jost, G., Moore, R.D., Menounos, B., & Wheate, R. (2012). Quantifying the contribution of glacier runoff to streamflow in the upper Columbia River Basin, Canada. *Hydrology and Earth System Sciences*, *16*(3), 849–860. https://doi.org/10.5194/hess-16-849-2012

Kamaraj, M., & Rangarajan, S. (2022). Predicting the future land use and land cover changes for Bhavani basin, Tamil Nadu, India, using QGIS MOLUSCE plugin. *Environmental Science and Pollution Research*, *29*(57), 86337–86348. https://doi.org/10.1007/s11356-021-17904-6

Keddy, P.A. (2011). Wetland ecology: principles and conservation. *Choice Reviews Online*, *48*(08), 48–4471. https://doi.org/10.5860/choice.48-4471

Keddy, P., & Reznicek, A. (1986). Great Lakes Vegetation Dynamics: The Role of Fluctuating Water Levels and Buried Seeds. *Journal of Great Lakes Research*, *12*(1), 25–36. https://doi.org/10.1016/s0380-1330(86)71697-3

Kendall, M.G. (1957). Rank Correlation Methods. *Biometrika*, *44*(1/2), 298. https://doi.org/10.2307/2333282

Kienzle, S.W. (2006). The Use of the Recession Index as an Indicator for Streamflow Recovery After a Multi-Year Drought. *Water Resources Management*, *20*(6), 991–1006. https://doi.org/10.1007/s11269-006-9019-1

Knowles, N., Dettinger, M.D., & Cayan, D.R. (2006). Trends in Snowfall versus Rainfall in the Western United States. *Journal of Climate*, *19*(18), 4545–4559. https://doi.org/10.1175/jcli3850.1

Kołos, A., & Banaszuk, P. (2013). Mowing as a tool for wet meadows restoration: Effect of long-term management on species richness and composition of sedge-dominated wetland. *Ecological Engineering*, *55*, 23–28. https://doi.org/10.1016/j.ecoleng.2013.02.008

Koomen, E., & Beurden, J.B. (2011). *Land-Use Modelling in Planning Practice*. Springer Science & Business Media.

Kundzewicz, Z., Krysanova, V., Benestad, R., Hov, Ø., Piniewski, M., & Otto, I. (2017). Uncertainty in climate change impacts on water resources. *Environmental Science & Policy*, *79*, 1–8. https://doi.org/10.1016/j.envsci.2017.10.008

Lau, K.H., & Kam, B.H. (2005). A Cellular Automata Model for Urban Land-Use Simulation. *Environment and Planning B Planning and Design*, *32*(2), 247–263. https://doi.org/10.1068/b31110

Leipe, S.C., & Carey, S.K. (2021). Rapid shrub expansion in a subarctic mountain basin revealed by repeat airborne LiDAR. *Environmental Research Communications*, *3*(7), 071001. https://doi.org/10.1088/2515-7620/ac0e0c

Levenberg, K. (1944). A method for the solution of certain non-linear problems in least squares. *Quarterly of Applied Mathematics*, *2*(2), 164–168. https://doi.org/10.1090/qam/10666

Li, K., Coe, M., Ramankutty, N., & De Jong, R. (2007). Modeling the hydrological impact of land-use change in West Africa. *Journal of Hydrology*, *337*(3–4), 258–268. https://doi.org/10.1016/j.jhydrol.2007.01.038

Löffler, J., Anschlag, K., Baker, B., Finch, O., Wundram, D., Diekkrüger, B., Schröder, B., Pape, R., & Lundberg, A. (2011). Mountain ecosystem response to global change. *Erdkunde*, *65*(2), 189–213. https://doi.org/10.3112/erdkunde.2011.02.06

Lottig, N.R., Buffam, I., & Stanley, E.H. (2013). Comparisons of wetland and drainage lake influences on stream dissolved carbon concentrations and yields in a north temperate lake-rich region. *Aquatic Sciences*, *75*(4), 619–630. https://doi.org/10.1007/s00027-013-0305-8

MacDonald, R.J., Byrne, J.M., Kienzle, S.W., & Larson, R.P. (2010). Assessing the Potential

Impacts of Climate Change on Mountain Snowpack in the St. Mary River Watershed, Montana. *Journal of Hydrometeorology*, *12*(2), 262–273. https://doi.org/10.1175/2010jhm1294.1

Mahoney, J. M., & Rood, S. B. (1998). Streamflow requirements for cottonwood seedling recruitment—An integrative model. *Wetlands*, *18*(4), 634–645. https://doi.org/10.1007/bf03161678

Mann, H. B. (1945). Nonparametric Tests Against Trend. *Econometrica*, *13*(3), 245. https://doi.org/10.2307/1907187

Marquardt, D.W. (1963). An Algorithm for Least-Squares Estimation of Nonlinear Parameters. *Journal of the Society for Industrial and Applied Mathematics*, *11*(2), 431–441. https://doi.org/10.1137/0111030

McClymont, A.F., Hayashi, M., Bentley, L.R., Muir, D., & Ernst, E. (2010). Groundwater flow and storage within an alpine meadow-talus complex. *Hydrology and Earth System Sciences*, *14*(6), 859–872. https://doi.org/10.5194/hess-14-859-2010

Middelkoop, H., Daamen, K., Gellens, D., Grabs, W., Kwadijk, J. C. J., Lang, H., Parmet, B. W. a. H., Schädler, B., Schulla, J., & Wilke, K. (2001). Impact of climate change on hydrological regimes and water resources management in the Rhine Basin. *Climatic Change*, *49*(1/2), 105–128. https://doi.org/10.1023/a:1010784727448

Milly, P. C. D., Dunne, K. A., & Vecchia, A. V. (2005). Global pattern of trends in streamflow and water availability in a changing climate. *Nature*, *438*(7066), 347–350. https://doi.org/10.1038/nature04312

Milner, A.M., Khamis, K., Battin, T.J., Brittain, J.E., Barrand, N.E., Füreder, L., Cauvy-Fraunié, S., Gíslason, G.M., Jacobsen, D., Hannah, D.M., Hodson, A.J., Hood, E., Lencioni, V., Ólafsson, J.S., Robinson, C.T., Tranter, M., & Brown, L.E. (2017). Glacier shrinkage driving global changes in downstream systems. *Proceedings of the National Academy of Sciences*, *114*(37), 9770–9778. https://doi.org/10.1073/pnas.1619807114

Mirmasoudi, S., Byrne, J., MacDonald, R., Johnson, D., & Kroebel, R. (2019). Modelling historical and potential future climate impacts on Keremeos Creek, an Okanagan-Similkameen watershed, British Columbia, Canada: Part I. Forecasting change in spring and summer water supply and demand. *Canadian Water Resources Journal / Revue Canadienne Des Ressources Hydriques*, *44*(4), 350–366. https://doi.org/10.1080/07011784.2019.1640137

Moore, R.D., Fleming, S.W., Menounos, B., Wheate, R., Fountain, A., Stahl, K., Holm, K., & Jakob, M. (2008). Glacier change in western North America: influences on hydrology, geomorphic hazards and water quality. *Hydrological Processes*, *23*(1), 42–61. https://doi.org/10.1002/hyp.7162

Moore, R.D., Pelto, B., Menounos, B., & Hutchinson, D. (2020). Detecting the Effects of Sustained Glacier Wastage on Streamflow in Variably Glacierized Catchments. *Frontiers in Earth Science*, *8*. https://doi.org/10.3389/feart.2020.00136

Moradkhani, H., Baird, R. G., & Wherry, S. A. (2010). Assessment of climate change impact on floodplain and hydrologic ecotones. *Journal of Hydrology*, *395*(3–4), 264–278.

https://doi.org/10.1016/j.jhydrol.2010.10.038

Moser, K., Baron, J., Brahney, J., Oleksy, I., Saros, J., Hundey, E., Sadro, S., Kopáček, J., Sommaruga, R., Kainz, M., Strecker, A., Chandra, S., Walters, D., Preston, D., Michelutti, N., Lepori, F., Spaulding, S., Christianson, K., Melack, J., & Smol, J. (2019). Mountain lakes: Eyes on global environmental change. *Global and Planetary Change*, *178*, 77–95. https://doi.org/10.1016/j.gloplacha.2019.04.001

Muhammad, R., Zhang, W., Abbas, Z., Guo, F., & Gwiazdzinski, L. (2022). Spatiotemporal Change Analysis and Prediction of Future Land Use and Land Cover Changes Using QGIS MOLUSCE Plugin and Remote Sensing Big Data: A Case Study of Linyi, China. *Land*, *11*(3), 419. https://doi.org/10.3390/land11030419

Nash, J., & Sutcliffe, J. (1970). River flow forecasting through conceptual models part I — A discussion of principles. *Journal of Hydrology*, *10*(3), 282–290. https://doi.org/10.1016/0022-1694(70)90255-6

NextGIS (2017) MOLUSCE-quick and convenient aanalysis of Land- Cover Changes. https:// nextg is. com/ blog/ molus ce/ (accessed 25 February 2023)

Nohara, D., Kitoh, A., Hosaka, M., & Oki, T. (2006). Impact of Climate Change on River Discharge Projected by Multimodel Ensemble. *Journal of Hydrometeorology*, *7*(5), 1076–1089. https://doi.org/10.1175/jhm531.1

Peters, D., Caissie, D., Monk, W., Rood, S., & St-Hilaire, A. (2015). An ecological perspective on floods in Canada. *Canadian Water Resources Journal / Revue Canadienne Des Ressources Hydriques*, *41*(1–2), 288–306. https://doi.org/10.1080/07011784.2015.1070694

Polzin, M. L., & Rood, S. B. (2006). Effective disturbance: Seedling safe sites and patch recruitment of riparian cottonwoods after a major flood of a mountain river. *Wetlands*, *26*(4), 965–980. https://doi.org/10.1672/0277-5212(2006)26

Rahman, M.T.U., Tabassum, F., Rasheduzzaman, M., Saba, H., Sarkar, L., Ferdous, J., Uddin, S.Z., & Islam, A.Z.M.Z. (2017). Temporal dynamics of land use/land cover change and its prediction using CA-ANN model for southwestern coastal Bangladesh. *Environmental Monitoring and Assessment*, *189*(11). https://doi.org/10.1007/s10661-017-6272-0

Rodrigues, I.S., Hopkinson, C., Chasmer, L., MacDonald, R.J., Bayley, S.E., & Brisco, B. (2024). Multi-decadal floodplain classification and trend analysis in the Upper Columbia River valley, British Columbia. Hydrology and Earth System Sciences, 28(10), 2203–2221. https://doi.org/10.5194/hess-28-2203-2024

Rood, S. B., Samuelson, G. M., Braatne, J. H., Gourley, C. R., Hughes, F. M., & Mahoney, J. M. (2005). Managing river flows to restore floodplain forests. Frontiers in Ecology and the Environment, 3(4), 193-201. https://doi.org/10.1890/1540-9295(2005)003[0193:MRFTRF]2.0.CO;2

Rood, S. B., Braatne, J. H., & Hughes, F. M. R. (2003). Ecophysiology of riparian cottonwoods:

stream flow dependency, water relations and restoration. *Tree Physiology*, *23*(16), 1113–1124. https://doi.org/10.1093/treephys/23.16.1113

Rood, S. B., Kalischuk, A. R., & Mahoney, J. M. (1998). Initial cottonwood seedling recruitment following the flood of the century of the Oldman River, Alberta, Canada. *Wetlands*, *18*(4), 557–570. https://doi.org/10.1007/bf03161672

Rooney, R.C., Carli, C., & Bayley, S.E. (2013). River Connectivity Affects Submerged and Floating Aquatic Vegetation in Floodplain Wetlands. *Wetlands*, *33*(6), 1165–1177. https://doi.org/10.1007/s13157-013-0471-4

Schnorbus, M., Werner, A., & Bennett, K. (2012). Impacts of climate change in three hydrologic regimes in British Columbia, Canada. *Hydrological Processes*, *28*(3), 1170–1189. https://doi.org/10.1002/hyp.9661

Shrestha, M., Acharya, S.C., & Shrestha, P.K. (2017). Bias correction of climate models for hydrological modelling – are simple methods still useful? *Meteorological Applications*, *24*(3), 531–539. https://doi.org/10.1002/met.1655

Silva, W.P.D., Silva, C.M., Cavalcanti, C.G., Silva, D.D., Soares, I.B., Oliveira, J.A., & Silva, C.D. (2004). LAB fit curve fitting: a software in portuguese for treatment of experimental data. *Revista Brasileira de Ensino de Física*, 26, 419-427. https://doi.org/10.1590/S1806-11172004000400018

Sparks, R.E. (1995). Need for Ecosystem Management of Large Rivers and Their Floodplains. *BioScience*, *45*(3), 168–182. https://doi.org/10.2307/1312556

Stahl, K., & Moore, R. D. (2006). Influence of watershed glacier coverage on summer streamflow in British Columbia, Canada. *Water Resources Research*, *42*(6). https://doi.org/10.1029/2006wr005022

Steiger, J., Tabacchi, E., Dufour, S., Corenblit, D., & Peiry, J.L. (2005). Hydrogeomorphic processes affecting riparian habitat within alluvial channel–floodplain river systems: a review for the temperate zone. *River Research and Applications*, 21(7), 719-737. https://doi.org/10.1002/rra.879

Stewart, I.T.: Changes in snowpack and snowmelt runoff for key mountain regions. Hydrological Processes: An International Journal, 23(1), 78-94, https://doi.org/10.1002/hyp.7128, 2009.

Stewart, I.T., Cayan, D.R., & Dettinger, M.D. (2005). Changes toward Earlier Streamflow Timing across Western North America. *Journal of Climate*, *18*(8), 1136–1155. https://doi.org/10.1175/jcli3321.1

Swart, N.C., Cole, J.N., Kharin, V.V., Lazare, M., Scinocca, J.F., Gillett, N.P., ... & Winter, B. (2019). The Canadian earth system model version 5 (CanESM5. 0.3). *Geoscientific Model Development*, 12(11), 4823-4873. https://doi.org/10.5194/gmd-12-4823-2019

Teuling, A.J., De Badts, E. a. G., Jansen, F.A., Fuchs, R., Buitink, J., Van Dijke, A.J. H., & Sterling, S. M. (2019). Climate change, reforestation/afforestation, and urbanization impacts on

evapotranspiration and streamflow in Europe. *Hydrology and Earth System Sciences*, *23*(9), 3631–3652. https://doi.org/10.5194/hess-23-3631-2019

Teutschbein, C., & Seibert, J. (2012). Bias correction of regional climate model simulations for hydrological climate-change impact studies: Review and evaluation of different methods. *Journal of Hydrology*, *456–457*, 12–29. https://doi.org/10.1016/j.jhydrol.2012.05.052

Tsuruta, K., & Schnorbus, M.A. (2021). Exploring the operational impacts of climate change and glacier loss in the upper Columbia River Basin, Canada. *Hydrological Processes*, *35*(7). https://doi.org/10.1002/hyp.14253

Thomson, A.M., Calvin, K.V., Smith, S.J., Kyle, G.P., Volke, A., Patel, P., Delgado-Arias, S., Bond-Lamberty, B., Wise, M. A., Clarke, L. E., & Edmonds, J. A. (2011). RCP4.5: a pathway for stabilization of radiative forcing by 2100. *Climatic Change*, *109*(1–2), 77–94. https://doi.org/10.1007/s10584-011-0151-4

Van Der Valk, A.G. (2005). Water-level fluctuations in North American prairie wetlands. *Hydrobiologia*, *539*(1), 171–188. https://doi.org/10.1007/s10750-004-4866-3

VanShaar, J. R., Haddeland, I., & Lettenmaier, D.P. (2002). Effects of land-cover changes on the hydrological response of interior Columbia River basin forested catchments. *Hydrological Processes*, *16*(13), 2499–2520. https://doi.org/10.1002/hyp.1017

Wang, W.Y., Wang, Q.J., Wang, C.Y., Shi, H. L., Li, Y., & Wang, G. (2005). The effect of land management on carbon and nitrogen status in plants and soils of alpine meadows on the Tibetan plateau. *Land Degradation and Development*, *16*(5), 405–415. https://doi.org/10.1002/ldr.661

Wang, X., Parisien, M., Taylor, S.W., Candau, J., Stralberg, D., Marshall, G.A., Little, J.M., & Flannigan, M.D. (2017). Projected changes in daily fire spread across Canada over the next century. *Environmental Research Letters*, *12*(2), 025005. https://doi.org/10.1088/1748-9326/aa5835

Wang, X., Studens, K., Parisien, M., Taylor, S.W., Candau, J., Boulanger, Y., & Flannigan, M.D. (2020). Projected changes in fire size from daily spread potential in Canada over the 21st century. *Environmental Research Letters*, *15*(10), 104048. https://doi.org/10.1088/1748-9326/aba101

Weiland, F. C. S., Van Beek, L. P. H., Kwadijk, J. C. J., & Bierkens, M. F. P. (2012). Global patterns of change in discharge regimes for 2100. *Hydrology and Earth System Sciences*, *16*(4), 1047–1062. https://doi.org/10.5194/hess-16-1047-2012

Werner, A.T., Schnorbus, M.A., Shrestha, R.R., & Eckstrand, H.D. (2013). Spatial and Temporal Change in the Hydro-Climatology of the Canadian Portion of the Columbia River Basin under Multiple Emissions Scenarios. *ATMOSPHERE-OCEAN*, *51*(4), 357–379. https://doi.org/10.1080/07055900.2013.821400

Williamson, C.E., Dodds, W., Kratz, T.K., & Palmer, M.A. (2008). Lakes and streams as sentinels of environmental change in terrestrial and atmospheric processes. *Frontiers in Ecology and the Environment*, 6(5), 247-254. https://doi.org/10.1890/070140

Wulder, M.A., Roy, D.P., Radeloff, V.C., Loveland, T.R., Anderson, M.C., Johnson, D.M., Healey, S., Zhu, Z., Scambos, T.A., Pahlevan, N., Hansen, M., Gorelick, N., Crawford, C.J., Masek, J.G., Hermosilla, T., White, J.C., Belward, A.S., Schaaf, C., Woodcock, C. E., Cook, B.D. (2022). Fifty years of Landsat science and impacts. *Remote Sensing of Environment*, *280*, 113195. https://doi.org/10.1016/j.rse.2022.113195

Yatoo, S.A., Sahu, P., Kalubarme, M.H., & Kansara, B.B. (2020). Monitoring land use changes and its future prospects using cellular automata simulation and artificial neural network for Ahmedabad city, India. *GeoJournal*, *87*(2), 765–786. https://doi.org/10.1007/s10708-020-10274-5

Yin, Z., Zhang, C., Fan, X., Zhang, N., Zhao, X., & Von Gadow, K. (2023). Effects of tree density and herbaceous plants on tree seedling survival across the growing and non-growing season in a temperate forest. *Forest Ecology and Management*, *545*, 121234. https://doi.org/10.1016/j.foreco.2023.121234

Zhang, H., Huang, G.H., Wang, D., & Zhang, X. (2011). Multi-period calibration of a semi-distributed hydrological model based on hydroclimatic clustering. *Advances in Water Resources*, *34*(10), 1292–1303. https://doi.org/10.1016/j.advwatres.2011.06.005

Zhang, T., Li, D., East, A.E., Walling, D.E., Lane, S., Overeem, I., Beylich, A.A. , Koppes, M., & Lu, X. (2022a). Warming-driven erosion and sediment transport in cold regions. Nature Reviews Earth & Environment, 1-20. https://doi.org/10.1038/s43017-022-00362-0

Zhang, L., Wang, X., Wang, J., Liao, L., Lei, S., Liu, G., & Zhang, C. (2022). Alpine meadow degradation depresses soil nitrogen fixation by regulating plant functional groups and diazotrophic community composition. *Plant and Soil*, *473*(1–2), 319–335. https://doi.org/10.1007/s11104-021-05287-z

Zheng, J., Wang, W., Ding, Y., Liu, G., Xing, W., Cao, X., & Chen, D. (2019). Assessment of climate change impact on the water footprint in rice production: Historical simulation and future projections at two representative rice cropping sites of China. *The Science of the Total Environment*, *709*, 136190. https://doi.org/10.1016/j.scitotenv.2019.136190

Zwieback, S., Chang, Q., Marsh, P., & Berg, A. (2019). Shrub tundra ecohydrology: rainfall interception is a major component of the water balance. *Environmental Research Letters*, *14*(5), 055005. https://doi.org/10.1088/1748-9326/ab1049

Chapter 4: Aquatic and Riparian Land Cover Trends across Mountainous Headwater Basins in Alberta, Canada

Abstract

Mountain headwaters of the Eastern Slopes of Alberta (ES) are the primary source of freshwater of major easterly flowing basins in western Canada, supplying a significant volume of water to about four million people. However, increasing temperatures are altering mountain aquatic (open water areas, lakes, reservoirs, rivers, ponds, wetlands) and riparian vegetation (herbaceous and woody/shrub) ecosystems, particularly in the snowmelt-dominated (mid-May to mid-July) and rainfall-dominated (late-July to mid-September) periods. This study quantified changes in landcover areas (i.e., open water, non-woody, woody/shrub, and barren) within the ES using a Random Forest classification applied to the Landsat imagery archive spanning 1984 to 2023. Historical aerial photographs and the annual-based land cover classification of Canada, along with the Wetland Inventory of Alberta, were used combined as a reference dataset to identify the training and validation pixels. Furthermore, an elevation-based land cover evaluation was performed, to quantify the land cover changes in the subalpine (≤ 2300 m) and alpine (> 2300 m) regions of the ES.

Utilizing independent historical and recent aerial photographs, the land cover classifier achieved an average validation kappa of 0.75 during the snowmelt-dominated period and 0.72 during the rainfall-dominated period. Over the long term of many years, as open water area and non-woody plants decline, woody vegetation and barren increases in the ES, indicating this region is drying out. Over 40 years, during snowmelt-dominated periods, subalpine regions showed significant (p-value<0.05) increases in open water area (+1.9%), non-woody vegetation (+1.9%), and woody/shrub cover (+0.5%), whereas barren have decreased (-4.4%). Similar changes were observed in alpine regions, where open water (+0.1%) and non-woody vegetation (+0.2%) increased while barren areas decreased (-0.1%). In the rainfall-dominated period, subalpine regions experienced a significant decline in open water (-2.2%), accompanied by an expansion of barren (+2.1%) and a vegetation shift from non-woody (-4.4%) to woody/shrub (+4.4%). Alpine regions mirrored this trend, with open water (-0.3%) and non-woody vegetation (-0.3%) declining as barren areas increased (+0.6%).

Keywords: Mountainous Environments; Hydrology; Water Resources; Remote Sensing

4.1.Introduction

Global climate change has exhibited significant variability and complexity, characterized by a pronounced increase in air temperatures (20 ~ 40% faster than the global average) in temperate latitudes (Intergovernmental Panel on Climate Change, 2021). In the Eastern Slopes of Alberta (ES) (Canada) changes have been documented as a consequence of climate warming (Stewart et al., 2005; Clarke et al., 2015; Zheng et al., 2021). Air temperatures have increased over recent decades (Zhang et al., 2000), contributing to an earlier snowmelt (Stewart et al., 2004; Stewart et al., 2005) and accelerated glacier melt (Hopkinson and Young, 1998; Clarke et al., 2015). These shifts have resulted in higher river discharge over a shorter period and have led to an earlier expansion of open water and lake surfaces during the spring season (MacDonald et al., 1993; Shugar et al., 2020; Zheng et al., 2021). However, during the early to late summer season, in the ES recent studies have found that as temperatures increase, river discharge decreases (Chassé et al., 2013; Déry et al., 2016). This can be explained as higher air temperatures increase evaporation rates from open water areas and reduce recharge to important water stores, such as high-elevation wetlands and groundwater; thus, resulting in reduced river discharge (Fontrodona Bach et al., 2018; Teuling et al., 2019). Three key elements mediate this relationship: first, warmer temperatures accelerate snowmelt, leading to an initial surge in river discharge that later declines as snow reserves diminish (Barnett et al., 2005; Mote et al., 2005); second, while glacial retreat temporarily boosts summer flows, long-term ice loss removes this buffer, increasing the likelihood of late-season drought (Jost et al., 2012; Tennant et al., 2012); and third, soil moisture feedbacks, as drier soils absorb more meltwater, further reducing runoff (Berghuijs et al., 2014). Therefore, the combination of atmospheric and cryospheric changes can reduce water inputs into regions and ecosystems that rely on glacier and snow melt for water supply during the rainfall-dominated period (late-July to mid-September), such as mountain aquatic environments and riparian vegetation zones in the ES (Barnett et al., 2005).

Mountain aquatic and riparian vegetation ecosystems within the ES are adapted to the snowmelt-dominated period (mid-May to mid-July) for water accumulation and storage, making them particularly sensitive to climate-induced changes (Mercer, 2018). Variations in the timing of snowmelt can dictate whether intermittent open water areas remain wet or dry during late summer. When snowmelt occurs earlier than usual, water is released before peak evaporative demand in late summer, often resulting in a temporal mismatch between water supply and ecosystem demand.

Early snowmelt advances the delivery of water to the landscape at a time when the vapour pressure deficit (i.e., a measure of atmospheric drying potential) is still relatively low (Ruzzante and Gleeson, 2025). As the season progresses into the late summer, a vapour pressure deficit typically increases due to higher temperatures and lower relative humidity, intensifying evapotranspiration rates (Massmann et al., 2019). If snowmelt has already been depleted by this time, soil moisture and shallow groundwater reserves are more likely to face reduction (Harpold and Molotch, 2015), increasing the risk of water shortages in wetlands and riparian areas. The separation of supply and demand may result in the drying out of intermittent wetlands, alterations in vegetation composition (such as the encroachment of woody and shrub vegetation), and a reduced resilience of mountain aquatic ecosystems in the face of extended warm and dry conditions (Mastrotheodoros et al., 2020).

Furthermore, because of the elevation range (1000 m ~ 3400 m) in the ES, the mountainous region can be divided into subalpine (≤2300 m) and alpine (>2300 m). The 2300-meter elevation in the ES is a fundamental divide of water movement over the landscape. Below 2300 meters, the subalpine zone serves as a seasonal water bank, where winter snowfall melts regularly each summer, supplying water for wetlands, forests, and river flows with effects far downstream (Petrone et al., 2003). Above 2300 meters, the alpine rules change; glaciers and permanent snowfields act as the "water reserves," gradually releasing water in late summer when subalpine regions have run dry (Menounos et al., 2019). Moreover, subalpine and alpine aquatic and riparian vegetation areas provide a variety of ecosystem services, such as, sediment retention (Johnston, 1991), nutrient removal (Campbell et al., 2000), and aquatic life support (Windell et al., 1986). However, although subalpine and alpine aquatic and riparian vegetation offer numerous ecosystem benefits, their vulnerability to climate change remains poorly quantified on mountainous land cover areas (based on water and vegetation cover, e.g., open water, riparian non-woody, riparian woody/shrub, and barren) of the ES. For instance, some wetlands shrink into barren areas while others transition into woody and shrub-dominated zones, as drying soils favour woody invasion (Brunbjerg et al., 2022). Nonetheless, these changes are hardly straightforward; glacial retreat, for example, exposes new barren land where open water first expands (Shugar et al., 2020) only to later contract as sediment fills these basins (Carrivick and Heckmann, 2017). Likewise, earlier snowmelt could momentarily increase riparian vegetation prior to drought stress causing die-offs (Selmants et al., 2023). Therefore, understanding the effects of climate change on mountainous environments may reveal how alpine and subalpine aquatic and riparian vegetation areas are

responding to these gradual climatological shifts.

To ascertain whether the land cover is changing, physically grid-based hydrological models have been used in recent research to estimate the ecological changes of inland aquatic environments and the land cover of riparian vegetation ecosystems globally (Avis et al., 2011; Mastrotheodoros et al., 2020). However, grid-based simulations provide results in simulated changes over grids of several hundred kilometers. Important regional elements such as topography, land cover, and land use are not considered in the modelling process. Alternatively, remotely sensed data could be used, since it is critical for tracking land cover changes in remote regions like the ES. The 30-meter Landsat archive (1984–present) facilitates detecting changes in land cover at a fine scale in mountain aquatic and riparian vegetation areas, including wetland drying to shifts in riparian vegetation.

The Landsat imagery archive has facilitated studies of land cover extent changes in mountain aquatic and riparian ecosystems by providing at least 50 years of continuous data (Wulder et al., 2022). Since the launch of Landsat MSS in 1972, the Landsat program has offered a valuable balance between spatial resolution and large-scale coverage, delivering moderate temporal resolution for the investigation of seasonal patterns and change over time. Moreover, both supervised (e.g., Random Forest, Maximum Likelihood) and unsupervised (e.g., Iso-clustering, K-Means) classification methods can analyze historical Landsat imagery to track land cover changes in mountain wetlands and riparian zones over time (Rodrigues et al., 2024). Overall, embedding historical Landsat imagery archives with supervised classification facilitates the understanding and quantification of climate change effects on land cover in the ES.

This study aims to investigate the response of aquatic and riparian land cover to changing natural conditions within the ES, Canada, from 1984 – 2023. The objectives are to quantify and assess multi-decadal mountainous land cover extent (i.e., open water, riparian non-woody, riparian woody/shrub, and barren) trends and changes in the subalpine (≤ 2300 m) and alpine (> 2300 m) regions of the ES over the last 40 years. To achieve this, landcovers were classified using the historical Landsat archive using Random Forest during the snowmelt- and rainfall-dominated period in four key headwater basins in the ES. Meanwhile, local air temperature and precipitation data were analyzed to better comprehend the observed land cover trends. As far as the author knows, this study is the first to analyze the mountain aquatic and riparian vegetation land cover trends and changes over broad areas.

4.2. Methods

4.2.1. Study Region

Mountain aquatic and riparian vegetation land cover extent (spatial area covered by a specific landcover type, e.g., open water, riparian non-woody, riparian woody/shrub, and barren) in the Eastern Slopes of Alberta (ES) are located in the Montane Cordillera Ecozone, with a latitude range of 49° to 54.5° (Figure 4.1). The study area location spans four primary drainage basin headwaters: Oldman River, Bow River, North Saskatchewan, and Athabasca. These watersheds were chosen for this work due to their vital source of water supply to downstream users in the Prairies and into Boreal Forest. In addition, the intersection of the Montane Cordillera Ecozone and the Red Deer River watershed, specifically the headwater section, was merged with the Bow River watershed. The merging of the Red Deer River with the Bow River watersheds is unlikely to alter the conclusions of this study, given that the adjacent watersheds possess comparable physiographic characteristics (elevation range: 1200–3400 m; mean slope: 15–25°) and demonstrated analogous hydrological responses to climate influences (Philipsen et al., 2018; Whitfield et al., 2021), as both watersheds are situated within similar latitude and ecozone.

The regional climatic normal (Table 4.1 lists the hydroclimatological and physical characteristics of the watersheds) data shows that the average temperature is 2ºC (standard deviation ±14 ºC), and the average annual total precipitation is 700 mm (standard deviation ±110 mm) (Alberta Climate Information Service, 2023). The land cover extent in the research region was based on two datasets: (i) the maximum open water area identified by the Global Surface Water Explorer (Pekel et al., 2016), as well as (ii) the limits of lakes and rivers of the province of Alberta (Government of Alberta, 2016). The two datasets were merged and a buffer zone of 90 meters was created surrounding this new dataset. This buffer zone aims to identify and evaluate land cover changes over time in areas surrounding to open water, including non-woody riparian zones, woody/shrub riparian zones, and barren areas. The choice of a 90 meters buffer width was based on the literature, which shows that this riparian vegetation buffer effectively captures the transitional ecotone between aquatic and terrestrial ecosystems, while also considering the usual floodplain widths found in temperate regions (Naiman et al., 2005; Décamps et al., 2004). This distance achieves a balance between ecological importance and analytical feasibility, as narrower buffers (e.g., 60 m) might overlook critical edge effects, while wider buffers may hide the identification of land cover changes related to riparian interfaces (Gregory et al., 1991; Fernandes et al., 2014).

Moreover, if a permanent glacier land cover (glacier that has not changed from 1984 to 2022, i.e., 100% frequency; detected with the historical land cover classification data of Canada (Hermosilla et al., 2022)) was identified within the 90 meters buffer, this area was masked out from the sub-sample buffered research region. The sub-sample buffered research region, covering about 1668 km^2, was created by merging the intersection of the maximum open water area identified by the Global Surface Water Explorer, the boundaries of lakes and rivers in Alberta, a 90-meter buffer zone, the natural borders of the Rocky Mountains, and the watersheds of the Athabasca, North Saskatchewan, Bow, and Oldman Rivers.

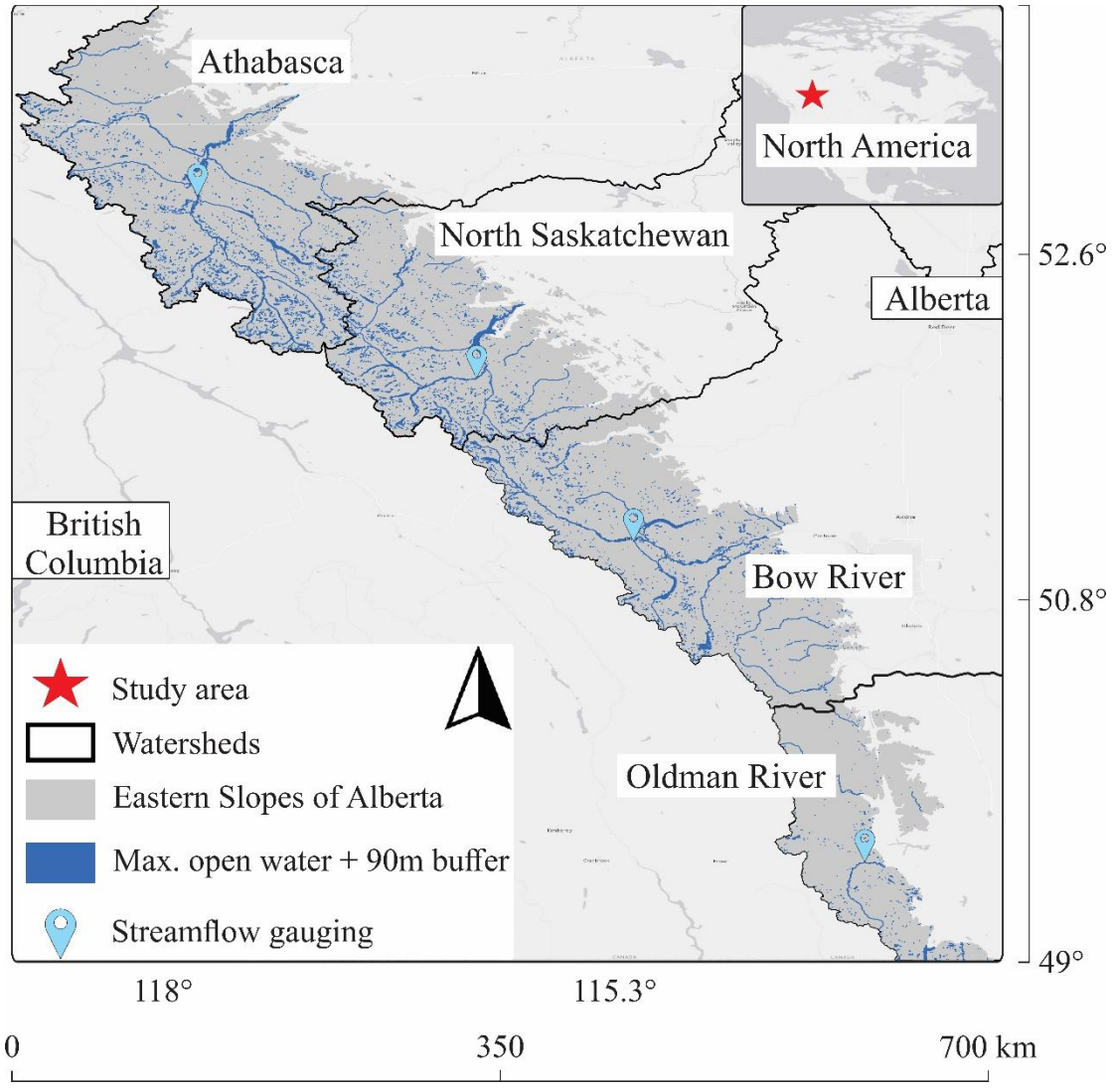

Fig. 4.1. Study area location in land cover zones, township weather stations, and streamflow gauging in the Eastern Slopes of Alberta

Table 4.1. Hydroclimatological and physical characteristics of the Eastern Slopes of Alberta watersheds.

Watersheds / Parameters		Oldman River	Bow River	North Saskatchewan	Athabasca
Climate (Köppen)		Dfc and Td			
Sub-sample buffered research area (km^2)		100	479	452	637
Altitude range (m a.s.l)		1165 ~ 2894	1188 ~ 3403	1218 ~ 3391	956 ~ 3420
Historical monthly average 1984 – 2023	Air temperature (ºC) – min., max. (average)	-53.2 ~ +29.7 (+1.4)	-56.9 ~ +29.9 (-0.5)	-58.1 ~ +31.3 (-1.3)	-58.2 ~ +30.9 (-1.4)
	Precipitation average (mm $year^{-1}$)	728	700	704	683

Dfc – Subartic; Td – Tundra; Sub-sample buffered research area –Maximum open water area merged with rivers and buffered by 90 meters, which includes the land covers open water, riparian non-woody, riparian woody/shrub, and barren; Altitude range (Average) – The altitude range of land cover (Shuttle Radar Topography Mission, 2023); Historical monthly average from the Interpolated Weather data from the Alberta Townships 1984 – 2023 (Alberta Climate Information Service, 2023)

4.2.2. Data

All historical datasets utilized span the years 1984 to 2023. Multidecadal land cover in ES was generated using historical Landsat 5 and 8 imagery archives. Gridded historical air temperature data (Alberta Climate Information Service, 2023) were utilized to identify air temperature trends in each watershed of ES. Historical river discharge data were utilized to identify the snowmelt-dominated period (nival) and the rainfall-dominated period (pluvial) of river flow. Subsequently, these periods were employed to generate two mosaic images (using the best available pixel, i.e., cloud and snow/ice-free pixels, per nival and pluvial period), representing the snowmelt-dominated and rainfall-dominated periods of each year.

4.2.2.1. Remote sensing dataset

The Landsat 5 (Thematic Mapper TM) and 8 (Operational Land Imager OLI) archives (1984–2023) (Collection 2, Tier 1, Level 2 reflectance) were accessed through the Google Earth

Engine (GEE). GEE includes cloud-free composites and Landsat processing techniques for calculating at-sensor surface reflectance. This platform was utilized to classify the mountain aquatic environment and riparian vegetation land cover extent. The four land cover classes are: Open water: lakes, reservoirs, rivers, ponds, and wetlands; Non-woody: Herbaceous vegetation; Woody/Shrub: Woody and Shrubby vegetation; Barren: rock rubble, barren/exposed land/soil, and wildfire-burned area. The area affected by wildfire (i.e., wildfire-burned area) can be regarded as barren or exposed soil, particularly after a fire event that consumes vegetation (Lutes et al., 2006). Moreover, the spectral reflectance of these wildfire-burned areas frequently resembles that of exposed or bare soil, particularly in the shortwave infrared band (Pleniou and Koutsias, 2013).

Cloud and snow/ice-free pixels were chosen, and the median reflectance result was used to create two composition images for each year: one for the period for the snowmelt-dominated (nival) period, and another for the rainfall-dominated (pluvial) period. Historical aerial photographs (1985, 1987, 1988, 1993, 1994, 2002, 2003, 2020, 2021) (Alberta Government, 2024), the Wetland Inventory of Alberta (Hird et al., 2017; DeLancey et al., 2019; ABMI, 2021), and the historical Canadian annual-based land cover classification (Hermosilla et al., 2022) were employed in conjunction as a reference dataset to assign the training and validation pixels throughout the land cover classification process.

4.2.2.2. Air temperature and river discharge dataset

Daily air temperature (°C) between 1984 and 2023 was obtained by utilizing the Interpolated Weather data from the Alberta Townships (Alberta Climate Information Service, 2023). This dataset is known for its extensive historical record dating back to 1901. Furthermore, the Alberta Township dataset was crucial for this study due to the limited availability of historical, continuous, and spatially distributed hydroclimatic measurements in the alpine and subalpine regions of the ES. This gridded interpolation data offers more spatially representative estimates compared to depending on one or two weather stations per watershed, which can lead to high uncertainty caused by elevation biases and microclimate variability (Bertoncini and Pomeroy et al., 2025). The data for each township location were estimated using Hybrid Inverse Distance Cubed weighting for precipitation and linear Inverse Distance weighting for air temperature. Both methods were weighted based on the eight nearest weather station observations. These methods consider spatial variation in elevation throughout the ES (Alberta Climate Information Service, 2023).

Information regarding the interpolation methodology is available in Alberta Climate Information Service, (2023). The average of all Townships (spatial resolution of 10 km) contained in each watershed was used to represent each watershed. Supplementary material A of Chapter 4 shows all used townships numbers per watershed.

The historical (1984 – 2023) river discharge data were acquired for each watershed: Oldman River – Castle River in the Ranger Station (Number: 05AA028; Location: 49°23'50" N, 114°20'23" W; Streamflow gauging watershed area: 375 km^2) (Environment Canada, 2024a); Bow River – Bow River at Banff (05BB001; 51°10'20" N, 115°34'18" W) (Environment Canada, 2024b; 2210 km^2); North Saskatchewan – North Saskatchewan River at Whirlpool Point (05DA009; 52°00'04" N, 116°28'15" W; 1920 km^2) (Environment Canada, 2024c); Athabasca – Athabasca River Near Jasper (07AA002; 52°54'36" N, 118°03'31" W) (Environment Canada, 2024d; 3870 km^2). The selection of these river gauges is based on their comprehensive and concurrently accessible temporal river discharge data spanning from 1984 to 2023 across all watersheds of ES.. In addition, the river gauges are located in the central area of each basin headwater.

4.2.3. Modelling framework, remote sensing and air temperature data collection

The land cover extent trend and change analysis conducted in the ES followed a series of seven steps, as seen in Figure 4.2: i) remote sensing, air temperature, and river discharge data; ii) season identification; iii) land cover classification; iv) reference dataset and accuracy evaluation; v) post-classification process; vi) trend and change analysis; vii) changes in land cover relative to variance with elevation.

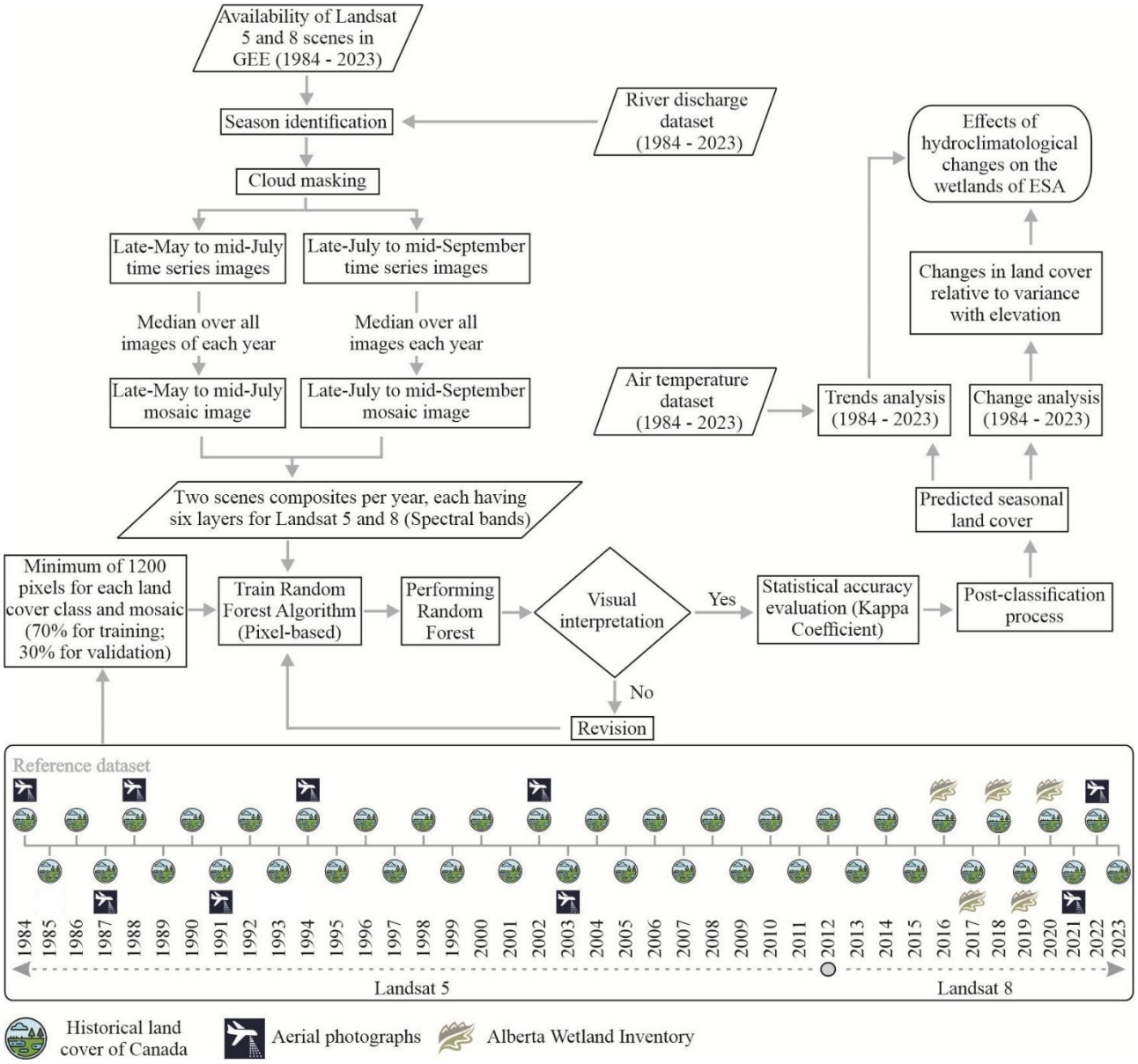

Fig. 4.2. Methodological flowchart for the seasonal spatiotemporal (1984–2023) assessment of the wetlands land cover extent trends and changes in the Eastern Slopes of Alberta

4.2.4. Season identification

Direct river discharge measurements (streamflow gauging) can be used to identify the peak discharge period (as per Rodrigues et al., 2024) and demonstrate the year-round nival (herein referred to as snowmelt-dominated period) and pluvial (herein referred to as rainfall-dominated period) period of the river flow. This separation indicates an arbitrarily chosen point in time at which the snowpack has been significantly reduced as a source of melt-driven river flow.

Therefore, to approximate the duration/period of snowmelt- and rainfall-dominated periods, peak flow and baseflow were separated applying some assumptions. Firstly, the baseflow threshold utilized for the used streamflow gauging was: Oldman River watershed in the Ranger Station 10 $m^3 s^{-1}$, Bow River at Banff 45 $m^3 s^{-1}$, North Saskatchewan River at Whirlpool Point 75 $m^3 s^{-1}$, Athabasca River Near Jasper 95 $m^3 s^{-1}$; the reason for the selection of these values was the observation that the discharge normally increased only beyond these values. Therefore, the snowmelt-dominated period initiates at the time river discharge surpasses baseflow threshold (consistent change point, i.e., when river discharge values normally increased only above these baseflow values) to the peak discharge. The snowmelt-dominated period continues until the river discharge falls to a level at least 20% lower than the peak discharge, thereby inhibiting the formation of subsequent peaks. A threshold of 20% below peak discharge was chosen, as it was observed (historical streamflow gauging data used in ES) that 90% of peak discharge events had occurred after the drop of 20%. After that, the rainfall-dominated period starts; the rainfall-dominated period ends by the end of summer season (i.e., September 15). September 15 was chosen as end of rainfall-dominated period since the average first snowfall day in subalpine and alpine regions of the ES usually occurs during mid-September (September 10–20) (Harder et al., 2015; DeBeer et al., 2015). The watershed area of each streamflow gauging was utilized to normalize river discharge, thereby facilitating the comparison of hydrographs. Figure 4.3 shows how two periods were identified.

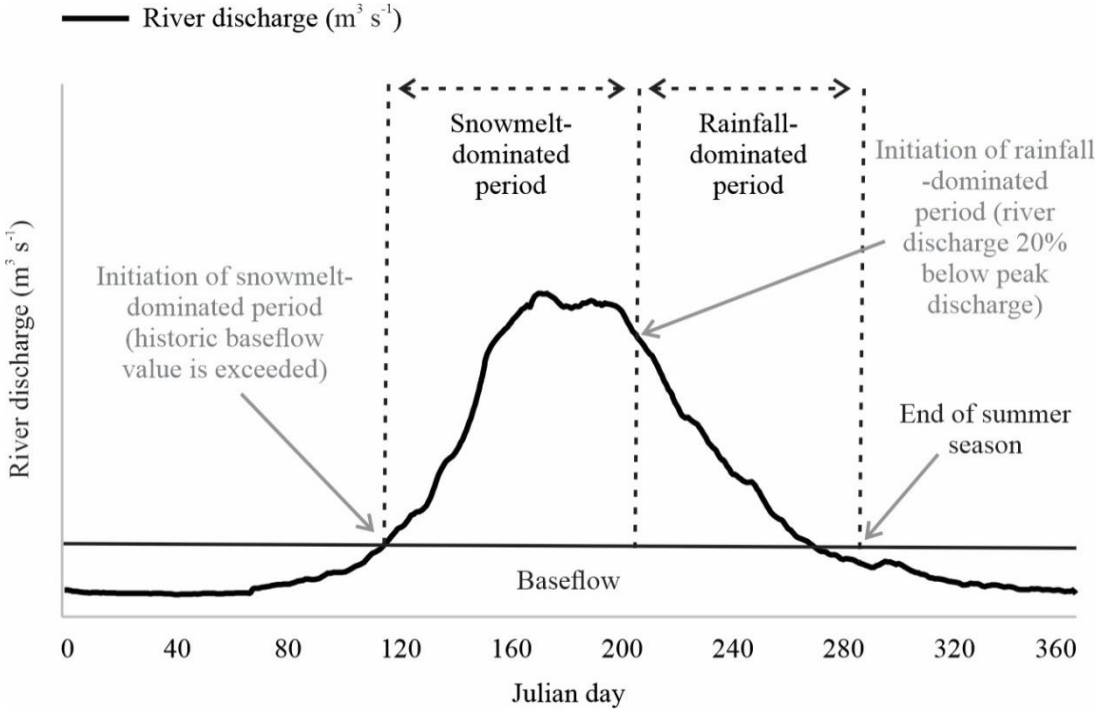

Fig. 4.3. Snowmelt- and rainfall-dominated periods identification using river discharge measurements

However, as the investigation focused on the ES and employed four streamflow gauges to identify the snowmelt-dominated and rainfall-dominated periods, each watershed had its unique snowmelt- and rainfall-dominated period interval. Thus, the Julian days from the start and end of each period within each watershed were averaged to standardize both periods for the ES. In the end, the snowmelt-dominated and rainfall-dominated periods time span were used in GEE to classify the land cover for each period.

4.2.5. Land cover classification, reference dataset, and accuracy evaluation

The Random Forest algorithm (Breiman, 2001) was performed within the GEE, to predict a raster with four land cover classes: Open water, Non-woody vegetation, Woody/Shrub, and Barren. The Random Forest routine was utilized since it is non-parametric and does not require previous knowledge of the ecological drivers or features of the prediction/classification outputs (Menze et al., 2009). The four land cover classes were selected as they capture hydrological and ecological wetlands characteristics in the ES. For instance, open water and barren areas reflect surface hydrology and disturbance regimes (e.g., drying cycles), while non-woody and woody/shrub vegetation represent dominant biological responses to moisture availability and successional stages

(Hogg and Hurdle, 1995). Furthermore, the land cover classes align with wetland classification systems used in similar mountain regions (National Wetlands Working Group, 1997). In addition, these land covers are detectable via remote sensing, enabling consistent monitoring of land cover dynamics (Adam et al., 2022). Cloud-covered and snow/ice pixels were excluded throughout the land cover classification procedure using the quality band of Landsat (i.e., *Bitmask for pixel_qa*) within GEE. The attributes of this band were generated using the C Function (a method that leverages bit-mapped values for the analysis of Landsat archive) of the Mask algorithm (Foga et al., 2017). This band combined with the Mask algorithm flags undesirable pixels (e.g., clouds and snow/ice) with the class name or "unused". This method preserves spectral integrity by utilizing per-band median calculations per period (snowmelt-dominated and rainfall-dominated), effectively minimizing transient noise caused by single-date anomalies. The resulting composite illustrates standard reflectance conditions for effective land cover classification, derived from recognized best available pixel methodologies (White et al., 2014). Only composite images with a total extent of more than 80% (i.e., cloud-pixel threshold < 20%) were utilized for the trend analysis (as per Bian et al., 2020; DeLancey et al., 2019; Hermosilla et al., 2022; Roy et al., 2016).

However, collecting ground-truth (i.e., field-collected samples) historical training and validation data in vast and rugged terrains poses significant challenges due to their distant and inaccessible nature, often requiring transportation by airplane or helicopter (Mahdianpari et al., 2020). For this study, different remote sensing data sources were used: aerial photographs (Alberta Government, 2024), the Wetland Inventory of Alberta (Hird et al., 2017; DeLancey et al., 2019; ABMI, 2021) and the historical Canadian land cover classification (Hermosilla et al., 2022) (for more details see the supplementary material B of Chapter 4) to generate training samples per each year (Supplementary material C of Chapter 4).

The historical land cover classification data of Canada (Hermosilla et al., 2022; with an overall accuracy of ~80%) was used to assign training pixels inside the ES. The analysis utilized nine land cover classes from the historical annual land cover dataset. One class was dedicated to open water, such as, Open water (Producer's accuracy of 65%). Two of the classes represented non-woody, specifically Bryoides (mosses, liverworts, and hornworts; Producer's accuracy of 82%) and Wetland (marsh and fen; Producer's accuracy of 65%). Four classes represented woody and shrub vegetation, namely Shrubs (Producer's accuracy of 88%), Coniferous (Producer's accuracy of 93%), Broadleaf (Producer's accuracy of 70%), and Mixed wood (Producer's accuracy of 62%).

Two classes represented Barren, specifically rock rubble (Producer's accuracy of 40%) and barren/exposed land/soil (Producer's accuracy of 82%). In addition, four classes from the Wetland Inventory of Alberta (ABMI, 2021; overall classification accuracy of 85%) provided another source of training pixels. From this inventory, four main classes were used: woody/shrub vegetation were represented by Swamp (Producer's accuracy of 69%); two classes represented non-woody vegetation, namely Marsh (Producer's accuracy of 64.4%) and Fen (Producer's accuracy of 68%); and open water (Producer's accuracy of 89.8%), which stands for permanent and seasonal open water areas.

To identify the training/validation pixels within areas of unchanging land cover class (i.e., 100% frequency), a frequency analysis (i.e., "equals to frequency" routine on the land cover dataset from each year in ArcGIS Pro) was performed on the historical land cover of Canada dataset (from 1984 – 2022). The 1984 land cover raster was chosen as the reference raster since it was the initial year of the record and was considered to be "undisturbed" or "unchanged". The permanent land cover raster was subsequently imported into GEE as an asset to mask out permanent zones inside the ES that were identified as possible training regions for the allocation of training/validation pixels. Thus, training/validation pixels were allocated within these training areas and utilized throughout the entire time series.

However, in the years with available higher resolution imagery (i.e., periodically across time: Aerial photographs (resolution of printed images: 2000 dots per inch) – 1984 (Photo color – Black and white; Scale – 1:30000), 1987 (Black and white; 1:20000), 1988 (Black and white; 1:20000), 1991 (Black and white; 1:50000), 1994 (Black and white; 1:50000), 2002 (Colored; 1:20000), 2003 (Red, green, and blue; 1:30000), 2020 (Red, green, and blue; 1:4000), 2021 (Red, green, and blue; 1:4000) (Alberta Government, 2024); Wetland Inventory of Alberta – 2016 to 2020, overall accuracy of ~90%), which by expert interpretive identification of land cover class was possible to increase by 50 the number of training/validation pixels per land cover class and watershed in these years with more reference datasets.

The aerial photos were obtained from the Government of Alberta and were manually orthorectified in ArcGIS Pro using ground control points. The identification of these ground control points was achieved by comparing aerial photographs with stable landscape features, including road intersections, rock outcrops, and river confluences, which were distinctly visible and remained unchanged in the World Imagery basemap. On average, ten ground control points were placed per

image, with careful distribution across both the center and corners to ensure spatial accuracy throughout the extent of the image. This manual registration process was applied to the first aerial photo in each flight path. For the subsequent images within the same path, the Auto Georeference tool in ArcGIS Pro was used. This tool identifies tie points automatically by comparing spectral patterns and spatial relationships between the manually georeferenced image and adjacent overlapping images, facilitating efficient and consistent alignment across sequential aerials. This approach ensured accurate georegistration while balancing precision and processing efficiency for the full image set.

In addition, to reduce uncertainty, the training/validation pixels were assigned a minimum distance of 90 meters from the permanent class within the boundary. This was done to mitigate the influence of edge effects or the presence of mixed pixels. The Random Forest model was trained using 1500 trees (as per Rodrigues et al., 2024). For each land cover class (i.e., Open water, Non-woody, Woody/Shrub, and Barren), in addition to the 50 from aerial photos, 300 pixels were assigned (as suggested by Congalton and Green, 2019). The training dataset consisted of 70% of the allotted pixels, while the remaining 30% were reserved for validation purposes, i.e., out of bag. Therefore, a total of 4800 permanent training/validation pixels (from unchanging land cover class of the historical land cover of Canada dataset; Hermosilla et al., 2022) were randomly dispersed throughout the ES inside the image mosaic and maintaining a minimum distance of 90 meters within the permanent land cover boundary, with 1200 training/validation pixels per class and per watershed.

The training/validation pixels for each class were allocated to specific regions of ES, as per supplementary material section C of Chapter 4. For instance, the training/validation of open water pixels were in large lakes such as Waterton Lake and Crowsnest lake for the Oldman River watershed; Spray Lake and Minnewanka lake for the Bow River watershed; Abraham Lake, Chephren Lake, and Peyto lake for the North Saskatchewan watershed; Maligne lake and Medicine Lake for the Athabasca watershed. The non-woody vegetation was situated along the border of the large lakes, while the woody/shrub vegetation class was found in the riparian vegetation corridor of the main river, such as the Oldman River for the Oldman River watershed, Bow River for the Bow River watershed, North Saskatchewan River for the North Saskatchewan watershed, and Athabasca River for the Athabasca watershed. The training/validation pixels of barren were allocated along the border of the large and small lakes.

The classification was conducted using five bands (or six layers) from each Landsat TM and OLI sensors: SWIR (Short Wave Infrared; Bands 6 and 7 in OLI; Band 7 in TM), NIR (Near Infrared; Band 5 in OLI; Bands 4 and 5 in TM), Red (Band 4 in OLI; Band 3 in TM), Green (Band 3 in OLI; Band 2 in TM), and Blue (Band 2 in OLI; Band 1 in TM). The Kappa coefficient was computed to assess the accuracy of the Random Forest simulated land cover. The Kappa values reported were obtained from the validation dataset, which consisted of a randomly selected 30% subset of the reference data. Although the Random Forest algorithm naturally produces accuracy and Kappa statistics for the training set, these metrics were omitted from the final evaluation as they often overestimate model performance due to the tendency for overfitting. This conservative approach guarantees that our assessment of accuracy truly represents the model's predictive ability when applied to independent data. A confusion matrix was computed for each land cover classification within each watershed from 1984 to 2023. Subsequently, these results were averaged to generate two overall confusion matrix: one for the snowmelt-dominated period and the other for the rainfall-dominated period.

4.2.6. Post-classification process

A cross-validation assessment was conducted comparing the results of the Random Forest algorithm land cover classification (polygons and regions) with historical (1980's) and current (2020's) aerial photos taken at the same location. Six aerial photos, spanning historical years 1988, 1991, and 1994, as well as current years 2020 and 2021, were utilized to conduct cross-validation in the Oldman River, Bow River, and Athabasca watersheds. The cross-validation was not carried out in North Saskatchewan because there were no current aerial photos available. Cross-validation is a common method used to verify the accuracy of land cover classification (as per Amani et al., 2021). In addition to the visual interpretation, a confusion matrix was created to compare the land cover classification raster (from section 4.2.5) with the images used in this section. A total of 500 pixels for each land cover class were created using these aerial photos. This results in a cumulative total of 2000 validation pixels per image and year. The Kappa coefficient was also computed to evaluate the accuracy of the land cover predicted by the Random Forest model. This comparison demonstrates how the land cover classification was represented when compared to these historical and current higher spatial resolution datasets. It also indicated whether the land cover class was inside the right sample region. Thus, regions without significant changes and regions with major changes were

selected to ensure both scenarios were appropriately detected throughout time.

4.2.7. Temporal trend and spatial change analysis

The Mann-Kendall method, as described by Kendall in 1975 and Mann in 1945, was used to conduct a trend analysis over the land cover extent per period (snowmelt- and rainfall-dominated), annual (grouping all land cover extents from each period), and in the daily average air temperature (performed through the *pyMannKendall* code, Hussain and Mahmud, 2019) over the past (1984 to 2023). The Mann-Kendall method (Kendall, 1975, Mann, 1945), is a nonparametric test used to detect trends in a series. It considers three hypotheses: i) no trend, ii) positive trend, and iii) negative trend. The degree of the changes was evaluated through the nonparametric Sen's slope and Kendall's tau (τ) coefficient. The trend method was considered significant when the p-value $\leq$ 0.05.

The assessment of land cover change utilized the mode (which represents the most frequently occurring value) of the land cover maps (of the snowmelt- and rainfall-dominated period) from 1984 to 1988 (referred to as the 1980s) and from 2018 to 2022 (referred to as the 2020s). The mode of the land cover maps was determined in the Google Earth Engine using the "*.mode()*" tool. This tool determines the most frequently occurring value at each pixel across all land cover maps from each period (i.e., snowmelt- and rainfall-dominated). This approach avoids the selection of a dry or wet year and instead uses 'typical' characteristics on a per pixel basis. To evaluate the land cover transition from 1980s to 2020s raster dataset, ArcGIS Pro's Change Detection Wizard and pixel value change approach were employed.

4.2.8. Changes in land cover relative to variance with elevation

This analysis aims to elucidate in which elevations the land cover changes are occurring in the ES, i.e., Subalpine (lower or equal than 2300 meters elevation; Alberta Parks, 2015), or in Alpine (higher than 2300 meters; Alberta Parks, 2015) regions. The elevation threshold of 2300 meters was chosen as it generally represents the treeline limit in mountainous areas (Trant et al., 2020; Körner and Körner, 2021). The elevation was defined from the digital elevation model of the Shuttle Radar Topography Mission; spatial resolution of 30 meters (Shuttle Radar Topography Mission, 2023). With the elevation dataset (specifically altering by increments of 100 meters), the mode (1980s and 2020s) of the periodic land cover datasets were used to determine land cover areas

per elevation. The Tabulate Area tool in ArcGIS Pro created elevation-specific land cover areas. Hence, evaluating the alterations in land cover along the elevation gradient of each watershed from the 1980s to the 2020s. Furthermore, independent regions (not used in training the Random Forest algorithm) from the historical and contemporary aerial photographs, Landsat 5 and Sentinel 2 archive was used to illustrate land cover changes in subalpine and alpine regions of ES.

4.3. Results

4.3.1. Snow-melting and rainfall-driven season identification

The average snowmelt-dominated period onset time starts differently in each watershed, such as, April 27 (Julian day 118) for the Oldman River, May 17 (Julian day 138) for the Bow River, May 28 (Julian day 149) for the North Saskatchewan, and May 19 (Julian day 140) for the Athabasca. Thus, the average start date for the ES's snowmelt-dominated period is May 15 (Julian day 136).

The snowmelt-dominated period ends when the river peak discharge drops below 20%. Thus, using the chosen definition, the end of the snowmelt-dominated period for each basin occurs on June 17 (Julian day 169) for the Oldman River, July 14 (Julian day 196) for the Bow River, August 15 (Julian day 228) for the North Saskatchewan, and August 1 (Julian day 214) for the Athabasca. Therefore, the snowmelt-dominated period in the ES typically ends on July 20 (Julian day 202). When the snowmelt-dominated period ends, the rainfall-dominated period starts. The rainfall-dominated period ends on September 15 (the end of the summer season). Figure 4.4 shows the start and conclusion of snowmelt- and rainfall-dominated periods in each watershed, and the averaged time periods for the ES.

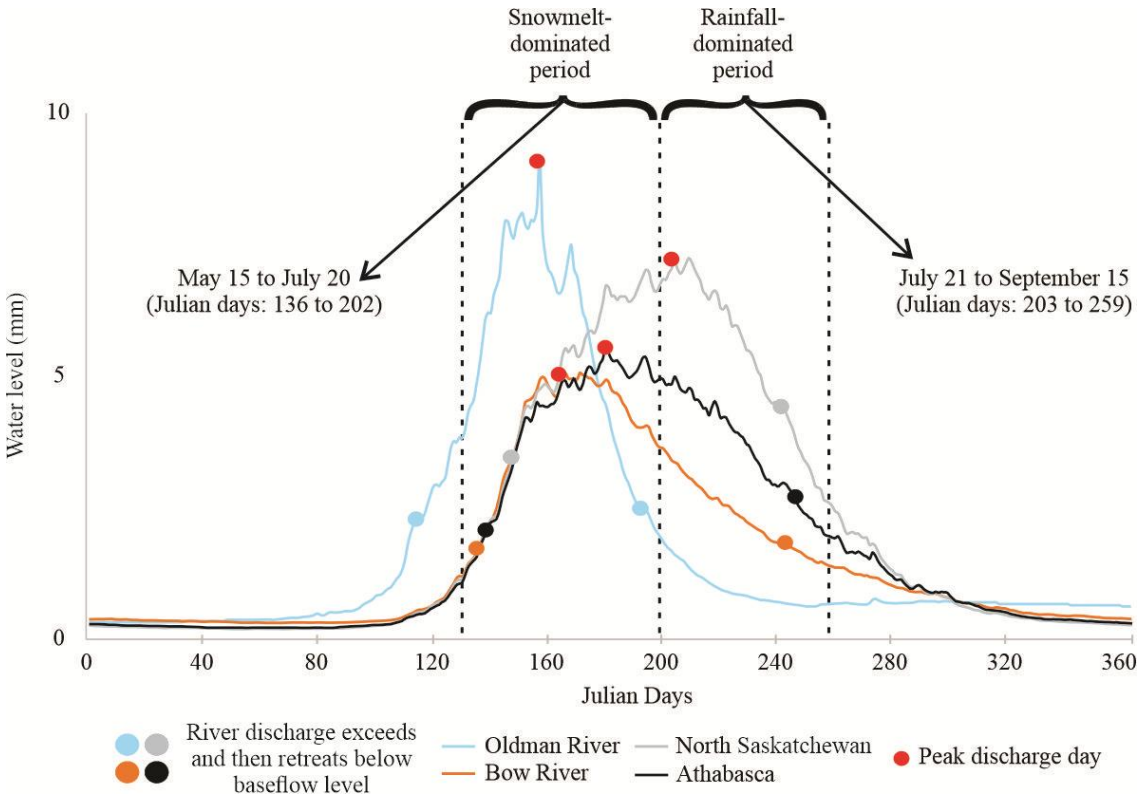

Fig. 4.4. Snowmelt- and rainfall-dominated periods identification using the daily average river discharge from 1984 to 2023 normalized by streamflow gaging watershed area.

4.3.2. Supervised classification accuracy

Supervised classifications were conducted in mosaic images using a total through time of 330,800 training and validation pixels during both periods: snowmelt-dominated (Number of mosaics per years represented – Oldman River: 30; Bow River: 28; North Saskatchewan: 29; Athabasca: 27); rainfall-dominated (Number of mosaics – Oldman River: 39; Bow River: 35; North Saskatchewan: 36; Athabasca: 36). 231,560 pixels were allocated for training purposes, and 99,240 pixels were utilized for validation. In the Snowmelt-dominated period the average omission errors for open water were 0.07 with a standard deviation of ± 0.3. The omission errors for non-woody, woody/shrub, and barren were estimated as 0.10 ± 0.01, 0.10 ± 0.02, and 0.09 ± 0.03, respectively. Meanwhile, higher omission errors were found during Rainfall-dominated period (open water: 0.10 ± 0.02; non-woody: 0.14 ± 0.04; woody/shrub: 0.13 ± 0.03; Barren: 0.12 ± 0.03). Tables 4.2 (snowmelt-dominated period) and 4.3 (rainfall-dominated period) shows the confusion matrix average (with total accuracy, omission and commission errors) of the reference (x–axis) and

classified (y–axis) land cover maps from 1984 to 2023 across all watersheds within the ES. Overall, the average validation kappa coefficient during both periods in ES was 0.86 ± 0.05 (All confusion matrix detailing all years, periods and land cover classes is included in the Supplementary Material D of Chapter 4; it includes the following: total accuracy, omission and commission errors).

Table 4.2. Average validation confusion matrix with commission and omission errors between the reference and classified land cover in the ES during snowmelt-dominated period (i.e., May 15 to July 20)

Land Cover Classes	Open Water	Non-Woody	Woody / Shrub	Barren	Marginal total	Commission Error	Kappa Index
Open Water	88	3	2	3	95	0.07±0.2	
Non-Woody	2	86	4	2	95	0.10±0.3	
Woody/Shrub	2	4	86	3	95	0.10±0.2	
Barren	2	3	3	87	95	0.08±0.2	0.88±0.5
Marginal total	95	95	95	95	380		
Omission Error	0.07±0.3	0.10±0.1	0.10±0.2	0.09±0.3			

Table 4.3. Average validation confusion matrix with commission and omission errors between the reference and classified land cover in the ES during rainfall-dominated period (i.e., July 21 to September 15)

Land Cover Classes	Open Water	Non-Woody	Woody / Shrub	Barren	Marginal total	Commission Error	Kappa Index
Open Water	85	4	3	4	96	0.11±0.2	
Non-Woody	3	83	6	4	96	0.14±0.3	
Woody/Shrub	3	6	82	5	96	0.14±0.4	
Barren	4	4	4	85	96	0.11±0.2	0.83±0.6
Marginal total	95	96	95	96	382		
Omission Error	0.10±0.2	0.14±0.4	0.13±0.3	0.12±0.3			

In both periods the best classified land cover class was open water, followed by barren, non-woody, and woody/shrub. Moreover, the non-woody and woody/shrub land cover classes were a source of confusion for the random forest algorithm, particularly during the rainfall-dominated period when a higher degree of confusion was observed between these two land cover classes. Figure 4.5 displays the average commission and omission errors separated by watershed and year (Figure 4.5a), in addition to the yearly average for the ES (Figure 4.5b). All years utilizing available higher resolution imagery, such as aerial photographs and the Wetland Inventory of Alberta,

exhibited average commission and omission errors below 0.10. Figure 4.6 depicts depicts the historical (1984 to 2023) kappa coefficient from all watersheds (Figure 4.6a) and an average for the ES (Figure 4.6b).

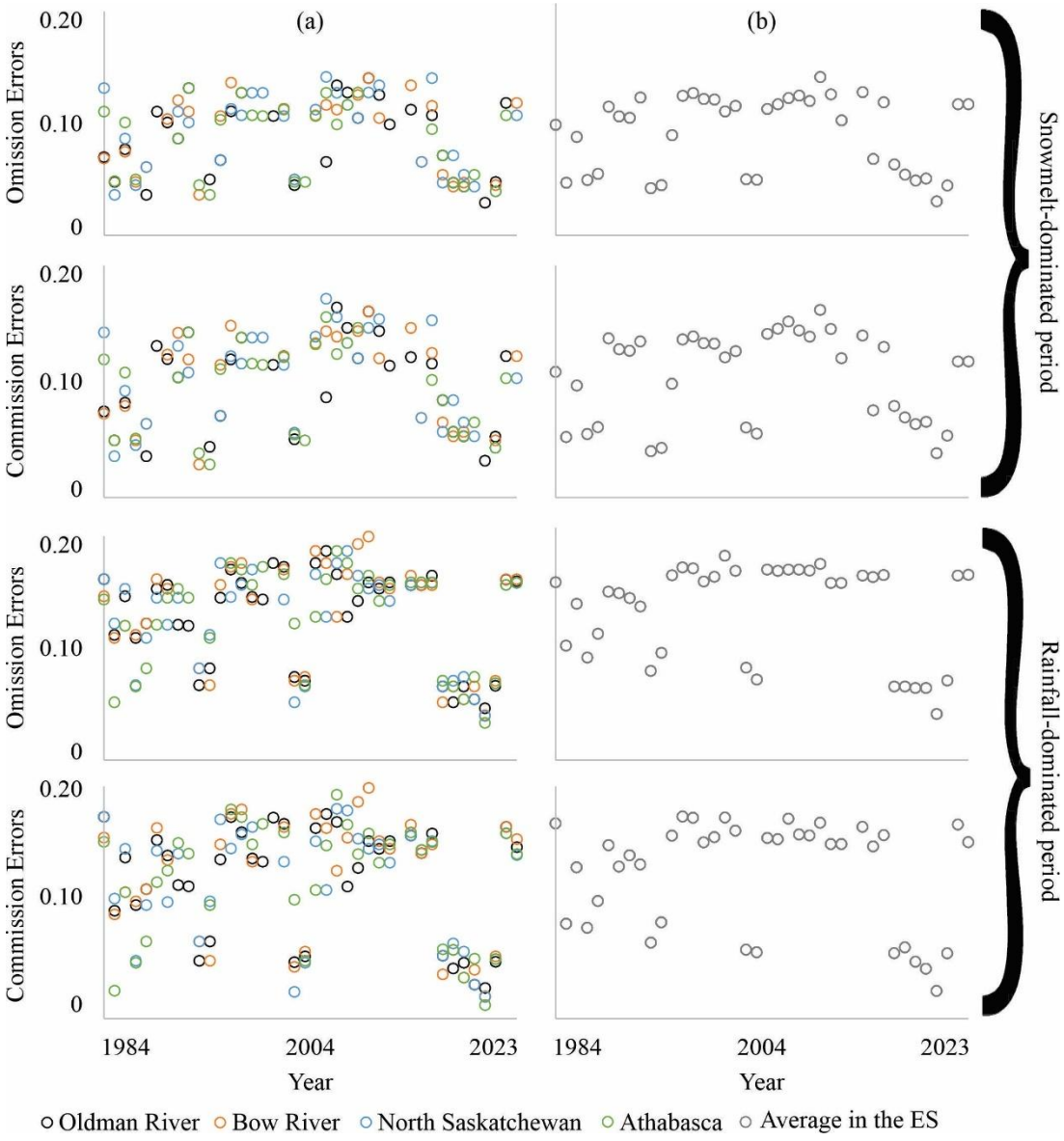

Fig. 4.5. Average errors of commission and omission within watersheds (a) and the average for the ES (b) during the snowmelt-dominated and rainfall-dominated period from 1984 to 2023.

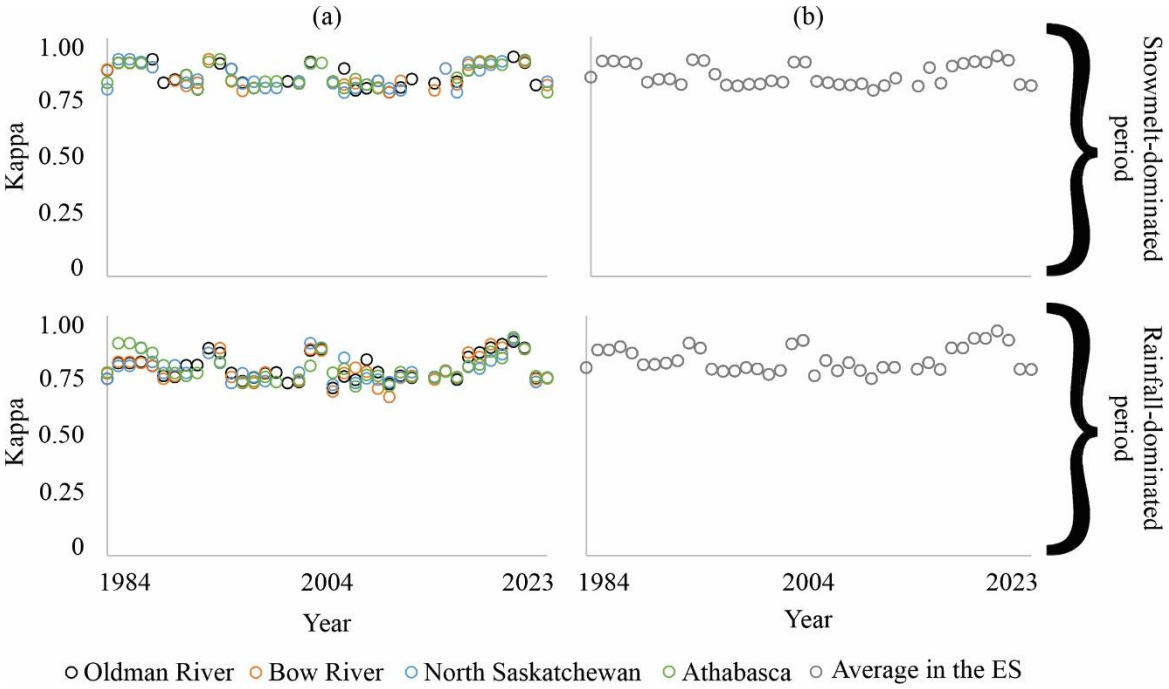

Fig. 4.6. Kappa coefficient within watersheds (a) and the average for the ES (b) during the snowmelt-dominated and rainfall-dominated period from 1984 to 2023.

4.3.3. Cross validation assessment

In the ES, the results of the Random Forest algorithm land cover classification were favorable in comparison to independent regions (not used in training the Random Forest algorithm) of aerial photographs from the past and present, as illustrated in Figure 4.7. Tables 4.4 to 4.7 present the confusion matrix, including total accuracy, omission, and commission errors, for the reference (x-axis) and classified (y-axis) land cover maps during the snowmelt-dominated period (Tables 4.4 and 4.5) and the rainfall-dominated period (Tables 4.6 and 4.7) from the 1980s and 2020s, utilizing independent regions within the ES. The kappa coefficient for the snowmelt-dominated period was 0.76 in the 1980s and 0.74 in the 2020s. During the rainfall-dominated period, the kappa coefficient was 0.72 in the 1980s and 0.71 in the 2020s. In both periods the best classified land cover class was open water. The Random Forest algorithm faced confusion between non-woody and woody/shrub land cover classes, especially during the rainfall-dominated period, when the distinction between these two classes became more challenging. The higher omission and commission errors between non-woody (Omission errors: 0.24 to 0.28; Commission errors: 0.24 to 0.42) and woody/shrub

(Omission errors: 0.15 to 0.24; Commission errors: 0.24 to 0.42) vegetation highlighted this confusion.

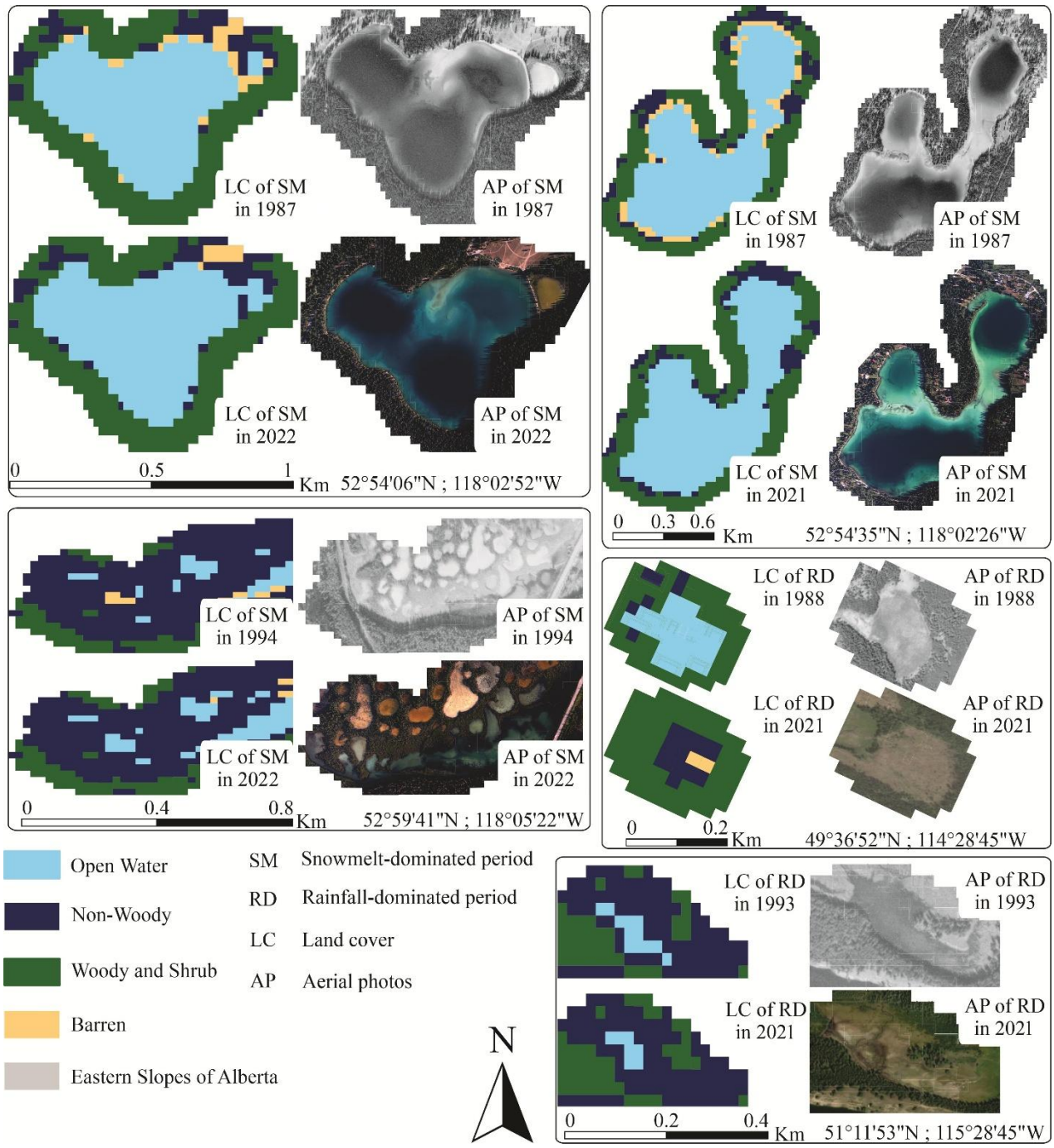

Fig. 4.7. Comparison of the past and present land cover (LC) classification with aerial photos (AP) in the Eastern Slopes of Alberta

Table 4.4. Validation confusion matrix with commission and omission errors between the reference and classified land cover in the ES during snowmelt-dominated period (i.e., May 15 to July 20) of 1980s

Land Cover Classes	Open Water	Non-Woody	Woody / Shrub	Barren	Marginal total	Commission Error	Kappa Index
Open Water	463	32	19	56	570	0.19	
Non-Woody	9	351	60	42	462	0.24	
Woody/Shrub	9	51	416	19	495	0.16	
Barren	39	28	3	403	473	0.15	0.76
Marginal total	520	462	498	520	2000		
Omission Error	0.11	0.24	0.16	0.23			

Table 4.5. Validation confusion matrix with commission and omission errors between the reference and classified land cover in the ES during snowmelt-dominated period (i.e., May 15 to July 20) of 2020s

Land Cover Classes	Open Water	Non-Woody	Woody / Shrub	Barren	Marginal total	Commission Error	Kappa Index
Open Water	449	35	22	70	576	0.22	
Non-Woody	44	358	47	63	512	0.30	
Woody/Shrub	5	91	408	7	511	0.20	
Barren	2	4	1	394	401	0.02	0.74
Marginal total	500	488	478	534	2000		
Omission Error	0.10	0.27	0.15	0.26			

Table 4.6. validation confusion matrix with commission and omission errors between the reference and classified land cover in the ES during rainfall-dominated period (i.e., July 21 to September 15) of 1980s

Land Cover Classes	Open Water	Non-Woody	Woody / Shrub	Barren	Marginal total	Commission Error	Kappa Index
Open Water	454	14	16	28	512	0.11	
Non-Woody	98	346	108	47	599	0.42	
Woody/Shrub	4	107	371	3	485	0.24	
Barren	12	5	1	386	404	0.04	0.72
Marginal total	568	472	496	464	2000		
Omission Error	0.20	0.27	0.25	0.17			

Table 4.7. validation confusion matrix with commission and omission errors between the reference and classified land cover in the ES during rainfall-dominated period (i.e., July 21 to September 15) of 2020s

Land Cover Classes	Open Water	Non-Woody	Woody / Shrub	Barren	Marginal total	Commission Error	Kappa Index
Open Water	446	13	18	58	535	0.17	
Non-Woody	46	349	94	67	556	0.37	
Woody/Shrub	4	118	374	6	502	0.25	
Barren	4	7	7	389	407	0.04	0.71
Marginal total	500	487	493	520	2000		
Omission Error	0.11	0.28	0.24	0.25			

4.3.4. Temporal land cover extent trends and changes

The trend analysis revealed that the yearly mean daily air temperature exhibited positive trends (Supplementary materials E of Chapter 4), with an approximate annual increase of 0.05 °C $year^{-1}$ across all watersheds. Additionally, open water and non-woody areas experienced an annual negative trend of -0.21 km^2 $year^{-1}$ and -0.46 km^2 $year^{-1}$, respectively, from 1984 to 2023. Conversely, the extent of woody/shrub and barren areas experienced a positive trend of +0.51 km^2 $year^{-1}$ and +0.16 km^2 $year^{-1}$, respectively (Figure 4.8).

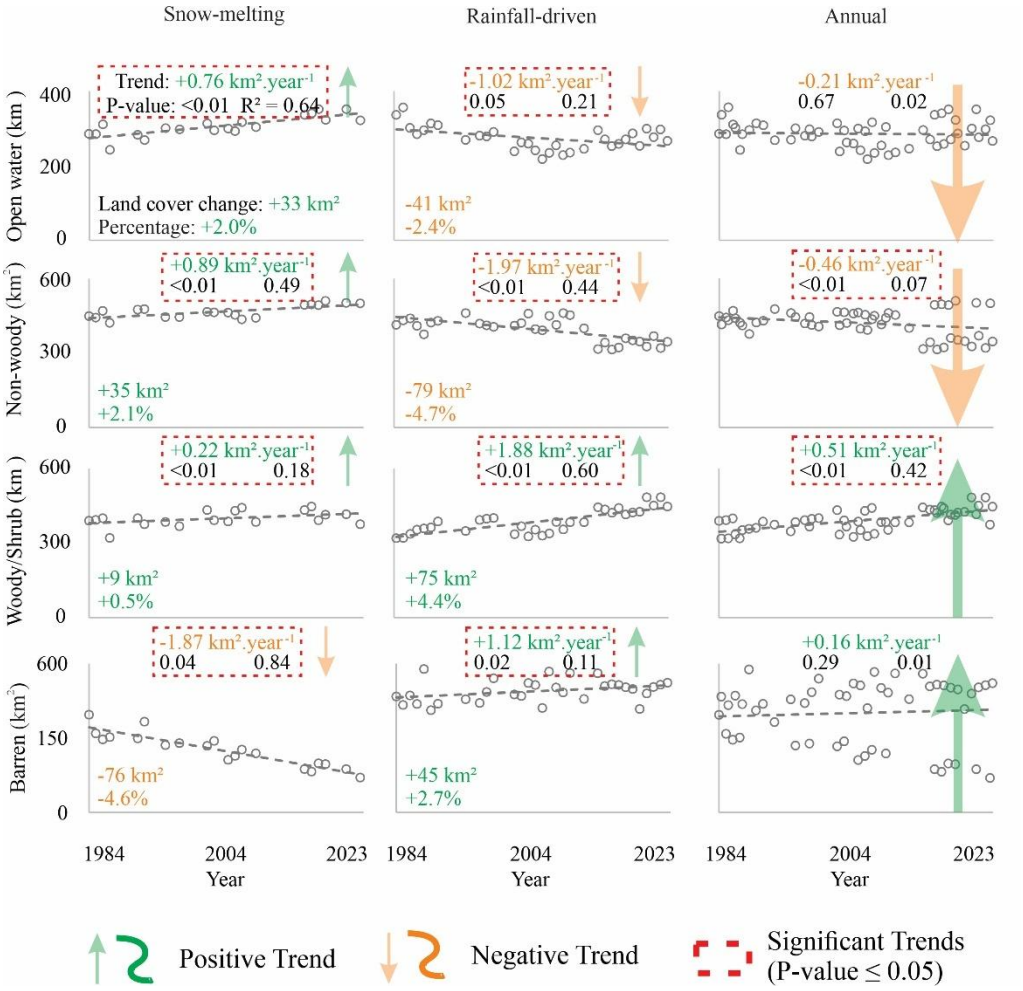

Fig. 4.8. Trends and changes of land cover extent per period in the Eastern Slopes of Alberta region from 1984 to 2023. The % has been normalized by the sub-sample buffered research area within the ES (1668 km^2).

In relation to the periodic trends and changes, in the snowmelt-dominated period, all watersheds exhibited substantial positive trends in air temperatures, with values ranging from 0.04 to 0.08 °C year^{-1} (Supplementary materials E of Chapter 4). During the same period, a statistically significant (p-value ≤ 0.05) increase of open water in the ES (+0.76 km^2 year^{-1}; +33 km^2 or +2.0%) was observed (Figure 4.9a). This phenomenon led to an expansion of the non-woody (+0.89 km^2 year^{-1}; +35 km^2 or +2.1%) and woody and shrub (+0.22 km^2 year^{-1}; +9 km^2 or +0.5%) areas (Figure 4.9a). Meanwhile, barren land cover has experienced a significant reduction (-1.87 km^2 year^{-1}; -76 km^2 or -4.6%) (Figure 4.9a).

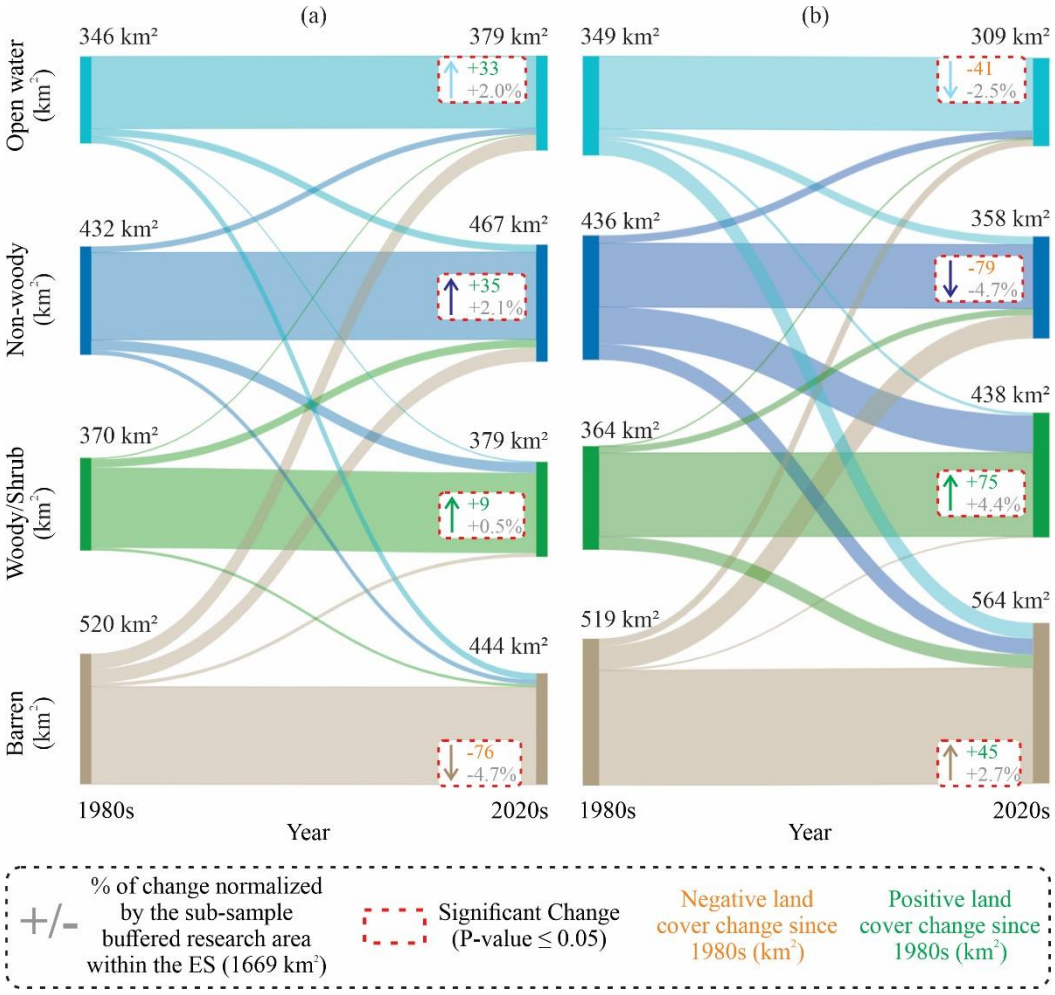

Fig. 4.9. Sankey diagram depicting the land cover change (km^2) from 1980s to 2020s during the snowmelt- (a) and rainfall-dominated period (b). The Sankey also presents the percentage of change normalized by the sub-sample buffered research area within the ES (1668 km^2).

In the rainfall-dominated period, significant positive trends in the average air temperature were observed during the rainfall-dominated period, with values ranging from 0.07 to 0.09 °C $year^{-1}$, as illustrated in in the Supplementary Materials E of Chapter 4. Furthermore, significant negative trends of open water were observed (-1.02 km^2 $year^{-1}$; -41 km^2 or -2.4%) (Figure 4.9b). The open water (-1.02 km^2 $year^{-1}$; -41 km^2 or -2.4%) has been replaced with barren (+1.12 km^2 $year^{-1}$; +45 km^2 or +2.7 %) and then non-woody vegetation. Moreover, barren is becoming non-woody, indicating new vegetation growth, while the main loss of non-woody (-1.97 km^2 $year^{-1}$; -79 km^2 or -4.7 %) is to woody and shrub (+1.88 km^2 $year^{-1}$; +75 km^2 or +4.4 %), suggesting a successional process (Figure 4.9b). Furthermore, during the rainfall-dominated period, changes in land cover

from woody/shrub and non-woody vegetation to barren areas were noted, likely as a result of episodic disturbances such as wildfires. Table 4.8 and 4.9 depicts the land cover area trends and changes, respectively, per watershed and period in ES. Finally, supplementary materials F and G of Chapter 4show the trends graphs and changes results, respectively, of each land cover by watershed.

Table 4.8. Land cover trends (km^2 $year^{-1}$) per watershed and period (SM: snowmelt-dominated; RF: rainfall-dominated; Annual) in the ES.

Land cover class	Period	Oldman River	Bow River	North Saskatchewan	Athabasca
Open water	SM	+0.05*	+0.21*	+0.21*	+0.29*
	RF	-0.10*	-0.28*	-0.28*	-0.36*
	Annual	-0.04*	-0.03	-0.09*	-0.11
Non woody	SM	+0.24*	+0.23*	+0.19*	+0.23*
	RF	+0.15*	-0.40*	-0.40*	-1.32*
	Annual	+0.08*	-0.12	-0.15	-0.27*
Woody/Shrub	SM	-0.05	+0.08	+0.14	+0.05
	RF	-0.15*	+0.98*	+0.47*	+0.58*
	Annual	-0.05*	+0.37*	+0.10*	+0.12*
Barren	SM	-0.24*	-0.52*	-0.54	-0.57*
	RF	+0.10	-0.30*	+0.22	+1.10*
	Annual	+0.01	-0.25*	+0.14	+0.26

*: There is a significant temporal trend at the 5% level; Green: Positive trends; Orange: Negative trends; SM: Snowmelt-dominated period; RF: Rainfall-dominated period.

Table 4.9. Land cover changes (%) per watershed and period in the ES. Land cover changes normalized by the sub-sample buffered research area within the ES (1668 km^2).

Land cover class	Period	Oldman River	Bow River	North Saskatchewan	Athabasca
Open water	SM	+0.2	+0.6	+0.5	+0.8
	RF	-0.3	-0.7	-0.7	-0.8
Non woody	SM	+0.6	+0.5	+0.4	+0.5
	RF	+0.4	-0.9	-1.0	-3.2
Woody/Shrub	SM	-0.1	+0.2	+0.3	+0.2
	RF	-0.4	+2.3	+1.1	+1.3
Barren	SM	-0.6	-1.2	-1.2	-1.5
	RF	+0.3	-0.7	+0.5	+2.7

Green: Positive changes; Orange: Negative changes; SM: Snowmelt-dominated period; RF: Rainfall-dominated period.

4.3.5. Land cover change over variable elevations

The study revealed that elevation demonstrated an influence on the direction and magnitude of land cover changes (Supplementary materials H of Chapter 4 show the land cover changes by 100 meters elevation). During the snowmelt-dominated period, an increase in open water was observed in the alpine (i.e., above 2300 meters) (+0.1%), and the subalpine regions (i.e., below 2300 meters) (+1.9%). In the same period an increase of non-woody vegetation in the subalpine (+1.9%) and alpine (+0.2%) was observed. Meanwhile, a slightly increase of woody and shrub vegetation was observed in the subalpine regions (+0.6%), while no change has been noticed in the alpine. In contrast, barren land cover has decreased in the subalpine (-4.0%) and alpine (-0.4%) regions.

In the rainfall-dominated period, the open water areas experienced a decline in the subalpine (-2.2%) and alpine (-0.2%). In response, non-woody vegetation decreased in the subalpine (-4.3%) and alpine (-0.4%). This drying pattern allowed woody and shrubs encroachment into subalpine (+4.3%) and alpine (+0.1%) areas. In addition, due to the reduction of open water in

these zones, barren have replaced into subalpine (+2.1%) and alpine (+0.5%). Figure 4.10 depicts a hypsometric curve (with 100 meters increments) of land cover area change in the alpine (≥ 2300 m) and subalpine (< 2300 m) of the ES. Figure 4.11 presents a summary of the land cover change in the alpine and subalpine of the ES since 1984. Table 4.10 shows the land cover change area per elevation, period and watershed in the ES. Supplementary materials I of Chapter 4 presents the Sankey diagram land cover change area per period, watershed and in subalpine and alpine regions of the ES. Figure 4.12 illustrates the variations in spatial characteristics across different watersheds and periods in alpine and subalpine regions, respectively.

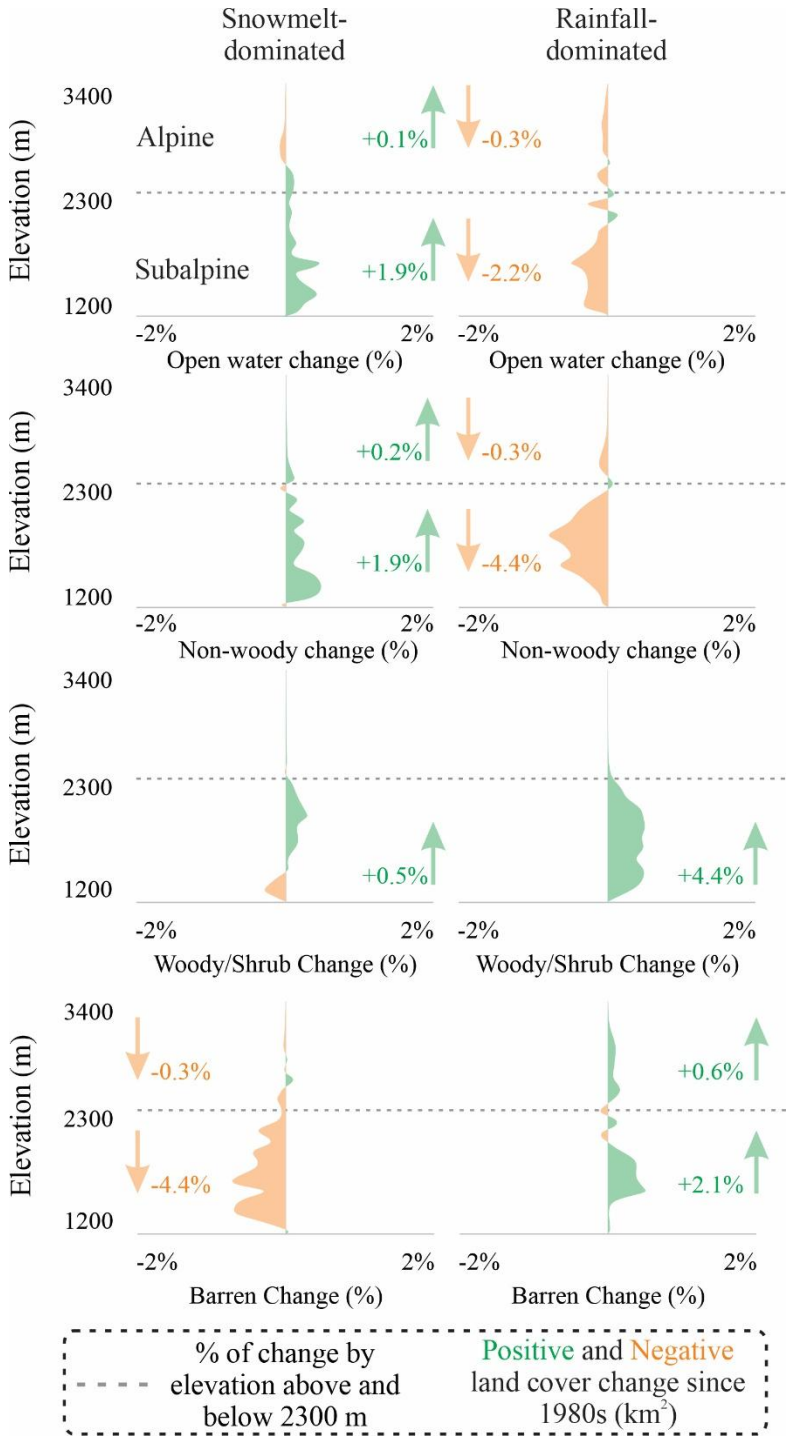

Fig. 4.10. Hypsometric curve (with 100 meters increments) of land cover area change (%) by period and watershed in the subalpine (< 2300 m) and alpine (≥ 2300 m) regions of the ES from the 1980s to the 2020s. The percentage of change is normalized by the total area of the Eastern Slopes of Alberta (1668 km²).

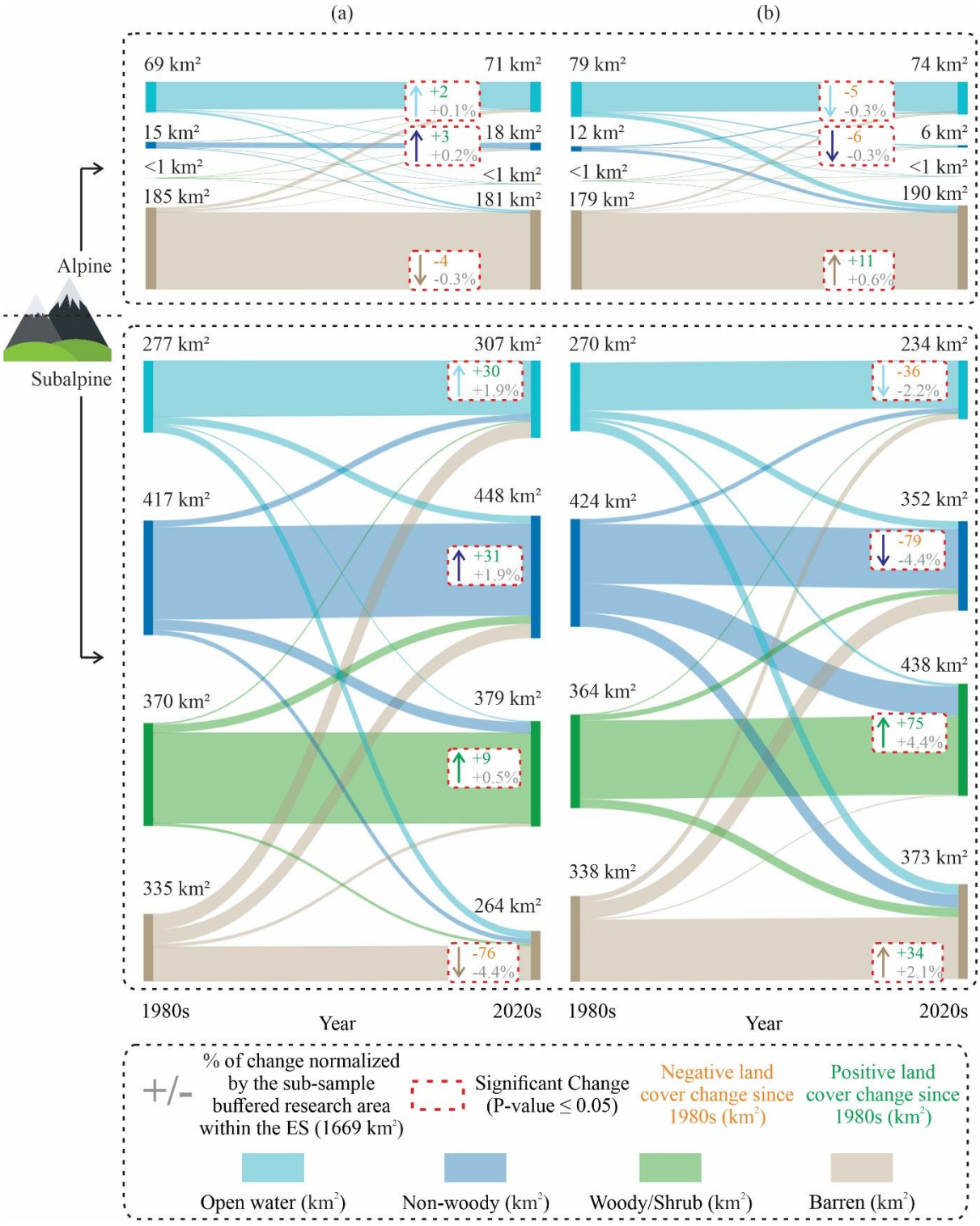

Fig. 4.11. Sankey diagram showing the land cover change area (km^2) and percentage (%) from 1980s to 2020s in alpine and subalpine regions normalized by the sub-sample buffered research area within the ES in the snowmelt-dominated (a) and rainfall-dominated (b) period.

Table 4.10. Land cover changes (%) in alpine and subalpine regions per watershed and period in the ES. Land cover changes normalized by the sub-sample buffered research area within the ES (1668 km^2).

Land cover class	Region	Period	Oldman River	Bow River	North Saskatchewan	Athabasca
Open water	Alpine	SM	<+0.1	<-0.1	<+0.1	+0.1
		RF	<-0.1	-0.3	-0.1	+0.2
	Subalpine	SM	+0.2	+0.6	+0.4	+0.7
		RF	-0.3	-0.4	-0.6	-1.0
Non woody	Alpine	SM	<+0.1	<+0.1	<+0.1	+0.1
		RF	<-0.1	+0.1	-0.2	-0.3
	Subalpine	SM	+0.6	+0.5	+0.4	+0.4
		RF	+0.4	-1.0	-0.8	-2.9
Woody / Shrub	Alpine	SM	-	-	-	-
		RF	-	-	<+0.1	<+0.1
	Subalpine	SM	-0.1	+0.2	+0.3	+0.2
		RF	-0.4	+2.3	+1.1	+1.3
Barren	Alpine	SM	-0.1	<-0.1	-0.1	-0.2
		RF	+0.1	+0.3	+0.3	+0.1
	Subalpine	SM	-0.5	-1.2	-1.1	-1.2
		RF	+0.2	-1.0	+0.2	+2.6

Green: Positive changes; Orange: Negative changes; SM: Snowmelt-dominated period; RF: Rainfall-dominated period; <+0.1: lower than +0.1%; <-0.1: lower than -0.1%; -: no change.

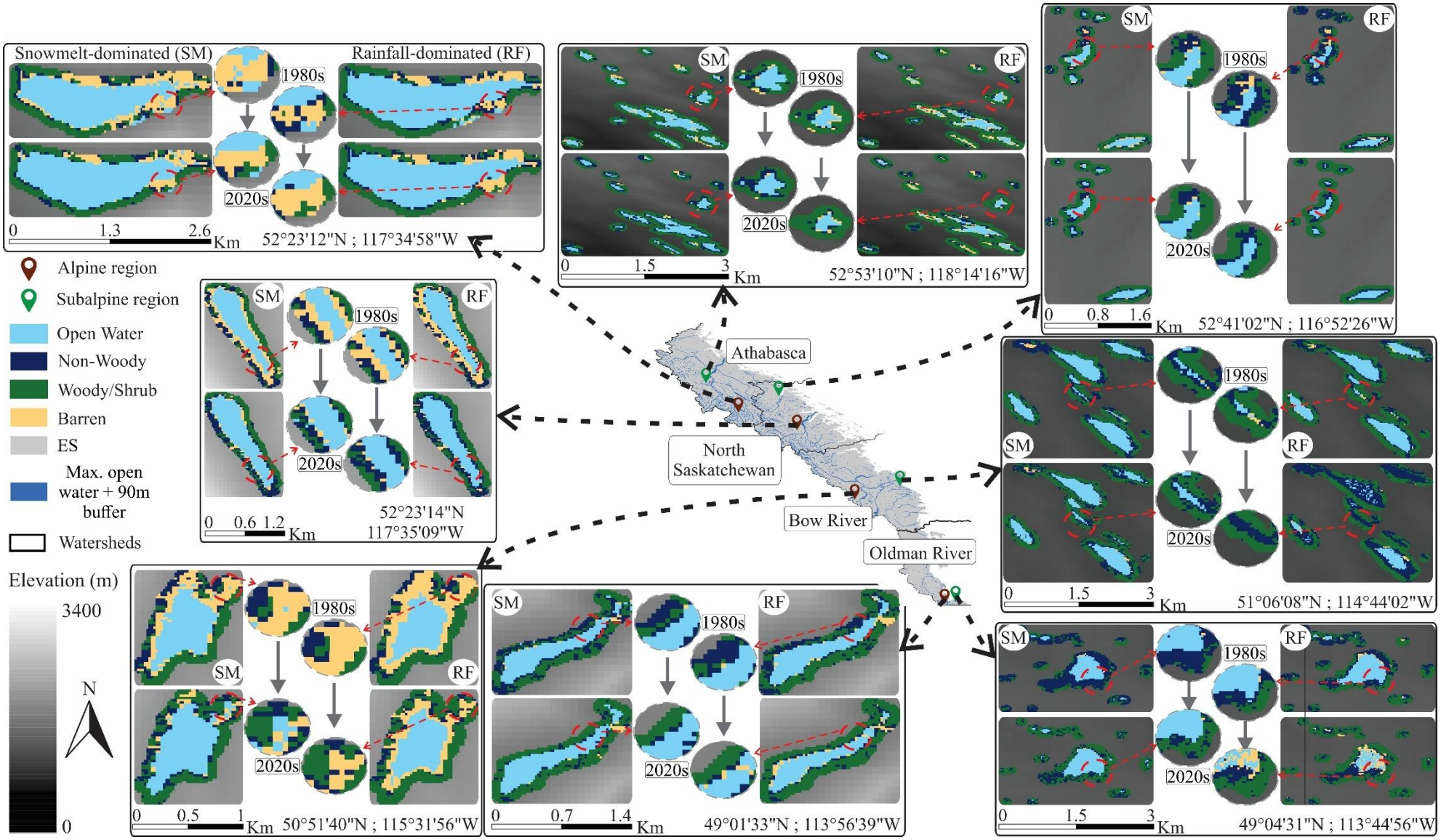

Fig. 4.12. Land cover change from 1980s to 2020s during the snowmelt- and rainfall-dominated period in the alpine and subalpine elevations of the ES

4.4. Discussion

4.4.1. Season identification

In temperate mountain environments, the active hydrological period spans from May–September, when the snow and glaciers start to melt. In the Eastern Slopes of Alberta (ES), the snowmelt-dominated period represents the spring and mid-summer season, which commences in mid-May and becomes less dominant (i.e., gradually transits to rainfall-dominated period, since snow- and glacier-melt continues through to the Fall and first snowfalls) in mid-July. The rainfall-dominated period is characterized by the mid-summer to late summer season, starting in the late-July and ending mid-September. Historically, the snowmelt-dominated period has always supported (through the snow- and glacier-melt) the rainfall-dominated period, essentially in the dry years, supplying water flow for many aquatic species (Milner et al. 2017). However, climate change has accelerated the hydrological cycle (i.e., increase of the air temperature, leading to earlier snow and glacier melting, higher rates of evapotranspiration, and growing-season length) (Zhang et al., 2000; Dyurgerov, 2003; Stewart et al., 2004; Stewart et al., 2005; Huntington, 2006; Wang et al., 2023), as a result, the snowmelt-dominated period has seen a rapid expansion of open water, while the rainfall-dominated period has seen a reduction in the open water areas.

The decrease in open water areas in the ES can have a direct effect on the surrounding herbaceous, non-woody vegetation. The strong link between open water and non-woody vegetation indicates that a reduction in open water areas can lead to the reduction or disappearance of water-reliant non-woody plants, a trend that historical data has confirmed for both types of land cover. Consequently, this decline in non-woody vegetation areas is likely to give way to an increase in woody and shrub vegetation, which has been increasing over time. The encroachment of woody and shrubs can affect water movement and evapotranspiration (Cui et al., 2022), potentially resulting in reduced soil moisture (Deng et al., 2021), and, ultimately, a drier environment that is primed for wildfires.

Furthermore, the river gauges from each watershed in the ES indicate that variations in basin area or flow are likely to result in a corresponding increase in lag time within the basin. As such, an increase in flow lags could delay the separation time of snowmelt- and rainfall-dominated period. For instance, the choice of Castle River in the Ranger Station (with the smaller watershed area) to represent the Oldman River basin was based on the fact that this watershed is narrower

relative to other northern basins, so the smaller sub-basin is likely more representative of flow lengths throughout the headwater.

4.4.2. Supervised classification benefits and limitations

This study's land cover classification employed various types of data for training and validation, resulting in an overall kappa average of 0.85, with higher accuracy during snowmelt-dominated period (mid-May to mid-July). In the snowmelt-dominated, open water, non-woody, woody/shrub, and barren were simpler to differentiate. During the rainfall-dominated (late-July to mid-September) period, there is higher greening in the non-woody and woody/shrub vegetation, which induces some degree of confusion between the vegetated classes. The non-woody and woody/shrub land cover class sometimes merge, which reduce kappa during rainfall-dominated period. Furthermore, the years with additional higher spatial resolution imagery (1984, 1987, 1988, 1991, 1994, 2002, 2003, 2016, 2017, 2018, 2019, 2020, 2021) for further training and validation were those that Random Forest demonstrated superior performance (average validation kappa of 0.93). This demonstrates how the land cover classification is enhanced by the addition of high-quality training/validation sites.

On the other hand, the post-validation kappa results were reduced in comparison to the historical supervised classification accuracy. For instance, in the snowmelt-dominated period, the range varied from 0.74 to 0.76, while in the rainfall-dominated period varied from 0.71 to 0.72. The rationale for this relates to the use of land cover change areas in the post-validation process, rather than solely focusing on regions that remained constant or unchanged throughout the years, such as the permanent training/validation pixels mentioned in section 4.2.5. The use of predominantly permanent pixels from Hermosilla et al. (2022) has proven to be an innovative method for classifying land cover. However, it also highlights the importance of incorporating training/validation pixels in land cover change areas into the land cover classification process on an annual basis, thereby enhancing the accuracy of the classification.

In the ES, the accuracy of land cover classes from the reference datasets varies. The accuracy of the Wetland Inventory of Alberta varies by elevation and vegetation structure. For instance, open water maintains the highest accuracy (88-92% across studies) due to its distinct spectral signature, though small alpine ponds (<0.1 ha) show 12-15% omission errors from shadow effects. Marshes achieve moderate accuracy (78-84%) but suffer seasonal variability, as late-lying

snowpack causes 9-11% commission errors into barren classes (DeLancey et al., 2019). Fens prove particularly challenging (70-76% accuracy) due to spectral mixing with wet meadows at tree line (Hird et al., 2017). Swamps demonstrate the least reliability (65-72%) due to several factors: dense shrub canopies hide groundwater signals, alpine krummholz is often incorrectly identified as swamp, and snow-loading affects winter synthetic aperture data backscatter (ABMI, 2021).

On the other hand, while the Canadian Historical Land Cover (Hermosilla et al., 2022) datasets provided a baseline for training data, this dataset demonstrated both precise and imprecise land cover classification in the ES. The high accuracy for open water (89–92%) demonstrates that permanent water bodies can be reliably detected even in rugged terrain. The moderate accuracy (75–80%) for non-woody vegetation highlights a key challenge in mountain hydrology: the spectral similarity observed between marshes and fens at the peak of the growing season. This uncertainty reflects the experience of field ecologists that these ecosystems operate along a dynamic ecological gradient (Zoltai and Vitt, 1995). The challenge increases in alpine regions, where late-lying snow patches are frequently misidentified as barren ground, which may lead to an underestimation of the extent of these climate-sensitive ecosystems.

However, by grouping some of the mountainous land covers into single classes the inherent variability of this ecosystem is simplified. For instance, using Hermosilla et al., (2022), Bryoides, marsh, and fen were grouped as non-woody vegetation, while shrubs, coniferous, broadleaf, and mixed wood were grouped as woody/shrub vegetation. Meanwhile, in the Wetland Inventory of Alberta (ABMI, 2021), non-woody vegetation was categorised as marsh and fen, while woody/shrub vegetation was classified as swamp. However, this simplification requires meticulous execution, employing stable training pixels (National Wetlands Working Group, 1997).

The use of results of classification processes as training data sources is not ideal, however, necessary in our scarce-data mountainous environment. To address these limitations, the use of permanent land cover pixels (unchanged from 1984 to 2023) as training anchors has the potential to enhance the reliability of the final land cover classification, as demonstrated by other studies. For instance, Pekel et al. (2016) enhanced classification accuracy in alpine zones by 11.7% when compared to traditional methods (one-time imagery, often summer scenes, or averages data across limited time), especially for shrub-wetland/upland detection. This method decreased seasonal snow misclassification errors from 15% to 6.2% by utilizing stable spectral baselines (Gorelick et al.,

2017). Thus, the use of unchanged simplified grouped land cover classes to allocate training and validation pixels over time showed an overall kappa average accuracy of 0.86.

In addition, to further validate the land cover classification, a confusion matrix regarding the land cover change classes (e.g., open water to non-woody, open water to woody/shrub, non-woody to woody/shrub, etc.) should be created using an independent dataset, for instance, the use of aerial photographs. This approach would help quantify errors of omission and commission between mapped (Random Forest algorithm results) and actual land cover changes (detected by aerial photography) while identifying systematic biases in the classification process. For robust validation, the reference data should be strategically sampled to represent all change classes proportionally and include challenging edge cases (e.g., partially vegetated open water areas or mixed shrub-water boundaries), ensuring the accuracy assessment reflects real-world land cover change conditions.

Furthermore, only composite images with a minimum total extent of more than 80% (i.e., cloud-pixel threshold of the image composite with < 20%) were utilized for the trend analysis. Therefore, certain years were excluded; for instance, in the overall picture of the entire ES composite, twelve were missed during the snowmelt-dominated period and three during the rainfall-dominated period. However, the exclusion of cloudy days can introduce a bias in the results, especially when studying seasonal or interannual trends in land cover dynamics. Cloudy periods are not random; they usually coincide with particular seasons (e.g., spring and early summer in the ES tend to be wetter and cloudier) or with significant climate events like El Niño and La Niña or Pacific Decadal Oscillation phases (Patterson et al., 2013). Filtering out clouds may unintentionally overrepresent drier, sunnier conditions and underrepresent wetter periods, so distorting the understanding of seasonal dynamics or long-term trends (Ju and Roy, 2008; White et al., 2014). Comparing the temporal distribution of accepted versus rejected images relative to the full climatological record (e.g., snowmelt- and rainfall-dominated periods) would help to investigate this bias.

Although the Landsat archive has proven to be quite beneficial in long-term wetland monitoring due to its extensive historical archive dating back to the 1980s. The 16-day revisit cycle and 30-meter spatial resolution are suitable for tracking extensive wetland changes over time. However, Sentinel-2 provides improved detail, greater precision in defining wetland boundaries, and enhanced accuracy in identifying smaller or fragmented wetlands due to its higher spatial resolution of 10 meters and more frequent revisit intervals (~5 days). The multispectral properties,

especially in the red-edge and shortwave infrared ranges, enhance the classification of various types of wetlands. The drawback lies in its limited timeline data availability (2015 – present). A significant benefit of Sentinel-1 (A and B from 2014 to 2021; C from 2024 – present) is its radar-based technology, which allows for cloud-penetrating capabilities. This ensures data acquisition is possible regardless of weather conditions, thereby aiding regions that frequently experience cloud cover. Its sensitivity to surface moisture renders it particularly useful for monitoring hydrological changes in wetlands and for detecting flooding. Nonetheless, the application of Sentinel-1 in mountainous regions requires careful terrain correction (Small, 2011), the integration of digital elevation models (Twele et al., 2016), and the fusion with optical imagery to address challenges in land cover interpretation (Zebker and Villasenor, 1992). In conclusion, although Landsat 8 is effective for analyzing historical trends, Sentinel-2 provides enhanced spatial and temporal resolution for precise wetland mapping, while Sentinel-1 guarantees reliable data collection, especially in areas with frequent cloud cover. Combining these databases allows for the utilization of their unique strengths, leading to a more precise and thorough wetland inventory.

Another method to mitigate this bias is to employ gap-filling strategies such as harmonic regression (Zhu et al., 2010) and evaluating how sensitive the results are to the missing observations. To ensure reliability, gap-filling methods need to be validated using observed data, such as aerial or in-situ geotagged photos. Nonetheless, the lack of consistent annual aerial or in-situ geotagged photos coverage in the ES creates uncertainty in efforts to use gap-filling methods.

Overall, even the most permanent training pixels may not completely shield against the constantly shifting complexities of Earth's surface. The reference pixels may remain unchanged; however, the spectral truth evolves due to sensor upgrades (e.g., Landsat 5 to Landsat 8, which involves slight alterations in the spectral resolution of their bands) (Roy et al., 2014), phenological variations (leaf-on/leaf-off) and seasonal dynamics (moisture levels, flooding cycles) (Zhang et al., 2003), disturbances (e.g., wildfires, floods, droughts, logging, or grazing; even if the class of the pixel has not permanently altered, the spectral signal will appear different) (Foody 2002).

4.4.3. Effects of hydroclimatological changes on the aquatic and riparian ecosystem of ES

The increase of open water areas during the snowmelt-dominated period is directly linked to the annual increase in air temperature of 0.04 to 0.06 °C in the ES, which is consistent with

findings from previous researchers (Luckman 1998; Stewart et al., 2004; Castellazzi et al., 2019; Musselman et al., 2021). The rise in air temperature has caused significant changes in the mountainous environments, such as, decrease in the amount of seasonal snowpack (Mote et al., 2005) and an earlier spring snowmelt (DeBeer et al., 2021; Rood et al., 2008; Stewart et al., 2004). These changes have led to increased river discharge (Brahney et al., 2017), expanded open water and lakes (Hauer et al., 1997), and a decline in groundwater levels due to the partially frozen and difficult-to-infiltrate soil (Millar et al., 2018).

Moreover, the western side of the ES has the largest portion of the snowfall and is home of the glaciers, which melt during the summer and late summer months. Consequently, with the rise in air temperature in recent years (Luckman, 1998; Trant et al., 2020), there has been an earlier melting of snowpack and glaciers (Moore et al., 2009; DeBeer et al., 2021). The earlier melting of snowpack during the snowmelt-period results in increased river discharge (Musselman et al., 2018), which promotes the expansion of connected open water areas. On the other hand, the snowpack that has built up during late fall, winter, and early spring in disconnected open water areas is experiencing earlier melting than in previous years, when the process was more gradual throughout the summer, thus, leading to an expansion of open water. Those processes accounts for the upward trend in the open water throughout the snowmelt-dominated period in the subalpine regions.

At a broader scale, Bevington and Menounos (2022) conducted a study in 14,329 glaciers in British Columbia and Alberta, Canada, between 1984 and 2020 using Landsat archives, whose showed an increase in the rate of glacier area loss after 2011. The increase resulted in area shrinkage rates of -49 km^2 $year^{-1}$ (before 2011) and -340 km^2 $year^{-1}$ (after 2011), leading to a total loss of -8%. In consequence, the extent of proglacial lakes or open water areas expanded to 565 km^2 in 2020. These findings are consistent with Armstrong et al., (2022), who utilized field- and satellite-based data to demonstrate that the Athabasca Glacier had a reduction in thickness of 60 meters between 1961 and 2020. In the Saskatchewan Glacier, Western ES, Kinnard et al. (2022) demonstrated a total decrease of -26.79 meters, between the years 1979 and 2016. The significant decrease in glacier size and the consequent increase in open water are directly associated with the observed increase of open water extent in the alpine region of the ES, as demonstrated by this research. Moreover, in the case of glacier melting and expansion (or genesis) of open water area in alpine regions, this connection is due to local geology and earlier snow- and glaciers-melt into areas of topographic depressions, thus causing lakes.

The results of this study are also associated with the Government of Alberta report, which indicated that the Athabasca rivers exhibited significant positive trends from 1912 to 2001 (Seneka, 2004). On the other hand, St Jacques et al. (2010) observed that the North Saskatchewan (1911 to 2007), Bow River (1912 to 2007), and the Oldman River (1912 to 2001) had seen significant negative trends.

The significant (p-value ≤ 0.05) increase in open water during the snowmelt-dominated period led to an expansion of water-dependent non-woody vegetation and a slightly encroachment of woody and shrub in the ES in subalpine and alpine regions (as illustrated in Figure 4.11). In contrast, a significant decrease in barren was observed in both regions, which is attributed to the significant expansion of open water throughout the snowmelt-dominated period. In the end of snowmelt-dominated period, in subalpine regions, the open water areas will retreat, but the soil and barren will still be moist. This will allow the non-woody and woody and shrub vegetation to expand into these moist and dry subalpine regions. The non-woody and woody and shrub vegetation expansion over the snowmelt-period supports the research by Rodrigues et al. (2024), who also observed a positive trend of woody and shrub growth in the Upper Columbia River floodplain valley from 1984 to 2022. The floodplain is located in British Columbia, on the West of the ES, and between the latitudes of the North Saskatchewan and Oldman River watersheds. On the other hand, in alpine regions connected to glaciers and with topographic depressions, open water areas are likely to continue to expand during the summer.

However, the reduced snowpack and early melt are leading to a rapid increase of open water during the snowmelt-dominated period, which are reducing the open water areas during late summer (i.e., rainfall-dominated period), particularly in disconnected open water areas. During the rainfall-dominated period, the subalpine and alpine regions in the ES are seeing a decrease (except in the alpine region of Athabasca, which increased) in open water areas. As a result, in the subalpine regions, water-dependent non-woody vegetation are drying out, thus, woody and shrub vegetation is gradually encroaching into the intermittent open water areas. In alpine regions, the reduction of open water areas is creating space for barren land and a slight increase in woody and shrub vegetation. The woody and shrub expansion are consistent with Conway and Danby (2014), Harsch et al. (2009), and Whited et al. (2025), who observed positive trends in the extension and filling of treeline and rapid riparian vegetation encroachment linked to glacier retreat in other mountainous environments.

In contrast to the overall decline in open water during rainfall-dominated period, the Athabasca watershed showed an increase of open water areas in the alpine regions (Supplementary materials H of Chapter 4). This positive trend might be related to the glacier melting, resulting in an expansion of open water areas and lakes during rainfall-dominated period. These results agree with Zemp et al. (2015) and Bevington and Menounos (2022) which has seen an increase in open water areas in alpine regions when glacier retreat over the summer and late summer periods. However, glacier melting in Athabasca alpine regions appear to be reaching its apex (Rood et al., 2004). Once peak glacier melting in Athabasca is over, its alpine open water areas trends may relate to other ES watersheds, which are having a negative trend. Overall, Figure 4.13 provides a concise overview of the land cover feedback resulting from the effects of hydroclimatological changes in ES's watersheds from 1984 onwards.

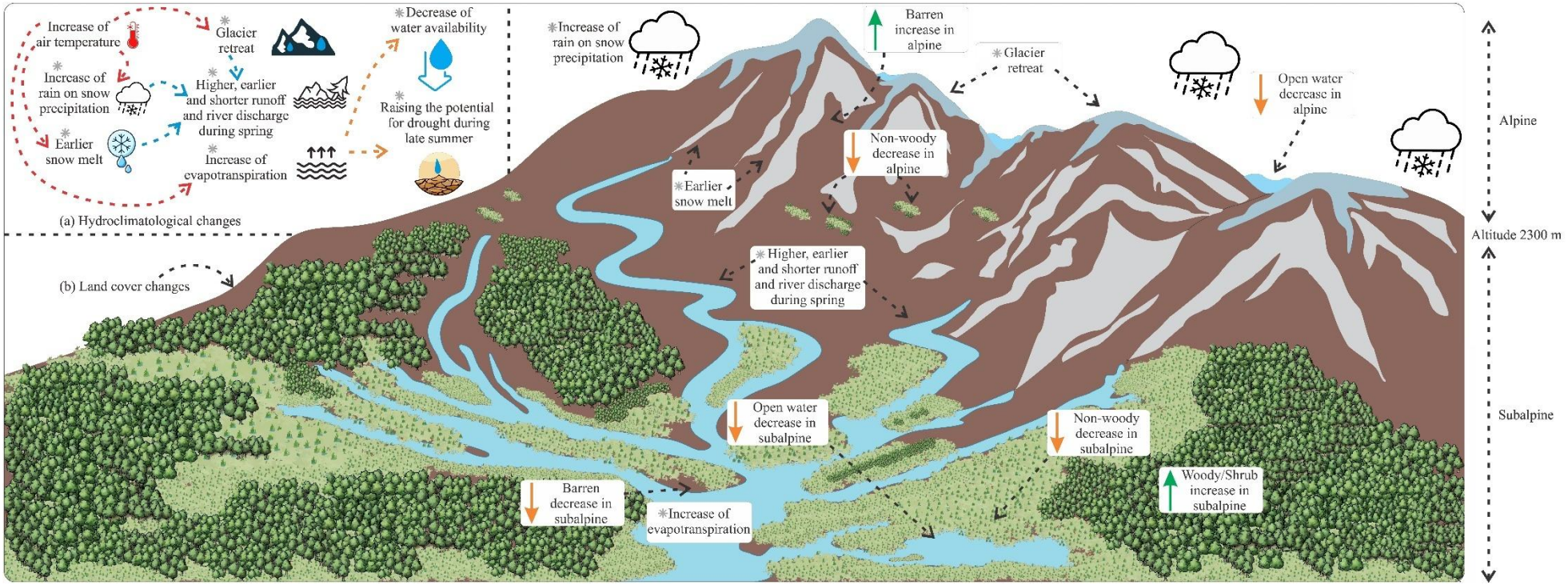

Fig. 4.13. Hydroclimatological changes (a) and the landcover feedback (b) in the Eastern Slopes of Alberta

* - Hydroclimatological changes based on literature: Increase of rain on snow precipitation from DeBeer et al. (2015), Notarnicola (2022), Whitfield and Shook (2019); Earlier snow melt from DeBeer et al. (2021) and Stewart et al. (2004); Glaciers wastage from Zemp et al. (2015); Higher, earlier, and shorter runoff and river discharge Rodrigues et al., (2024) and ; Increase of evapotranspiration from Kasurinen et al. (2014); Decrease of water availability from Barnett et al. (2005); Raising the potential for drought during late summer from Wheaton et al. (2008).

Moreover, according to Fernandes et al. (2007), the increasing evaporative demands in the Easter Slopes of Alberta will decrease the open water areas, allowing the expansion of non-woody plants and later encroachment of woody and shrub vegetation (Burkinshaw, 2005; Burkinshaw and Bork, 2009; Roush, 2009). The expansion of vegetation on land can affect various aspects of the hydrological cycle in a region, such as higher evapotranspiration rates by herbaceous and woody plants (Donohue et al., 2007), the increase of the precipitation interception by the canopy trees (Owens et al., 2006), lower runoff (Bonan, 2008), decreases of the groundwater recharge (Breeuwer et al. 2009; Potvin et al. 2015), and streamflow (Tennesen, 2008).

Furthermore, the increase in air temperatures during the rainfall-dominated period (0.06 ~ 0.09 °C $year^{-1}$) has influenced the timing of the start (earlier) and end (delayed) of the vegetation growing season in the Northern Hemisphere (Lian et al., 2020; Yan et al., 2023), which is attributed to the more frequent occurrence of Pacific Warm episodes (Cai et al., 2014). The vegetation community composition (i.e., density, distribution, and phenology) is the immediate ecosystem to respond to these abiotic changes (Danby and Hik, 2007; Myers-Smith and Hik, 2018). Climate change can promote the expansion of coniferous vegetation (Sanz-Elorza et al., 2003; Moffat et al., 2016; Wookey et al., 2009). In the high-latitude ecosystems of Canada, the combination of higher temperatures and drier late summers has led to the growth of shrub and woody species (Wang et al., 2022). This phenomenon is referred to as shrubification, as described by Leipe and Carey (2021) and Tremblay et al. (2012). These positive trends of woody and shrub encroachment relates well to all watersheds of ES.

Nonetheless, the drying of the wetland is not the only trajectory of land cover change, as wildfires have been occurring with increasing frequency over the years (Wang et al., 2025). Wildfires often transform dense vegetation, including woody plants, shrubs, or herbaceous areas, to ashes or bare soil (Farid et al., 2024). For instance, the Oldman River showed a negative trend of woody and shrub species, possibly due to the massive wildfire of 2017 that burned 75% of woody and non-woody species (Eisenberg et al., 2019; Buunk, 2021). Treating wildfire areas as barren in this study will likely lead to a rapid increase in woody and shrub growth, thus overestimating the extent to which the region is becoming shrubbier. Therefore, it is necessary to mask wildfire regions to accurately identify true vegetation trends separate from the effects of post-fire succession. This approach would prevent the misclassification of early-successional vegetation as stable shrubland or forest, avoid the artificial inflation of greening trends in areas that have burned, ensures temporal

consistency in land cover classification, and allows for the differentiation between anthropogenic changes and disturbance-recovery cycles.

In the ES, wildfires have impacted wetland dynamics, resulting in both short-term (<5 years) and long-term (>10 years) consequences (Alberta Wildfire, 2023; Wilkinson et al., 2021). Short-term impacts involve a notable expansion of barren areas due to ash deposition and a delay in vegetation recovery (Hood and Bayley, 2008). In contrast, long-term changes highlight an increase in shrub dominance and a decrease in open water in regions where peat layers have burned (Turetsky et al., 2015). The interactions of climate significantly enhance these transformations, especially through the rapid snowmelt occurring in burned watersheds (Burles and Boon, 2011). On the other hand, beaver activity aided in the recovery of marshes burned regions (Fairfax and Whittle, 2021), showcasing the resilience of nature. Overall, the combined impacts of fire and climate are fundamentally transforming these wetland ecosystems (Schneider et al., 2023).

Changes in the composition and arrangement of vegetation has resulted in intricate interactions between soil, plants, and the atmosphere. These interactions affect the way water is received, retained, and released in the ES, consequently influencing the regional climate cycle. This impact is primarily mediated through the albedo feedback and energy distribution (Bonan, 2008; Chapin et al., 2005; Lafleur and Humphreys, 2018). The characteristics of vegetation, such as its type, height, and density, have a considerable influence on the accumulation of snow and rainfall, as well as the interception and infiltration of water (Liu et al., 2022; Sturm et al., 2005; Zwieback et al., 2019). Additionally, an increase in the height and coverage of shrubs enhances the ability to trap snow (Pomeroy et al., 2006). Vegetation has an impact on the speed and timing of snow melting and evapotranspiration (Brümmer et al., 2012; Kasurinen et al., 2014). For instance, tall shrubs speed up the melting process by emitting longwave radiation (Marsh et al., 2010), while also reducing turbulent fluxes by shading the soil and decreasing evaporation (Endrizzi and Marsh, 2010).

All in all, the air temperature and precipitation are the primary climatological factors that influence the alpine regions of the ES. The air temperature controls the duration and rate of snowmelt, while precipitation determines the amount of snowfall. These factors play a crucial role in driving changes in these non-woodies and woody ecosystems (Mote et al., 2005). Global warming has various impacts on alpine regions, such as the degradation of permafrost (Walvoord and Kurylyk, 2016), the retreat of glaciers (Zemp et al., 2015), and changes in precipitation

quantity, timing, and phase (e.g., liquid, or solid, or mixed of both, such as rain-on-snow) (DeBeer et al., 2015, DeBeer et al., 2021; Notarnicola, 2022; Whitfield and Shook, 2019). In addition, warming also has the tendency to elevate the occurrence of rain-on-snow events in mountainous areas (McCabe et al., 2007; Ye, et al., 2008). As average temperatures near the freezing point, there is an increased chance that temperatures will exceed the thresholds at which precipitation occurs as rain rather than snow (Gottlieb and Mankin, 2024). For instance, in the Canadian Rocky Mountains, this shift from snowfall to rain is leading to an increase of runoff by 50% in the spring, as reported by Musselman et al. (2018). The results align with the observed increase of open water extent during the snowmelt-dominated period, which is related to the expansion of water-dependent non-woody vegetation area.

Overall, alpine ecosystem is undergoing some of the fastest climate-related changes on Earth and seem to be warming up faster than other ecosystems worldwide (Masson-Delmotte et al., 2018; Pepin et al., 2015). Rising temperatures are leading to a reduction in the average snowfall and spring snowpack in ES (Marty and Blanchet, 2012; Mote et al., 2005; Gottlieb and Mankin, 2024), as well as the shrinkage or disappearance of glaciers (Beniston et al., 2018; Zemp et al., 2015). Overall, continuous changes in land cover and river flow patterns (Huss and Hock, 2018; Poloczanska et al., 2019) may lead to catastrophic or potentially irreversible outcomes in these ecosystems.

4.5. Conclusion

This study provides insights into different patterns and transformations in land cover in the Eastern Slopes of Alberta (ES), Canada, throughout the past four decades. Snowmelt- (May 15 to July 20) and rainfall-dominated period (July 20 to September 15) were identified, which allowed the land cover classification in these two periods. The observed increase in open water during the snowmelt-dominated period can be attributed to the positive trends in air temperature, which affects earlier snow- and glaciers- melt in the study area, leading to the fast seasonal spread of open water in places that were previously covered by barren. In the rainfall-dominated period, the ES are becoming drier as a result of the open water areas reduction. The reason for this phenomenon may be attributed to rising temperatures, decreased-, earlier-, and phase-change precipitation, and higher evapotranspiration rates.

Furthermore, based on the evaluation of land cover change with respect to elevation, in the snowmelt-dominated period, open water, non-woody, and woody/shrub vegetation have increased

while barren has decreased in both subalpine (≤ 2300 m) and alpine (> 2300 m) regions. In contrast, during the rainfall-dominated period, the reduction of open water areas has increased barren land cover. Barren areas are transitioning to non-woody vegetation. Meanwhile, there is a transformation of habitat from non-woody to woody and shrub in both altitudes, indicating a process of succession.

The decrease in open water creates opportunities for the spread of non-woody areas that were previously covered by water. Drier conditions are transforming non-woody areas into shrub and woody vegetation. The transition from herbaceous to woody plants is a natural succession. However, in alpine and subalpine of the ES, climate change has accelerated the encroachment of woody ecotones. However, caution is necessary in interpreting these results, since wildfires were considered as barren land cover. This is likely to result in a rapid increase in woody/shrub increase, thereby overestimating the degree to which the region is becoming more shrubby. Thus, masking wildfire regions is essential to accurately identify authentic vegetation trends associated with hydroclimatic changes, independent of the effects of post-fire succession. As far as the author knows, this study is the first to analyze the alpine and subalpine land cover trends on a broad scale during the nival and pluvial period in four key headwater basins in of the Rocky Mountains of Canada.

Acknowledgements

The authors received funding provided by the Natural Sciences and Engineering Research Council of Canada (NSERC; grant no. 2017-04362), Alberta Innovates, the Nexen Fellowship in Water Resources, the Columbia Wetlands Stewardship Partners and the Shuswap Band's Columbia Headwaters Aquatic Restoration Secwépemc Strategy (CHARS) project.

4.6. References

ABMI. 2021. "ABMI Wetland Inventory – Metadata." Edmonton, Alberta, Canada.

Adam, E., Mutanga, O., & Rugege, D. (2022). Remote sensing of wetlands in mountain regions: A review. *Remote Sensing, 14*(3), 492. https://doi.org/10.3390/rs14030492

Alberta Climate Information Service (ACIS) https://acis.alberta.ca (December, 2023)

Alberta Government: Air Photos. Province of Alberta, https://www.alberta.ca/air-photos (last access: 15 April 2024), 2024.

Alberta Parks. (2015). Natural Regions and Subregions of Alberta. A Framework for Alberta's Parks. Alberta Tourism, Parks and Recreation. Edmonton, Alberta. 72pp.

Alberta Wildfire. (2023). *Eastern Slopes wildfire impacts report (1984–2023)*. Alberta Agriculture and Forestry.

Amani, M., Mahdavi, S., Kakooei, M., Ghorbanian, A., Brisco, B., DeLancey, E., Toure, S., & Reyes, E. L. (2021). Wetland Change Analysis in Alberta, Canada Using Four Decades of Landsat Imagery. *IEEE Journal of Selected Topics in Applied Earth Observations and Remote Sensing*, *14*, 10314–10335. https://doi.org/10.1109/jstars.2021.3110460

Armstrong, W. H., Polashenski, D., Truffer, M., Horne, G., Hanson, J. B., Hawley, R. L., Hengst, A. M., Vowels, L., Menounos, B., & Van Wychen, W. (2022). Declining Basal Motion Dominates the Long-Term Slowing of Athabasca Glacier, Canada. *Journal of Geophysical Research Earth Surface*, *127*(10). https://doi.org/10.1029/2021jf006439

Avis, C. A., Weaver, A. J., & Meissner, K. J. (2011). Reduction in areal extent of high-latitude wetlands in response to permafrost thaw. Nature Geoscience, 4(7), 444–448. https://doi.org/10.1038/ngeo1160

Bach, A. F., Van Der Schrier, G., Melsen, L. A., Tank, A. M. G. K., & Teuling, A. J. (2018). Widespread and Accelerated Decrease of Observed Mean and Extreme Snow Depth Over Europe. *Geophysical Research Letters*, *45*(22). https://doi.org/10.1029/2018gl079799

Barnett, T. P., Adam, J. C., & Lettenmaier, D. P. (2005). Potential impacts of a warming climate on water availability in snow-dominated regions. *Nature*, *438*(7066), 303–309. https://doi.org/10.1038/nature04141

Beniston, M., Farinotti, D., Stoffel, M., Andreassen, L. M., Coppola, E., Eckert, N., Fantini, A., Giacona, F., Hauck, C., Huss, M., Huwald, H., Lehning, M., López-Moreno, J., Magnusson, J., Marty, C., Morán-Tejéda, E., Morin, S., Naaim, M., Provenzale, A., . . . Vincent, C. (2018). The European mountain cryosphere: a review of its current state, trends, and future challenges. *The Cryosphere*, *12*(2), 759–794. https://doi.org/10.5194/tc-12-759-2018

Berghuijs, W. R., Woods, R. A., & Hrachowitz, M. (2014). A precipitation shift from snow towards rain leads to a decrease in streamflow. *Nature Climate Change*, *4*(7), 583–586. https://doi.org/10.1038/nclimate2246

Bertoncini, A., & Pomeroy, J. W. (2025). Quantifying spatiotemporal and elevational precipitation gauge network uncertainty in the Canadian Rockies. Hydrology and Earth System Sciences, 29, 983–1000. https://doi.org/10.5194/hess-29-983-2025

Bevington, A. R., & Menounos, B. (2022). Accelerated change in the glaciated environments of western Canada revealed through trend analysis of optical satellite imagery. *Remote Sensing of Environment*, *270*, 112862. https://doi.org/10.1016/j.rse.2021.112862

Bian, J., Li, A., Lei, G., Zhang, Z., & Nan, X. (2020). Global high-resolution mountain green cover index mapping based on Landsat images and Google Earth Engine. *ISPRS Journal of Photogrammetry and Remote Sensing*, *162*, 63–76. https://doi.org/10.1016/j.isprsjprs.2020.02.011

Bonan, G. B. (2008). Forests and Climate Change: Forcings, Feedbacks, and the Climate Benefits of Forests. *Science*, *320*(5882), 1444–1449. https://doi.org/10.1126/science.1155121

Bork, E. W., & Su, J. G. (2007). Integrating LIDAR data and multispectral imagery for enhanced classification of rangeland vegetation. *Remote Sensing of Environment, 111*(1), 11–24. https://doi.org/10.1016/j.rse.2007.03.011

Brahney, J., Weber, F., Foord, V., Janmaat, J., & Curtis, P. J. (2017). Evidence for a climate-driven hydrologic regime shift in the Canadian Columbia Basin. *Canadian Water Resources Journal / Revue Canadienne Des Ressources Hydriques*, *42*(2), 179–192. https://doi.org/10.1080/07011784.2016.1268933

Breeuwer, A., Robroek, B. J., Limpens, J., Heijmans, M. M., Schouten, M. G., & Berendse, F. (2008). Decreased summer water table depth affects peatland vegetation. *Basic and Applied Ecology*, *10*(4), 330–339. https://doi.org/10.1016/j.baae.2008.05.005

Breiman, L. (2001). Random forests. *Machine Learning*, *45*(1), 5–32. https://doi.org/10.1023/a:1010933404324

Brunbjerg, A. K., Fløjgaard, C., Frøslev, T. G., Andersen, D. K., Bruun, H. H., Dalby, L., Goldberg, I., Lehmann, L. J., Moeslund, J. E., & Ejrnæs, R. (2022). Scrub encroachment promotes biodiversity in temperate European wetlands under eutrophic conditions. *Ecology and Evolution*, *12*(11). https://doi.org/10.1002/ece3.9445

Brümmer, C., Black, T. A., Jassal, R. S., Grant, N. J., Spittlehouse, D. L., Chen, B., Nesic, Z., Amiro, B. D., Arain, M. A., Barr, A. G., Bourque, C. P., Coursolle, C., Dunn, A. L., Flanagan, L. B., Humphreys, E. R., Lafleur, P. M., Margolis, H. A., McCaughey, J. H., & Wofsy, S. C. (2011). How climate and vegetation type influence evapotranspiration and water use efficiency in Canadian forest, peatland and grassland ecosystems. *Agricultural and Forest Meteorology*, *153*, 14–30. https://doi.org/10.1016/j.agrformet.2011.04.008

Buunk, C. J. (2021). Mountains on fire: Making sense of change in Waterton Lakes National Park (Doctoral dissertation).

Burkinshaw, A. M., & Bork, E. W. (2009). Shrub Encroachment Impacts the Potential for Multiple Use Conflicts on Public Land. *Environmental Management*, *44*(3), 493–504. https://doi.org/10.1007/s00267-009-9328-2

Burkinshaw, A. M. (2005). Shrub encroachment onto floodplain meadows within the Rocky Mountain Forest Reserve, Alberta.

Burles, K., & Boon, S. (2011). Snowmelt energy balance in a burned forest plot, Crowsnest Pass, Alberta, Canada. *Hydrological Processes*, 25(6), 923–935. https://doi.org/10.1002/hyp.8067

Cai, W., Borlace, S., Lengaigne, M., Van Rensch, P., Collins, M., Vecchi, G., Timmermann, A., Santoso, A., McPhaden, M. J., Wu, L., England, M. H., Wang, G., Guilyardi, E., & Jin, F. (2014). Increasing frequency of extreme El Niño events due to greenhouse warming. *Nature Climate Change*, *4*(2), 111–116. https://doi.org/10.1038/nclimate2100

Campbell, D. H., Baron, J. S., Tonnessen, K. A., Brooks, P. D., & Schuster, P. F. (2000). Controls

on nitrogen flux in alpine/subalpine watersheds of Colorado. *Water Resources Research*, *36*(1), 37–47. https://doi.org/10.1029/1999wr900283

Carrivick, J. L., & Heckmann, T. (2017). Short-term geomorphological evolution of proglacial systems. *Geomorphology*, *287*, 3–28. https://doi.org/10.1016/j.geomorph.2017.01.037

Castellazzi, P., Burgess, D., Rivera, A., Huang, J., Longuevergne, L., & Demuth, M. N. (2019). Glacial Melt and Potential Impacts on Water Resources in the Canadian Rocky Mountains. *Water Resources Research*, *55*(12), 10191–10217. https://doi.org/10.1029/2018wr024295

Chapin, F. S., Sturm, M., Serreze, M. C., McFadden, J. P., Key, J. R., Lloyd, A. H., McGuire, A. D., Rupp, T. S., Lynch, A. H., Schimel, J. P., Beringer, J., Chapman, W. L., Epstein, H. E., Euskirchen, E. S., Hinzman, L. D., Jia, G., Ping, C., Tape, K. D., Thompson, C. D. C., Welker, J. M. (2005). Role of Land-Surface Changes in Arctic Summer Warming. *Science*, *310*(5748), 657–660. https://doi.org/10.1126/science.1117368

Chassé, J., Lambert, N., & Lavoie, D. (2013). Precipitation, Evaporation and Freshwater Flux over Canada from Six Global Climate Models. Canadian Technical Report of Hydrography and Ocean Sciences, 287.

Clarke, G. K. C., Jarosch, A. H., Anslow, F. S., Radić, V., & Menounos, B. (2015). Projected deglaciation of western Canada in the twenty-first century. *Nature Geoscience*, *8*(5), 372–377. https://doi.org/10.1038/ngeo2407

Conway, A. J., & Danby, R. K. (2014). Recent advance of forest–grassland ecotones in southwestern Yukon. *Canadian Journal of Forest Research*, *44*(5), 509–520. https://doi.org/10.1139/cjfr-2013-0429

Congalton, R. G., & Green, K. (2019). *Assessing the Accuracy of Remotely Sensed Data: Principles and Practices, Third Edition*. CRC Press.

Cui, J., Lian, X., Huntingford, C., Gimeno, L., Wang, T., Ding, J., He, M., Xu, H., Chen, A., Gentine, P., & Piao, S. (2022). Global water availability boosted by vegetation-driven changes in atmospheric moisture transport. *Nature Geoscience*, *15*(12), 982–988. https://doi.org/10.1038/s41561-022-01061-7

Danby, R. K., & Hik, D. S. (2007). Variability, contingency and rapid change in recent subarctic alpine tree line dynamics. *Journal of Ecology*, *95*(2), 352–363. https://doi.org/10.1111/j.1365-2745.2006.01200.x

DeBeer, C. M., Wheater, H. S., Pomeroy, J. W., Barr, A. G., Baltzer, J. L., Johnstone, J. F., Turetsky, M. R., Stewart, R. E., Hayashi, M., Van Der Kamp, G., Marshall, S., Campbell, E., Marsh, P., Carey, S. K., Quinton, W. L., Li, Y., Razavi, S., Berg, A., McDonnell, J. J., . . . Pietroniro, A. (2021). Summary and synthesis of Changing Cold Regions Network (CCRN) research in the interior of western Canada – Part 2: Future change in cryosphere, vegetation, and hydrology. *Hydrology and Earth System Sciences*, *25*(4), 1849–1882. https://doi.org/10.5194/hess-25-1849-2021

DeBeer, C. M., Wheater, H. S., Carey, S. K., & Chun, K. P. (2015). Recent climatic, cryospheric, and hydrological changes over the interior of western Canada: a synthesis and review. *Hydrology and Earth System Sciences*. https://doi.org/10.5194/hessd-12-8615-2015

DeLancey, E. R., Simms, J. F., Mahdianpari, M., Brisco, B., Mahoney, C., & Kariyeva, J. (2019). Comparing Deep Learning and Shallow Learning for Large-Scale Wetland Classification in Alberta, Canada. *Remote Sensing*, *12*(1), 2. https://doi.org/10.3390/rs12010002

Deng, Y., Li, X., Shi, F., & Hu, X. (2021). Woody plant encroachment enhanced global vegetation greening and ecosystem water-use efficiency. *Global Ecology and Biogeography*, *30*(12), 2337–2353. https://doi.org/10.1111/geb.13386

Décamps, H., Pinay, G., Naiman, R. J., Petts, G. E., McClain, M. E., Hillbricht-Ilkowska, A., Hanley, T. A., Holmes, R. M., Quinn, J., Gibert, J., Planty-Tabacchi, A. M., Schiemer, F., Tabacchi, E., & Zalewski, M. (2004). Riparian zones: Where biogeochemistry meets biodiversity in management practice. Polish Journal of Ecology, 52(1), 3–18.

Déry, S. J., Stadnyk, T. A., MacDonald, M. K., & Gauli-Sharma, B. (2016). Recent trends and variability in river discharge across northern Canada. *Hydrology and Earth System Sciences*, *20*(12), 4801–4818. https://doi.org/10.5194/hess-20-4801-2016

Donohue, R. J., McVICAR, T. R., & Roderick, M. L. (2009). Climate-related trends in Australian vegetation cover as inferred from satellite observations, 1981–2006. *Global Change Biology*, *15*(4), 1025–1039. https://doi.org/10.1111/j.1365-2486.2008.01746.x

Donohue, R. J., Roderick, M. L., & McVicar, T. R. (2007). On the importance of including vegetation dynamics in Budyko's hydrological model. *Hydrology and Earth System Sciences*, *11*(2), 983–995. https://doi.org/10.5194/hess-11-983-2007

Dyurgerov, M. (2003). Mountain and subpolar glaciers show an increase in sensitivity to climate warming and intensification of the water cycle. *Journal of Hydrology*, *282*(1–4), 164–176. https://doi.org/10.1016/s0022-1694(03)00254-3

Eisenberg, C., Anderson, C. L., Collingwood, A., Sissons, R., Dunn, C. J., Meigs, G. W., Hibbs, D. E., Murphy, S., Kuiper, S. D., SpearChief-Morris, J., Bear, L. L., Johnston, B., & Edson, C. B. (2019). Out of the Ashes: Ecological Resilience to Extreme Wildfire, Prescribed Burns, and Indigenous Burning in Ecosystems. *Frontiers in Ecology and Evolution*, *7*. https://doi.org/10.3389/fevo.2019.00436

Endrizzi, S., & Marsh, P. (2010). Observations and modeling of turbulent fluxes during melt at the shrub-tundra transition zone 1: point scale variations. *Hydrology Research*, *41*(6), 471–491. https://doi.org/10.2166/nh.2010.149

Environment Canada.: "HYDAT database". Environment Canada. Accessed June, 2024. https://wateroffice.ec.gc.ca/report/historical_e.html?stn=05AA028, 2024a

Environment Canada.: "HYDAT database". Environment Canada. Accessed June, 2024. https://wateroffice.ec.gc.ca/report/historical_e.html?stn=05BB001, 2024b

Environment Canada.: “HYDAT database”. Environment Canada. Accessed June, 2024. https://wateroffice.ec.gc.ca/report/historical_e.html?stn=05DA009, 2024c

Environment Canada.: “HYDAT database”. Environment Canada. Accessed June, 2024. https://wateroffice.ec.gc.ca/report/historical_e.html?stn=07AA002, 2024d

Fernandes, R., Korolevych, V., & Wang, S. (2007). Trends in Land Evapotranspiration over Canada for the Period 1960–2000 Based on In Situ Climate Observations and a Land Surface Model. *Journal of Hydrometeorology*, *8*(5), 1016–1030. https://doi.org/10.1175/jhm619.1

Fairfax, E., & Whittle, A. J. (2021). Smokey the Beaver: Beaver-dammed riparian corridors stay green during wildfire throughout the western United States. *Ecological Applications*, 102(1), e01795. https://doi.org/10.1002/bes2.1795

Farid, A., Alam, M. K., Goli, V. S. N. S., Akin, I. D., Akinleye, T., Chen, X., Cheng, Q., Cleall, P., Cuomo, S., Foresta, V., Ge, S., Iervolino, L., Iradukunda, P., Luce, C. H., Koda, E., Mickovski, S. B., O’Kelly, B. C., Paleologos, E. K., Peduto, D., Winkler, J. (2024). A review of the occurrence and causes for wildfires and their impacts on the geoenvironment. *Fire*, *7*(8), 295. https://doi.org/10.3390/fire7080295

Fernandes, M. R., Aguiar, F. C., & Ferreira, M. T. (2014). Assessing riparian vegetation structure and the influence of land use using landscape metrics and geostatistical tools. Landscape and Urban Planning, 120, 226–236. https://doi.org/10.1016/j.landurbplan.2013.09.002

Foody, G. M. (2002). Status of land cover classification accuracy assessment. Remote Sensing of Environment, 80(1), 185–201. https://doi.org/10.1016/s0034-4257(01)00295-4

Foga, S., Scaramuzza, P. L., Guo, S., Zhu, Z., Dilley, R. D., Beckmann, T., Schmidt, G. L., Dwyer, J. L., Hughes, M. J., & Laue, B. (2017). Cloud detection algorithm comparison and validation for operational Landsat data products. *Remote Sensing of Environment*, *194*, 379–390. https://doi.org/10.1016/j.rse.2017.03.026

Gorelick, N., Hancher, M., Dixon, M., Ilyushchenko, S., Thau, D., & Moore, R. (2017). Google Earth Engine: Planetary-scale geospatial analysis for everyone. *Remote Sensing of Environment, 202*, 18–27. https://doi.org/10.1016/j.rse.2017.06.031

Gottlieb, A. R., & Mankin, J. S. (2024). Evidence of human influence on Northern Hemisphere snow loss. *Nature*, *625*(7994), 293–300. https://doi.org/10.1038/s41586-023-06794-y

Government of Alberta – Boundary Files, Reference Guide, Second edition, 2016 Census. Statistics Canada Catalogue no. 92-160-G.

Gregory, S. V., Swanson, F. J., McKee, W. A., & Cummins, K. W. (1991). An ecosystem perspective of riparian zones. BioScience, 41(8), 540–551. https://doi.org/10.2307/1311607

Harder, P., Pomeroy, J. W., & Westbrook, C. J. (2015). Hydrological resilience of a Canadian Rockies headwaters basin subject to changing climate, extreme weather, and forest management. *Hydrological Processes*, *29*(18), 3905–3924. https://doi.org/10.1002/hyp.10596

Harpold, A. A., & Molotch, N. P. (2015). Sensitivity of soil water availability to changing snowmelt timing in the western U.S. *Geophysical Research Letters*, *42*(19), 8011–8020. https://doi.org/10.1002/2015gl065855

Harsch, M. A., Hulme, P. E., McGlone, M. S., & Duncan, R. P. (2009). Are treelines advancing? A global meta-analysis of treeline response to climate warming. *Ecology Letters*, *12*(10), 1040–1049. https://doi.org/10.1111/j.1461-0248.2009.01355.x

Hauer, F. R., Baron, J. S., Campbell, D. H., Fausch, K. D., Hostetler, S. W., Leavesley, G. H., Leavitt, P. R., Mcknight, D. M., & Stanford, J. A. (1997). Assessment of climate change and freshwater ecosystems of the rocky mountains, USA and Canada. *Hydrological Processes*, *11*(8), 903–924. https://doi.org/10.1002/(sici)1099-1085(19970630)11:8

Hermosilla, T., Wulder, M. A., White, J. C., & Coops, N. C. (2022). Land cover classification in an era of big and open data: Optimizing localized implementation and training data selection to improve mapping outcomes. *Remote Sensing of Environment*, *268*, 112780. https://doi.org/10.1016/j.rse.2021.112780

Hird, J., DeLancey, E., McDermid, G., & Kariyeva, J. (2017). Google Earth Engine, Open-Access Satellite Data, and Machine Learning in Support of Large-Area Probabilistic Wetland Mapping. *Remote Sensing*, *9*(12), 1315. https://doi.org/10.3390/rs9121315

Hogg, E. H., & Hurdle, P. A. (1995). The Aspen Parkland in Western Canada: a Dry-Climate analogue for the future Boreal forest? In *Springer eBooks* (pp. 391–400). https://doi.org/10.1007/978-94-017-0942-2_37

Hood, G. A., & Bayley, S. E. (2008). Beaver (Castor canadensis) mitigate the effects of climate on the area of open water in boreal wetlands in western Canada. Biological Conservation, 141(2), 556–567. https://doi.org/10.1016/j.biocon.2007.12.003

Hopkinson, C., & Young, G. J. (1998). The effect of glacier wastage on the flow of the Bow River at Banff, Alberta, 1951–1993. *Hydrological Processes*, *12*(10–11), 1745–1762. https://doi.org/10.1002/(sici)1099-1085(199808/09)12:10/11

Huntington, T. G. (2005). Evidence for intensification of the global water cycle: Review and synthesis. *Journal of Hydrology*, *319*(1–4), 83–95. https://doi.org/10.1016/j.jhydrol.2005.07.003

Hussain, M., & Mahmud, I. (2019). pyMannKendall: a python package for non parametric Mann Kendall family of trend tests. *The Journal of Open Source Software*, *4*(39), 1556. https://doi.org/10.21105/joss.01556

Huss, M., & Hock, R. (2018). Global-scale hydrological response to future glacier mass loss. *Nature Climate Change*, *8*(2), 135–140. https://doi.org/10.1038/s41558-017-0049-x

Intergovernmental Panel on Climate Change. (2021). *Climate change 2021: The physical science basis. Contribution of Working Group I to the Sixth Assessment Report*. Cambridge University Press. https://www.ipcc.ch/report/ar6/wg1/

Johnston, C. A. (1991). Sediment and nutrient retention by freshwater wetlands: Effects on surface water quality. *Critical Reviews in Environmental Control*, *21*(5–6), 491–565. https://doi.org/10.1080/10643389109388425

Jost, G., Moore, R. D., Menounos, B., & Wheate, R. (2012). Quantifying the contribution of glacier runoff to streamflow in the upper Columbia River Basin, Canada. *Hydrology and Earth System Sciences*, *16*(3), 849–860. https://doi.org/10.5194/hess-16-849-2012

Ju, J., & Roy, D. P. (2008). The availability of cloud-free Landsat ETM+ data over the conterminous United States and globally. *Remote Sensing of Environment, 112*(3), 1196–1211. https://doi.org/10.1016/j.rse.2007.08.011

Kasurinen, V., Alfredsen, K., Kolari, P., Mammarella, I., Alekseychik, P., Rinne, J., Vesala, T., Bernier, P., Boike, J., Langer, M., Marchesini, L. B., Van Huissteden, K., Dolman, H., Sachs, T., Ohta, T., Varlagin, A., Rocha, A., Arain, A., Oechel, W., Berninger, F. (2014). Latent heat exchange in the boreal and arctic biomes. *Global Change Biology*, *20*(11), 3439–3456. https://doi.org/10.1111/gcb.12640

Kendall, M. G. (1957). Rank Correlation Methods. *Biometrika*, *44*(1/2), 298. https://doi.org/10.2307/2333282

Kinnard, C., Larouche, O., Demuth, M. N., & Menounos, B. (2022). Modelling glacier mass balance and climate sensitivity in the context of sparse observations: application to Saskatchewan Glacier, western Canada. *The Cryosphere*, *16*(8), 3071–3099. https://doi.org/10.5194/tc-16-3071-2022

Körner, C. (2021). *Alpine Plant Life: Functional Plant Ecology of High Mountain Ecosystems*. Springer Nature.

Lafleur, P. M., & Humphreys, E. R. (2018). Tundra shrub effects on growing season energy and carbon dioxide exchange. *Environmental Research Letters*, *13*(5), 055001. https://doi.org/10.1088/1748-9326/aab863

Lantz, T. C., Gergel, S. E., & Henry, G. H. R. (2010). Response of green alder (Alnus viridis subsp. fruticosa) patch dynamics and plant community composition to fire and regional temperature in north-western Canada. *Journal of Biogeography*, *37*(8), 1597–1610. https://doi.org/10.1111/j.1365-2699.2010.02317.x

Leipe, S. C., & Carey, S. K. (2021). Rapid shrub expansion in a subarctic mountain basin revealed by repeat airborne LiDAR. *Environmental Research Communications*, *3*(7), 071001. https://doi.org/10.1088/2515-7620/ac0e0c

Levenberg, K. (1944). A method for the solution of certain non-linear problems in least squares. *Quarterly of Applied Mathematics*, *2*(2), 164–168. https://doi.org/10.1090/qam/10666

Lian, X., Piao, S., Li, L. Z. X., Li, Y., Huntingford, C., Ciais, P., Cescatti, A., Janssens, I. A., Peñuelas, J., Buermann, W., Chen, A., Li, X., Myneni, R. B., Wang, X., Wang, Y., Yang, Y., Zeng, Z., Zhang, Y., & McVicar, T. R. (2020). Summer soil drying exacerbated by earlier spring greening of northern vegetation. *Science Advances*, *6*(1). https://doi.org/10.1126/sciadv.aax0255

Liu, Y., Cui, Z., Huang, Z., López-Vicente, M., Zhao, J., Ding, L., & Wu, G. (2022). Shrub encroachment in alpine meadows increases the potential risk of surface soil salinization by redistributing soil water. *CATENA*, *219*, 106593. https://doi.org/10.1016/j.catena.2022.106593

Luckman, B. H. (1998). Landscape and climate change in the central Canadian Rockies during the 20th century. *Canadian Geographies / Géographies Canadiennes*, *42*(4), 319–336. https://doi.org/10.1111/j.1541-0064.1998.tb01349.x

Lutes, D. C., Keane, R. E., Caratti, J. F., Key, C. H., Benson, N. C., Sutherland, S., & Gangi, L. J. (2006). *FIREMON: Fire effects monitoring and inventory system*. https://doi.org/10.2737/rmrs-gtr-164

MacDonald, G. M., Edwards, T. W. D., Moser, K. A., Pienitz, R., & Smol, J. P. (1993). Rapid response of treeline vegetation and lakes to past climate warming. *Nature*, *361*(6409), 243–246. https://doi.org/10.1038/361243a0

Mahdianpari, M., Jafarzadeh, H., Granger, J. E., Mohammadimanesh, F., Brisco, B., Salehi, B., Homayouni, S., & Weng, Q. (2020). A large-scale change monitoring of wetlands using time series Landsat imagery on Google Earth Engine: a case study in Newfoundland. *GIScience & Remote Sensing*, *57*(8), 1102–1124. https://doi.org/10.1080/15481603.2020.1846948

Mann, H. B. (1945). Nonparametric Tests Against Trend. *Econometrica*, *13*(3), 245. https://doi.org/10.2307/1907187

Marquardt, D. W. (1963). An Algorithm for Least-Squares Estimation of Nonlinear Parameters. *Journal of the Society for Industrial and Applied Mathematics*, *11*(2), 431–441. https://doi.org/10.1137/0111030

Marsh, P., Bartlett, P., MacKay, M., Pohl, S., & Lantz, T. (2010). Snowmelt energetics at a shrub tundra site in the western Canadian Arctic. *Hydrological Processes*, *24*(25), 3603–3620. https://doi.org/10.1002/hyp.7786

Marty, C., & Blanchet, J. (2011). Long-term changes in annual maximum snow depth and snowfall in Switzerland based on extreme value statistics. *Climatic Change*, *111*(3–4), 705–721. https://doi.org/10.1007/s10584-011-0159-9

Massmann, A., Gentine, P., & Lin, C. (2019). When does vapor pressure deficit drive or reduce evapotranspiration? *Journal of Advances in Modeling Earth Systems*, *11*(10), 3305–3320. https://doi.org/10.1029/2019ms001790

Masson-Delmotte, V., Zhai, P., Pörtner, H., Roberts, D., Skea, J., Priyadarshi, R., Pirani, A., Moufouma-Okia, W., Péan, C., Pidcock, R., Connors, S., Matthews, J. R., Chen, Y., Zhou, X., Gomis, M., Lonnoy, E., Maycock, T., Tignor, M., & Waterfield, T. (2019). Global Warming of 1.5°C. An IPCC Special Report on the impacts of global warming of 1.5°C above pre-industrial levels and related global greenhouse gas emission pathways, in the context of strengthening the global response to the threat of climate change,sustainable development, and efforts to eradicate poverty. In *IPCC (Intergovernmental Panel on Climate Change)*. http://www.vliz.be/en/imis?module=ref&refid=323552

Mastrotheodoros, T., Pappas, C., Molnar, P., Burlando, P., Manoli, G., Parajka, J., Rigon, R., Szeles, B., Bottazzi, M., Hadjidoukas, P., & Fatichi, S. (2020). More green and less blue water in the Alps during warmer summers. *Nature Climate Change*, *10*(2), 155–161. https://doi.org/10.1038/s41558-019-0676-5

McCabe, G. J., Clark, M. P., & Hay, L. E. (2007). Rain-on-Snow Events in the Western United States. *Bulletin of the American Meteorological Society*, *88*(3), 319–328. https://doi.org/10.1175/bams-88-3-319

Menounos, B., Hugonnet, R., Shean, D., Gardner, A., Howat, I., Berthier, E., Pelto, B., Tennant, C., Shea, J., Noh, M., Brun, F., & Dehecq, A. (2018). Heterogeneous changes in western North American glaciers linked to decadal variability in zonal wind strength. *Geophysical Research*

Letters, *46*(1), 200–209. https://doi.org/10.1029/2018gl080942

Menze, B. H., Kelm, B. M., Masuch, R., Himmelreich, U., Bachert, P., Petrich, W., & Hamprecht, F. A. (2009). A comparison of random forest and its Gini importance with standard chemometric methods for the feature selection and classification of spectral data. *BMC Bioinformatics*, *10*(1). https://doi.org/10.1186/1471-2105-10-213

Mercer, J. J. (2018). Insights into mountain wetland resilience to climate change: An evaluation of the hydrological processes contributing to the hydrodynamics of alpine wetlands in the Canadian Rocky Mountains. https://harvest.usask.ca/bitstream/10388/11257/1/MERCER-THESIS-2018.pdf

Millar, D. J., Cooper, D. J., & Ronayne, M. J. (2018). Groundwater dynamics in mountain peatlands with contrasting climate, vegetation, and hydrogeological setting. *Journal of Hydrology*, *561*, 908–917. https://doi.org/10.1016/j.jhydrol.2018.04.050

Milner, A. M., Khamis, K., Battin, T. J., Brittain, J. E., Barrand, N. E., Füreder, L., Cauvy-Fraunié, S., Gíslason, G. M., Jacobsen, D., Hannah, D. M., Hodson, A. J., Hood, E., Lencioni, V., Ólafsson, J. S., Robinson, C. T., Tranter, M., & Brown, L. E. (2017). Glacier shrinkage driving global changes in downstream systems. *Proceedings of the National Academy of Sciences*, *114*(37), 9770–9778. https://doi.org/10.1073/pnas.1619807114

Moffat, N. D., Lantz, T. C., Fraser, R. H., & Olthof, I. (2016). Recent Vegetation Change (1980–2013) in the Tundra Ecosystems of the Tuktoyaktuk Coastlands, NWT, Canada. *Arctic Antarctic and Alpine Research*, *48*(3), 581–597. https://doi.org/10.1657/aaar0015-063

Moore, R. D., Fleming, S. W., Menounos, B., Wheate, R., Fountain, A., Stahl, K., Holm, K., & Jakob, M. (2008). Glacier change in western North America: influences on hydrology, geomorphic hazards and water quality. *Hydrological Processes*, *23*(1), 42–61. https://doi.org/10.1002/hyp.7162

Mote, P. W., Hamlet, A. F., Clark, M. P., & Lettenmaier, D. P. (2005). Declining mountain snowpack in Western North America. *Bulletin of the American Meteorological Society*, *86*(1), 39–50. https://doi.org/10.1175/bams-86-1-39

Musselman, K. N., Addor, N., Vano, J. A., & Molotch, N. P. (2021). Winter melt trends portend widespread declines in snow water resources. *Nature Climate Change*, *11*(5), 418–424. https://doi.org/10.1038/s41558-021-01014-9

Musselman, K. N., Lehner, F., Ikeda, K., Clark, M. P., Prein, A. F., Liu, C., Barlage, M., & Rasmussen, R. (2018). Projected increases and shifts in rain-on-snow flood risk over western North America. *Nature Climate Change*, *8*(9), 808–812. https://doi.org/10.1038/s41558-018-0236-4

Myers-Smith, I. H., & Hik, D. S. (2017). Climate warming as a driver of tundra shrubline advance. *Journal of Ecology*, *106*(2), 547–560. https://doi.org/10.1111/1365-2745.12817

Naiman, R. J., Décamps, H., & McClain, M. E. (2005). Riparia: Ecology, conservation, and management of streamside communities. Elsevier Academic Press.

National Wetlands Working Group. (1997). The Canadian wetland classification system (2nd ed.). Wetlands Research Centre, University of Waterloo.

Notarnicola, C. (2022). Overall negative trends for snow cover extent and duration in global mountain regions over 1982–2020. *Scientific Reports*, *12*(1). https://doi.org/10.1038/s41598-022-16743-w

Owens, M. K., Lyons, R. K., & Alejandro, C. L. (2006). Rainfall partitioning within semiarid juniper communities: effects of event size and canopy cover. *Hydrological Processes*, *20*(15), 3179–3189. https://doi.org/10.1002/hyp.6326

Owens, M. K., Lyons, R. K., & Alejandro, C. L. (2006). Rainfall partitioning within semiarid juniper communities: effects of event size and canopy cover. *Hydrological Processes*, *20*(15), 3179–3189. https://doi.org/10.1002/hyp.6326

Patterson, R. T., Chang, A. S., Prokoph, A., Roe, H. M., & Swindles, G. T. (2013). Influence of the Pacific Decadal Oscillation, El Niño-Southern Oscillation and solar forcing on climate and primary productivity changes in the northeast Pacific. *Quaternary International*, *310*, 124–139. https://doi.org/10.1016/j.quaint.2013.02.001

Pepin, N., Bradley, R. S., Diaz, H. F., Baraer, M., Caceres, E. B., Forsythe, N., Fowler, H., Greenwood, G., Hashmi, M. Z., Liu, X. D., Miller, J. R., Ning, L., Ohmura, A., Palazzi, E., Rangwala, I., Schöner, W., Severskiy, I., Shahgedanova, M., Wang, M. B., . . . Yang, D. Q. (2015). Elevation-dependent warming in mountain regions of the world. *Nature Climate Change*, *5*(5), 424–430. https://doi.org/10.1038/nclimate2563

Petrone, R. M., Price, J. S., Carey, S. K., & Waddington, J. M. (2003). Statistical characterization of the spatial variability of soil moisture in a cutover peatland. *Hydrological Processes*, *18*(1), 41–52. https://doi.org/10.1002/hyp.1309

Philipsen, L. J., Gill, K. M., Shepherd, A., & Rood, S. B. (2018). Climate change and hydrology at the prairie margin: Historic and prospective future flows of Canada's Red Deer and other Rocky Mountain rivers. *Hydrological Processes*, *32*(17), 2669–2684. https://doi.org/10.1002/hyp.13180

Pleniou, M., & Koutsias, N. (2013). Sensitivity of spectral reflectance values to different burn and vegetation ratios: A multi-scale approach applied in a fire affected area. *ISPRS Journal of Photogrammetry and Remote Sensing*, *79*, 199–210. https://doi.org/10.1016/j.isprsjprs.2013.02.016

Poloczanska, E., Mintenbeck, K., Portner, H. O., Roberts, D., & Levin, L. A. (2018). The IPCC special report on the ocean and cryosphere in a changing climate. In 2018 Ocean Sciences Meeting. AGU.

Pomeroy, J., Bewley, D., Essery, R., Hedstrom, N., Link, T., Granger, R., Sicart, J., Ellis, C., & Janowicz, J. (2006). Shrub tundra snowmelt. *Hydrological Processes*, *20*(4), 923–941. https://doi.org/10.1002/hyp.6124

Potvin, L. R., Kane, E. S., Chimner, R. A., Kolka, R. K., & Lilleskov, E. A. (2014). Effects of water table position and plant functional group on plant community, aboveground production, and peat properties in a peatland mesocosm experiment (PEATcosm). *Plant and Soil*, *387*(1–2), 277–294. https://doi.org/10.1007/s11104-014-2301-8

Rodrigues, I. S., Hopkinson, C., Chasmer, L., MacDonald, R. J., Bayley, S. E., & Brisco, B. (2024).

Multi-decadal floodplain classification and trend analysis in the Upper Columbia River valley, British Columbia. *Hydrology and Earth System Sciences*, *28*(10), 2203–2221. https://doi.org/10.5194/hess-28-2203-2024

Rood, S. B., Pan, J., Gill, K. M., Franks, C. G., Samuelson, G. M., & Shepherd, A. (2007). Declining summer flows of Rocky Mountain rivers: Changing seasonal hydrology and probable impacts on floodplain forests. *Journal of Hydrology*, *349*(3–4), 397–410. https://doi.org/10.1016/j.jhydrol.2007.11.012

Rood, S. B., Samuelson, G., Weber, J., & Wywrot, K. (2004). Twentieth-century decline in streamflows from the hydrographic apex of North America. *Journal of Hydrology*, *306*(1–4), 215–233. https://doi.org/10.1016/j.jhydrol.2004.09.010

Roush, W. M. (2009). A substantial upward shift of the alpine treeline ecotone in the southern Canadian Rocky Mountains (Doctoral dissertation).

Roy, D. P., Kovalskyy, V., Zhang, H. K., Vermote, E. F., Yan, L., Kumar, S. S., & Egorov, A. (2016). Characterization of Landsat-7 to Landsat-8 reflective wavelength and normalized difference vegetation index continuity. Remote Sensing of Environment, 185, 57–70. https://doi.org/10.1016/j.rse.2015.12.024

Roy, D., Wulder, M., Loveland, T., CE, W., Allen, R., Anderson, M., Helder, D., Irons, J., Johnson, D., Kennedy, R., Scambos, T., Schaaf, C., Schott, J., Sheng, Y., Vermote, E., Belward, A., Bindschadler, R., Cohen, W., Gao, F., Zhu, Z. (2014). Landsat-8: Science and product vision for terrestrial global change research. *Remote Sensing of Environment*, *145*, 154–172. https://doi.org/10.1016/j.rse.2014.02.001

Ruzzante, S. W., & Gleeson, T. (2025). Rising temperatures drive lower summer minimum flows across hydrologically diverse catchments in British Columbia. *Water Resources Research*, *61*(2). https://doi.org/10.1029/2024wr038057

Sanz-Elorza, M., Dana, E. D., González, A., & Sobrino, E. (2003). Changes in the High-mountain Vegetation of the Central Iberian Peninsula as a Probable Sign of Global Warming. *Annals of Botany*, *92*(2), 273–280. https://doi.org/10.1093/aob/mcg130

Schneider, R. R., Devito, K., & Bayne, E. (2023). Cumulative effects of wildfire and climate change on Alberta's mountain wetlands. *Environmental Reviews*, 31(1), 1–15. https://doi.org/10.1139/er-2022-0066

Selmants, P. C., Conrad, C. R., Wilson, T. S., & Villarreal, M. L. (2023). Resilience of riparian vegetation productivity to early 21st century drought in northern California, USA. *Ecosphere*, *14*(8). https://doi.org/10.1002/ecs2.4638

Seneka, M. (2004). Trends in historical annual flows for major rivers in Alberta. Alberta Environment, Environmental Monitoring & Evaluation Branch, Evaluation & Reporting Section, Water Assessment Team.

Shugar, D. H., Burr, A., Haritashya, U. K., Kargel, J. S., Watson, C. S., Kennedy, M. C., Bevington, A. R., Betts, R. A., Harrison, S., & Strattman, K. (2020). Rapid worldwide growth of glacial lakes since 1990. *Nature Climate Change*, *10*(10), 939–945. https://doi.org/10.1038/s41558-020-0855-4

Shuttle Radar Topography Mission. 2023 (Digital Object Identifier – DOI): /10.5066/F7F76B1X. Accessed November, 2023. https://earthexplorer.usgs.gov/

Small, D. (2011). Flattening Gamma: Radiometric terrain correction for SAR imagery. *IEEE Transactions on Geoscience and Remote Sensing*, 49(8), 3081–3093. https://doi.org/10.1109/TGRS.2011.2120616

Stewart, I. T., Cayan, D. R., & Dettinger, M. D. (2005). Changes toward Earlier Streamflow Timing across Western North America. *Journal of Climate*, *18*(8), 1136–1155. https://doi.org/10.1175/jcli3321.1

Stewart, I. T., Cayan, D. R., & Dettinger, M. D. (2004). Changes in Snowmelt Runoff Timing in Western North America under a `Business as Usual' Climate Change Scenario. *Climatic Change*, *62*(1–3), 217–232. https://doi.org/10.1023/b:clim.0000013702.22656.e8

St Jacques, J., Sauchyn, D. J., & Zhao, Y. (2010). Northern Rocky Mountain streamflow records: Global warming trends, human impacts or natural variability? *Geophysical Research Letters*, *37*(6). https://doi.org/10.1029/2009gl042045

Sturm, M., Douglas, T., Racine, C., & Liston, G. E. (2005). Changing snow and shrub conditions affect albedo with global implications. *Journal of Geophysical Research Atmospheres*, *110*(G1). https://doi.org/10.1029/2005jg000013

Tennant, C., Menounos, B., Wheate, R., & Clague, J. J. (2012). Area change of glaciers in the Canadian Rocky Mountains, 1919 to 2006. *The Cryosphere*, *6*(6), 1541–1552. https://doi.org/10.5194/tc-6-1541-2012

Tennesen, M. (2008). When Juniper and Woody Plants Invade, Water May Retreat. *Science*, *322*(5908), 1630–1631. https://doi.org/10.1126/science.322.5908.1630

Teuling, A. J., De Badts, E. a. G., Jansen, F. A., Fuchs, R., Buitink, J., Van Dijke, A. J. H., & Sterling, S. M. (2019). Climate change, reforestation/afforestation, and urbanization impacts on evapotranspiration and streamflow in Europe. *Hydrology and Earth System Sciences*, *23*(9), 3631–3652. https://doi.org/10.5194/hess-23-3631-2019

Trant, A., Higgs, E., & Starzomski, B. M. (2020). A century of high elevation ecosystem change in the Canadian Rocky Mountains. *Scientific Reports*, *10*(1). https://doi.org/10.1038/s41598-020-66277-2

Tremblay, B., Lévesque, E., & Boudreau, S. (2012). Recent expansion of erect shrubs in the Low Arctic: evidence from Eastern Nunavik. *Environmental Research Letters*, *7*(3), 035501. https://doi.org/10.1088/1748-9326/7/3/035501

Turetsky, M. R., Benscoter, B., Page, S., Rein, G., van der Werf, G. R., & Watts, A. (2015). Global vulnerability of peatlands to fire and carbon loss. Nature Geoscience, 8(1), 11–14. https://doi.org/10.1038/ngeo2325

Twele, A., Cao, W., Plank, S., & Martinis, S. (2016). Sentinel-1-based flood mapping: A fully automated processing chain. *International Journal of Remote Sensing*, 37(13), 2990–3004. https://doi.org/10.1080/01431161.2016.1192304

Walvoord, M. A., & Kurylyk, B. L. (2016). Hydrologic Impacts of Thawing Permafrost—A Review. *Vadose Zone Journal*, *15*(6), 1–20. https://doi.org/10.2136/vzj2016.01.0010

Wang, J., Liu, D., Ciais, P., & Peñuelas, J. (2022). Decreasing rainfall frequency contributes to earlier leaf onset in northern ecosystems. *Nature Climate Change*, *12*(4), 386–392. https://doi.org/10.1038/s41558-022-01285-w

Wang, W. W., Wang, X., Flannigan, M. D., Guindon, L., Swystun, T., Castellanos-Acuna, D., Wu, W., & Wang, G. (2025). Canadian forests are more conducive to high severity fires in recent decades. Science, 387, 91–97. https://doi.org/10.1126/science.ado1006

Wang, Y., Meili, N., & Fatichi, S. (2023). Evidence and Controls of the Acceleration of the Hydrological Cycle Over Land. *Water Resources Research*, *59*(8). https://doi.org/10.1029/2022wr033970

Wheaton, E., Kulshreshtha, S., Wittrock, V., & Koshida, G. (2008). Dry times: hard lessons from the Canadian drought of 2001 and 2002. *Canadian Geographies / Géographies Canadiennes*, *52*(2), 241–262. https://doi.org/10.1111/j.1541-0064.2008.00211.x

White, J. C., Wulder, M. A., Hobart, G. W., Luther, J. E., Hermosilla, T., Griffiths, P., Coops, N. C., Hall, R. J., Hostert, P., Dyk, A., & Guindon, L. (2014). Pixel-Based Image Compositing for Large-Area Dense Time Series Applications and Science. *Canadian Journal of Remote Sensing*, *40*(3), 192–212. https://doi.org/10.1080/07038992.2014.945827

Whited, D., Pitman, K. J., Moore, J. W., Sergeant, C. J., Sexton, E., & Connor, M. (2025). Rapid riparian vegetation development and channel stabilization linked to glacier retreat within a large transboundary watershed. *Earth Surface Processes and Landforms*, *50*(1). https://doi.org/10.1002/esp.6045

Whitfield, P. H., Kraaijenbrink, P. D. A., Shook, K. R., & Pomeroy, J. W. (2021). The spatial extent of hydrological and landscape changes across the mountains and prairies of Canada in the Mackenzie and Nelson River basins based on data from a warm-season time window. Hydrology and Earth System Sciences, 25(5), 2513–2541. https://doi.org/10.5194/hess-25-2513-2021

Whitfield, P. H., & Shook, K. R. (2019). Changes to rainfall, snowfall, and runoff events during the autumn–winter transition in the Rocky Mountains of North America. *Canadian Water Resources Journal / Revue Canadienne Des Ressources Hydriques*, *45*(1), 28–42. https://doi.org/10.1080/07011784.2019.1685910

Windell, J. T., Willard, B. E., Cooper, D. J., Foster, S. Q., Knud-Hansen, C. F., Rink, L. P., & Kiladis, G. N. (1986). *An ecological characterization of Rocky Mountain montane and subalpine wetlands*. U. S. Fish & Wildlife Service Biological Report.

Wookey, P. A., Aerts, R., Bardgett, R. D., Baptist, F., Bråthen, K. A., Cornelissen, J. H. C., Gough, L., Hartley, I. P., Hopkins, D. W., Lavorel, S., & Shaver, G. R. (2008). Ecosystem feedbacks and cascade processes: understanding their role in the responses of Arctic and alpine ecosystems to environmental change. *Global Change Biology*, *15*(5), 1153–1172. https://doi.org/10.1111/j.1365-2486.2008.01801.x

Wulder, M. A., Roy, D. P., Radeloff, V. C., Loveland, T. R., Anderson, M. C., Johnson, D. M., Healey, S., Zhu, Z., Scambos, T. A., Pahlevan, N., Hansen, M., Gorelick, N., Crawford, C. J., Masek, J. G., Hermosilla, T., White, J. C., Belward, A. S., Schaaf, C., Woodcock, C. E., . . . Cook, B. D. (2022). Fifty years of Landsat science and impacts. *Remote Sensing of Environment*, *280*, 113195. https://doi.org/10.1016/j.rse.2022.113195

Wulder, M., Li, Z., Campbell, E., White, J., Hobart, G., Hermosilla, T., & Coops, N. (2018). A National Assessment of Wetland Status and Trends for Canada's Forested Ecosystems Using 33 Years of Earth Observation Satellite Data. *Remote Sensing*, *10*(10), 1623. https://doi.org/10.3390/rs10101623

Yan, W., Yang, F., Zhou, J., & Wu, R. (2023). Droughts force temporal change and spatial migration of vegetation phenology in the northern Hemisphere. *Agricultural and Forest Meteorology*, *341*, 109685. https://doi.org/10.1016/j.agrformet.2023.109685

Ye, H., Yang, D., & Robinson, D. (2008). Winter rain on snow and its association with air temperature in northern Eurasia. *Hydrological Processes*, *22*(15), 2728–2736. https://doi.org/10.1002/hyp.7094

Zebker, H. A., & Villasenor, J. (1992). Decorrelation in interferometric radar echoes. *IEEE Transactions on Geoscience and Remote Sensing*, 30(5), 950–959. https://doi.org/10.1109/36.175330

Zemp, M., Frey, H., Gärtner-Roer, I., Nussbaumer, S. U., Hoelzle, M., Paul, F., Haeberli, W., Denzinger, F., Ahlstrøm, A. P., Anderson, B., Bajracharya, S., Baroni, C., Braun, L. N., Cáceres, B. E., Casassa, G., Cobos, G., Dávila, L. R., Granados, H. D., Demuth, M. N., . . . Vincent, C. (2015). Historically unprecedented global glacier decline in the early 21st century. *Journal of Glaciology*, *61*(228), 745–762. https://doi.org/10.3189/2015jog15j017

Zhang, X., Vincent, L. A., Hogg, W., & Niitsoo, A. (2000). Temperature and precipitation trends in Canada during the 20th century. *Atmosphere-Ocean*, *38*(3), 395–429. https://doi.org/10.1080/07055900.2000.9649654

Zhang, X., Friedl, M. A., Schaaf, C. B., Strahler, A. H., Hodges, J. C., Gao, F., Reed, B. C., & Huete, A. (2003). Monitoring vegetation phenology using MODIS. Remote Sensing of Environment, 84(3), 471–475. https://doi.org/10.1016/s0034-4257(02)00135-9

Zheng, G., Allen, S. K., Bao, A., Ballesteros-Cánovas, J. A., Huss, M., Zhang, G., Li, J., Yuan, Y., Jiang, L., Yu, T., Chen, W., & Stoffel, M. (2021). Increasing risk of glacial lake outburst floods from future Third Pole deglaciation. *Nature Climate Change*, *11*(5), 411–417. https://doi.org/10.1038/s41558-021-01028-3

Zhu, X., Chen, J., Gao, F., Chen, X., & Masek, J. G. (2010). An enhanced spatial and temporal adaptive reflectance fusion model for complex heterogeneous regions. *Remote Sensing of Environment*, *114*(11), 2610–2623. https://doi.org/10.1016/j.rse.2010.05.032

Zoltai, S. C., & Vitt, D. H. (1995). Canadian wetlands: Environmental gradients and classification. *Vegetatio*, *118*(1), 131–137. https://doi.org/10.1007/BF00045195

Zwieback, S., Chang, Q., Marsh, P., & Berg, A. (2019). Shrub tundra ecohydrology: rainfall interception is a major component of the water balance. *Environmental Research Letters*, *14*(5), 055005. https://doi.org/10.1088/1748-9326/ab1049

Chapter 5: **Trends in the extent of water bodies related to evapotranspiration rates in the Eastern Slopes of Alberta, Canada**

Abstract

Evapotranspiration (ET) is a major factor controlling the hydrological dynamics of open water areas and forest regions, as it limits excessive amplification of open water areas by slowing the expansion rate, and it can also amplify forest ecosystem ET losses. This study aims to evaluate past (1984–2023) trends of open water areas (hydroclimatic models: air temperature and precipitation vs open water area; average RMSE and %RMSE: training 6.79 km^2 and 10.2%; validation 7.36 km^2 and 12.7%) and evaporation rates (Penman method) in the Eastern Slopes of Alberta (ES), Canada. Furthermore, the proportion (P%) of open water area evaporation relative to forest ecosystem ET (applying forest ecosystem coefficient to open water evaporation rates) in ES was evaluated. The open water areas, evaporation rates (+0.028 mm $year^{-1}$), and forest ecosystem ET (+0.015 mm $year^{-1}$) exhibited positive trends during the snowmelt-dominated period (mid-May to mid-July), which were correlated with increasing trends in air temperature. During the rainfall-dominated period (late-July to mid-September), open water area is decreasing. Meanwhile, evaporation and forest ecosystem ET exhibited positive trends at +0.014 mm $year^{-1}$ and +0.008 mm $year^{-1}$, respectively. The historical P% during the snowmelt-dominated period was 2.4%, which was higher than during the rainfall-dominated (2.1%) period (late-July to mid-September).

Keywords: Modelling; Hydrology; Water Resources; Mountain Wetlands

5.1. Introduction

Historical trends and changes in precipitation and air temperature are affecting land cover, runoff processes, and water balance (Jiang et al., 2015). For example, evaporation rates are increasing (Kasurinen et al., 2014; Fernandes et al., 2007), leading to a reduction in the size of inland open water areas (Rood et al., 2008; Rasouli et al., 2013). Furthermore, water cycle fluxes are accelerating due to rising air temperatures (Koutsoyiannis, 2020). This is evident in mountain regions like the Eastern Slopes of Alberta (ES), Canada, where above-average warming is occurring (Gobiet et al., 2014; Chiarle et al., 2021). As a result, glaciers and snow cover are melting at a faster rate since 1980s (Pelto, 2020), and changes in precipitation quantity, timing, and phase, i.e., raising the frequency of rain-on-snow events (McCabe et al., 2007; Ye, et al., 2008). During the snowmelt-dominated period (mid-May to mid-July), snowmelt is occurring earlier, leading to an increase in volume and peak river discharge (as per, Vormoor et al., 2015; Stewart et al., 2004; Stewart et al., 2005; Rodrigues et al., 2024a). These changes have contributed to the expansion of open water areas during the snowmelt-dominated period (according to Chapter 4).

In contrast, during the rainfall-dominated period (late-July to mid-September) in the ES, river flow and open water areas are decreasing (DeBeer et al., 2015; Rood et al., 2008). In the ES, the convergence of increased open water areas during the snowmelt-dominated period (according to Chapter 4), combined with positive trends of evaporation rates (Kasurinen et al., 2014; Fernandes et al., 2007), may result in increased water volume losses during this period. During the rainfall-dominated period, the persistent increase in evaporation rates may intensify water resources depletion (Mastrotheodoros et al., 2020), increase drought risk (Peterson et al., 2021), and exacerbate ecosystem stress (Brodribb et al., 2020). Drier conditions and vegetation stress set a dangerous cycle in the ES whereby plants lose moisture, fire risk increases, and wildfires that change the land cover results. While open water areas are reducing due to the increase of evaporation losses, the fires turn mature forests into shrubs and grasses, which may increase the forest ecosystem evapotranspiration (ET) within just a few years post-fire (Brantley et al., 2024; Poulos et al., 2021).

Evaporation rates can be accurately estimated using the equation developed by Penman (1948), which is one of the most complete methods developed over the last 200 years (McMahon et al., 2016). Penman incorporates the primary factors that influence evaporation, such as energy balance and aerodynamic components. Furthermore, Penman has been tested in several

mountainous lakes and reservoirs around the globe (Zolá et al., 2019; Rosenberry et al., 2007; Zhao and Gao, 2019). However, despite extensive research on evaporation rates in response to climate change (Wang et al., 2018), there is uncertainty whether this hydrological process is increasing or decreasing during the snowmelt- and rainfall-dominated periods in the ES. Moreover, the open water evaporation rates volume loss in response to rapid changes in open water areas of ES during the snowmelt-dominated period remains unknown.

Another source of water flux to the atmosphere is represented through forest ecosystem ET (i.e., the integration of all plant transpiration, evaporated intercepted moisture, and soil evaporation at the ecosystem or flux footprint scale). Forest ecosystem ET in the ES is responsible for most atmospheric water losses due to their larger area relative to open water areas. This hydrological process can be accurately measured using eddy covariance tower (Langs, 2019), nevertheless, scaling these measurements to the regional level of the ES can be challenging. In a manner to effectively estimate forest ecosystem ET on a larger scale, forest ecosystem coefficients can be incorporated into evapotranspiration equations (as per Mata-González et al., 2005; Martel et al., 2017; Costa et al., 2021). While the evaporation and forest ecosystem ET rates in the ES are generally known, the proportion of open water evaporation volume in relation to the forest ecosystem ET volumes in the ES have not been quantified. Thus, with the shifting open water areas discussed in chapter 4, it is essential to investigate how these changes will impact regional water losses. To contextualize this within water resources, an estimation of the total forest ecosystem ET losses from vegetated areas is required.

The ES has a crucial role in providing freshwater for human activities like industry, irrigation, and home usage, as well as for the natural environment (Viviroli et al., 2007). This water tower is responsible for ~70% of the annual runoff of the Saskatchewan-Nelson River and Peace River (Ashmore and Church, 2001). Furthermore, this region provides over 90% of streamflow to downstream users, serving around 6.7 million people in the Canadian Prairie Provinces (Martz et al., 2007). The primary driver of streamflow in the ES is the melting of snow, with highest levels occurring between June ~ July (i.e., snowmelt-dominated period) (Rood et al., 2008; Whitfield and Pomeroy, 2017). In the rainfall-dominated period, glacier melt, and rainfall help maintain the flow of water in streams (Bash and Marshall, 2014). However, higher rates of glacier meltwater have been noticed (Hopkinson and Young, 1998; Castellazzi et al., 2019; Moore et al., 2009), which are expected to disappear in future decades.

However, the implementation of a full hydrological model to evaluate hydrological changes in a large and remote area like the ES can be difficult, since usually they require a lot of parameters (e.g., soil characteristics, land cover, watershed topographic characteristics, vegetation attributes, etc.) and variables (e.g., historical hydroclimatic dataset) (Craig et al., 2020). Thus, hydroclimatic-based models (e.g., bivariate models based on air temperature and precipitation) can be used as a parsimonious alternative to simulate open water areas (Sen et al., 2012), since air temperature and precipitation are the main drivers of change in open water areas in mountain environment. Thus, forcing hydroclimatic-based models and a reference method for evaporation estimates (for example, Penman, 1948) by historical hydroclimatic datasets provides an approach to evaluate open water area and evaporation rates in the ES. This framework can enable an evaluation of past trends in open water areas and evaporation losses, thereby facilitating a deeper understanding of patterns, direction, rates, and drivers of change across large and spatially mountainous ecosystems.

Here, it was investigated the long-term historical patterns (1984–2023) of open water area and evaporation rates in the ES. The study addresses the following core question: How are open water extent and evaporation processes in mountain headwaters of the ES changing in the last 40 years? To answer this, it was quantified historical open water areas using hydroclimatic modeling during both snowmelt- and rainfall-dominated periods. Historical evaporation rates were estimated using the Penman (1948) equation, applied to both periods. Additionally, the proportion of open water evaporation volume in relation to the forest ecosystem ET volumes in the ES was estimated. These analyses provide an integrated view of open water surface dynamics under shifting climatic conditions and support a better understanding of the hydrological sensitivity of the ES region.

5.2. Methods and data

5.2.1. Study Area

The Eastern Slopes of Alberta (ES) is within the Montane Cordillera Ecozone of Canada (Figure 5.1). This region is characterized by four primary watersheds: Oldman River, Bow River (that was combined with the headwaters of the Red Deer River), North Saskatchewan, and Athabasca. The headwaters of the Red Deer River watershed were merged into the Bow River watershed. Due to their comparable latitude and ecozone, the watersheds of the Red Deer River and Bow River exhibit similar physiographic characteristics (elevation range: 1200–3400 m; mean slope: 15–25°) and hydrological responses to climatic factors (Philipsen et al., 2018; Whitfield et

al., 2021). Merging them is unlikely to change the results of this study. The average climatic normals (from 1984 to 2023) are, air temperature of 2ºC (±14 ºC), annual precipitation of 700 mm (±110 mm), wind speed of 3.5 m s^{-1} (±1.5 m s^{-1}), and relative air humidity of 60% (±12.4%) (Alberta Climate Information Service, 2023). Throughout the last four decades, the historical air temperature in the ES has shown a positive trend of +0.06 °C $year^{-1}$ (as per Chapter 4). Figure 5.2 shows the historical average monthly air temperature (ºC), wind speed (m s^{-1}), net radiation (MJ m^{-2} d^{-1}), relative humidity (%), and precipitation (mm). The open water areas shown in Figure 5.1 were extracted from the Global Surface Water Explorer database (Pekel et al., 2016), which were merged with the lakes and rivers boundaries (Government of Alberta, 2016).

Fig. 5.1. a) ES location in North America; b) Canadian Eastern Slopes of Alberta region

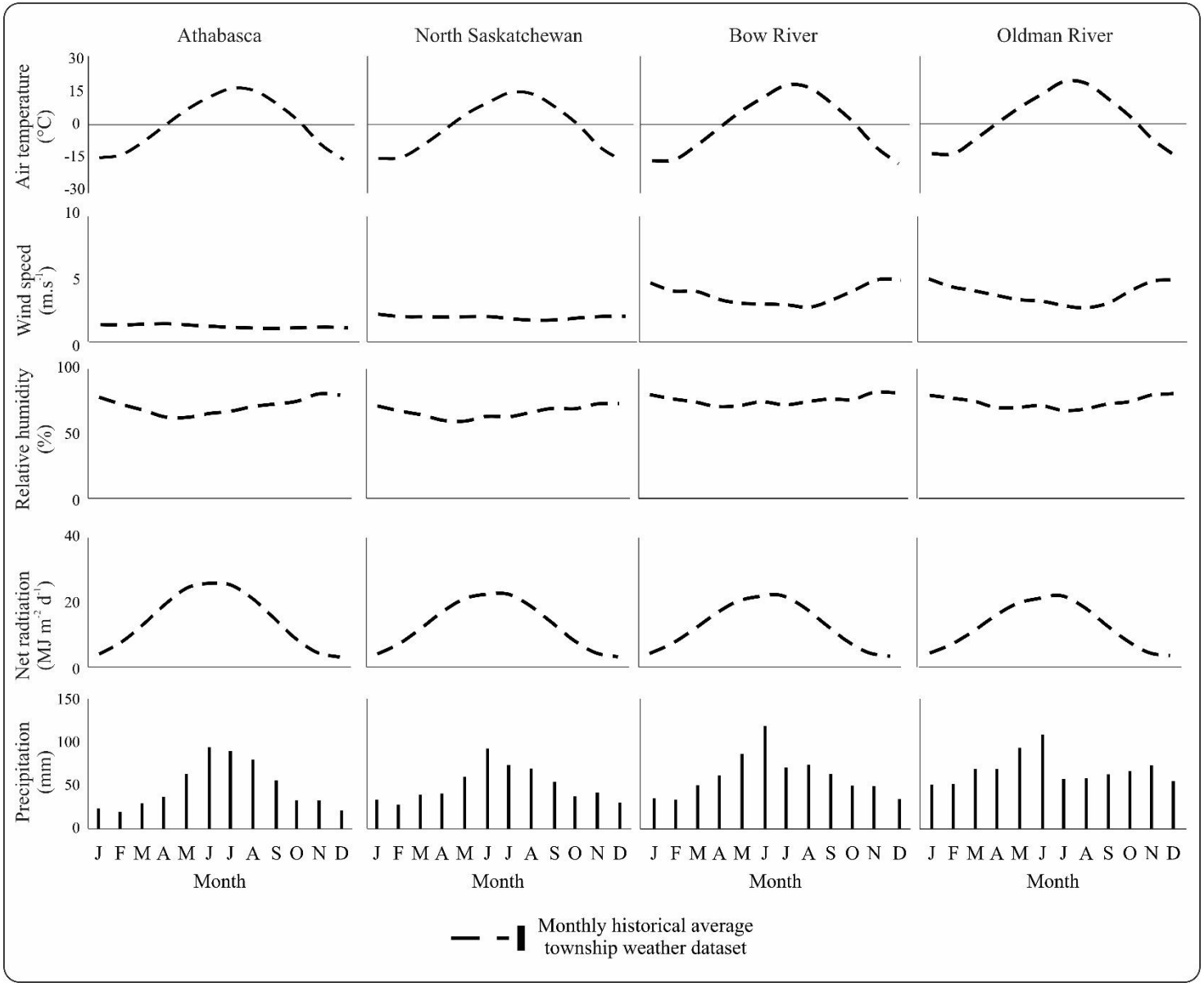

Fig. 5.2. Meteorological observed datasets, where, Obs – Historical monthly averages at township weather datasets (1984 to 2023)

The ES region warms more throughout the spring and early summer, as seen in Figure 5.2. This trend is directly related to higher net radiation. Three main radiative processes account for this seasonal amplification (2.3°C since 1950; Vincent et al., 2020). Initially, the earlier occurrence of snowmelt (advancing by 2.1 days per decade; Mudryk et al., 2018) leads to a reduction in surface albedo by 40–60% (Yang et al., 2001), resulting in an increase in absorbed solar radiation by 25–35 W m^{-2}. Secondly, the increase in CO_2 levels (~420 ppm in 2023; NOAA, 2023) enhances the absorption of longwave radiation. Concurrently, spring cloud cover is decreasing by 5% each decade, as noted by Bush and Lemmen in 2022, which intensifies the input of shortwave radiation. The changes resulted in a shift to drier soils (>30%), altering the energy flux from latent to sensible heat (Bonan, 2019) and causing near-surface temperatures to rise disproportionately in April–June (+3.1°C vs +1.7°C annual; Zhang et al., 2019). With MODIS land surface temperature patterns matching Clouds and the Earth's Radiant Energy System radiation anomalies (r=0.82; Zhan and Liang, 2023), eddy covariance data confirm net radiation drives 68±7% of spring warming ($p<0.01$; Mioduszewski et al., 2014). These feedbacks help to explain why mountain springs warm two times faster than winters (IPCC, 2023).

5.2.2. Data sets

Historical (1984 – 2023) open water areas from four primary watersheds in the ES were acquired in Chapter 4, using land cover classification in the ES (from 1984 to 2023) during the snowmelt-dominated (Mid-May to mid-July) and rainfall-dominated period (Late-July to mid-September).

Historical (1984 – 2023) air temperature (T_{air}) (°C) (average, minimum, and maximum), precipitation (P) (mm day^{-1}), wind speed (m s^{-1}), relative humidity (%), and total incoming solar radiation (MJ m^{-2} day^{-1}) was collected using the Interpolated Weather data from Alberta Townships. This dataset was chosen due to its extensive historical series dating back to 1901 (Alberta Climate Information Service, 2023). Estimates for each township location were derived using Hybrid Inverse Distance Cubed weighting for precipitation and linear Inverse Distance weighting for air temperature. The wind speed was interpolated from township stations using sector-based Inverse Distance Weighting. Net radiation was derived using a modified Food and Agriculture Organization Penman-Monteith approach (Allen et al., 1998). These methods consider spatial variation in elevation throughout the ES (Alberta Climate Information Service, 2023). The two methods were weighed according to the observations from the eight nearest weather stations. Details on the

interpolation methodology can be found in the Alberta Climate Information Service (2023). To ensure proper representation of each catchment's hydroclimatic data, each watershed was characterized by the average of all Townships (spatial resolution of 10 km) within it. Supplementary material A of Chapter 5 displays all utilized township numbers for each watershed.

5.2.3. Modelling framework

A four-phase approach was used to evaluate the historical trends in the open water area and rates of forest ET in the ES, as seen in Figure 5.3: i) Development of hydroclimatic-based models to simulate open water area; ii) Open water area and evaporation simulation forced with historical (1984-2023) hydroclimatic dataset using the Interpolated Weather data from Alberta Townships; iii) Proportion (%) of open water evaporation volume to forest ET volume; iv) Trend analysis over the past (1984 to 2023).

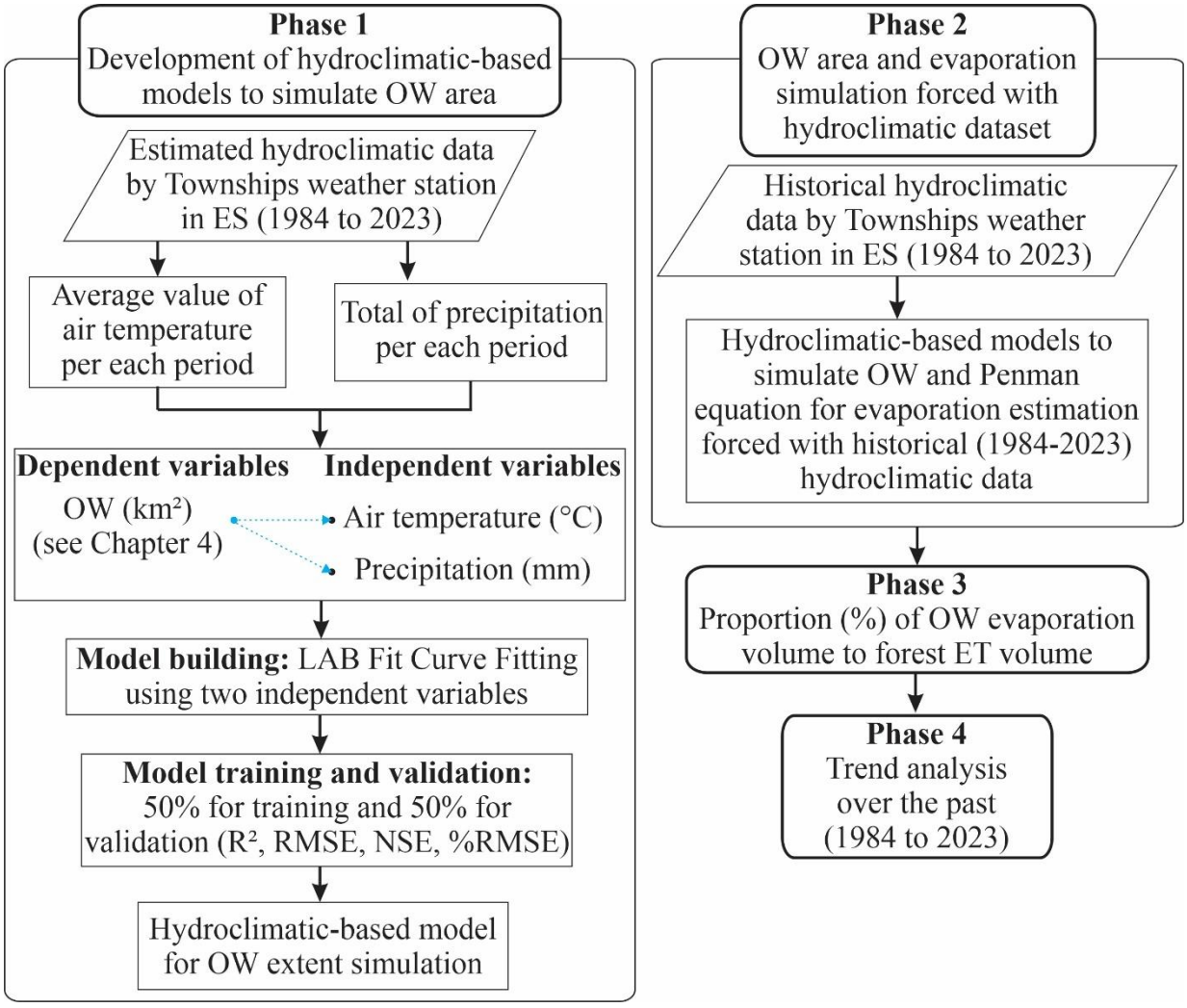

Fig. 5.3. Methodological flowchart for assessing historical changes in open water (OW) areas, OW evaporation, and forest ecosystem ET in ES.
R^2: coefficient of determination; RMSE: root mean square error; NSE: Nash-Sutcliffe efficiency coefficient; %RMSE: percentage root mean square error.

5.2.4. Phase 1: Development of hydroclimatic-based models to simulate open water area

Hydroclimatic models based on average monthly air temperature (T_{air}) (°C) and monthly total precipitation (P) (mm) were created to estimate open water area during the snowmelt- and rainfall-dominated period in the ES, since glacier melt, snow melt, and rainfall are the primary factors influencing changes on open water areas in the ES (Rodrigues et al., 2024a; Sen et al., 2012). To estimate the extent of open water in the ES, separate models were created for each period (i.e., snowmelt- and rainfall-dominated period) and for each watershed (Oldman River, Bow River, North Saskatchewan, Athabasca). The models to simulate monthly open water area were developed based on reference open water area (km^2) supplied in Chapter 4 (from 1984 to 2023) as the response variable, T_{air} and P as inputs. T_{air} and open water were averaged, and cumulative P was totalized for each period (snowmelt- and rainfall-dominated period). Average open water area (km^2) was projected for each period and watershed of ES.

The hydroclimatic-based models were designed using the LABFit software (Silva et al., 2004), which employs a statistical modelling technique known as the Levenberg-Marquardt optimization method (Levenberg, 1944; Marquardt, 1963), commonly referred to as damped least-squares. This method is powerful as it integrates a gradient descent algorithm, utilized in machine learning to determine the coefficients of a function that minimizes a cost function, with a Gauss-Newton algorithm, which addresses non-linear least squares problems identified by the minimum residual of the selected non-linear function (Silva et al., 2004).

The optimal non-linear regression form between the T_{air} and P and open water area was found using reduced chi-square (i.e., non-linear function around 1 is optimal) using LABFit library, which offers around 500 pre-defined non-linear and linear regression functions. The open water data from 1984 to 2023 were divided into two equal parts: 50% for training (even years 1984, 1986, etc.) and the remaining 50% (odd years) for validation. Training and validation were sampled from alternating years due to the substantial alterations seen in montane wetlands globally, especially after the 2000s (Avis et al., 2011; Zhang et al., 2012).

5.2.5. Phase 2: Open water area and evaporation simulation forced with historical (1984-2023) hydroclimatic dataset

The hydroclimatic-based models (section 5.2.4), and Penman (1948) equation (supplementary material B of Chapter 5), were driven by the historical (1984-2023) Alberta townships hydroclimatic dataset (1984 – 2023). The open water areas and evaporation were examined using the historical Alberta townships hydroclimatic dataset: a hydroclimatic-based model and Penman (1948) equation driven by the average of all townships within each watershed of ES. To assess whether the estimated open water area accurately reflects the reference open water area, historical-modelled open water area was compared (using Nash-Sutcliffe coefficient) against reference (as per Chapter 4) open water areas during the period of overlap from 1984 to 2023.

5.2.6. Phase 3: Proportion (%) of open water evaporation volume to forest ecosystem evapotranspiration volume

Evaporation from open water areas has a significant impact/reduction in water availability; nonetheless, forest regions could potentially result in even higher ET losses in ES, due to their larger coverage relative to open water areas. This analysis seeks to evaluate the proportion (P%) (in percentage %) of the evaporated open water volume compared with forest ecosystem ET volume in each watershed of the ES from 1984 to 2023. Hydroclimatic-based models (developed in section 5.2.4) were used to estimate open water areas (results from section 5.2.5). The forest areas spanning from 1984 to 2022 were determined using the historical annual-based land cover classification of Canada (Hermosilla et al. in 2022). The selection of this historical land cover dataset was based on overall accuracy of 83% (±4.1%) in Coniferous, and Mixed wood land covers. In this dataset, a frequency analysis was conducted using the "equals to frequency" procedure in ArcGIS Pro to determine the permanent forest area (PFA) per watershed in the ES. Coniferous vegetation was chosen as the reference forest since it predominantly constitutes the vegetation type of the ES (Meyn et al., 2010; Rhemtulla et al., 2002; Dawe et al., 2020). The PFA in the ES was used as reference forest area for all years. Supplementary material C of Chapter 5 illustrates the PFA (in km^2) for each watershed. To calculate the forest ET within ES, evaporation rates determined by Penman (1948) (which can be considered the maximum or potential water loss to the atmosphere, as evaporation rates are from open water surfaces where there is no surface resistance) were multiplied by a forest ecosystem coefficient (a division of forest ecosystem ET measured by Eddy covariance

tower, and open water evaporation estimated by Penman equation), providing an estimate of forest ET.

The forest ecosystem coefficient was based on Langs (2019), which investigated mature conifers (i.e., *Picea engelmannii and Abies lasiocarpa*) ET rates during growing seasons (early June to late September) of 2016 (Wet year) and 2017 (Dry year) located in Kananaskis River Valley, Fortress Mountain (50°49'32.7" N, 115°11'48.2" W), within the Eastern Slopes of Alberta. Langs (2019) determined the forest ecosystem ET (i.e., evaporation from soil, sublimation from snow, and transpiration via plant stomata during photosynthesis) using an Eddy Covariance Tower. Therefore, a periodic forest ecosystem coefficient was determined by dividing daily forest ecosystem ET to daily open water evaporation rates during the snowmelt- and rainfall-dominated period in 2016 and 2017. The open water evaporation rates, estimated through the Penman equation, were obtained from hydroclimatic parameters (air temperature, wind speed, relative humidity, and net radiation) recorded by Langs (2019) during the same timeframe and location where forest ecosystem ET was recorded. Thus, evaporation volume (m^3) per period from open water area (V_{ow}) was divided by the total PFA ET volume (m^3) (V_{PFA}) (Equation 5.1).

$$P\% = \frac{V_{ow}}{V_{PFA}} \tag{5.1}$$

This analysis compared the proportion of evaporation volume losses in open water areas with the volume losses due to forest ecosystem evapotranspiration in PFA of ES in each watershed.

5.2.7. Phase 4: Trend analysis over the past (1984 to 2023)

A temporal study was conducted to examine annual trends of open water area (i.e., total open water area in Alpine and Subalpine regions per watershed of the ES), open water evaporation, and forest ecosystem ET in the ES since 1984 to 2023. The trend analysis was conducted using Mann-Kendall approach, as described by Kendall in 1975 and Mann in 1945. The assessment was conducted with *pyMannKendall* code (Hussain and Mahmud, 2019). The null hypothesis posits that there is an absence of any discernible pattern or trend in the series. Three hypotheses were assessed: i) absence of a trend, ii) presence of a positive trend, and iii) presence of a negative trend. A significance threshold of $p \leq 0.05$ was applied. The extent of changes was assessed using nonparametric Sen's slope and Kendall's tau (τ) coefficient, which quantifies the association between variables.

5.2.8. Statistical comparison

In section 5.2.4 (Phase 1), the performance of the hydroclimatic models was evaluated using the coefficient of determination (R^2), root mean square error (RMSE), Nash-Sutcliffe efficiency coefficient (NSE) as introduced by Nash and Sutcliffe (1970), and the percentage root mean square error (%RMSE).

5.3. Results

5.3.1. Hydroclimatic-based models performance

Figure 5.4 (a, b) illustrates the training and validation performance of the hydroclimatic models developed using air temperature and precipitation data for each watershed in the Eastern Slopes of Alberta (ES). Snowmelt-dominated period models exhibited the highest level of accuracy. Figure 5.4c shows a visual comparison between modelled and reference values of open water across each watershed of ES. Overall, the results suggest that the hydroclimatic-based models captured the total open water area dynamic throughout the 1984 to 2023 period.

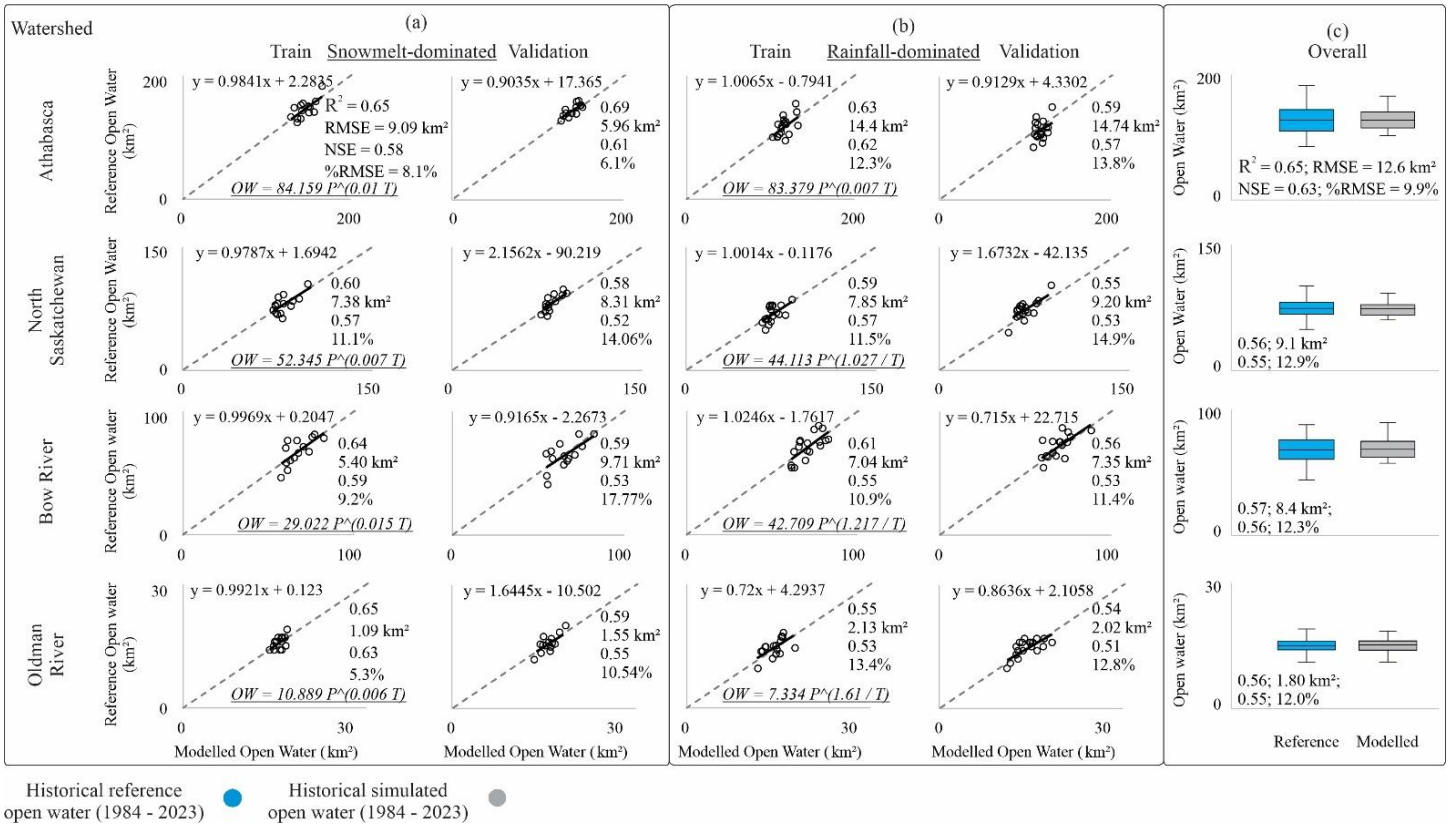

Fig. 5.4. Performance (i.e., R^2, RMSE, NSE, and %RMSE) of the hydroclimatic-based models for

snowmelt- (a) and rainfall-dominated period (b), and the overall (i.e., train and validation data) variation of reference and modeled open water per watershed (c) from 1984 to 2023

5.3.2. Historical trends

5.3.2.1. Historical trends of open water areas in the ES

Air temperature has been increasing (0.05 °C $year^{-1}$ across all watersheds of the ES; Supplementary materials E of Chapter 4) in the ES. Historical open water area of the ES from 1984 to 2023 is shown in Figure 5.5, during the snowmelt-dominated period, i.e., mid-May to mid-July (Figure 5.5a), and rainfall-dominated period, i.e., late-July to mid-September (Figure 5.5b). Historically (from 1984 to 2023), there was a significant ($p \leq 0.05$) increase of open water area in all watersheds of the ES..

Meanwhile, in the rainfall-dominated period, open water area has decreased in all watersheds of the ES (Figure 5.5b). Figure 5.5 also illustrates a comparison between reference and modelled open water during the overlapped period (from 1984 to 2023). Table 5.1 depicts the historical (1984–2023) open water area trends per watershed, and period (i.e., snowmelt- and rainfall-dominated) in ES. Supplementary materials D of Chapter 5 illustrates historical trends of open water per watershed in ES. Supplementary materials E of Chapter 4 illustrates historical trends of air temperature for each watershed in ES.

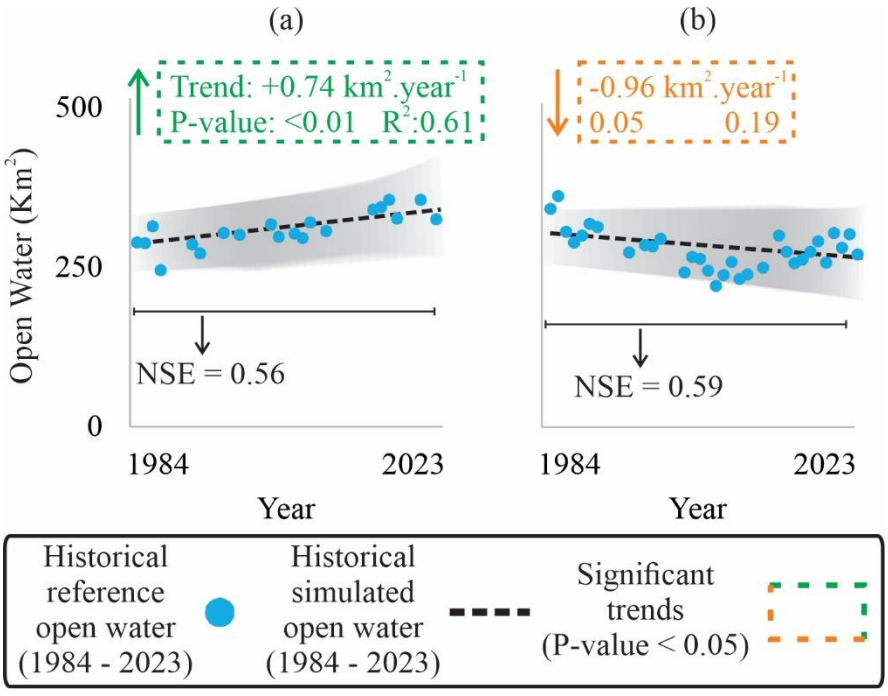

Fig. 5.5. Temporal changes of open water area in the ES during snowmelt-dominated (a), and rainfall-dominated period (b) in the from 1984 – 2023 based on hydroclimatic models driven by the historical Alberta townships hydroclimatic dataset. Shaded areas represent 95% confidence intervals for historical simulated open water area.

Table 5.1. Historical trends of open water area (1984 – 2023; km^2 $year^{-1}$) per watershed and period (snowmelt- and rainfall-dominated), in the ES.

	Period	Oldman River	Bow River	North Saskatchewan	Athabasca
Open water area	SM	+0.05*	+0.21*	+0.20*	+0.27*
	RD	-0.08*	-0.26*	-0.25*	-0.35*

*: There is a significant temporal trend at the 5% level; Green: Positive trends; Orange: Negative trends; SM: Snowmelt-dominated period; RD: Rainfall-dominated period.

5.3.2.2. Historical trends of open water evaporation in the ES

Historical evaporation rates from 1984 to 2023 in all watersheds of the ES during the snowmelt-dominated period (Figure 5.6a) presented significant ($p \leq 0.05$) positive trends. During the rainfall-dominated period (Figure 5.6b), all watersheds exhibited a non-significant ($p > 0.05$) positive trends in evaporation rates. Table 5.2 depicts the historical (1984–2023) open water evaporation rates per watershed, period (i.e., snowmelt- and rainfall-dominated) in the ES. The supplementary materials E of Chapter 5 illustrates historical trends of evaporation per period and watershed in ES.

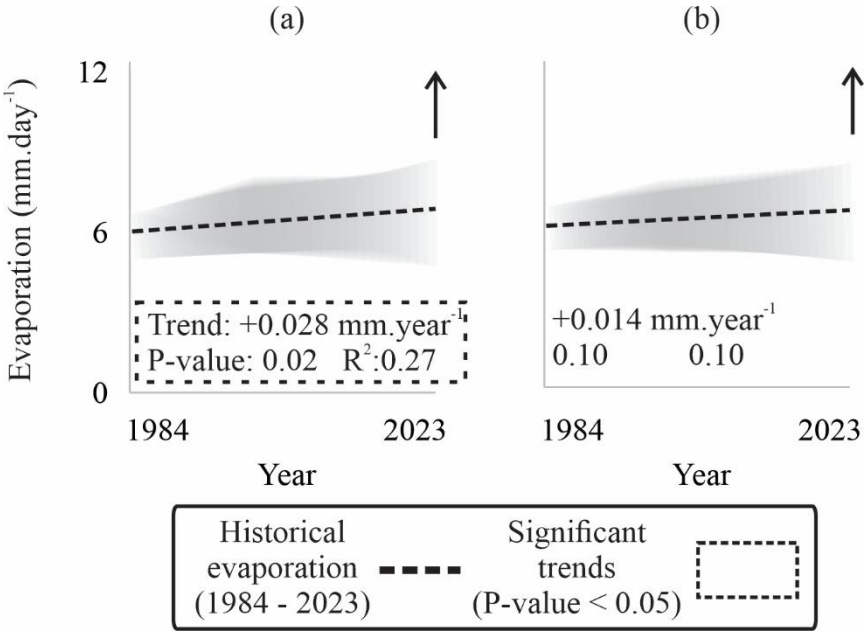

Fig. 5.6. Average trends of open water evaporation in the ES during the snowmelt-dominated (a), and rainfall-dominated period (b) in the historical period (1984 – 2023). Shaded areas represent 95% confidence intervals for historical open water evaporation.

Table 5.2. Historical trends of open water evaporation (1984 – 2023; mm year^{-1}) per watershed and period (snowmelt- and rainfall-dominated) in the ES.

	Period	Oldman River	Bow River	North Saskatchewan	Athabasca
Open water evaporation	SM	+0.026*	+0.023*	+0.025*	+0.037*
	RD	+0.013	+0.018	+0.015	+0.011

*: There is a significant temporal trend at the 5% level; Green: Positive trends; SM: Snowmelt-dominated period; RD: Rainfall-dominated period.

5.3.2.3. Historical trends of forest ecosystem evapotranspiration in ES

The average values of the forest ecosystem coefficient for the years 2016 (0.44) and 2017

(0.55) were 0.49. Historical forest ecosystem ET rates from 1984 to 2023 in all watersheds of the ES during the snowmelt-dominated period (Figure 5.7a) showed significant ($p \leq 0.05$) positive trends. In the rainfall-dominated period (Figure 5.7b), forest ecosystem ET rates in all watersheds demonstrated a non-significant ($p > 0.05$) positive trend. Table 5.3 shows the historical (1984–2023) forest ecosystem ET rates per watershed, and period (i.e., snowmelt- and rainfall-dominated) in the ES. Historical trends of forest ecosystem ET rates per period and watershed in the ES are illustrated in Figures the supplementary materials F of Chapter 5.

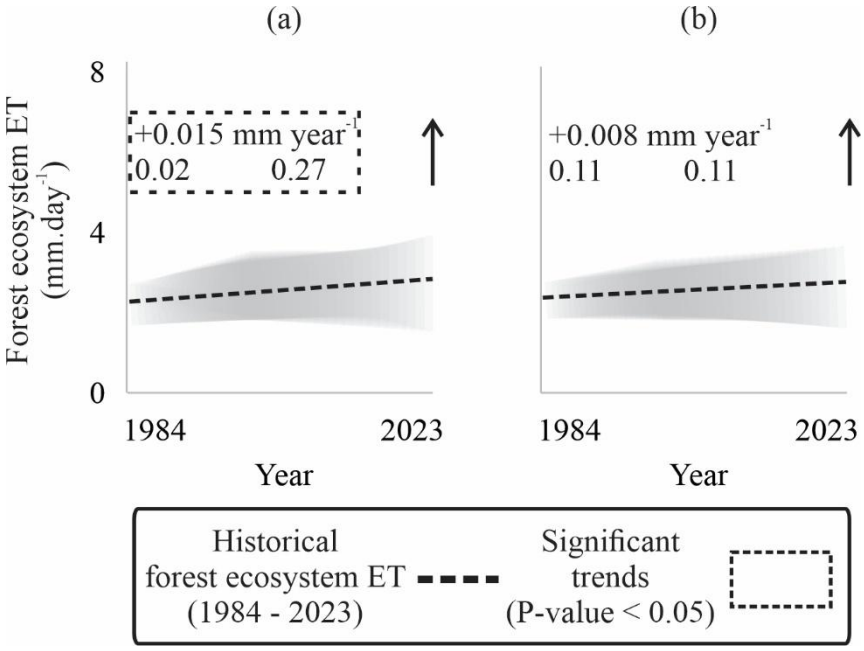

Fig. 5.7. Average trends of forest ecosystem ET in the ES during snowmelt-dominated (a), and rainfall- dominated period (b) in the historical period (1984 – 2014). Shaded areas represent the 95% confidence intervals for the historical forest ecosystem ET.

Table 5.3. Historical trends of forest ecosystem ET (1984 – 2023; mm year^{-1}) per watershed and period (snowmelt- and rainfall-dominated) in the ES.

	Period	Oldman River	Bow River	North Saskatchewan	Athabasca
Forest ecosystem ET	SM	+0.014*	+0.011*	+0.013	+0.019*
	RD	+0.007	+0.010	+0.008	+0.007

*: There is a significant temporal trend at the 5% level; Green: Positive trends; SM: Snowmelt-dominated period; RD: Rainfall-dominated period.

5.3.3. Volume of open water evaporation in proportion (P%) to the volume of forest ecosystem evapotranspiration

Forest areas in the ES contribute significantly to water atmospheric losses because of their larger size compared to open water areas. Supplementary material C of Chapter 5 displays the permanent forest areas (PFA) of ES, with a total of 24,872 km^2 (i.e., Oldman River: 4883 km^2; Bow River: 7976 km^2; North Saskatchewan: 4600 km^2; Athabasca: 7413 km^2). Table 5.4 displays the average historical P% of open water evaporation volume to forest ecosystem ET volume per watershed and period in ES. The supplementary materials G of Chapter 5 depicts historical (1984 – 2023) P% of open water area evaporation volume to PFA ET volume per watershed in ES, categorized by period and year.

Historically, average P% (P%$_A$) of open water evaporation volume compared to forest ecosystem ET in the snowmelt-dominated period was 2.4% (Table 5.4), varying between 0.7% (Oldman River) and 3.8% (Athabasca) depending on the watershed. During the rainfall-dominated period, historical P%$_A$ was 2.1%, varying between 0.5% (Oldman River) and 3.4% (Athabasca). Table 5.4 shows historical P%$_A$ in all watersheds and periods of the ES.

Table 5.4. Historical $P\%_A$ between evaporation volume in open water areas and ET volume in permanent forest areas (PFA) in all watersheds and periods of the ES

Watershed	Period	$P\%_A$ (OW_E/PFA_{ET})
ES	SM	2.4%
	RD	2.1%
Athabasca	SM	3.8%
	RD	3.4%
North Saskatchewan	SM	3.2%
	RD	2.9%
Bow River	SM	1.7%
	RD	1.6%
Oldman River	SM	0.7%
	RD	0.5%

OW_E: Open Water Areas evaporation volume (m^3 day^{-1}); PFA_{ET}: Permanent Forest Areas evapotranspiration volume (m^3 day^{-1}); Historic period (1984 – 2023).

Overall, open water evaporation volume losses are relatively minor when compared to ET losses from PFA in ES, which showed a historical $P\%_A$ of 2.2%. This is since the PFA are larger in size compared to open water areas in ES. As a result, it is anticipated that there will be greater volumes of ET losses in forest regions.

5.4. Discussion

5.4.1. Hydroclimatic-based models to estimate open water area

The major hydroclimatological drivers of change in open water areas in the ES are the air temperature and precipitation, which relates to the satisfactory accuracy found (average NSE of 0.56 for training and validation during snowmelt- and rainfall-dominated period) in the parsimonious hydroclimatic-based models. Furthermore, given the lack of data regarding actual/field-based measured historical open water area in ES, it was necessary to adopt a straightforward simple (i.e., parsimonious hydroclimatic-based model for the open water area), yet

conceptually sound, modelling approach for the open water areas, nonetheless allowing us to satisfactorily reproduce reference (as per Chapter 4) open water area in the ES.

The model design utilized hydroclimatological interpolated datasets from Township data provided by Alberta Agriculture, Forestry and Rural Development, as there were no ES weather stations that offered continuous air temperature and precipitation measurements throughout the entire study period from 1984 to 2023. Thus, if in-situ weather measurements were used, part of air temperature and precipitation time series would come from one station, and the other portion and timeline from another station, which would lead to greater uncertainty rather than using the average air temperature and precipitation of all townships within each watershed of ES. Furthermore, relying on just one or two weather stations per watershed for a vast region like the ES may not provide a sufficiently accurate representation to develop hydroclimatic-based models. In summary, the hydroclimatic-based models captured the total open water area dynamic throughout the 1984 to 2023 period, presenting average NSE during the snowmelt-dominated period of 0.57 (training: 0.59; validation: 0.55), and 0.55 during the rainfall-dominated period (training: 0.57; validation: 0.54).

The higher accuracy of the hydroclimatic models during the snowmelt-dominated period can be attributed to positive trends in open water area during this period in all watersheds, enhancing models' capability to identify these changes. Furthermore, the expansion of open water areas during the snowmelt-dominated period could be associated with historical increase in air temperature (0.05 °C $year^{-1}$ across all the ES). Air temperature increases leads to an earlier glacier and snow cover melting (Pelto, 2020; Huss and Hock, 2018; Diro and Sushama, 2020), increasing the open water areas during the snowmelt-dominated period in all watersheds. Historically, glaciers provided meltwater primarily during the pluvial period; however, climate change has altered this dynamic. Earlier snowpack disappearance now exposes glacier ice to solar radiation weeks sooner, starting major melt during the nival period (Huss and Hock, 2018). The Eastern Slopes of Alberta, where glacier melt begins, has advanced by 3.1 days per decade since 1980, illustrating this change particularly well (Derksen et al., 2022). Two effects arise from nival streamflow, now incorporating an increasing portion of “irrecoverable” glacier storage loss and a decline in the reliability of pluvial water supplies as glaciers diminish (Milner et al., 2017). This explains why glaciers, previously regarded as summer buffers, now contribute to late-season shortages and pose risks of nival flooding.

In the rainfall-dominated period, river flow is more dynamic and is closely linked to

precipitation patterns. Changes in quantity, timing, and phase of precipitation (McCabe et al., 2007; Ye et al., 2008) will directly impact river discharge volumes, timing, and magnitude (Vormoor et al., 2015; Stewart et al., 2004; Stewart et al., 2005), leading to changes in the connected open water areas. In addition, the reference historical open water areas (according to Chapter 4) aligned with the historical open water areas simulations (hydroclimatic-based models) , exhibiting a historical (1984 to 2023) annual NSE of 0.55.

5.4.2. Open water and forest ecosystem evapotranspiration in ES

The historical increase of open water areas in the snowmelt-dominated period, along with positive trends of open water evaporation and forest ecosystem evapotranspiration (ET) during this period, could potentially intensify water volume losses associated with ET processes. At least 80% of ET can be attributed to air temperature, therefore, an increase in air temperature is likely to lead to a rise in ET rates (Priestley and Taylor, 1972; Samani, 2000). In the same domain, warming climate is also leading to earlier spring glacier- and snow-melt (DeBeer et al., 2015; Diro and Sushama, 2020; Huss and Hock, 2018; Stewart et al., 2004), which increases river discharge (Brahney et al., 2017), and open water areas (Hauer et al., 1997), in addition, impacting/changing precipitation quantity, timing, and phase (McCabe et al., 2007; Ye, et al., 2008).

More specifically, the substantial historical increase in open water area within the Athabasca watershed suggests a sequence of interconnected hydrological alterations across various elevation zones. In alpine regions (>2300 m), the retreat of glaciers leads to sporadic releases of accumulated meltwater (Huss and Hock, 2018), while subalpine areas (≤2300 m) show responses mainly influenced by precipitation, particularly during intensified rainfall events (Pomeroy et al., 2020). During the snowmelt-dominated period, episodes of rain-on-snow greatly increase the creation of open water areas (Koch et al., 2012). The historical increase of open water areas stem from: elevation-dependent warming rates, non-linear glacier depletion curves, and increasing precipitation variability attributed to historical climate change (DeBeer et al., 2015). This demonstrates why lower elevation open water areas may see consistent increases, while alpine systems exhibit "boom-bust" hydrology as glaciers recede.

In the rainfall-dominated period, all watersheds experienced significant decreases in open water areas. However, as per Chapter 4, this negative trend in open water area is not followed in alpine regions (>2300 meters) of the Athabasca watershed, which showed positive trends of open

water areas since 1984 to 2023. The peculiar expansion of the open water area relates to the meltwater from glaciers, which helps to sustain the water flow in streams (Bash and Marshall, 2014). However, historical climate change has led to increased glacier meltwater rates (Castellazzi et al., 2019; Moore et al., 2009), which are not offset during winter, consequently, glaciers are projected to disappear within the next 40 years as a result of increasing air temperatures (Huss and Hock, 2018; Derksen et al., 2022). Thus, once the glaciers have disappeared, the alpine region of the Athabasca watershed is likely to align with the negative trends of open water area observed in Oldman, Bow River, and North Saskatchewan during the rainfall-dominated period.

Furthermore, the precipitation phase change is observed by the increasing of frequency of rain-on-snow precipitation in the snowmelt-dominated period (López-Moreno et al., 2021). This leads to a quick rise in runoff within watersheds due to the presence of frozen soil from the Winter season. Thus, groundwater levels are expected to decline due to partially frozen and difficult-to-infiltrate soil (Millar et al., 2018). Moreover, in the western mountain range of US, negative projections in snowpack are expected to reduce groundwater recharge to this mountain system (Meixner et al., 2016). Projected declines in snowpack, coupled with increasing air temperatures, will lead to higher ET rates and reduced groundwater recharge in higher mountainous areas (Somers and McKenzie, 2020). For instance, Goulden and Bales (2014) assessed the connection between precipitation, ET, and elevation in California's Sierra Nevada. Employing a space-for-time method, a 28% rise in ET was projected throughout King's River watershed, which followed a projected 26% reduction in river flow by 2100. Decreases in groundwater storage will lead to reduced water availability for plants, particularly during the rainfall-dominated period, when ET rates are high.

During the rainfall-dominated period, significant and negative historical open water area trends may have been influenced by changes in precipitation onset (i.e., higher concentrations or volumes of precipitation during the snowmelt-dominated period) and phase (i.e., forecasted increasing frequency of rain-on-snow events during the snowmelt-dominated period) (McCabe et al., 2007; Ye, et al., 2008). Moreover, positive trends of evaporation rates were found during the snowmelt- and rainfall-dominated periods, leading to a significant reduction in open water areas. The positive trend of air temperature increases the vapor pressure deficit and ultimately leading to increased open water evaporation rates (Ma and Zhang, 2022; Mintz and Walker, 1993).

Meanwhile, warmer temperatures and changes in precipitation can also affect the onset and termination of vegetation growth (Fu et al., 2019), resulting in an earlier spring green-up and later

fall senescence (Chen et al., 2024; Jeong et al., 2011). Changes in vegetation greening and senescence can directly impact local ecohydrology by altering albedo (Bonan, 2008), energy partitioning (Chapin et al., 2005), rainfall interception and accumulation of snow (Pomeroy et al., 2006; Zwieback et al., 2019). Vegetation has an impact on surface energy balance, which in turn affects vegetation transpiration rate (Tanner et al., 1960; Brümmer et al., 2012; Kasurinen et al., 2014; Kool et al., 2014), which will likely increase with earlier spring growth onset, thereby lowering groundwater storage (Chen et al., 2022). In a warming climate, vegetation is likely to encroach into previously cold-limited higher elevations, which will increase ET rates and decrease groundwater recharge (Goulden et al., 2012). The decrease in soil moisture and groundwater recharge (Barnett et al., 2005) has the potential to increase the frequency of droughts, especially in the rainfall-dominated period (Wheaton et al., 2008). The increased drought occurrence may increase the likelihood of wildfire activity (Balling et al., 1992; Lantz et al., 2010), particularly in pine and spruce forests, which are the predominant species in the ES (Meyn et al., 2010; Xiao and Zhuang, 2007). In summary, expansion of vegetation growth season in northern ecosystems has the potential to affect water availability during both periods, by enhancing plant growth and ET rates (Lian et al., 2020; Zhou et al., 2020; Piao et al., 2019).

Furthermore, the climate of the ES is impacted by the Pacific Decadal Oscillation, which accounts for the occurrence of El Niño (Pacific Ocean warm episodes defined by above-average sea surface temperatures) and La Niña (Pacific Ocean cold episodes marked by below-average sea surface temperatures) events. The frequency of warm episodes of the Pacific Decadal Oscillation has increased over the years (Gan et al., 2023; Wang et al., 2017), with the primary explanation likely being the ongoing emissions of greenhouse gases (Cai et al., 2014). The consequences of this phenomenon include increased air temperatures, changes in precipitation patterns (quantity, timing, and phase), earlier glacier and snowmelt, expanded open water areas during the snowmelt-dominated period, prolonged vegetation growth season, higher rates of forest ecosystem ET, decreased groundwater levels during the rainfall-dominated period, and increased occurrence of droughts and wildfires. Figure 5.8 provides an overview of land cover feedback resulting from historical climate change effects in ES.

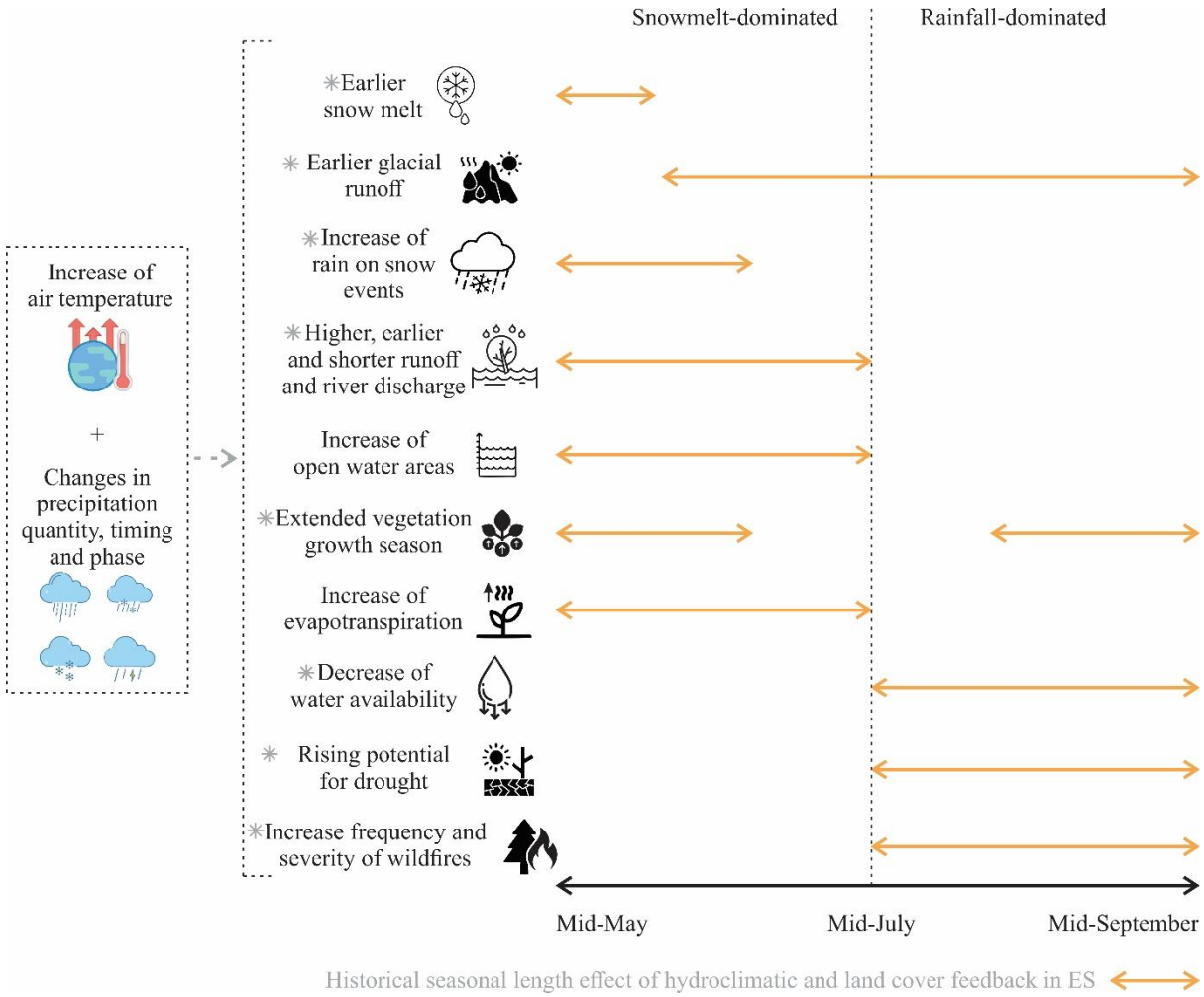

Fig. 5.8. Seasonal length of historical hydroclimatological parameters and land cover feedback resulting from increase of air temperature and precipitation changes in ES

* - Hydroclimatological and land cover changes based on literature: Earlier snow melt from DeBeer et al. (2015) and Stewart et al. (2004); Earlier glacial runoff from Hopkinson and Young, (1998), Castellazzi et al. (2019), and Moore et al. (2009); Increase of rain on snow events from Ye et al., (2008) and McCabe et al. (2007); Higher, earlier, and shorter runoff and river discharge Vormoor et al. (2015), Stewart et al. (2004), and Stewart et al. (2005); Extended vegetation phenology Jeong et al. (2011) and Piao et al. (2019); Decrease of water availability from Barnett et al. (2005), Kienzle (2006); Rising potential for drought from Meyn et al. (2010), Wheaton et al. (2008), Xiao and Zhuang, (2007); Increase the frequency and severity of wildfires Balling et al. (1992), Lantz et al. (2010), Travers-Smith et al. (2022).

Overall, the ES has changed over the past (1984 – 2023), including rising air temperatures,

alterations in precipitation patterns, and positive trends in ET processes. In the snowmelt-dominated period, the combination of early melting of glaciers and snow, together with rain falling on snow and increased intensity of rainfall, may cause an increase in the open water areas. In addition, in early to mid-May, the thawing of soils in the subalpine regions of the Canadian Rockies facilitates the infiltration (i.e., groundwater recharge) of rainfall and snowmelt (Woo and Marsh, 2005). In alpine regions or on north-facing slopes, soil frost may persist into late spring, especially during years characterized by heavy snowfall or cold winters (Hayashi, 2013). As a result, earlier snowmelt is likely to enhance soil infiltration in subalpine areas. In alpine regions, there will likely be a reduction, as the soil may remain frozen, hindering the infiltration of surface water, which includes snowmelt, glacier runoff, and rainfall, into the soil (DeBeer et al., 2015; Koch et al., 2012). Moreover, extension of vegetation growth season will lead to higher forest ecosystem ET rates and a decrease in groundwater storage. Over the rainfall-dominated period, increased frequency of droughts is expected, which can expand wildfire season. Figure 5.9 provides a summary of the historical (1984-2023) environmental challenges in the ES.

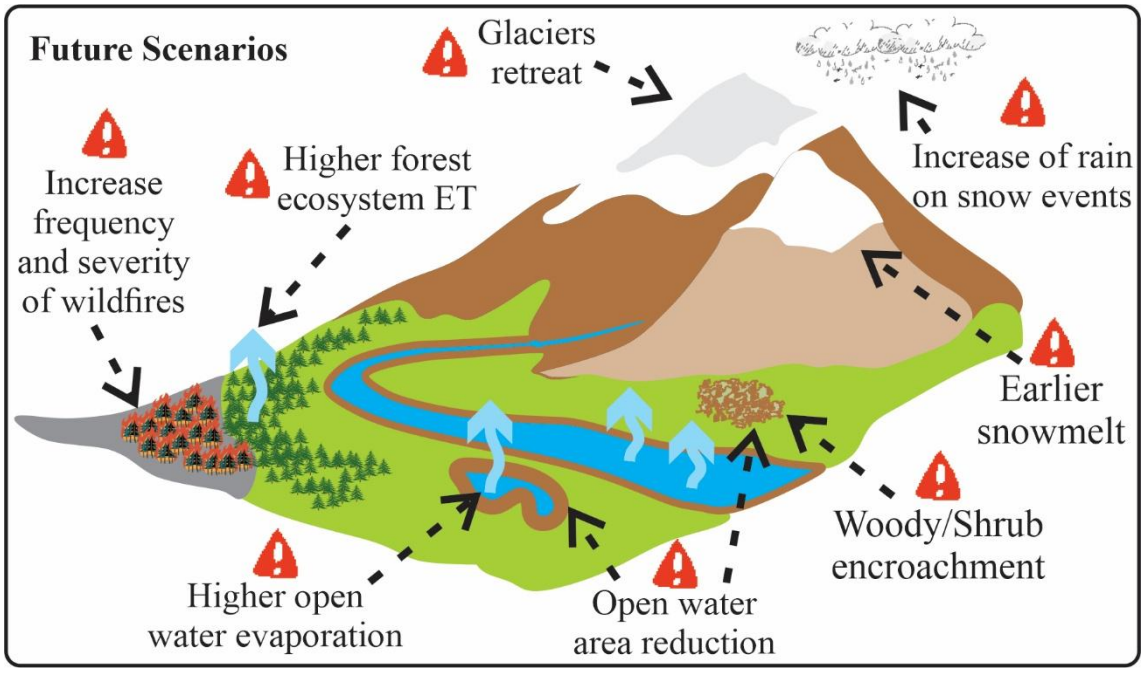

Fig. 5.9. A conceptual representation illustrating the historical environmental challenges in the Eastern Slopes of Alberta.

Changes based on literature: Earlier snow melt from DeBeer et al. (2015) and Stewart et al. (2004); Glacier retreat from Hopkinson and Young, (1998), Castellazzi et al. (2019), and Moore et al.

(2009); Increase of rain on snow events from Ye et al., (2008), McCabe et al. (2006), Pomeroy et al., (2015), Musselman et al., (2018); Woody/Shrub encroachment from Rodrigues et al. (2024b) and Whited et al. (2025); Increase frequency and severity of wildfires from Balling et al. (1992), Lantz et al. (2010), Travers-Smith et al. (2022).

5.4.3. Evaporation volume by open water vs forest ecosystem evapotranspiration

This study estimated forest ecosystem ET in the ES multiplying daily open water evaporation rate (using Penman, 1948) by forest ecosystem coefficient of 0.49; the forest ecosystem coefficient was determined by dividing daily ecosystem ET measured by Eddy covariance tower (Langs, 2019) to open water evaporation estimated by Penman (1948). Eddy Covariance Towers are considered the standard method for acquiring reference forest ecosystem ET data (Scott et al., 2004, 2021; Fang et al., 2020). Furthermore, the Penman (1948) has proven effective in measuring open water evaporation across different mountainous lakes and reservoirs around the globe (Zolá et al., 2019; Rosenberry et al., 2007; Zhao and Gao, 2019). Therefore, using those two datasets seems to be a reliable method for estimating a forest ecosystem coefficient in the ES. Moreover, the forest ecosystem coefficient found for this study aligns with previous research, as per Allen et al. (1998), Allen (2000), Brümmer et al., (2011), Kuriata-Potasznik and Szymczyk (2016), and Kachholz and Tränckner (2020), who reported a forest ecosystem coefficient between 0.40 and 0.80. In addition, a variety of studies have incorporated a forest ecosystem coefficient into evapotranspiration equations and rates, in the end, considering this estimation as reference data for forest ecosystem ET (Mata-González et al., 2005; Martel et al., 2017; Costa et al., 2021; Rodrigues et al., 2024c).

The historical proportion (P%) of evaporated open water volume in relation to permanent forest areas (PFA) ET volume in the ES was higher during the snowmelt-dominated period when compared to the rainfall-dominated period (as per Table 5.1). Higher historical P% in the snowmelt-dominated period is related to positive trends of evaporation rates and expansion of open water areas in ES. The Athabasca watershed had the highest historical P% throughout all periods, which may be attributed to higher historical trends of open water areas in this watershed. The Oldman River watershed had the lowest historical P%, mostly as a result of its large PFA and the relatively smaller open water area. Furthermore, positive trends in historical air temperatures are prolonging vegetation growing season (Pettorelli et al., 2007; Trant et al., 2020), leading to an increase in forest area over time, along with historical rising of forest ecosystem ET rates.

In Alpine regions (>2300 meters), during the rainfall-dominated period, mountainous areas that lack snow cover may promote the growth and spread of deciduous and tree line vegetation (McCaffrey and Hopkinson, 2020; Mekonnen et al., 2019). Vegetation change can alter the P% of forest ecosystem ET to open water evaporation during the rainfall-dominated (snow-free) period (Wang et al., 2014), as well as impact ground thermal and local moisture conditions (Domine et al., 2016; Myers-Smith and Hik, 2013; Paradis et al., 2016; Sturm et al., 2005; Wilcox et al., 2019), carbon and nutrient cycling (Lafleur and Humphreys, 2018) and terrain stability (Lara et al., 2016). The vegetation shifting, often referred to as "greening", alongside the increased occurrence of droughts, can lead to a higher frequency of wildfires, which, in normal circumstances wildfires are advantageous for the distribution of plant seeds (Habeck and Mutch, 1973). Nevertheless, the likelihood and occurrence of more catastrophic wildfires are escalating over time, driven by drier late summer conditions, coupled with increase of fire fuel (like dry vegetation), and a decrease in soil moisture (Lantz et al., 2010; Travers-Smith et al., 2022; Jain et al., 2024).

In the future, the P% of ET volumes from PFA to evaporation volume from open water areas may exceed the historical P% presented here, particularly if the increased frequency and severity of wildfires in the ES persists over the years, leading to a reduction in forest areas and therefore decreasing ET volume via PFA. In the Canadian Boreal Forest, Kang et al., (2006) and Bond-Lamberty et al., (2009) found that wildfires decreased forest transpiration rates by -3.8 ~ -38% (varying by forest type) and increased soil evaporation by ~ +13%. In contrast, post-fire shrubs and grasses that are regenerating can exhibit more anisohydric behavior, maintaining prolonged stomatal opening even as leaf water potential declines, and may sustain higher transpiration rates compared to pre-fire vegetation (Brantley et al., 2024; Cooper et al., 2018; Poulos et al., 2021). Baur et al. (2024) conducted a global investigation into the effects of wildfires on the relationship between plant and soil water content, utilizing remote sensing techniques to analyze soil moisture, vegetation water content, and burned area. The authors observed a significant impact of fire on plant–soil water interactions, resulting in an ~17% increase in soil moisture loss and a ~62% rise in vegetation water content, both of which correlate positively with high fire severity. Furthermore, post-fire vegetation also tended to have less control on their water content, leading to anisohydric behavior. This could potentially hinder the increase of P% during the snowmelt-dominated period, as this period coincides with the peak of vegetation regeneration (i.e., spring and summer) and the higher historical forest ecosystem ET rates.

Wildfires will expose soil as trees burn down, leading to a decrease in precipitation interception. The combination of earlier glacier and snow melt, rain-on-snow events, and higher intensity of rainfall will elevate the likelihood of higher floods and erosive processes (Musselman et al., 2018), resulting in greater siltation of lakes, rivers, and open water areas (Moore et al., 2009). Shallower open water areas have a limited capacity to store energy, leading to sudden and significant temperature changes in these water bodies (Campos et al., 2016), resulting in increased rates of evaporation.

5.5. Modelling Limitations

This study presents a method for estimating open water areas, open water evaporation, and forest ecosystem ET in the ES since 1984 to 2023. This research offers a straightforward yet effective solution to the ES's urgent need for modelling approaches that dynamically integrate historical hydroclimatic datasets into the water cycle over extended timescales. As a result, the primary objective was to enhance understanding of historical changes in open water areas and evapotranspiration processes within the ES watersheds. As such, the limitations in this modeling approach must be addressed.

The decreasing role of glacier melting in open water on the ES presents a non-linear (essentially in the rainfall-dominated period) air temperature-driven hydrological relationship. As temperatures rise, the melting of glaciers releases meltwater that has been stored for long periods. Nonetheless, the quantity of meltwater generated for each degree of warming has decreased over time because of the retreat and thinning of glaciers. As a result, a 1°C increase today results in less meltwater compared to the same increase experienced 40 years ago (Milner et al., 2017; Huss and Hock, 2018). Empirical models (e.g., hydroclimatic models) that relate open water to air temperature and precipitation are unable to inherently address this diminishing storage buffer, as they do not incorporate data on glacial mass balance trends. That could be the reason snowmelt-dominated period models exhibited higher accuracy, because the rainfall period is when open water areas are being influenced by long-term storage from deglaciation that the model cannot account for. As the system evolves, the hydroclimatic-based modelling framework utilized (calibrated under conditions with active glacier input) may gradually lose its reliability. Therefore, if these hydroclimatic models are used to forecast open water areas, it is crucial to proceed with caution, as projections might underestimate open water losses and misrepresent the timing and extent of open

water reduction, as these empirical models do not specifically model glacier mass balance and meltwater contributions. It is essential to recognize this limitation as uncertainty when interpreting long-term changes in open water, especially in glacier-fed watersheds of the ES where the depletion of storage is increasing (Pradhananga and Pomeroy, 2022). Future research may incorporate glacial inventory data or physically based models (represent the actual physical processes controlling the water cycle, for instance, precipitation, infiltration, runoff, evapotranspiration, and groundwater flow, using equations based on physics, chemistry, and biology) to more effectively constrain these non-stationary dynamics. Furthermore, incorporating additional hydroclimatological factors, including surface temperature, groundwater, and shortwave or longwave radiation, can enhance the precision of open water area projections.

The limitations of hydroclimatic models in estimating open water areas are subject to their simplicity when compared to full hydrological models (e.g., Raven hydrological modelling; Craig et al., 2020), as the second one (in theory) should deliver superior accuracy. Running a full hydrological model is intended to improve analysis, however parsimonious hydroclimatic models can be used in data-poor places such as mountain regions. Nevertheless, our findings are consistent with the literature, for example, Fernandes et al. (2007) evaluated the trends of evapotranspiration across Canada using the Ecological Assimilation of Land and Climate Observations land surface model and discovered significant positive trends in evapotranspiration in the Canadian Rocky Mountains, which is in accordance with our results. Finally, a comparison of the uncertainties between the hydroclimatic and full hydrological models would assist in determining whether the parsimonious model can accurately represent open water areas compared with a more complex model.

Moreover, the spatial variability of land surface characteristics, especially elevation, are important for estimating evapotranspiration and other related flux calculations in different types of landscapes (Allen et al., 1998; McCabe and Wood, 2006). Utilizing a single average elevation value for clear sky radiation and other weather-related factors may cause systematic bias because land area is not evenly distributed across elevation gradients within watersheds (Zhang et al., 2016). This simplification does not take into account the complex hypsometric relationships that affect temperature, radiation, and vapour pressure, which are important parts of Penman-type evapotranspiration models (Allen et al., 1998). On the other hand, GIS-based hypsometric modelling methods that take into account how meteorological variables change with elevation have

shown that they can improve the accuracy and spatial representation of evapotranspiration estimates across different types of terrain (McCabe and Wood, 2006; Pepin et al., 2015). Understanding these uncertainties is crucial for accurately and transparently interpreting model outputs. Ignoring elevation variability may result in either under- or over-estimation of evapotranspiration, which can subsequently impact watershed-scale water balance assessments and management decisions.

Furthermore, it is important to recognize that systematic biases may arise when applying a single meteorological input, such as average temperatures and elevations, across heterogeneous land cover types like forests and open water bodies within the ES. For instance, when open water areas are primarily found at lower, warmer elevations and forested regions are located at higher, cooler elevations, relying on a single average elevation may result in a significant underestimation of forest ET (Marks et al., 1999; Zhang et al., 2025). This would therefore skew the forest-to-open water ET ratio downward, possibly misrepresenting their respective hydrological contributions. Conversely, in alpine or pro-glacial zones where open water expansion is significant, lower temperatures might imply reduce ET rates; however, increased wind speeds, often channelized over these lakes, can elevate the vapor pressure deficit and thus enhance evaporation, partially offsetting cooler temperature effects (Dingman, 2015). The presence of these counteracting factors indicates that elevation-related biases in ET estimates might offset one another to some extent; however, the overall impact remains unclear without spatially explicit modelling. Incorporating elevation-dependent meteorological data through GIS-based hypsometric methods or distributed modeling frameworks is essential for minimizing biases and enhancing the reliability of watershed-scale ET assessments (Sharma and Irmak, 2016; Pepin et al., 2015). Thus, recognizing and tackling these elevation-related uncertainties enhances the clarity of ET estimations and guides improved water resource management strategies across different landscape conditions.

The choice of a simple (i.e., multiplying evaporation rates, which were determined by the Penman equation, by forest ecosystem coefficient to estimate forest ecosystem ET), yet conceptually sound, representation of forest ecosystem ET estimation was necessary, nonetheless allowing to estimate this important hydrological flux in all basins of ES. Furthermore, it is crucial to underscore the complexities of the study area, which encompasses subalpine ($\leq$ 2300 meters) and Alpine ($>$ 2300 meters) regions. Therefore, distributed models may enhance ET processes estimations by capturing the altitude effect and dynamic in all watersheds of ES. For instance, Liu et al., (2003) estimated ET in the whole Canada at daily steps and 1 km spatial resolution using the

boreal ecosystem productivity simulator, which is driven by remotely sensed leaf area index and land cover maps as well as daily meteorological data. Liu et al., (2003) reported that average ET in forest areas ranged from 200 to 500 mm per year. In the Canadian Boreal Forest, coniferous and aspen forest ET ranges from 100 to 410 mm $year^{-1}$ during summer season (Black et al., 1996; Baldocchi et al., 1997; Jarvis et al., 1997; McCaughey et al., 1997a; Blanken et al., 2001; Eaton and Rouse, 2001). Low transpiration rates (< 200 mm $year^{-1}$) observed in Canadian Boreal Forest may be attributed to the shallow root zones and strong regulation of transpiration by stomata. (McCaughey et al., 1997b). Moreover, other studies in temperate regions used sap flow systems to measure daily forest transpiration worldwide. For instance, in Norunda Forest, North of Uppsala in central Sweden, Lundblad and Lindroth, (2002) measured pine and spruce transpiration, resulting in mean values ranging between 1.3 to 4.6 mm day^{-1} according to the species. At the northern edge of Bavarian Alps, Germany, Matyssek et al., (2009) compared mountainous and sub-alpine forests transpiration, reporting that these plants can reach between 2.5 ~ 6 mm day^{-1}.

The aforementioned findings relate to our results, which showed an historical (1984–2023) average daily forest ecosystem ET of 3.3 $mm.day^{-1}$ during the snowmelt-dominated period (May 15 to July 20, or 66 days), and an average of 2.7 $mm.day^{-1}$ in the rainfall-dominated period (July 21 to September 15, or 61 days). When the periodic average daily forest ecosystem ET values are multiplied by the number of days in each period, the annual ET average value is 382.5 mm $year^{-1}$, which aligns with literature range (Black et al., 1996; Baldocchi et al., 1997; Jarvis et al., 1997; McCaughey et al., 1997a; Blanken et al., 2001; Eaton and Rouse, 2001). Furthermore, the estimation of historical ET processes can be enhanced using remote sensing techniques (Williamson, 2020; Chen and Liu, 2020; Zhu et al., 2022). However, remote sensing methods are unable to replicate long-term changes in ET estimations, as satellite imagery has only been accessible since the 1980s. Nevertheless, Chen et al. (2021) have shown that the temporal issue can be resolved by combining ET remote sensing techniques with reanalysis datasets.

In addition, while the Alberta Township Climate dataset has limitations, it offers a spatially consistent source of estimates for temperature, precipitation, wind, humidity, and total incoming solar radiation across the Eastern Slopes of Alberta. This data set provides daily records since 1984, with elevation-aware adjustments (Alberta Climate Information Service, 2023). The interpolated data serves as valuable resources for regional trend analysis and model inputs, demonstrating reasonable accuracy in temperature and precipitation (RMSE ~0.8°C and RMSE ~4.3 mm/month,

respectively). Nonetheless, limitations remain in alpine and subalpine regions, where wind speeds are underestimated (~10%), whereas total incoming solar radiation (overestimation ~12%), and relative humidity (overestimation ~8%) are overestimated. Moreover, the Alberta Township dataset proved essential for this study given the scarcity of historical, continuous, and spatially distributed hydroclimatic measurements in alpine and subalpine regions of the Eastern Slopes. While imperfect, its gridded interpolation approach provides more spatially representative estimates than relying on one or two weather station per watershed, which can introduce substantial uncertainty due to elevation biases and microclimate variability (Bertoncini and Pomeroy et al., 2025).

5.6. Conclusion

The results of this work help to elucidate the historical trends in open water area and forest ecosystem ET processes in the Eastern Slopes of Alberta (ES), Canada. The hydroclimatic-based models exhibited an average RMSE of 6.8 km^2 and a %RMSE of 10.2% during training, while the validation phase showed an average of RMSE of 7.4 km^2 and a %RMSE of 12.7%. The positive trends in air temperature have resulted in significant positive trends in historical open water areas during the snowmelt-dominated period in all watersheds of ES. However, non-significant decreases in the open water area were predicted for the rainfall-dominated period.

Commensurate with increasing air temperature trends, significant positive historical trends of open water evaporation and forest ecosystem ET were, respectively, observed for the snowmelt and rainfall-dominated period. The $P\%_A$ of evaporated open water volume compared with historical ET volume in forest areas was higher in the snowmelt-dominated period (2.4%) than in the rainfall-dominated period (2.1%), as open water areas are expanding.

However, this modelling approach has shown some limitations, such as, hydroclimatic models are unable to address glacier storage buffer reduction because they do not consider glacial mass balance changes. Snowmelt-dominated period models may be more accurate because long-term storage from deglaciation affects open water areas during the rainfall-dominated period, which the model cannot account for. Despite its limitations, the Alberta Township Climate dataset provides spatially consistent hydroclimatic variable estimates across the ES. This study relied on the Alberta Township dataset since alpine and subalpine portions of the ES lack historical, continuous, and geographically dispersed hydroclimatic observations. The imperfect gridded interpolation

method delivers more spatially representative estimates than using one or two weather stations per watershed, which can contribute significant error because of elevation biases and microclimate variability.

Overall, our research offers a parsimonious solution to model the potential effects of historical hydroclimatic change on open water areas and ET losses. Future studies in the ES should consider the effects of ET losses on the overall basin yields, hence framing evapotranspiration changes to a quantifiable impact on water security.

Acknowledgements

The authors received funding provided by the Natural Sciences and Engineering Research Council of Canada (NSERC; grant no. 2017-04362), Alberta Innovates, the Nexen Fellowship in Water Resources, the Columbia Wetlands Stewardship Partners and the Shuswap Band's Columbia Headwaters Aquatic Restoration Secwépemc Strategy (CHARS) project.

5.7. References

Alberta Climate Information Service (ACIS) https://acis.alberta.ca (December, 2023)

Allen, R. G., Pereira, L. S., Raes, D., & Smith, M. (1998). Crop evapotranspiration: Guidelines for computing crop water requirements (FAO Irrigation and Drainage Paper No. 56). Food and Agriculture Organization of the United Nations. https://www.fao.org/3/x0490e/x0490e00.htm

Allen, R. (2000). Using the FAO-56 dual crop coefficient method over an irrigated region as part of an evapotranspiration intercomparison study. Journal of Hydrology, 229(1–2), 27–41. https://doi.org/10.1016/s0022-1694(99)00194-8

Allen, R. G., Pereira, L. S., Raes, D., & Smith, M. (1998). Crop evapotranspiration : guidelines for computing crop water requirements. In FAO eBooks (Issue 1). http://ci.nii.ac.jp/naid/10018074422

Ashmore, P., & Church, M. (2001). The impact of climate change on rivers and river processes in Canada. https://doi.org/10.4095/211891

Avis, C. A., Weaver, A. J., & Meissner, K. J. (2011). Reduction in areal extent of high-latitude wetlands in response to permafrost thaw. Nature Geoscience, 4(7), 444–448. https://doi.org/10.1038/ngeo1160

Baldocchi, D. D., Vogel, C. A., & Hall, B. (1997). Seasonal variation of energy and water vapor exchange rates above and below a boreal jack pine forest canopy. Journal of Geophysical Research Atmospheres, 102(D24), 28939–28951. https://doi.org/10.1029/96jd03325

Balling, R. C., Meyer, G. A., & Wells, S. G. (1992). Relation of surface climate and burned area in

Yellowstone National Park. Agricultural and Forest Meteorology, 60(3–4), 285–293. https://doi.org/10.1016/0168-1923(92)90043-4

Barnett, T. P., Adam, J. C., & Lettenmaier, D. P. (2005). Potential impacts of a warming climate on water availability in snow-dominated regions. Nature, 438(7066), 303–309. https://doi.org/10.1038/nature04141

Bash, E. A., & Marshall, S. J. (2014). Estimation of glacial melt contributions to the Bow River, Alberta, Canada, using a radiation-temperature melt model. Annals of Glaciology, 55(66), 138–152. https://doi.org/10.3189/2014aog66a226

Baur, M. J., Friend, A. D., & Pellegrini, A. F. A. (2024). Widespread and systematic effects of fire on plant–soil water relations. Nature Geoscience, 17(11), 1115–1120.

Bertoncini, A., & Pomeroy, J. W. (2025). Quantifying spatiotemporal and elevational precipitation gauge network uncertainty in the Canadian Rockies. Hydrology and Earth System Sciences, 29, 983–1000. https://doi.org/10.5194/hess-29-983-2025

Black, T. A., Hartog, G. D., Neumann, H. H., Blanken, P., Yang, P., Russell, C., Nesic, Z., Lee, X., Chen, S. G., Staebler, R., & Novak, M. D. (1996). Annual cycles of water vapour and carbon dioxide fluxes in and above a boreal aspen forest. Global Change Biology, 2(3), 219–229. https://doi.org/10.1111/j.1365-2486.1996.tb00074.x

Blanken, P., Black, T., Neumann, H., Hartog, G. D., Yang, P., Nesic, Z., & Lee, X. (2001). The seasonal water and energy exchange above and within a boreal aspen forest. Journal of Hydrology, 245(1–4), 118–136. https://doi.org/10.1016/s0022-1694(01)00343-2

Bonan, G. (2019). *Climate change and terrestrial ecosystem modeling*. https://doi.org/10.1017/9781107339217

Bonan, G. B. (2008). Forests and Climate Change: Forcings, Feedbacks, and the Climate Benefits of Forests. Science, 320(5882), 1444–1449. https://doi.org/10.1126/science.1155121

Bond-lamberty, B., Peckham, S. D., Gower, S. T., & Ewers, B. E. (2009). Effects of fire on regional evapotranspiration in the central Canadian boreal forest. Global Change Biology, 15(5), 1242–1254. https://doi.org/10.1111/j.1365-2486.2008.01776.x

Brahney, J., Weber, F., Foord, V., Janmaat, J., & Curtis, P. J. (2017). Evidence for a climate-driven hydrologic regime shift in the Canadian Columbia Basin. Canadian Water Resources Journal / Revue Canadienne Des Ressources Hydriques, 42(2), 179–192. https://doi.org/10.1080/07011784.2016.1268933

Brantley, S. T., Stuber, O. S., Holder, D. L., & Taylor, R. S. (2024). Fire exclusion alters forest evapotranspiration: A comprehensive water budget analysis in longleaf pine woodlands. *Ecological Monographs*, *94*(4). https://doi.org/10.1002/ecm.1623

Brodribb, T. J., Powers, J., Cochard, H., & Choat, B. (2020). Hanging by a thread? Forests and drought. Science, 368(6488), 261–266. https://doi.org/10.1126/science.aat7631

Brümmer, C., Black, T. A., Jassal, R. S., Grant, N. J., Spittlehouse, D. L., Chen, B., Nesic, Z., Amiro, B. D., Arain, M. A., Barr, A. G., Bourque, C. P., Coursolle, C., Dunn, A. L., Flanagan, L. B., Humphreys, E. R., Lafleur, P. M., Margolis, H. A., McCaughey, J. H., & Wofsy, S. C. (2011).

How climate and vegetation type influence evapotranspiration and water use efficiency in Canadian forest, peatland and grassland ecosystems. Agricultural and Forest Meteorology, 153, 14–30. https://doi.org/10.1016/j.agrformet.2011.04.008

Bush, E., & Lemmen, D.S. (2022). *Canada's Changing Climate Report*. Govt. of Canada.

Cai, W., Borlace, S., Lengaigne, M., Van Rensch, P., Collins, M., Vecchi, G., Timmermann, A., Santoso, A., McPhaden, M. J., Wu, L., England, M. H., Wang, G., Guilyardi, E., & Jin, F. (2014). Increasing frequency of extreme El Niño events due to greenhouse warming. Nature Climate Change, 4(2), 111–116. https://doi.org/10.1038/nclimate2100

Campos, J. N., Neto, I. E. L., Studart, T. M., & Nascimento, L. S. (2016). Trade-off between reservoir yield and evaporation losses as a function of lake morphology in semi-arid Brazil. Anais Da Academia Brasileira De Ciências, 88(2), 1113–1125. https://doi.org/10.1590/0001-3765201620150124

Cannon, A. J., Sobie, P., & Murdock, T. Q. (2015). Bias correction of GCM precipitation by quantile mapping: How well do methods preserve changes in quantiles and extremes? *Journal of Climate, 28*(17), 6938-6959. https://doi.org/10.1175/JCLI-D-14-00754.1

Castellazzi, P., Burgess, D., Rivera, A., Huang, J., Longuevergne, L., & Demuth, M. N. (2019). Glacial Melt and Potential Impacts on Water Resources in the Canadian Rocky Mountains. Water Resources Research, 55(12), 10191–10217. https://doi.org/10.1029/2018wr024295

Chapin, F. S., Sturm, M., Serreze, M. C., McFadden, J. P., Key, J. R., Lloyd, A. H., McGuire, A. D., Rupp, T. S., Lynch, A. H., Schimel, J. P., Beringer, J., Chapman, W. L., Epstein, H. E., Euskirchen, E. S., Hinzman, L. D., Jia, G., Ping, C., Tape, K. D., Thompson, C. D. C., Welker, J. M. (2005). Role of Land-Surface Changes in Arctic Summer Warming. Science, 310(5748), 657–660. https://doi.org/10.1126/science.1117368

Chen, S., Fu, Y. H., Geng, X., Hao, Z., Tang, J., Zhang, X., Xu, Z., & Hao, F. (2022). Influences of Shifted Vegetation Phenology on Runoff Across a Hydroclimatic Gradient. Frontiers in Plant Science, 12. https://doi.org/10.3389/fpls.2021.802664

Chen, Y., & Kirwan, M. L. (2024). Rapid greening in mangroves. Nature Ecology & Evolution, 8(2), 186–187. https://doi.org/10.1038/s41559-023-02247-x

Chen, J. M., & Liu, J. (2019). Evolution of evapotranspiration models using thermal and shortwave remote sensing data. Remote Sensing of Environment, 237, 111594. https://doi.org/10.1016/j.rse.2019.111594

Chen, X., Su, Z., Ma, Y., Trigo, I., & Gentine, P. (2021). Remote Sensing of Global Daily Evapotranspiration based on a Surface Energy Balance Method and Reanalysis Data. Journal of Geophysical Research Atmospheres, 126(16). https://doi.org/10.1029/2020jd032873

Chiarle, M., Geertsema, M., Mortara, G., & Clague, J. J. (2021). Relations between climate change and mass movement: Perspectives from the Canadian Cordillera and the European Alps. Global and Planetary Change, 202, 103499. https://doi.org/10.1016/j.gloplacha.2021.103499

Cooper, C. E., Aparecido, L. M., Muir, J. P., Morgan, C. L., Heilman, J. L., & Moore, G. W. (2018). Transpiration in recovering mixed loblolly pine and oak stands following wildfire in the Lost Pines region of Texas. Ecohydrology, 12(1). https://doi.org/10.1002/eco.2052

Costa, J. A., Navarro-Hevia, J., Costa, C. a. G., & De Araújo, J. C. (2021). Temporal dynamics of evapotranspiration in semiarid native forests in Brazil and Spain using remote sensing. Hydrological Processes, 35(3). https://doi.org/10.1002/hyp.14070

Craig, J. R., Brown, G., Chlumsky, R., Jenkinson, R. W., Jost, G., Lee, K., Mai, J., Serrer, M., Sgro, N., Shafii, M., Snowdon, A. P., & Tolson, B. A. (2020b). Flexible watershed simulation with the Raven hydrological modelling framework. Environmental Modelling & Software, 129, 104728. https://doi.org/10.1016/j.envsoft.2020.104728

Dawe, D. A., Peters, V. S., & Flannigan, M. D. (2019). Post-fire regeneration of endangered limber pine (Pinus flexilis) at the northern extent of its range. Forest Ecology and Management, 457, 117725. https://doi.org/10.1016/j.foreco.2019.117725

DeBeer, C. M., Wheater, H. S., Carey, S. K., & Chun, K. P. (2015). Recent climatic, cryospheric, and hydrological changes over the interior of western Canada: a synthesis and review. Hydrology and Earth System Sciences. https://doi.org/10.5194/hessd-12-8615-2015

Derksen, C., Burgess, D., Duguay, C., Howell, S., Murdyk, L., Smith, S., Thackeray, C., & Kirchmeier-Young, M. (2019). *Changes in snow, ice, and permafrost across Canada*. https://doi.org/10.4095/308279

Dingman, S. L. (2015). *Physical hydrology* (3rd ed.). Waveland Press.

Diro, G. T., & Sushama, L. (2019). Contribution of Snow Cover Decline to Projected Warming Over North America. Geophysical Research Letters, 47(1). https://doi.org/10.1029/2019gl084414

Domine, F., Barrere, M., & Morin, S. (2016). The growth of shrubs on high Arctic tundra at Bylot Island: impact on snow physical properties and permafrost thermal regime. Biogeosciences, 13(23), 6471–6486. https://doi.org/10.5194/bg-13-6471-2016

Eaton, A. K., & Rouse, W. R. (2001). Controls on evapotranspiration at a subarctic sedge fen. Hydrological Processes, 15(18), 3423–3431. https://doi.org/10.1002/hyp.1029

Fang, B., Lei, H., Zhang, Y., Quan, Q., Yang, D., (2020a). Spatio-temporal patterns of evapotranspiration based on upscaling eddy covariance measurements in the dryland of the North China Plain. Agric. For. Meteorol. 281, 107844.

Fernandes, R., Korolevych, V., & Wang, S. (2007). Trends in Land Evapotranspiration over Canada for the Period 1960–2000 Based on In Situ Climate Observations and a Land Surface Model. Journal of Hydrometeorology, 8(5), 1016–1030. https://doi.org/10.1175/jhm619.1

Fu, Y. H., Piao, S., Delpierre, N., Hao, F., Hänninen, H., Geng, X., Peñuelas, J., Zhang, X., Janssens, I. A., & Campioli, M. (2019). Nutrient availability alters the correlation between spring leaf-out and autumn leaf senescence dates. Tree Physiology, 39(8), 1277–1284. https://doi.org/10.1093/treephys/tpz041

Gaertner, B. A., Zegre, N., Warner, T., Fernandez, R., He, Y., & Merriam, E. R. (2018). Climate, forest growing season, and evapotranspiration changes in the central Appalachian Mountains, USA. The Science of the Total Environment, 650, 1371–1381. https://doi.org/10.1016/j.scitotenv.2018.09.129

Gan, R., Liu, Q., Huang, G., Hu, K., & Li, X. (2023). Greenhouse warming and internal variability

increase extreme and central Pacific El Niño frequency since 1980. Nature Communications, 14(1). https://doi.org/10.1038/s41467-023-36053-7

Gobiet, A., Kotlarski, S., Beniston, M., Heinrich, G., Rajczak, J., & Stoffel, M. (2013). 21st century climate change in the European Alps—A review. The Science of the Total Environment, 493, 1138–1151. https://doi.org/10.1016/j.scitotenv.2013.07.050

Goulden, M. L., & Bales, R. C. (2014). Mountain runoff vulnerability to increased evapotranspiration with vegetation expansion. Proceedings of the National Academy of Sciences, 111(39), 14071–14075. https://doi.org/10.1073/pnas.1319316111

Goulden, M. L., Anderson, R. G., Bales, R. C., Kelly, A. E., Meadows, M., & Winston, G. C. (2012). Evapotranspiration along an elevation gradient in California's Sierra Nevada. Journal of Geophysical Research Atmospheres, 117(G3). https://doi.org/10.1029/2012jg002027

Government of Alberta – Boundary Files, Reference Guide, Second edition, 2016 Census. Statistics Canada Catalogue no. 92-160-G.

Habeck, J. R., & Mutch, R. W. (1973). Fire-Dependent Forests in the Northern Rocky Mountains. Quaternary Research, 3(3), 408–424. https://doi.org/10.1016/0033-5894(73)90006-9

Hauer, F. R., Baron, J. S., Campbell, D. H., Fausch, K. D., Hostetler, S. W., Leavesley, G. H., Leavitt, P. R., Mcknight, D. M., & Stanford, J. A. (1997). Assessment of climate change and freshwater ecosystems of the Rocky Mountains, USA and Canada. Hydrological Processes, 11(8), 903–924. https://doi.org/10.1002/(sici)1099-1085(19970630)11:8

Hayashi, M. (2013). The cold vadose zone: Hydrological and ecological significance of frozen-soil processes. Vadose Zone Journal, 12(4). https://doi.org/10.2136/vzj2013.03.0064

Hermosilla, T., Wulder, M. A., White, J. C., & Coops, N. C. (2022). Land cover classification in an era of big and open data: Optimizing localized implementation and training data selection to improve mapping outcomes. Remote Sensing of Environment, 268, 112780. https://doi.org/10.1016/j.rse.2021.112780

Hopkinson, C., & Young, G. J. (1998). The effect of glacier wastage on the flow of the Bow River at Banff, Alberta, 1951–1993. Hydrological Processes, 12(10–11), 1745–1762. https://doi.org/10.1002/(sici)1099-1085(199808/09)12:10/11

Hussain, M., & Mahmud, I. (2019). pyMannKendall: a python package for non parametric Mann Kendall family of trend tests. The Journal of Open Source Software, 4(39), 1556. https://doi.org/10.21105/joss.01556

Huss, M., & Hock, R. (2018). Global-scale hydrological response to future glacier mass loss. Nature Climate Change, 8(2), 135–140. https://doi.org/10.1038/s41558-017-0049-x

IPCC. (2023). *AR6 Synthesis Report*. https://www.ipcc.ch/report/ar6/syr/

Jain, P., Barber, Q. E., Taylor, S. W., Whitman, E., Acuna, D. C., Boulanger, Y., Chavardès, R. D., Chen, J., Englefield, P., Flannigan, M., Girardin, M. P., Hanes, C. C., Little, J., Morrison, K., Skakun, R. S., Thompson, D. K., Wang, X., & Parisien, M. (2024). Drivers and Impacts of the Record-Breaking 2023 Wildfire Season in Canada. Nature Communications, 15(1). https://doi.org/10.1038/s41467-024-51154-7

Jarvis, P. G., Massheder, J. M., Hale, S. E., Moncrieff, J. B., Rayment, M., & Scott, S. L. (1997). Seasonal variation of carbon dioxide, water vapor, and energy exchanges of a boreal black spruce forest. Journal of Geophysical Research Atmospheres, 102(D24), 28953–28966. https://doi.org/10.1029/97jd01176

Jeong, S., Ho, C., Gim, H., & Brown, M. E. (2011). Phenology shifts at start vs. end of growing season in temperate vegetation over the Northern Hemisphere for the period 1982-2008. Global Change Biology, 17(7), 2385–2399. https://doi.org/10.1111/j.1365-2486.2011.02397.x

Jiang, R., Gan, T. Y., Xie, J., Wang, N., & Kuo, C. (2015). Historical and potential changes of precipitation and temperature of Alberta subjected to climate change impact: 1900–2100. Theoretical and Applied Climatology, 127(3–4), 725–739. https://doi.org/10.1007/s00704-015-1664-y

Ju, J., & Masek, J. G. (2016). The vegetation greenness trend in Canada and US Alaska from 1984–2012 Landsat data. Remote Sensing of Environment, 176, 1–16. https://doi.org/10.1016/j.rse.2016.01.001

Kachholz, F., & Tränckner, J. (2020). Long-Term Modelling of an Agricultural and Urban River Catchment with SWMM Upgraded by the Evapotranspiration Model UrbanEVA. Water, 12(11), 3089. https://doi.org/10.3390/w12113089

Kang, S., Kimball, J. S., & Running, S. W. (2005). Simulating effects of fire disturbance and climate change on boreal forest productivity and evapotranspiration. The Science of the Total Environment, 362(1–3), 85–102. https://doi.org/10.1016/j.scitotenv.2005.11.014

Kasurinen, V., Alfredsen, K., Kolari, P., Mammarella, I., Alekseychik, P., Rinne, J., Vesala, T., Bernier, P., Boike, J., Langer, M., Marchesini, L. B., Van Huissteden, K., Dolman, H., Sachs, T., Ohta, T., Varlagin, A., Rocha, A., Arain, A., Oechel, W., . . . Berninger, F. (2014). Latent heat exchange in the boreal and arctic biomes. *Global Change Biology*, *20*(11), 3439–3456. https://doi.org/10.1111/gcb.12640

Kendall, M.G. (1957). Rank Correlation Methods. Biometrika, 44(1/2), 298. https://doi.org/10.2307/2333282

Kienzle, S. W. (2006). The Use of the Recession Index as an Indicator for Streamflow Recovery After a Multi-Year Drought. Water Resources Management, 20(6), 991–1006. https://doi.org/10.1007/s11269-006-9019-1

Koch, J. C., Ewing, S. A., Striegl, R., & McKnight, D. M. (2012). Rapid runoff via shallow throughflow and deeper preferential flow in a boreal catchment underlain by frozen silt (Alaska, USA). *Hydrogeology Journal*, *21*(1), 93–106. https://doi.org/10.1007/s10040-012-0934-3

Kool, D., Agam, N., Lazarovitch, N., Heitman, J., Sauer, T., & Ben-Gal, A. (2014). A review of approaches for evapotranspiration partitioning. Agricultural and Forest Meteorology, 184, 56–70. https://doi.org/10.1016/j.agrformet.2013.09.003

Koutsoyiannis, D. (2020). Revisiting the global hydrological cycle: is it intensifying? Hydrology and Earth System Sciences, 24(8), 3899–3932. https://doi.org/10.5194/hess-24-3899-2020

Kuriata-Potasznik, A. B., & Szymczyk, S. (2016). Variability of the water availability in a river lake system – A case study of Lake Symsar. Journal of Water and Land Development, 31(1), 87–96.

https://doi.org/10.1515/jwld-2016-0039

Lafleur, P. M., & Humphreys, E. R. (2018). Tundra shrub effects on growing season energy and carbon dioxide exchange. Environmental Research Letters, 13(5), 055001. https://doi.org/10.1088/1748-9326/aab863

Langs, L. (2019). Quantifying coniferous subalpine tree transpiration and source water under seasonal and hydrological stress in the Canadian Rocky Mountains, Kananaskis, Alberta. https://libuwspaceprd02.uwaterloo.ca/handle/10012/14741

Lantz, T. C., Gergel, S. E., & Henry, G. H. R. (2010). Response of green alder (Alnus viridis subsp. fruticosa) patch dynamics and plant community composition to fire and regional temperature in north-western Canada. Journal of Biogeography, 37(8), 1597–1610. https://doi.org/10.1111/j.1365-2699.2010.02317.x

Lara, M. J., Genet, H., McGuire, A. D., Euskirchen, E. S., Zhang, Y., Brown, D. R. N., Jorgenson, M. T., Romanovsky, V., Breen, A., & Bolton, W. R. (2015). Thermokarst rates intensify due to climate change and forest fragmentation in an Alaskan boreal forest lowland. Global Change Biology, 22(2), 816–829. https://doi.org/10.1111/gcb.13124

Levenberg, K. (1944). A method for the solution of certain non-linear problems in least squares. Quarterly of Applied Mathematics, 2(2), 164–168. https://doi.org/10.1090/qam/10666

Lian, X., Piao, S., Li, L. Z. X., Li, Y., Huntingford, C., Ciais, P., Cescatti, A., Janssens, I. A., Peñuelas, J., Buermann, W., Chen, A., Li, X., Myneni, R. B., Wang, X., Wang, Y., Yang, Y., Zeng, Z., Zhang, Y., & McVicar, T. R. (2020). Summer soil drying exacerbated by earlier spring greening of northern vegetation. Science Advances, 6(1). https://doi.org/10.1126/sciadv.aax0255

Liu, J., Chen, J. M., & Cihlar, J. (2003). Mapping evapotranspiration based on remote sensing: An application to Canada's landmass. Water Resources Research, 39(7). https://doi.org/10.1029/2002wr001680

López-Moreno, J. I., Pomeroy, J. W., Morán-Tejeda, E., Revuelto, J., Navarro-Serrano, F. M., Vidaller, I., & Alonso-González, E. (2021). Changes in the frequency of global high mountain rain-on-snow events due to climate warming. Environmental Research Letters, 16(9), 094021. https://doi.org/10.1088/1748-9326/ac0dde

Lundblad, M., & Lindroth, A. (2002). Stand transpiration and sapflow density in relation to weather, soil moisture and stand characteristics. Basic and Applied Ecology, 3(3), 229–243. https://doi.org/10.1078/1439-1791-00099

Ma, N., & Zhang, Y. (2022). Increasing Tibetan Plateau terrestrial evapotranspiration primarily driven by precipitation. Agricultural and Forest Meteorology, 317, 108887. https://doi.org/10.1016/j.agrformet.2022.108887

Mann, H. B. (1945). Nonparametric Tests Against Trend. Econometrica, 13(3), 245. https://doi.org/10.2307/1907187

Marks, D., Domingo, J., Susong, D., Link, T., & Garen, D. (1999). A spatially distributed energy balance snowmelt model for application in mountain basins. *Hydrological Processes*, *13*(12–13), 1935–1959. https://doi.org/10.1002/(sici)1099-1085(199909)13:12/13

Mata-González, R., McLendon, T., & Martin, D. W. (2005). The Inappropriate Use of Crop Transpiration coefficients (KC) to estimate evapotranspiration in arid ecosystems: a review. Arid Land Research and Management, 19(3), 285–295. https://doi.org/10.1080/15324980590951469

McCabe, M. F., & Wood, E. F. (2006). Scale influences on the remote estimation of evapotranspiration using multiple satellite sensors. Remote Sensing of Environment, 105(4), 271–285. https://doi.org/10.1016/j.rse.2006.07.006

McCaughey, J. H., Lafleur, P. M., Joiner, D. W., Bartlett, P. A., Costello, A. M., Jelinski, D. E., & Ryan, M. G. (1997a). Magnitudes and seasonal patterns of energy, water, and carbon exchanges at a boreal young jack pine forest in the BOREAS northern study area. Journal of Geophysical Research Atmospheres, 102(D24), 28997–29007. https://doi.org/10.1029/97jd00239

McCaughey, J. H., B. D. Amiro, A. W. Robertson, and D. Spittlehouse (1997b) Forest environments, in The Surface Climates of Canada, edited by W. G. Bailey, T. R. Oke, and W. R. Rouse, pp. 247–276, McGill-Queen's Univ. Press, Montreal, Canada.

McMahon, T. A., Finlayson, B. L., & Peel, M. C. (2016). Historical developments of models for estimating evaporation using standard meteorological data. Wiley Interdisciplinary Reviews Water, 3(6), 788–818. https://doi.org/10.1002/wat2.1172

Mekonnen, Z. A., Riley, W. J., Randerson, J. T., Grant, R. F., & Rogers, B. M. (2019). Expansion of high-latitude deciduous forests driven by interactions between climate warming and fire. Nature Plants, 5(9), 952–958. https://doi.org/10.1038/s41477-019-0495-8

Marquardt, D.W. (1963). An Algorithm for Least-Squares Estimation of Nonlinear Parameters. Journal of the Society for Industrial and Applied Mathematics, 11(2), 431–441. https://doi.org/10.1137/0111030

Martz, L., Armstrong, R., & Pietroniro, E. (2007). The South Saskatchewan River Basin: Physical Geography. In "Climate Change and Water SSRB Final Technical Report." In Prairie Adaptation Research Collaborative, Regina, Canada (pp. 31–40). https://espace.library.uq.edu.au/view/UQ:388633

Mastrotheodoros, T., Pappas, C., Molnar, P., Burlando, P., Manoli, G., Parajka, J., Rigon, R., Szeles, B., Bottazzi, M., Hadjidoukas, P., & Fatichi, S. (2020). More green and less blue water in the Alps during warmer summers. Nature Climate Change, 10(2), 155–161. https://doi.org/10.1038/s41558-019-0676-5

Matyssek, R., Wieser, G., Patzner, K., Blaschke, H., & Häberle, K. (2009). Transpiration of forest trees and stands at different altitude: consistencies rather than contrasts? European Journal of Forest Research, 128(6), 579–596. https://doi.org/10.1007/s10342-008-0243-5

Meyn, A., Taylor, S. W., Flannigan, M. D., Thonicke, K., & Cramer, W. (2009). Relationship between fire, climate oscillations, and drought in British Columbia, Canada, 1920–2000. Global Change Biology, 16(3), 977–989. https://doi.org/10.1111/j.1365-2486.2009.02061.x

McCabe, G. J., Clark, M. P., & Hay, L. E. (2007). Rain-on-Snow Events in the Western United States. Bulletin of the American Meteorological Society, 88(3), 319–328. https://doi.org/10.1175/bams-88-3-319

McCaffrey, D. R., & Hopkinson, C. (2020). Modeling Watershed-Scale Historic Change in the

Alpine Treeline Ecotone Using Random Forest. Canadian Journal of Remote Sensing, 46(6), 715–732. https://doi.org/10.1080/07038992.2020.1865792

Myers-Smith, I. H., Kerby, J. T., Phoenix, G. K., et al. (2020). Complexity revealed in the greening of the Arctic. Nature Climate Change, 10(2), 106–117. https://doi.org/10.1038/s41558-019-0688-1

Meixner, T., Manning, A. H., Stonestrom, D. A., Allen, D. M., Ajami, H., Blasch, K. W., Brookfield, A. E., Castro, C. L., Clark, J. F., Gochis, D. J., Flint, A. L., Neff, K. L., Niraula, R., Rodell, M., Scanlon, B. R., Singha, K., & Walvoord, M. A. (2016). Implications of projected climate change for groundwater recharge in the western United States. Journal of Hydrology, 534, 124–138. https://doi.org/10.1016/j.jhydrol.2015.12.027

Millar, D. J., Cooper, D. J., & Ronayne, M. J. (2018). Groundwater dynamics in mountain peatlands with contrasting climate, vegetation, and hydrogeological setting. Journal of Hydrology, 561, 908–917. https://doi.org/10.1016/j.jhydrol.2018.04.050

Milner, A. M., Khamis, K., Battin, T. J., Brittain, J. E., Barrand, N. E., Füreder, L., Cauvy-Fraunié, S., Gíslason, G. M., Jacobsen, D., Hannah, D. M., Hodson, A. J., Hood, E., Lencioni, V., Ólafsson, J. S., Robinson, C. T., Tranter, M., & Brown, L. E. (2017). Glacier shrinkage driving global changes in downstream systems. Proceedings of the National Academy of Sciences, 114(37), 9770–9778. https://doi.org/10.1073/pnas.1619807114

Mintz, Y., & Walker, G. K. (1993). Global Fields of Soil Moisture and Land Surface Evapotranspiration Derived from Observed Precipitation and Surface Air Temperature. Journal of Applied Meteorology, 32(8), 1305–1334. https://doi.org/10.1175/1520-0450(1993)032

Mioduszewski, J. R., Rennermalm, A. K., Robinson, D. A., & Mote, T. L. (2014). Attribution of snowmelt onset in Northern Canada. *Journal of Geophysical Research Atmospheres*, *119*(16), 9638–9653. https://doi.org/10.1002/2013jd021024

Moore, R. D., Fleming, S. W., Menounos, B., Wheate, R., Fountain, A., Stahl, K., Holm, K., & Jakob, M. (2008). Glacier change in western North America: influences on hydrology, geomorphic hazards and water quality. Hydrological Processes, 23(1), 42–61. https://doi.org/10.1002/hyp.7162

Mudryk, L. R., Derksen, C., Howell, S., Laliberté, F., Thackeray, C., Sospedra-Alfonso, R., Vionnet, V., Kushner, P. J., & Brown, R. (2018). Canadian snow and sea ice: historical trends and projections. *the Cryosphere*, *12*(4), 1157–1176. https://doi.org/10.5194/tc-12-1157-2018

Musselman, K. N., Lehner, F., Ikeda, K., Clark, M. P., Prein, A. F., Liu, C., Barlage, M., & Rasmussen, R. (2018). Projected increases and shifts in rain-on-snow flood risk over western North America. Nature Climate Change, 8(9), 808–812. https://doi.org/10.1038/s41558-018-0236-4

Myers-Smith, I. H., & Hik, D. S. (2017). Climate warming as a driver of tundra shrubline advance. Journal of Ecology, 106(2), 547–560. https://doi.org/10.1111/1365-2745.12817

Nash, J., & Sutcliffe, J. (1970). River flow forecasting through conceptual models part I — A discussion of principles. Journal of Hydrology, 10(3), 282–290. https://doi.org/10.1016/0022-1694(70)90255-6

National Oceanic and Atmospheric Administration (NOAA). (2023). Trends in atmospheric carbon dioxide. Global Monitoring Laboratory. https://gml.noaa.gov/ccgg/trends/global.html

Paradis, M., Lévesque, E., & Boudreau, S. (2016). Greater effect of increasing shrub height on winter versus summer soil temperature. Environmental Research Letters, 11(8), 085005. https://doi.org/10.1088/1748-9326/11/8/085005

Pekel, J., Cottam, A., Gorelick, N., & Belward, A. S. (2016). High-resolution mapping of global surface water and its long-term changes. Nature, 540(7633), 418–422. https://doi.org/10.1038/nature20584

Pelto, M., WGMS Network. (2020). Alpine glaciers [in State of the Climate in 2019]. Bulletin of the American Meteorological Society, 101(8), S37–S38. doi.org/10.1175/2020BAMSStateoftheClimate.1.

Pendergrass, A. G., Meehl, G. A., Pulwarty, R., Hobbins, M., Hoell, A., AghaKouchak, A., Bonfils, C. J. W., Gallant, A. J. E., Hoerling, M., Hoffmann, D., Kaatz, L., Lehner, F., Llewellyn, D., Mote, P., Neale, R. B., Overpeck, J. T., Sheffield, A., Stahl, K., Svoboda, M., Woodhouse, C. A. (2020). Flash droughts present a new challenge for subseasonal-to-seasonal prediction. Nature Climate Change, 10(3), 191–199. https://doi.org/10.1038/s41558-020-0709-0

Penman, H. L. (1956). Estimating evaporation. Transactions American Geophysical Union, 37(1), 43–50. https://doi.org/10.1029/tr037i001p00043

Penman, H. L. (1948). Natural evaporation from open water, bare soil and grass. Proceedings of the Royal Society of London a Mathematical and Physical Sciences, 193(1032), 120–145. https://doi.org/10.1098/rspa.1948.0037

Pepin, N., Bradley, R. S., Diaz, H. F., Baraer, M., Caceres, E. B., Forsythe, N., Fowler, H., Greenwood, G., Hashmi, M. Z., Liu, X. D., Miller, J. R., Ning, L., Ohmura, A., Palazzi, E., Rangwala, I., Schöner, W., Severskiy, I., Shahgedanova, M., Wang, M. B., . . . Yang, D. Q. (2015). Elevation-dependent warming in mountain regions of the world. *Nature Climate Change*, *5*(5), 424–430. https://doi.org/10.1038/nclimate2563

Peterson, T. J., Saft, M., Peel, M. C., & John, A. (2021). Watersheds may not recover from drought. Science, 372(6543), 745–749. https://doi.org/10.1126/science.abd5085

Pettorelli, N., Pelletier, F., Von Hardenberg, A., Festa-Bianchet, M., & CôTé, S. D. (2007). Early onset of vegetation growth vs. Rapid green-up: impacts on Juvenile mountain ungulates. Ecology, 88(2), 381–390. https://doi.org/10.1890/06-0875

Pomeroy, J., Bewley, D., Essery, R., Hedstrom, N., Link, T., Granger, R., Sicart, J., Ellis, C., & Janowicz, J. (2006). Shrub tundra snowmelt. Hydrological Processes, 20(4), 923–941. https://doi.org/10.1002/hyp.6124

Pomeroy, J. W., Fang, X., & Ellis, C. (2020). Sensitivity of snowmelt hydrology in Marmot Creek, Alberta, to forest cover disturbance. Hydrological Processes, 34(26), 5308-5323. https://doi.org/10.1002/hyp.9248

Pomeroy, J. W., Fang, X., & Rasouli, K. (2015). Sensitivity of snow processes to warming in the Canadian Rockies. In: Cold Regions Hydrology in a Changing Climate (pp. 95–104). IAHS Publ. 371.

Poulos, H. M., Barton, A. M., Koch, G. W., Kolb, T. E., & Thode, A. E. (2021). Wildfire severity and vegetation recovery drive post-fire evapotranspiration in a southwestern pine-oak forest,

Arizona, USA. Remote Sensing in Ecology and Conservation, 7(4), 579–591. https://doi.org/10.1002/rse2.210

Piao, S., Liu, Q., Chen, A., Janssens, I. A., Fu, Y., Dai, J., Liu, L., Lian, X., Shen, M., & Zhu, X. (2019). Plant phenology and global climate change: Current progresses and challenges. Global Change Biology, 25(6), 1922–1940. https://doi.org/10.1111/gcb.14619

Pradhananga, D., & Pomeroy, J. W. (2022). Recent hydrological response of glaciers in the Canadian Rockies to changing climate and glacier configuration. Hydrology and Earth System Sciences, 26(10), 2605–2616. https://doi.org/10.5194/hess-26-2605-2022

Priestley, C. H. B., & Taylor, R. J. (1972). On the Assessment of Surface Heat Flux and Evaporation Using Large-Scale Parameters. Monthly Weather Review, 100(2), 81–92. https://doi.org/10.1175/1520-0493(1972)100

Rasouli, K., Hernández-Henr&Amp;Iacute;Quez, M. A., & Déry, S. J. (2013). Streamflow input to Lake Athabasca, Canada. Hydrology and Earth System Sciences, 17(5), 1681–1691. https://doi.org/10.5194/hess-17-1681-2013

Rhemtulla, J. M., Hall, R. J., Higgs, E. S., & Macdonald, S. E. (2002). Eighty years of change: vegetation in the montane ecoregion of Jasper National Park, Alberta, Canada. Canadian Journal of Forest Research, 32(11), 2010–2021. https://doi.org/10.1139/x02-112

Rodrigues, I. S., Hopkinson, C., Chasmer, L., MacDonald, R. J., Bayley, S. E., & Brisco, B. (2024a). Multi-decadal floodplain classification and trend analysis in the Upper Columbia River valley, British Columbia. Hydrology and Earth System Sciences, 28(10), 2203–2221. https://doi.org/10.5194/hess-28-2203-2024

Rodrigues, I. S., Hopkinson, C., Chasmer, L., MacDonald, R. J., & Bayley, S. E. (2024b). Warmer air temperatures predicted to result in wetland drying in the Upper Columbia River Valley, British Columbia, Canada. The Science of the Total Environment, 959, 178261. https://doi.org/10.1016/j.scitotenv.2024.178261

Rodrigues, I. S., Rodrigues, G. P., Costa, C. a. G., Hopkinson, C., & De Araújo, J. C. (2024c). Connectivity of evapotranspiration processes in a Brazilian dryland reservoir using remote sensing. Agricultural and Forest Meteorology, 351, 110017. https://doi.org/10.1016/j.agrformet.2024.110017

Rood, S. B., Pan, J., Gill, K. M., Franks, C. G., Samuelson, G. M., & Shepherd, A. (2008). Declining summer flows of Rocky Mountain rivers: Changing seasonal hydrology and probable impacts on floodplain forests. Journal of Hydrology, 349(3–4), 397–410. https://doi.org/10.1016/j.jhydrol.2007.11.012

Rosenberry, D. O., Winter, T. C., Buso, D. C., & Likens, G. E. (2007). Comparison of 15 evaporation methods applied to a small mountain lake in the northeastern USA. Journal of Hydrology, 340(3–4), 149–166. https://doi.org/10.1016/j.jhydrol.2007.03.018

Rouse, W. R., Oswald, C. J., Binyamin, J., Spence, C., Schertzer, W. M., Blanken, P. D., Bussières, N., & Duguay, C. R. (2005). The role of Northern lakes in a regional energy balance. *Journal of Hydrometeorology*, *6*(3), 291–305. https://doi.org/10.1175/jhm421.1

Samani, Z. (2000). Estimating Solar Radiation and Evapotranspiration Using Minimum Climatological Data. Journal of Irrigation and Drainage Engineering, 126(4), 265–267.

https://doi.org/10.1061/(asce)0733-9437(2000)126:4(265

Schaaf, C. B., Gao, F., Strahler, A. H., Lucht, W., Li, X., Tsang, T., Strugnell, N. C., Zhang, X., Jin, Y., Muller, J., Lewis, P., Barnsley, M., Hobson, P., Disney, M., Roberts, G., Dunderdale, M., Doll, C., D'Entremont, R. P., Hu, B., . . . Roy, D. (2002). First operational BRDF, albedo nadir reflectance products from MODIS. *Remote Sensing of Environment*, *83*(1–2), 135–148. https://doi.org/10.1016/s0034-4257(02)00091-3

Scott, R. L., Edwards, E. A., Shuttleworth, W., Huxman, T. E., Watts, C., & Goodrich, D. C. (2004). Interannual and seasonal variation in fluxes of water and carbon dioxide from a riparian woodland ecosystem. Agricultural and Forest Meteorology, 122(1–2), 65–84. https://doi.org/10.1016/j.agrformet.2003.09.001

Scott, R. L., Knowles, J. F., Nelson, J. A., Gentine, P., Li, X., Barron-Gafford, G., Bryant, R., & Biederman, J. A. (2020). Water Availability Impacts on Evapotranspiration Partitioning. Agricultural and Forest Meteorology, 297, 108251. https://doi.org/10.1016/j.agrformet.2020.108251

Sen, O. L., Bozkurt, D., Vogler, J. B., Fox, J., Giambelluca, T. W., & Ziegler, A. D. (2012). Hydro-climatic effects of future land-cover/land-use change in montane mainland southeast Asia. Climatic Change, 118(2), 213–226. https://doi.org/10.1007/s10584-012-0632-0

Sharma, V., Kilic, A., & Irmak, S. (2016). Impact of scale/resolution on evapotranspiration from Landsat and MODIS images. *Water Resources Research*, *52*(3), 1800–1819. https://doi.org/10.1002/2015wr017772

Silva, W.P.D., Silva, C.M., Cavalcanti, C.G., Silva, D.D., Soares, I.B., Oliveira, J.A., & Silva, C.D. (2004). LAB fit curve fitting: a software in portuguese for treatment of experimental data. Revista Brasileira de Ensino de Física, 26, 419-427. https://doi.org/10.1590/S1806-11172004000400018

Somers, L. D., & McKenzie, J. M. (2020). A review of groundwater in high mountain environments. Wiley Interdisciplinary Reviews Water, 7(6). https://doi.org/10.1002/wat2.1475

Stewart, I. T., Cayan, D. R., & Dettinger, M. D. (2005). Changes toward Earlier Streamflow Timing across Western North America. Journal of Climate, 18(8), 1136–1155. https://doi.org/10.1175/jcli3321.1

Stewart, I. T., Cayan, D. R., & Dettinger, M. D. (2004). Changes in Snowmelt Runoff Timing in Western North America under a `Business as Usual' Climate Change Scenario. Climatic Change, 62(1–3), 217–232. https://doi.org/10.1023/b:clim.0000013702.22656.e8

Sturm, M., Douglas, T., Racine, C., & Liston, G. E. (2005). Changing snow and shrub conditions affect albedo with global implications. Journal of Geophysical Research Atmospheres, 110(G1). https://doi.org/10.1029/2005jg000013

Tanner, C. B. (1960). Energy Balance Approach to Evapotranspiration from Crops. Soil Science Society of America Journal, 24(1), 1–9. https://doi.org/10.2136/sssaj1960.03615995002400010012x

Trant, A., Higgs, E., & Starzomski, B. M. (2020). A century of high elevation ecosystem change in the Canadian Rocky Mountains. Scientific Reports, 10(1). https://doi.org/10.1038/s41598-020-66277-2

Travers-Smith, H., Lantz, T. C., Fraser, R. H., & Kokelj, S. V. (2022). Changes in surface water dynamics across northwestern Canada are influenced by wildfire and permafrost thaw. Environmental Research Letters, 17(11), 114021. https://doi.org/10.1088/1748-9326/ac97f7

Vincent, L. A., Zhang, X., Brown, R. D., Feng, Y., Mekis, E., Milewska, E. J., Wan, H., & Wang, X. L. (2015). Observed trends in Canada's climate and influence of Low-Frequency variability modes. *Journal of Climate*, *28*(11), 4545–4560. https://doi.org/10.1175/jcli-d-14-00697.1

Viviroli, D., Dürr, H. H., Messerli, B., Meybeck, M., & Weingartner, R. (2007). Mountains of the world, water towers for humanity: Typology, mapping, and global significance. Water Resources Research, 43(7). https://doi.org/10.1029/2006wr005653

Vormoor, K., Lawrence, D., Heistermann, M., & Bronstert, A. (2015). Climate change impacts on the seasonality and generation processes of floods – projections and uncertainties for catchments with mixed snowmelt/rainfall regimes. Hydrology and Earth System Sciences, 19(2), 913–931. https://doi.org/10.5194/hess-19-913-2015

Wang, G., Cai, W., Gan, B., Wu, L., Santoso, A., Lin, X., Chen, Z., & McPhaden, M. J. (2017). Continued increase of extreme El Niño frequency long after 1.5 °C warming stabilization. Nature Climate Change, 7(8), 568–572. https://doi.org/10.1038/nclimate3351

Wang, L., Good, S. P., & Caylor, K. K. (2014). Global synthesis of vegetation control on evapotranspiration partitioning. Geophysical Research Letters, 41(19), 6753–6757. https://doi.org/10.1002/2014gl061439

Wang, W., Lee, X., Xiao, W., Liu, S., Schultz, N., Wang, Y., Zhang, M., & Zhao, L. (2018). Global lake evaporation accelerated by changes in surface energy allocation in a warmer climate. Nature Geoscience, 11(6), 410–414. https://doi.org/10.1038/s41561-018-0114-8

Wheaton, E., Kulshreshtha, S., Wittrock, V., & Koshida, G. (2008). Dry times: hard lessons from the Canadian drought of 2001 and 2002. Canadian Geographies / Géographies Canadiennes, 52(2), 241–262. https://doi.org/10.1111/j.1541-0064.2008.00211.x

Whited, D., Pitman, K. J., Moore, J. W., Sergeant, C. J., Sexton, E., & Connor, M. (2025). Rapid riparian vegetation development and channel stabilization linked to glacier retreat within a large transboundary watershed. Earth Surface Processes and Landforms, 50(1). https://doi.org/10.1002/esp.6045

Whitfield, P. H., & Pomeroy, J. W. (2017). Assessing the quality of the streamflow record for a long-term reference hydrometric station: Bow River at Banff. Canadian Water Resources Journal / Revue Canadienne Des Ressources Hydriques, 42(4), 391–415. https://doi.org/10.1080/07011784.2017.1399086

Wilcox, E. J., Keim, D., De Jong, T., Walker, B., Sonnentag, O., Sniderhan, A. E., Mann, P., & Marsh, P. (2019). Tundra shrub expansion may amplify permafrost thaw by advancing snowmelt timing. Arctic Science, 5(4), 202–217. https://doi.org/10.1139/as-2018-0028

Williamson, J. (2020). Assessing the role of tree growth patterns on the spatial variability of evapotranspiration on a subalpine transition zone in Kananaskis, Alberta. https://uwspace.uwaterloo.ca/bitstream/10012/15941/3/Williamson_Jessica.pdf (Master's thesis, University of Waterloo).

Woo, M.-K., & Marsh, P. (2005). Snow, frozen soils and permafrost hydrology in Canada, 1999–2002. Hydrological Processes, 19(1), 215–229. https://doi.org/10.1002/hyp.5772

Xiao, J., & Zhuang, Q. (2007). Drought effects on large fire activity in Canadian and Alaskan forests. Environmental Research Letters, 2(4), 044003. https://doi.org/10.1088/1748-9326/2/4/044003

Yang, F., Kumar, A., Wang, W., Juang, H. H., & Kanamitsu, M. (2001). Snow–Albedo Feedback and Seasonal Climate Variability over North America. *Journal of Climate*, *14*(22), 4245–4248. https://doi.org/10.1175/1520-0442(2001)014

Ye, H., Yang, D., & Robinson, D. (2008). Winter rain on snow and its association with air temperature in northern Eurasia. Hydrological Processes, 22(15), 2728–2736. https://doi.org/10.1002/hyp.7094

Zhang, X., Flato, G., Kirchmeier-Young, M., Vincent, L., Wan, H., Wang, X., Rong, R., Fyfe, J., Li, G., Kharin, V.V. (2019): Changes in Temperature and Precipitation Across Canada; Chapter 4 in Bush, E. and Lemmen, D.S. (Eds.) Canada's Changing Climate Report. Government of Canada, Ottawa, Ontario, pp 112-193.

Zhang, X., He, J., Zhang, J., Polyakov, I., Gerdes, R., Inoue, J., & Wu, P. (2012). Enhanced poleward moisture transport and amplified northern high-latitude wetting trend. Nature Climate Change, 3(1), 47–51. https://doi.org/10.1038/nclimate1631

Zhang, Y., He, T., Liang, S., Ma, Y., & Yao, Y. (2025). A novel approach for estimating evapotranspiration by considering topographic effects in radiation over mountainous terrain. *Agricultural and Forest Meteorology*, *366*, 110468. https://doi.org/10.1016/j.agrformet.2025.110468

Zhao, G., & Gao, H. (2019). Estimating reservoir evaporation losses for the United States: Fusing remote sensing and modeling approaches. Remote Sensing of Environment, 226, 109–124. https://doi.org/10.1016/j.rse.2019.03.015

Zhou, X., Geng, X., Yin, G., Hänninen, H., Hao, F., Zhang, X., & Fu, Y. H. (2019). Legacy effect of spring phenology on vegetation growth in temperate China. Agricultural and Forest Meteorology, 281, 107845. https://doi.org/10.1016/j.agrformet.2019.107845

Zhu, W., Tian, S., Wei, J., Jia, S., & Song, Z. (2022). Multi-scale evaluation of global evapotranspiration products derived from remote sensing images: Accuracy and uncertainty. Journal of Hydrology, 611, 127982. https://doi.org/10.1016/j.jhydrol.2022.127982

Zolá, R. P., Bengtsson, L., Berndtsson, R., Martí-Cardona, B., Satgé, F., Timouk, F., Bonnet, M., Mollericon, L., Gamarra, C., & Pasapera, J. (2019). Modelling Lake Titicaca's daily and monthly evaporation. Hydrology and Earth System Sciences, 23(2), 657–668. https://doi.org/10.5194/hess-23-657-2019

Zwieback, S., Chang, Q., Marsh, P., & Berg, A. (2019). Shrub tundra ecohydrology: rainfall interception is a major component of the water balance. Environmental Research Letters, 14(5), 055005. https://doi.org/10.1088/1748-9326/ab1049

Chapter 6: Conclusion and Recommendations

Temperate montane headwater wetlands are among the most significant ecosystems in Canada, as they have a direct impact on the hydrology and ecology of the downstream region. Innovative methodologies were implemented in this investigation to assess the historical trends and changes of the Upper Columbia floodplain (British Columbia) (showed in Chapters 2 and 3) through the integration of hydroclimatic modelling, field observations, and remote sensing data. The methods from Chapters 2 and 3 were subsequently expanded and implemented on the Eastern slopes of Alberta (Alberta), depicted in Chapters 4 and 5.

6.1. Outcomes

The thesis explored historical and projected trends in the temperate montane and mountainous wetlands of British Columbia and Alberta, respectively. Chapter 2 illustrated that the Upper Columbia floodplain has already been affected by the warming climate, which has altered the regional hydrology. The peak flow occurred eleven days earlier, and its duration has been reduced by eleven days, resulting in increased discharges in a shorter period. Further, the wetlands are drying out, which is accompanied by increase of the woody/shrubby area and a decrease in aquatic habitat. In Chapter 3, land cover and river discharge projections (2020-2040s) indicate a decline in open water areas in the Upper Columbia River floodplain during late summer (August-mid-September), aligning with RCP 4.5 forecasts. The peak open water area in the floodplain is projected to change from summer (late-May to July) to spring (April to mid-May) under RCP 4.5 and 8.5. Meanwhile, Chapter 4 assessed the historical trends and changes of the wetlands in the Eastern Slopes of Alberta. The trend analysis during the snowmelt-dominated period (late-May to mid-July) revealed an increase in open water area and a decrease in barren in the subalpine (≤ 2300 m) and alpine (> 2300 m) regions. The reduction of open water area has resulted in an increase in barren and a habitat change from non-woody to woody and shrub in both altitudes during the rainfall-dominated period (late-July to mid-September). In Chapter 5, the historical (1984–2023) evapotranspiration rates exhibited positive trends over the snowmelt- and rainfall-dominated period. Meanwhile, the historical open water area evaporation relative to forest ecosystem ET (P%) during the snowmelt-dominated period was higher (2.4%) than during the rainfall-dominated (2.1%) period. Overall, the annual decline of open water is accompanied by an

increase in woody vegetation, which suggests that wetlands in both regions are drying out. To the author's knowledge, this is the first historical (1984 to 2023) large-scale analysis per period conducted at the main watershed level in the Eastern Slopes of Alberta.

6.2. Recommendations and Next Steps

This wetland assessment framework has the potential to enhance the past and future monitoring of mountain headwaters and floodplain ecosystems. Opportunities to improve and better quantify (i) historical and (ii) projected open water areas, as well as the (iii) evapotranspiration rates across the temperate montane environment could be explored. For instance, one recommendation is to execute a full hydrological model (i.e., a model that simulates the dynamics of water movement, retention, and complete water balance over time within a hydrologic system) and compare its outputs to the seasonal parsimonious hydroclimatic model. This would aid in determining whether the seasonal parsimonious model can accurately depict historical and projected river discharge and open water area in comparison to a more complex model. This assessment would demonstrate the threshold at which a more complex or parsimonious model is valid. Moreover, in light of the absence of reference or in-situ forest evapotranspiration data, a straightforward (by incorporating a forest ecosystem coefficient into evaporation equation outputs) representation of forest transpiration was implemented, thereby enabling the estimation of this critical hydrological flux in all basins of the Eastern Slopes of Alberta. However, the application of distributed or remote sensing models can enhance the estimation of evapotranspiration.

Meanwhile, climate is changing, leading to positive trends of open water areas during spring and summer, and negative trends in the late summer. This, in turn, may affect the onset and termination of woody/shrub vegetation growth, resulting in an earlier spring green-up and later fall senescence. Also, the extended greening season may increase evapotranspiration rates, which could result in negative trends in soil moisture and groundwater. This scenario may result in more frequent droughts, especially in the late summer, which can increase the wildfire frequency.

Thus, the subsequent phase of this investigation will involve the extension of the open water detection method (which was developed in Chapters 2 to 5) to evaluate the extent to which the open water areas are and will be altered across the entire province of Alberta.

Therefore, testing the accuracy of these methodologies in other natural ecosystems, such as the Boreal Forest and Prairie in Alberta, in addition to the Mountain Cordillera. On top of that, to investigate how riparian forests within and outside of the Eastern Slopes of Alberta are increasing or decreasing and why. In addition, assessing which hydrological processes would be impacted, such as, interception, soil moisture, groundwater, runoff, and evapotranspiration as land cover is changing. Overall, to assess how these changes will impact the open water area and volume in the province of Alberta.

7. Supplementary Materials Chapter 4

Supplementary Material A

4.1. Townships per watershed

Oldman watershed townships: T001R27W4, T002R28W4, T003R01W5, T004R03W5, T005R03W5, T006R04W5 T007R04W5, T008R04W5, T009R04W5, T010R04W5, T011R05W5, T012R04W5, T013R05W5.

Bow River townships: T014R05W5, T015R05W5, T016R05W5, T017R06W5, T018R07W5, T019R09W5, T020R09W5, T021R10W5, T022R10W5, T023R10W5, T024R10W5, T025R10W5, T026R10W5, T027R10W5, T027R10W5, T028R10W5, T029R10W5.

North Saskatchewan townships: T030R10W5, T031R11W5, T032R12W5, T033R13W5, T034R14W5, T034R18W5, T035R18W5, T036R19W5, T037R20W5, T038R21W5, T039R20W5, T040R20W5, T041R20W5, T042R20W5.

Athabasca townships: T045R23W5, T046R24W5, T047R24W5, T048R25W5, T049R26W5, T050R02W6, T050R27W5, T051R04W6.

Supplementary Material B

4.2. The followings are detailed descriptions of the reference datasets.

(i) The Historical Land Cover (created by the Hermosilla et al., 2022) is a high spatial resolution (30m) land cover maps for Canada's ecosystems (1984-2019) (Overall accuracy of 80%). These time-series land cover maps were produced from annual time-series of Landsat image composites, forest change information, and ancillary topographic and hydrologic data. It was used (i) a refined training pool derived from existing land cover products using airborne and spaceborne measures of forest structure; (ii) selection of training samples proportionally to the land cover distribution using a distance weighted approach; and (iii) generation of regional classification models using a 150x150 km tiling system.

(ii) Wetland Inventory of Alberta (ABMI): The ABMI plots are spatially explicit polygons that are attributed to high-resolution three-dimensional (3D) image interpretation. They encompass information regarding the structure, forest type, wetland morphology, and wetland class. The ABMI plots have been subjected to ground-truthing and are accurate (90%) compared to field data (Hird et al., 2017; DeLancey et al., 2020; ABMI, 2021). The ABMI reference samples are comprised of 839 photo plots (sites) that are 3 × 7 km in size and contain comprehensive datasets that define land cover classes. These polygons are extremely detailed and are interpreted using 3-D imagery with a spatial resolution of approximately 0.5 m. The land cover map was validated using a variety of reference samples from the bog, fen, marsh, wetland, shallow water, deep water, and forest. In the "ABMI 3X7 photoplot land cover dataset data model (*Alberta Biodiversity Monit. Inst.*, 2016)", additional information regarding these reference samples is available.

4.3. Allocation of training pixels method

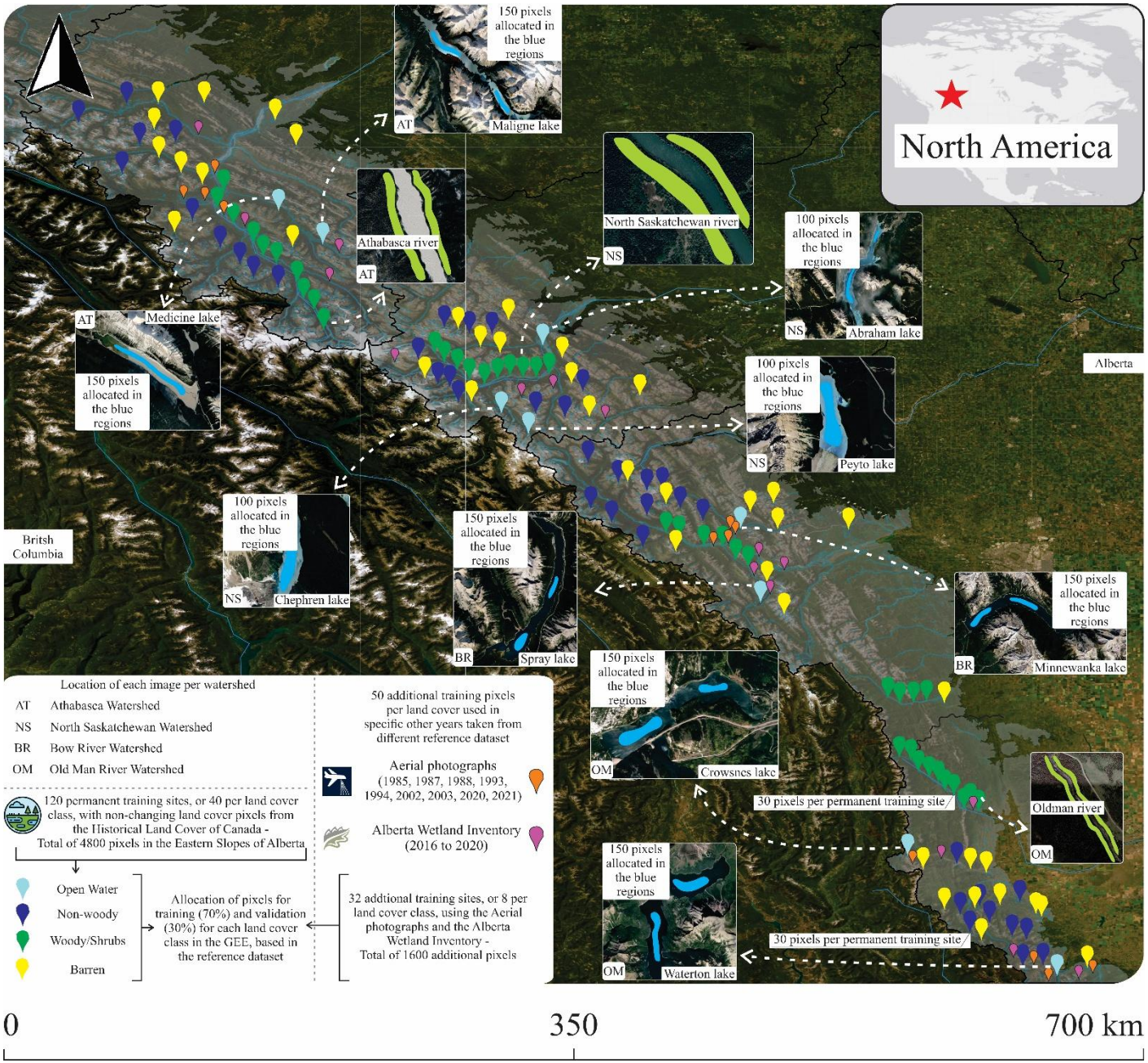

Fig. S4.1. Location of the training pixels per land cover and watershed

Supplementary Material C

4.4. Confusion matrix, total accuracy, omission, and commission of the validation dataset

4.4.1. Oldman River Basin

4.4.1.1. Season: Snow-melting (Mid-May to mid-July)

Table S4.1. Confusion Matrix with commission and omission errors from Mid-May to mid-July 1984

Classes	Open Water	Non-Woody	Woody / Shrub	Barren	Marginal total	Comission Error	Total Accuracy	Kappa Index
Open Water	101	2	0	2	105	0.04		
Non-Woody	0	100	5	0	105	0.05		
Woody/Shrub	1	4	99	2	105	0.06		
Barren	0	2	3	100	105	0.05	95.1%	0.94
Marginal total	102	108	107	104	420			
Omission Error	0.01	0.08	0.08	0.03				

Table S4.2. Confusion Matrix with commission and omission errors from Mid-May to mid-July 1985

Classes	Open Water	Non-Woody	Woody / Shrub	Barren	Marginal total	Comission Error	Total Accuracy	Kappa Index
Open Water	85	2	1	2	90	0.06		
Non-Woody	0	83	5	2	90	0.08		
Woody/Shrub	0	5	84	2	90	0.07		
Barren	2	3	2	83	90	0.08	92.9%	0.91
Marginal total	87	93	92	89	360			
Omission Error	0.02	0.11	0.09	0.06				

Table S4.3. Confusion Matrix with commission and omission errors from Mid-May to mid-July 1986

Classes	Open Water	Non-Woody	Woody / Shrub	Barren	Marginal total	Comission Error	Total Accuracy	Kappa Index
Open Water	84	3	1	2	90	0.07		
Non-Woody	2	83	5	2	90	0.08		
Woody/Shrub	1	5	82	2	90	0.09	92.3%	0.90
Barren	2	3	2	84	90	0.07		
Marginal total	88	93	89	90	360			

Omission Error	0.04761905	0.11	0.08	0.07				

Table S4.4. Confusion Matrix with commission and omission errors from Mid-May to mid-July 1988

Classes	Open Water	Non-Woody	Woody / Shrub	Barren	Marginal total	Comission Error	Total Accuracy	Kappa Index
Open Water	103	2	0	1	105	0.02		
Non-Woody	1	101	2	1	105	0.03		
Woody/Shrub	1	3	100	2	105	0.05		
Barren	1	1	2	101	105	0.04	96.4%	0.95
Marginal total	105	107	104	104	420			
Omission Error	0.02564103	0.05	0.04	0.03				

Table S4.5. Confusion Matrix with commission and omission errors from Mid-May to mid-July 1989

Classes	Open Water	Non-Woody	Woody / Shrub	Barren	Marginal total	Comission Error	Total Accuracy	Kappa Index
Open Water	81	3	2	4	90	0.10		
Non-Woody	3	80	5	3	90	0.12		
Woody/Shrub	3	5	79	3	90	0.12		
Barren	2	4	3	81	90	0.10	88.9%	0.85
Marginal total	89	92	89	91	360			
Omission Error	0.09	0.13	0.11	0.11				

Table S4.6. Confusion Matrix with commission and omission errors from Mid-May to mid-July 1990

Classes	Open Water	Non-Woody	Woody / Shrub	Barren	Marginal total	Comission Error	Total Accuracy	Kappa Index
Open Water	82	2	2	3	90	0.09		
Non-Woody	3	80	4	2	90	0.11		
Woody/Shrub	2	5	80	3	90	0.11		
Barren	2	4	3	81	90	0.10	89.9%	0.87
Marginal total	90	91	89	90	360			
Omission Error	0.09	0.11	0.10	0.10				

Table S4.7. Confusion Matrix with commission and omission errors from Mid-May to mid-July 1991

Classes	Open Water	Non-Woody	Woody / Shrub	Barren	Marginal total	Comission Error	Total Accuracy	Kappa Index
Open Water	83	2	2	3	90	0.08	91.3%	0.88

Non-Woody	3	82	3	2	90	0.09
Woody/Shrub	2	3	81	3	90	0.10
Barren	2	2	3	83	90	0.08
Marginal total	91	89	89	91	360	
Omission Error	0.08	0.08	0.09	0.09		

Table S4.8. Confusion Matrix with commission and omission errors from Mid-May to mid-July 1992

Classes	Open Water	Non-Woody	Woody / Shrub	Barren	Marginal total	Comission Error	Total Accuracy	Kappa Index
Open Water	80	3	4	3	90	0.11		
Non-Woody	4	78	5	4	90	0.14		
Woody/Shrub	3	6	75	6	90	0.16		
Barren	4	4	3	80	90	0.12	86.8%	0.82
Marginal total	90	90	87	92	360			
Omission Error	0.11	0.14	0.14	0.14				

Table S4.9. Confusion Matrix with commission and omission errors from Mid-May to mid-July 1994

Classes	Open Water	Non-Woody	Woody / Shrub	Barren	Marginal total	Comission Error	Total Accuracy	Kappa Index
Open Water	101	2	1	1	105	0.04		
Non-Woody	2	99	4	1	105	0.06		
Woody/Shrub	2	3	99	2	105	0.06		
Barren	1	1	2	101	105	0.04	95.0%	0.93
Marginal total	105	105	106	104	420			
Omission Error	0.04	0.05	0.07	0.04				

Table S4.10. Confusion Matrix with commission and omission errors from Mid-May to mid-July 1995

Classes	Open Water	Non-Woody	Woody / Shrub	Barren	Marginal total	Comission Error	Total Accuracy	Kappa Index
Open Water	86	2	1	1	90	0.04		
Non-Woody	2	83	4	2	90	0.08		
Woody/Shrub	3	2	83	3	90	0.08		
Barren	2	2	2	84	90	0.06	93.3%	0.91
Marginal total	93	87	89	91	360			
Omission Error	0.07	0.05	0.07	0.07				

Table S4.11. Confusion Matrix with commission and omission errors from Mid-May to mid-July 1996

Classes	Open Water	Non-Woody	Woody / Shrub	Barren	Marginal total	Comission Error	Total Accuracy	Kappa Index
Open Water	81	4	2	3	90	0.10		
Non-Woody	3	80	5	3	90	0.12		
Woody/Shrub	3	5	79	4	90	0.12		
Barren	3	3	3	81	90	0.10	88.9%	0.85
Marginal total	90	91	89	90	360			
Omission Error	0.10	0.13	0.12	0.10				

Table S4.12. Confusion Matrix with commission and omission errors from Mid-May to mid-July 1997

Classes	Open Water	Non-Woody	Woody / Shrub	Barren	Marginal total	Comission Error	Total Accuracy	Kappa Index
Open Water	80	3	2	4	90	0.11		
Non-Woody	4	78	5	4	90	0.13		
Woody/Shrub	2	6	78	4	90	0.14		
Barren	4	4	4	78	90	0.14	87.3%	0.83
Marginal total	90	91	89	90	360			
Omission Error	0.11	0.14	0.13	0.13				

Table S4.13. Confusion Matrix with commission and omission errors from Mid-May to mid-July 2000

Classes	Open Water	Non-Woody	Woody / Shrub	Barren	Marginal total	Comission Error	Total Accuracy	Kappa Index
Open Water	83	2	2	3	90	0.08		
Non-Woody	2	81	4	3	90	0.10		
Woody/Shrub	4	4	78	4	90	0.13		
Barren	4	3	3	80	90	0.12	89.3%	0.86
Marginal total	93	90	88	89	360			
Omission Error	0.11	0.10	0.11	0.11				

Table S4.14. Confusion Matrix with commission and omission errors from Mid-May to mid-July 2001

Classes	Open Water	Non-Woody	Woody / Shrub	Barren	Marginal total	Comission Error	Total Accuracy	Kappa Index
Open Water	81	2	3	4	90	0.10		
Non-Woody	4	78	5	3	90	0.13	88.7%	0.85
Woody/Shrub	3	4	79	4	90	0.12		
Barren	4	3	3	81	90	0.10		

Marginal total	91	87	90	92	360
Omission Error	0.11	0.10	0.12	0.12	

Table S4.15. Confusion Matrix with commission and omission errors from Mid-May to mid-July 2002

Classes	Open Water	Non-Woody	Woody / Shrub	Barren	Marginal total	Comission Error	Total Accuracy	Kappa Index
Open Water	102	2	1	1	105	0.03		
Non-Woody	2	99	3	1	105	0.05		
Woody/Shrub	2	2	100	2	105	0.05		
Barren	1	2	2	100	105	0.05	95.5%	0.94
Marginal total	106	105	106	103	420			
Omission Error	0.04	0.05	0.06	0.03				

Table S4.16. Confusion Matrix with commission and omission errors from Mid-May to mid-July 2005

Classes	Open Water	Non-Woody	Woody / Shrub	Barren	Marginal total	Comission Error	Total Accuracy	Kappa Index
Open Water	86	2	2	1	90	0.05		
Non-Woody	2	84	3	2	90	0.07		
Woody/Shrub	2	2	83	3	90	0.07		
Barren	2	2	2	84	90	0.07	93.4%	0.91
Marginal total	92	89	90	90	360			
Omission Error	0.07	0.06	0.07	0.07				

Table S4.17. Confusion Matrix with commission and omission errors from Mid-May to mid-July 2006

Classes	Open Water	Non-Woody	Woody / Shrub	Barren	Marginal total	Comission Error	Total Accuracy	Kappa Index
Open Water	80	4	2	4	90	0.11		
Non-Woody	2	76	8	4	90	0.16		
Woody/Shrub	2	6	78	5	90	0.14		
Barren	2	5	5	78	90	0.13	86.5%	0.82
Marginal total	86	91	93	90	360			
Omission Error	0.07	0.17	0.16	0.14				

Table S4.18. Confusion Matrix with commission and omission errors from Mid-May to mid-July 2007

Classes	Open	Non-	Woody /	Barren	Marginal	Comission	Total	Kappa

	Water	Woody	Shrub		total	Error	Accuracy	Index
Open Water	81	4	2	4	90	0.10		
Non-Woody	2	77	7	4	90	0.14		
Woody/Shrub	3	6	77	5	90	0.15		
Barren	2	5	4	79	90	0.12	87.2%	0.83
Marginal total	87	92	90	91	360			
Omission Error	0.08	0.16	0.15	0.13				

Table S4.19. Confusion Matrix with commission and omission errors from Mid-May to mid-July 2008

Classes	Open Water	Non-Woody	Woody / Shrub	Barren	Marginal total	Comission Error	Total Accuracy	Kappa Index
Open Water	83	2	2	3	90	0.08		
Non-Woody	1	80	6	3	90	0.11		
Woody/Shrub	3	5	78	4	90	0.13		
Barren	2	3	4	81	90	0.10	89.5%	0.86
Marginal total	89	90	90	91	360			
Omission Error	0.06	0.11	0.13	0.12				

Table S4.20. Confusion Matrix with commission and omission errors from Mid-May to mid-July 2009

Classes	Open Water	Non-Woody	Woody / Shrub	Barren	Marginal total	Comission Error	Total Accuracy	Kappa Index
Open Water	79	3	3	4	90	0.12		
Non-Woody	2	77	7	4	90	0.14		
Woody/Shrub	4	5	75	5	90	0.16		
Barren	3	5	5	78	90	0.14	85.9%	0.81
Marginal total	88	90	90	92	360			
Omission Error	0.10	0.15	0.17	0.15				

Table S4.21. Confusion Matrix with commission and omission errors from Mid-May to mid-July 2010

Classes	Open Water	Non-Woody	Woody / Shrub	Barren	Marginal total	Comission Error	Total Accuracy	Kappa Index
Open Water	80	3	3	3	90	0.11		
Non-Woody	2	78	6	3	90	0.13		
Woody/Shrub	4	5	78	4	90	0.14	87.4%	0.83
Barren	3	5	4	79	90	0.13		
Marginal total	89	91	92	89	360			

Omission Error	0.10	0.14	0.15	0.12				

Table S4.22. Confusion Matrix with commission and omission errors from Mid-May to mid-July 2011

Classes	Open Water	Non-Woody	Woody / Shrub	Barren	Marginal total	Comission Error	Total Accuracy	Kappa Index
Open Water	82	3	2	3	90	0.09		
Non-Woody	2	80	6	2	90	0.11		
Woody/Shrub	4	3	81	2	90	0.10		
Barren	3	3	3	82	90	0.09	90.1%	0.87
Marginal total	90	90	91	89	360			
Omission Error	0.10	0.10	0.11	0.08				

Table S4.23. Confusion Matrix with commission and omission errors from Mid-May to mid-July 2013

Classes	Open Water	Non-Woody	Woody / Shrub	Barren	Marginal total	Comission Error	Total Accuracy	Kappa Index
Open Water	81	3	2	4	90	0.10		
Non-Woody	2	79	5	3	90	0.12		
Woody/Shrub	4	3	79	3	90	0.12		
Barren	3	4	3	80	90	0.11	88.8%	0.85
Marginal total	90	89	90	91	360			
Omission Error	0.10	0.11	0.12	0.12				

Table S4.24. Confusion Matrix with commission and omission errors from Mid-May to mid-July 2015

Classes	Open Water	Non-Woody	Woody / Shrub	Barren	Marginal total	Comission Error	Total Accuracy	Kappa Index
Open Water	82	2	2	4	90	0.09		
Non-Woody	3	79	5	4	90	0.12		
Woody/Shrub	4	3	80	3	90	0.12		
Barren	3	4	3	81	90	0.10	89.3%	0.86
Marginal total	92	88	89	92	360			
Omission Error	0.11	0.11	0.10	0.12				

Table S4.25. Confusion Matrix with commission and omission errors from Mid-May to mid-July 2016

Classes	Open Water	Non-Woody	Woody / Shrub	Barren	Marginal total	Comission Error	Total Accuracy	Kappa Index
Open Water	99	3	2	2	105	0.05	92.9%	0.90

Non-Woody	2	97	5	2	105	0.08
Woody/Shrub	2	4	96	3	105	0.09
Barren	2	2	2	98	105	0.07
Marginal total	105	106	104	105	420	
Omission Error	0.06	0.09	0.08	0.06		

Table S4.26. Confusion Matrix with commission and omission errors from Mid-May to mid-July 2017

Classes	Open Water	Non-Woody	Woody / Shrub	Barren	Marginal total	Comission Error	Total Accuracy	Kappa Index
Open Water	101	3	1	1	105	0.04		
Non-Woody	1	100	3	1	105	0.05		
Woody/Shrub	2	2	99	2	105	0.06		
Barren	1	1	2	101	105	0.04	95.3%	0.94
Marginal total	105	106	104	105	420			
Omission Error	0.04	0.06	0.05	0.04				

Table S4.27. Confusion Matrix with commission and omission errors from Mid-May to mid-July 2018

Classes	Open Water	Non-Woody	Woody / Shrub	Barren	Marginal total	Comission Error	Total Accuracy	Kappa Index
Open Water	102	2	1	1	105	0.03		
Non-Woody	2	99	3	1	105	0.05		
Woody/Shrub	2	2	99	2	105	0.06		
Barren	1	1	1	102	105	0.03	95.6%	0.94
Marginal total	106	104	104	106	420			
Omission Error	0.04	0.05	0.05	0.04				

Table S4.28. Confusion Matrix with commission and omission errors from Mid-May to mid-July 2020

Classes	Open Water	Non-Woody	Woody / Shrub	Barren	Marginal total	Comission Error	Total Accuracy	Kappa Index
Open Water	119	1	0	0	120	0.01		
Non-Woody	0	115	4	1	120	0.04		
Woody/Shrub	1	3	116	1	120	0.04		
Barren	1	2	1	116	120	0.03	97.1%	0.96
Marginal total	120	121	121	118	480			
Omission Error	0.01	0.05	0.04	0.02				

Table S4.29. Confusion Matrix with commission and omission errors from Mid-May to mid-July 2021

Classes	Open Water	Non-Woody	Woody / Shrub	Barren	Marginal total	Comission Error	Total Accuracy	Kappa Index
Open Water	102	1	1	1	105	0.03		
Non-Woody	2	99	3	1	105	0.05		
Woody/Shrub	2	2	99	2	105	0.06		
Barren	1	2	2	100	105	0.05	95.2%	0.94
Marginal total	106	104	105	104	420			
Omission Error	0.04	0.05	0.06	0.04				

Table S4.30. Confusion Matrix with commission and omission errors from Mid-May to mid-July 2022

Classes	Open Water	Non-Woody	Woody / Shrub	Barren	Marginal total	Comission Error	Total Accuracy	Kappa Index
Open Water	81	3	2	4	90	0.10		
Non-Woody	4	78	5	4	90	0.13		
Woody/Shrub	4	5	78	3	90	0.13		
Barren	3	4	4	80	90	0.11	88.2%	0.84
Marginal total	92	89	88	91	360			
Omission Error	0.11	0.13	0.11	0.12				

4.4.1.2. Season: Rainfall-driven (Late-July to mid-September)

Table S4.31. Confusion Matrix with commission and omission errors from Late-July to mid-September 1984

Classes	Open Water	Non-Woody	Woody / Shrub	Barren	Marginal total	Comission Error	Total Accuracy	Kappa Index
Open Water	76	5	4	5	90	0.16		
Non-Woody	3	74	8	5	90	0.18		
Woody/Shrub	3	8	75	5	90	0.17		
Barren	4	5	5	77	90	0.14	83.8%	0.78
Marginal total	85	92	92	92	360			
Omission Error	0.11	0.19	0.18	0.16				

Table S4.32. Confusion Matrix with commission and omission errors from Late-July to mid-September 1985

Classes	Open Water	Non-Woody	Woody / Shrub	Barren	Marginal total	Comission Error	Total Accuracy	Kappa Index

Open Water	95	5	2	2	105	0.09		
Non-Woody	1	94	7	3	105	0.11		
Woody/Shrub	2	5	93	5	105	0.12		
Barren	3	6	5	91	105	0.13	88.7%	0.85
Marginal total	101	111	107	101	420			
Omission Error	0.06	0.15	0.13	0.10				

Table S4.33. Confusion Matrix with commission and omission errors from Late-July to mid-September 1986

Classes	Open Water	Non-Woody	Woody / Shrub	Barren	Marginal total	Comission Error	Total Accuracy	Kappa Index
Open Water	77	5	4	4	90	0.14		
Non-Woody	3	76	7	5	90	0.16		
Woody/Shrub	3	7	76	4	90	0.15		
Barren	4	4	4	78	90	0.13	85.3%	0.80
Marginal total	87	92	90	91	360			
Omission Error	0.1137931	0.18	0.16	0.14				

Table S4.34. Confusion Matrix with commission and omission errors from Late-July to mid-September 1987

Classes	Open Water	Non-Woody	Woody / Shrub	Barren	Marginal total	Comission Error	Total Accuracy	Kappa Index
Open Water	96	5	2	2	105	0.09		
Non-Woody	2	93	7	3	105	0.11		
Woody/Shrub	2	5	93	4	105	0.11		
Barren	3	6	5	92	105	0.13	89.0%	0.85
Marginal total	103	109	107	101	420			
Omission Error	0.07	0.15	0.13	0.09				

Table S4.35. Confusion Matrix with commission and omission errors from Late-July to mid-September 1988

Classes	Open Water	Non-Woody	Woody / Shrub	Barren	Marginal total	Comission Error	Total Accuracy	Kappa Index
Open Water	95	3	4	3	105	0.10		
Non-Woody	3	91	7	4	105	0.14		
Woody/Shrub	3	6	91	5	105	0.13		
Barren	3	5	5	93	105	0.12	87.8%	0.84
Marginal total	104	105	107	105	420			
Omission Error	0.08959538	0.13	0.15	0.12				

Table S4.36. Confusion Matrix with commission and omission errors from Late-July to mid-September 1989

Classes	Open Water	Non-Woody	Woody / Shrub	Barren	Marginal total	Comission Error	Total Accuracy	Kappa Index
Open Water	76	5	4	5	90	0.16		
Non-Woody	3	75	7	5	90	0.17		
Woody/Shrub	4	7	75	4	90	0.16		
Barren	4	4	4	79	90	0.13	84.7%	0.80
Marginal total	86	92	90	92	360			
Omission Error	0.12	0.18	0.16	0.15				

Table S4.37. Confusion Matrix with commission and omission errors from Late-July to mid-September 1990

Classes	Open Water	Non-Woody	Woody / Shrub	Barren	Marginal total	Comission Error	Total Accuracy	Kappa Index
Open Water	76	5	4	5	90	0.15		
Non-Woody	3	75	7	5	90	0.17		
Woody/Shrub	4	7	75	4	90	0.17		
Barren	5	4	4	78	90	0.14	84.3%	0.79
Marginal total	88	91	89	92	360			
Omission Error	0.13	0.18	0.16	0.15				

Table S4.38. Confusion Matrix with commission and omission errors from Late-July to mid-September 1991

Classes	Open Water	Non-Woody	Woody / Shrub	Barren	Marginal total	Comission Error	Total Accuracy	Kappa Index
Open Water	99	3	2	2	105	0.06		
Non-Woody	2	97	5	1	105	0.07		
Woody/Shrub	2	4	97	2	105	0.08		
Barren	1	2	3	99	105	0.06	93.3%	0.91
Marginal total	104	106	107	104	420			
Omission Error	0.04	0.08	0.09	0.05				

Table S4.39. Confusion Matrix with commission and omission errors from Late-July to mid-September 1992

Classes	Open Water	Non-Woody	Woody / Shrub	Barren	Marginal total	Comission Error	Total Accuracy	Kappa Index
Open Water	80	3	4	3	90	0.11		
Non-Woody	4	78	5	3	90	0.13	88.0%	0.84
Woody/Shrub	3	5	77	6	90	0.15		

Barren	4	2	2	82	90	0.09		
Marginal total	90	88	87	95	360			
Omission Error	0.10963455	0.11	0.12	0.13				

Table S4.40. Confusion Matrix with commission and omission errors from Late-July to mid-September 1993

Classes	Open Water	Non-Woody	Woody / Shrub	Barren	Marginal total	Comission Error	Total Accuracy	Kappa Index
Open Water	80	3	3	4	90	0.11		
Non-Woody	4	79	5	3	90	0.12		
Woody/Shrub	3	5	78	4	90	0.13		
Barren	3	4	4	79	90	0.12	87.9%	0.84
Marginal total	90	90	90	90	360			
Omission Error	0.11	0.13	0.13	0.12				

Table S4.41. Confusion Matrix with commission and omission errors from Late-July to mid-September 1994

Classes	Open Water	Non-Woody	Woody / Shrub	Barren	Marginal total	Comission Error	Total Accuracy	Kappa Index
Open Water	98	3	2	2	105	0.06		
Non-Woody	2	96	6	2	105	0.09		
Woody/Shrub	2	5	95	3	105	0.09		
Barren	3	3	4	96	105	0.09	91.8%	0.89
Marginal total	105	106	107	102	420			
Omission Error	0.06	0.10	0.11	0.06				

Table S4.42. Confusion Matrix with commission and omission errors from Late-July to mid-September 1995

Classes	Open Water	Non-Woody	Woody / Shrub	Barren	Marginal total	Comission Error	Total Accuracy	Kappa Index
Open Water	79	4	4	4	90	0.13		
Non-Woody	4	75	6	5	90	0.17		
Woody/Shrub	3	5	75	6	90	0.16		
Barren	5	3	3	79	90	0.12	85.5%	0.81
Marginal total	91	88	88	94	360			
Omission Error	0.14	0.14	0.14	0.16				

Table S4.43. Confusion Matrix with commission and omission errors from Late-July to mid-September 1996

Classes	Open Water	Non-Woody	Woody / Shrub	Barren	Marginal total	Comission Error	Total Accuracy	Kappa Index
Open Water	76	5	4	6	90	0.16		
Non-Woody	5	73	8	3	90	0.19		
Woody/Shrub	5	8	72	6	90	0.20		
Barren	6	3	3	78	90	0.14	83.0%	0.77
Marginal total	92	89	87	92	360			
Omission Error	0.17	0.18	0.17	0.16				

Table S4.44. Confusion Matrix with commission and omission errors from Late-July to mid-September 1997

Classes	Open Water	Non-Woody	Woody / Shrub	Barren	Marginal total	Comission Error	Total Accuracy	Kappa Index
Open Water	76	4	4	6	90	0.15		
Non-Woody	5	75	7	3	90	0.17		
Woody/Shrub	4	6	74	5	90	0.18		
Barren	6	3	3	78	90	0.13	84.2%	0.79
Marginal total	92	89	87	93	360			
Omission Error	0.17	0.16	0.15	0.16				

Table S4.45. Confusion Matrix with commission and omission errors from Late-July to mid-September 1998

Classes	Open Water	Non-Woody	Woody / Shrub	Barren	Marginal total	Comission Error	Total Accuracy	Kappa Index
Open Water	78	4	4	5	90	0.14		
Non-Woody	5	76	6	3	90	0.16		
Woody/Shrub	4	5	75	5	90	0.17		
Barren	5	3	3	79	90	0.12	85.4%	0.81
Marginal total	92	89	87	92	360			
Omission Error	0.16	0.14	0.14	0.15				

Table S4.46. Confusion Matrix with commission and omission errors from Late-July to mid-September 1999

Classes	Open Water	Non-Woody	Woody / Shrub	Barren	Marginal total	Comission Error	Total Accuracy	Kappa Index
Open Water	77	4	4	5	90	0.14		
Non-Woody	5	76	6	3	90	0.15		
Woody/Shrub	4	5	75	5	90	0.16		
Barren	5	3	3	80	90	0.12	85.7%	0.81
Marginal total	91	89	87	93	360			
Omission	0.15	0.14	0.14	0.14				

Error

Table S4.47. Confusion Matrix with commission and omission errors from Late-July to mid-September 2000

Classes	Open Water	Non-Woody	Woody / Shrub	Barren	Marginal total	Comission Error	Total Accuracy	Kappa Index
Open Water	75	6	5	5	90	0.17		
Non-Woody	6	73	7	4	90	0.19		
Woody/Shrub	5	6	72	6	90	0.20		
Barren	5	4	4	77	90	0.15	82.4%	0.77
Marginal total	92	89	88	91	360			
Omission Error	0.18	0.18	0.18	0.16				

Table S4.48. Confusion Matrix with commission and omission errors from Late-July to mid-September 2001

Classes	Open Water	Non-Woody	Woody / Shrub	Barren	Marginal total	Comission Error	Total Accuracy	Kappa Index
Open Water	76	6	4	5	90	0.16		
Non-Woody	6	74	7	4	90	0.18		
Woody/Shrub	4	6	74	6	90	0.18		
Barren	5	5	5	75	90	0.16	82.8%	0.77
Marginal total	91	90	89	90	360			
Omission Error	0.17	0.18	0.17	0.16				

Table S4.49. Confusion Matrix with commission and omission errors from Late-July to mid-September 2002

Classes	Open Water	Non-Woody	Woody / Shrub	Barren	Marginal total	Comission Error	Total Accuracy	Kappa Index
Open Water	99	2	2	2	105	0.06		
Non-Woody	2	96	6	2	105	0.09		
Woody/Shrub	2	4	96	3	105	0.08		
Barren	3	3	2	98	105	0.07	92.6%	0.90
Marginal total	105	105	107	104	420			
Omission Error	0.06	0.08	0.10	0.06				

Table S4.50. Confusion Matrix with commission and omission errors from Late-July to mid-September 2003

Classes	Open Water	Non-Woody	Woody / Shrub	Barren	Marginal total	Comission Error	Total Accuracy	Kappa Index
Open Water	100	2	2	2	105	0.05	92.9%	0.91
Non-Woody	2	97	5	2	105	0.08		

Woody/Shrub	2	4	96	3	105	0.09
Barren	2	3	2	98	105	0.07
Marginal total	106	105	105	104	420	
Omission Error	0.06	0.08	0.09	0.06		

Table S4.51. Confusion Matrix with commission and omission errors from Late-July to mid-September 2004

Classes	Open Water	Non-Woody	Woody / Shrub	Barren	Marginal total	Comission Error	Total Accuracy	Kappa Index
Open Water	75	6	4	5	90	0.17		
Non-Woody	6	73	7	4	90	0.19		
Woody/Shrub	4	7	73	6	90	0.19		
Barren	5	4	5	76	90	0.16	82.4%	0.77
Marginal total	91	90	88	91	360			
Omission Error	0.17	0.19	0.17	0.17				

Table S4.52. Confusion Matrix with commission and omission errors from Late-July to mid-September 2005

Classes	Open Water	Non-Woody	Woody / Shrub	Barren	Marginal total	Comission Error	Total Accuracy	Kappa Index
Open Water	74	6	5	5	90	0.18		
Non-Woody	7	72	7	5	90	0.20		
Woody/Shrub	5	7	72	7	90	0.20		
Barren	5	5	5	75	90	0.17	81.3%	0.75
Marginal total	91	90	88	91	360			
Omission Error	0.18	0.20	0.19	0.18				

Table S4.53. Confusion Matrix with commission and omission errors from Late-July to mid-September 2006

Classes	Open Water	Non-Woody	Woody / Shrub	Barren	Marginal total	Comission Error	Total Accuracy	Kappa Index
Open Water	77	6	3	4	90	0.15		
Non-Woody	5	74	7	4	90	0.18		
Woody/Shrub	3	7	73	7	90	0.19		
Barren	5	3	5	77	90	0.15	83.4%	0.78
Marginal total	90	90	88	92	360			
Omission Error	0.15	0.18	0.17	0.16				

Table S4.54. Confusion Matrix with commission and omission errors from Late-July to mid-September 2007

Classes	Open Water	Non-Woody	Woody / Shrub	Barren	Marginal total	Comission Error	Total Accuracy	Kappa Index
Open Water	81	4	2	4	90	0.10		
Non-Woody	2	77	7	4	90	0.14		
Woody/Shrub	3	6	77	5	90	0.15		
Barren	2	5	4	79	90	0.12	87.2%	0.83
Marginal total	87	92	90	91	360			
Omission Error	0.08	0.16	0.15	0.13				

Table S4.55. Confusion Matrix with commission and omission errors from Late-July to mid-September 2008

Classes	Open Water	Non-Woody	Woody / Shrub	Barren	Marginal total	Comission Error	Total Accuracy	Kappa Index
Open Water	79	5	3	4	90	0.12		
Non-Woody	2	76	8	4	90	0.16		
Woody/Shrub	3	6	76	5	90	0.16		
Barren	3	5	4	78	90	0.13	85.8%	0.81
Marginal total	87	92	90	91	360			
Omission Error	0.09	0.17	0.16	0.14				

Table S4.56. Confusion Matrix with commission and omission errors from Late-July to mid-September 2009

Classes	Open Water	Non-Woody	Woody / Shrub	Barren	Marginal total	Comission Error	Total Accuracy	Kappa Index
Open Water	78	5	3	4	90	0.13		
Non-Woody	3	75	8	5	90	0.17		
Woody/Shrub	3	7	75	6	90	0.17		
Barren	4	6	5	75	90	0.17	84.1%	0.79
Marginal total	88	93	90	89	360			
Omission Error	0.11	0.19	0.17	0.16				

Table S4.57. Confusion Matrix with commission and omission errors from Late-July to mid-September 2010

Classes	Open Water	Non-Woody	Woody / Shrub	Barren	Marginal total	Comission Error	Total Accuracy	Kappa Index
Open Water	78	5	3	4	90	0.13		
Non-Woody	3	75	8	5	90	0.17		
Woody/Shrub	3	6	75	6	90	0.16		
Barren	4	5	5	77	90	0.15	84.7%	0.80
Marginal total	88	91	90	91	360			
Omission	0.11	0.18	0.17	0.16				

Error

Table S4.58. Confusion Matrix with commission and omission errors from Late-July to mid-September 2011

Classes	Open Water	Non-Woody	Woody / Shrub	Barren	Marginal total	Comission Error	Total Accuracy	Kappa Index
Open Water	77	5	4	5	90	0.15		
Non-Woody	4	74	8	5	90	0.17		
Woody/Shrub	3	6	75	6	90	0.17		
Barren	4	5	5	77	90	0.15	84.1%	0.79
Marginal total	87	91	91	92	360			
Omission Error	0.12	0.18	0.17	0.16				

Table S4.59. Confusion Matrix with commission and omission errors from Late-July to mid-September 2013

Classes	Open Water	Non-Woody	Woody / Shrub	Barren	Marginal total	Comission Error	Total Accuracy	Kappa Index
Open Water	77	5	3	5	90	0.14		
Non-Woody	3	75	8	4	90	0.17		
Woody/Shrub	3	6	75	5	90	0.16		
Barren	4	5	5	76	90	0.15	84.3%	0.79
Marginal total	88	91	91	91	360			
Omission Error	0.12	0.18	0.17	0.16				

Table S4.60. Confusion Matrix with commission and omission errors from Late-July to mid-September 2014

Classes	Open Water	Non-Woody	Woody / Shrub	Barren	Marginal total	Comission Error	Total Accuracy	Kappa Index
Open Water	77	5	3	5	90	0.14		
Non-Woody	4	74	8	5	90	0.17		
Woody/Shrub	3	7	74	6	90	0.18		
Barren	4	5	3	78	90	0.14	84.3%	0.79
Marginal total	88	92	88	93	360			
Omission Error	0.12	0.19	0.15	0.16				

Table S4.61. Confusion Matrix with commission and omission errors from Late-July to mid-September 2015

Classes	Open Water	Non-Woody	Woody / Shrub	Barren	Marginal total	Comission Error	Total Accuracy	Kappa Index
Open Water	77	5	3	5	90	0.15	83.5%	0.78
Non-Woody	4	74	8	5	90	0.18		

Woody/Shrub	4	7	74	6	90	0.18
Barren	4	6	4	76	90	0.15
Marginal total	88	92	88	92	360	
Omission Error	0.13	0.19	0.16	0.17		

Table S4.62. Confusion Matrix with commission and omission errors from Late-July to mid-September 2016

Classes	Open Water	Non-Woody	Woody / Shrub	Barren	Marginal total	Comission Error	Total Accuracy	Kappa Index
Open Water	100	2	2	2	105	0.05		
Non-Woody	1	98	5	2	105	0.07		
Woody/Shrub	2	4	97	2	105	0.08		
Barren	2	2	2	98	105	0.06	93.4%	0.91
Marginal total	105	105	105	104	420			
Omission Error	0.05	0.07	0.08	0.05				

Table S4.63. Confusion Matrix with commission and omission errors from Late-July to mid-September 2017

Classes	Open Water	Non-Woody	Woody / Shrub	Barren	Marginal total	Comission Error	Total Accuracy	Kappa Index
Open Water	101	2	2	1	105	0.04		
Non-Woody	1	98	4	2	105	0.07		
Woody/Shrub	2	3	98	2	105	0.07		
Barren	1	2	2	101	105	0.04	94.9%	0.93
Marginal total	105	104	105	105	420			
Omission Error	0.04	0.06	0.07	0.04				

Table S4.64. Confusion Matrix with commission and omission errors from Late-July to mid-September 2018

Classes	Open Water	Non-Woody	Woody / Shrub	Barren	Marginal total	Comission Error	Total Accuracy	Kappa Index
Open Water	99	2	2	2	105	0.06		
Non-Woody	2	97	4	2	105	0.08		
Woody/Shrub	2	4	97	2	105	0.07		
Barren	2	2	2	99	105	0.05	93.4%	0.91
Marginal total	105	105	105	105	420			
Omission Error	0.06	0.08	0.07	0.05				

Table S4.65. Confusion Matrix with commission and omission errors from Late-July to mid-September 2019

Classes	Open Water	Non-Woody	Woody / Shrub	Barren	Marginal total	Comission Error	Total Accuracy	Kappa Index
Open Water	101	2	1	2	105	0.04		
Non-Woody	2	99	3	2	105	0.06		
Woody/Shrub	2	3	98	2	105	0.07		
Barren	1	2	2	100	105	0.05	94.6%	0.93
Marginal total	105	106	104	105	420			
Omission Error	0.04	0.07	0.05	0.05				

Table S4.66. Confusion Matrix with commission and omission errors from Late-July to mid-September 2020

Classes	Open Water	Non-Woody	Woody / Shrub	Barren	Marginal total	Comission Error	Total Accuracy	Kappa Index
Open Water	116	2	2	2	120	0.04		
Non-Woody	1	113	3	2	120	0.06		
Woody/Shrub	2	4	113	1	120	0.06		
Barren	1	2	1	116	120	0.04	95.4%	0.94
Marginal total	119	121	119	121	480			
Omission Error	0.03	0.06	0.05	0.04				

Table S4.67. Confusion Matrix with commission and omission errors from Late-July to mid-September 2021

Classes	Open Water	Non-Woody	Woody / Shrub	Barren	Marginal total	Comission Error	Total Accuracy	Kappa Index
Open Water	99	2	2	2	105	0.06		
Non-Woody	2	98	4	2	105	0.07		
Woody/Shrub	2	4	97	3	105	0.08		
Barren	2	2	2	99	105	0.06	93.4%	0.91
Marginal total	105	105	105	105	420			
Omission Error	0.06	0.07	0.08	0.06				

Table S4.68. Confusion Matrix with commission and omission errors from Late-July to mid-September 2022

Classes	Open Water	Non-Woody	Woody / Shrub	Barren	Marginal total	Comission Error	Total Accuracy	Kappa Index
Open Water	77	5	3	5	90	0.15		
Non-Woody	4	74	8	5	90	0.18		
Woody/Shrub	4	7	74	6	90	0.18		
Barren	4	5	4	77	90	0.14	83.8%	0.78
Marginal total	88	91	88	93	360			
Omission	0.13	0.19	0.16	0.17				

Error

Table S4.69. Confusion Matrix with commission and omission errors from Late-July to mid-September 2023

Classes	Open Water	Non-Woody	Woody / Shrub	Barren	Marginal total	Comission Error	Total Accuracy	Kappa Index
Open Water	76	5	3	5	90	0.15		
Non-Woody	4	74	8	4	90	0.17		
Woody/Shrub	3	7	74	6	90	0.18		
Barren	4	5	4	78	90	0.14	84.0%	0.79
Marginal total	87	92	89	92	360			
Omission Error	0.12714777	0.19	0.17	0.16				

4.4.2. Bow River Basin

4.4.2.1. Season: Snow-melting (Mid-May to mid-July)

Table S4.70. Confusion Matrix with commission and omission errors from Mid-May to mid-July 1984

Classes	Open Water	Non-Woody	Woody / Shrub	Barren	Marginal total	Comission Error	Total Accuracy	Kappa Index
Open Water	85	2	1	2	90	0.06		
Non-Woody	1	83	5	2	90	0.07		
Woody/Shrub	0	4	84	2	90	0.06		
Barren	2	3	2	83	90	0.08	93.1%	0.91
Marginal total	88	92	92	88	360			
Omission Error	0.04	0.09	0.08	0.06				

Table S4.71. Confusion Matrix with commission and omission errors from Mid-May to mid-July 1985

Classes	Open Water	Non-Woody	Woody / Shrub	Barren	Marginal total	Comission Error	Total Accuracy	Kappa Index
Open Water	102	2	0	1	105	0.03		
Non-Woody	1	100	3	1	105	0.05		
Woody/Shrub	1	4	99	2	105	0.06		
Barren	1	2	3	99	105	0.06	95.1%	0.94
Marginal total	105	108	104	103	420			
Omission Error	0.03	0.07	0.05	0.04				

Table S4.72. Confusion Matrix with commission and omission errors from Mid-May to mid-July 1986

Classes	Open Water	Non-Woody	Woody / Shrub	Barren	Marginal total	Comission Error	Total Accuracy	Kappa Index
Open Water	84	3	1	2	90	0.06		
Non-Woody	2	82	4	2	90	0.09		
Woody/Shrub	1	4	83	2	90	0.08		
Barren	2	3	2	84	90	0.07	92.5%	0.90
Marginal total	89	92	89	90	360			
Omission Error	0.05387205	0.10	0.07	0.07				

Table S4.73. Confusion Matrix with commission and omission errors from Mid-May to mid-July 1987

Classes	Open Water	Non-Woody	Woody / Shrub	Barren	Marginal total	Comission Error	Total Accuracy	Kappa Index
Open Water	101	2	0	2	105	0.04		
Non-Woody	0	100	5	0	105	0.05		
Woody/Shrub	1	4	99	2	105	0.06		
Barren	0	2	3	100	105	0.05	95.1%	0.94
Marginal total	102	108	107	104	420			
Omission Error	0.01	0.08	0.08	0.03				

Table S4.74. Confusion Matrix with commission and omission errors from Mid-May to mid-July 1988

Classes	Open Water	Non-Woody	Woody / Shrub	Barren	Marginal total	Comission Error	Total Accuracy	Kappa Index
Open Water	100	2	2	2	105	0.05		
Non-Woody	2	98	4	1	105	0.06		
Woody/Shrub	2	4	97	2	105	0.07		
Barren	1	2	3	99	105	0.06	93.9%	0.92
Marginal total	104	107	106	103	420			
Omission Error	0.04322767	0.08	0.08	0.04				

Table S4.75. Confusion Matrix with commission and omission errors from Mid-May to mid-July 1990

Classes	Open Water	Non-Woody	Woody / Shrub	Barren	Marginal total	Comission Error	Total Accuracy	Kappa Index
Open Water	82	3	2	3	90	0.09		
Non-Woody	3	80	3	4	90	0.11	89.6%	0.86
Woody/Shrub	2	5	80	4	90	0.12		
Barren	2	3	3	81	90	0.10		

Marginal total	89	90	89	92	360			
Omission Error	0.09	0.11	0.10	0.11				

Table S4.76. Confusion Matrix with commission and omission errors from Mid-May to mid-July 1991

Classes	Open Water	Non-Woody	Woody / Shrub	Barren	Marginal total	Comission Error	Total Accuracy	Kappa Index
Open Water	81	4	2	3	90	0.10		
Non-Woody	4	79	4	4	90	0.13		
Woody/Shrub	3	5	78	4	90	0.13		
Barren	3	4	4	79	90	0.12	87.9%	0.84
Marginal total	90	91	89	90	360			
Omission Error	0.11	0.14	0.12	0.13				

Table S4.77. Confusion Matrix with commission and omission errors from Mid-May to mid-July 1992

Classes	Open Water	Non-Woody	Woody / Shrub	Barren	Marginal total	Comission Error	Total Accuracy	Kappa Index
Open Water	81	3	2	4	90	0.10		
Non-Woody	3	80	5	3	90	0.12		
Woody/Shrub	3	5	79	3	90	0.12		
Barren	2	4	3	81	90	0.10	88.9%	0.85
Marginal total	89	92	89	91	360			
Omission Error	0.09	0.13	0.11	0.11				

Table S4.78. Confusion Matrix with commission and omission errors from Mid-May to mid-July 1993

Classes	Open Water	Non-Woody	Woody / Shrub	Barren	Marginal total	Comission Error	Total Accuracy	Kappa Index
Open Water	103	2	0	1	105	0.02		
Non-Woody	1	101	2	1	105	0.03		
Woody/Shrub	1	3	100	2	105	0.05		
Barren	1	1	2	101	105	0.04	96.4%	0.95
Marginal total	105	107	104	104	420			
Omission Error	0.03	0.05	0.04	0.03				

Table S4.79. Confusion Matrix with commission and omission errors from Mid-May to mid-July 1995

Classes	Open	Non-	Woody /	Barren	Marginal	Comission	Total	Kappa

	Water	Woody	Shrub		total	Error	Accuracy	Index
Open Water	83	2	2	3	90	0.08		
Non-Woody	2	81	4	3	90	0.10		
Woody/Shrub	4	4	78	4	90	0.13		
Barren	4	3	3	80	90	0.12	89.3%	0.86
Marginal total	93	90	88	89	360			
Omission Error	0.11	0.10	0.11	0.11				

Table S4.80. Confusion Matrix with commission and omission errors from Mid-May to mid-July 1996

Classes	Open Water	Non-Woody	Woody / Shrub	Barren	Marginal total	Comission Error	Total Accuracy	Kappa Index
Open Water	79	4	3	4	90	0.12		
Non-Woody	4	77	5	5	90	0.15		
Woody/Shrub	3	5	77	5	90	0.14		
Barren	3	5	4	78	90	0.13	86.3%	0.82
Marginal total	90	91	89	91	360			
Omission Error	0.12	0.16	0.13	0.14				

Table S4.81. Confusion Matrix with commission and omission errors from Mid-May to mid-July 1997

Classes	Open Water	Non-Woody	Woody / Shrub	Barren	Marginal total	Comission Error	Total Accuracy	Kappa Index
Open Water	80	3	2	4	90	0.11		
Non-Woody	4	78	5	4	90	0.13		
Woody/Shrub	2	6	78	4	90	0.14		
Barren	4	4	4	78	90	0.14	87.3%	0.83
Marginal total	90	91	89	90	360			
Omission Error	0.11	0.14	0.13	0.13				

Table S4.82. Confusion Matrix with commission and omission errors from Mid-May to mid-July 2001

Classes	Open Water	Non-Woody	Woody / Shrub	Barren	Marginal total	Comission Error	Total Accuracy	Kappa Index
Open Water	81	2	3	4	90	0.10		
Non-Woody	4	78	5	3	90	0.13		
Woody/Shrub	3	4	79	4	90	0.12	88.7%	0.85
Barren	4	3	3	81	90	0.10		
Marginal total	91	87	90	92	360			

Omission Error	0.11	0.10	0.12	0.12				

Table S4.83. Confusion Matrix with commission and omission errors from Mid-May to mid-July 2002

Classes	Open Water	Non-Woody	Woody / Shrub	Barren	Marginal total	Comission Error	Total Accuracy	Kappa Index
Open Water	101	2	1	1	105	0.04		
Non-Woody	2	99	4	1	105	0.06		
Woody/Shrub	2	3	99	2	105	0.06		
Barren	1	1	2	101	105	0.04	95.0%	0.93
Marginal total	105	105	106	104	420			
Omission Error	0.04	0.05	0.07	0.04				

Table S4.84. Confusion Matrix with commission and omission errors from Mid-May to mid-July 2004

Classes	Open Water	Non-Woody	Woody / Shrub	Barren	Marginal total	Comission Error	Total Accuracy	Kappa Index
Open Water	82	2	2	4	90	0.09		
Non-Woody	3	79	5	4	90	0.12		
Woody/Shrub	4	3	80	3	90	0.12		
Barren	3	4	3	81	90	0.10	89.3%	0.86
Marginal total	92	88	89	92	360			
Omission Error	0.10	0.11	0.10	0.12				

Table S4.85. Confusion Matrix with commission and omission errors from Mid-May to mid-July 2005

Classes	Open Water	Non-Woody	Woody / Shrub	Barren	Marginal total	Comission Error	Total Accuracy	Kappa Index
Open Water	81	4	2	4	90	0.10		
Non-Woody	3	78	5	4	90	0.13		
Woody/Shrub	4	3	79	3	90	0.12		
Barren	3	4	3	80	90	0.11	88.3%	0.84
Marginal total	90	89	90	91	360			
Omission Error	0.11	0.12	0.12	0.12				

Table S4.86. Confusion Matrix with commission and omission errors from Mid-May to mid-July 2006

Classes	Open Water	Non-Woody	Woody / Shrub	Barren	Marginal total	Comission Error	Total Accuracy	Kappa Index
Open Water	81	3	2	4	90	0.10	88.8%	0.85

Non-Woody	2	79	5	3	90	0.12
Woody/Shrub	4	3	79	3	90	0.12
Barren	3	4	3	80	90	0.11
Marginal total	90	89	90	91	360	
Omission Error	0.10	0.11	0.12	0.12		

Table S4.87. Confusion Matrix with commission and omission errors from Mid-May to mid-July 2008

Classes	Open Water	Non-Woody	Woody / Shrub	Barren	Marginal total	Comission Error	Total Accuracy	Kappa Index
Open Water	80	3	3	3	90	0.11		
Non-Woody	2	78	6	3	90	0.13		
Woody/Shrub	4	5	78	4	90	0.14		
Barren	3	5	4	79	90	0.13	87.4%	0.83
Marginal total	89	91	92	89	360			
Omission Error	0.10	0.14	0.15	0.12				

Table S4.88. Confusion Matrix with commission and omission errors from Mid-May to mid-July 2009

Classes	Open Water	Non-Woody	Woody / Shrub	Barren	Marginal total	Comission Error	Total Accuracy	Kappa Index
Open Water	79	3	3	4	90	0.12		
Non-Woody	2	77	7	4	90	0.14		
Woody/Shrub	4	5	75	5	90	0.16		
Barren	3	5	5	78	90	0.14	85.9%	0.81
Marginal total	88	90	90	92	360			
Omission Error	0.10	0.15	0.17	0.15				

Table S4.89. Confusion Matrix with commission and omission errors from Mid-May to mid-July 2010

Classes	Open Water	Non-Woody	Woody / Shrub	Barren	Marginal total	Comission Error	Total Accuracy	Kappa Index
Open Water	83	2	2	3	90	0.08		
Non-Woody	1	80	6	3	90	0.11		
Woody/Shrub	3	5	78	4	90	0.13		
Barren	2	3	4	81	90	0.10	89.5%	0.86
Marginal total	89	90	90	91	360			
Omission Error	0.06	0.11	0.13	0.12				

Table S4.90. Confusion Matrix with commission and omission errors from Mid-May to mid-July 2013

Classes	Open Water	Non-Woody	Woody / Shrub	Barren	Marginal total	Comission Error	Total Accuracy	Kappa Index
Open Water	80	4	2	4	90	0.11		
Non-Woody	2	76	8	4	90	0.16		
Woody/Shrub	2	6	78	5	90	0.14		
Barren	2	5	5	78	90	0.13	86.5%	0.82
Marginal total	86	91	93	90	360			
Omission Error	0.07	0.17	0.16	0.14				

Table S4.91. Confusion Matrix with commission and omission errors from Mid-May to mid-July 2014

Classes	Open Water	Non-Woody	Woody / Shrub	Barren	Marginal total	Comission Error	Total Accuracy	Kappa Index
Open Water	86	2	2	1	90	0.05		
Non-Woody	2	84	3	2	90	0.07		
Woody/Shrub	2	2	83	3	90	0.07		
Barren	2	2	2	84	90	0.07	93.4%	0.91
Marginal total	92	89	90	90	360			
Omission Error	0.07	0.06	0.07	0.07				

Table S4.92. Confusion Matrix with commission and omission errors from Mid-May to mid-July 2015

Classes	Open Water	Non-Woody	Woody / Shrub	Barren	Marginal total	Comission Error	Total Accuracy	Kappa Index
Open Water	81	3	4	3	90	0.10		
Non-Woody	4	79	3	4	90	0.12		
Woody/Shrub	2	5	78	5	90	0.13		
Barren	5	3	2	80	90	0.11	88.4%	0.85
Marginal total	92	89	88	91	360			
Omission Error	0.12	0.11	0.11	0.13				

Table S4.93. Confusion Matrix with commission and omission errors from Mid-May to mid-July 2016

Classes	Open Water	Non-Woody	Woody / Shrub	Barren	Marginal total	Comission Error	Total Accuracy	Kappa Index
Open Water	101	2	1	2	105	0.04		
Non-Woody	2	99	3	2	105	0.06	94.6%	0.93
Woody/Shrub	2	3	98	2	105	0.07		
Barren	1	2	2	100	105	0.05		

Marginal total	105	106	104	105	420
Omission Error	0.04	0.07	0.05	0.05	

Table S4.94. Confusion Matrix with commission and omission errors from Mid-May to mid-July 2017

Classes	Open Water	Non-Woody	Woody / Shrub	Barren	Marginal total	Comission Error	Total Accuracy	Kappa Index
Open Water	102	2	1	1	105	0.03		
Non-Woody	2	99	3	1	105	0.05		
Woody/Shrub	2	2	99	2	105	0.06		
Barren	1	1	1	102	105	0.03	95.6%	0.94
Marginal total	106	104	104	106	420			
Omission Error	0.04	0.05	0.05	0.04				

Table S4.95. Confusion Matrix with commission and omission errors from Mid-May to mid-July 2018

Classes	Open Water	Non-Woody	Woody / Shrub	Barren	Marginal total	Comission Error	Total Accuracy	Kappa Index
Open Water	101	3	1	1	105	0.04		
Non-Woody	1	100	3	1	105	0.05		
Woody/Shrub	2	2	99	2	105	0.06		
Barren	1	1	2	101	105	0.04	95.3%	0.94
Marginal total	105	106	104	105	420			
Omission Error	0.04	0.06	0.05	0.04				

Table S4.96. Confusion Matrix with commission and omission errors from Mid-May to mid-July 2021

Classes	Open Water	Non-Woody	Woody / Shrub	Barren	Marginal total	Comission Error	Total Accuracy	Kappa Index
Open Water	102	1	1	1	105	0.03		
Non-Woody	2	100	3	1	105	0.05		
Woody/Shrub	2	2	99	2	105	0.05		
Barren	1	2	2	100	105	0.05	95.5%	0.94
Marginal total	106	104	105	105	420			
Omission Error	0.04	0.04	0.05	0.04				

Table S4.97. Confusion Matrix with commission and omission errors from Mid-May to mid-July 2023

Classes	Open	Non-	Woody /	Barren	Marginal	Comission	Total	Kappa

	Water	Woody	Shrub		total	Error	Accuracy	Index
Open Water	81	3	2	4	90	0.10		
Non-Woody	4	78	5	4	90	0.13		
Woody/Shrub	4	5	78	3	90	0.13		
Barren	3	4	4	80	90	0.11	88.2%	0.84
Marginal total	92	89	88	91	360			
Omission Error	0.11	0.13	0.11	0.12				

4.4.2.2. Season: Rainfall-driven (Late-July to mid-September)

Table S4.98. Confusion Matrix with commission and omission errors from Late-July to mid-September 1984

Classes	Open Water	Non-Woody	Woody / Shrub	Barren	Marginal total	Comission Error	Total Accuracy	Kappa Index
Open Water	77	5	4	4	90	0.14		
Non-Woody	3	76	7	5	90	0.16		
Woody/Shrub	3	7	76	4	90	0.15		
Barren	4	4	4	78	90	0.13	85.3%	0.80
Marginal total	87	92	90	91	360			
Omission Error	0.11	0.18	0.16	0.14				

Table S4.99. Confusion Matrix with commission and omission errors from Late-July to mid-September 1985

Classes	Open Water	Non-Woody	Woody / Shrub	Barren	Marginal total	Comission Error	Total Accuracy	Kappa Index
Open Water	96	5	2	2	105	0.09		
Non-Woody	2	93	7	3	105	0.11		
Woody/Shrub	2	5	93	4	105	0.11		
Barren	3	6	5	92	105	0.13	89.0%	0.85
Marginal total	103	109	107	101	420			
Omission Error	0.07	0.15	0.13	0.09				

Table S4.100. Confusion Matrix with commission and omission errors from Late-July to mid-September 1986

Classes	Open Water	Non-Woody	Woody / Shrub	Barren	Marginal total	Comission Error	Total Accuracy	Kappa Index

Open Water	80	3	4	3	90	0.11		
Non-Woody	4	78	5	3	90	0.13		
Woody/Shrub	3	5	77	6	90	0.15		
Barren	4	2	2	82	90	0.09	88.0%	0.84
Marginal total	90	88	87	95	360			
Omission Error	0.10963455	0.11	0.12	0.13				

Table S4.101. Confusion Matrix with commission and omission errors from Late-July to mid-September 1987

Classes	Open Water	Non-Woody	Woody / Shrub	Barren	Marginal total	Comission Error	Total Accuracy	Kappa Index
Open Water	95	5	2	2	105	0.09		
Non-Woody	1	94	7	3	105	0.11		
Woody/Shrub	2	5	93	5	105	0.12		
Barren	3	6	5	91	105	0.13	88.7%	0.85
Marginal total	101	111	107	101	420			
Omission Error	0.06	0.15	0.13	0.10				

Table S4.102. Confusion Matrix with commission and omission errors from Late-July to mid-September 1988

Classes	Open Water	Non-Woody	Woody / Shrub	Barren	Marginal total	Comission Error	Total Accuracy	Kappa Index
Open Water	95	3	4	3	105	0.10		
Non-Woody	3	91	7	4	105	0.14		
Woody/Shrub	3	6	91	5	105	0.13		
Barren	3	5	5	93	105	0.12	87.8%	0.84
Marginal total	104	105	107	105	420			
Omission Error	0.08959538	0.13	0.15	0.12				

Table S4.103. Confusion Matrix with commission and omission errors from Late-July to mid-September 1989

Classes	Open Water	Non-Woody	Woody / Shrub	Barren	Marginal total	Comission Error	Total Accuracy	Kappa Index
Open Water	76	5	4	5	90	0.16		
Non-Woody	3	74	8	5	90	0.18		
Woody/Shrub	3	8	75	5	90	0.17		
Barren	4	5	5	77	90	0.14	83.8%	0.78
Marginal total	85	92	92	92	360			
Omission Error	0.11	0.19	0.18	0.16				

Table S4.104. Confusion Matrix with commission and omission errors from Late-July to mid-September 1990

Classes	Open Water	Non-Woody	Woody / Shrub	Barren	Marginal total	Comission Error	Total Accuracy	Kappa Index
Open Water	76	5	4	5	90	0.16		
Non-Woody	3	75	7	5	90	0.17		
Woody/Shrub	4	7	75	4	90	0.16		
Barren	4	4	4	79	90	0.13	84.7%	0.80
Marginal total	86	92	90	92	360			
Omission Error	0.12	0.18	0.16	0.15				

Table S4.105. Confusion Matrix with commission and omission errors from Late-July to mid-September 1993

Classes	Open Water	Non-Woody	Woody / Shrub	Barren	Marginal total	Comission Error	Total Accuracy	Kappa Index
Open Water	98	3	2	2	105	0.06		
Non-Woody	2	96	6	2	105	0.09		
Woody/Shrub	2	5	95	3	105	0.09		
Barren	3	3	4	96	105	0.09	91.8%	0.89
Marginal total	105	106	107	102	420			
Omission Error	0.06	0.10	0.11	0.06				

Table S4.106. Confusion Matrix with commission and omission errors from Late-July to mid-September 1994

Classes	Open Water	Non-Woody	Woody / Shrub	Barren	Marginal total	Comission Error	Total Accuracy	Kappa Index
Open Water	99	3	2	2	105	0.06		
Non-Woody	2	97	5	1	105	0.07		
Woody/Shrub	2	4	97	2	105	0.08		
Barren	1	2	3	99	105	0.06	93.3%	0.91
Marginal total	104	106	107	104	420			
Omission Error	0.04	0.08	0.09	0.05				

Table S4.107. Confusion Matrix with commission and omission errors from Late-July to mid-September 1995

Classes	Open Water	Non-Woody	Woody / Shrub	Barren	Marginal total	Comission Error	Total Accuracy	Kappa Index
Open Water	76	5	4	5	90	0.15		
Non-Woody	3	75	7	5	90	0.17		
Woody/Shrub	4	7	75	4	90	0.17	84.3%	0.79
Barren	5	4	4	78	90	0.14		
Marginal	88	91	89	92	360			

total								
Omission Error	0.13	0.18	0.16	0.15				

Table S4.108. Confusion Matrix with commission and omission errors from Late-July to mid-September 1996

Classes	Open Water	Non-Woody	Woody / Shrub	Barren	Marginal total	Comission Error	Total Accuracy	Kappa Index
Open Water	76	6	4	5	90	0.16		
Non-Woody	6	74	7	4	90	0.18		
Woody/Shrub	4	6	74	6	90	0.18		
Barren	5	5	5	75	90	0.16	82.8%	0.77
Marginal total	91	90	89	90	360			
Omission Error	0.17	0.18	0.17	0.16				

Table S4.109. Confusion Matrix with commission and omission errors from Late-July to mid-September 1997

Classes	Open Water	Non-Woody	Woody / Shrub	Barren	Marginal total	Comission Error	Total Accuracy	Kappa Index
Open Water	75	6	5	5	90	0.17		
Non-Woody	6	73	7	4	90	0.19		
Woody/Shrub	5	6	72	6	90	0.20		
Barren	5	4	4	77	90	0.15	82.4%	0.77
Marginal total	92	89	88	91	360			
Omission Error	0.18	0.18	0.18	0.16				

Table S4.110. Confusion Matrix with commission and omission errors from Late-July to mid-September 1998

Classes	Open Water	Non-Woody	Woody / Shrub	Barren	Marginal total	Comission Error	Total Accuracy	Kappa Index
Open Water	77	4	4	5	90	0.14		
Non-Woody	5	76	6	3	90	0.15		
Woody/Shrub	4	5	75	5	90	0.16		
Barren	5	3	3	80	90	0.12	85.7%	0.81
Marginal total	91	89	87	93	360			
Omission Error	0.15	0.14	0.14	0.14				

Table S4.111. Confusion Matrix with commission and omission errors from Late-July to mid-September 2001

Classes	Open Water	Non-Woody	Woody / Shrub	Barren	Marginal total	Comission Error	Total Accuracy	Kappa Index
Open Water	76	5	4	6	90	0.16	83.0%	0.77

Non-Woody	5	73	8	3	90	0.19
Woody/Shrub	5	8	72	6	90	0.20
Barren	6	3	3	78	90	0.14
Marginal total	92	89	87	92	360	
Omission Error	0.17	0.18	0.17	0.16		

Table S4.112. Confusion Matrix with commission and omission errors from Late-July to mid-September 2002

Classes	Open Water	Non-Woody	Woody / Shrub	Barren	Marginal total	Comission Error	Total Accuracy	Kappa Index
Open Water	100	2	2	2	105	0.05		
Non-Woody	2	97	5	2	105	0.08		
Woody/Shrub	2	4	96	3	105	0.09		
Barren	2	3	2	98	105	0.07	92.9%	0.91
Marginal total	106	105	105	104	420			
Omission Error	0.06	0.08	0.09	0.06				

Table S4.113. Confusion Matrix with commission and omission errors from Late-July to mid-September 2003

Classes	Open Water	Non-Woody	Woody / Shrub	Barren	Marginal total	Comission Error	Total Accuracy	Kappa Index
Open Water	99	2	2	2	105	0.06		
Non-Woody	2	96	6	2	105	0.09		
Woody/Shrub	2	4	96	3	105	0.08		
Barren	3	3	2	98	105	0.07	92.6%	0.90
Marginal total	105	105	107	104	420			
Omission Error	0.06	0.08	0.10	0.06				

Table S4.114. Confusion Matrix with commission and omission errors from Late-July to mid-September 2004

Classes	Open Water	Non-Woody	Woody / Shrub	Barren	Marginal total	Comission Error	Total Accuracy	Kappa Index
Open Water	74	6	5	5	90	0.18		
Non-Woody	7	72	7	5	90	0.20		
Woody/Shrub	5	7	72	7	90	0.20		
Barren	5	5	5	75	90	0.17	81.3%	0.75
Marginal total	91	90	88	91	360			
Omission Error	0.18	0.20	0.19	0.18				

Table S4.115. Confusion Matrix with commission and omission errors from Late-July to mid-September 2005

Classes	Open Water	Non-Woody	Woody / Shrub	Barren	Marginal total	Comission Error	Total Accuracy	Kappa Index
Open Water	75	6	4	5	90	0.17		
Non-Woody	6	73	7	4	90	0.19		
Woody/Shrub	4	7	73	6	90	0.19		
Barren	5	4	5	76	90	0.16	82.4%	0.77
Marginal total	91	90	88	91	360			
Omission Error	0.17	0.19	0.17	0.17				

Table S4.116. Confusion Matrix with commission and omission errors from Late-July to mid-September 2006

Classes	Open Water	Non-Woody	Woody / Shrub	Barren	Marginal total	Comission Error	Total Accuracy	Kappa Index
Open Water	81	4	2	4	90	0.10		
Non-Woody	2	77	7	4	90	0.14		
Woody/Shrub	3	6	77	5	90	0.15		
Barren	2	5	4	79	90	0.12	87.2%	0.83
Marginal total	87	92	90	91	360			
Omission Error	0.08	0.16	0.15	0.13				

Table S4.117. Confusion Matrix with commission and omission errors from Late-July to mid-September 2007

Classes	Open Water	Non-Woody	Woody / Shrub	Barren	Marginal total	Comission Error	Total Accuracy	Kappa Index
Open Water	77	6	3	4	90	0.15		
Non-Woody	5	74	7	4	90	0.18		
Woody/Shrub	3	7	73	7	90	0.19		
Barren	5	3	5	77	90	0.15	83.4%	0.78
Marginal total	90	90	88	92	360			
Omission Error	0.15	0.18	0.17	0.16				

Table S4.118. Confusion Matrix with commission and omission errors from Late-July to mid-September 2008

Classes	Open Water	Non-Woody	Woody / Shrub	Barren	Marginal total	Comission Error	Total Accuracy	Kappa Index
Open Water	75	6	4	5	90	0.17		
Non-Woody	5	72	8	6	90	0.20		
Woody/Shrub	5	8	71	7	90	0.22		
Barren	4	6	6	74	90	0.18	80.7%	0.74
Marginal total	89	92	88	92	360			
Omission	0.16	0.22	0.20	0.20				

Error

Table S4.119. Confusion Matrix with commission and omission errors from Late-July to mid-September 2009

Classes	Open Water	Non-Woody	Woody / Shrub	Barren	Marginal total	Comission Error	Total Accuracy	Kappa Index
Open Water	74	7	4	6	90	0.18		
Non-Woody	5	71	8	6	90	0.22		
Woody/Shrub	5	8	71	7	90	0.21		
Barren	4	6	6	73	90	0.19	80.0%	0.73
Marginal total	88	91	89	92	360			
Omission Error	0.16	0.23	0.21	0.20				

Table S4.120. Confusion Matrix with commission and omission errors from Late-July to mid-September 2010

Classes	Open Water	Non-Woody	Woody / Shrub	Barren	Marginal total	Comission Error	Total Accuracy	Kappa Index
Open Water	77	5	4	5	90	0.15		
Non-Woody	4	74	8	5	90	0.17		
Woody/Shrub	3	6	75	6	90	0.17		
Barren	4	5	5	77	90	0.15	84.1%	0.79
Marginal total	87	91	91	92	360			
Omission Error	0.12	0.18	0.17	0.16				

Table S4.121. Confusion Matrix with commission and omission errors from Late-July to mid-September 2011

Classes	Open Water	Non-Woody	Woody / Shrub	Barren	Marginal total	Comission Error	Total Accuracy	Kappa Index
Open Water	78	5	3	4	90	0.13		
Non-Woody	3	75	8	5	90	0.17		
Woody/Shrub	3	6	75	6	90	0.16		
Barren	4	5	5	77	90	0.15	84.7%	0.80
Marginal total	88	91	90	91	360			
Omission Error	0.11	0.18	0.17	0.16				

Table S4.122. Confusion Matrix with commission and omission errors from Late-July to mid-September 2013

Classes	Open Water	Non-Woody	Woody / Shrub	Barren	Marginal total	Comission Error	Total Accuracy	Kappa Index
Open Water	77	5	3	5	90	0.15	83.5%	0.78
Non-Woody	4	74	8	5	90	0.18		

Woody/Shrub	4	7	74	6	90	0.18
Barren	4	6	4	76	90	0.15
Marginal total	88	92	88	92	360	
Omission Error	0.13	0.19	0.16	0.17		

Table S4.123. Confusion Matrix with commission and omission errors from Late-July to mid-September 2014

Classes	Open Water	Non-Woody	Woody / Shrub	Barren	Marginal total	Comission Error	Total Accuracy	Kappa Index
Open Water	77	5	3	5	90	0.14		
Non-Woody	4	74	8	5	90	0.17		
Woody/Shrub	3	7	74	6	90	0.18		
Barren	4	5	3	78	90	0.14	84.3%	0.79
Marginal total	88	92	88	93	360			
Omission Error	0.12	0.19	0.15	0.16				

Table S4.124. Confusion Matrix with commission and omission errors from Late-July to mid-September 2015

Classes	Open Water	Non-Woody	Woody / Shrub	Barren	Marginal total	Comission Error	Total Accuracy	Kappa Index
Open Water	77	5	3	5	90	0.14		
Non-Woody	3	75	8	4	90	0.17		
Woody/Shrub	3	6	75	5	90	0.16		
Barren	4	5	5	76	90	0.15	84.3%	0.79
Marginal total	88	91	91	91	360			
Omission Error	0.12	0.18	0.17	0.16				

Table S4.125. Confusion Matrix with commission and omission errors from Late-July to mid-September 2016

Classes	Open Water	Non-Woody	Woody / Shrub	Barren	Marginal total	Comission Error	Total Accuracy	Kappa Index
Open Water	101	2	2	1	105	0.04		
Non-Woody	1	98	4	2	105	0.07		
Woody/Shrub	2	3	98	2	105	0.07		
Barren	1	2	2	101	105	0.04	94.9%	0.93
Marginal total	105	104	105	105	420			
Omission Error	0.04	0.06	0.07	0.04				

Table S4.126. Confusion Matrix with commission and omission errors from Late-July to mid-September 2017

Classes	Open Water	Non-Woody	Woody / Shrub	Barren	Marginal total	Comission Error	Total Accuracy	Kappa Index
Open Water	100	2	2	2	105	0.05		
Non-Woody	1	98	5	2	105	0.07		
Woody/Shrub	2	4	97	2	105	0.08		
Barren	2	2	2	98	105	0.06	93.4%	0.91
Marginal total	105	105	105	104	420			
Omission Error	0.05	0.07	0.08	0.05				

Table S4.127. Confusion Matrix with commission and omission errors from Late-July to mid-September 2018

Classes	Open Water	Non-Woody	Woody / Shrub	Barren	Marginal total	Comission Error	Total Accuracy	Kappa Index
Open Water	101	2	1	2	105	0.04		
Non-Woody	2	99	3	2	105	0.06		
Woody/Shrub	2	3	98	2	105	0.07		
Barren	1	2	2	100	105	0.05	94.6%	0.93
Marginal total	105	106	104	105	420			
Omission Error	0.04	0.07	0.05	0.05				

Table S4.128. Confusion Matrix with commission and omission errors from Late-July to mid-September 2019

Classes	Open Water	Non-Woody	Woody / Shrub	Barren	Marginal total	Comission Error	Total Accuracy	Kappa Index
Open Water	99	2	2	2	105	0.06		
Non-Woody	2	97	4	2	105	0.08		
Woody/Shrub	2	4	97	2	105	0.07		
Barren	2	2	2	99	105	0.05	93.4%	0.91
Marginal total	105	105	105	105	420			
Omission Error	0.06	0.08	0.07	0.05				

Table S4.129. Confusion Matrix with commission and omission errors from Late-July to mid-September 2020

Classes	Open Water	Non-Woody	Woody / Shrub	Barren	Marginal total	Comission Error	Total Accuracy	Kappa Index
Open Water	117	1	1	2	120	0.03		
Non-Woody	1	114	2	3	120	0.05		
Woody/Shrub	2	3	114	1	120	0.05	96.0%	0.95
Barren	1	2	1	116	120	0.03		
Marginal total	121	120	118	122	480			

Omission Error	0.03	0.05	0.04	0.04				

Table S4.130. Confusion Matrix with commission and omission errors from Late-July to mid-September 2021

Classes	Open Water	Non-Woody	Woody / Shrub	Barren	Marginal total	Comission Error	Total Accuracy	Kappa Index
Open Water	331	6	8	5	350	0.05		
Non-Woody	8	321	12	9	350	0.08		
Woody/Shrub	9	12	320	9	350	0.09		
Barren	8	7	6	329	350	0.06	92.9%	0.91
Marginal total	356	346	346	352	1400			
Omission Error	0.07	0.07	0.08	0.07				

Table S4.131. Confusion Matrix with commission and omission errors from Late-July to mid-September 2022

Classes	Open Water	Non-Woody	Woody / Shrub	Barren	Marginal total	Comission Error	Total Accuracy	Kappa Index
Open Water	77	5	3	5	90	0.14		
Non-Woody	3	75	8	5	90	0.17		
Woody/Shrub	4	7	73	6	90	0.19		
Barren	4	5	4	77	90	0.15	83.8%	0.78
Marginal total	89	92	88	92	360			
Omission Error	0.13	0.19	0.16	0.16				

Table S4.132. Confusion Matrix with commission and omission errors from Late-July to mid-September 2023

Classes	Open Water	Non-Woody	Woody / Shrub	Barren	Marginal total	Comission Error	Total Accuracy	Kappa Index
Open Water	77	5	3	5	90	0.15		
Non-Woody	4	74	8	4	90	0.18		
Woody/Shrub	3	7	74	6	90	0.17		
Barren	4	5	5	77	90	0.15	83.8%	0.78
Marginal total	88	91	90	92	360			
Omission Error	0.13	0.18	0.17	0.16				

4.4.3. North Saskatchewan Basin

4.4.3.1. Season: Snow-melting (Mid-May to mid-July)

Table S4.133. Confusion Matrix with commission and omission errors from Mid-May to mid-July 1984

Classes	Open Water	Non-Woody	Woody / Shrub	Barren	Marginal total	Comission Error	Total Accuracy	Kappa Index
Open Water	103	2	0	1	105	0.02		
Non-Woody	1	101	2	1	105	0.03		
Woody/Shrub	1	3	100	2	105	0.05		
Barren	1	1	2	101	105	0.04	96.4%	0.95
Marginal total	105	107	104	104	420			
Omission Error	0.03	0.05	0.04	0.03				

Table S4.134. Confusion Matrix with commission and omission errors from Mid-May to mid-July 1985

Classes	Open Water	Non-Woody	Woody / Shrub	Barren	Marginal total	Comission Error	Total Accuracy	Kappa Index
Open Water	80	3	4	3	90	0.11		
Non-Woody	4	78	5	4	90	0.14		
Woody/Shrub	3	6	75	6	90	0.16		
Barren	4	4	3	80	90	0.12	86.8%	0.82
Marginal total	90	90	87	92	360			
Omission Error	0.11	0.14	0.14	0.14				

Table S4.135. Confusion Matrix with commission and omission errors from Mid-May to mid-July 1986

Classes	Open Water	Non-Woody	Woody / Shrub	Barren	Marginal total	Comission Error	Total Accuracy	Kappa Index
Open Water	83	2	2	3	90	0.08		
Non-Woody	3	82	3	2	90	0.09		
Woody/Shrub	2	3	81	3	90	0.10		
Barren	2	2	3	83	90	0.08	91.3%	0.88
Marginal total	91	89	89	91	360			
Omission Error	0.08	0.08	0.09	0.09				

Table S4.136. Confusion Matrix with commission and omission errors from Mid-May to mid-July 1987

Classes	Open Water	Non-Woody	Woody / Shrub	Barren	Marginal total	Comission Error	Total Accuracy	Kappa Index
Open Water	102	2	1	1	105	0.03	95.5%	0.94
Non-Woody	2	99	3	1	105	0.05		

Woody/Shrub	2	2	100	2	105	0.05
Barren	1	2	2	100	105	0.05
Marginal total	106	105	106	103	420	
Omission Error	0.04	0.05	0.06	0.03		

Table S4.137. Confusion Matrix with commission and omission errors from Mid-May to mid-July 1988

Classes	Open Water	Non-Woody	Woody / Shrub	Barren	Marginal total	Comission Error	Total Accuracy	Kappa Index
Open Water	100	2	2	2	105	0.05		
Non-Woody	2	98	4	1	105	0.06		
Woody/Shrub	2	4	97	2	105	0.07		
Barren	1	2	3	99	105	0.06	93.9%	0.92
Marginal total	104	107	106	103	420			
Omission Error	0.04322767	0.08	0.08	0.04				

Table S4.138. Confusion Matrix with commission and omission errors from Mid-May to mid-July 1991

Classes	Open Water	Non-Woody	Woody / Shrub	Barren	Marginal total	Comission Error	Total Accuracy	Kappa Index
Open Water	81	3	2	4	90	0.10		
Non-Woody	3	80	5	3	90	0.12		
Woody/Shrub	3	5	79	3	90	0.12		
Barren	2	4	3	81	90	0.10	88.9%	0.85
Marginal total	89	92	89	91	360			
Omission Error	0.09	0.13	0.11	0.11				

Table S4.139. Confusion Matrix with commission and omission errors from Mid-May to mid-July 1992

Classes	Open Water	Non-Woody	Woody / Shrub	Barren	Marginal total	Comission Error	Total Accuracy	Kappa Index
Open Water	82	2	2	3	90	0.11		
Non-Woody	3	80	4	2	90	0.13		
Woody/Shrub	2	5	80	3	90	0.14		
Barren	2	4	3	81	90	0.13	87.4%	0.83
Marginal total	90	91	89	90	360			
Omission Error	0.10	0.14	0.15	0.12				

Table S4.140. Confusion Matrix with commission and omission errors from Mid-May to mid-July 1995

Classes	Open Water	Non-Woody	Woody / Shrub	Barren	Marginal total	Comission Error	Total Accuracy	Kappa Index
Open Water	86	2	1	1	90	0.04		
Non-Woody	2	83	4	2	90	0.08		
Woody/Shrub	3	2	83	3	90	0.08		
Barren	2	2	2	84	90	0.06	93.3%	0.91
Marginal total	93	87	89	91	360			
Omission Error	0.07	0.05	0.07	0.07				

Table S4.141. Confusion Matrix with commission and omission errors from Mid-May to mid-July 1996

Classes	Open Water	Non-Woody	Woody / Shrub	Barren	Marginal total	Comission Error	Total Accuracy	Kappa Index
Open Water	81	2	3	4	90	0.10		
Non-Woody	4	78	5	3	90	0.13		
Woody/Shrub	3	4	79	4	90	0.12		
Barren	4	3	3	81	90	0.10	88.7%	0.85
Marginal total	91	87	90	92	360			
Omission Error	0.11	0.10	0.12	0.12				

Table S4.142. Confusion Matrix with commission and omission errors from Mid-May to mid-July 1997

Classes	Open Water	Non-Woody	Woody / Shrub	Barren	Marginal total	Comission Error	Total Accuracy	Kappa Index
Open Water	82	2	2	4	90	0.09		
Non-Woody	3	79	5	4	90	0.12		
Woody/Shrub	4	3	80	3	90	0.12		
Barren	3	4	3	81	90	0.10	89.3%	0.86
Marginal total	92	88	89	92	360			
Omission Error	0.10	0.11	0.10	0.12				

Table S4.143. Confusion Matrix with commission and omission errors from Mid-May to mid-July 1998

Classes	Open Water	Non-Woody	Woody / Shrub	Barren	Marginal total	Comission Error	Total Accuracy	Kappa Index
Open Water	80	3	2	4	90	0.11		
Non-Woody	4	78	5	4	90	0.13	87.3%	0.83
Woody/Shrub	2	6	78	4	90	0.14		
Barren	4	4	4	78	90	0.14		

Marginal total	90	91	89	90	360			
Omission Error	0.11	0.14	0.13	0.13				

Table S4.144. Confusion Matrix with commission and omission errors from Mid-May to mid-July 1999

Classes	Open Water	Non-Woody	Woody / Shrub	Barren	Marginal total	Comission Error	Total Accuracy	Kappa Index
Open Water	80	3	2	4	90	0.11		
Non-Woody	4	78	5	4	90	0.13		
Woody/Shrub	2	6	78	4	90	0.14		
Barren	4	4	4	78	90	0.14	87.3%	0.83
Marginal total	90	91	89	90	360			
Omission Error	0.11	0.14	0.13	0.13				

Table S4.145. Confusion Matrix with commission and omission errors from Mid-May to mid-July 2001

Classes	Open Water	Non-Woody	Woody / Shrub	Barren	Marginal total	Comission Error	Total Accuracy	Kappa Index
Open Water	83	2	2	3	90	0.08		
Non-Woody	2	81	4	3	90	0.10		
Woody/Shrub	4	4	78	4	90	0.13		
Barren	4	3	3	80	90	0.12	89.3%	0.86
Marginal total	93	90	88	89	360			
Omission Error	0.11	0.10	0.11	0.11				

Table S4.146. Confusion Matrix with commission and omission errors from Mid-May to mid-July 2002

Classes	Open Water	Non-Woody	Woody / Shrub	Barren	Marginal total	Comission Error	Total Accuracy	Kappa Index
Open Water	101	2	1	1	105	0.04		
Non-Woody	2	99	4	1	105	0.06		
Woody/Shrub	2	3	99	2	105	0.06		
Barren	1	1	2	101	105	0.04	95.0%	0.93
Marginal total	105	105	106	104	420			
Omission Error	0.04	0.05	0.07	0.04				

Table S4.147. Confusion Matrix with commission and omission errors from Mid-May to mid-July 2004

Classes	Open Water	Non-Woody	Woody / Shrub	Barren	Marginal total	Comission Error	Total Accuracy	Kappa Index

Open Water	81	3	2	4	90	0.10		
Non-Woody	2	79	5	3	90	0.12		
Woody/Shrub	4	3	79	3	90	0.12		
Barren	3	4	3	80	90	0.11	88.8%	0.85
Marginal total	90	89	90	91	360			
Omission Error	0.10	0.11	0.12	0.12				

Table S4.148. Confusion Matrix with commission and omission errors from Mid-May to mid-July 2005

Classes	Open Water	Non-Woody	Woody / Shrub	Barren	Marginal total	Comission Error	Total Accuracy	Kappa Index
Open Water	79	4	3	4	90	0.13		
Non-Woody	3	77	7	3	90	0.15		
Woody/Shrub	4	5	76	5	90	0.16		
Barren	4	4	5	78	90	0.13	85.8%	0.81
Marginal total	90	90	90	90	360			
Omission Error	0.13	0.15	0.16	0.13				

Table S4.149. Confusion Matrix with commission and omission errors from Mid-May to mid-July 2006

Classes	Open Water	Non-Woody	Woody / Shrub	Barren	Marginal total	Comission Error	Total Accuracy	Kappa Index
Open Water	80	3	2	4	90	0.11		
Non-Woody	4	78	5	4	90	0.13		
Woody/Shrub	2	6	78	4	90	0.14		
Barren	4	4	4	78	90	0.14	87.3%	0.83
Marginal total	90	91	89	90	360			
Omission Error	0.11	0.14	0.13	0.13				

Table S4.150. Confusion Matrix with commission and omission errors from Mid-May to mid-July 2007

Classes	Open Water	Non-Woody	Woody / Shrub	Barren	Marginal total	Comission Error	Total Accuracy	Kappa Index
Open Water	81	4	2	4	90	0.10		
Non-Woody	3	78	5	4	90	0.13		
Woody/Shrub	4	3	79	3	90	0.12		
Barren	3	4	3	80	90	0.11	88.3%	0.84
Marginal total	90	89	90	91	360			
Omission Error	0.11	0.12	0.12	0.12				

Table S4.151. Confusion Matrix with commission and omission errors from Mid-May to mid-July 2008

Classes	Open Water	Non-Woody	Woody / Shrub	Barren	Marginal total	Comission Error	Total Accuracy	Kappa Index
Open Water	83	2	2	3	90	0.08		
Non-Woody	1	80	6	3	90	0.11		
Woody/Shrub	3	5	78	4	90	0.13		
Barren	2	3	4	81	90	0.10	89.5%	0.86
Marginal total	89	90	90	91	360			
Omission Error	0.06	0.11	0.13	0.12				

Table S4.152. Confusion Matrix with commission and omission errors from Mid-May to mid-July 2009

Classes	Open Water	Non-Woody	Woody / Shrub	Barren	Marginal total	Comission Error	Total Accuracy	Kappa Index
Open Water	81	4	2	4	90	0.10		
Non-Woody	2	77	7	4	90	0.14		
Woody/Shrub	3	6	77	5	90	0.15		
Barren	2	5	4	79	90	0.12	87.2%	0.83
Marginal total	87	92	90	91	360			
Omission Error	0.08	0.16	0.15	0.13				

Table S4.153. Confusion Matrix with commission and omission errors from Mid-May to mid-July 2010

Classes	Open Water	Non-Woody	Woody / Shrub	Barren	Marginal total	Comission Error	Total Accuracy	Kappa Index
Open Water	80	4	2	4	90	0.11		
Non-Woody	2	76	8	4	90	0.16		
Woody/Shrub	2	6	78	5	90	0.14		
Barren	2	5	5	78	90	0.13	86.5%	0.82
Marginal total	86	91	93	90	360			
Omission Error	0.07	0.17	0.16	0.14				

Table S4.154. Confusion Matrix with commission and omission errors from Mid-May to mid-July 2014

Classes	Open Water	Non-Woody	Woody / Shrub	Barren	Marginal total	Comission Error	Total Accuracy	Kappa Index
Open Water	86	2	2	1	90	0.05	93.4%	0.91
Non-Woody	2	84	3	2	90	0.07		

Woody/Shrub	2	2	83	3	90	0.07
Barren	2	2	2	84	90	0.07
Marginal total	92	89	90	90	360	
Omission Error	0.07	0.06	0.07	0.07		

Table S4.155. Confusion Matrix with commission and omission errors from Mid-May to mid-July 2015

Classes	Open Water	Non-Woody	Woody / Shrub	Barren	Marginal total	Comission Error	Total Accuracy	Kappa Index
Open Water	79	3	3	4	90	0.12		
Non-Woody	2	77	7	4	90	0.14		
Woody/Shrub	4	5	75	5	90	0.16		
Barren	3	5	5	78	90	0.14	85.9%	0.81
Marginal total	88	90	90	92	360			
Omission Error	0.10	0.15	0.17	0.15				

Table S4.156. Confusion Matrix with commission and omission errors from Mid-May to mid-July 2016

Classes	Open Water	Non-Woody	Woody / Shrub	Barren	Marginal total	Comission Error	Total Accuracy	Kappa Index
Open Water	101	3	1	1	105	0.04		
Non-Woody	1	100	3	1	105	0.05		
Woody/Shrub	2	2	99	2	105	0.06		
Barren	1	1	2	101	105	0.04	95.3%	0.94
Marginal total	105	106	104	105	420			
Omission Error	0.04	0.06	0.05	0.04				

Table S4.157. Confusion Matrix with commission and omission errors from Mid-May to mid-July 2017

Classes	Open Water	Non-Woody	Woody / Shrub	Barren	Marginal total	Comission Error	Total Accuracy	Kappa Index
Open Water	99	3	2	2	105	0.05		
Non-Woody	2	97	5	2	105	0.08		
Woody/Shrub	2	4	96	3	105	0.09		
Barren	2	2	2	98	105	0.07	92.9%	0.90
Marginal total	105	106	104	105	420			
Omission Error	0.06	0.09	0.08	0.06				

Table S4.158. Confusion Matrix with commission and omission errors from Mid-May to mid-July 2018

Classes	Open Water	Non-Woody	Woody / Shrub	Barren	Marginal total	Comission Error	Total Accuracy	Kappa Index
Open Water	101	2	1	2	105	0.04		
Non-Woody	2	99	3	2	105	0.06		
Woody/Shrub	2	3	98	2	105	0.07		
Barren	1	2	2	100	105	0.05	94.6%	0.93
Marginal total	105	106	104	105	420			
Omission Error	0.04	0.07	0.05	0.05				

Table S4.159. Confusion Matrix with commission and omission errors from Mid-May to mid-July 2019

Classes	Open Water	Non-Woody	Woody / Shrub	Barren	Marginal total	Comission Error	Total Accuracy	Kappa Index
Open Water	102	2	1	1	105	0.03		
Non-Woody	2	99	3	1	105	0.05		
Woody/Shrub	2	2	99	2	105	0.06		
Barren	1	1	1	102	105	0.03	95.6%	0.94
Marginal total	106	104	104	106	420			
Omission Error	0.04	0.05	0.05	0.04				

Table S4.160. Confusion Matrix with commission and omission errors from Mid-May to mid-July 2021

Classes	Open Water	Non-Woody	Woody / Shrub	Barren	Marginal total	Comission Error	Total Accuracy	Kappa Index
Open Water	103	1	1	1	105	0.02		
Non-Woody	1	100	3	1	105	0.05		
Woody/Shrub	1	2	100	2	105	0.05		
Barren	1	2	2	101	105	0.04	96.1%	0.95
Marginal total	106	104	105	106	420			
Omission Error	0.03	0.04	0.05	0.04				

Table S4.161. Confusion Matrix with commission and omission errors from Mid-May to mid-July 2023

Classes	Open Water	Non-Woody	Woody / Shrub	Barren	Marginal total	Comission Error	Total Accuracy	Kappa Index
Open Water	82	3	2	4	90	0.09		
Non-Woody	4	79	4	4	90	0.13	89.3%	0.86
Woody/Shrub	4	5	79	2	90	0.12		
Barren	3	3	3	82	90	0.09		

Marginal total	92	89	88	92	360			
Omission Error	0.11	0.11	0.10	0.11				

4.4.3.2. Season: Rainfall-driven (Late-July to mid-September)

Table S4.162. Confusion Matrix with commission and omission errors from Late-May to July 1984

Classes	Open Water	Non-Woody	Woody / Shrub	Barren	Marginal total	Comission Error	Total Accuracy	Kappa Index
Open Water	76	5	4	5	90	0.16		
Non-Woody	3	74	8	5	90	0.18		
Woody/Shrub	3	8	75	5	90	0.17		
Barren	4	5	5	77	90	0.14	83.8%	0.78
Marginal total	85	92	92	92	360			
Omission Error	0.11	0.19	0.18	0.16				

Table S4.163. Confusion Matrix with commission and omission errors from Late-May to July 1985

Classes	Open Water	Non-Woody	Woody / Shrub	Barren	Marginal total	Comission Error	Total Accuracy	Kappa Index
Open Water	95	3	4	3	105	0.10		
Non-Woody	3	91	7	4	105	0.14		
Woody/Shrub	3	6	91	5	105	0.13		
Barren	3	5	5	93	105	0.12	87.8%	0.84
Marginal total	104	105	107	105	420			
Omission Error	0.09	0.13	0.15	0.12				

Table S4.164. Confusion Matrix with commission and omission errors from Late-May to July 1986

Classes	Open Water	Non-Woody	Woody / Shrub	Barren	Marginal total	Comission Error	Total Accuracy	Kappa Index
Open Water	76	5	4	5	90	0.16		
Non-Woody	3	75	7	5	90	0.17		
Woody/Shrub	4	7	75	4	90	0.16		
Barren	4	4	4	79	90	0.13	84.7%	0.80
Marginal total	86	92	90	92	360			
Omission Error	0.12	0.18	0.16	0.15				

Table S4.165. Confusion Matrix with commission and omission errors from Late-May to July 1987

Classes	Open Water	Non-Woody	Woody / Shrub	Barren	Marginal total	Comission Error	Total Accuracy	Kappa Index
Open Water	99	3	2	2	105	0.06		
Non-Woody	2	97	5	1	105	0.07		
Woody/Shrub	2	4	97	2	105	0.08		
Barren	1	2	3	99	105	0.06	93.3%	0.91
Marginal total	104	106	107	104	420			
Omission Error	0.04	0.08	0.09	0.05				

Table S4.166. Confusion Matrix with commission and omission errors from Late-May to July 1988

Classes	Open Water	Non-Woody	Woody / Shrub	Barren	Marginal total	Comission Error	Total Accuracy	Kappa Index
Open Water	96	5	2	2	105	0.09		
Non-Woody	2	93	7	3	105	0.11		
Woody/Shrub	2	5	93	4	105	0.11		
Barren	3	6	5	92	105	0.13	89.0%	0.85
Marginal total	103	109	107	101	420			
Omission Error	0.06725146	0.15	0.13	0.09				

Table S4.167. Confusion Matrix with commission and omission errors from Late-May to July 1989

Classes	Open Water	Non-Woody	Woody / Shrub	Barren	Marginal total	Comission Error	Total Accuracy	Kappa Index
Open Water	79	4	4	4	90	0.13		
Non-Woody	4	75	6	5	90	0.17		
Woody/Shrub	3	5	75	6	90	0.16		
Barren	5	3	3	79	90	0.12	85.5%	0.81
Marginal total	91	88	88	94	360			
Omission Error	0.14	0.14	0.14	0.16				

Table S4.168. Confusion Matrix with commission and omission errors from Late-May to July 1990

Classes	Open Water	Non-Woody	Woody / Shrub	Barren	Marginal total	Comission Error	Total Accuracy	Kappa Index
Open Water	80	3	3	4	90	0.11		
Non-Woody	4	79	5	3	90	0.12	87.9%	0.84
Woody/Shrub	3	5	78	4	90	0.13		
Barren	3	4	4	79	90	0.12		

Marginal total	90	90	90	90	360			
Omission Error	0.11	0.13	0.13	0.12				

Table S4.169. Confusion Matrix with commission and omission errors from Late-May to July 1991

Classes	Open Water	Non-Woody	Woody / Shrub	Barren	Marginal total	Comission Error	Total Accuracy	Kappa Index
Open Water	79	4	4	4	90	0.13		
Non-Woody	4	75	6	5	90	0.17		
Woody/Shrub	3	5	75	6	90	0.16		
Barren	5	3	3	79	90	0.12	85.5%	0.81
Marginal total	91	88	88	94	360			
Omission Error	0.14	0.14	0.14	0.16				

Table S4.170. Confusion Matrix with commission and omission errors from Late-May to July 1993

Classes	Open Water	Non-Woody	Woody / Shrub	Barren	Marginal total	Comission Error	Total Accuracy	Kappa Index
Open Water	98	3	2	2	105	0.06		
Non-Woody	2	96	6	2	105	0.09		
Woody/Shrub	2	5	95	3	105	0.09		
Barren	3	3	4	96	105	0.09	91.8%	0.89
Marginal total	105	106	107	102	420			
Omission Error	0.06	0.10	0.11	0.06				

Table S4.171. Confusion Matrix with commission and omission errors from Late-May to July 1994

Classes	Open Water	Non-Woody	Woody / Shrub	Barren	Marginal total	Comission Error	Total Accuracy	Kappa Index
Open Water	95	5	2	2	105	0.09		
Non-Woody	1	94	7	3	105	0.11		
Woody/Shrub	2	5	93	5	105	0.12		
Barren	3	6	5	91	105	0.13	88.7%	0.85
Marginal total	101	111	107	101	420			
Omission Error	0.06	0.15	0.13	0.10				

Table S4.172. Confusion Matrix with commission and omission errors from Late-May to July 1995

Classes	Open	Non-	Woody /	Barren	Marginal	Comission	Total	Kappa

	Water	Woody	Shrub		total	Error	Accuracy	Index
Open Water	75	6	5	5	90	0.17		
Non-Woody	6	73	7	4	90	0.19		
Woody/Shrub	5	6	72	6	90	0.20		
Barren	5	4	4	77	90	0.15	82.4%	0.77
Marginal total	92	89	88	91	360			
Omission Error	0.18	0.18	0.18	0.16				

Table S4.173. Confusion Matrix with commission and omission errors from Late-May to July 1996

Classes	Open Water	Non-Woody	Woody / Shrub	Barren	Marginal total	Comission Error	Total Accuracy	Kappa Index
Open Water	78	4	4	5	90	0.14		
Non-Woody	5	76	6	3	90	0.16		
Woody/Shrub	4	5	75	5	90	0.17		
Barren	5	3	3	79	90	0.12	85.4%	0.81
Marginal total	92	89	87	92	360			
Omission Error	0.16	0.14	0.14	0.15				

Table S4.174. Confusion Matrix with commission and omission errors from Late-May to July 1997

Classes	Open Water	Non-Woody	Woody / Shrub	Barren	Marginal total	Comission Error	Total Accuracy	Kappa Index
Open Water	76	5	4	5	90	0.15		
Non-Woody	3	75	7	5	90	0.17		
Woody/Shrub	4	7	75	4	90	0.17		
Barren	5	4	4	78	90	0.14	84.3%	0.79
Marginal total	88	91	89	92	360			
Omission Error	0.13	0.18	0.16	0.15				

Table S4.175. Confusion Matrix with commission and omission errors from Late-May to July 1998

Classes	Open Water	Non-Woody	Woody / Shrub	Barren	Marginal total	Comission Error	Total Accuracy	Kappa Index
Open Water	76	5	4	6	90	0.16		
Non-Woody	5	73	8	3	90	0.19		
Woody/Shrub	5	8	72	6	90	0.20	83.0%	0.77
Barren	6	3	3	78	90	0.14		
Marginal total	92	89	87	92	360			

Omission Error	0.17	0.18	0.17	0.16				

Table S4.176. Confusion Matrix with commission and omission errors from Late-May to July 2001

Classes	Open Water	Non-Woody	Woody / Shrub	Barren	Marginal total	Comission Error	Total Accuracy	Kappa Index
Open Water	77	4	4	5	90	0.14		
Non-Woody	5	76	6	3	90	0.15		
Woody/Shrub	4	5	75	5	90	0.16		
Barren	5	3	3	80	90	0.12	85.7%	0.81
Marginal total	91	89	87	93	360			
Omission Error	0.15	0.14	0.14	0.14				

Table S4.177. Confusion Matrix with commission and omission errors from Late-May to July 2002

Classes	Open Water	Non-Woody	Woody / Shrub	Barren	Marginal total	Comission Error	Total Accuracy	Kappa Index
Open Water	101	2	2	1	105	0.04		
Non-Woody	1	98	4	2	105	0.07		
Woody/Shrub	2	3	98	2	105	0.07		
Barren	1	2	2	101	105	0.04	94.9%	0.93
Marginal total	105	104	105	105	420			
Omission Error	0.04	0.06	0.07	0.04				

Table S4.178. Confusion Matrix with commission and omission errors from Late-May to July 2003

Classes	Open Water	Non-Woody	Woody / Shrub	Barren	Marginal total	Comission Error	Total Accuracy	Kappa Index
Open Water	99	2	2	2	105	0.06		
Non-Woody	2	97	4	2	105	0.08		
Woody/Shrub	2	4	97	2	105	0.07		
Barren	2	2	2	99	105	0.05	93.4%	0.91
Marginal total	105	105	105	105	420			
Omission Error	0.06	0.08	0.07	0.05				

Table S4.179. Confusion Matrix with commission and omission errors from Late-May to July 2004

Classes	Open Water	Non-Woody	Woody / Shrub	Barren	Marginal total	Comission Error	Total Accuracy	Kappa Index
Open Water	77	6	3	4	90	0.15	83.4%	0.78

Non-Woody	5	74	7	4	90	0.18
Woody/Shrub	3	7	73	7	90	0.19
Barren	5	3	5	77	90	0.15
Marginal total	90	90	88	92	360	
Omission Error	0.15	0.18	0.17	0.16		

Table S4.180. Confusion Matrix with commission and omission errors from Late-May to July 2005

Classes	Open Water	Non-Woody	Woody / Shrub	Barren	Marginal total	Comission Error	Total Accuracy	Kappa Index
Open Water	81	4	2	4	90	0.10		
Non-Woody	2	77	7	4	90	0.14		
Woody/Shrub	3	6	77	5	90	0.15		
Barren	2	5	4	79	90	0.12	87.2%	0.83
Marginal total	87	92	90	91	360			
Omission Error	0.08	0.16	0.15	0.13				

Table S4.181. Confusion Matrix with commission and omission errors from Late-May to July 2006

Classes	Open Water	Non-Woody	Woody / Shrub	Barren	Marginal total	Comission Error	Total Accuracy	Kappa Index
Open Water	75	6	4	5	90	0.17		
Non-Woody	6	73	7	4	90	0.19		
Woody/Shrub	4	7	73	6	90	0.19		
Barren	5	4	5	76	90	0.16	82.4%	0.77
Marginal total	91	90	88	91	360			
Omission Error	0.17	0.19	0.17	0.17				

Table S4.182. Confusion Matrix with commission and omission errors from Late-May to July 2007

Classes	Open Water	Non-Woody	Woody / Shrub	Barren	Marginal total	Comission Error	Total Accuracy	Kappa Index
Open Water	74	6	5	5	90	0.18		
Non-Woody	7	72	7	5	90	0.20		
Woody/Shrub	5	7	72	7	90	0.20		
Barren	5	5	5	75	90	0.17	81.3%	0.75
Marginal total	91	90	88	91	360			
Omission Error	0.18	0.20	0.19	0.18				

Table S4.183. Confusion Matrix with commission and omission errors from Late-May to July 2008

Classes	Open Water	Non-Woody	Woody / Shrub	Barren	Marginal total	Comission Error	Total Accuracy	Kappa Index
Open Water	77	5	3	5	90	0.15		
Non-Woody	4	74	8	5	90	0.18		
Woody/Shrub	4	7	74	6	90	0.18		
Barren	4	6	4	76	90	0.15	83.5%	0.78
Marginal total	88	92	88	92	360			
Omission Error	0.13	0.19	0.16	0.17				

Table S4.184. Confusion Matrix with commission and omission errors from Late-May to July 2009

Classes	Open Water	Non-Woody	Woody / Shrub	Barren	Marginal total	Comission Error	Total Accuracy	Kappa Index
Open Water	78	5	3	4	90	0.13		
Non-Woody	3	75	8	5	90	0.17		
Woody/Shrub	3	6	75	6	90	0.16		
Barren	4	5	5	77	90	0.15	84.7%	0.80
Marginal total	88	91	90	91	360			
Omission Error	0.11	0.18	0.17	0.16				

Table S4.185. Confusion Matrix with commission and omission errors from Late-May to July 2010

Classes	Open Water	Non-Woody	Woody / Shrub	Barren	Marginal total	Comission Error	Total Accuracy	Kappa Index
Open Water	77	5	3	5	90	0.14		
Non-Woody	4	74	8	5	90	0.17		
Woody/Shrub	3	7	74	6	90	0.18		
Barren	4	5	3	78	90	0.14	84.3%	0.79
Marginal total	88	92	88	93	360			
Omission Error	0.12	0.19	0.15	0.16				

Table S4.186. Confusion Matrix with commission and omission errors from Late-May to July 2011

Classes	Open Water	Non-Woody	Woody / Shrub	Barren	Marginal total	Comission Error	Total Accuracy	Kappa Index
Open Water	79	5	3	4	90	0.12		
Non-Woody	2	76	8	4	90	0.16	85.8%	0.81
Woody/Shrub	3	6	76	5	90	0.16		
Barren	3	5	4	78	90	0.13		

Marginal total	87	92	90	91	360			
Omission Error	0.09	0.17	0.16	0.14				

Table S4.187. Confusion Matrix with commission and omission errors from Late-May to July 2013

Classes	Open Water	Non-Woody	Woody / Shrub	Barren	Marginal total	Comission Error	Total Accuracy	Kappa Index
Open Water	77	5	3	5	90	0.14		
Non-Woody	3	75	8	4	90	0.17		
Woody/Shrub	3	6	75	5	90	0.16		
Barren	4	5	5	76	90	0.15	84.3%	0.79
Marginal total	88	91	91	91	360			
Omission Error	0.12	0.18	0.17	0.16				

Table S4.188. Confusion Matrix with commission and omission errors from Late-May to July 2014

Classes	Open Water	Non-Woody	Woody / Shrub	Barren	Marginal total	Comission Error	Total Accuracy	Kappa Index
Open Water	77	5	4	5	90	0.15		
Non-Woody	4	74	8	5	90	0.17		
Woody/Shrub	3	6	75	6	90	0.17		
Barren	4	5	5	77	90	0.15	84.1%	0.79
Marginal total	87	91	91	92	360			
Omission Error	0.12	0.18	0.17	0.16				

Table S4.189. Confusion Matrix with commission and omission errors from Late-May to July 2015

Classes	Open Water	Non-Woody	Woody / Shrub	Barren	Marginal total	Comission Error	Total Accuracy	Kappa Index
Open Water	78	5	3	4	90	0.13		
Non-Woody	3	75	8	5	90	0.17		
Woody/Shrub	3	7	75	6	90	0.17		
Barren	4	6	5	75	90	0.17	84.1%	0.79
Marginal total	88	93	90	89	360			
Omission Error	0.11	0.19	0.17	0.16				

Table S4.190. Confusion Matrix with commission and omission errors from Late-May to July 2016

Classes	Open	Non-	Woody /	Barren	Marginal	Comission	Total	Kappa

	Water	Woody	Shrub		total	Error	Accuracy	Index
Open Water	100	2	2	2	105	0.05		
Non-Woody	1	98	5	2	105	0.07		
Woody/Shrub	2	4	97	2	105	0.08		
Barren	2	2	2	98	105	0.06	93.4%	0.91
Marginal total	105	105	105	104	420			
Omission Error	0.05	0.07	0.08	0.05				

Table S4.191. Confusion Matrix with commission and omission errors from Late-May to July 2017

Classes	Open Water	Non-Woody	Woody / Shrub	Barren	Marginal total	Comission Error	Total Accuracy	Kappa Index
Open Water	100	2	2	2	105	0.05		
Non-Woody	2	97	5	2	105	0.08		
Woody/Shrub	2	4	96	3	105	0.09		
Barren	2	3	2	98	105	0.07	92.9%	0.91
Marginal total	106	105	105	104	420			
Omission Error	0.06	0.08	0.09	0.06				

Table S4.192. Confusion Matrix with commission and omission errors from Late-May to July 2018

Classes	Open Water	Non-Woody	Woody / Shrub	Barren	Marginal total	Comission Error	Total Accuracy	Kappa Index
Open Water	99	2	2	2	105	0.06		
Non-Woody	2	96	6	2	105	0.09		
Woody/Shrub	2	4	96	3	105	0.08		
Barren	3	3	2	98	105	0.07	92.6%	0.90
Marginal total	105	105	107	104	420			
Omission Error	0.06	0.08	0.10	0.06				

Table S4.193. Confusion Matrix with commission and omission errors from Late-May to July 2019

Classes	Open Water	Non-Woody	Woody / Shrub	Barren	Marginal total	Comission Error	Total Accuracy	Kappa Index
Open Water	101	2	1	2	105	0.04		
Non-Woody	2	99	3	2	105	0.06		
Woody/Shrub	2	3	98	2	105	0.07	94.6%	0.93
Barren	1	2	2	100	105	0.05		
Marginal total	105	106	104	105	420			

Omission Error	0.04	0.07	0.05	0.05				

Table S4.194. Confusion Matrix with commission and omission errors from Late-May to July 2020

Classes	Open Water	Non-Woody	Woody / Shrub	Barren	Marginal total	Comission Error	Total Accuracy	Kappa Index
Open Water	117	1	1	2	120	0.03		
Non-Woody	1	115	2	3	120	0.05		
Woody/Shrub	2	3	114	1	120	0.05		
Barren	2	2	2	115	120	0.04	96.1%	0.95
Marginal total	122	120	118	121	480			
Omission Error	0.04	0.04	0.03	0.04				

Table S4.195. Confusion Matrix with commission and omission errors from Late-May to July 2021

Classes	Open Water	Non-Woody	Woody / Shrub	Barren	Marginal total	Comission Error	Total Accuracy	Kappa Index
Open Water	100	2	2	2	105	0.05		
Non-Woody	2	97	4	3	105	0.08		
Woody/Shrub	2	4	97	3	105	0.08		
Barren	3	2	2	98	105	0.07	93.1%	0.91
Marginal total	107	104	104	105	420			
Omission Error	0.07	0.07	0.07	0.07				

Table S4.196. Confusion Matrix with commission and omission errors from Late-May to July 2022

Classes	Open Water	Non-Woody	Woody / Shrub	Barren	Marginal total	Comission Error	Total Accuracy	Kappa Index
Open Water	78	5	3	5	90	0.14		
Non-Woody	3	75	8	4	90	0.17		
Woody/Shrub	4	7	74	5	90	0.18		
Barren	4	5	4	77	90	0.14	84.3%	0.79
Marginal total	89	92	88	91	360			
Omission Error	0.13	0.18	0.16	0.15				

Table S4.197. Confusion Matrix with commission and omission errors from Late-May to July 2023

Classes	Open Water	Non-Woody	Woody / Shrub	Barren	Marginal total	Comission Error	Total Accuracy	Kappa Index
Open Water	77	5	3	5	90	0.14	84.2%	0.79

Non-Woody	4	74	7	4	90	0.17
Woody/Shrub	3	6	75	6	90	0.17
Barren	4	5	5	77	90	0.15
Marginal total	89	90	89	92	360	
Omission Error	0.13	0.18	0.16	0.16		

4.4.4. Athabasca Basin

4.4.4.1. Season: Snow-melting (Mid-May to mid-July)

Table S4.198. Confusion Matrix with commission and omission errors from Mid-May to mid-July 1984

Classes	Open Water	Non-Woody	Woody / Shrub	Barren	Marginal total	Comission Error	Total Accuracy	Kappa Index
Open Water	102	2	0	1	105	0.03		
Non-Woody	1	100	3	1	105	0.05		
Woody/Shrub	1	4	99	2	105	0.06		
Barren	1	2	3	99	105	0.06	95.1%	0.94
Marginal total	105	108	104	103	420			
Omission Error	0.03	0.07	0.05	0.04				

Table S4.199. Confusion Matrix with commission and omission errors from Mid-May to mid-July 1985

Classes	Open Water	Non-Woody	Woody / Shrub	Barren	Marginal total	Comission Error	Total Accuracy	Kappa Index
Open Water	81	3	2	4	90	0.10		
Non-Woody	3	80	5	3	90	0.12		
Woody/Shrub	3	5	79	3	90	0.12		
Barren	2	4	3	81	90	0.10	88.9%	0.85
Marginal total	89	92	89	91	360			
Omission Error	0.09	0.13	0.11	0.11				

Table S4.200. Confusion Matrix with commission and omission errors from Mid-May to mid-July 1986

Classes	Open Water	Non-Woody	Woody / Shrub	Barren	Marginal total	Comission Error	Total Accuracy	Kappa Index
Open Water	82	2	2	3	90	0.09		
Non-Woody	3	80	4	2	90	0.11	89.9%	0.87
Woody/Shrub	2	5	80	3	90	0.11		

Barren	2	4	3	81	90	0.10		
Marginal total	90	91	89	90	360			
Omission Error	0.09	0.11	0.10	0.10				

Table S4.201. Confusion Matrix with commission and omission errors from Mid-May to mid-July 1987

Classes	Open Water	Non-Woody	Woody / Shrub	Barren	Marginal total	Comission Error	Total Accuracy	Kappa Index
Open Water	101	2	1	1	105	0.04		
Non-Woody	2	99	4	1	105	0.06		
Woody/Shrub	2	3	99	2	105	0.06		
Barren	1	1	2	101	105	0.04	95.0%	0.93
Marginal total	105	105	106	104	420			
Omission Error	0.04	0.05	0.07	0.04				

Table S4.202. Confusion Matrix with commission and omission errors from Mid-May to mid-July 1991

Classes	Open Water	Non-Woody	Woody / Shrub	Barren	Marginal total	Comission Error	Total Accuracy	Kappa Index
Open Water	102	2	1	1	105	0.03		
Non-Woody	2	99	3	1	105	0.05		
Woody/Shrub	2	2	100	2	105	0.05		
Barren	1	2	2	100	105	0.05	95.5%	0.94
Marginal total	106	105	106	103	420			
Omission Error	0.04	0.05	0.06	0.03				

Table S4.203. Confusion Matrix with commission and omission errors from Mid-May to mid-July 1992

Classes	Open Water	Non-Woody	Woody / Shrub	Barren	Marginal total	Comission Error	Total Accuracy	Kappa Index
Open Water	80	3	4	3	90	0.11		
Non-Woody	4	78	5	4	90	0.14		
Woody/Shrub	3	6	75	6	90	0.16		
Barren	4	4	3	80	90	0.12	86.8%	0.82
Marginal total	90	90	87	92	360			
Omission Error	0.11	0.14	0.14	0.14				

Table S4.204. Confusion Matrix with commission and omission errors from Mid-May to mid-July 1993

Classes	Open Water	Non-Woody	Woody / Shrub	Barren	Marginal total	Comission Error	Total Accuracy	Kappa Index
Open Water	83	2	2	3	90	0.08		
Non-Woody	3	82	3	2	90	0.09		
Woody/Shrub	2	3	81	3	90	0.10		
Barren	2	2	3	83	90	0.08	91.3%	0.88
Marginal total	91	89	89	91	360			
Omission Error	0.08	0.08	0.09	0.09				

Table S4.205. Confusion Matrix with commission and omission errors from Mid-May to mid-July 1994

Classes	Open Water	Non-Woody	Woody / Shrub	Barren	Marginal total	Comission Error	Total Accuracy	Kappa Index
Open Water	103	2	0	1	105	0.02		
Non-Woody	1	101	2	1	105	0.03		
Woody/Shrub	1	3	100	2	105	0.05		
Barren	1	1	2	101	105	0.04	96.4%	0.95
Marginal total	105	107	104	104	420			
Omission Error	0.03	0.05	0.04	0.03				

Table S4.206. Confusion Matrix with commission and omission errors from Mid-May to mid-July 1995

Classes	Open Water	Non-Woody	Woody / Shrub	Barren	Marginal total	Comission Error	Total Accuracy	Kappa Index
Open Water	81	3	3	3	90	0.07		
Non-Woody	4	78	5	3	90	0.12		
Woody/Shrub	4	4	79	3	90	0.11		
Barren	2	2	2	84	90	0.10	90.0%	0.87
Marginal total	91	87	89	93	360			
Omission Error	0.11	0.10	0.12	0.07				

Table S4.207. Confusion Matrix with commission and omission errors from Mid-May to mid-July 1997

Classes	Open Water	Non-Woody	Woody / Shrub	Barren	Marginal total	Comission Error	Total Accuracy	Kappa Index
Open Water	80	3	2	4	90	0.11		
Non-Woody	4	78	5	4	90	0.13	87.3%	0.83
Woody/Shrub	2	6	78	4	90	0.14		
Barren	4	4	4	78	90	0.14		

Marginal total	90	91	89	90	360
Omission Error	0.11	0.14	0.13	0.13	

Table S4.208. Confusion Matrix with commission and omission errors from Mid-May to mid-July 1998

Classes	Open Water	Non-Woody	Woody / Shrub	Barren	Marginal total	Comission Error	Total Accuracy	Kappa Index
Open Water	82	2	2	4	90	0.09		
Non-Woody	3	79	5	4	90	0.12		
Woody/Shrub	4	3	80	3	90	0.12		
Barren	3	4	3	81	90	0.10	89.3%	0.86
Marginal total	92	88	89	92	360			
Omission Error	0.10	0.11	0.10	0.12				

Table S4.209. Confusion Matrix with commission and omission errors from Mid-May to mid-July 1999

Classes	Open Water	Non-Woody	Woody / Shrub	Barren	Marginal total	Comission Error	Total Accuracy	Kappa Index
Open Water	83	2	2	3	90	0.08		
Non-Woody	2	81	4	3	90	0.10		
Woody/Shrub	4	4	78	4	90	0.13		
Barren	4	3	3	80	90	0.12	89.3%	0.86
Marginal total	93	90	88	89	360			
Omission Error	0.11	0.10	0.11	0.11				

Table S4.210. Confusion Matrix with commission and omission errors from Mid-May to mid-July 2001

Classes	Open Water	Non-Woody	Woody / Shrub	Barren	Marginal total	Comission Error	Total Accuracy	Kappa Index
Open Water	81	3	2	4	90	0.10		
Non-Woody	2	79	5	3	90	0.12		
Woody/Shrub	4	3	79	3	90	0.12		
Barren	3	4	3	80	90	0.11	88.8%	0.85
Marginal total	90	89	90	91	360			
Omission Error	0.10	0.11	0.12	0.12				

Table S4.211. Confusion Matrix with commission and omission errors from Mid-May to mid-July 2002

Classes	Open	Non-	Woody /	Barren	Marginal	Comission	Total	Kappa

	Water	Woody	Shrub		total	Error	Accuracy	Index
Open Water	101	2	0	2	105	0.04		
Non-Woody	0	100	5	0	105	0.05		
Woody/Shrub	1	4	99	2	105	0.06		
Barren	0	2	3	100	105	0.05	95.1%	0.94
Marginal total	102	108	107	104	420			
Omission Error	0.01	0.08	0.08	0.03				

Table S4.212. Confusion Matrix with commission and omission errors from Mid-May to mid-July 2003

Classes	Open Water	Non-Woody	Woody / Shrub	Barren	Marginal total	Comission Error	Total Accuracy	Kappa Index
Open Water	101	2	0	2	105	0.04		
Non-Woody	0	100	5	0	105	0.05		
Woody/Shrub	1	4	99	2	105	0.06		
Barren	0	2	3	100	105	0.05	95.1%	0.94
Marginal total	102	108	107	104	420			
Omission Error	0.01	0.08	0.08	0.03				

Table S4.213. Confusion Matrix with commission and omission errors from Mid-May to mid-July 2004

Classes	Open Water	Non-Woody	Woody / Shrub	Barren	Marginal total	Comission Error	Total Accuracy	Kappa Index
Open Water	83	2	2	3	90	0.08		
Non-Woody	2	81	4	3	90	0.10		
Woody/Shrub	4	4	78	4	90	0.13		
Barren	4	3	3	80	90	0.12	89.3%	0.86
Marginal total	93	90	88	89	360			
Omission Error	0.11	0.10	0.11	0.11				

Table S4.214. Confusion Matrix with commission and omission errors from Mid-May to mid-July 2005

Classes	Open Water	Non-Woody	Woody / Shrub	Barren	Marginal total	Comission Error	Total Accuracy	Kappa Index
Open Water	80	3	2	4	90	0.11		
Non-Woody	4	78	5	4	90	0.13		
Woody/Shrub	2	6	78	4	90	0.14	87.3%	0.83
Barren	4	4	4	78	90	0.14		
Marginal total	90	91	89	90	360			

Omission Error	0.11	0.14	0.13	0.13				

Table S4.215. Confusion Matrix with commission and omission errors from Mid-May to mid-July 2006

Classes	Open Water	Non-Woody	Woody / Shrub	Barren	Marginal total	Comission Error	Total Accuracy	Kappa Index
Open Water	82	3	2	3	90	0.09		
Non-Woody	2	80	6	2	90	0.11		
Woody/Shrub	4	3	81	2	90	0.10		
Barren	3	3	3	82	90	0.09	90.1%	0.87
Marginal total	90	90	91	89	360			
Omission Error	0.10	0.10	0.11	0.08				

Table S4.216. Confusion Matrix with commission and omission errors from Mid-May to mid-July 2007

Classes	Open Water	Non-Woody	Woody / Shrub	Barren	Marginal total	Comission Error	Total Accuracy	Kappa Index
Open Water	81	4	2	4	90	0.10		
Non-Woody	3	78	5	4	90	0.13		
Woody/Shrub	4	3	79	3	90	0.12		
Barren	3	4	3	80	90	0.11	88.3%	0.84
Marginal total	90	89	90	91	360			
Omission Error	0.11	0.12	0.12	0.12				

Table S4.217. Confusion Matrix with commission and omission errors from Mid-May to mid-July 2008

Classes	Open Water	Non-Woody	Woody / Shrub	Barren	Marginal total	Comission Error	Total Accuracy	Kappa Index
Open Water	81	4	2	4	90	0.10		
Non-Woody	2	77	7	4	90	0.14		
Woody/Shrub	3	6	77	5	90	0.15		
Barren	2	5	4	79	90	0.12	87.2%	0.83
Marginal total	87	92	90	91	360			
Omission Error	0.08	0.16	0.15	0.13				

Table S4.218. Confusion Matrix with commission and omission errors from Mid-May to mid-July 2015

Classes	Open Water	Non-Woody	Woody / Shrub	Barren	Marginal total	Comission Error	Total Accuracy	Kappa Index
Open Water	84	2	2	2	90	0.07	90.5%	0.87

Non-Woody	2	81	5	2	90	0.10
Woody/Shrub	3	5	80	2	90	0.11
Barren	3	3	3	81	90	0.10
Marginal total	92	91	89	88	360	
Omission Error	0.09	0.11	0.10	0.08		

Table S4.219. Confusion Matrix with commission and omission errors from Mid-May to mid-July 2016

Classes	Open Water	Non-Woody	Woody / Shrub	Barren	Marginal total	Comission Error	Total Accuracy	Kappa Index
Open Water	99	3	2	2	105	0.05		
Non-Woody	2	97	5	2	105	0.08		
Woody/Shrub	2	4	96	3	105	0.09		
Barren	2	2	2	98	105	0.07	92.9%	0.90
Marginal total	105	106	104	105	420			
Omission Error	0.06	0.09	0.08	0.06				

Table S4.220. Confusion Matrix with commission and omission errors from Mid-May to mid-July 2017

Classes	Open Water	Non-Woody	Woody / Shrub	Barren	Marginal total	Comission Error	Total Accuracy	Kappa Index
Open Water	101	3	1	1	105	0.04		
Non-Woody	1	100	3	1	105	0.05		
Woody/Shrub	2	2	99	2	105	0.06		
Barren	1	1	2	101	105	0.04	95.3%	0.94
Marginal total	105	106	104	105	420			
Omission Error	0.04	0.06	0.05	0.04				

Table S4.221. Confusion Matrix with commission and omission errors from Mid-May to mid-July 2018

Classes	Open Water	Non-Woody	Woody / Shrub	Barren	Marginal total	Comission Error	Total Accuracy	Kappa Index
Open Water	102	2	1	1	105	0.03		
Non-Woody	2	99	3	1	105	0.05		
Woody/Shrub	2	2	99	2	105	0.06		
Barren	1	1	1	102	105	0.03	95.6%	0.94
Marginal total	106	104	104	106	420			
Omission Error	0.04	0.05	0.05	0.04				

Table S4.222. Confusion Matrix with commission and omission errors from Mid-May to mid-July 2019

Classes	Open Water	Non-Woody	Woody / Shrub	Barren	Marginal total	Comission Error	Total Accuracy	Kappa Index
Open Water	101	2	1	2	105	0.04		
Non-Woody	2	99	3	2	105	0.06		
Woody/Shrub	2	3	98	2	105	0.07		
Barren	1	2	2	100	105	0.05	94.6%	0.93
Marginal total	105	106	104	105	420			
Omission Error	0.04	0.07	0.05	0.05				

Table S4.223. Confusion Matrix with commission and omission errors from Mid-May to mid-July 2021

Classes	Open Water	Non-Woody	Woody / Shrub	Barren	Marginal total	Comission Error	Total Accuracy	Kappa Index
Open Water	103	1	1	1	105	0.02		
Non-Woody	1	100	3	1	105	0.05		
Woody/Shrub	1	2	100	2	105	0.05		
Barren	1	2	2	101	105	0.04	96.1%	0.95
Marginal total	106	104	105	106	420			
Omission Error	0.03	0.04	0.05	0.04				

Table S4.224. Confusion Matrix with commission and omission errors from Mid-May to mid-July 2023

Classes	Open Water	Non-Woody	Woody / Shrub	Barren	Marginal total	Comission Error	Total Accuracy	Kappa Index
Open Water	79	3	3	4	90	0.12		
Non-Woody	2	77	7	4	90	0.14		
Woody/Shrub	4	5	75	5	90	0.16		
Barren	3	5	5	78	90	0.14	85.9%	0.81
Marginal total	88	90	90	92	360			
Omission Error	0.10	0.15	0.17	0.15				

4.4.4.2. Season: Rainfall-driven (Late-July to mid-September) 36

Table S4.225. Confusion Matrix with commission and omission errors from Late-May to July 1984

Classes	Open Water	Non-Woody	Woody / Shrub	Barren	Marginal total	Comission Error	Total Accuracy	Kappa Index
Open Water	101	2	2	1	105	0.04		
Non-Woody	1	98	4	2	105	0.07		
Woody/Shrub	2	3	98	2	105	0.07		
Barren	1	2	2	101	105	0.04	94.9%	0.93
Marginal total	105	104	105	105	420			
Omission Error	0.04	0.06	0.07	0.04				

Table S4.226. Confusion Matrix with commission and omission errors from Late-May to July 1985

Classes	Open Water	Non-Woody	Woody / Shrub	Barren	Marginal total	Comission Error	Total Accuracy	Kappa Index
Open Water	77	4	4	5	90	0.14		
Non-Woody	5	76	6	3	90	0.15		
Woody/Shrub	4	5	75	5	90	0.16		
Barren	5	3	3	80	90	0.12	85.7%	0.81
Marginal total	91	89	87	93	360			
Omission Error	0.15	0.14	0.14	0.14				

Table S4.227. Confusion Matrix with commission and omission errors from Late-May to July 1986

Classes	Open Water	Non-Woody	Woody / Shrub	Barren	Marginal total	Comission Error	Total Accuracy	Kappa Index
Open Water	80	3	4	3	90	0.11		
Non-Woody	4	78	5	3	90	0.13		
Woody/Shrub	3	5	77	6	90	0.15		
Barren	4	2	2	82	90	0.09	88.0%	0.84
Marginal total	90	88	87	95	360			
Omission Error	0.11	0.11	0.12	0.13				

Table S4.228. Confusion Matrix with commission and omission errors from Late-May to July 1987

Classes	Open Water	Non-Woody	Woody / Shrub	Barren	Marginal total	Comission Error	Total Accuracy	Kappa Index
Open Water	99	2	2	2	105	0.06		
Non-Woody	2	97	4	2	105	0.08		
Woody/Shrub	2	4	97	2	105	0.07	93.4%	0.91
Barren	2	2	2	99	105	0.05		
Marginal total	105	105	105	105	420			

Omission Error	0.06	0.08	0.07	0.05				

Table S4.229. Confusion Matrix with commission and omission errors from Late-May to July 1988

Classes	Open Water	Non-Woody	Woody / Shrub	Barren	Marginal total	Comission Error	Total Accuracy	Kappa Index
Open Water	98	3	2	2	105	0.06		
Non-Woody	2	96	6	2	105	0.09		
Woody/Shrub	2	5	95	3	105	0.09		
Barren	3	3	4	96	105	0.09	91.8%	0.89
Marginal total	105	106	107	102	420			
Omission Error	0.06	0.10	0.11	0.06				

Table S4.230. Confusion Matrix with commission and omission errors from Late-May to July 1989

Classes	Open Water	Non-Woody	Woody / Shrub	Barren	Marginal total	Comission Error	Total Accuracy	Kappa Index
Open Water	80	3	3	4	90	0.11		
Non-Woody	4	79	5	3	90	0.12		
Woody/Shrub	3	5	78	4	90	0.13		
Barren	3	4	4	79	90	0.12	87.9%	0.84
Marginal total	90	90	90	90	360			
Omission Error	0.11	0.13	0.13	0.12				

Table S4.231. Confusion Matrix with commission and omission errors from Late-May to July 1990

Classes	Open Water	Non-Woody	Woody / Shrub	Barren	Marginal total	Comission Error	Total Accuracy	Kappa Index
Open Water	79	4	4	4	90	0.13		
Non-Woody	4	75	6	5	90	0.17		
Woody/Shrub	3	5	75	6	90	0.16		
Barren	5	3	3	79	90	0.12	85.5%	0.81
Marginal total	91	88	88	94	360			
Omission Error	0.14	0.14	0.14	0.16				

Table S4.232. Confusion Matrix with commission and omission errors from Late-May to July 1991

Classes	Open Water	Non-Woody	Woody / Shrub	Barren	Marginal total	Comission Error	Total Accuracy	Kappa Index
Open Water	76	5	4	5	90	0.16	84.7%	0.80

Non-Woody	3	75	7	5	90	0.17
Woody/Shrub	4	7	75	4	90	0.16
Barren	4	4	4	79	90	0.13
Marginal total	86	92	90	92	360	
Omission Error	0.12	0.18	0.16	0.15		

Table S4.233. Confusion Matrix with commission and omission errors from Late-May to July 1992

Classes	Open Water	Non-Woody	Woody / Shrub	Barren	Marginal total	Comission Error	Total Accuracy	Kappa Index
Open Water	79	4	4	4	90	0.13		
Non-Woody	4	75	6	5	90	0.17		
Woody/Shrub	3	5	75	6	90	0.16		
Barren	5	3	3	79	90	0.12	85.5%	0.81
Marginal total	91	88	88	94	360			
Omission Error	0.14	0.14	0.14	0.16				

Table S4.234. Confusion Matrix with commission and omission errors from Late-May to July 1994

Classes	Open Water	Non-Woody	Woody / Shrub	Barren	Marginal total	Comission Error	Total Accuracy	Kappa Index
Open Water	96	5	2	2	105	0.09		
Non-Woody	2	93	7	3	105	0.11		
Woody/Shrub	2	5	93	4	105	0.11		
Barren	3	6	5	92	105	0.13	89.0%	0.85
Marginal total	103	109	107	101	420			
Omission Error	0.07	0.15	0.13	0.09				

Table S4.235. Confusion Matrix with commission and omission errors from Late-May to July 1996

Classes	Open Water	Non-Woody	Woody / Shrub	Barren	Marginal total	Comission Error	Total Accuracy	Kappa Index
Open Water	75	6	5	5	90	0.17		
Non-Woody	6	73	7	4	90	0.19		
Woody/Shrub	5	6	72	6	90	0.20		
Barren	5	4	4	77	90	0.15	82.4%	0.77
Marginal total	92	89	88	91	360			
Omission Error	0.18	0.18	0.18	0.16				

Table S4.236. Confusion Matrix with commission and omission errors from Late-May to July 1997

Classes	Open Water	Non-Woody	Woody / Shrub	Barren	Marginal total	Comission Error	Total Accuracy	Kappa Index
Open Water	76	5	4	6	90	0.16		
Non-Woody	5	73	8	3	90	0.19		
Woody/Shrub	5	8	72	6	90	0.20		
Barren	6	3	3	78	90	0.14	83.0%	0.77
Marginal total	92	89	87	92	360			
Omission Error	0.17	0.18	0.17	0.16				

Table S4.237. Confusion Matrix with commission and omission errors from Late-May to July 1998

Classes	Open Water	Non-Woody	Woody / Shrub	Barren	Marginal total	Comission Error	Total Accuracy	Kappa Index
Open Water	76	5	4	5	90	0.15		
Non-Woody	3	75	7	5	90	0.17		
Woody/Shrub	4	7	75	4	90	0.17		
Barren	5	4	4	78	90	0.14	84.3%	0.79
Marginal total	88	91	89	92	360			
Omission Error	0.13	0.18	0.16	0.15				

Table S4.238. Confusion Matrix with commission and omission errors from Late-May to July 1999

Classes	Open Water	Non-Woody	Woody / Shrub	Barren	Marginal total	Comission Error	Total Accuracy	Kappa Index
Open Water	76	6	4	5	90	0.16		
Non-Woody	6	74	7	4	90	0.18		
Woody/Shrub	4	6	74	6	90	0.18		
Barren	5	5	5	75	90	0.16	82.8%	0.77
Marginal total	91	90	89	90	360			
Omission Error	0.17	0.18	0.17	0.16				

Table S4.239. Confusion Matrix with commission and omission errors from Late-May to July 2001

Classes	Open Water	Non-Woody	Woody / Shrub	Barren	Marginal total	Comission Error	Total Accuracy	Kappa Index
Open Water	77	6	3	4	90	0.15		
Non-Woody	5	74	7	4	90	0.18	83.4%	0.78
Woody/Shrub	3	7	73	7	90	0.19		
Barren	5	3	5	77	90	0.15		

Marginal total	90	90	88	92	360			
Omission Error	0.15	0.18	0.17	0.16				

Table S4.240. Confusion Matrix with commission and omission errors from Late-May to July 2002

Classes	Open Water	Non-Woody	Woody / Shrub	Barren	Marginal total	Comission Error	Total Accuracy	Kappa Index
Open Water	95	3	4	3	105	0.10		
Non-Woody	3	91	7	4	105	0.14		
Woody/Shrub	3	6	91	5	105	0.13		
Barren	3	5	5	93	105	0.12	87.8%	0.84
Marginal total	104	105	107	105	420			
Omission Error	0.09	0.13	0.15	0.12				

Table S4.241. Confusion Matrix with commission and omission errors from Late-May to July 2003

Classes	Open Water	Non-Woody	Woody / Shrub	Barren	Marginal total	Comission Error	Total Accuracy	Kappa Index
Open Water	99	3	2	2	105	0.06		
Non-Woody	2	97	5	1	105	0.07		
Woody/Shrub	2	4	97	2	105	0.08		
Barren	1	2	3	99	105	0.06	93.3%	0.91
Marginal total	104	106	107	104	420			
Omission Error	0.04	0.08	0.09	0.05				

Table S4.242. Confusion Matrix with commission and omission errors from Late-May to July 2004

Classes	Open Water	Non-Woody	Woody / Shrub	Barren	Marginal total	Comission Error	Total Accuracy	Kappa Index
Open Water	81	4	2	4	90	0.10		
Non-Woody	2	77	7	4	90	0.14		
Woody/Shrub	3	6	77	5	90	0.15		
Barren	2	5	4	79	90	0.12	87.2%	0.83
Marginal total	87	92	90	91	360			
Omission Error	0.08	0.16	0.15	0.13				

Table S4.243. Confusion Matrix with commission and omission errors from Late-May to July 2005

Classes	Open	Non-	Woody /	Barren	Marginal	Comission	Total	Kappa

	Water	Woody	Shrub		total	Error	Accuracy	Index
Open Water	76	5	4	5	90	0.16		
Non-Woody	3	74	8	5	90	0.18		
Woody/Shrub	3	8	75	5	90	0.17		
Barren	4	5	5	77	90	0.14	83.8%	0.78
Marginal total	85	92	92	92	360			
Omission Error	0.11	0.19	0.18	0.16				

Table S4.244. Confusion Matrix with commission and omission errors from Late-May to July 2006

Classes	Open Water	Non-Woody	Woody / Shrub	Barren	Marginal total	Comission Error	Total Accuracy	Kappa Index
Open Water	74	6	5	5	90	0.18		
Non-Woody	7	72	7	5	90	0.20		
Woody/Shrub	5	7	72	7	90	0.20		
Barren	5	5	5	75	90	0.17	81.3%	0.75
Marginal total	91	90	88	91	360			
Omission Error	0.18	0.20	0.19	0.18				

Table S4.245. Confusion Matrix with commission and omission errors from Late-May to July 2007

Classes	Open Water	Non-Woody	Woody / Shrub	Barren	Marginal total	Comission Error	Total Accuracy	Kappa Index
Open Water	75	6	4	5	90	0.17		
Non-Woody	6	73	7	4	90	0.19		
Woody/Shrub	4	7	73	6	90	0.19		
Barren	5	4	5	76	90	0.16	82.4%	0.77
Marginal total	91	90	88	91	360			
Omission Error	0.17	0.19	0.17	0.17				

Table S4.246. Confusion Matrix with commission and omission errors from Late-May to July 2008

Classes	Open Water	Non-Woody	Woody / Shrub	Barren	Marginal total	Comission Error	Total Accuracy	Kappa Index
Open Water	78	5	3	4	90	0.13		
Non-Woody	3	75	8	5	90	0.17		
Woody/Shrub	3	6	75	6	90	0.16	84.7%	0.80
Barren	4	5	5	77	90	0.15		
Marginal total	88	91	90	91	360			

Omission Error	0.11	0.18	0.17	0.16				

Table S4.247. Confusion Matrix with commission and omission errors from Late-May to July 2009

Classes	Open Water	Non-Woody	Woody / Shrub	Barren	Marginal total	Comission Error	Total Accuracy	Kappa Index
Open Water	77	5	3	5	90	0.15		
Non-Woody	4	74	8	5	90	0.18		
Woody/Shrub	4	7	74	6	90	0.18		
Barren	4	6	4	76	90	0.15	83.5%	0.78
Marginal total	88	92	88	92	360			
Omission Error	0.13	0.19	0.16	0.17				

Table S4.248. Confusion Matrix with commission and omission errors from Late-May to July 2010

Classes	Open Water	Non-Woody	Woody / Shrub	Barren	Marginal total	Comission Error	Total Accuracy	Kappa Index
Open Water	79	5	3	4	90	0.12		
Non-Woody	2	76	8	4	90	0.16		
Woody/Shrub	3	6	76	5	90	0.16		
Barren	3	5	4	78	90	0.13	85.8%	0.81
Marginal total	87	92	90	91	360			
Omission Error	0.09	0.17	0.16	0.14				

Table S4.249. Confusion Matrix with commission and omission errors from Late-May to July 2011

Classes	Open Water	Non-Woody	Woody / Shrub	Barren	Marginal total	Comission Error	Total Accuracy	Kappa Index
Open Water	77	5	3	5	90	0.14		
Non-Woody	4	74	8	5	90	0.17		
Woody/Shrub	3	7	74	6	90	0.18		
Barren	4	5	3	78	90	0.14	84.3%	0.79
Marginal total	88	92	88	93	360			
Omission Error	0.12	0.19	0.15	0.16				

Table S4.250. Confusion Matrix with commission and omission errors from Late-May to July 2013

Classes	Open Water	Non-Woody	Woody / Shrub	Barren	Marginal total	Comission Error	Total Accuracy	Kappa Index
Open Water	78	5	3	4	90	0.13	84.1%	0.79

Non-Woody	3	75	8	5	90	0.17
Woody/Shrub	3	7	75	6	90	0.17
Barren	4	6	5	75	90	0.17
Marginal total	88	93	90	89	360	
Omission Error	0.11	0.19	0.17	0.16		

Table S4.251. Confusion Matrix with commission and omission errors from Late-May to July 2014

Classes	Open Water	Non-Woody	Woody / Shrub	Barren	Marginal total	Comission Error	Total Accuracy	Kappa Index
Open Water	77	5	4	5	90	0.15		
Non-Woody	4	74	8	5	90	0.17		
Woody/Shrub	3	6	75	6	90	0.17		
Barren	4	5	5	77	90	0.15	84.1%	0.79
Marginal total	87	91	91	92	360			
Omission Error	0.12	0.18	0.17	0.16				

Table S4.252. Confusion Matrix with commission and omission errors from Late-May to July 2015

Classes	Open Water	Non-Woody	Woody / Shrub	Barren	Marginal total	Comission Error	Total Accuracy	Kappa Index
Open Water	77	5	3	5	90	0.14		
Non-Woody	4	74	7	4	90	0.17		
Woody/Shrub	3	6	75	6	90	0.17		
Barren	4	5	5	77	90	0.15	84.2%	0.79
Marginal total	89	90	89	92	360			
Omission Error	0.13	0.18	0.16	0.16				

Table S4.253. Confusion Matrix with commission and omission errors from Late-May to July 2016

Classes	Open Water	Non-Woody	Woody / Shrub	Barren	Marginal total	Comission Error	Total Accuracy	Kappa Index
Open Water	100	2	2	2	105	0.05		
Non-Woody	2	97	5	2	105	0.08		
Woody/Shrub	2	4	96	3	105	0.09		
Barren	2	3	2	98	105	0.07	92.9%	0.91
Marginal total	106	105	105	104	420			
Omission Error	0.06	0.08	0.09	0.06				

Table S4.254. Confusion Matrix with commission and omission errors from Late-May to July 2017

Classes	Open Water	Non-Woody	Woody / Shrub	Barren	Marginal total	Comission Error	Total Accuracy	Kappa Index
Open Water	100	2	2	2	105	0.05		
Non-Woody	1	98	5	2	105	0.07		
Woody/Shrub	2	4	97	2	105	0.08		
Barren	2	2	2	98	105	0.06	93.4%	0.91
Marginal total	105	105	105	104	420			
Omission Error	0.05	0.07	0.08	0.05				

Table S4.255. Confusion Matrix with commission and omission errors from Late-May to July 2018

Classes	Open Water	Non-Woody	Woody / Shrub	Barren	Marginal total	Comission Error	Total Accuracy	Kappa Index
Open Water	101	2	1	2	105	0.04		
Non-Woody	2	99	3	2	105	0.06		
Woody/Shrub	2	3	98	2	105	0.07		
Barren	1	2	2	100	105	0.05	94.6%	0.93
Marginal total	105	106	104	105	420			
Omission Error	0.04	0.07	0.05	0.05				

Table S4.256. Confusion Matrix with commission and omission errors from Late-May to July 2019

Classes	Open Water	Non-Woody	Woody / Shrub	Barren	Marginal total	Comission Error	Total Accuracy	Kappa Index
Open Water	99	2	2	2	105	0.06		
Non-Woody	2	96	6	2	105	0.09		
Woody/Shrub	2	4	96	3	105	0.08		
Barren	3	3	2	98	105	0.07	92.6%	0.90
Marginal total	105	105	107	104	420			
Omission Error	0.06	0.08	0.10	0.06				

Table S4.257. Confusion Matrix with commission and omission errors from Late-May to July 2020

Classes	Open Water	Non-Woody	Woody / Shrub	Barren	Marginal total	Comission Error	Total Accuracy	Kappa Index
Open Water	117	1	1	1	120	0.02		
Non-Woody	1	116	2	2	120	0.04	96.7%	0.96
Woody/Shrub	2	2	115	1	120	0.04		
Barren	1	2	1	116	120	0.03		

Marginal total	121	120	119	121	480			
Omission Error	0.03	0.04	0.03	0.04				

Table S4.258. Confusion Matrix with commission and omission errors from Late-May to July 2021

Classes	Open Water	Non-Woody	Woody / Shrub	Barren	Marginal total	Comission Error	Total Accuracy	Kappa Index
Open Water	100	2	2	2	105	0.05		
Non-Woody	2	97	4	3	105	0.08		
Woody/Shrub	2	4	97	3	105	0.08		
Barren	3	2	2	98	105	0.07	93.1%	0.91
Marginal total	107	104	104	105	420			
Omission Error	0.07	0.07	0.07	0.07				

Table S4.259. Confusion Matrix with commission and omission errors from Late-May to July 2022

Classes	Open Water	Non-Woody	Woody / Shrub	Barren	Marginal total	Comission Error	Total Accuracy	Kappa Index
Open Water	78	5	3	5	90	0.14		
Non-Woody	3	75	8	4	90	0.17		
Woody/Shrub	4	7	74	5	90	0.18		
Barren	4	5	4	77	90	0.14	84.3%	0.79
Marginal total	89	92	88	91	360			
Omission Error	0.13	0.18	0.16	0.15				

Table S4.260. Confusion Matrix with commission and omission errors from Late-May to July 2023

Classes	Open Water	Non-Woody	Woody / Shrub	Barren	Marginal total	Comission Error	Total Accuracy	Kappa Index
Open Water	77	5	4	5	90	0.15		
Non-Woody	4	74	8	5	90	0.17		
Woody/Shrub	3	6	75	6	90	0.17		
Barren	4	5	5	77	90	0.15	84.1%	0.79
Marginal total	87	91	91	92	360			
Omission Error	0.12	0.18	0.17	0.16				

Supplementary Material E

4.5. Land cover changes in proportion of variance with elevation

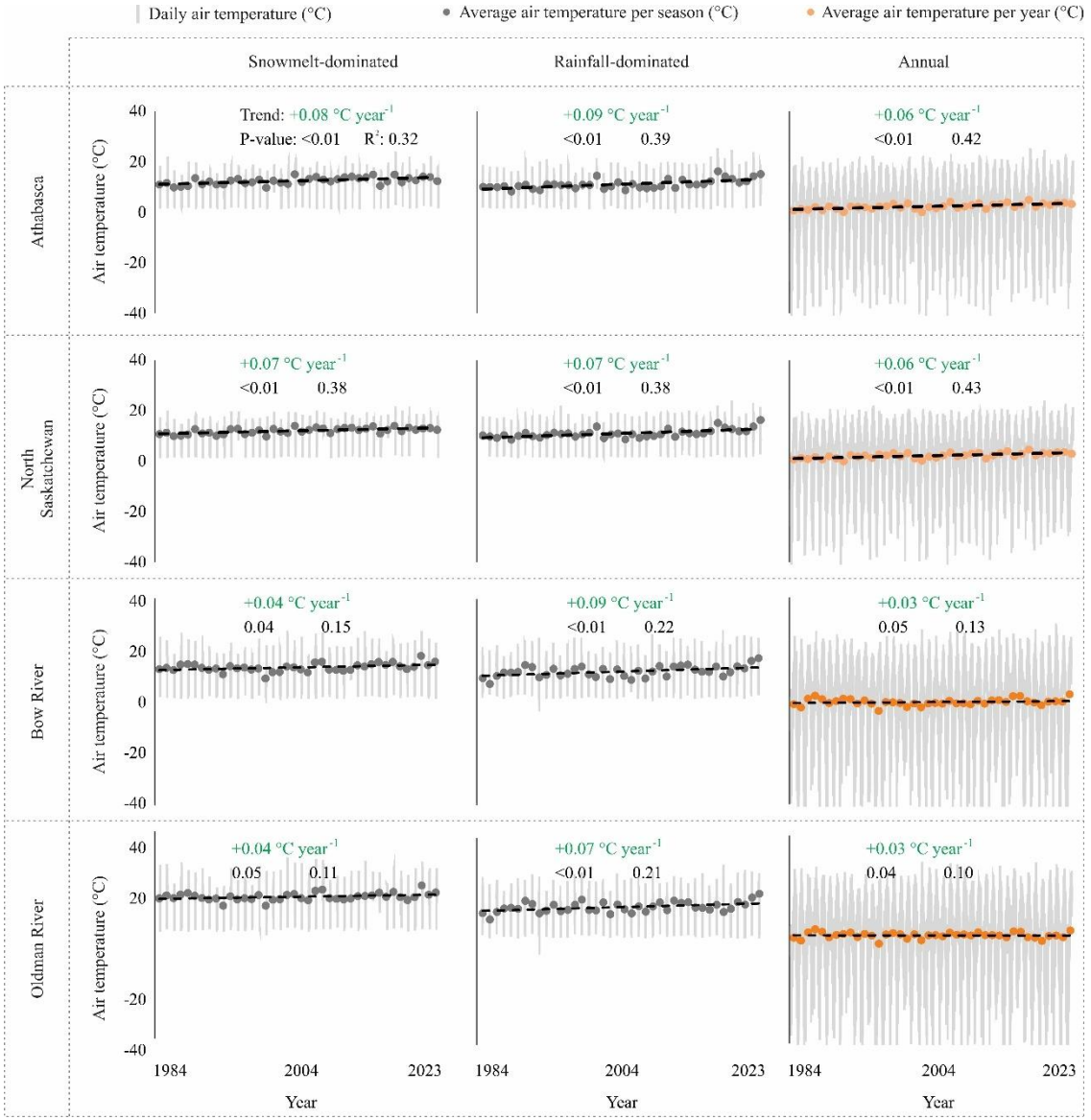

Fig**. S4.2.** Trends of the daily average air temperature.

4.6. Land cover extent trends

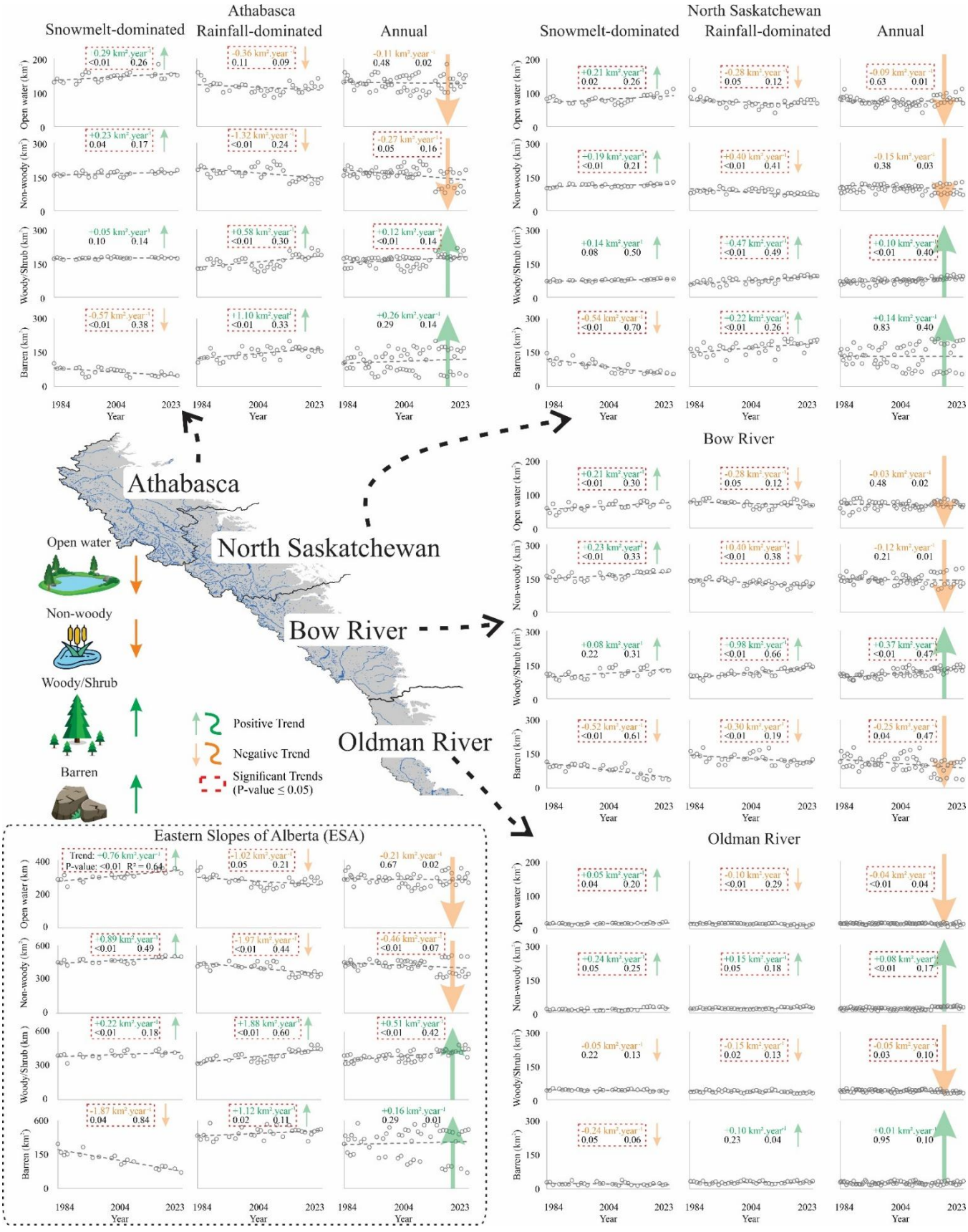

Fig. S4.3. Trends (a) of the land cover extent per season, per watershed and at all ES region from 1984 to 2023

4.7. Land cover changes

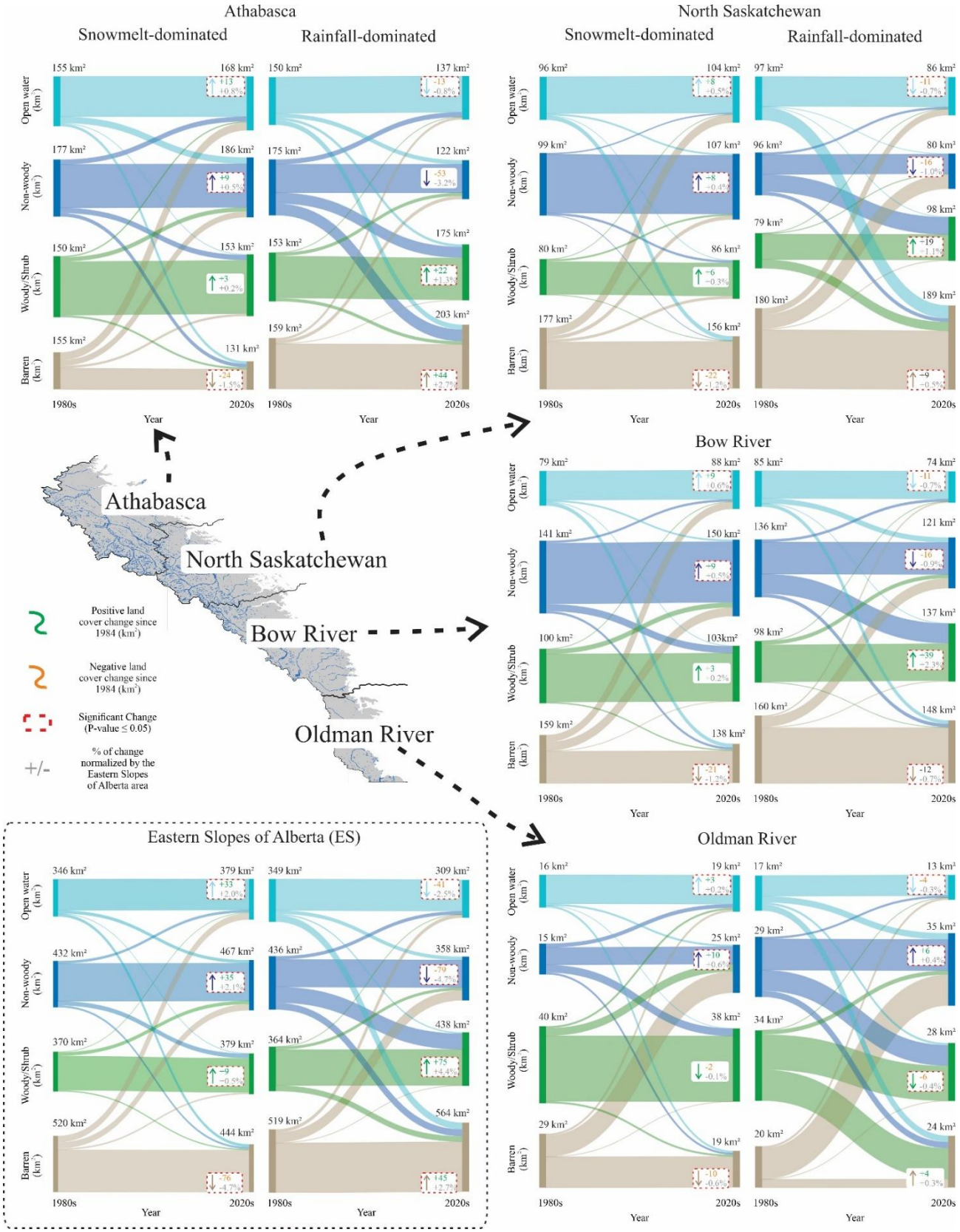

Fig. S4.4. Sankey diagram of the land cover changes in the Eastern Slopes of Alberta per period from 1980s to 2020s. The percentage of change are normalized by the total area of the Eastern Slopes of Alberta (1668 km^2).

Supplementary Material H

4.8. Land cover changes in proportion of variance with elevation

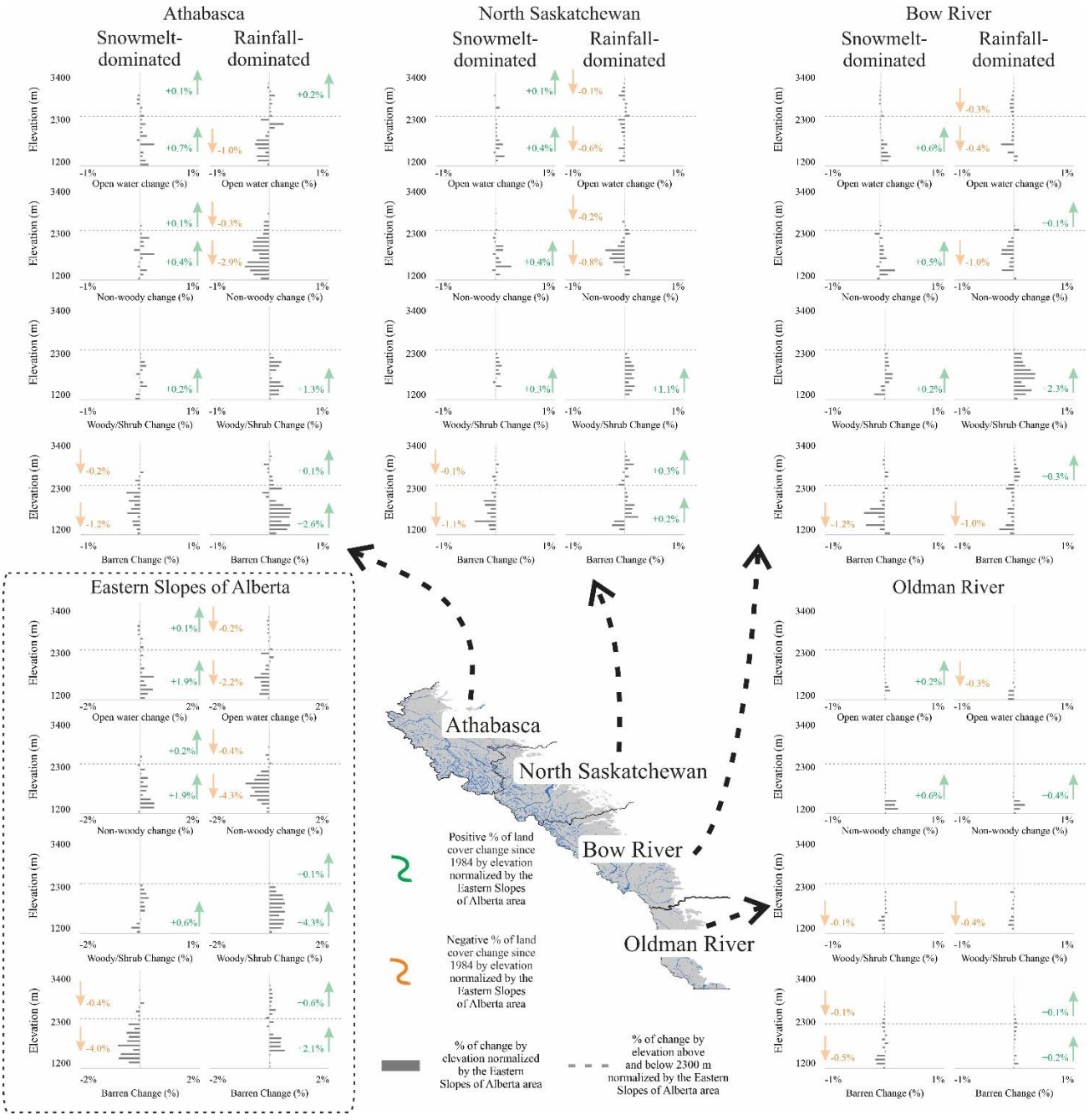

Fig. S4.5. Total land cover area changes (%) per period and watershed in the subalpine (< 2300 m) and alpine (≥ 2300 m) regions of the Eastern Slopes of Alberta from 1980s to 2020s. The percentage of change are normalized by the total area of the Eastern Slopes of Alberta (1668 km^2).

Supplementary Material I

4.9. Land cover changes in subalpine and alpine regions of the ES

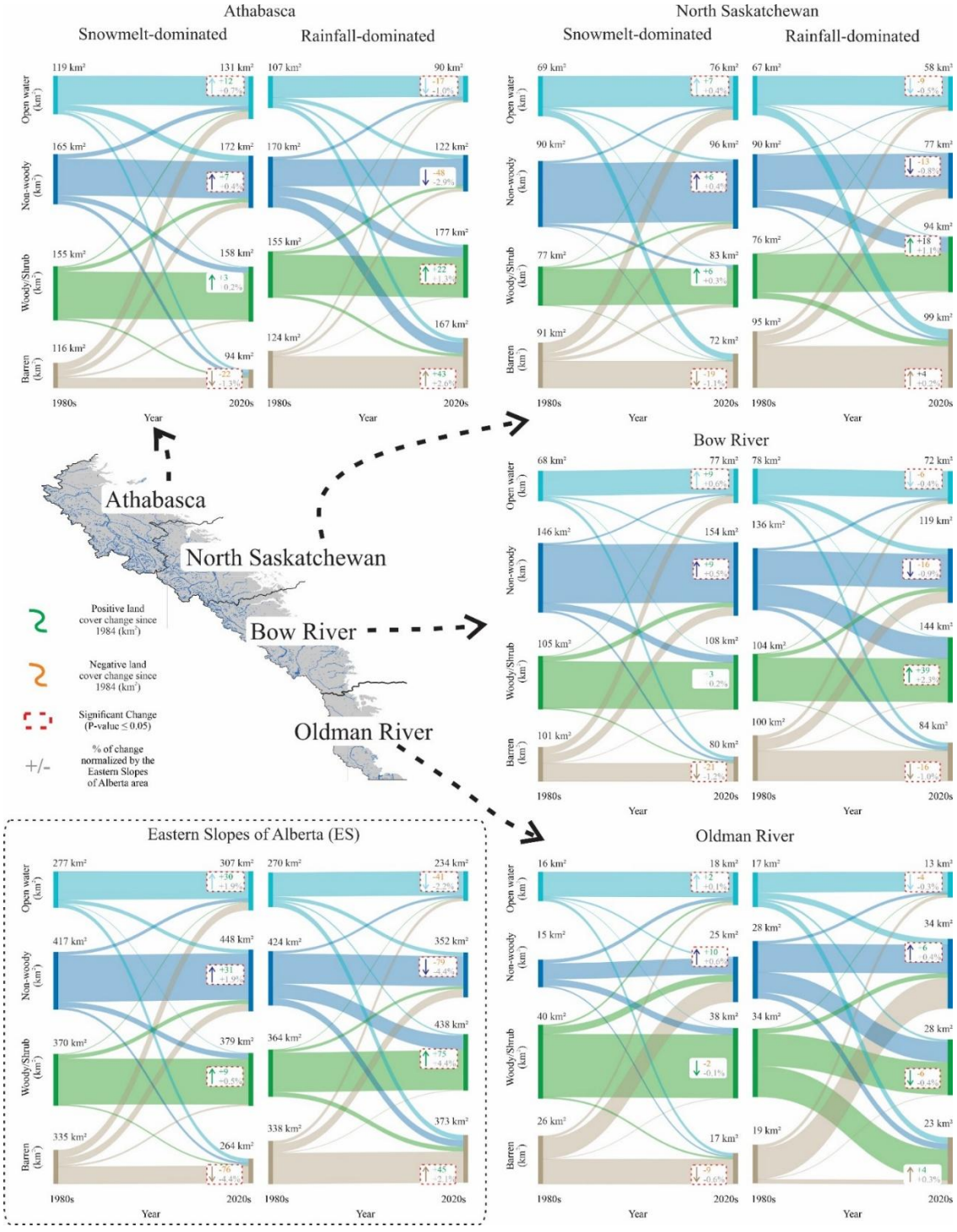

Fig. **S4.6.** Sankey diagram of the land cover changes in the subalpine region of the Eastern Slopes of Alberta per period from 1980s to 2020s. The percentage of change are normalized by the total area of the Eastern Slopes of Alberta (1668 km^2).

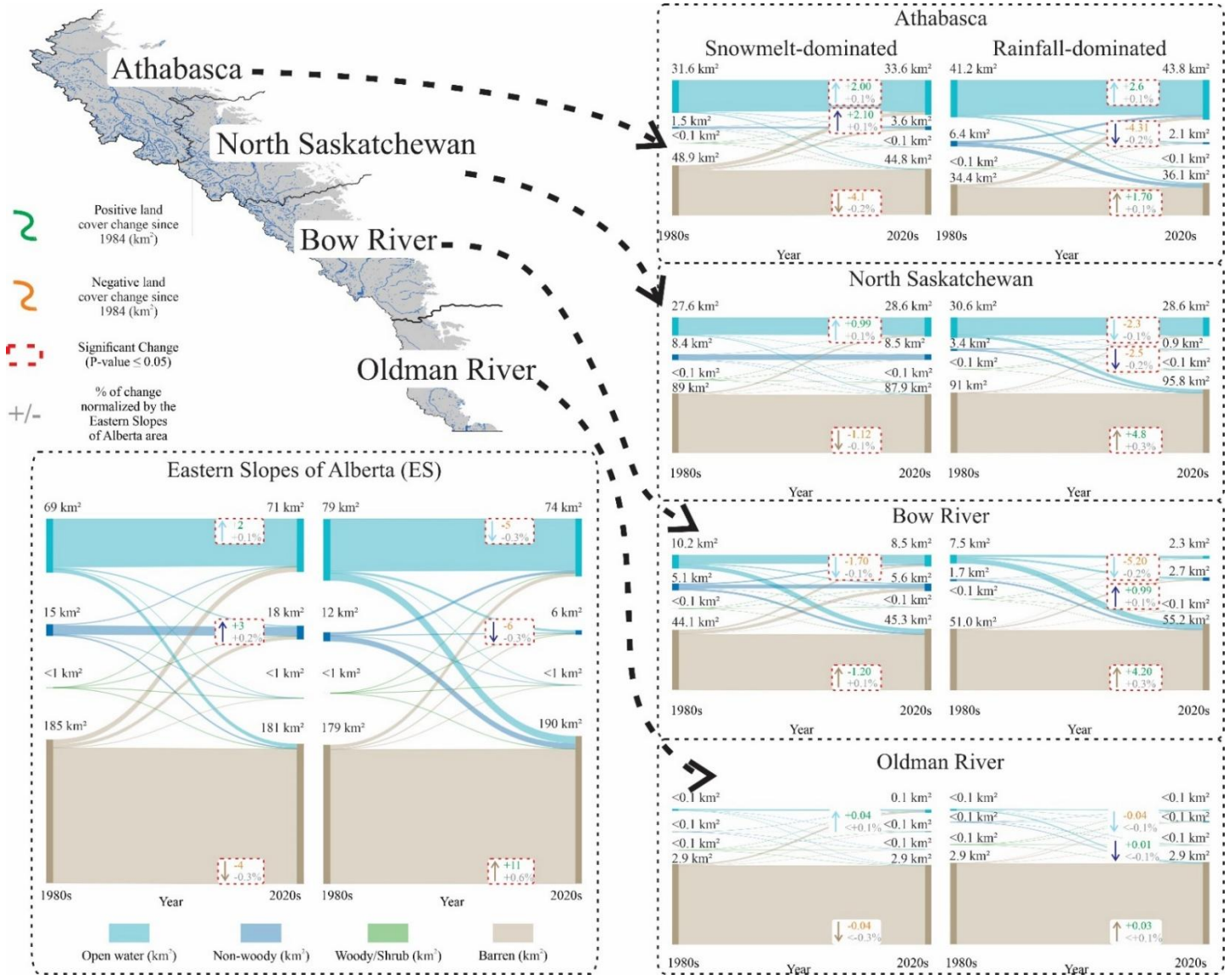

Fig. **S4.7.** Sankey diagram of the land cover changes in alpine region of the Eastern Slopes of Alberta per period from 1980s to 2020s. The percentage of change are normalized by the total area of the Eastern Slopes of Alberta (1668 km^2).

8. Supplementary Materials Chapter 5

Supplementary Material A

5.1. Townships per watershed

Oldman watershed townships: T001R27W4, T002R28W4, T003R01W5, T004R03W5, T005R03W5, T006R04W5 T007R04W5, T008R04W5, T009R04W5, T010R04W5, T011R05W5, T012R04W5, T013R05W5.

Bow River townships: T014R05W5, T015R05W5, T016R05W5, T017R06W5, T018R07W5, T019R09W5, T020R09W5, T021R10W5, T022R10W5, T023R10W5, T024R10W5, T025R10W5, T026R10W5, T027R10W5, T027R10W5, T028R10W5, T029R10W5.

North Saskatchewan townships: T030R10W5, T031R11W5, T032R12W5, T033R13W5, T034R14W5, T034R18W5, T035R18W5, T036R19W5, T037R20W5, T038R21W5, T039R20W5, T040R20W5, T041R20W5, T042R20W5.

Athabasca townships: T045R23W5, T046R24W5, T047R24W5, T048R25W5, T049R26W5, T050R02W6, T050R27W5, T051R04W6.

Supplementary Material B

5.3. Penman evaporation model

The Penman equation (1948) was utilised to calculate evaporation rates within the ES, as shown in Equation 5.3. The selection of this model was based on its specific purpose of estimating open water evaporation and its successful validation in several mountainous water bodies (Pillco Zolá et al., 2019; Rosenberry et al., 2007; Zhao and Gao, 2019).

$$E = \frac{\Delta}{\Delta+\gamma} \cdot \frac{R_n}{\lambda v} + \frac{\gamma}{\Delta+\gamma} \cdot f(u)\cdot(e_s - e_a) \quad (5.3)$$

Equation 5.3 defines E as the open-water evaporation rate (mm/d); R_n represents the net radiation received at the water surface ($MJ.m^{-2}.d^{-1}$); Δ is the slope of the saturation vapour pressure curve ($kPa.^oC^{-1}$) at air temperature; γ is the psychrometric coefficient (assumed 0.0665 $kPa.^oC^{-1}$); ρ is the density of water (1000 $kg.m^{-3}$); λv is the latent heat of vaporization (assumed 2.5 $MJ.kg^{-1}$), ($e_s - e_a$) is the difference between saturation and partial water vapour pressure (kPa), and f(u) is a function used to account for the advective drying effects of wind ($mm.d^{-1}.kPa^{-1}$). In Equation 5.4, u is the wind speed at 2 m height ($m.s^{-1}$). The wind function was measured using the method established by Penman in 1956.

$$f(u)=1.313+1.381\ u \quad (5.4)$$

The method to obtain Δ is described in Annex 2 of the Food and Agriculture Organisation of the United Nations protocol-56 (Allen et al., 1998) and showed in Equation 5.5.

$$\Delta=\frac{4098\ e_s}{(T+237.3)^2} \quad (5.5)$$

Where T represents the average air temperature (ºC), and e_s (saturation vapor pressure) was derived from the maximum (T_{max}) and minimum (T_{min}) air temperature (Allen et al., 1998), as per in Equation 5.6.

$$e_s=\frac{e^o(T_{max}) + e^o(T_{min})}{2} \quad (5.6)$$

The saturation vapour pressure (e^o) is related to average air temperature. This relationship is expressed by Equation 5.7.

$$e^o(T) = 0.6108 \exp\left[\frac{17.27T}{T+237.3}\right] \quad (5.7)$$

Subsequently, e_a was determined by the average relative humidity (RH) (%) and the saturation vapour pressure (e_s), as shown in Equation 5.8.

$$e_a = \frac{RH}{100}\, e_s \quad (5.8)$$

The R_n was estimated based on the difference between net incoming short-wave radiation ($R_{ns}\downarrow$) and net outgoing longwave radiation ($R_{nl}\uparrow$) estimated based on Food and Agriculture Organisation-56 method, i.e., Allen et al., 1998), as per Equation 5.9. The Food and Agriculture Organization Penman convention utilizes Equation 5.9 because it considers the typical daily norm, where $R_{ns}\downarrow$ is the radiation input (net incoming) to the earth's surface, while $R_{nl}\uparrow$ represents the primary radiation loss (net outgoing) through emission.

$$R_n = R_{ns}\downarrow - R_{nl}\uparrow \quad (5.9)$$

The R_{ns} was estimated by Equation 5.10, using the total incoming solar radiation (R_s), and the open water albedo (α) considered as 0.05 (as a common value for open water in the literature; Schaaf et al., 2002; Rouse et al., 2005).

$$R_{ns}\downarrow = R_s\,(1 - \alpha) \quad (5.10)$$

The method to obtain R_{nl} is described in equation 5.11, by using the Stefan-Boltzmann law (Food and Agriculture Organization, protocol-56), using maximum and minimum air temperatures

$$R_{nl}\uparrow = \sigma \left(\frac{T_{max}^4 + T_{min}^4}{2}\right)(0.34 - 0.14\sqrt{e_a})\left(1.35\frac{R_{ns}}{R_{so}} - 0.35\right) \quad (5.11)$$

The σ represents the Stefan-Boltzmann constant (4.903×10^{-9} MJ K^{-4} m^{-2} d^{-1}). R_{so} represents the clear sky radiation value and it was calculated according to the Food and Agriculture Organization, protocol-56, showed in Equation 5.12.

$$R_{so} = (0.75 + 0.00002\, z)\, R_a \quad (5.12)$$

Where z is the elevation (m), and R_a represents the extraterrestrial radiation (MJ m^{-2} d^{-1}). When the Penman method was implemented in each watershed of the ES, the average elevation of each watershed was considered during the application of Equation 5.12. Therefore, considering 1500 m

for the Oldman River, 1735 m for the Bow River, 1885 m for the North Saskatchewan, and 1950 m for the Athabasca watershed. R_a was calculated using Equation 5.13, following the Food and Agriculture Organization, protocol-56.

$$R_a = \frac{1440}{\pi} G_{sc}\, d_r\, [w_s \sin\phi\ \sin\delta + \cos\phi\ \cos\delta \sin w_s] \tag{5.13}$$

Where the solar constant (0.082 MJ m^{-2} min^{-1}) is represented by the G_{sc}, d_r is the inverse Earth-Sun distance factor, π is a mathematical constant (3.14159) that represents the ratio of a circle's circumference to its diameter, w_s represents the sunset hour angel (radians), ϕ is the latitude in radians, and δ represents the solar declination (radians). The central latitude (ϕ) of each watershed was considered during the application of Equation 5.13. Therefore, considering 0.864 radians (49.5º N in the Livingstone Range, High Rock Junction) for the Oldman River, 0.892 radians (51.1º N from Banff to Kananaskis) for the Bow River, 0.911 radians (52.2º N in the Columbia Icefield, David Thompson Corridor) for the North Saskatchewan, and 0.930 radians (53.3º N Jasper National Park, Tonquin Valley) for the Athabasca watershed. The d_r was calculated by Equation 5.14.

$$d_r = 1 + 0.033 \cos\left(\frac{2\pi J}{365}\right) \tag{5.14}$$

The Julian days (1-365) are represented by *J*. The δ was estimated by Equation 5.15. Later, w_s was estimated by the Equation 5.16.

$$\delta = 0.409\, sin\left(\frac{2\pi J}{365} - 1.39\right) \tag{5.15}$$

$$w_s = arccos[-tan\phi\ tan\delta] \tag{5.16}$$

Supplementary Material C

5.4. Permanent forest areas per watershed in ESA

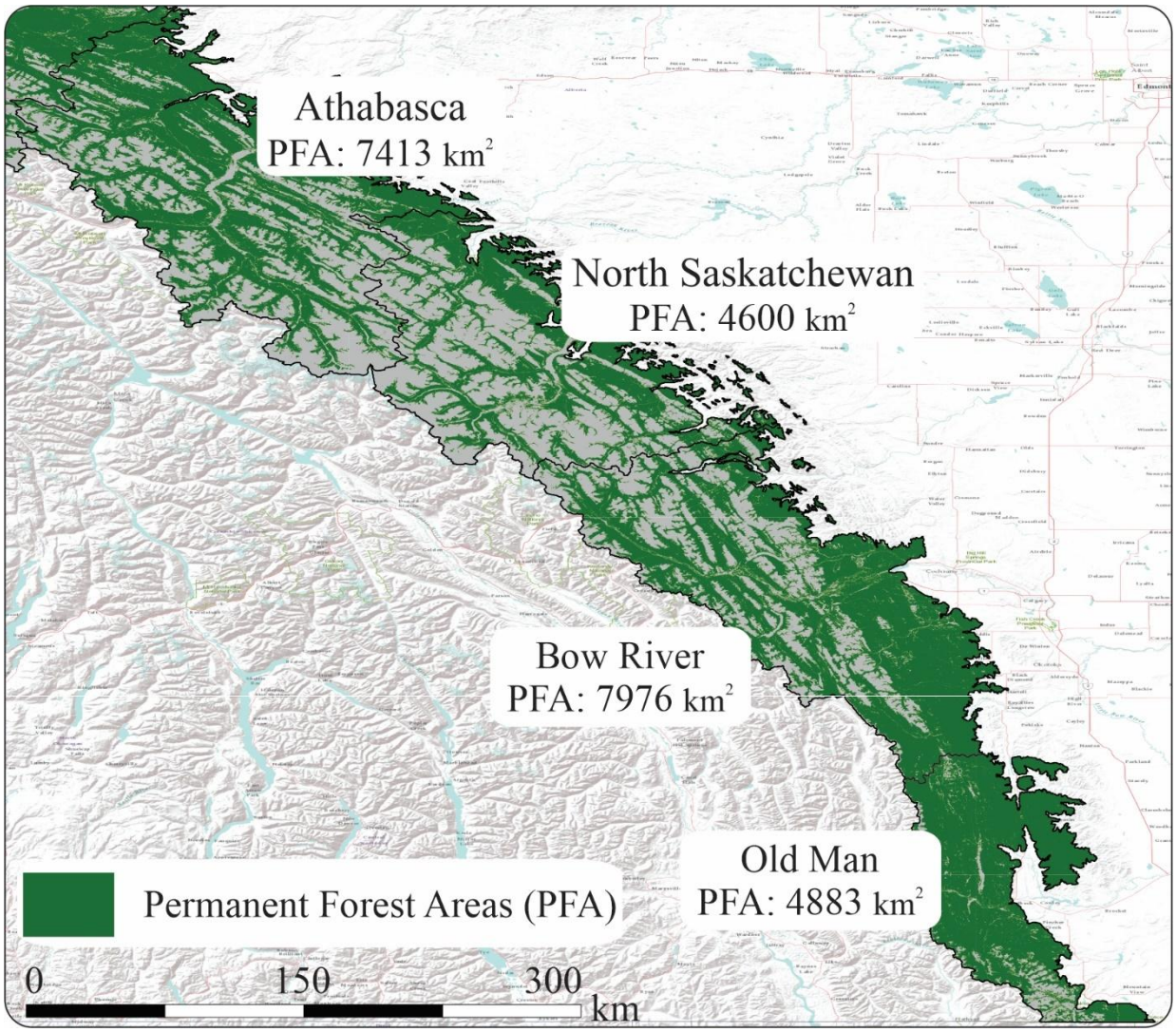

Fig. S5.1 Permanent Forest areas per watershed in ESA since 1984 to 2022

Supplementary Material D

5.5. Projected trends of open water per watershed in ES

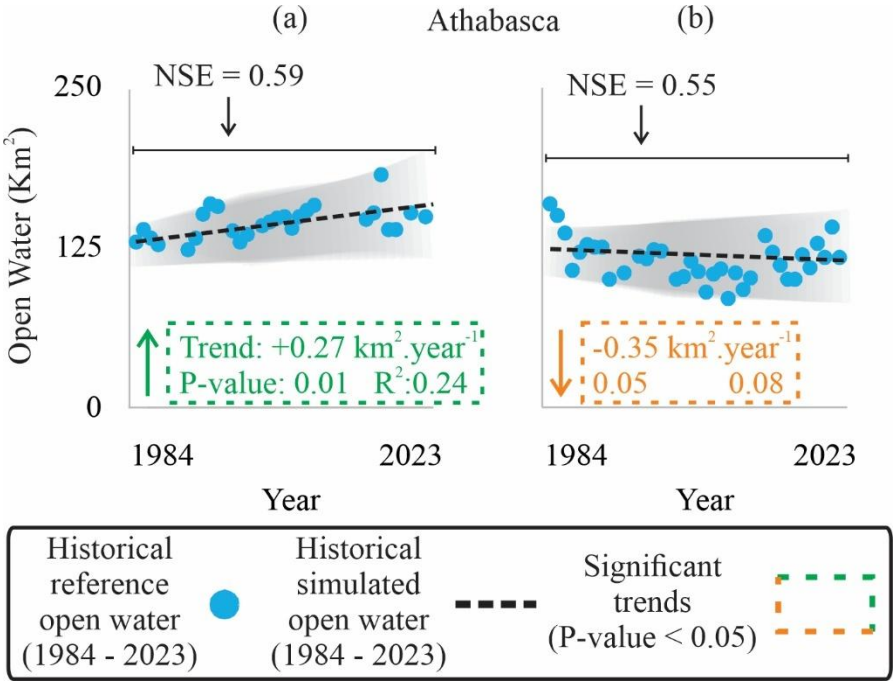

Fig. S5.2. Temporal trends of open water area in the Athabasca watershed during Snowmelt- (a), and Rainfall-dominated period (b) in the simulated historical period (1984 – 2023) compared (NSE) with historical reference open water area. Shaded areas represent the 95% confidence intervals for the historical simulated open water extent.

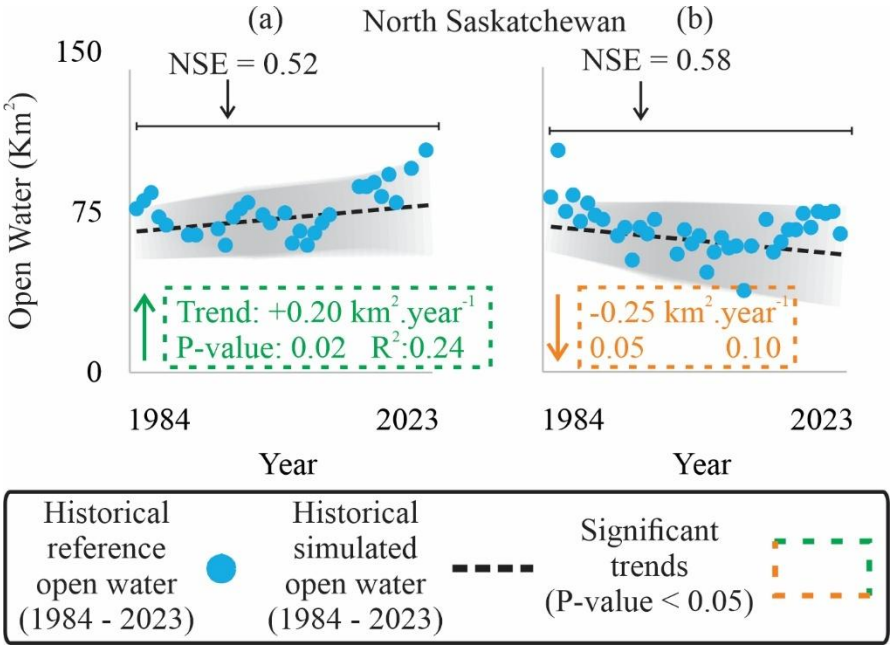

Fig. S5.3. Temporal trends of open water area in the North Saskatchewan watershed during Snowmelt- (a), and Rainfall-dominated period (b) in the simulated historical period (1984 – 2023) compared (NSE) with historical reference open water area. Shaded areas represent the 95% confidence intervals for the historical simulated open water extent.

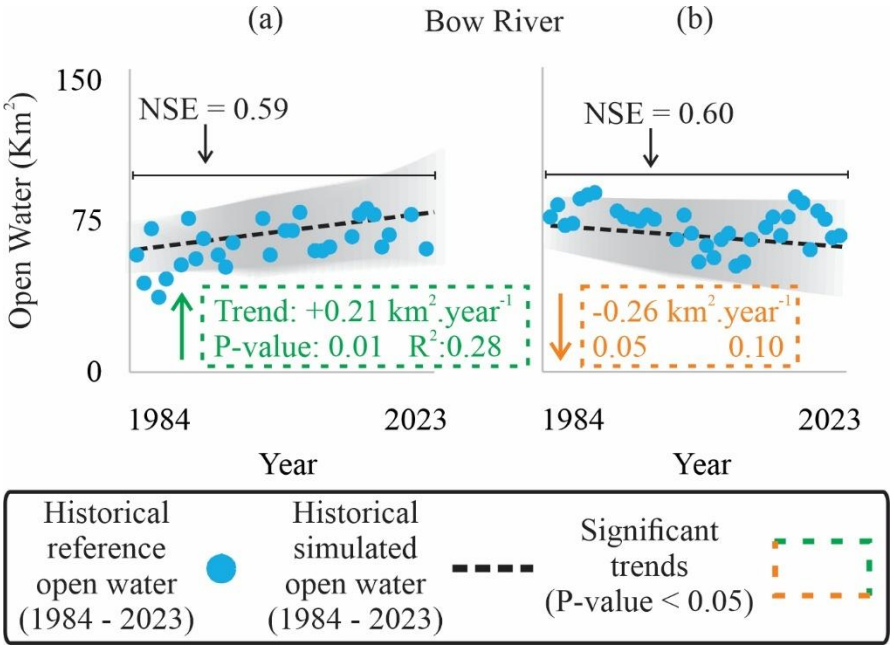

Fig. S4. Temporal trends of open water area in the Bow River watershed during Snowmelt- (a), and Rainfall-dominated period (b) in the simulated historical period (1984 – 2014) compared (NSE) with historical reference open water area. Shaded areas represent the 95% confidence intervals for the historical simulated open water extent.

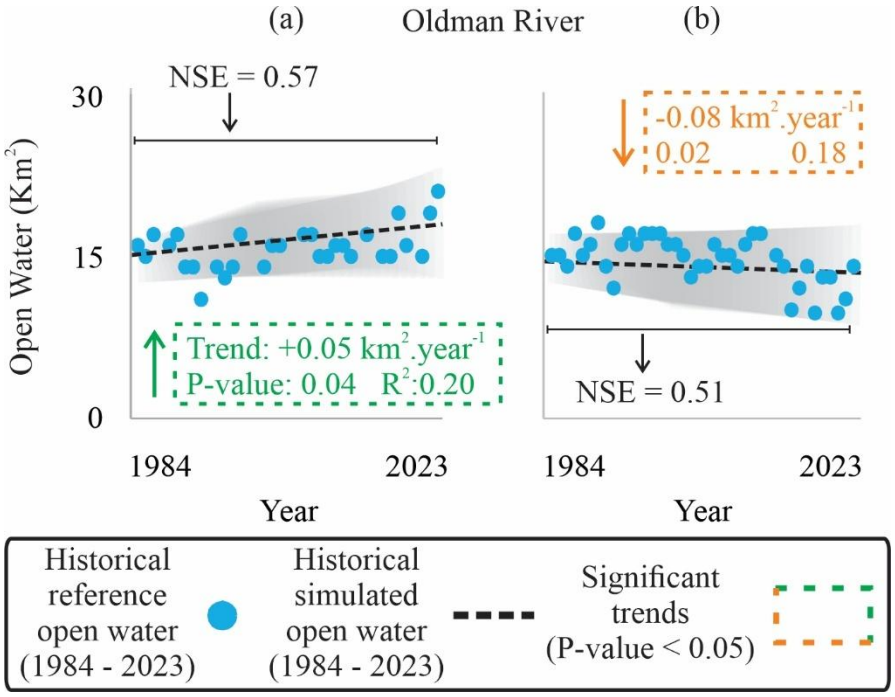

Fig. S5.5. Temporal trends of open water area in the Oldman River watershed during Snowmelt-(a), and Rainfall-dominated period (b) in the simulated historical period (1984 – 2023) compared (NSE) with historical reference open water area. Shaded areas represent the 95% confidence intervals for the historical simulated open water extent.

Supplementary Material E

5.7. Projected trends of evaporation per watershed in ES

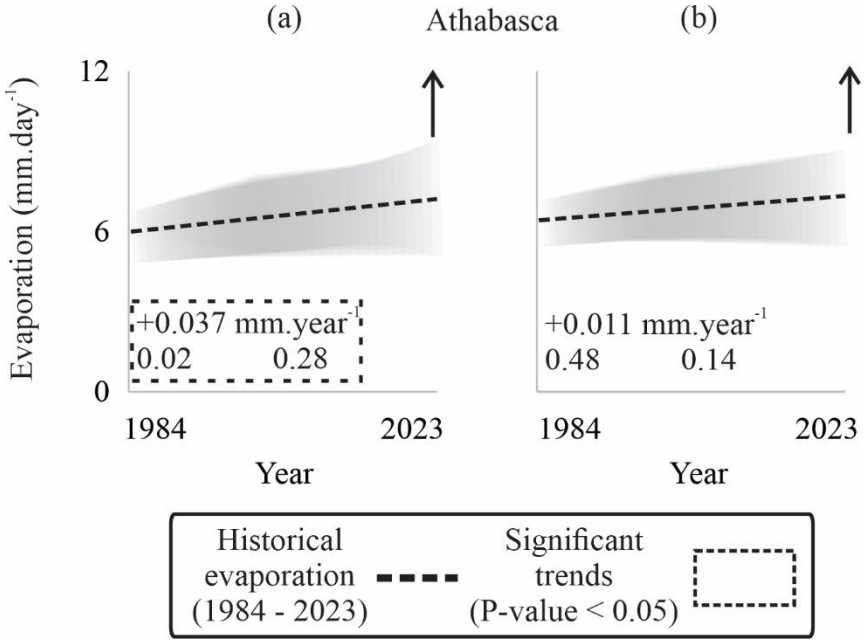

Fig. S5.6. Trends of open water evaporation in the Athabasca watershed during Snowmelt- (a), and Rainfall-dominated period (b) in the simulated historical period (1984 – 2023). Shaded areas represent the represent the 95% confidence intervals for the historical open water evaporation.

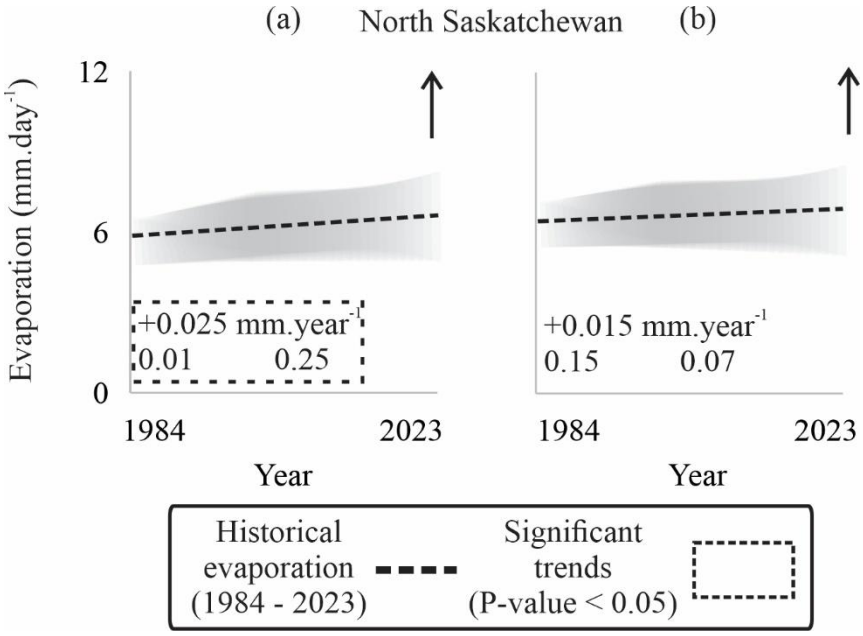

Fig. S5.7. Trends of open water evaporation in the North Saskatchewan watershed during Snowmelt- (a), and Rainfall-dominated period (b) in the simulated historical period (1984 – 2023). Shaded areas represent the represent the 95% confidence intervals for the historical open water evaporation.

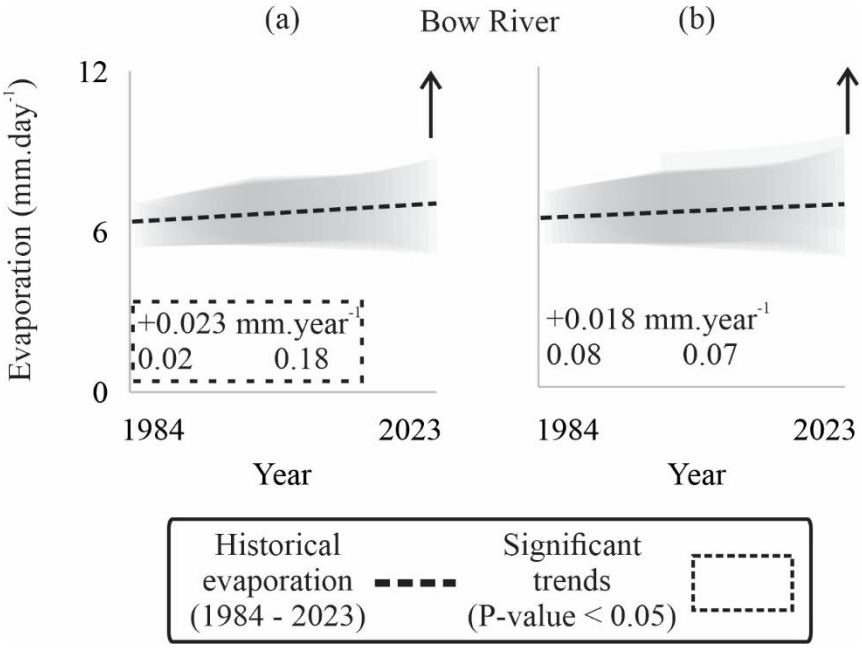

Fig. S5.8. Trends of open water evaporation in the Bow River watershed during Snowmelt- (a), and Rainfall-dominated period (b) in the simulated historical period (1984 – 2023). Shaded areas represent the represent the 95% confidence intervals for the historical open water evaporation.

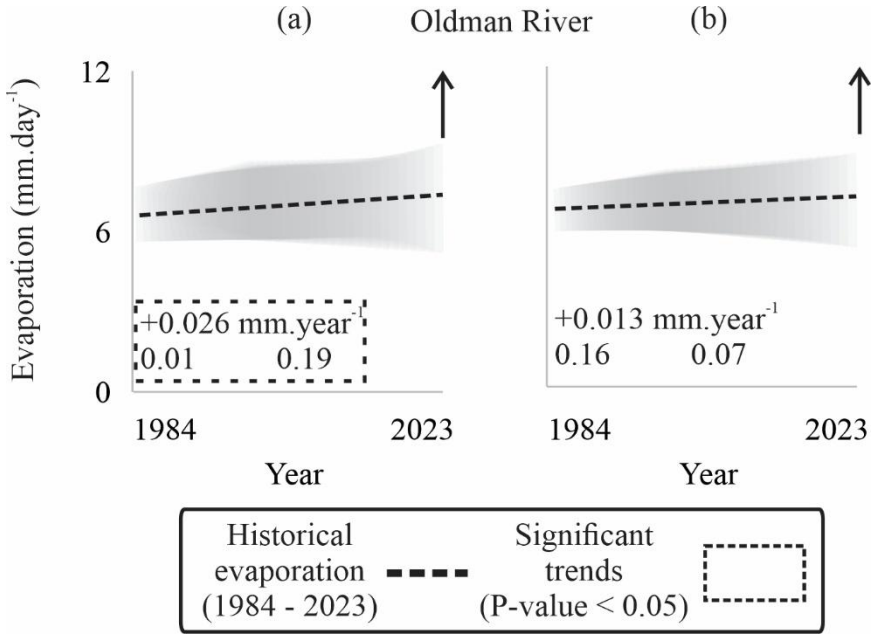

Fig. S5.9. Trends of open water evaporation in the Oldman River watershed during Snowmelt- (a), and Rainfall-dominated period (b) in the simulated historical period (1984 – 2023). Shaded areas represent the represent the 95% confidence intervals for the historical open water evaporation.

Supplementary Material F

5.8. Projected trends of forest transpiration per watershed in ES

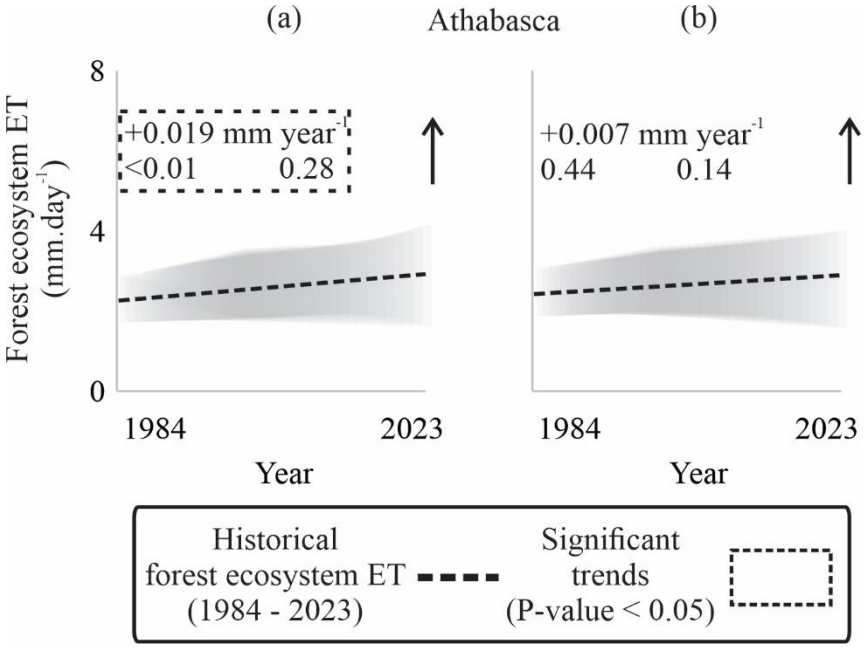

Fig. S5.10. Trends of forest ecosystem ET rates in the Athabasca watershed during Snowmelt- (a), and Rainfall-dominated period (b) in the historical period (1984 – 2023). Shaded areas represent the represent the 95% confidence intervals for the historical forest ecosystem ET.

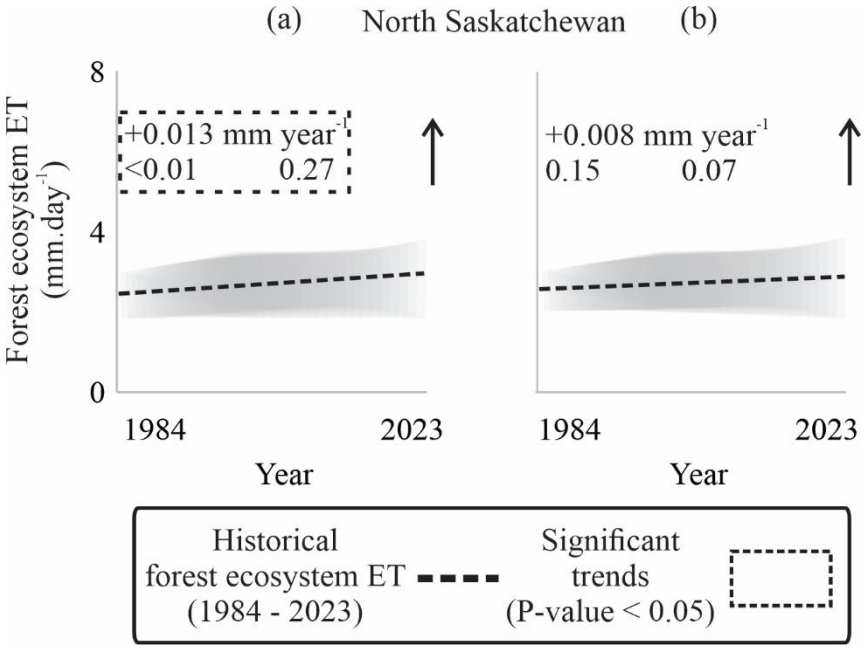

Fig. S5.11. Trends of forest ecosystem ET rates in the North Saskatchewan watershed during Snowmelt- (a), and Rainfall-dominated period (b) in the historical period (1984 – 2023). Shaded areas represent the represent the 95% confidence intervals for the forest ecosystem ET.

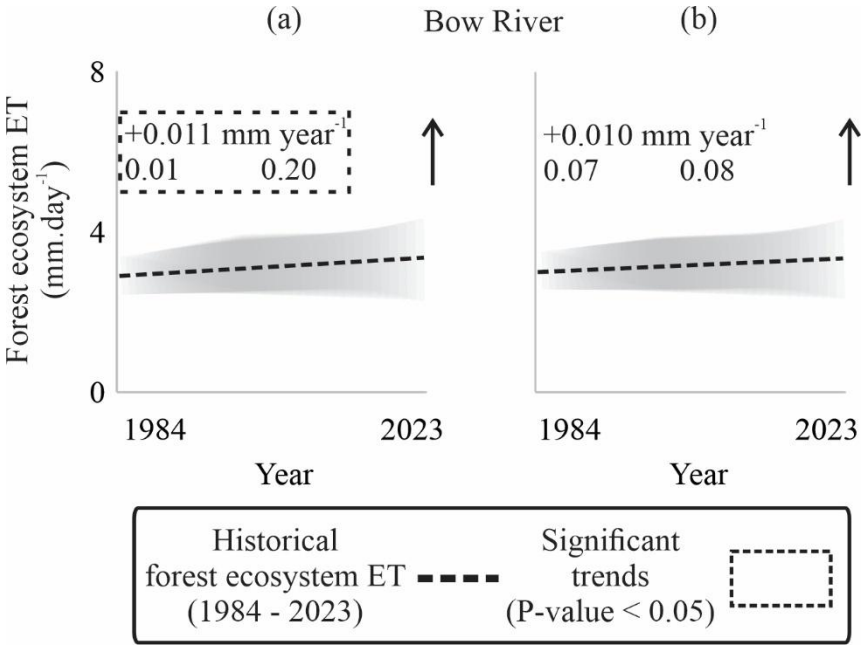

Fig. S5.12. Trends of forest ecosystem ET rates in the Bow River watershed during Snowmelt- (a), and Rainfall-dominated period (b) in the historical period (1984 – 2023). Shaded areas represent the represent the 95% confidence intervals for the forest ecosystem ET.

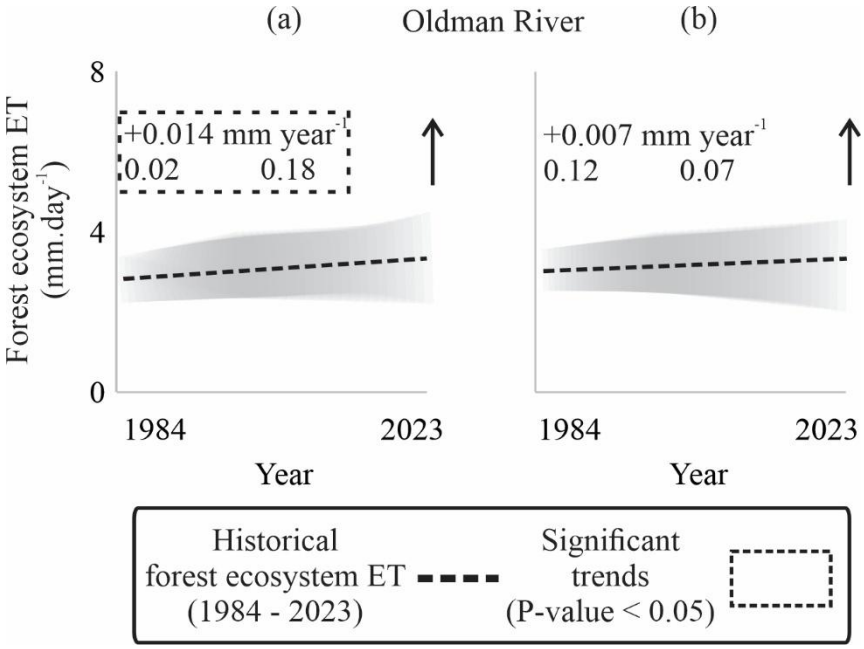

Fig. S5.13. Trends of forest ecosystem ET rates in the Oldman River watershed during Snowmelt-(a), and Rainfall-dominated period (b) in the historical period (1984 – 2023). Shaded areas represent the represent the 95% confidence intervals for the historical forest ecosystem ET.

Supplementary Material G

5.9. Ratio of evapotranspiration volume per watershed in ES

5.9.1. Athabasca Watershed

Table S5.1.

Historical (1984 to 2014) proportion (P%) between evaporation volume in open water areas and ET volume in permanent forest areas in the Athabasca watershed during Snowmelt-dominated period (Late May to mid-July)

Year	Average evaporation of OW (mm day^{-1})	OW Area (km^2)	Evaporation volume of OW (m^3 day^{-1})	Average ET of PFA (mm day^{-1})	PFA Area (km^2)	ET volume of PFA (m^3 day^{-1})	P% (OW_E/PFA_{ET})
1984	5.21	155	805272	2.6	7413	18915362	4.3%
1985	6.88	131	901350	3.4	7413	24981206	3.6%
1986	6.60	124	817182	3.2	7413	23986555	3.4%
1987	6.69	131	878461	3.3	7413	24315702	3.6%
1988	5.85	130	760802	2.9	7413	21264919	3.6%
1989	6.32	151	952586	3.1	7413	22958168	4.1%
1990	6.76	137	924464	3.3	7413	24544980	3.8%
1991	5.09	153	779879	2.5	7413	18488068	4.2%
1992	5.68	144	815275	2.8	7413	20627675	4.0%
1993	6.77	129	870327	3.3	7413	24576213	3.5%
1994	5.96	143	850388	2.9	7413	21666321	3.9%
1995	6.38	144	917026	3.1	7413	23167565	4.0%
1996	6.34	148	940076	3.1	7413	23035932	4.1%
1997	5.77	141	813938	2.8	7413	20964605	3.9%
1998	6.42	154	987619	3.1	7413	23328166	4.2%
1999	6.22	128	798955	3.0	7413	22589210	3.5%
2000	6.78	145	979130	3.3	7413	24612587	4.0%
2001	6.43	134	859628	3.2	7413	23372578	3.7%

2002	8.28	133	1100773	4.1	7413	30073584	3.7%
2003	6.92	156	1080461	3.4	7413	25133914	4.3%
2004	6.70	142	951910	3.3	7413	24335208	3.9%
2005	6.73	163	1098091	3.3	7413	24454583	4.5%
2006	6.86	145	997015	3.4	7413	24900271	4.0%
2007	7.18	147	1054407	3.5	7413	26066918	4.0%
2008	8.37	147	1228039	4.1	7413	30395997	4.0%
2009	6.67	153	1022321	3.3	7413	24242853	4.2%
2010	6.77	158	1068082	3.3	7413	24584193	4.3%
2011	6.71	157	1050149	3.3	7413	24357838	4.3%
2012	7.19	152	1094534	3.5	7413	26121023	4.2%
2013	7.53	178	1343343	3.7	7413	27368956	4.9%
2014	6.41	173	1109240	3.1	7413	23297476	4.8%
2015	6.19	133	821196	3.0	7413	29822298	2.8%
2016	7.29	135	980659	3.6	7413	35120366	2.8%
2017	7.58	158	1201515	3.7	7413	36543405	3.3%
2018	7.09	134	951560	3.5	7413	34159751	2.8%
2019	7.68	134	1026529	3.8	7413	36998079	2.8%
2020	7.06	155	1094909	3.5	7413	34012691	3.2%
2021	7.02	149	1042441	3.4	7413	33807603	3.1%
2022	7.44	146	1087924	3.6	7413	35851264	3.0%
2023	6.28	150	939759	3.1	7413	30262000	3.1%

OW_E: Open Water Areas evaporation volume (m^3 day^{-1}); PFA_{ET}: Permanent Forest Areas evapotranspiration volume (m^3 day^{-1})

Table S5.2.

Historical (1984 to 2023) proportion (P%) between evaporation volume in open water areas and ET volume in permanent forest areas in the Athabasca watershed during Rainfall-dominated period (late-July to mid-September)

Year	Average evaporation of OW (mm day^{-1})	OW Area (km^2)	Evaporation volume of OW ($m^3\ day^{-1}$)	Average ET of PFA (mm day^{-1})	PFA Area (km^2)	ET volume of PFA ($m^3\ day^{-1}$)	P% (OW_E/PFA_{ET})
1984	5.16	115	594881	2.5	7413	18756250	3.2%
1985	5.15	124	639229	2.5	7413	18713477	3.4%
1986	4.41	119	522838	2.2	7413	16010123	3.3%
1987	6.31	116	733535	3.1	7413	22928638	3.2%
1988	4.68	117	547115	2.3	7413	16997174	3.2%
1989	5.20	119	618812	2.5	7413	18889197	3.3%
1990	5.15	123	632708	2.5	7413	18712217	3.4%
1991	5.55	118	656911	2.7	7413	20149452	3.3%
1992	4.82	116	561003	2.4	7413	17515513	3.2%
1993	6.17	114	706049	3.0	7413	22412328	3.2%
1994	5.30	123	653550	2.6	7413	19258799	3.4%
1995	5.15	125	642446	2.5	7413	18706185	3.4%
1996	4.55	126	573134	2.2	7413	16530426	3.5%
1997	5.20	118	613626	2.5	7413	18900122	3.2%
1998	5.39	120	646255	2.6	7413	19564192	3.3%
1999	6.47	118	765408	3.2	7413	23491282	3.3%
2000	7.05	122	861209	3.5	7413	25626139	3.4%
2001	5.26	126	663338	2.6	7413	19122251	3.5%
2002	5.26	124	653836	2.6	7413	19118113	3.4%
2003	5.30	115	611190	2.6	7413	19238574	3.2%
2004	4.51	118	533161	2.2	7413	16397172	3.3%
2005	4.92	121	594815	2.4	7413	17869452	3.3%
2006	6.21	121	749389	3.0	7413	22574204	3.3%

2007	4.66	115	535211	2.3	7413	16917379	3.2%
2008	5.76	118	680469	2.8	7413	20924067	3.3%
2009	7.25	119	861506	3.6	7413	26351655	3.3%
2010	6.52	133	869637	3.2	7413	23690412	3.7%
2011	5.27	120	634022	2.6	7413	19146584	3.3%
2012	6.16	116	713393	3.0	7413	22385490	3.2%
2013	5.74	130	746547	2.8	7413	20836614	3.6%
2014	6.13	121	743898	3.0	7413	22253337	3.3%
2015	6.23	121	754365	3.1	7413	22629665	3.3%
2016	6.44	126	811477	3.2	7413	23392463	3.5%
2017	6.06	138	834874	3.0	7413	22012162	3.8%
2018	6.67	129	859634	3.3	7413	24227908	3.5%
2019	6.32	134	845297	3.1	7413	22956578	3.7%
2020	6.35	126	800994	3.1	7413	23065550	3.5%
2021	6.44	124	799352	3.2	7413	23392463	3.4%
2022	6.67	133	889031	3.3	7413	24227908	3.7%
2023	6.27	137	857047	3.1	7413	22774960	3.8%

5.9.2. North Saskatchewan Watershed

Table S5.3.

Historical (1984 to 2023) proportion (P%) between evaporation volume in open water areas and ET volume in permanent forest areas in the North Saskatchewan watershed during Snowmelt-dominated period (Late May to mid-July)

Year	Average evaporation of OW (mm day^{-1})	OW Area (km^2)	Evaporation volume of OW ($m^3\ day^{-1}$)	Average ET of PFA (mm day^{-1})	PFA Area (km^2)	ET volume of PFA ($m^3\ day^{-1}$)	P% (OW_E/PFA_{ET})
1984	5.31	81	429387	2.60	4600	11977530	3.6%
1985	6.30	71	450189	3.09	4600	14206845	3.2%
1986	6.50	70	452670	3.18	4600	14644776	3.1%
1987	6.59	73	483390	3.23	4600	14864147	3.3%
1988	5.70	70	401285	2.80	4600	12858516	3.1%
1989	5.85	77	449197	2.87	4600	13179301	3.4%
1990	6.06	71	432948	2.97	4600	13662307	3.2%
1991	5.32	78	413299	2.61	4600	11991280	3.4%
1992	5.33	74	396604	2.61	4600	12020211	3.3%
1993	6.55	72	471258	3.21	4600	14769857	3.2%
1994	6.19	78	482527	3.03	4600	13958875	3.5%
1995	5.98	75	451689	2.93	4600	13487703	3.3%
1996	5.84	76	445280	2.86	4600	13169651	3.4%
1997	5.96	75	446034	2.92	4600	13430614	3.3%
1998	6.93	77	532858	3.40	4600	15625501	3.4%
1999	6.34	70	443735	3.11	4600	14291273	3.1%
2000	6.66	76	503207	3.26	4600	15017555	3.4%
2001	5.92	73	430429	2.90	4600	13347725	3.2%
2002	6.67	72	481433	3.27	4600	15029187	3.2%
2003	5.74	80	458031	2.81	4600	12942067	3.5%
2004	6.11	75	460562	2.99	4600	13768913	3.3%
2005	6.67	81	539884	3.27	4600	15028391	3.6%

2006	6.57	78	511442	3.22	4600	14810873	3.5%
2007	6.72	76	510352	3.29	4600	15147999	3.4%
2008	6.80	78	530250	3.33	4600	15331478	3.5%
2009	6.43	81	520569	3.15	4600	14495734	3.6%
2010	6.40	80	510556	3.13	4600	14417491	3.5%
2011	6.94	78	540592	3.40	4600	15645704	3.5%
2012	6.40	76	487387	3.13	4600	14419662	3.4%
2013	6.87	85	585305	3.36	4600	15474057	3.8%
2014	6.08	84	509529	2.98	4600	13705482	3.7%
2015	6.14	73	444900	3.01	4600	18343967	2.4%
2016	6.27	76	474527	3.07	4600	18750306	2.5%
2017	6.89	80	548549	3.38	4600	20599294	2.7%
2018	6.40	73	469991	3.14	4600	19134716	2.5%
2019	6.83	73	499531	3.35	4600	20433538	2.4%
2020	6.39	80	509439	3.13	4600	19102295	2.7%
2021	6.06	78	470986	2.97	4600	18107218	2.6%
2022	6.84	76	521474	3.35	4600	20446176	2.6%
2023	6.15	76	469072	3.01	4600	18390522	2.6%

Table S5.4.

Historical (1984 to 2023) proportion (P%) between evaporation volume in open water areas and ET volume in permanent forest areas in the North Saskatchewan watershed during Rainfall-dominated period (late-July to mid-September)

Year	Average evaporation of OW (mm day^{-1})	OW Area (km^2)	Evaporation volume of OW ($m^3\ day^{-1}$)	Average ET of PFA (mm day^{-1})	PFA Area (km^2)	ET volume of PFA ($m^3\ day^{-1}$)	P% (OW_E/PFA_{ET})
1984	5.24	69	361432	2.57	4600	11816577	3.1%
1985	4.90	66	322721	2.40	4600	11033997	2.9%
1986	4.50	70	312820	2.21	4600	10144055	3.1%
1987	6.28	67	418045	3.08	4600	14162172	3.0%
1988	5.32	72	385302	2.61	4600	11984581	3.2%
1989	4.92	67	328784	2.41	4600	11082465	3.0%
1990	5.44	64	349686	2.66	4600	12256812	2.9%
1991	5.35	69	368696	2.62	4600	12069118	3.1%
1992	5.45	66	359094	2.67	4600	12280540	2.9%
1993	5.58	63	349549	2.73	4600	12566334	2.8%
1994	5.50	65	356842	2.69	4600	12391762	2.9%
1995	4.43	63	280838	2.17	4600	9977257	2.8%
1996	4.42	66	291826	2.17	4600	9959183	2.9%
1997	5.25	67	352108	2.57	4600	11839366	3.0%
1998	5.16	63	324042	2.53	4600	11622753	2.8%
1999	6.06	65	393680	2.97	4600	13655568	2.9%
2000	6.19	57	354476	3.03	4600	13942794	2.5%
2001	5.13	75	385086	2.51	4600	11557600	3.3%
2002	5.18	64	329719	2.54	4600	11666736	2.8%
2003	5.64	60	339669	2.76	4600	12705317	2.7%
2004	4.65	68	318450	2.28	4600	10484680	3.0%
2005	5.11	69	352223	2.50	4600	11519158	3.1%

2006	5.77	64	371124	2.83	4600	13003419	2.9%
2007	4.93	60	296789	2.41	4600	11108348	2.7%
2008	5.62	63	354032	2.75	4600	12661611	2.8%
2009	6.50	62	404140	3.18	4600	14650067	2.8%
2010	6.24	60	377093	3.06	4600	14069481	2.7%
2011	4.48	65	292772	2.20	4600	10107873	2.9%
2012	5.75	60	347037	2.82	4600	12952351	2.7%
2013	5.58	68	376786	2.73	4600	12572261	3.0%
2014	5.72	64	367046	2.80	4600	12894776	2.8%
2015	5.28	62	327345	2.59	4600	11901120	2.8%
2016	6.71	65	433270	3.29	4600	15124340	2.9%
2017	6.05	58	352870	2.96	4600	13636700	2.6%
2018	5.84	60	347767	2.86	4600	13163360	2.6%
2019	6.83	63	430229	3.35	4600	15394820	2.8%
2020	5.57	66	369106	2.73	4600	12554780	2.9%
2021	6.61	62	408755	3.24	4600	14898940	2.7%
2022	6.74	59	400266	3.30	4600	15191960	2.6%
2023	6.21	64	395367	3.04	4600	13997340	2.8%

5.9.3. Bow River Watershed

Table S5.5.

Historical (1984 to 2023) proportion (P%) between evaporation volume in open water areas and ET volume in permanent forest areas in the Bow River watershed during Snowmelt-dominated period (Late May to mid-July)

Year	Average evaporation of OW (mm day^{-1})	OW Area (km^2)	Evaporation volume of OW ($m^3\ day^{-1}$)	Average ET of PFA (mm day^{-1})	PFA Area (km^2)	ET volume of PFA ($m^3\ day^{-1}$)	P% (OW_E/PFA_{ET})
1984	5.74	81	464714	2.81	7976	22423538	2.1%
1985	6.84	62	426399	3.35	7976	26728620	1.6%
1986	7.04	58	408379	3.45	7976	27523607	1.5%
1987	7.09	66	465958	3.47	7976	27694355	1.7%
1988	6.22	60	373172	3.05	7976	24296754	1.5%
1989	6.31	73	459794	3.09	7976	24662691	1.9%
1990	6.60	61	405799	3.24	7976	25810418	1.6%
1991	5.70	75	426855	2.79	7976	22288545	1.9%
1992	5.77	67	384064	2.83	7976	22552002	1.7%
1993	7.20	63	451400	3.53	7976	28130936	1.6%
1994	6.64	75	494858	3.25	7976	25941030	1.9%
1995	6.47	70	451394	3.17	7976	25275769	1.8%
1996	6.28	72	449046	3.08	7976	24534840	1.8%
1997	6.49	69	449988	3.18	7976	25369675	1.8%
1998	7.36	72	532709	3.61	7976	28775772	1.9%
1999	6.86	59	406968	3.36	7976	26795137	1.5%
2000	7.19	70	500622	3.52	7976	28096331	1.8%
2001	6.49	65	419060	3.18	7976	25345944	1.7%
2002	7.15	63	452952	3.51	7976	27961913	1.6%
2003	6.12	80	488162	3.00	7976	23928567	2.0%
2004	6.57	70	460485	3.22	7976	25673319	1.8%

2005	7.10	82	581381	3.48	7976	27762777	2.1%
2006	7.04	75	529374	3.45	7976	27523426	1.9%
2007	7.22	71	511415	3.54	7976	28200550	1.8%
2008	7.25	74	540073	3.55	7976	28349766	1.9%
2009	6.87	82	559901	3.36	7976	26831916	2.1%
2010	6.90	80	552328	3.38	7976	26967713	2.0%
2011	7.38	75	555781	3.62	7976	28850724	1.9%
2012	6.77	71	481479	3.32	7976	26471724	1.8%
2013	7.24	92	665328	3.55	7976	28287179	2.4%
2014	6.43	87	558512	3.15	7976	25144401	2.2%
2015	6.62	64	426411	3.24	7976	34328077	1.2%
2016	6.71	70	469091	3.29	7976	34811586	1.3%
2017	7.33	79	577245	3.59	7976	38010977	1.5%
2018	6.89	65	449835	3.38	7976	35719022	1.3%
2019	7.39	65	478678	3.62	7976	38320398	1.2%
2020	6.84	79	536707	3.35	7976	35436161	1.5%
2021	6.49	75	488637	3.18	7976	33648461	1.5%
2022	7.33	72	527236	3.59	7976	37981147	1.4%
2023	6.57	72	470019	3.22	7976	34044003	1.4%

Table S5.6.

Historical (1984 to 2023) proportion (P%) between evaporation volume in open water areas and ET volume in permanent forest areas in the Bow River watershed during Rainfall-dominated period (late-July to mid-September)

Year	Average evaporation of OW (mm day^{-1})	OW Area (km^2)	Evaporation volume of OW ($m^3\ day^{-1}$)	Average ET of PFA (mm day^{-1})	PFA Area (km^2)	ET volume of PFA ($m^3\ day^{-1}$)	P% (OW_E/PFA_{ET})
1984	5.72	68	390869	2.80	7976	22364815	1.7%
1985	5.48	66	359540	2.69	7976	21435580	1.7%
1986	4.93	69	338121	2.41	7976	19249739	1.8%
1987	6.89	66	453867	3.38	7976	26942453	1.7%
1988	5.97	71	426181	2.92	7976	23318754	1.8%
1989	5.49	66	364203	2.69	7976	21466248	1.7%
1990	5.98	64	382206	2.93	7976	23360345	1.6%
1991	5.85	68	399416	2.87	7976	22873038	1.7%
1992	6.05	65	395388	2.97	7976	23660745	1.7%
1993	6.17	62	384572	3.03	7976	24129873	1.6%
1994	6.04	65	390392	2.96	7976	23622422	1.7%
1995	4.86	63	306656	2.38	7976	19011673	1.6%
1996	4.88	66	320774	2.39	7976	19084850	1.7%
1997	5.84	66	387353	2.86	7976	22811264	1.7%
1998	5.66	62	353043	2.78	7976	22134318	1.6%
1999	6.71	65	432842	3.29	7976	26224731	1.7%
2000	6.76	57	385145	3.31	7976	26415586	1.5%
2001	5.67	74	420912	2.78	7976	22151652	1.9%
2002	5.73	63	363233	2.81	7976	22393402	1.6%
2003	6.26	60	375248	3.07	7976	24471602	1.5%
2004	5.19	68	351187	2.54	7976	20283136	1.7%
2005	5.74	68	391563	2.81	7976	22429008	1.7%
2006	6.41	64	408805	3.14	7976	25048874	1.6%

2007	5.63	60	335330	2.76	7976	21985883	1.5%
2008	6.21	62	388380	3.05	7976	24288887	1.6%
2009	7.11	62	438554	3.48	7976	27776997	1.6%
2010	6.77	60	408013	3.32	7976	26463826	1.5%
2011	4.99	65	323838	2.45	7976	19507916	1.7%
2012	6.37	60	381561	3.12	7976	24900790	1.5%
2013	6.12	67	411880	3.00	7976	23934860	1.7%
2014	6.28	64	400204	3.08	7976	24527130	1.6%
2015	5.82	62	358474	2.85	7976	22745957	1.6%
2016	5.00	64	321907	2.45	7976	19541200	1.6%
2017	6.68	58	388822	3.27	7976	26107043	1.5%
2018	6.91	59	409937	3.39	7976	27005938	1.5%
2019	6.23	63	391811	3.05	7976	24348335	1.6%
2020	6.76	66	446563	3.31	7976	26419702	1.7%
2021	6.97	62	429135	3.42	7976	27240433	1.6%
2022	6.98	59	413434	3.42	7976	27279515	1.5%
2023	6.67	64	423963	3.27	7976	26067961	1.6%

5.9.4. Oldman River Watershed

Table S5.7.

Historical (1984 to 2023) proportion (P%) between evaporation volume in open water areas and ET volume in permanent forest areas in the Oldman River watershed during Snowmelt-dominated period (Late May to mid-July)

Year	Average evaporation of OW (mm day^{-1})	OW Area (km^2)	Evaporation volume of OW (m^3 day^{-1})	Average ET of PFA (mm day^{-1})	PFA Area (km^2)	ET volume of PFA (m^3 day^{-1})	P% (OW_E/PFA_{ET})
1984	6.11	16	96816	2.99	4883	14612757	0.7%
1985	6.96	16	109706	3.41	4883	16646416	0.7%
1986	7.90	16	128655	3.87	4883	18892405	0.7%
1987	6.95	15	106815	3.41	4883	16634491	0.6%
1988	6.41	15	98772	3.14	4883	15345727	0.6%
1989	6.89	15	106249	3.38	4883	16488095	0.6%
1990	6.77	15	101242	3.32	4883	16192022	0.6%
1991	5.55	16	86319	2.72	4883	13285048	0.6%
1992	6.15	16	98339	3.01	4883	14721449	0.7%
1993	7.75	16	120984	3.80	4883	18543072	0.7%
1994	6.58	16	103865	3.23	4883	15754260	0.7%
1995	6.81	18	119356	3.34	4883	16293673	0.7%
1996	6.39	16	102260	3.13	4883	15296598	0.7%
1997	6.82	15	104469	3.34	4883	16316244	0.6%
1998	7.09	16	110929	3.47	4883	16965464	0.7%
1999	7.32	15	107605	3.59	4883	17523486	0.6%
2000	7.51	17	125442	3.68	4883	17957834	0.7%
2001	7.16	17	120185	3.51	4883	17133535	0.7%
2002	7.35	15	110316	3.60	4883	17595395	0.6%
2003	6.58	18	121138	3.23	4883	15751560	0.8%
2004	6.69	18	118823	3.28	4883	16016231	0.7%

2005	7.18	18	128873	3.52	4883	17185120	0.7%
2006	7.59	18	136925	3.72	4883	18169037	0.8%
2007	7.44	18	131019	3.65	4883	17800518	0.7%
2008	7.36	17	126967	3.61	4883	17616126	0.7%
2009	7.34	18	130107	3.60	4883	17566024	0.7%
2010	7.41	17	129628	3.63	4883	17739984	0.7%
2011	7.64	17	131177	3.74	4883	18279539	0.7%
2012	7.12	17	120303	3.49	4883	17040143	0.7%
2013	7.59	18	135741	3.72	4883	18158143	0.7%
2014	6.78	19	130520	3.32	4883	16224156	0.8%
2015	6.71	16	106864	3.29	4883	16043094	0.7%
2016	6.74	17	114160	3.30	4883	16121939	0.7%
2017	7.11	18	127937	3.48	4883	17008001	0.8%
2018	7.19	16	116819	3.52	4883	17210404	0.7%
2019	7.55	17	125266	3.70	4883	18062589	0.7%
2020	6.85	17	118071	3.36	4883	16394106	0.7%
2021	6.34	17	107766	3.11	4883	15172939	0.7%
2022	7.35	17	122697	3.60	4883	17574360	0.7%
2023	6.98	16	115023	3.42	4883	16709465	0.7%

Table S5.8.

Historical (1984 to 2023) proportion (P%) between evaporation volume in open water areas and ET volume in permanent forest areas in the Oldman River watershed during Rainfall-dominated period (late-July to mid-September)

Year	Average evaporation of OW (mm day^{-1})	OW Area (km^2)	Evaporation volume of OW (m^3 day^{-1})	Average ET of PFA (mm day^{-1})	PFA Area (km^2)	ET volume of PFA (m^3 day^{-1})	P% (OW_E/PFA_{ET})
1984	5.60	11	62092	2.75	4883	13406701	0.5%
1985	5.97	11	65744	2.92	4883	14280012	0.5%
1986	5.51	11	61014	2.70	4883	13192889	0.5%
1987	6.41	12	79357	3.14	4883	15343323	0.5%
1988	6.20	11	71254	3.04	4883	14827059	0.5%
1989	6.62	12	81092	3.24	4883	15844155	0.5%
1990	6.55	12	75582	3.21	4883	15678675	0.5%
1991	6.11	14	86109	2.99	4883	14617419	0.6%
1992	6.72	11	76132	3.29	4883	16070868	0.5%
1993	6.66	12	78861	3.26	4883	15926659	0.5%
1994	6.58	11	73643	3.23	4883	15751717	0.5%
1995	5.93	11	66530	2.90	4883	14179735	0.5%
1996	5.26	12	61756	2.58	4883	12593570	0.5%
1997	6.61	10	67996	3.24	4883	15817788	0.4%
1998	5.75	11	61873	2.82	4883	13761027	0.4%
1999	7.13	11	81112	3.49	4883	17052120	0.5%
2000	7.44	11	83316	3.65	4883	17807715	0.5%
2001	5.24	14	73598	2.57	4883	12543578	0.6%
2002	6.13	8	50523	3.00	4883	14659886	0.3%
2003	6.36	12	75383	3.12	4883	15213741	0.5%
2004	5.76	12	71525	2.82	4883	13784747	0.5%
2005	6.42	13	81580	3.15	4883	15371759	0.5%

2006	6.75	13	85183	3.31	4883	16158407	0.5%
2007	6.24	9	58911	3.06	4883	14925426	0.4%
2008	6.50	10	67703	3.18	4883	15545002	0.4%
2009	7.25	11	78285	3.55	4883	17355284	0.5%
2010	6.78	11	77166	3.32	4883	16232296	0.5%
2011	5.91	12	71356	2.90	4883	14141588	0.5%
2012	7.15	10	73474	3.50	4883	17114689	0.4%
2013	6.24	13	81348	3.06	4883	14940485	0.5%
2014	6.15	12	75558	3.01	4883	14718835	0.5%
2015	5.30	11	60591	2.60	4883	12683937	0.5%
2016	6.31	11	67990	3.09	4883	15095093	0.5%
2017	6.08	13	76253	2.98	4883	14545083	0.5%
2018	6.78	11	73848	3.32	4883	16210534	0.5%
2019	6.72	11	73776	3.29	4883	16086650	0.5%
2020	7.08	11	74781	3.47	4883	16947103	0.4%
2021	6.19	11	65279	3.03	4883	14816299	0.4%
2022	6.84	11	72179	3.35	4883	16359367	0.4%
2023	6.73	11	70910	3.30	4883	16094743	0.4%